UNCLASSIFIED

AD NUMBER

AD828243

NEW LIMITATION CHANGE

TO

Approved for public release, distribution unlimited

FROM

Distribution authorized to U.S. Gov't. agencies and their contractors; Administrative/Operational Use; MAR 1968. Other requests shall be referred to Air Force Rocket Propulsion Laboratory, Edwards AFB, CA.

AUTHORITY

AFRPL ltr dtd 20 Dec 1971

THIS PAGE IS UNCLASSIFIED

AD 828 243

AFRPL-TR-68-22

AD828243

FINAL REPORT ON THE DEVELOPMENT OF ANALYTICAL TECHNIQUES FOR BELLOWS AND DIAPHRAGM DESIGN

T. M. Trainer, L. E. Hulbert, J. F. Lestingi,
R. E. Keith, et al.

Battelle Memorial Institute
Columbus Laboratories

TECHNICAL REPORT NO. AFRPL-TR-68-22

March, 1968

REPRODUCED BY
NATIONAL TECHNICAL
INFORMATION SERVICE
US DEPARTMENT OF COMMERCE
SPRINGFIELD, VA. 22161

Air Force Rocket Propulsion Laboratory
Research and Technology Division
Air Force Systems Command
Edwards Air Force Base
California

NOTICES

When U. S. Government drawings, specifications, or other data are used for any purpose other than a definitely related Government procurement operation, the fact that the Government may have formulated, furnished, or in any way supplied the said drawings, specifications, or other data, is not to be regarded by implication or otherwise, or in any manner licensing the holder or any other person or corporation, or conveying any rights or permission to manufacture, use, or sell any patented invention that may in any way be related thereto.

If this copy is not needed, return to AFRPL (RPRPD), Edwards, California 93523.

Unclassified

Security Classification

DOCUMENT CONTROL DATA - R&D

(Security classification of title, body of abstract and indexing annotation must be entered when the overall report is classified)

1 ORIGINATING ACTIVITY *(Corporate author)*
Battelle Memorial Institute
Columbus Laboratories
505 King Avenue, Columbus, Ohio 43201

2a. REPORT SECURITY CLASSIFICATION
Unclassified

2b GROUP

3. REPORT TITLE
Final Report on the Development of Analytical Techniques for Bellows and Diaphragm Design

4. DESCRIPTIVE NOTES *(Type of report and inclusive dates)* Summary of program activities from March 1, 1965 to March 11, 1968, under USAS Contract No. 04(611)-10532

5. AUTHOR(S) *(Last name, first name, initial)*
Trainer, T. M., Hulbert, L. E., Lestingi, J. F., Keith, R. E., et al.

6. REPORT DATE	7a TOTAL NO. OF PAGES	7b. NO. OF REFS
March 11, 1968	582 (+ 9)	81

8a CONTRACT OR GRANT NO.	9a. ORIGINATOR'S REPORT NUMBER(S)
AF 04(611)-10532	
b. PROJECT NO. AFS No. 750 G	
c. AFSC Project No. 6753	9b OTHER REPORT NO(S) *(Any other numbers that may be assigned this report)*
d. AFSC Task No. 675304	AFRPL-TR-68-22

10. AVAILABILITY/LIMITATION NOTICES

[illegible] (RPR/Stinfo), Edwards, California 93523

11. SUPPLEMENTARY NOTES	12. SPONSORING MILITARY ACTIVITY
	Air Force Rocket Propulsion Laboratory Research and Technology Division Air Force Systems Command

13 ABSTRACT

A 3-year program was conducted to establish analytical design procedures, stress-analysis methods, techniques for manufacturing control, and other factors essential to the successful design and fabrication of metallic bellows and diaphragms. These objectives were accomplished through the identification of parameters pertinent to bellows and diaphragm design and fabrication, the development of improved stress-analysis and buckling-analysis procedures utilizing a digital computer, the investigation of selected aspects of corrosion, and the laboratory verification of theoretically predicted performance characteristics such as spring rate, effective area, vibration response, and fatigue life for representative formed and welded bellows and diaphragms. Extensive theoretical and experimental information is presented in the report as well as guidelines to assist in the analysis and design of bellows and diaphragms.

DD FORM 1473

14. KEY WORDS (Continued)	LINK A		LINK B		LINK C	
	ROLE	WT	ROLE	WT	ROLE	WT
Diaphragm Analysis						
Diaphragm Configuration						
Diaphragm Design						
Diaphragm Evaluation						
Diaphragm Manufacturing						
Direct Integration						
Effective Area						
Elastic Analysis						
End-Face Seals						
Expansion Joints						
Fatigue Prediction						
Finite Difference						
Flexible Connectors						
Formed Bellows						
Hermetic Seals						
Hydraulic Actuators						
Hydraulic Motors						
Inconel 718						
Instrumentation						
Linear Shell Analysis						
Low-Cycle Fatigue						
Metal Hose						
Metallic Bellows						
Metallic Diaphragms						
Motion Transducers						
Nonlinear Shell Analysis						
Plastic Collapse						
Runge-Kutta						
Shaft Seals						
Shell Buckling						
Shells of Revolution						
Shock Absorbers						
Spring Rate						
Squirm						
Stainless Steel						
Strain Gages						
Stress Analysis						
Temperature Sensors						
Transducers						
Vibration of Bellows						
Volume Compensators						
Welded Bellows						

14. KEY WORDS	LINK A		LINK B		LINK C	
	ROLE	WT	ROLE	WT	ROLE	WT
Accumulators						
Adams-Bashford						
Adams-Moulton						
AM-350						
Aneroid Capsules						
Axisymmetric Shells						
Bellows						
Bellows Analysis						
Bellows Configuration						
Bellows Design						
Bellows Evaluation						
Bellows Manufacturing						
Computer Solutions						
Corrosion						
Diaphragms						

INSTRUCTIONS

1. ORIGINATING ACTIVITY: Enter the name and address of the contractor, subcontractor, grantee, Department of Defense activity or other organization *(corporate author)* issuing the report.

2a. REPORT SECURITY CLASSIFICATION: Enter the overall security classification of the report. Indicate whether "Restricted Data" is included. Marking is to be in accordance with appropriate security regulations.

2b. GROUP: Automatic downgrading is specified in DoD Directive 5200.10 and Armed Forces Industrial Manual. Enter the group number. Also, when applicable, show that optional markings have been used for Group 3 and Group 4 as authorized.

3. REPORT TITLE: Enter the complete report title in all capital letters. Titles in all cases should be unclassified. If a meaningful title cannot be selected without classification, show title classification in all capitals in parenthesis immediately following the title.

4. DESCRIPTIVE NOTES: If appropriate, enter the type of report, e.g., interim, progress, summary, annual, or final. Give the inclusive dates when a specific reporting period is covered.

5. AUTHOR(S): Enter the name(s) of author(s) as shown on or in the report. Enter last name, first name, middle initial. If military, show rank and branch of service. The name of the principal author is an absolute minimum requirement.

6. REPORT DATE: Enter the date of the report as day, month, year; or month, year. If more than one date appears on the report, use date of publication.

7a. TOTAL NUMBER OF PAGES: The total page count should follow normal pagination procedures, i.e., enter the number of pages containing information.

7b. NUMBER OF REFERENCES: Enter the total number of references cited in the report.

8a. CONTRACT OR GRANT NUMBER: If appropriate, enter the applicable number of the contract or grant under which the report was written.

8b, 8c, & 8d. PROJECT NUMBER: Enter the appropriate military department identification, such as project number, subproject number, system numbers, task number, etc.

9a. ORIGINATOR'S REPORT NUMBER(S): Enter the official report number by which the document will be identified and controlled by the originating activity. This number must be unique to this report.

9b. OTHER REPORT NUMBER(S): If the report has been assigned any other report numbers *(either by the originator or by the sponsor)*, also enter this number(s).

If the report has been furnished to the Office of Technical Services, Department of Commerce, for sale to the public, indicate this fact and enter the price, if known.

11. SUPPLEMENTARY NOTES: Use for additional explanatory notes.

12. SPONSORING MILITARY ACTIVITY: Enter the name of the departmental project office or laboratory sponsoring *(paying for)* the research and development. Include address.

13. ABSTRACT: Enter an abstract giving a brief and factual summary of the document indicative of the report, even though it may also appear elsewhere in the body of the technical report. If additional space is required, a continuation sheet shall be attached.

It is highly desirable that the abstract of classified reports be unclassified. Each paragraph of the abstract shall end with an indication of the military security classification of the information in the paragraph, represented as *(TS), (S), (C), or (U)*

There is no limitation on the length of the abstract. However, the suggested length is from 150 to 225 words.

14. KEY WORDS. Key words are technically meaningful terms or short phrases that characterize a report and may be used as index entries for cataloging the report. Key words must be selected so that no security classification is required. Identifiers, such as equipment model designation, trade name, military project code name, geographic location, may be used as key words but will be followed by an indication of technical context. The assignment of links, rules, and weights is optional

DDC REPORT BIBLIOGRAPHY SEARCH CONTROL NO. /FAYE1

AD-828 243 13/11
BATTELLE MEMORIAL INST COLUMBUS OHIO COLUMBUS LABS

DEVELOPMENT OF ANALYTICAL TECHNIQUES FOR BELLOWS AND DIAPHRAGM DESIGN. (U)

DESCRIPTIVE NOTE: FINAL REPT. 1 MAR 65-11 MAR 68,
MAR 68 607P TRAINER,T. M. ;HULBERT,L. E. ;LESTINGI,J. F. ;KEITH,R. E. ;
CONTRACT: AF 04(611)-10532
PROJ: AF-6753
TASK: 675304
MONITOR: AFRPL TR-68-22

UNCLASSIFIED REPORT
DISTRIBUTION: NO FOREIGN WITHOUT APPROVAL OF AIR FORCE ROCKET PROPULSION LAB., ATTN: RPPR-STINFO, EDWARDS AFB, CALIF. 93523.

DESCRIPTORS: (*BELLOWS, DESIGN), (*DIAPHRAGMS(MECHANICS), DESIGN), STRESSES, MANUFACTURING METHODS, BUCKLING(MECHANICS), CONFIGURATION, SEALS, CORROSION-RESISTANT ALLOYS, DEFLECTION, FORCE(MECHANICS), VIBRATION, FATIGUE(MECHANICS), CORROSION, COPPER ALLOYS, PERFORMANCE(ENGINEERING), ALUMINUM ALLOYS, MAGNESIUM ALLOYS, NICKEL ALLOYS, TITANIUM ALLOYS, STAINLESS STEEL, STEEL, IRON ALLOYS, COBALT ALLOYS, REFRACTORY METALS (U)
IDENTIFIERS: STRESS ANALYSIS (U)

A 3-YEAR PROGRAM WAS CONDUCTED TO ESTABLISH ANALYTICAL DESIGN PROCEDURES, STRESS-ANALYSIS METHODS, TECHNIQUES FOR MANUFACTURING CONTROL, AND OTHER FACTORS ESSENTIAL TO THE SUCCESSFUL DESIGN AND FABRICATION OF METALLIC BELLOWS AND DIAPHRAGMS. THESE OBJECTIVES WERE ACCOMPLISHED THROUGH THE IDENTIFICATION OF PARAMETERS PERTINENT TO BELLOWS AND DIAPHRAGM DESIGN AND FABRICATION, THE DEVELOPMENT OF IMPROVED STRESS-ANALYSIS AND BUCKLING-ANALYSIS PROCEDURES UTILIZING A DIGITAL COMPUTER, THE INVESTIGATION OF SELECTED ASPECTS OF CORROSION, AND THE LABORATORY VERIFICATION OF THEORETICALLY PREDICTED PERFORMANCE CHARACTERISTICS SUCH AS SPRING RATE, EFFECTIVE AREA, VIBRATION RESPONSE, AND FATIGUE LIFE FOR REPRESENTATIVE FORMED AND WELDED BELLOWS AND DIAPHRAGMS. EXTENSIVE THEORETICAL AND EXPERIMENTAL INFORMATION IS PRESENTED IN THE REPORT AS WELL AS GUIDELINES TO ASSIST IN THE ANALYSIS AND DESIGN OF BELLOWS AND DIAPHRAGMS. (AUTHOR) (U)

AFRPL-TR-68-22

FINAL REPORT ON THE DEVELOPMENT OF ANALYTICAL TECHNIQUES FOR BELLOWS AND DIAPHRAGM DESIGN

T. M. Trainer, L. E. Hulbert, J. F. Lestingi,
R. E. Keith, et al.

Battelle Memorial Institute
Columbus Laboratories

TECHNICAL REPORT NO. AFRPL-TR-68-22

March, 1968

Air Force Rocket Propulsion Laboratory
Research and Technology Division
Air Force Systems Command
Edwards Air Force Base
California

FOREWORD

This report summarizes research conducted under USAF Contract No. 04 (611)-10532 from March 1, 1965, to March 11, 1968. The contract was established under Air Force Program Structure No. 750G, AFSC Project No. 6753, AFSC Task No. 675304. The work was performed by the Battelle Memorial Institute Columbus Laboratories for the Air Force Rocket Propulsion Laboratory, Research and Technology Division, Edwards Air Force Base, with Capt. John L. Feldman and Messrs. A. D'Arcangelo and Roy A. Silver serving as contract monitors. The principal contributors to the report were: Dr. L. E. Hulbert, Division Chief; Dr. H. J. Grover, Senior Fellow; Dr. R. E. Keith, Associate Fellow; Dr. J. C. Gerdeen, E. C. Rodabaugh, and J. D. Jackson, Senior Research Engineers, Dr. J. F. Lestingi, Research Engineer; and T. M. Trainer, Program Manager.

This technical report has been reviewed and is approved.

John L. Feldman
Capt., USAF
Project Engineer

ABSTRACT

A 3-year program was conducted to establish analytical design procedures, stress-analysis methods, techniques for manufacturing control, and other factors essential to the successful design and fabrication of metallic bellows and diaphragms. These objectives were accomplished through the identification of parameters pertinent to bellows and diaphragm design and fabrication, the development of improved stress-analysis and buckling-analysis procedures utilizing a digital computer, the investigation of selected aspects of corrosion, and the laboratory verification of theoretically predicted performance characteristics such as spring rate, effective area, vibration response, and fatigue life for representative formed and welded bellows and diaphragms. Extensive theoretical and experimental information is presented in the report as well as guidelines to assist in the analysis and design of bellows and diaphragms.

TABLE OF CONTENTS

	Page
INTRODUCTION	1
DESCRIPTIONS OF BELLOWS AND DIAPHRAGMS	2
Bellows Convolutions	2
Bellows Assemblies	5
Bellows Applications	8
Diaphragm Configurations	10
Diaphragm Applications	11
PERFORMANCE CHARACTERISTICS OF BELLOWS AND DIAPHRAGMS	12
Stresses in Bellows and Diaphragms	13
Spring Rates of Bellows and Diaphragms	19
Effective Area of Bellows and Diaphragms	23
Elastic Buckling and Plastic Collapse of Bellows and Diaphragms	24
Vibration of Bellows and Diaphragms	30
Flow Losses	35
Fatigue of Bellows and Diaphragms	37
Corrosion of Bellows and Diaphragms	39
Characteristics Important to Instrumentation Applications	41
MATERIALS FOR BELLOWS AND DIAPHRAGMS	44
Copper Alloys	45
Aluminum and Magnesium Alloys	47
Nickel and Cupro-Nickel Alloys	47
Titanium Alloys	48
Stainless Steels	48
Low-Alloy Steels	50
Other Iron-Base Alloys	50
Nickel- and Cobalt-Base Alloys	50
Refractory Metals	51
Other Alloys	52
MANUFACTURING CONSIDERATIONS	53
Formed Bellows	53
Welded Bellows and Diaphragms	58
Deposited Bellows	61
End-Fitting Design	63
Surface Irregularities	65
Cleanliness	65
In-Process Inspection	65
CONCLUSIONS AND RECOMMENDATIONS	69
REFERENCES	73

Preceding page blank

TABLE OF CONTENTS
(Continued)

		Page
APPENDIX A.	THEORETICAL ANALYSIS OF ELASTIC DEFORMATIONS OF BELLOWS AND DIAPHRAGMS.	A-1
APPENDIX B.	DESCRIPTION OF COMPUTING PROGRAM NONLIN	B-1
APPENDIX C.	THEORETICAL DEVELOPMENT AND LISTING OF COMPUTER PROGRAM	C-1
APPENDIX D.	PARAMETER ANALYSES	D-1
APPENDIX E.	STRESS ANALYSIS OF A 3-INCH, ONE-PLY FORMED BELLOWS - TYPE 321 STAINLESS STEEL	E-1
APPENDIX F.	STRESS ANALYSIS OF A 1-INCH ONE-PLY FORMED BELLOWS - TYPE 321 STAINLESS STEEL	F-1
APPENDIX G.	STRESS ANALYSIS OF A 3- AND A 1-INCH TWO-PLY FORMED BELLOWS - TYPE 321 STAINLESS STEEL	G-1
APPENDIX H.	STRESS ANALYSIS OF A 3-1/2-INCH WELDED BELLOWS - TYPE 347 STAINLESS STEEL	H-1
APPENDIX I.	STRESS ANALYSIS OF 4-INCH STAINLESS STEEL DIAPHRAGMS	I-1
APPENDIX J.	ELASTIC BUCKLING AND PLASTIC COLLAPSE OF BELLOWS	J-1
APPENDIX K.	LOW-CYCLE FATIGUE AND FATIGUE-LIFE PREDICTION . .	K-1
APPENDIX L.	FATIGUE ANALYSIS OF FORMED BELLOWS - TYPE 321 STAINLESS STEEL.	L-1
APPENDIX M.	FATIGUE ANALYSIS OF FORMED BELLOWS - INCONEL 718	M-1
APPENDIX N.	FATIGUE ANALYSIS OF WELDED BELLOWS AND DIAPHRAGMS	N-1
APPENDIX O.	EVALUATION OF THE CORROSION BEHAVIOR OF BELLOWS AND DIAPHRAGM MATERIALS FOR AEROSPACE APPLICATIONS.	O-1
APPENDIX P.	INSPECTION AND MEASUREMENT OF BELLOWS AND DIAPHRAGMS.	P-1
APPENDIX Q.	TEST EQUIPMENT AND PROCEDURES.	Q-1

LIST OF FIGURES

Page

Report Body

Figure 1. Typical Bellows Assemblies 6

Figure 2. Manufacturing Flow Sheet for Formed Bellows 54

Figure 3. Manufacturing Flow Sheet for Welded Bellows and Diaphragms . . . 59

Figure 4. Manufacturing Flow Sheet for Deposited Bellows. 62

Figure 5. Typical Bellows End-Fitting Joints 64

Report Appendixes

The report appendixes contain 333 figures. In the interest of brevity, and in recognition of the dependency of the figures on the associated texts, an independent listing of these figures has not been prepared.

LIST OF TABLES

Report Body

Table 1. Major Bellows Convolutions and Characteristics. 3

Table 2. Theoretical and Experimental Stresses for Typical Formed Bellows 14

Table 3. Theoretical and Experimental Strains for Convolution Crowns of Typical Formed Bellows 16

Table 4. Theoretical and Experimental Stresses for Typical Welded Bellows 18

Table 5. Theoretical and Experimental Spring Rates for Typical Formed Bellows 21

Table 6. Theoretical and Experimental Spring Rates for Typical Welded Bellows. 22

Table 7. Theoretical and Experimental Effective Areas for Typical Formed and Welded Bellows 24

Table 8. Theoretical and Experimental Values of the Lateral Bending Stiffness D for Typical Formed and Welded Bellows 26

Table 9. Relation Between Bending Stiffness D and Spring Constant k for Typical Formed and Welded Bellows. 26

LIST OF TABLES
(Continued)

Page

Table 10. Theoretical and Experimental Natural Vibration Frequencies for Typical Formed and Welded Bellows 33

Table 11. Hysteresis Effects at Zero Defiection for Stainless Steel Formed Bellows 43

Table 12. Typical Bellows and Diaphragm Alloys 46

Report Appendixes

The report appendixes contain 178 tables. In the interest of brevity, and in recognition of the dependency of the tables on the associated texts, an independent listing of these tables has not been prepared.

ABBREVIATIONS AND SYMBOLS APPEARING IN REPORT BODY*

F	Axial force on bellows, lb
N_ϕ	Meridional membrane resultant force, lb/in.
Q	Effective shear resultant force in direction normal to the shell, lb/in.
ϕ	Angle between normal to bellows surface and its axis of revolution, deg
r	Radial distance from bellows axis to a point on the bellows, in.
k	Bellows spring rate, lb/in.
L_o	Length of bellows included in mathematical model used for analysis, in.
L_c	Total live length of bellows, in.
δ	Assumed axial deflection imposed on mathematical model of bellows, in.
A	Effective area of bellows or diaphragm, sq. in.
p	Internal pressure in bellows, psi
$\overline{R}$	Effective radius or average radius of the bellows or diaphragm, in.
D	Lateral bending stiffness of a bellows, lb-in.^{2}
E	Modulus of elasticity, psi
I	Moment of inertia of the bellows cross section, in.^{4}
R_o, R_i	Outside and inside radii of bellows or diaphragm, in.
α	Correction factor for Seide bending formula for bellows
σ_T	Total bending stress, psi
σ_p	Stress due to pressure, psi
σ_Δ	Stress due to axial deflection, psi
σ_M	Additional stress caused by sidewise buckling of bellows, psi
d	Nominal bellows diameter, in.
h	Bellows thickness, in.
f_n	Natural frequency of bellows accordion vibration mode, cps
g	Acceleration rate due to gravity, in./sec^2
f_L	Natural frequency of bellows bending vibration mode, cps
W_m	Weight of vibrating bellows, lb.

*Individual listings of abbreviations and symbols have been prepared for each Appendix, where applicable.

INTRODUCTION

The Air Force Rocket Propulsion Laboratory has a primary responsibility of providing advanced technology for rocket propulsion systems through exploratory development programs. As a part of this mission, improvements in the performance and reliability of fluid-system components (valves and regulators) are being pursued vigorously. This is being accomplished by investigations into individual component parts or modules, i.e., seals, fittings, seats, poppets, and actuators.

The Air Force Rocket Propulsion Laboratory initiated a contract with the Battelle Memorial Institute Columbus Laboratories to investigate analytical design procedures, stress-analysis methods, techniques for manufacturing control, and other factors essential to the successful design and fabrication of bellows and diaphragms.

The initial phase of the program involved a literature and industry survey to determine the present state of the art of bellows and diaphragms. Technical Report No. AFRPL-TR-65-215 (AD479056) was prepared to summarize the results of the survey and present recommendations for activities during the remainder of the program. The first half of the program was summarized in Technical Report No. AFRPL-TR-66-181 (AD801842). The following report summarizes the entire program. Because of the scarcity of theoretical and experimental information on bellows and diaphragms, an attempt has been made to prepare a reference that will be useful to manufacturers, users, and government agencies responsible for the purchase of bellows and diaphragms. Detailed data from all phases of the program have been included, and guidelines have been prepared to assist in the analysis and design of bellows and diaphragms.

The report is divided into two major parts. The first part (the report body) summarizes in essentially narrative form the principal features of bellows and diaphragms, their primary performance characteristics, and the major associated manufacturing aspects. The second part (the Appendixes) gives detailed summaries of the investigations conducted during the program. Although discussions of the data have been prepared, further study of the data by the reader will undoubtedly yield additional insight and understanding.

DESCRIPTIONS OF BELLOWS AND DIAPHRAGMS

Bellows and diaphragms are thin elements whose deflection characteristics are utilized to provide movement in the structure of fluid systems. Generally, these items are used when the need for motion is combined with the need for a hermetic seal.

Bellows and diaphragms are made in many sizes and shapes from a variety of materials. This program has been concerned with the types of metallic bellows and diaphragms used in aerospace tubing systems, and in components such as valves and regulators. By mutual agreement with the Air Force, consideration has been given solely to configurations operated either totally or largely within the elastic state. Thus, no work has been done with bellows and diaphragms used as expulsion devices.

This report section summarizes the principal types of metallic bellows and diaphragms of interest, and describes typical assemblies and applications. Because some confusion exists as to terminology, an attempt has been made to use terms which are consistent with current practice and clarity.

Bellows Convolutions

Most metallic bellows are cylindrical elements which contain annular circumferential corrugations. In flexible hose, the corrugations may be formed in a continuous helix. Some bellows are not cylindrical but have elliptical or other noncircular cross sections. However, these shapes are sufficiently unusual that they have not been included in the program.

Bellows are generally classified according to one of the four primary methods of manufacture, i.e. (1) formed, (2) welded, (3) deposited, or (4) machined. Within these classifications, the bellows are usually categorized according to the appearance of the convolution cross section, as shown in Table 1.

Formed Bellows

Formed bellows are usually made from butt-welded tubing that has been fabricated from sheet metal with closely controlled thickness. Formed bellows constitute at least 75 percent of the bellows which are manufactured. They can be produced in many materials and sizes, and at a cost much lower than that for other types of bellows. Diameters up to 4 feet can be obtained, and one manufacturer advertises diameters up to 50 feet. In comparison with welded bellows (see below), formed bellows have a higher spring rate and require more ductile materials. However, because of the absence of circumferential welds, they are more reliable than welded bellows.

Although Table 1 shows only single-ply configurations, most formed bellows can be made with multiple plies. Three- and four-ply bellows are common. Multiple plies are used to provide a greater resistance to pressure and a lower spring rate than would be obtained with a single ply equal in thickness to the total thickness of the multiple plies. The major types of formed bellows are described briefly.

TABLE 1. MAJOR BELLOWS CONVOLUTIONS AND CHARACTERISTICS

	Convolution Shape	Axial Spring Rate	Long Stroke Capability	Resistance to Diff. Pressure
FORMED				
Semitoroidal		Very high	Very poor	Very good
U-shaped		Medium	Fair	Fair
U-shaped, ext. ring support		High	Fair	Very good
U-shaped, int. ring support		High	Fair	Very good
U-shaped, ext. T-ring support		High	Fair	Very good
S-shaped	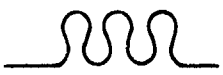	Medium	Fair	Fair
S-shaped, ext. ring support		High	Fair	Very good
Toroidal, ext. pressure		Very high	Poor	Excellent
Toroidal, int. pressure		Very high	Poor	Excellent
WELDED				
Flat		Medium	Fair	Good
Stepped	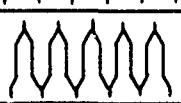	Low	Good	Fair
Single sweep	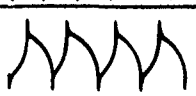	Medium	Good	Good
Nested ripple		Very low	Excellent	Poor
DEPOSITED				
U-shaped (can be varied)		Low	Good	Fair
MACHINED				
Rectangular		High	Fair	Excellent

Semitoroidal. Semitoroidal bellows are attractive for materials with relatively low ductility. The form also offers good pressure capability and stability. The convolutions may be truly semicircular, elliptical, or some combination of curves. A low deflection capability per convolution and a high spring rate are major limitations of this configuration.

U-Shaped. When flat sections are placed between the semitoroidal sections, a U-shaped, or flat-plate, bellows configuration is formed. Over 50 percent of all the bellows are of this type. The shape is amenable to any of the methods for manufacturing formed bellows, a variety of performance characteristics can be achieved by varying the radii and depth of convolution, and supporting devices are easily installed externally or internally.

S-Shaped. The S-shaped bellows is similar to the U-shaped bellows. By slanting the straight sections between the semitoroidal sections, or by connecting the semitoroidal sections with curved sections, it is possible to form more convolutions and thus achieve more deflection per unit length. The S-shaped bellows is not as easy to manufacture and not as amenable to the use of supporting devices as the U-shaped bellows.

Toroidal. Toroidal bellows have been developed to reduce the pressure-induced stresses in the bellows. By using a shape which is essentially circular, the effects of pressure are more evenly distributed along the convolution. In addition, the stresses in the convolution are less affected by an increase in bellows diameter than is the case with the other convolution shapes. The Marquette Coppersmithing Company claims that their OMEGA shape distributes the stresses more evenly than a true toroidal bellows. Zallea Brothers advertise a HyPTor, or modified toroidal shape which is satisfactory for intermediate pressures and is more flexible than a true toroidal shape. Although the toroidal bellows permit high operating pressures, they are more difficult to manufacture than the other formed bellows and have a high spring rate.

Rippled-Sidewall. Rippled-sidewall bellows are formed bellows that have convolution shapes similar to those of welded bellows. These bellows are relatively new and the manufacturing methods are still being improved. The bellows are almost as compact as welded bellows and are less expensive. The fatigue life of rippled-sidewall bellows is more predictable than that for welded bellows because of the absence of circumferential welds. If very ductile materials are used, rippled-sidewall bellows can be made with low spring rates. However, some rippled-sidewall bellows have spring rates as high as or higher than those for formed bellows. It is difficult to summarize the characteristics associated with this new type of bellows, and performance data must be obtained from each manufacturer.

Welded Bellows

Approximately 20 percent of the manufactured bellows have welded convolutions. Welded bellows are made up of shaped diaphragms which are alternately welded together at the inner and outer diameters. Although they are more expensive to manufacture than formed bellows, welded bellows offer three significant advantages over formed

bellows: (1) a wider choice of materials, (2) more deflection per unit length, resulting in shorter assemblies or longer strokes, and (3) a wider choice of performance characteristics because of a greater variety of convolute dimensions and shapes. A few companies offer a two-ply welded bellows, but most welded bellows have a single ply. In general, welded bellows are available in sizes from 1/2 inch to 7 inches outside diameter. Bellows in excess of 12 inches in diameter have been produced.

Table 1 summarizes the major types of welded convolutions, and their primary characteristics. Most welded bellows are of the nested-ripple configuration because this design makes maximum use of the advantages of low spring rate and compactness. However, the other configurations have attractive characteristics for certain applications. Despite the impressive welding techniques that have been developed by the manufacturers of welded bellows, the large amount of welding required (approximately 18 inches per convolution in a 3-inch-OD bellows) makes fatigue failure less predictable for welded bellows than for other types of bellows.

Deposited Bellows

Two kinds of deposited bellows are commercially available: chemically deposited and electrodeposited. Both methods can be used to produce any shape that can be deposited on a machined mandrel. In each method an aluminum mandrel is machined for each bellows, and after the bellows material is deposited, the mandrel is dissolved. The primary advantages of the processes are the ability to produce: (1) very thin-walled bellows, (2) bellows having no welds, (3) very small bellows, and (4) special shaped bellows. Chemically deposited bellows can be made with wall thicknesses from 0.0003 inch to 0.005 inch, and with diameters from 0.060 inch to 12 inches. Electrodeposited or electroplated bellows are usually produced in nickel or nickel-cobalt alloy. Sizes are available from 0.063 inch to 1.250 inches in diameter, with wall thicknesses varying from 0.0003 inch to 0.006 inch.

Machined Bellows

Machined bellows are turned or ground from bar stock, tubing, or forged rings of most materials used in other types of metallic bellows, as well as of materials not found in sheet stock. High-strength, high-endurance, heat-treatable tool steels, in addition to high-strength, low-modulus titanium alloys can be used. The design of machined bellows is customized, with most machined bellows having high spring rates. Machined bellows have been made from 1/4 inch to 60 inches in diameter, for pressures as high as 12,000 psi.

Bellows Assemblies

Although bellows can be used in an extremely wide variety of ways, certain types of assemblies have become relatively common. In general, these assemblies, some of which are shown in Figure 1, prevent certain types of motion and limit other types of motion.

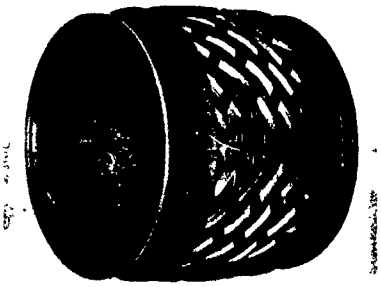

Braided Assembly

Slide Assembly

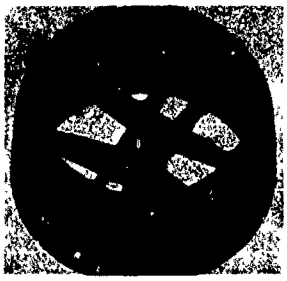

Internally Linked Assembly

Internal Gimbal Assembly

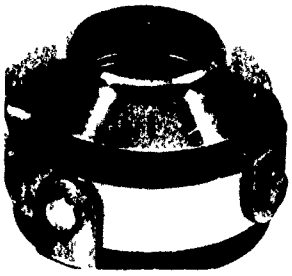

External Gimbal Assembly

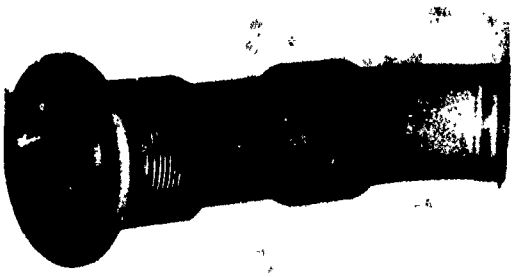

Universal Assembly

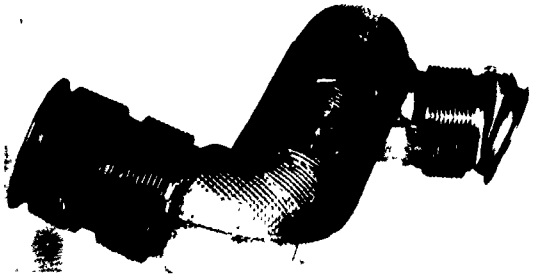

Insulated Universal Assembly

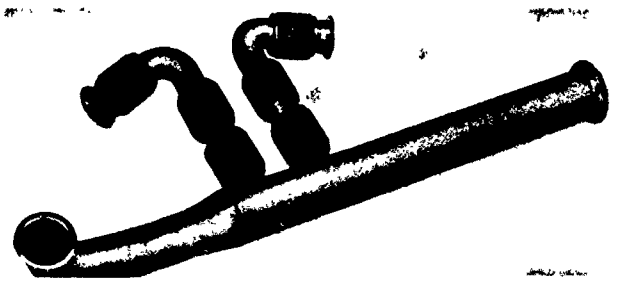

Ducting Assembly

(Permission has been granted to use the above reproductions by the Aeroquip Corporation/Marman Division, Los Angeles, California)

FIGURE 1. TYPICAL BELLOWS ASSEMBLIES

Braided

Bellows can be distorted by internal pressure in a manner referred to as "squirm". When squirm occurs, the bellows deflects as a column, causing plastic distortion in one or more convolutions. Metal braiding is commonly used to provide external support for such bellows and to protect the bellows from external damage. This configuration is most common in flexible metal hoses. Braiding may cause abrasion of the bellows and it may accelerate corrosion of the bellows.

Sleeve

A bellows may be provided with an internal sleeve to reduce fluid-scrubbing contact with the bellows. Such contact can cause flow losses, abrasion, noise, and flow-induced vibration which can lead to early failure. The length of the internal sleeve can also be used to limit the amount of axial compression of the bellows.

Slide

A slide assembly is similar to a sleeve assembly except that telescoping sleeves provide axial guiding and prevent squirm. Slide assemblies are attractive for systems subjected to high surge pressures and temperatures.

Universal

A universal assembly contains two bellows joined by a common connector for the purpose of absorbing any combination of the three basic movements, i.e., axial deflection, lateral deflection, and angular deflection. Limit rods are often used to distribute the movement between the two bellows and to stabilize the common connector. This configuration can tolerate more lateral deflection or offset than one bellows equal in length to the two bellows.

Internally Linked

Internally linked assemblies utilize struts inside the bellows in the flow stream to limit movement in all directions. Such assemblies are simple, compact, and lightweight, but they introduce significant flow losses.

Hinged

A hinged bellows is designed to permit angular deflection in one plane only by the use of a pair of pins through hinge plates attached to the ends. The hinges and hinge pins must be designed to resist external forces and thrust due to internal pressure.

Gimbaled

Gimbaled bellows assemblies provide for angular deflection in any direction from the tubing axis. Internal or external gimbals can be used. They are made with two

sets of hinge plates attached to a gimbal ring and function in a manner similar to a universal joint.

Pressure Balanced

A pressure-balanced bellows assembly is designed to absorb axial movement and/or lateral deflection while absorbing the end thrust by means of tie devices interconnecting the flow bellows with an opposed bellows also subjected to line pressure. This type of assembly is normally used where a change of direction occurs in a run of tubing.

Bellows Applications

Bellows are used primarily in two ways: (1) as motion compensators and (2) as calibrated transducers. Typical applications are discussed briefly.

Expansion Joints

Many bellows are used as expansion joints to compensate for movement occurring in tubing as a result of temperature changes and/or external loading. With the wide variety of tubing systems, movement can be transmitted to a bellows as compression, extension, offset, rotation, or combinations of these motions. Many of the "standard" bellows assemblies were developed to compensate for thermal changes in industrial tubing and piping systems.

Flexible Connectors

Bellows are often used to compensate for structural deflections, misalignment, and tolerance accumulation. These functions may be fulfilled by a short, plain bellows or by relatively long, flexible metal hoses with metal braiding or other types of exterior covering.

Pressure and Temperature Sensors

One of the most common uses for bellows is the actuation of some device as a function of a change in the pressure or temperature of a fluid system. The fluid may be external or internal to the bellows. For temperature sensing, the bellows system often incorporates a liquid whose vapor pressure reflects the temperature being sensed. The vapor pressure is then used to actuate the bellows. When the bellows moves in response to pressure changes, the movement is utilized to actuate a device such as a valve or switch. Because the bellows responds very quickly to changes, the movement can be used both as a proportioning signal and an on-off signal. Diaphragms and Bourdon tubes are also used extensively for these functions.

Reciprocating Shaft Seals

Although most reciprocating shafts are sealed with some kind of packing, increasingly stringent operating requirements have resulted in the wider use of bellows for sealing. In a number of aerospace valve configurations, formed and welded bellows have been utilized to provide: (1) hermetic sealing in the closed position, (2) opening forces (from controlled pressure differentials), and (3) closing forces (from the spring rate of the bellows). The use of metallic bellows makes possible the provision of these features over a wide temperature range for a variety of corrosive and reactive fluids.

End-Face Seals

The ability of a bellows to provide sealing and to act as a spring and motion compensator makes it ideal as a means of pressing face seals together on rotating shafts. Because of their compact construction and low spring rate, welded bellows are commonly used in face-seal assemblies.

Hydraulic Motors and Actuators

For small power requirements, particularly for remote operation, bellows can be used for converting mechanical work to hydraulic work or for converting hydraulic work to mechanical work. For example, a liquid-filled system may consist of two bellows connected by tubing. The movement of one bellows causes movement of the other bellows.

Vibration Dampeners

Just as springs with frictional elements for energy adsorption are used as vibration dampeners in mechanical systems, bellows may be used as vibration dampeners for fluid-containing structures. Because the bellows itself responds to certain vibration frequencies, care must be taken to assure that the bellows is not excited by the frequencies transmitted from the system structure.

Accumulators and Shock Absorbers

In a hydraulic system, a bellows can function as a flexible container to maintain oil flow or to absorb surge pressures. The primary requirements are long stroke, resistance to high differential pressure, and quick response.

Volume Compensators

For liquid systems of small volume, bellows furnish an attractive means of compensating for fluid expansion or contraction Hermetically sealed floated instruments such as gyros and accelerometers are typical applications.

Flexible Couplings

Although bellows are not usually designed to transmit torsional loads, bellows have been found to be attractive for transmitting small torques, particularly for instrumentation-type equipment. The bellows can tolerate some misalignment and the torsional stiffness of the bellows insures accurate rotational transmission. Bellows-type flexible couplings are available for shafts up to 1/2 inch in diameter.

Diaphragm Configurations

A diaphragm is a thin disk-like element which deflects in a direction substantially perpendicular to its flexible surface. Metallic diaphragms are classified as flat, or nearly flat, and corrugated. They are used primarily as actuators to transform pressure into linear motion and force. Corrugated diaphragms are preferred for aerospace components such as valves and regulators because their average sensitivity over a large range of pressure is greater than that of flat diaphragms of the same size, their zero-position under no-load is more stable, much larger deflections can be obtained without permanent deformation, and a variety of pressure-deflection characteristics may be obtained for a given size diaphragm by using different depths or shapes of corrugations. This report is concerned only with corrugated diaphragms.

In contrast with the variety of information on bellows sizes and shapes contained in the open literature and listed in catalogs, little information is available on commercially available corrugated diaphragms. The most complete discussion of possible diaphragm configurations and their performance characteristics is contained in a publication by Newell[1]*.

In general, the work reported by Newell[1] and by Wildhack, et al.,[2] shows that increasing the number of corrugations increases the initial flexibility as well as the average flexibility over the usable range, although diaphragms with more corrugations may be more nonlinear. Diaphragms with shallower corrugations exhibit better initial flexibilities within limits, but at the expense of decreasing the linear range. According to Wildhack, et al.,[2] diaphragms made with triangular and trapezoidal shapes provide linear force-deflection characteristics for deflections up to at least 2 percent of the diameter, with the trapezoidal shape being slightly stiffer and the triangular shape being slightly more flexible than the corresponding diaphragm with the same number of circular corrugations. Although empirical relationships have been developed, the design of corrugated diaphragms is reported to be largely a process of trial and error.

According to a survey by Giannini Controls,[3] corrugated diaphragms are manufactured in sizes from 0.875 to 6.0 inches in diameter, and are usually joined together in pairs to form a capsule. They can be used to sense pressures from 0.5 to 400 psi; however, the majority of units are used to sense pressures from 5 to 100 psi, and most units are less than 2.5 inches in diameter. Most diaphragms will not be more than 1 percent nonlinear if the displacement is kept below 2 percent of the diameter. If nonlinearity of more than 1 percent is acceptable, displacements up to 5 or 6 percent can be obtained.

*References are given on page 73.

Diaphragm Applications

The publication by Newell[1] lists 15 major and several minor application classifications for corrugated diaphragms. The most important applications from the standpoint of this program are: (1) pressure and temperature sensors, (2) reciprocating shaft seals, and (3) volume compensators. Since these applications have been discussed previously for bellows, they will not be repeated. It should be noted that the primary advantages of diaphragms as compared with bellows are greater sensitivity and more compact shape for some components. Low deflection and low pressure capability are the primary limitations of diaphragms, although the pressure capability is often increased by the use of supporting springs and stops.

PERFORMANCE CHARACTERISTICS OF BELLOWS AND DIAPHRAGMS

Bellows and diaphragms are usually used to provide motion in some part of a liquid or gaseous system while maintaining a hermetic seal between the system and its environment. In such applications, a bellows or a diaphragm may be subjected to different combinations of pressure and deflection loading. When the application is that of a calibrated transducer in an instrument, the primary characteristics of the bellows or diaphragm which determine satisfactory performance are: spring rate, effective area, effective volume, and those material characteristics which cause changes in reading, such as hysteresis, inelasticity, creep, etc. When the application is that of a motion compensator, the primary bellows and diaphragm performance characteristics are spring rate, effective area, buckling pressure, fatigue life, corrosion resistance, and vibration response. When a bellows is used in a tubing system, flow losses and flow-induced vibration are also important characteristics. Motion compensation was of primary interest to this program, and the associated performance characteristics are discussed in this report section. For completeness, brief comments are also included concerning the characteristics associated with instrument applications.

To obtain reliable estimates of most bellows characteristics, a basic requirement is the accurate prediction of the stresses and strains at each point of the bellows under the given loading conditions. Most manufacturers have developed approximate procedures for predicting maximum stresses and strains in their standard bellow lines. These procedures are based on beam or plate theory or, in some instances, on simplified shell theory. The application of such procedures usually includes provision for empirical correction factors which have been determined from tests on sample bellows. Once these formulas have been established experimentally, they can be utilized in the design of similar bellows. However, these procedures do not give detailed stress calculations in all parts of the bellows, and each empirically established formula is applicable only to bellows very similar to the ones tested.

One of the principal objectives of the current research was the development of a unified procedure for accurately predicting the detailed stresses and deflections in bellows and diaphragms of any cross-sectional shape. Because of the complex shape of many types of bellows and diaphragms, it became clear early in the study that a computer program would be required as part of the procedure.

After considerable investigation, it was decided that the most useful available computer program was one developed by Dr. A. Kalnins of Lehigh University (formerly of Yale University). A modification of this computer program, called MOLSA, was used in the early part of the research. Later, MOLSA was replaced by a computer program NONLIN, which was developed by Dr. J. F. Lestingi*. Program NONLIN provided for the analysis of the geometrically nonlinear elastic deformations of bellows and diaphragms, as well as for the analysis of linear deformations as accomplished by MOLSA. A discussion of the selection and evaluation of the computer programs is given in Appendix A. Appendix B gives a detailed description of the computing program NONLIN. It is believed that program NONLIN will become a standard tool for estimating stresses and strains in bellows and diaphragms.

*Now at the University of Akron

Appendixes D, E, F, G, and H give detailed results of the theoretical analyses of typical formed and welded bellows, and a comparison of these analyses with experimental results. These investigations are summarized here.

Stresses in Bellows and Diaphragms

Program MOLSA was first evaluated through comparisons of computer results with theoretical and experimental results for bellows and diaphragms reported in the literature. These comparisons demonstrated the general applicability and reliability of the computing program. To evaluate MOLSA and NONLIN in more detail, a major part of the research consisted of: (1) formulating a procedure that yielded accurate mathematical models of formed and welded bellows and of diaphragms, (2) utilizing these mathematical models in the computing program to obtain predictions of stresses and strains in representative bellows or diaphragms under typical loads, and (3) comparing these predictions with experimentally determined stresses and strains.

After some investigation, it was determined that no nondestructive method would provide sufficiently accurate dimensions for the mathematical model. The method finally adopted involved encapsulating the bellows or diaphragm, sectioning it along a diameter, polishing the sectioned specimen, and measuring the required dimensions with a traveling microscope. Each specimen chosen for encapsulation was one of several that were made at the same time with the same set of dies, so that the specimens of each lot were very similar. It was believed that the predicted stresses and strains based on the analysis of the mathematical model of the encapsulated specimen could be used to predict the stresses and strains in other specimens of the same lot.

To check the analytically predicted stresses, 1/64-inch strain gages were mounted on one specimen of each lot. For formed bellows, gages were mounted on the outside surface of selected bellows crowns and on the inside surface of selected bellows roots. On welded bellows, the strain gages could be mounted only on the bellows flats near the crown weld. On the diaphragm, it was possible to mount strain gages at several radial positions. Appendix Q contains a detailed description of the placement of the gages, of the conduct of the tests, and of the methods used to select representative measured strains for calculating experimentally determined stresses.

Stresses in Formed Bellows

Analysis of Stresses in Formed Bellows. In order to test the general applicability of the analysis procedure for formed bellows, it was decided to test formed bellows in three sizes and two materials. Type 347 stainless steel bellows were obtained with inside diameters of 1 inch, 3 inches, and 5 inches. Bellows made from Inconel 718 were obtained with inside diameters of 1 inch and 3 inches. The configurations were analyzed utilizing the computing program NONLIN as applied to mathematical models obtained from careful measurement of encapsulated specimens. The stresses and strains obtained from these analyses were compared with strains measured by strain gages on a convolution near the center of each strain-gaged bellows.

Table 2 shows a comparison of the theoretically calculated and experimentally determined stresses in the different formed bellows loaded by internal pressure and by

TABLE 2. THEORETICAL AND EXPERIMENTAL STRESSES FOR TYPICAL FORMED BELLOWS

			Theoretical and Experimental Stresses, psi[a]									
			5-Inch, One-Ply SS Bellows		3-Inch, One-Ply SS Bellows		1-Inch, One-Ply SS Bellows		3-Inch, One-Ply Inconel Bellows		1-Inch, One-Ply Inconel Bellows	
			Stresses	% Diff.	Stresses	% Diff.	Stresses	% Diff.	Stresses	% Diff.	Stresses	% Diff.
Deflection Stresses	Convolution Crown	Meridional:										
		Theoretical	+19,294		+16,987		+35,048		+22,879		+58,568	
				+0.2		-14.1		-8.5		-0.3		-25.3
		Experimental	+19,330		+14,580		+32,075		+22,177		+43,741	
		Circumferential:										
		Theoretical	+10,791		+9,887		+19,803		+9,742		+21,684	
				+12.6		-1.1		+14.9		+10.4		-15.2
		Experimental	+12,150		+9,780		+22,750		+10,867		+18,392	
	Convolution Root	Meridional:										
		Theoretical	+22,943		+20,623		+48,931		+25,592		(c)	
				+6.7		-8.1		-14.8		-0.3		(c)
		Experimental	+24,482		+18,963		+41,695		+24,724		(c)	
		Circumferential:										
		Theoretical	+2,727		+2,935		+9,097		+7,445		(c)	
				(b)		(b)		(b)		(b)		(c)
		Experimental	+2,911		+2,697		+7,750		+7,187		(c)	
Pressure Stresses	Convolution Crown	Meridional:										
		Theoretical	-57,112		-50,446		-35,865		-57,348		-23,790	
				-4.3		-13.8		-28.1		-10.8		-17.4
		Experimental	-54,655		-43,500		-25,775		-51,133		-19,660	
		Circumferential:										
		Theoretical	-16,242		-20,098		-18,570		-16,490		-6,845	
				+9.9		-1.5		-54.0		+5.8		-6.1
		Experimental	-17,850		-19,800		-8,550		-17,476		-6,425	
	Convolution Root	Meridional:										
		Theoretical	+66,024		+58,709		+44,235		+45,599		(c)	
				-13.4		+0.6		-29.6		-32.5		(c)
		Experimental	+57,145		+59,064		+31,150		+30,761		(c)	
		Circumferential:										
		Theoretical	+26,268		+19,559		+13,620		+13,470		(c)	
				(b)		(b)		(b)		(b)		(c)
		Experimental	+22,767		+19,388		+9,585		+10,500		(c)	

(a) Plus values indicate tensile stresses; minus values indicate compressive stresses.

(b) These values are similar to the meridional values because of the method of calculating the experimental circumferential stresses at the convolution root – no circumferential strain gages were used at this location.

(c) Strain gages could not be placed on the convolution root of this bellows.

axial compression. This comparison shows excellent agreement between the theoretical and experimental stresses for the 3- and 5-inch bellows, and somewhat poorer agreement for the 1-inch Inconel and the 1-inch stainless steel bellows. All stresses for the larger bellows agreed within 15 percent except for one measurement on the 3-inch Inconel bellows. For the 1-inch bellows, the theoretical meridional stresses (which were the largest stresses) agreed with the experimental stresses to within 30 percent. The source of error was not determined. Since it was believed that the resolution of this discrepancy would require a considerable effort, and since the theoretical predictions for the small bellows were always conservative, it was decided to postpone further investigation of this problem. However, computer programs are now being developed for the analysis of 3-dimensional bodies of revolution (as opposed to shells of revolution). It is believed that the use of these programs will permit investigation of the applicability of the theory of thin shells to the analysis of bellows in which there are limited sections with small radius-to-thickness ratios.

As described in Appendix Q, data from only two meridional strain gages were used to calculate the experimental values of the crown meridional stresses on the middle convolution. A further check on the theoretical predictions of the stresses at the crown was made by comparing the theoretical meridional crown strain with the strains measured by all five of the meridional crown gages that were used on each bellows. The results of this comparison are summarized in Table 3. This table lists the theroetically predicted crown strains for internal pressure and axial compression, the representative strains as obtained from the two crown gages used to determine the representative stresses reported in Table 2, the largest strains and the smallest strains measured at one or the other of the five gages, and the overall average of the strains of all five gages. Both internal pressure and axial deflection are included. An examination of Table 3 leads to the following conclusions: (1) in almost every case the averaged value of the strains for the five gages was closer to the theoretical value than the average of the two gages used earlier, (2) there was considerable improvement in the correlation between the theoretical predictions and measured strains for both 1-inch bellows, and (3) except for the maximum deflection strain measured in the 3-inch Inconel bellows, all measured strains were either very close to or were less than the theoretically predicted strains.

It is believed that the correlation between the theoretical and experimental results reported here gives impressive evidence of the accuracy and applicability of the analysis procedure in predicting stresses and strains in formed bellows.

Discussion of Stresses in Formed Bellows. Formed bellows are used in systems that must be subjected to relatively high pressures and in applications where relatively high spring rates and small axial deflections can be tolerated. The formed bellows designed for a given application is always a compromise between a deep U-shaped bellows with larger deflection capability and a shallow convolution semitoroidal-type bellows with more pressure capability. Within the constraints imposed by spring-rate requirements and minimum buckling loads, the selected bellows should have the lowest maximum stresses under the most severe combinations of the operating pressure and deflection.

In selecting the best formed bellows configuration, the parametric studies of formed bellows discussed in Appendix D will be helpful. As shown in Appendix D, the deflection and pressure stress patterns vary greatly, depending on the general bellows configuration. Because the pressure and deflection stresses are combined algebraically,

TABLE 3. THEORETICAL AND EXPERIMENTAL STRAINS FOR CONVOLUTION CROWNS OF TYPICAL FORMED BELLOWS

	Meridional Deflection Strains, μin./in.			%	Meridional Pressure Strains, μin./in.			%
	Theoretical	Experimental		Diff.	Theoretical	Experimental		Diff.
5-Inch, One-Ply, Stainless Steel Bellows	+554	Rep.	+541	-2.3	-1801	Rep.	-1700	-5.6
		Max	+600	+8.3		Max	-1932	+7.3
		Avg	+525	-3.4		Avg	-1728	-4.1
		Min	+439	-20.8		Min	-1600	-11.2
3-Inch, One-Ply Stainless Steel Bellows	+484	Rep.	+401	-17.2	-1532	Rep.	-1295	-15.5
		Max	+437	-9.7		Max	-1557	+1.6
		Avg	+409	-15.5		Avg	-1326	-13.4
		Min	+394	-18.6		Min	-1166	-24.0
1-Inch, One-Ply Stainless Steel Bellows	+1004	Rep.	+871	-13.3	-1045	Rep.	-800	-23.4
		Max	+1073	+6.9		Max	-1049	+0.5
		Avg	+922	-8.2		Avg	-895	-14.3
		Min	+735	-26.9		Min	-789	-24.4
3-Inch, One-Ply Inconel Bellows	+643	Rep.	+610	-5.1	-1690	Rep.	-1480	-12.4
		Max	+755	+17.5		Max	-1539	-8.9
		Avg	+649	+1.0		Avg	-1409	-16.6
		Min	+599	-6.8		Min	-1326	-21.5
1-Inch, One-Ply Inconel Bellows	+1676	Rep.	+1233	-26.4	-700	Rep.	-572	-18.3
		Max	+1432	-14.6		Max	-675	-3.6
		Avg	+1305	-22.2		Avg	-606	-13.5
		Min	+1188	-29.1		Min	-551	-21.3

the parametric curves in Appendix D can be used to estimate the best approximate configuration for each application. To determine the pressure and deflection stresses accurately in the final bellows configuration, however, it is necessary to calculate the stresses for the exact bellows dimensions. This can be readily accomplished with the computing program NONLIN.

Stresses in Welded Bellows

Analysis of Stresses in Welded Bellows. The procedures for the theoretical and experimental stress analysis of welded bellows are generally the same as for the formed bellows. A comparison of the theoretically predicted and experimentally determined stresses for four typical welded bellows made of two representative materials is given in Table 4. A review of Table 4 shows fair agreement between the theoretical and experimental stresses. This agreement is significant since the strain gages were placed in regions where the stresses were varying rapidly so that the stresses measured by the gages were affected considerably by the location of the strain gages. Moreover, the comparison between the experimental and theoretical stresses depended upon the determination of the radial location of each strain gage.

Although the data accumulated for the welded bellows were not as extensive as that obtained for formed bellows, it is believed that the applicability of the theoretical-analysis procedure to welded bellows has been demonstrated.

Discussion of Stresses in Welded Bellows. Welded bellows are used in applications involving moderate pressures and large axial movement at low spring rates. In contrast to formed bellows, the maximum pressure and deflection stresses in welded bellows of standard design always occur near the root and crown welds. This is extremely undesirable since it means that the maximum stresses occur in a notched heat-affected zone. The change in section resulting from the weld bead also represents a possible source of stress concentration.

One of the most significant results of this research program has been the discovery that it is possible to redesign nested-ripple welded bellows so that the stresses near the crown and root welds are virtually eliminated. This design change involves tilting the bellows flats with respect to the axis of the bellows. Appendix D gives a discussion of an investigation of the optimum tilt angle for two bellows configurations. These results show that (1) it is possible to find a tilt angle for the flats that achieves dramatic reduction in the stresses in the weld areas for both axial deflection and pressure loading and (2) tilting the flats raises the spring rate by less than 20 percent.

By reducing the stresses near the welds, so that the maximum stresses occur away from the weld areas and in an area where the metal has the properties of the original sheet material, the fatigue life of welded bellows should be significantly improved. It is believed that this slight design change alone should result in a major improvement in the operating characteristics of welded bellows if optimum tilted flat configurations can be found for most types of welded bellows convolution shapes.

TABLE 4. THEORETICAL AND EXPERIMENTAL STRESSES FOR TYPICAL WELDED BELLOWS

		Theoretical and Experimental Stresses, psi[a]							
		3-1/2-Inch SS Bellows		1-1/2-Inch SS Bellows		3-Inch AM-350 Bellows		1-1/2-Inch AM-350 Bellows	
		Stresses	% Diff	Stresses	% Diff	Stresses	% Diff	Stresses	% Diff
Deflection Stresses	Meridional								
	Theoretical	+28,050	-28.1	+40,760	0.0	+63,220	-38.9	+66,350	-15.4
	Experimental	+20,166		+40,760		+38,730		+56,160	
	Circumferential								
	Theoretical	+10,402	+26.2	+13,200	-37.3	+20,520	-53.4	+ 9,640	+4.3
	Experimental	+13,133		+ 8,268		+9,570		+10,050	
Pressure Stresses	Meridional								
	Theoretical	-14,486	-16.7	-8,840	-40.4	-8,160	-8.5	-5,954	-48.0
	Experimental	-12,067		-5,268		-7,470		-3,090	
	Circumferential								
	Theoretical	-4,149	-7.0	-1,140	+1.8	-460	-8.7	+34	+1,488
	Experimental	-3,858		-1,160		-420		+540	

(a) Plus values indicate tensile stresses; minus values indicate compressive stresses.

Stresses in Diaphragms

Analysis of Stresses in a Diaphragm. The diaphragm used for this study was a 4-inch convoluted diaphragm made of stainless steel. In contrast to the bellows, the diaphragm configuration allowed placement of strain gages at several positions. This permitted a far more detailed comparison of the theoretical and experimental stresses than was possible for the different bellows. The stress analysis of the diaphragm under upward and downward axial deflection of the hub and under pressure loading is discussed in detail in Appendix I. The comparison of the theoretical and experimental stresses in the diaphragm under the different loading conditions is shown in Figures I-18 through I-20. These figures demonstrate the impressive accuracy of the theoretical analysis technique in predicting stresses and strains in corrugated shells.

Discussion of Stresses in Diaphragms. Diaphragms have a wide application in pressure-measuring instruments and other systems where maximum sensitivity to change in pressure is desired. Corrugations have been added to diaphragms to increase their flexibility. When flexible corrugated diaphragms undergo large deflections of several times the thickness, they exhibit highly nonlinear behavior. This means that deflections and stresses cannot be accurately predicted with linear theory, but nonlinear theory must be used. Accurate nonlinear calculations are now possible with the use of computer program NONLIN, although the accuracy does decrease as the degree of nonlinearity increases. There were insufficient funds on the program to investigate this relationship in detail.

For the 4-inch diaphragms analyzed during this research program, it was found that the stresses were high near the outside edge, but highest near the inside edge adjacent to the hub. It was also found that care had to be taken in superimposing stresses from pressure and from central hub loading, because the nonlinear response was different for the individual loadings than for the combined loadings. For example, upward pressure loading and downward deflection loading of the hub produced maximum stresses of the same sign near the hub. Simple addition of stresses from the individual loadings gave a total stress which was appreciably different from the actual total stress under combined loading. Even though individual results may be fairly linear, combined loadings can result in nonlinear response due to higher combined deflection. Computer program NONLIN can be used for combined loadings as well, and such a calculation should be made if combined deflections are expected to be large.

Very large deflection loading of the 4-inch diaphragm produced fatigue failures at an inner convolution. This was probably a result of geometrical nonlinearity causing the location of maximum stress to shift from the hub to an inner convolution. It has not been determined whether NONLIN can be used for this degree of nonlinearity.

Spring Rates of Bellows and Diaphragms

The spring rate of a bellows or diaphragm can be defined as the average axial force necessary to deflect the bellows or diaphragm a unit distance, or as the ratio of a given axial force to the axial deflection caused by that force. The former value is usually supplied by the manufacturer. However, since many bellows and diaphragms

exhibit some spring-rate nonlinearity even in the "linear" region, the value for the latter calculation may be different from that for the former calculation. (For example, see Tables G-3 and G-4 of Appendix G.)

Spring rate is one of the important characteristics needed for the selection of bellows and diaphragms. Although it is quite easy to measure the spring rate of a bellows or diaphragm, this has always been one of the most difficult characteristics to predict accurately. The primary reason for this difficulty is that the spring rate in essence is an integration of the stresses in all parts of the bellows or diaphragm. Consequently, measured spring rates were expected to be a sensitive indication of the accuracy of the stresses calculated using the computing program NONLIN. It was found that, in almost every case, the theoretical spring rate predicted for each lot of experimental bellows was within the range of experimentally measured spring rates for that lot.

The spring rate of an analyzed configuration can be calculated very simply from the analyses of the axial deflection cases. In an analysis of a bellows or diaphragm, an assumed axial deflection, δ, is imposed on one end of the theoretical model. Once the stress analysis has been performed, the axial force, F, required to produce the deflection δ is found from the formula

$$F = 2\pi r \left(N_\phi \sin \phi + Q \cos \phi\right) \quad , \tag{1}$$

where $N\phi$ and Q are the meridional and transverse resultant forces at any point in the bellows or diaphragm, r is the radius of the point from the centerline, and ϕ is the angle between the normal to the shell and the axis at the point. Although this formula holds at every point, it is obviously more convenient to use at some point where ϕ is 0 deg or 90 deg, that is, at a point where the shell is either normal or parallel to the axis. Once F has been determined, the spring rate, k, of the bellows is calculated from the formula

$$k = \frac{F \ L_o}{\delta \ L_c} \quad , \tag{2}$$

where L_o is the axial length of the mathematical model, and L_c is the live length of the actual bellows. For a convoluted diaphragm, the spring rate is simply given by

$$k = F/\delta \quad ,$$

since the mathematical model on which the analysis is based is the same as the actual diaphragm.

The experimental determination of the spring rate is made by observing the increments of bellows or diaphragm deflection caused by increments of axial force.

Comparison of Theoretical and Experimental Spring Rates for Bellows

Table 5 shows the measured spring rates for the formed bellows test specimens, the average spring rate for each bellows type, and the theoretical spring rate calculated from each bellows model. In every case the predicted spring rate was within 10 percent of the averaged measured spring rate. Table 6 shows a similar comparison between the

TABLE 5. THEORETICAL AND EXPERIMENTAL SPRING RATES FOR TYPICAL FORMED BELLOWS

5-Inch, One-Ply Stainless Steel, 12 Convolutions				3-Inch, One-Ply Stainless Steel, 10 Convolutions				1-Inch, One-Ply Stainless Steel, 8 Convolutions			
Bellows	Compr. Spring Rate, lb/in.	Extens. Spring Rate, lb/in.	Comb. Spring Rate, lb/in.	Bellows	Compr. Spring Rate, lb/in.	Extens. Spring Rate, lb/in.	Comb. Spring Rate, lb/in.	Bellows	Compr. Spring Rate, lb/in.	Extens. Spring Rate, lb/in.	Comb. Spring Rate, lb/in.
JD87	294	332	313	JD61	138	152	145	JD23	73	80	77
JD88	302	316	309	JD62	155	179	167	JD24	-	-	-
JD89	287	316	302	JD63	152	193	173	JD25	76	93	85
JD90	296	324	310	JD64	148	174	161	JD26	78	89	84
JD91	288	324	306	JD65	163	184	174	JD27	78	85	82
JD93	272	302	287	JD66	168	187	178	JD28	70	85	78
JD94	279	314	297	JD67	155	182	169	JD30	76	85	81
JD95	280	321	301	JD69	151	166	159	JD31	80	85	83
JD96	287	322	305	JD70	156	187	172	JD32	68	82	75
JD97	283	317	300	JD71	172	198	185	JD33	82	89	86
JD98	284	316	300	JD72	174	194	184	JD34	74	78	76
Experimental Avg	287	319	303		158	181	170		77	85	81
Theoretical Avg	-	-	325		-	-	161		-	-	86

3-Inch, One-Ply Inconel, 14 Convolutions				1-Inch, One-Ply Inconel, 16 Convolutions			
Bellows	Compr. Spring Rate, lb/in.	Extens. Spring Rate, lb/in.	Comb. Spring Rate, lb/in.	Bellows	Compr. Spring Rate, lb/in.	Extens. Spring Rate, lb/in.	Comb. Spring Rate, lb/in.
JD119	139	145	142	JD107	76	76	76
JD120	125	131	128	JD108	82	82	82
JD121	137	143	140	JD109	78	78	78
JD122	-	-	-	JD110	-	-	-
JD123	139	145	142	JD111	90	90	90
JD125	131	133	132	JD112	79	75	77
JD126	136	140	138	JD113	77	79	78
JD127	133	139	136	JD114	79	81	80
JD128	136	142	139	JD115	82	82	82
JD129	136	142	139	JD116	79	79	79
				JD118	89	89	89
Experimental Avg	134	140	137		81	81	81
Theoretical Avg	-	-	140		-	-	89

TABLE 6. THEORETICAL AND EXPERIMENTAL SPRING RATES FOR TYPICAL WELDED BELLOWS

3-1/2-Inch Stainless Steel Spring Rate, lb/in.			1-1/2-Inch Stainless Steel Spring Rate, lb/in.			3-Inch AM-350 Spring Rate, lb/in.			1-1/2-Inch AM-350 Spring Rate, lb/in.		
Bellows	Compr.	Extens.	Bellows	Compr.	Extens.	Bellows	Compr.	Extens.	Bellows	Compr.	Extens.
Experimental											
JD131	84	81	JD143	112	98	JD155	171	139	JD167	127	121
JD132	65	82	JD144	80	100	JD156	154	148	JD168	121	108
JD133	68	82	JD145	74	98	JD157	150	146	JD169	105	105
JD134	60	70	JD146	76	89	JD159	141	141	JD170	111	100
JD135	62	85	JD147	83	91	JD160	150	146	JD172	114	111
JD137	89	78	JD148	79	98	JD161	146	145	JD173	108	105
JD138	86	78	JD149	91	87	JD162	156	146	JD174	118	111
JD139	69	83	JD151	83	121	JD163	156	143	JD175	114	105
JD140	66	81	JD152	80	111	JD164	143	138	JD176	121	105
JD141	95	78	JD153	77	100	JD165	150	148	JD177	105	108
JD142	63	81	JD154	77	111	JD166	146	145	JD178	111	111
Experimental Average											
	73	80		83	100		151	144		114	108
Theoretical Spring Rates (Nonlinear)											
	57	-		101	-		152	-		124	-

theoretical and experimental values of the spring rates for welded bellows. The theoretical spring rates for the welded bellows were calculated from a nonlinear deflection calculation. Although the agreement between the theory and experiment is not as striking for welded as for formed bellows, it is still very good.

Some appreciation of the variation in bellows behavior introduced by the welding in welded bellows can be gained by comparing the compressive-extension spring-rate relationships for formed and welded bellows. In formed bellows, the absolute spring-rate values varied, but the extension spring rate was almost always the higher value. Within a given lot of welded bellows, at least one or two bellows departed from the pattern relationship established by the majority of the lot. The variations in welded bellows spring rates can also be large. For example, compare the compression spring rates of JD134 (60 lb/in.) and JD141 (95 lb/in.), and the compression spring rate of JD135 (62 lb/in.) with the extension spring rate of JD135 (85 lb/in.). It is apparent that, for critical applications, the spring rates of each welded bellows must be determined experimentally.

Comparison of the Theoretical and Experimental Spring Rates for Diaphragms

Table I-7 compares the theoretical and experimental spring rates for a convoluted diaphragm. It is seen from this table that the calculated spring rates were somewhat higher than the experimentally measured spring rates. It is believed that this was caused primarily by differences in shape between the diaphragm on which the spring rate was measured and the diaphragm used to construct the mathematical model. Differences in shape in diaphragm convolutions might have a cumulative effect on the spring rate of the diaphragm, while differences in the convolutions of bellows tend to average out. It was shown in Appendix I that there was a significant chance that the diaphragm could interact with the hub as well as with the rim when it was deflected downward, and that this interaction could have a significant effect on the spring rate. However, it was not determined whether this had any bearing on the discrepancy between the measured and experimental spring rates.

Effective Area of Bellows and Diaphragms

The effective area of a bellows or a diaphragm is a measure of the axial force caused by internal or external pressure. If a bellows loaded by a pressure, p, is restrained by an axial force, F, so that its length under pressure equals the free length, then the effective area of the bellows is given as:

$$A = F/p \quad .$$

The effective area of a pressurized diaphragm held to its free position by an axial force on the hub is determined by the same formula.

The theoretical prediction of the effective area of either a bellows or a diaphragm is calculated quite easily from the analysis of the pressure-loaded and axially restrained bellows or diaphragm. The axial force for the diaphragm is obtained from the formula:

$$F = 2\pi r_1 Q + \pi r_o^2 p \quad , \tag{3}$$

where r_o is the radius of the hub and Q is the transverse shear at the edge of the hub. In a bellows the axial force is determined from the formula:

$$F = 2\pi r_o (Q \cos \phi - N_\phi \sin \phi) + \pi r_o^2 p \quad , \tag{4}$$

where Q and N_ϕ are the transverse and meridional stress resultants, r_o is the radius to the point at which Q and N_ϕ are determined and ϕ is the angle between the normal to the bellows surface at this point and the bellows axis. While this formula holds at any point of the bellows, it is most convenient to use at a point where ϕ is 0 or 90 deg. Both N_ϕ and Q are printed out by program NONLIN at each point of the bellows or diaphragm to facilitate this calculation.

Appendix D describes the parametric stress analysis of 24 formed bellows. Effective areas were calculated from analysis of each of these bellows under pressure loads. In every case the effective area was given to within 1-1/2 percent by the formula $A = \pi \bar{R}^2$, where $2\bar{R}$ is the average of the OD and ID of each bellows.

Comparisons of the experimentally determined and theoretically calculated effective areas for the formed- and welded-bellows test specimens are given in Table 7. The agreement between these results is good.

The theoretical effective area for the diaphragm JD181 was 7.55 $in.^2$ while the effective measured effective area of Diaphragm JD190 was 7.72 $in.^2$.

TABLE 7. THEORETICAL AND EXPERIMENTAL EFFECTIVE AREAS FOR TYPICAL FORMED AND WELDED BELLOWS

Bellows Size and Type	Bellows No.	Theoretical Effective Area, sq in.	Bellows No.	Experimental Effective Area, sq in.
Formed Bellows				
5-inch stainless steel	JD92	22.3	JD88	21.0
3-inch stainless steel	JD68	8.62	JD69	8.66
1-inch stainless steel	JD29	1.05	JD28	1.06
3-inch Inconel 718	JD124	8.41	JD122	8.33
1-inch Inconel 718	JD117	0.98	JD110	0.96
Welded Bellows				
3-inch stainless steel	JD136	8.10	JD131	8.25
1-inch stainless steel	JD171	1.37	JD167	1 26
3-1/2-inch AM-350	JD158	7.85	JD155	7.32
1-inch AM-350	JD150	1.30	JD143	1.27

Elastic Buckling and Plastic Collapse of Bellows and Diaphragms

The thin-wall construction of bellows and diaphragms makes them particularly susceptible to overstressing and excessive deformation due to pressure. Although bellows manufacturers usually provide pressure ratings for each bellows, standard rating definitions have not been established and the detailed procedures and calculations used to

determine the pressure ratings are often not available. More importantly, it has been established in the current research program that a bellows may be overstressed at low pressures and small deflections because of elastic buckling (partial squirm). Further, when combined with compression, internal pressures that are less than the maximum rated operating pressure may cause plastic collapse of the bellows (squirm) within the maximum deflection rating. Thus the response of bellows to internal pressure is an important consideration in their design.

Elastic Buckling of Bellows

As far as is known, the problem of elastic sidewise beam-column buckling, or partial squirm, is appreciated by few, if any, bellows designers, and estimates of stresses resulting from elastic buckling cannot presently be obtained from bellows manufacturers. However, as discussed in Appendix J, such stresses can be estimated if:

(1) The lateral bending stiffness D, lb-in.^{2} is calculated using the analysis procedure described in Appendix B

(2) Imperfections in the bellows are included in the analysis.

Calculation of Lateral Bending Stiffness, D. The buckling strength of a bellows as a beam column is proportional to its lateral bending stiffness, D. D is comparable to EI for conventional beams, where E = modulus of elasticity, psi, and I = moment of inertia, in.^{4}. Theoretical calculations and experimental measurements of D are shown in Table 8 for typical bellows analyzed in this research program. The bending stiffnesses increase with the nominal diameter, and are much lower for welded bellows than for formed bellows. The experimental values in Table 8 are average values for each bellows lot. The specific values of D showed some variation within each lot.

In the literature, the lateral bending stiffness, D, of a bellows has been related to the axial spring constant, k, by the Seide formula:

$$D = 0.500\, k\, \bar{R}^2\, L_c \quad , \tag{5}$$

where

$$\bar{R} = \frac{R_o + R_i}{2} = \text{average bellows radius}$$

L_c = total live convolution length of bellows.

The factor 0.500, which is exactly correct for a cylindrical shell, has been shown in this research program to be incorrect for some bellows. The Seide formula has been rewritten with a factor α:

$$D = \alpha\, k\, \bar{R}^2\, L_c \quad . \tag{6}$$

Theoretical and average experimental values of α are shown in Table 9 for typical bellows. The experimental range of α for all sizes of formed bellows tested was $0.356 \leq \alpha \leq 0.643$. Thus, $\alpha = 0.500$ can be used as an approximate average value for bellows, but for a more accurate determination, a computer calculation should be made.

TABLE 8. THEORETICAL AND EXPERIMENTAL VALUES OF THE LATERAL BENDING STIFFNESS D FOR TYPICAL FORMED AND WELDED BELLOWS

Nominal Bellows Diam, in.	Number of Plies	Material	Lateral Bending Stiffness, D, lb-in.^{2}	
			Theoretical(a)	Experimental Average
Formed Bellows				
1	1	321 SS	13.8	12.2
1	1	Inconel 718	15.4	16.4
3	1	321 SS	480.4	586.3
3	1	Inconel 718	--	413.4
3	2	321 SS	960.8	1007.3
5	1	321 SS	4507.0	4124.0
Welded Bellows				
1-1/2	1	347 SS	9.44	6.80
1-1/2	1	AM-350	12.83	8.02
3	1	AM-350	58.50	63.5
3-1/2	1	347 SS	37.90	44.5

(a) Calculated using the analysis procedure described in Appendix B.

TABLE 9. RELATION BETWEEN BENDING STIFFNESS D AND SPRING CONSTANT k FOR TYPICAL FORMED AND WELDED BELLOWS

Nominal Bellows Diam, in.	Number of Plies	Material	Factor α, $\frac{D}{k\bar{R}^2 L_c}$	
			Theoretical(a)	Experimental Average
Formed Bellows				
1	1	321 SS	0.480	0.434
1	1	Inconel 718	--	0.493
3	1	321 SS	0.540	0.583
3	1	Inconel 718	--	0.547
3	2	321 SS	0.540	0.501
5	1	321 SS	0.536	0.471
Welded Bellows				
1-1/2	1	347 SS	0.581	0.406
1-1/2	1	AM-350	0.699	0.430
3	1	AM-350	0.457	0.495
3-1/2	1	347 SS	0.537	0.575

(a) Calculated using the shell computer program for a mathematical model of an encapsulated and cross-sectioned specimen.

Calculation of Theoretical Critical Loading Conditions. With the bending stiffness D known, the Euler critical load for a perfectly straight bellows may be calculated from the formula:

$$P_{cr} = \frac{4\pi^2 D}{L_c^2} \quad . \tag{7}$$

For a bellows under internal pressure and axial compression, the equivalent axial load P_{cr} is a combination of a pressure force and a compression force as given by Equation (J-16) in Appendix J. Critical internal pressures without axial compression are given in Tables J-23 and J-24 for typical formed bellows and typical welded bellows, respectively If the bellows were perfectly made, these would be the conditions that would cause gross buckling, or squirm, of the bellows.

Calculation of Stresses Caused by Elastic Buckling. Although the critical buckling pressure calculated for one of the experimental formed bellows was more than 330 psi, the actual bellows tested were found to exhibit detectable sidewise movement at pressures of less than 80 psi. The reason for this was found to be that instead of being perfectly straight, the bellows were actually bowed slightly, so that they had the appearance of a slightly bent beam. (Deviations like this from the ideal shape are usually called "imperfections".) Because of this imperfection, internal pressure in the bellows induced a bending moment that tended to increase the bow, and the bellows began to deform sideways from the onset of the pressure loading. It was also observed that the ends of many of the test bellows had a sideways offset relative to each other, so that the bellows had a slight S-shape. This is another type of imperfection that will lead to an early sidewise deformation when the bellows is pressurized internally. Theoretically derived curves of load vs. sideways deflection are shown in Figure J-8 for two types of bowing imperfections.

The sidewise movement of a bellows introduces additional strains and stresses in the convolutions of the bellows. Thus, the total stress is:

$$\sigma_T = \sigma_p + \sigma_\Delta + \sigma_M \quad , \tag{8}$$

where σ_p and σ_Δ are the usual axisymmetric stresses from internal pressure p (psi) and compression Δ (in.) and σ_M is the additional asymmetric stress from sidewise bending of the bellows due to beam-column buckling. As shown in Appendix J, the stress σ_M can be determined from computer calculations using the mathematical model of the bellows if measurements are made of the bellows imperfections.

At the inner surface of an inner convolution of a 5-inch bellows, the meridional stresses were calculated to be:

$$\sigma_p = 40,000 \text{ psi}$$

and

$$\sigma_M = 11,500 \text{ psi}$$

for p = 78.6 psi and Δ = 0.0 in. The stress value 11,500 psi corresponded to a modest sidewise deflection of 0.004 in. Thus, elastic beam-column buckling of a bellows may

result in an appreciable increase in stress in the bellows. If this stress fluctuates with the other fluctuating stresses, the fatigue life of the bellows may be significantly reduced. (In the fatigue tests conducted during this research, the pressures were held constant, so this type of stress was probably not a factor in the fatigue failures.)

Plastic Collapse of Bellows

Plastic collapse of a bellows results in gross permanent deformation of the bellows which makes it unfit for further use. At the limit load at which collapse occurs, a sufficiently large region of the bellows convolutions becomes wholly plastic so that adjacent elastic or elastic-plastic regions of the convolutions no longer restrain the plastic region. Whereas initial buckling deflections can be analyzed using elasticity theory, the terminal-collapse state necessitates the use of the plasticity theory. Only axisymmetric plastic collapse under internal pressure was considered in detail during this program. However, comments are included on nonsymmetric plastic collapse, i.e., the permanent squirm which results when the elastic beam-column buckling loads are exceeded. Comments are also included on the plastic deformation of diaphragms.

Axisymmetric Plastic Collapse. The elastic solution for stresses in shells has been employed by Marcal and Turner[4] to obtain a lower bound on the axisymmetric collapse pressure for bellows. As a first approximation, this method was also tried in this study. The method consists of scaling up the maximum elastic stress state at a point in a shell to the plastic collapse value. In the 5-inch bellows the maximum stress occurred at the roots of the convolutions and was predominantly a bending state of stress. Scaling up the corresponding bending moment to the plastic collapse value gave a plastic collapse pressure of 116 psi.

Tests with these bellows showed that collapse occurred at internal pressures of about 260 to 270 psi. Even if allowance was made for strain hardening due to forming and fatigue-test cycling at the root, it did not appear that this accounted for the larger observed collapse pressure – particularly since the root area was also observed to remain relatively rigid at collapse. Thus, use of the elastic solution to predict lower bounds based upon maximum elastic stress did not provide sufficient accuracy.

Marcal and Turner had much better success. This is believed to be due to two different kinds of plastic collapse which are related to two different ranges of diameter-to-thickness ratios. The diameter-to-thickness ratio for the 5-inch bellows was $d/h = 5.0/0.010 = 500$, whereas the ratio for the bellows tested by Marcal and Turner ranged from 8.2 to 23.6. It is reasoned that a membrane stress state predominates at plastic collapse of the thin-walled bellows ($d/h = 500$), and that a bending-stress state predominates at plastic collapse of thick-walled bellows ($d/h \simeq 10$).

If the above reasoning is correct, then the maximum membrane stress calculated elastically should result in a better prediction of the collapse pressure. The following method was tried: the membrane stress resultants from the elastic computer solution were taken at the inflection point where the bending moment was 0, and were scaled up to the collapse value. The resulting calculation of 313 psi was quite close to the experimental values. It was believed that this was as close an approximation as could be made without conducting a complete detailed theoretical-plastic analysis, which was beyond the scope of the present program.

Theoretical predictions of collapse pressures were then made for other bellows. The pressures causing axisymmetric plastic collapse were found to be significantly higher than the elastic buckling pressures. Thus, beam-column buckling will be the mode of failure, unless the bellows is restrained, e.g., by a housing, guide rods, etc.

An interesting use of restraint has been reported by Newland[5], who analyzed the buckling resistance of a universal expansion joint. Such a joint incorporates two bellows joined by a length of rigid pipe. He has shown that, by providing a correctly designed supporting structure, the critical buckling pressure can be increased up to four times the value for the same system without supports.

A bellows clamped at both ends and subjected to external pressure will not buckle as a beam column, but it may buckle locally as a shell. The crowns of the formed bellows, which are parts of toroidal shells, will develop compressive hoop stresses under external pressure. Thus, the crowns may buckle[6] in a nonsymmetric mode, particularly if the shell thickness is small in relation to the radius of curvature of the crown. Welded bellows also may be subjected to local shell buckling in their leaves under external pressure. The analysis of shell buckling is very complicated and was beyond the scope of the present research program.

Bellows subjected to external pressure can be expected to have plastic-collapse pressures of about the same values as predicted for internal pressure collapse. For example, plastic-collapse internal pressures found for 5-inch formed bellows were 250 to 270 psi. External pressures of this magnitude, likewise, may cause plastic collapse.

It is difficult to predict whether elastic buckling or plastic collapse will be the dominant failure mode under external pressure. If the bellows is very thin, then elastic buckling may predominate. If not, plastic collapse may predominate. A combination of failure modes may also occur, i.e., elastic-plastic buckling. This is a problem that warrants further investigation.

Estimates related to axisymmetric plastic collapse pressures can usually be obtained from bellows manufacturers. Often called "maximum allowable pressure", or "proof pressure", the cited values usually incorporate a safety factor so the bellows will not suffer permanent deformation when the fluid system is given a proof-pressure test at the rated pressure. The values are usually based on tests in which the bellows is restrained at its free length and laterally supported. As described above, if the bellows is not given lateral support, deformation will occur at pressures much below the cited value. Even with lateral restraint, if the bellows has a large deflection loading, the bellows convolutions may collapse below the cited pressure value.

Some manufacturers list burst pressures for bellows. This may be the pressure at which axisymmetric collapse is expected. Since the material usually does not rupture at the initial stage of collapse, this value represents a safety factor for burst. A burst-pressure value can also represent a calculation based on the ultimate tensile strength of the bellows wall. As such, it has little practical meaning since rupture may take place at a lower pressure in a location where the bellows has creased during deformation.

Nonsymmetric Plastic Collapse. If the elastic beam-column buckling loads are exceeded, the highly stressed parts of the bellows convolutions will deform plastically and a state of permanent squirm deformation will result. Equation (8), above, can be used to calculate the pressure and axial compression required to cause stresses in the

plastic range and thus to predict the loading conditions that cause the beam-column type of plastic collapse. This collapse is essentially a continuation of the elastic buckling deformation beyond the elastic limit of the material, and it, too, depends upon the bowing and offset imperfections of each bellows.

This mode of failure is reasonably well known and squirm-producing combinations of pressure and deflection can be obtained from some manufacturers. However, some references have implied that a bellows which is "square" (length equal to or less than the diameter) will not squirm. On the contrary, many "square" bellows will squirm at less than their maximum compression rating when the internal pressure is equal to the maximum rated operating pressure.

Plastic Collapse of Diaphragms

Overpressure experiments were conducted on the 4-inch stainless steel corrugated diaphragms. The diaphragms exhibited plastic deformation at pressures as low as 12 to 17 psi. These initial plastic-collapse pressures were relatively small; the diaphragms withstood much higher pressures without burst (up to 300 psi), but they did so with a great change in shape. This behavior was attributed to favorable geometry change during deformation. As noted in Figure I-26, the diaphragms deformed from the corrugated shape toward a semitoroidal shape with flattening of the corrugations. Thus, large plastic (and permanent) deformations were possible without appreciable material stretching, but with appreciable bending at the roots and crowns of the corrugations, i.e., material was available in the corrugations to permit a grossly deformed shape without reducing the thickness.

Overload deflection experiments were also conducted. The central hub of a diaphragm was deflected with the outside rim clamped. Plastic deformations were first observed at a load of 13.7 pounds. Subsequent tests to higher loads (up to 26.3 pounds) showed that strain results for subsequent runs at a certain load level were essentially the same. These results indicated that the diaphragm could be cycled into the plastic range with repeated strain readings after very few cycles. However, the spring constant changed during cycling, and the load-deflection curves became quite nonlinear (concave upward).

It was found that the pressure and deflection load required to cause initial plastic deformation could be estimated by a lower-bound analysis. The maximum bending moments predicted by linear computer calculations (using NONLIN) were scaled up to the yield values. Lower bounds of 5.5 psi and 13.6 lb were estimated as compared with initial plastic loading values of 12 to 17 psi and 13.7 lb from the experiments.

The overload experiments indicated that corrugated diaphragms can withstand loads much beyond their initial plastic-collapse values. Accurate prediction of this kind of behavior would require an elastic-plastic theoretical analysis.

Vibration of Bellows and Diaphragms

The life of bellows and diaphragms may be drastically reduced if resonance causes amplitudes greater than those estimated for the normal operating conditions. Resonance

can occur in response to vibration of the supporting structure. Bellows in a fluid line can also experience flow-induced vibration.

Structurally Induced Vibration in Bellows

The general approach to a structurally induced vibration problem is to use a bellows which will not resonate with the structure, or to apply various dampening devices to the bellows. Formulas can be used to estimate resonant frequencies in a bellows. Because bellows are lightly damped structures, resonance must be prevented, and the adequacy of each assembly in the vibration environment must be demonstrated in the laboratory.

Vibration Formulas. The problem of structurally induced vibration in bellows was investigated in some depth by the Bell Aerosystems Company[7] as a part of a program on the design of expulsion bellows. Three modes were studied: (1) the longitudinal or accordion mode, (2) the transverse or beam mode, and (3) the liquid mode.

Bell was able to predict the accordion and beam vibration modes using formulas for a solid bar and beam when the constants used in the formulas were interpreted correctly. Calculations of the natural frequency for bellows clamped at both ends, undamped, and vented to atmosphere can be made by substituting the appropriate values in the frequency equations shown below.

Accordion Mode	Beam Mode
$f_n = 1/2\sqrt{\frac{kg}{W_m}}$	$f_L = \frac{A_n}{2\pi}\sqrt{\frac{kR_o^2 g}{2L_c^2 (W_m)}}$

(9)

where

f_n = fundamental natural frequency for the accordion mode, cps

f_L = fundamental natural frequency for the lateral beam mode in cps when the constant $A_n = 22$

k = axial spring rate of bellows, lb/in.

g = acceleration due to gravity, 386 in./sec^2

W_m = weight of metal in the convolutions, lb

R_o = outside diameter of the convolutions ÷ 2, in.

L_c = live length of the bellows.

The liquid mode, which occurs in the longitudinal direction when vibration-induced pressure surges in the contained liquid interact with the expulsion bellows, was more difficult to analyze. Although Bell developed an analysis approach for this problem, this mode usually does not occur in bellows used in aerospace components such as valves and regulators, and the accuracy of the analysis method was not investigated.

Investigation of Vibration Formulas. The applicability of Bell's accordion and beam-mode formulas for small bellows was evaluated during the current program through theoretical and experimental vibration analyses of each of the test bellows. Each analysis consisted of: (1) determining the weight and spring rate of the bellows, (2) calculating the natural frequency for the accordion and beam modes of vibration, and (3) subjecting the bellows to axial and transverse vibrations on a Caladyne shaker table. Since this work is not described in an appendix, it is reported in some detail here.

The estimated weight of the bellows was obtained by estimating the developed length of the bellows and multiplying this by the average thickness to obtain the volume of metal used in the bellows. As a check, a similar estimate was made of the weight of the end fittings and other parts of the test specimens not including the bellows. This weight was subtracted from the measured weight of the test specimen to obtain the bellows weight.

The axial spring rate of each bellows was obtained by measuring the load-deflection characteristics of the bellows, and then calculating the slope of the load-vs.-deflection curve. Since vibration of the bellows alternately places the individual convolutions under tensile and compressive loads, the spring-rate value used in the frequency equation was the average of the extension and compression spring rates.

When the theoretical resonant frequencies of the bellows had been calculated, the bellows were mounted in a fixture (see Appendix Q) and attached to the Caladyne shaker table. Each bellows was subjected to accordion and lateral-mode frequency scans from 100 cps to 10,000 cps to determine resonant frequencies. Since some indications of resonance by the acceleration meter on the shaker console were produced because of fixture vibration, each indicated resonant period was checked by means of stroboscopic observation to verify that the resonant behavior was associated with the bellows and not the fixture. In some cases the amplitude of lateral response was so slight that acceleration indications of resonance were meaningless and a touch sensing approach was used to detect the resonant periods.

Results of Theoretical and Experimental Analysis. Calculated and observed resonant frequencies for the test bellows are shown in Table 10. For the formed bellows, the experimental results for the accordion mode correlated very closely with the formula predictions. The experimental results for the lateral beam mode did not correlate well with the theoretical predictions, and it was concluded that the beam formula is not applicable to the type of bellows tested. Examination of the results in Table 10 showed that the experimental lateral frequencies were everywhere substantially less than the theoretical predictions of the classical beam theory. This was attributed to the effects of shear deformation and rotary inertia. These effects are known to result in lower frequencies than predicted by the classical theory and cause a greater reduction for shorter length beams.[8] Inclusion of these effects for the complicated geometry of a bellows was considered beyond the scope of the present program.

The results for the welded bellows were essentially the same as for the formed bellows: the calculated and observed values for the accordion mode were quite close, while the calculated and observed values for the beam mode disagreed more than for the formed bellows.

All the bellows tested exhibited low internal damping and extremely narrow resonant periods. Except for nonstandard modes of vibration caused by noncentroidal

TABLE 10. THEORETICAL AND EXPERIMENTAL NATURAL VIBRATION FREQUENCIES FOR TYPICAL FORMED AND WELDED BELLOWS

		Bellows Description			Natural Frequency Data, cps							
		Nominal	Number	Number of	Calculated f_n (Accordion Mode)		Observed f_n (Accordion Mode)		Calculated f_L (Lateral Mode)		Observed f_L (Lateral Mode)	
No.	Material	Size, in.	of Plys	Convolutions								
JD23	321 SS	1	1	8	1st	681	1st	715	1st	2400	1st	1180
					2nd	2043	2nd	2140				
					3rd	3405	3rd	3490				
JD35	321 SS	1	1	16	1st	376	1st	380	1st	601	1st	464
					2nd	1128	2nd	1160				
					3rd	1880	3rd	1930				
JD36	321 SS	1	2	16	1st	364	1st	382	1st	579	1st	470
					2nd	1092	2nd	1100				
					3rd	1820	3rd	1880				
JD66	321 SS	3	1	10	1st	337	1st	349	1st	1320	1st	610
					2nd	1011	2nd	1041				
					3rd	1685	3rd	1755				
JD81	321 SS	3	2	10	1st	320	1st	332	1st	1490	1st	612
					2nd	960	2nd	1030				
					3rd	1600	3rd	1650				
JD85	321 SS	3	1	20	1st	145	1st	152	1st	323	1st	218
					2nd	435	2nd	456				
					3rd	725	3rd	751				
JD86	321 SS	3	2	20	1st	162	1st	168	1st	340	1st	251
					2nd	486	2nd	498				
					3rd	810	3rd	835				
JD90	321 SS	5	1	12	1st	243	1st	252	1st	820	1st	425
					2nd	729	2nd	768				
					3rd	1215	3rd	1265				
JD99	321 SS	5	1	24	1st	122	1st	127	1st	220	1st	163
					2nd	366	2nd	370				
					3rd	610	3rd	645				
JD111	718 Inconel	1	1	16	1st	775	1st	770	1st	1892	1st	1122
					2nd	2325	2nd	2280				
					3rd	3875	3rd	3780				
JD125	718 Inconel	3	1	14	1st	339	1st	323	1st	1468	1st	581
					2nd	1017	2nd	970				
					3rd	1695	3rd	1580				
JD135	347 SS (welded)	3-1/2	1	8	1st	282	1st	270	1st	4550	1st	564
					2nd	846	2nd	828				
					3rd	1410	3rd	1345				
JD156	AM-350 (welded)	3	1	8	1st	468	1st	440	1st	11650	1st	860
					2nd	1403	2nd	1265				
					3rd	2340	3rd	1967				

excitation, bellows response to inputs other than true harmonics was practically negligible. Light applications of Coulomb damping eliminated bellows vibration altogether.

Flow-Induced Vibration in Bellows

Little theoretical work has been done on flow-induced vibration in bellows, and since this is not a problem in bellows used in aerospace components, this performance characteristic was not investigated during the current program. If flow-induced vibration occurs, it can often be prevented by a liner in the bellows which separates the convolutions from the flow stream. However, unexpected flow-induced vibration is a frequent cause of bellows failure in piping systems.

Vibration of Corrugated Diaphragms

The only publication found in the literature search that pertained to the analysis of the vibration of corrugated diaphragms is a paper by Akasaka and Takagishi.[9] Their analysis is very approximate: they predict the natural frequencies of a diaphragm with shallow corrugations using formulas for orthotropic flat plates. The corrugated diaphragm has less stiffness in the meridional direction than in circumferential direction. The authors have used the method of Haringx[10] to estimate the stiffnesses in the two directions. (Haringx conducted only static analysis.) They also include the effect of a concentrated mass (hub) at the center of the diaphragm. Their results of an experiment on one diaphragm agreed very well with the approximate formula. This diaphragm, however, was very shallow – the amplitude (half-depth) of the corrugations (0.85 mm) was only about twice the thickness (0.4 mm) and the half-wave pitch of the corrugations was very large (6 mm).

The formula of Akasaka and Takagishi is not considered applicable to nonshallow diaphragms, where the amplitude-to-pitch ratio is much greater than 0.1. The authors mention that "informal" experiments show that the formula predicts frequencies much too high. For nonshallow diaphragms, rotary inertia of the corrugations and other secondary effects must be accounted for. This is best accomplished by conducting a correct shell analysis of the diaphragm. This, however, was beyond the scope of the present program.

Akasaka and Takagishi show that the natural frequencies increase with increase of edge tensile force, as would be expected. It is also expected that the frequencies would be higher for a pressurized diaphragm.

Flow Losses

No work was done in the current program on the problem of flow losses in bellows because this performance characteristic is not of major importance for bellows in aerospace components. However, for completeness, the following material has been reproduced from the literature*.

ALTHOUGH satisfactory design data are available for turbulent flow in smooth tubes, rough tubes, channels, valves, and elbows, data for turbulent flow through unlined flexible hose and bellows are severely lacking. To fill this void, data from several sources, in addition to the authors experimental data, were correlated to provide a generalized method for predicting the pressure loss of both straight and bent flexible sections.

Generalized Method: Friction factors for straight flexible sections as a function of the flow parameter, Reynolds number, and the relative roughness of the internal diameter are shown in Fig. 1. These friction factors can be used in conjunction with the Darcy-Weisbach pressure-loss equation:

$$\Delta P = \frac{L}{d} \times \frac{V^2}{2g} \times \rho \qquad (1)$$

The hose selected determines the values of the physical dimensions. Using the values of the relative roughness, e/d, and the Reynolds number, $dV\rho/12\mu$, the value of the friction factor f is read from Fig. 1. Direct substitution permits solving for the pressure loss.

Specific data for various flexible hoses can be obtained.[1,2,3] For approximate calculations, typical physical dimensions are given in Table 1 for several nominal diameters.

[1]References are tabulated at end of article.

Nomenclature

- d = Inside diameter of bellows, in.
- e = Average height of convolution, in.
- f = Darcy-Weisbach friction factor
- g = Acceleration of gravity, ft per sec^2
  = 32.2 ft per sec^2
- L = Length of bellows, in.
- S_f = Cross-sectional area of bellows, sq in.
- S_t = Cross sectional flow area of fitting, sq in.
- V = Fluid velocity, ft per sec
- ΔP = Pressure loss, psf
- ρ = Fluid density, lb per cu ft
- μ = Fluid viscosity, lb per ft per sec

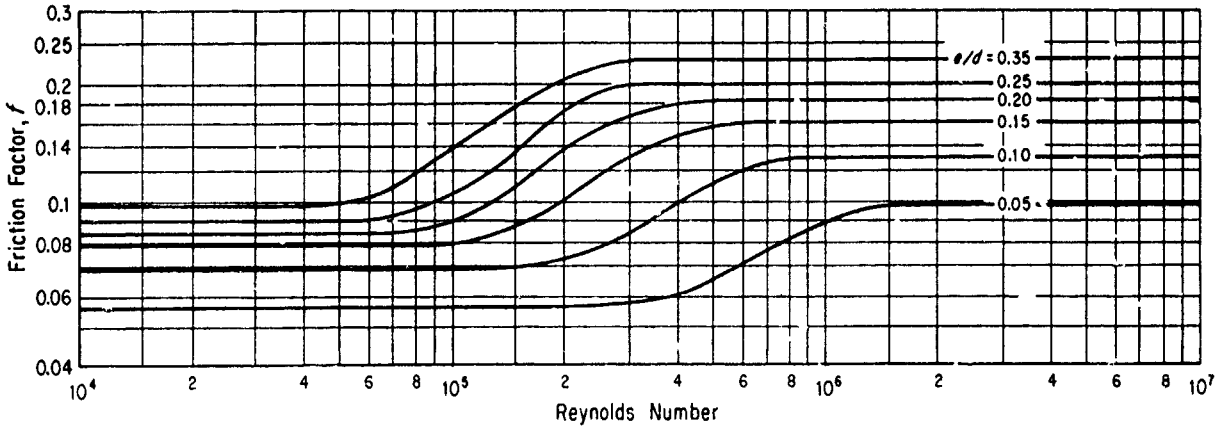

Fig. 1—Friction factors for flexible metal hose as a function of Reynolds number and relative roughness.

*Daniels, C. M., and Cleveland, J. R., "Determining Pressure Drop in Flexible Metal Hose", Adapted from MACHINE DESIGN, November 25, 1965. Copyright 1965 by The Penton Publishing Company, Cleveland, Ohio

Bend Losses: Since the flexible section is used to allow variable misalignment or bends in a tube or duct system, the pressure-loss factors of bent flexible sections are included as a function of bend radius, Fig. 2, and bend angle, Fig. 3.

To obtain the bend loss, first calculate the relative radius, R/d. From Fig. 2, find the total loss for a 90-deg bend as equivalent length, L/d. Obtain the bend-angle correction factor, C, from Fig. 3. To obtain the pressure loss, substitute $C(L/d)$ for L/d in Equation 1. Friction factor f is obtained from Fig. 1.

The same answer can be obtained by adding the inertia loss of the bend from Fig. 2 (corrected for bend angle by data from Fig. 3) to the length of the flexible hose. This latter method may be easier if the entire flexible hose is not used in the bend.

Table 1—Typical Dimensions of Flexible Sections

Nominal Size (in.)	Inside Diameter d(in.)	Outside Diameter (in.)	Wall Thickness (in.)	Height of Convolutions (in.)
3/16	0.188	0.308	0.006	0.034
¼	0.255	0.491	0.010	0.108
⅜	0.390	0.668	0.012	0.127
½	0.520	0.804	0.012	0.130
⅝	0.582	0.861	0.012	0.128
¾	0.750	1.190	0.014	0.206
1	1.000	1.398	0.012	0.187
1¼	1.284	1.850	0.016	0.267
1½	1.500	2.132	0.016	0.300
2	2.000	2.676	0.016	0.322
3	2.962	3.413	0.027	0.424
4	4.000	4.700	0.027	0.323

Connection Losses: Because the inside diameter of the flexible section seldom matches the inside diameter of the connecting tube or duct, expansion and contraction pressure losses are encountered. These follow the established analogies.[4]

$$K_e = \left(\frac{S_f}{S_t} - 1 \right)^2$$

$$K_c = 0.75 \left(1 - \frac{S_t}{S_f} \right)$$

The values of K calculated from these equations can be substituted for $f(L/d)$ in the Darcy-Weisbach equation to obtain pressure loss.

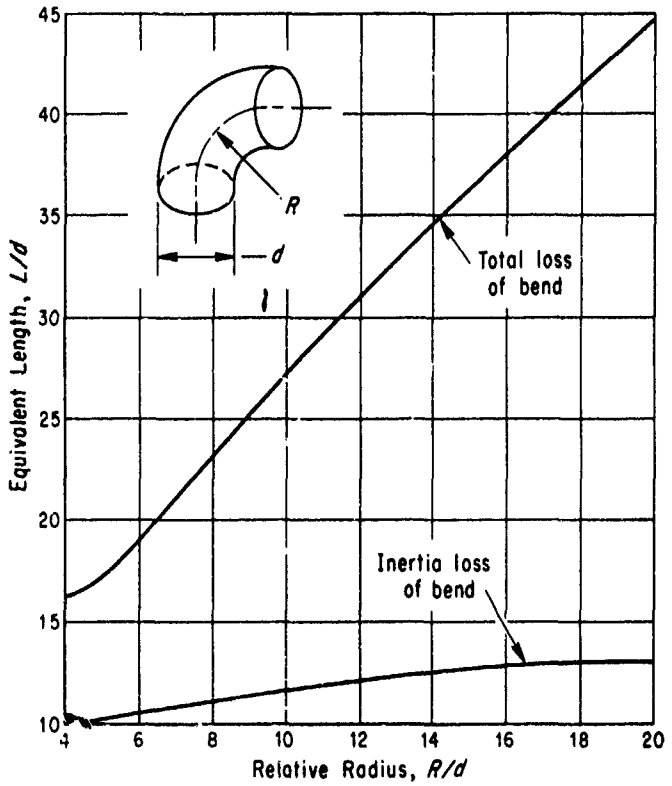

Fig. 2—Bend-loss factor for a 90-deg bend angle as a function of the ratio of elbow bend radius to the flexible hose diameter.

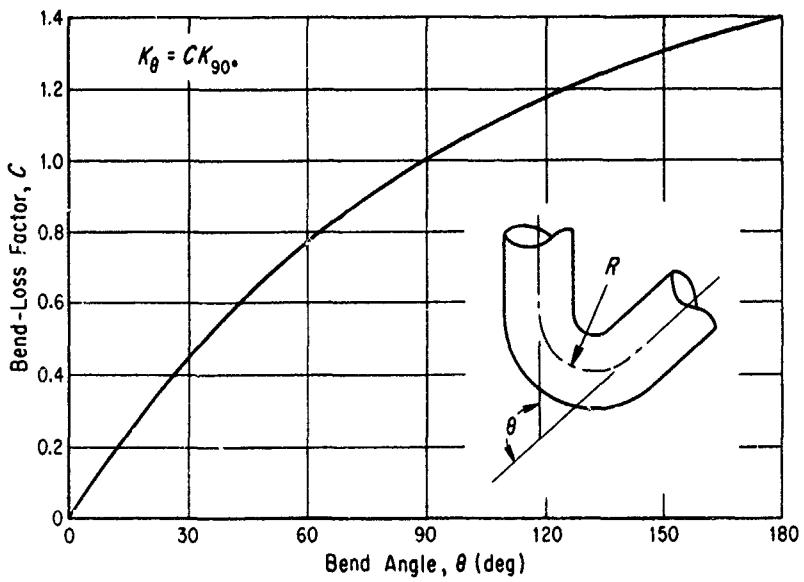

Fig. 3—Bend-loss factor in terms of a 90-deg bend loss.

REFERENCES

1. C. M. Daniels—"Pressure Losses in Flexible Metal Tubing," *Product Engineering*, Vol. 27, No. 4, April, 1956, pp. 223-227.
2. C. M. Daniels and R. E. Fenton—"Determining Pressure Drop in Flexible Metal Hose," MACHINE DESIGN, Oct. 13, 1960, pp. 195-198.
3. R. C. Hawthorne and H. C. Helms—"Flow in Corrugated Hose," *Product Engineering*, Vol. 34, No. 12, June, 1963, pp. 98-100.
4. J. H. Perry—*Chemical Engineers Handbook*, McGraw-Hill Book Co. Inc., New York, 1950, p. 388.

Fatigue of Bellows and Diaphragms

Fatigue failure is one of the most common types of failures in bellows and diaphragms. In normal service, the life of a bellows or diaphragm is determined by the cumulative effect of the deflection and pressure stresses (or strains) to which it is subjected. As summarized in the next section, corrosion can significantly reduce fatigue life. Fatigue life can also be reduced by stress concentration at points of geometrical discontinuity, material variations, residual stresses, and heat-affected material. On occasion, unexpected modes of deformation can cause high stresses which result in premature fatigue failure. Common causes of such overstressing are damage during shipment, improper installation, dynamic resonance, excessive stroke, and excessive pressure.

Until the present program, there has been no method by which the deflection and pressure stresses could be accurately evaluated for bellows and diaphragms. Thus, each manufacturer has been required to develop empirical design data based on fatigue tests of the manufacturer's bellows. With sufficient data, it has been possible to construct nomographs relating different fatigue life cycles to different percentages of maximum deflection and maximum pressure for the types of bellows tested. (Maximum deflection and pressure are those values, with appropriate safety factors, which will cause permanent deformation in the bellows.) Such nomographs are available from a number of bellows manufacturers.

It was demonstrated in the present research study that the computing program NONLIN could be used to accurately predict the elastic strains in bellows or diaphragms of any shape subjected to either axial deflection or internal pressure. One of the major tasks in the study was an investigation of the feasibility of using the theoretically predicted maximum strains in a bellows to predict the fatigue life of the bellows under a given cyclic load. The planned approach involved testing formed bellows, welded bellows, and diaphragms to establish their fatigue limits at different levels of cyclic strain as calculated by the program NONLIN. These experimental results were then to be compared with data obtained from standard fatigue tests made on metal coupons of the same material. If a correlation could be established between the fatigue lives of the bellows and diaphragms at the calculated strain ranges and the fatigue lives of the coupons at the same strain ranges, then the relatively ample coupon fatigue data available in the literature could be used, together with NONLIN, to predict fatigue life of bellows and diaphragms. Appendixes K through N give detailed descriptions of the fatigue tests conducted in the program and the results obtained. These results are summarized briefly here.

Formed Bellows

An investigation was carried out for formed bellows made of Type 321 stainless steel and Inconel 718. The results of this investigation showed that NONLIN could be used together with coupon data to estimate the minimum fatigue life of a formed bellows subject to the following limitations:

(1) The lifetime values estimated from coupon data may be optimistic because of variations of actual bellows from the geometric model on which the computations are based, and because of residual stresses and material variations which the theoretical treatment does not include.

(2) When such factors have been taken into account by a few fatigue tests on bellows formed by a similar process and from similar material, the stress analysis can be used to provide good interpolations and moderate extrapolations for different loadings and moderately different geometries.

Welded Bellows

In contrast to the formed-bellows fatigue tests, no satisfactory correlation could be obtained between the fatigue life and the theoretically predicted maximum strain for welded bellows made of either Type 347 stainless steel or AM-350. As discussed earlier, it was demonstrated that the strains predicted by Program NONLIN were satisfactorily accurate. However, the tests showed considerable variation both in fatigue life and failure location for bellows subjected to the same maximum strain range. This fatigue-life variation was apparently the result of manufacturing variations associated with the welding process (such variations are not accounted for by Program NONLIN). Significant variations in the fatigue life were observed both for bellows made by different manufacturers and for nominally identical bellows made by the same manufacturer.

As a result of the tests, it was concluded that the variability of the fatigue life resulting from manufacturing variations must be experimentally determined for each manufacturer's process. This requires the same type of testing that manufacturers currently perform to establish fatigue nomographs. Thus, although the computer program NONLIN can be used to analyze the stresses and strains in welded bellows and to aid in their design, the fatigue life of welded bellows must still be established experimentally. It must be emphasized that experimental determination of welded-bellows fatigue life must be based on a sufficiently large number of tests.

As discussed in Appendix N, it has been demonstrated that a combination of compression and pressure may reduce the life of welded bellows significantly. This occurs if the slight ballooning caused by the pressure causes the diaphragms of the bellows to interfere during compression, thereby greatly increasing the stresses at other points of the cross section. Although the analytical prediction of this condition would be very difficult, it can be determined experimentally because the diaphragm interference causes a significant change in the spring rate of the bellows. Since each welded bellows should be used as much in compression as possible to obtain the longest fatigue life (see Appendix N) these tests must be conducted to assure that diaphragm interference will not be encountered.

The tilted-edge welded-bellows configuration to be investigated in a follow-on program is expected to experience fatigue failure in the parent material rather than in the weld areas. If this is achieved, the procedure for estimating the fatigue life of formed bellows may be applicable to the tilt-edge configuration.

Diaphragms

Insufficient tests were conducted during the present program to provide the depth of understanding of fatigue-failure modes for diaphragms that was obtained for formed and welded bellows. It is believed that the fatigue characteristics of diaphragms are very similar to those of welded bellows when the maximum cyclic stress occurs in a weld area. When the maximum cyclic stress occurs at one of the convolutions, the failure mode is more like the failure mode of formed bellows. The nonlinear-stress-analysis program can be used as a basis for estimating the fatigue life of diaphragms.

Corrosion of Bellows and Diaphragms

Because of the thin materials of construction, bellows and diaphragms are very susceptible to corrosion-induced failure. To prevent this, three types of precaution must be taken. First, the bellows or diaphragm material must be selected so that little, if any, corrosion will occur under normal operating conditions. Second, the manufacturing procedures must be reviewed in detail to determine that corrosion will not be initiated during fabrication and that the finished item will be completely free of corrosive substances. Third, all system abnormalities must be reviewed for the possible creation or introduction of corrosive agents in the fluid systems.

An understanding of the different types of corrosion and of the applicable corrosion data is required to accomplish these objectives. Appendix O presents information pertinent to the corrosion of bellows and diaphragms in aerospace applications. Because corrosion rates are greatly affected by many factors, i.e., temperature, time, material composition, etc., care should be taken in extrapolating corrosion data. It may be necessary to conduct tests to simulate the expected corrosion conditions.

The prevention of fatigue failure is particularly important for bellows and diaphragms in aerospace applications. Because very few data were available concerning the effect of typical rocket fuels and oxidizers on the fatigue life of typical bellows and diaphragm materials, selected tests were conducted to obtain representative data (see Appendix O). The following guidelines summarize the results of these tests.

N_2O_4

At 200 F, a reduction in the design fatigue life (based on 200 F air data) should be made for most of the common alloys. A reduction of at least 50 percent is suggested for aluminum-base alloys and 60 percent for the austenitic stainless steels. Thus, if the air data suggest a 10,000-cycle life, a reduction of 60 percent to 4000 cycles should be applied to the 300-series stainless steels. A 60 percent reduction is also recommended for the martensitic or other high-strength steels, until such time as additional data are available.

Laboratory data suggest that titanium and its alloys have excellent resistance to impact-fatigue-type loading in N_2O_4 at 90 F [11] At 200 F, however, some reduction in design fatigue life is indicated particularly for the red grade of N_2O_4. No reductions may be necessary for the green grade of N_2O_4. This is based on the fact that at temperatures above, say, 100 F, titanium alloys have been found to stress-corrosion crack in red N_2O_4 but not in green N_2O_4.

The fatigue life of most metals would probably be reduced less as the temperature of the environment is lowered. However, since no data are available at this time, the same reduction in cycle life should be applied at room temperature as at 200 F. Above 200 F, a greater reduction in cycle life should be applied.

Hydrazine Fuels

At 200 F, no detrimental behavior was found for 6061-T6 aluminum alloy or Type 347 stainless steel in the UDMH-hydrazine mix. No correction for corrosion fatigue should, therefore, be required for other aluminum-base or stainless steel alloys in any hydrazine-type fuel. All corrosion data available to date indicate that hydrazine, UDMH, A-50, and monomethylhydrazine behave similarly for aluminum and stainless steels.

It is pointed out, however, that specification hydrazine can contain as much as 2.5 percent water. High water content would be expected to promote corrosion and thus could adversely affect fatigue life. In this case a particularly weak area might be at the juncture of the bellows and end fixtures, where galvanic effects from dissimilar metal contacts could lead to premature failures.

No recommendations can be made at this time about the fatigue behavior of other alloys in hydrazines because of the inherent danger of catalyzed decomposition of the fuel and the possible increased rate of corrosion.

ClF_3

In ClF_3, aluminum-base and nickel-base alloys (provided they have adequate general corrosion resistance) should provide a fatigue life equivalent to their respective air data. Thus, no correction for corrosion fatigue may be required up to 200 F.

Copper and many of its alloys show an equally high order of resistance to ClF_3 compared with the nickel-base alloys. It is believed that no corrosion fatigue will result in ClF_3 up to 200 F.

A correction for corrosion fatigue should be made for all stainless steels. A reduction by up to 60 percent of the air fatigue life is suggested as a reasonable value.

Titanium and titanium alloys are rapidly attacked by ClF_3 and should not be considered for such service.

Other Fluorine-Base Oxidizers

The behavior of aluminum-base and nickel-base alloys in other fluorine-base oxidizers such as fluorine, FLOX, NF_3, and N_2F_4, would be expected to be similar to that in ClF_3. Thus, no correction for corrosion-fatigue behavior is believed necessary up to 200 F.

In fluorine-type propellants, copper-base alloys would be expected to behave similarly to the nickel-base alloys, and should perform with little or no reduction in fatigue properties up to 200 F.

As with ClF_3, a reduction by 60 percent of the air-fatigue-life value is recommended for the stainless steels in other fluorine-base oxidizers.

It appears that corrosion-fatigue data on fluorine-base propellants should not be extrapolated at this time to other than the materials discussed above.

Consideration should also be given to the limited protection to physical damage afforded by the thin walls of bellows and diaphragms. In fluorine-base oxidizers this problem is especially serious because the protective fluoride film can be easily damaged by abrasion or by the mechanical motion of the bellows. Breakdown of the film in localized areas could lead to reduction in fatigue life. Thus abrasion vibration, impingement, high flow rates, etc., should be avoided.

Characteristics Important to Instrumentation Applications

Ideally, bellows and diaphragms would deflect exactly the same amount when an equal increment of force or pressure load was added or subtracted. Linearity of response can be prevented by geometrical aspects of the bellows and diaphragms. However, even when there is geometrical linearity and when the material remains well within the elastic limit, small departures from linearity can occur which are important to precision instruments. The term "anelasticity" has been used to denote the nonelastic behavior of solid materials in the low stress range. Included in this term are such effects as hysteresis, drift, aftereffect, recovery, and zero shift. Changes in temperature can affect response because of thermal expansion of the material and because of changes in the elastic modulus of the material. In addition, edge attachments, particularly of diaphragms, have been shown to affect linearity of response.

Anelastic Effects

Hysteresis is the difference between the deflections of a bellows or diaphragm at a given load for increasing and decreasing loads. Drift is the increase of deflection with time under a constant load. Aftereffect is the deflection remaining immediately after removal of the load, i.e., hysteresis at no load. Recovery is the decrease of aftereffect with time under no load. Zero shift is the permanent deformation, i.e., the difference in position before loading and sufficiently long after unloading for recovery to occur.

Since these anelastic effects stem from nonelastic behavior of the bellows or diaphragm material, the effects are not generally predictable from elastic analysis and there is, at present, no basic theory covering such behavior. However, there are some guidelines for design:

(1) Anelastic behavior generally causes larger errors at higher stresses. Hence, bellows or diaphragms designed to operate at a low peak stress are desirable for precision instruments.

(2) The various effects are interrelated, although details of the interrelation may be only approximately known. Thus, a bellows with a small drift under maximum load would be expected to have a small hysteresis (at half-load) and a small aftereffect.

(3) Relatively simple tests (such as measurement of drift) may be helpful in quality control to produce units of low hysteresis. However, some precautions must be used in the time schedules for anelastic determinations.

Some work, much of which is unpublished, has been done on the anelastic "errors" in certain types of corrugated diaphragms. Little corresponding work seems to have been done on bellows, probably because these are less frequently used in precision instruments in such a way that their anelastic behavior is critical.

A detailed study of anelastic effects in bellows and diaphragms was beyond the scope of this investigation. Such a study would, in fact, require special instrumentation and experimental techniques. Some measurements of hysteresis were made for large deflection cycles for formed bellows made of Type 321 stainless steel and Inconel 718. Values for the Type 321 bellows, with a cycle time of approximately 1 hour, are shown in Table 11. These values are reproduced only to indicate types of hysteresis which can occur in one- and two-ply stainless steel formed bellows at relatively high pressures and strain levels. (The deflections corresponded to those used in the fatigue tests.) The Inconel 718 bellows tested averaged about one-fourth the hysteresis exhibited by the stainless steel bellows.

Temperature Effects

Consider a bellows (or diaphragm) subject to a high internal pressure of a gas, with (for simplicity) essentially zero external pressure and negligible deflection constraint. If the temperature is now increased, the bellows deflection will change because of several factors: (1) an increase in gas pressure, (2) a thermal expansion of the bellows material, and (3) a change (usually a decrease) in elastic modulus of the bellows material. In a particular situation, these factors may counterbalance each other. In some aneroid capsules, a small internal pressure may be intentionally left to counterbalance (at one condition of temperature and loading, the effects of thermal expansion and thermoelasticity of the diaphragm material.

Thermal stresses in a bellows or diaphragm caused by a temperature change in the material can arise in two ways, depending on whether the bellows or diaphragm undergoes a uniform or a nonuniform temperature change. If the bellows or diaphragm undergoes a uniform temperature change, then thermal stresses will be induced in the bellows or diaphragm unless it is completely free to expand or contract. This type of thermal stress is easily calculated by calculating the amount of thermal expansion or contraction that would occur if the edges were free, and then using NONLIN to calculate the stresses in the bellows or diaphragm when the deflections (of opposite sign) are applied to the edges.

When the bellows or diaphragm undergoes a nonuniform temperature change, thermal stresses can occur even if the edges are completely free. These thermal stresses can be calculated in the same way that pressure stresses are calculated if provision is made for the temperature effects in the computer program. Although computing Program MOLSA provides for the calculation of temperature effects, the current version of NONLIN does not have this capability since calculation of thermal effects was beyond the scope of the present project.

TABLE 11. HYSTERESIS EFFECTS AT ZERO DEFLECTION FOR STAINLESS STEEL FORMED BELLOWS

	Local Strain Range[a], microinch/inch	Differences in Loading, lb, at Zero Deflection and Indicated Internal Pressure					
		0 Psi	8 Psi	16 Psi	25 Psi	33 Psi	50 Psi
3-Inch, One-Ply Bellows	3480	1.5	--	--	0	--	--
	5773	4.5	--	--	4	--	--
3-Inch, Two-Ply Bellows	4075	7	7.5	7	7	--	--
	6737	23	22.5	22	35	--	--
1-Inch, One-Ply Bellows	3389	0.5	--	--	--	--	0.5
	5931	1.5	--	--	--	--	1.75
1-Inch, Two-Ply Bellows	3050	0.5	--	0.25	--	0.75	0.75
	5084	1.5	--	2.0	--	1.7	1.5

(a) Maximum strain range at convolution root calculated from elastic theory.

MATERIALS FOR BELLOWS AND DIAPHRAGMS

The extent to which the service performance of bellows and diaphragms fulfills design predictions is strongly dependent upon the quality of the materials from which they are fabricated and the care taken in their manufacture. Material defects, weld discontinuities, forming irregularities, and postfabrication damage can all result in locally high stresses that may lead to premature failure.

Materials for formed bellows must be both weldable and formable. Although smaller bellows are usually made from seamless tubing, most bellows over an inch in diameter are made from sheet or strip formed into a cylinder and longitudinally seam welded. Welding is also the preferred method of end-fitting attachment. Most formed aerospace bellows today are made from one of the 300-series stainless steels. Inconel 718 is being used increasingly because of its higher yield strength and its relative immunity to stress corrosion. Titanium alloys are becoming candidate materials for formed aerospace bellows because of their corrosion resistance and their good strength-to-weight ratios.

Materials for welded bellows need not have the formability of materials for formed bellows. Therefore, in addition to the materials used for formed bellows, a variety of less formable alloys are used for welded bellows. It is difficult to rank the welded-bellows alloys in order of decreasing usage because so many different alloys are used to make welded bellows and no industry-wide figures are available. The 300-series stainless steels, Inconel 718, and AM-350 are among the most-used welded-bellows materials, however.

Materials for deposited bellows are made in situ by electroplating or chemical deposition onto machined aluminum mandrels that are later chemically dissolved. The most common material for electrodeposited bellows is nickel. Copper is also used. Chemically deposited bellows can be made from alloys which, though still over 90 percent nickel, contain significant percentages of other strengthening elements. Both types of deposited bellows can be made with composite metal walls consisting of layers of different metals. The deposited-bellows industry is relatively young, and further developments in deposited-bellows materials can be expected.

Whether the strip of sheet used in bellows manufacture is purchased to any special tolerances depends upon the end application of the bellows. When the spring rate is not critical – bellows intended for expansion joints, for example – the customary 10 percent mill-thickness tolerance is satisfactory. When the deflection characteristics must be more carefully controlled, materials may be selected from warehouse stock. In this way, thickness may be controlled to within about 5 percent on a given order. Rerolled materials from specialty metal fabricators provide the best commercially obtainable thickness tolerances, but are seldom used for making formed bellows. Manufacturers of welded bellows and diaphragms using rerolled materials claim thickness tolerances of ±0.0001 inch. A more commonly quoted tolerance is ±0.00025 inch over a 20-inch-strip width.

Opinions differ among manufacturers as to the desirability of a bright surface finish on the starting material. Some manufacturers claim an improvement in the fatigue life of bellows produced from bright-finished material (No. 2B finish), while others see

no difference. Some manufacturers also claim that the bright-finished material, containing more cold work than the dull or matte-finished material (No. 2D finish), is more difficult to form. There is a trend toward the use of bright-finished material.

Although there is some disagreement most manufacturers see no effect of "grain", or preferred orientation, in their starting material. The common materials from which formed bellows are fabricated, when produced under good control, are nearly isotropic, so preferred orientation does not appear to be a serious problem.

All manufacturers of bellows and diaphragms use relatively small tonnages of material. Consequently, they are able to purchase only materials melted according to usual commercial practice. Stainless steels, for example, are electric-furnace melted. Although the metallurgical quality of stainless steels is good by ordinary standards, some improvement of bellows uniformity might be achieved by the use of vacuum-melted materials with their lower inclusion contents. Such materials have become standard in bearings. Other alloys, such as Inconel 718, are sensitive to compositional variations. A commercial heat of Inconel 718 balanced for maximum high-temperature rupture strength will not have the maximum obtainable fatigue strength. The bellows manufacturer buying a relatively small quantity of sheet often has little control over the chemistry of the material. Quantity purchase of heats of specially controlled materials by large users of bellows, and release of these materials to bellows manufacturers might be a method of significantly improving the uniformity and quality of bellows throughout the industry.

To discuss materials logically, it is necessary to group them in a number of classifications. The properties of the materials grouped together in the following discussion are not identical, but they are similar enough so that they can be discussed in general terms. The metallic materials which are used in bellows and diaphragms are listed in Table 12 and the alloy groups are discussed in the following sections.

Copper Alloys

The copper alloys of interest to the designer are those with moderate-to-high strength. These include the beryllium coppers, certain bronzes, and other alloys with strengths above 50,000 psi. Yield strengths of 150,000 psi are readily obtained in beryllium copper by heat treatment. The proportional limit is fairly high for the higher strength alloys. Lower strength alloys have very low or no proportional limit. The toughness of the copper-base materials depends on the strength level. At low to intermediate strengths, the toughness is fairly high; at high strengths, toughness is not outstanding. These materials do not undergo a ductile-to-brittle transition on cooling. The creep strength of the copper-base alloys is only moderate.

Copper-base alloys have fairly high densities and, consequently, only moderate strength-to-density ratios. The copper-base alloys have moderate moduli of elasticity (15×10^6 to 20×10^6 psi). They have rather high coefficients of thermal expansion and moderate thermal conductivities.

Although many copper-base-alloy bellows and diaphragms are used in industrial and consumer products, their use in aerospace applications is limited by the severe aerospace corrosion, temperature, and stress environments and the availability of alloys with higher elastic moduli.

TABLE 12. TYPICAL BELLOWS AND DIAPHRAGM ALLOYS

Material	Type of Bellows			Outstanding Characteristics
	Formed	Welded	Deposited	
Copper Alloys				
Brass, Bronze, Beryllium Copper, Zirconium Copper	X		X	High proportional limit, good toughness
Aluminum Alloys				High strength-weight ratios, good toughness at low and intermediate stress levels at temperatures as low as -425 F
5083, 6061, 7075	X			
Nickel and Cupro-nickel Alloys				
Nickel 200, Monels 400, 404, K-500	X		X	Good corrosion resistance; low magnetic permeability
Titanium Alloys				High strength, high strength-weight ratio, good creep strength to 500 to 700 F
Ti-75A, Ti-6Al-4V	X			
Low-Alloy Steels				Extremely high strength, high proportional limit, high fatigue strength, good creep resistance
4130	X			
Standard Austenitic Stainless Steels				
304, 304L, 310, 316, 321, 347	X	X		Excellent toughness to -423 F, good fatigue and creep strength, good neutron-radiation resistance; good corrosion and oxidation resistance
Precipitation-Hardening Stainless Steels				
17-4 PH, 17-7 PH, PH 15-7 Mo, AM350	X	X		High strength, good creep strength, high fatigue strength
Other Iron-Base Alloys				
19-9 DL, A-286, Kovar	X	X		Ditto, plus sealability to hard glass (Kovar)
Nickel-Base Alloys - Group I				
Inconels 600, 625, X-750, and 718; Incoloy 825; Hastelloy C	X	X		Good high-temperature strength, good fatigue strength, good toughness, good creep resistance, and good strength-to-rupture
Nickel-Base Alloys - Group II				
M 252; Waspaloy; Udimet 700; René 41; René 62		X		Ditto
Cobalt-Base Alloys				
L 605		X		"
Refractory Metals				
Columbium		X		Good strength at extreme temperature, high proportional limit, excellent fatigue strength above transition temperature, excellent creep strength
Other Alloys				
Invar, (Ni-Span-C)		X		Zero thermal-expansion coefficient or constant elastic modulus

Aluminum and Magnesium Alloys

These materials are readily available in sheet form. From a mechanical- and physical-property standpoint, aluminum and magnesium are somewhat different. These alloys generally have low strengths. The maximum ultimate strength that can be obtained is of the order of 75,000 psi. The proportional limit of aluminum and magnesium alloys is poorly defined – the stress-strain relationships tend to be curves in the nominal elastic range. This indicates that a hysteresis problem may exist on repeated loadings.

These materials have fair fatigue strengths. However, aluminum alloys do not have true fatigue limits. In general, the longer the fatigue exposure, the lower the strength at which failure occurs. Aluminum alloys have good toughness at low-to-intermediate strength levels. The toughness is not so good at high strength levels. However, these alloys do not undergo a property transition during cooling below room temperature. In particular, the fracture properties do not change much at temperatures as low as -425 F.

Magnesium alloys do not have good fracture properties. They tend to exhibit brittle behavior in the presence of notches at practically all temperatures. Aluminum and magnesium alloys are not designed for use where creep is of importance; although they have reasonably good properties at room temperature, at slightly elevated temperatures (300 to 500 F), the creep strength drops off rapidly.

Both aluminum and magnesium alloys having low densities and moderate strengths are available. This combination means that fairly high strength-to-density ratios are available. Magnesium has the lowest density of commercial structural materials. Both materials have low moduli of elasticity. Aluminum alloys have high coefficients of thermal expansion and high thermal conductivities.

Nickel and Cupro-Nickel Alloys

The Monel alloys, which range from approximately 45Ni-55Cu to 85Ni-15Cu, are available as thin sheet. Yield and ultimate strengths are moderate, but their elastic moduli are higher than those of copper or aluminum alloys, around 25×10^6 psi. The Monels do not become brittle at low temperatures, and thus Monel alloys are frequently used for bellows intended for cryogenic service. Monels are often substituted for the stainless steels in steam piping systems where stress corrosion is encountered. Service temperatures are limited to the 400 to 500 F range by the relaxation properties of these alloys, though the alloys retain good oxidation resistance to 1000 F. Thermal-expansion coefficients and thermal conductivities are about average.

Some nickel formed bellows are used in chemical equipment, but nickel is used principally in deposited bellows. Well-established techniques are available for electrodeposition and chemical deposition of nickel. Small amounts of other elements can be codeposited with nickel to form alloys with improved strength properties. Although nickel is ferromagnetic at room temperature, most of the cupro-nickels are nonmagnetic down to liquid-nitrogen temperatures and below.

Titanium Alloys

The common titanium alloys are available in sheet and foil thicknesses. Various high-strength titanium alloys are available. Ultimate strengths of the order of 200,000 psi can be obtained with special heat treatments. The materials have moderately high proportional limits. Titanium alloys have good fatigue strengths, and toughness is good at room-temperature levels in materials with yield strengths of 100,000 psi or lower. At higher strength levels, the toughness is much lower unless care is taken to produce alloys with low interstitial (e.g., carbon, oxygen, nitrogen, and hydrogen) -alloy content. The titanium alloys have high creep strengths at intermediate temperatures (500 to 700 F).

Titanium alloys have densities about 60 percent that of steel. This, coupled with the possible high strength, leads to fairly high strength-to-density ratios. However, these high levels are usually obtained at a sacrifice in toughness. The modulus of elasticity of titanium alloys is about 15×10^6 psi, which is lower than that of most high-strength alloys. Titanium alloys have rather low coefficients of thermal expansion, as well as low thermal conductivities.

Aerospace bellows have been formed from titanium alloys, and some bellows manufacturers expect titanium bellows to displace a significant fraction of the nickel-base-alloy and stainless steel bellows presently popular.

Stainless Steels

Many varieties of stainless steels are commercially available. All stainless steels can be characterized as containing chromium in amounts of 12 percent or more. They will be discussed here in three classifications. Steels in the first classification contain fairly large amounts of nickel and up to about 20 percent chromium. The high nickel content causes these steels to have an austenitic structure. These steels are designated by AISI as the 300 Series.

Stainless steels in the second group contain almost no nickel. This group may contain up to 27 percent chromium and may be either ferritic or martensitic, depending on composition. These steels are classed as the 400 Series. In the third group are steels which have been modified through alloying and heat treating to produce high strengths. These are generally referred to as precipitation-hardening stainless steels.

Standard 300-Series Stainless Steels

In general, availability of these steels in thin sheet is excellent. Since the 300-Series stainless steels have been produced in relatively large tonnages for a number of years, and because they are nonheat-treatable alloys, they tend to have more uniform properties than many of the other candidate aerospace bellows and diaphragm materials. They have moderate strengths, but the strengths can be increased considerably by cold working. Heating during fabrication removes the strengthening effect of cold work. These materials are similar to aluminum alloys in that they do not have a proportional limit. This may lead to hysteresis effects under repeated stress cycles. The

300-Series stainless steels have excellent toughness down to -425 F. Because they do not have austenitic structures, they do not undergo a ductile-to-brittle fracture transition. These steels have good fatigue resistance and good creep strength at moderate temperatures and are used in steam power plants at temperatures as high as 1250 F.

The 300-Series steels have high density and a modulus of elasticity of about 30 x 10^6 psi. Because of their normally low strengths, they have low strength-to-density ratios. They have high coefficients of thermal expansion and the lowest thermal conductivity of all the steels. They have good neutron-radiation-damage resistance and, in the annealed condition, have quite low magnetic susceptibility.

The stabilized (Types 321 and 347) and low-carbon (Type 304L) stainless steels are widely used as bellows materials.

400-Series Stainless Steels

These steels are readily available in sheet form, and have been produced in heavy-foil thicknesses. They are not widely used as bellows materials, however. High strengths (up to 200,000 psi ultimate tensile strength) can be obtained in some by heat treatment. They have high proportional limits and fair fatigue properties. Since the 400-Series stainless steels are ferritic stainless steels, they undergo ductile-to-brittle fracture transitions as the temperature decreases. Since they have relatively poor toughness at room temperature, particularly at high strength levels, they may have very poor toughness at temperatures just slightly below room temperature. They have good creep strengths and are used as elevated-temperature structural materials. An outstanding attribute of the 400-Series stainless steel is their oxidation resistance.

The 400-Series stainless steels have high density and about the same modulus of elasticity as other steels. They have moderate coefficients of expansion and moderate thermal conductivities.

Precipitation-Hardening Stainless Steels

The availability of a number of these steels in thin sheet is excellent, since they have been used in structural sandwich materials for several years. Some welded bellows are made of precipitation-hardening stainless steels.

There are a number of subclassifications in this general classification. Two are considered here. One of these has an austenitic structure after the precipitation-hardening treatment (A-286 is typical of this class). The other class consists of those steels whose structures contain martensite plus ferrite or austenite after heat treatment. Such steels as 17-7 PH, AM-350, and PH 17-4 Mo are typical of the martensitic age-hardened stainless steels.

All of these materials have high strengths. Yield strengths of over 200,000 psi are obtained in commercial sheet. Fatigue strength is fairly high in terms of pounds per square inch, but is not so high expressed as a percentage of tensile strength. Unfortunately, the same thing can be said about most high-strength materials. The martensitic materials have fair toughness at room temperature and this persists down to about

-100 F, below which these materials have poor toughness. As strength increases, the toughness decreases. The austenitic steels have about the same room-temperature toughness as the martensitic steels, but the toughness persists to a much lower temperature. The martensitic alloys generally have good creep strengths at temperatures up to about 800 F, at which point a rapid drop in strength occurs. The austenitic materials have somewhat lower creep strengths at low-to-intermediate temperatures, but do not experience such a rapid drop in strength in the higher temperature range.

All of the precipitation-hardening stainless steels have high density and the modulus of elasticity is about the same as that of other steels (30×10^6 psi). The martensitic steels have moderate coefficients of thermal expansion and low thermal conductivities. The austenitic steels have low coefficients of thermal expansion and low thermal conductivities.

Low-Alloy Steels

The low-alloy steels contain chromium, but not enough to be classed as stainless steels. They are available in sheets down to the order of 0.050 inch thick. Some formed bellows for expansion joints have been made from this class of alloy. They attain their strengths through quench-and-temper heat treatment and some can be heat treated to very high strengths. Ultimate strengths of 300,000 psi have been obtained. These steels generally have high ratios of yield strength to ultimate strength. Their proportional limit is high. They have good fatigue strength in absolute terms, but it is only fair in terms of percentage of yield strength. Their toughness is fairly good at room temperatures at yield strengths below about 180,000 psi, but toughness decreases rapidly as the yield strength increases above this level. At the lower strength level, the toughness transition is likely to occur at temperatures only slightly below room temperature. Steels in this group generally have good creep resistance to temperatures of about 1000 F.

Although these steels have fairly high density, high yield-to-density ratios can be obtained because of the high strengths that are available. Their modulus of elasticity is the same as that of other steels. They have moderate coefficients of thermal expansion and moderate thermal conductivities.

Other Iron-Base Alloys

This group of heat-resistant alloys is identified separately in Table 12 because of composition. Their properties are similar to those of the nickel- and cobalt-base alloys discussed below.

Nickel- and Cobalt-Base Alloys

This class of materials has been produced in sheet, for use in gas-turbine engines, for several years. The availability in relatively thin sheet is good. Most nickel- and cobalt-base alloys are designed to have good strength at elevated temperatures. They

have moderate strength at room temperature, but retain this strength at very high temperatures. The less formable alloys that can be used only for welded bellows and diaphragms are listed separately in Table 12. These alloys, identified as Group II, can be used at somewhat higher temperatures than can the alloys under Group I. The nickel and cobalt alloys have moderately high proportional limits, good fatigue properties, and generally good toughness at low temperatures. Since they are designed primarily to be used as high-temperature alloys, they have good creep and rupture properties at high temperatures.

These alloys have fairly high densities and low strength-to-density ratios at room temperature. However, their strength-to-density ratios remain almost constant over a wide temperature range. The nickel-base alloys have moduli of elasticity of about 30 x 10^6 psi; the cobalt-base alloys have moduli of 36 x 10^6 psi. Both alloys have moderate coefficients of thermal expansion and moderate conductivities.

A number of nickel-base and cobalt-base heat-resistant alloys are used to make bellows, as shown in Table 12.

Refractory Metals

In this discussion, refractory metals include tungsten, molybdenum, tantalum, columbium, and their alloys. The availability of these materials is fairly good in thin sheet. However, the cost may be extremely high and availability is marginal if foil gages are needed. The refractory metals and their alloys have moderate strengths at room temperature. However, their strengths at high temperatures are excellent. They have the highest strengths of all metals above a temperature range of 1800 to 2000 F, and, in fact, are about the only usable metals above this temperature range. These materials oxidize rapidly above about 1200 F. At this temperature and higher, oxidation can become catastrophic and can lead to failure in extremely short periods of time. The refractory metals have high proportional limits. Their fatigue strengths are excellent when tested above the tough-to-brittle transition temperatures and fair even below the transition temperatures. The transition temperatures of the refractory metals vary over a wide range. Tungsten and molybdenum have toughness transition temperatures at about 800 F and 400 F, respectively. On the other hand, tantalum and columbium have good toughness down to -425 F. The creep strengths of these alloys are excellent at high temperatures. They have very high densities, which means that the strength-to-density ratios are low. However, if metallic materials are needed for service above 2000 F, there are no other choices but the refractory metals, and protective coatings are necessary for service in air at these temperatures. In general, these metals have low coefficients of thermal expansion and fairly high thermal conductivities.

Experience in fabricating bellows from the refractory metals is very limited, but some alloys are sufficiently formable and weldable for use in bellows.

Other Alloys

There are two types of nickel-base alloys which are not designed for high strength but are used for instrument diaphragms or bellows. Invar alloys are a group of special nickel alloys which are designed to have a nearly zero coefficient of thermal expansion over about a 150 F temperature range near room temperature. Ni-Span-C is a special nickel alloy which is designed to have a nearly constant elastic modulus and a low thermal-expansion coefficient over a fairly wide temperature range. It is used when it is important that the effects of temperature on stresses and deflections be minimized.

MANUFACTURING CONSIDERATIONS

The manufacturing processes for formed, welded, and deposited bellows are discussed in the following sections. Diaphragm manufacture is considered under welded bellows, since diaphragms are made by similar methods. Considerations common to all bellows and diaphragm manufacture are given separately.

Formed Bellows

The formed-bellows manufacturing process, shown in Figure 2, begins with the fabrication of a thin metal cylinder. For small bellows, the metal cylinder is usually a seamless tube. For bellows having diameters greater than 1 inch, the cylinder is fabricated from flat sheet or strip having a high-quality surface and containing no visible damage to the edges. After the sheet has been cut to size by a shearing operation, it is roll-formed to a cylindrical shape. Typically, the cylinder is somewhat overformed in order to assure that the edges will meet satisfactorily.

Longitudinal Seam Welding

The formed cylinder is then placed in a welding fixture consisting of a rigid backup and hold-down clamps, and a butt weld of the gas-tungsten-arc type (GTA; also known as TIG) is made along the mated edges of the sheet. The technology of making such welds is well advanced, and manufacturers are capable of making welds in material as thin as 0.003 inch. Most welds are longitudinal, but one manufacturer uses a helical weld for small bellows.

Depending on the cylinder-wall thickness and material, it may be necessary to add metal while making the weld. Metal addition is usually required for welds in sheets over about 0.01 inch thick to maintain a weld bead thicker than the base metal. If welding rod or wire of suitable composition is available for the material comprising the bellows, it can be fed into the arc as the weld is made. This procedure is known as cold-wire addition. Metal to form the weld bead can also be obtained by the melting during welding of a flange that has previously been bent up along the edge of the metal. Cold-wire addition gives better dimensional control of the resulting cylinder, but flange burndown is less likely to introduce contaminants into the weld. When conditions permit, a square-butt joint is made without any metal addition. Some bellows manufacturers are able to make seam welds in stainless steels without additions, but must make additions to welds in other alloys of the same thickness. In the formed bellows made of Type 321 stainless steel and Inconel 718 that were tested during the program, there was no noticeable tendency for fatigue failure to occur in the longitudinal butt welds, attesting to the reliability of this operation.

Before the GTA-welding-process technology had been developed sufficiently to make welds in very thin material, longitudinal weld seams were made using a resistance-lap seam-welded joint. Although some bellows are still made with this type of joint, the overlapped region is a stress raiser and may present cleaning problems.

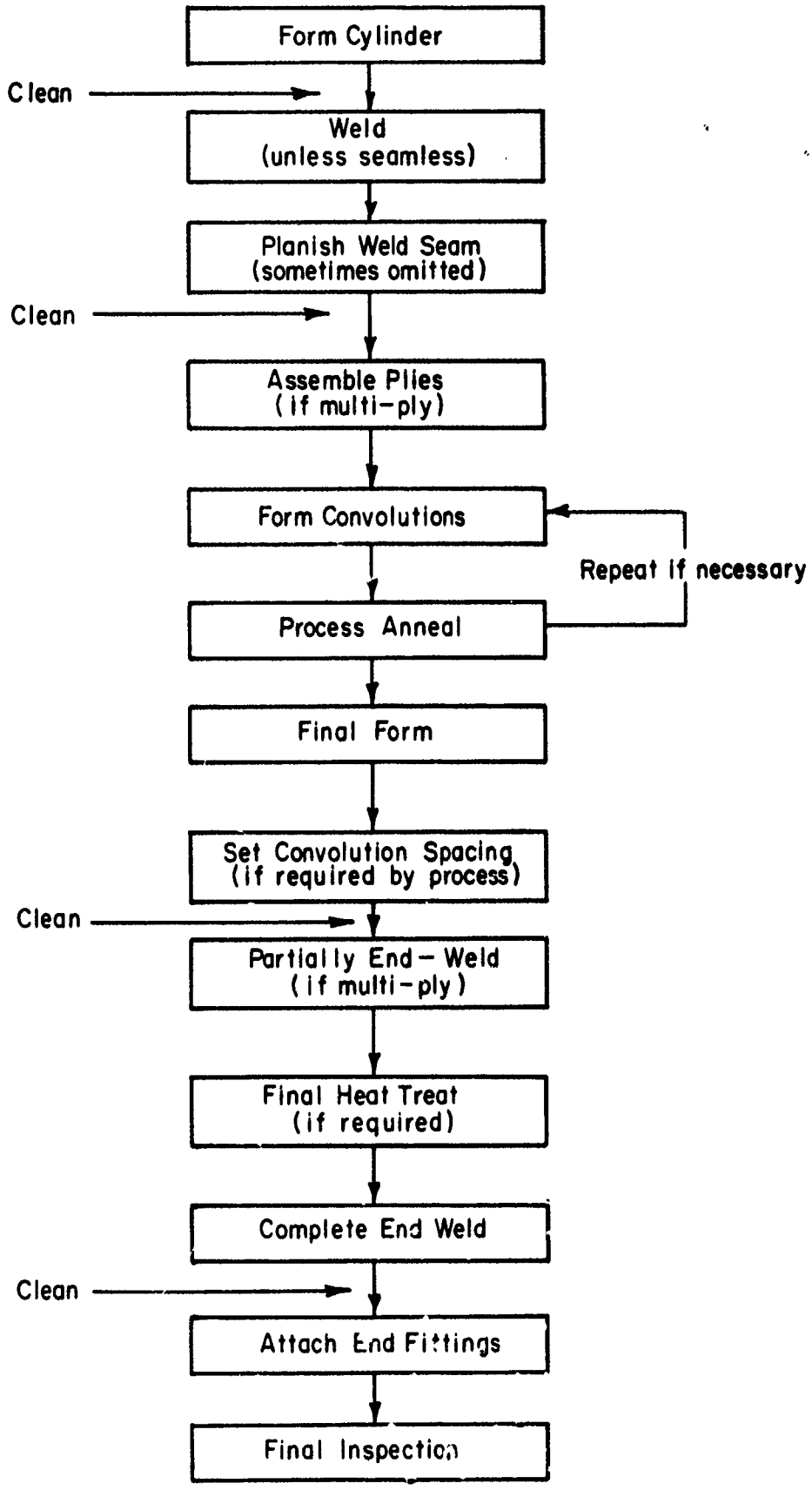

FIGURE 2. MANUFACTURING FLOW SHEET FOR FORMED BELLOWS

Planishing

Many manufacturers cold work the weld zone with a pair of crowned opposed rolls in a planishing operation. Planishing must be carefully controlled in order that the wall thickness in the vicinity of the weld zone is not reduced below the base-metal wall thickness. Total reduction of the weld bead by planishing should be limited to about 5 percent. Some manufacturers do not use planishing because of the danger of wall thinning, while others use it only for certain materials. Planishing cannot be used in those materials where the cold working might induce fusion-zone cracking.

Multi-Ply Bellows

In the fabrication of multi-ply bellows, a series of tubes, sized to fit closely one inside another, are cleaned and assembled ready for the forming operation. The cleaning at this stage is particularly important since it is exceedingly difficult, if not impossible, to remove contaminating materials that have been trapped between the plies once the convolutions have been formed. Best practice is to LOX clean the individual plies prior to assembly. This will insure that contaminants are not trapped between plies.

Forming

Almost every manufacturer uses a unique forming machine of proprietary design. Although these machines fall into several basic categories, there are differences in detail which may significantly affect the performance of the fabricated bellows. The basic categories of forming machines are as follows:

(1) Hydraulic, simultaneously formed convolutions
(2) Hydraulic, individually formed convolutions
(3) Hydrostatic, rubber pressure medium
(4) Mechanical rolls
(5) Mechanical expansion tools.

In the hydraulic process with simultaneous-convolution formation the ends of the tube are first closed by movable platens. The end sections of the bellows are constrained in cylindrical dies that may be part of the platens. A series of split rings, one less than the number of convolutions desired, is carefully spaced along the length of the tube. Hydraulic pressure is then applied to the interior of the tube, causing the tube to bulge outward between the split rings.

From this point, the processes of the various manufacturers differ. Some manufacturers leave the rings in place throughout the entire convolution-formation operation. Some manufacturers attach the rings to a pantograph during forming to maintain uniformity. Others remove the rings completely at this point and complete the convolution formation with the tube entirely free of restrictions except at the ends. This latter method is claimed to be advantageous, since it requires a minimum of contact of the tube with metallic tooling. During the formation of the convolutions, the platens must be moved together to accommodate the shortening of the tube. Some manufacturers accomplish the movement of the platens and the regulation of the hydraulic pressure by hand, while others have applied automatic controls to the process. Automatic controls are desirable from the standpoint of product uniformity.

It may be necessary to form the convolutions in several stages, depending upon the material and upon the depth of convolution desired relative to the tube diameter and wall thickness. Some manufacturers process-anneal their tubes following the initial bulging operation. Others find it necessary to stop several times during convolution formation, remove the split dies, clean, process-anneal, and reassemble the tube in the forming machine. Still other manufacturers restrict their product line to convolution depths that can be formed in their materials using a single operation, thus eliminating process-annealing. Manufacturers' processes also appear to differ widely in the amount of forming that can be accomplished between anneals.

Some manufacturers form each convolution individually, using essentially the same process as described above but with the hydraulic fluid confined to that region of the tube where the convolution is to be formed. The tube is first bulged. Then the external clamp holding the unformed portion of the tube is moved forward a preset distance to form a convolution. The operation is repeated after the tube is indexed to the next convolution position. It is claimed that this forming method gives more uniform convolutions than the methods in which convolutions are formed simultaneously.

A variant of the hydraulic process is one in which the hydraulic oil is replaced by a rubber form. Under pressure, the rubber acts as a hydrostatic fluid. Its use eliminates the need for the presence of oil. Oil can cause carburization and possible embrittlement of the metal if it is not completely removed prior to process annealing or final heat treatment. Residues from oil have also been known to cause pit-type corrosion.

Perhaps the oldest method of forming bellows is that of shaping the convolutions by mechanical tools while rotating the tube (called roll forming). As in the hydraulic processes, there is considerable variety among the machines for roll forming. Some roll-form tooling resembles a lathe on which the tube to be formed is slipped over a centered rotating grooved die. An external tool is then used to press the tube into the grooves in the die, one groove at a time. Another type of tooling makes use of two small coaxial wheels over which the tube is placed. While these wheels are rotated, thus rotating the tube, a third wheel is brought down between the other wheels, thus forming a convolution. The tube is then indexed one pitch distance, and the operation is repeated. Considerable ingenuity by the manufacturers who use the roll-forming process has led to the ability to roll form the convolutions outward as well as inward. However, roll-formed bellows are currently in disfavor among some users because of the possibility of creating surface defects and smearing metal over these defects in such a way that they are hidden. A second objection to roll-formed bellows that is often cited is the excessive wall thinning at the roots or crowns of the convolutions that may be encountered if forming is not done carefully enough. Successful hydraulic forming of bellows, on the other hand, constitutes a proof test of sorts.

It may be necessary to set the pitch of the formed convolutions in a separate operation if the manufacturing method used results in unacceptable variations in pitch. This is done using shaped rolls similar to roll-forming tooling, but using them in such a way that they are merely run around the circumferences of successive convolution without deepening them. Necessity to alter the pitch of the convolutions by more than about 15 percent in this way is an indication that convolution-forming dies may not be of the proper size for the bellows being produced.

Convolution Shapes

The closeness with which the desired convolution shape described by the design drawing is approximated by the actual bellows depends on a variety of factors. Different manufacturing processes differ in their ability to produce uniform convolutions. For a given manufacturing process and bellows material, convolution shapes will tend to be more uniform the thicker the wall and the larger the bellows diameter. Conical sections of the convolutions are seldom, if ever, flat over their entire depth, but tend to be arched.

The rippled-sidewall bellows, a type of formed bellows having relatively deep convolutions and corrugated, rather than arched, sidewalls, has been introduced within the last several years. The overall convolution shapes of these bellows are similar to welded bellows of the nested-ripple type shown in Table 1, except that there are no root and crown welds. Convolutions are formed by expanding the metal hydraulically into closed dies containing the corrugations and then collapsing the convolutions by compressing the roots and crowns.

Details of convolution shapes other than outer-torus radii are difficult to determine by nondestructive inspection methods. The only reliable method of determing convolution shapes that is presently available consists of encapsulation and diametral cross sectioning of a bellows.

Manufacturers sometimes alter the shapes of the end convolutions to decrease the likelihood of end effects. These alterations may consist of decreasing the convolution depths or increasing the convolution pitch.

Convolution Thickness

Formation of the convolutions in formed bellows is accompanied by local thinning of the metal. Whether the point of maximum thinning is located at the roots, crowns, or along the conical sections of the convolutions is determined by the ratio of convolution depth to pitch and to some extent by the details of the manufacturing process.

Some manufacturers claim to hold the amount of wall thinning during forming to 5 percent. Others allow 10 to 20 percent thinning. With the different manufacturing processes, there will be characteristic percentages of thinning for any given set of bellows dimensions. The wall thinning is accompanied by strain hardening of the material. The amount of strain hardening for a given amount of thinning depends in a subtle way upon the precise details of the metal flow during forming. The relationships of wall thinning, strain hardening, formability limits, and metal-flow directions are poorly understood as they apply to bellows fabrication. Although thinning in a convolution is acceptable, the convolutions should be similar to each other.

Sealing of Multi-Ply Bellows

Some multi-ply formed bellows, particularly those intended for steam piping service, are often left with the space between plies unsealed. Vent holes are even provided in the outer plies in some bellows. Unsealed construction is likely to be found in multi-ply bellows made from alloys that must be heat treated after forming.

The reason for this is that air and moisture trapped between plies of a sealed bellows may create sufficient internal pressure between the plies at high temperature to cause gross deformation and ballooning of the bellows. Unsealed multi-ply bellows have the disadvantage that corrosive agents can get between the plies, where they may cause premature failure by stress corrosion.

The best practice for the manufacture of multi-ply aerospace bellows would seem to be to weld the clean, formed plies together around most of their circumference at each end of the bellows, heat treat, and them complete the seal welds as soon as possible. The heat treatment should never be used as a method of burning out oil or other contaminants on or between plies of bellows. Such residues can cause carburization and embrittlement of the metal and may cause local corrosion.

Multi-ply bellows intended for low-temperature service should be sealed with only dry gas or vacuum between the plies, since moisture will freeze out in service, affecting the spring rate. Electron-beam welding in vacuum is probably the safest method of sealing multi-ply bellows.

Welded Bellows and Diaphragms

Figure 3 shows the steps in the manufacture of welded bellows and diaphragms. The blanking and forming processes are similar in principle for both products.

Blanking

The process begins with the blanking of doughnut-shaped disks, called diaphragms, from sheet material. The blanking operation must be carefully done, using dies that are in good adjustment to minimize the formation of burrs. Any burrs which are formed on the edges of the diaphragms must be removed to obtain good fitup for subsequent welding.

Forming

Corrugations in diaphragms are introduced by spinning, stamping, or by hydrostatic pressure. The spinning is done in a lathe by pressing the metal against a corrugated form. This results in a certain amount of cold working which improves the life of the diaphragm. Some manufacturers stamp the diaphragms first and finish them by spinning. Spinning is subject to the same possible objections as roll forming of formed bellows.

In the stamping process, two mating steel dies are generally used. Some dies are made so that they make contact only with the material on concave sides of the corrugations. The depth can be adjusted through a wide range. The die can be made such that the corrugations are formed in succession from the inside to the outside, thus drawing the material gradually from the outside. In order to reduce friction, a lubricant may be used between the material and the polished die.

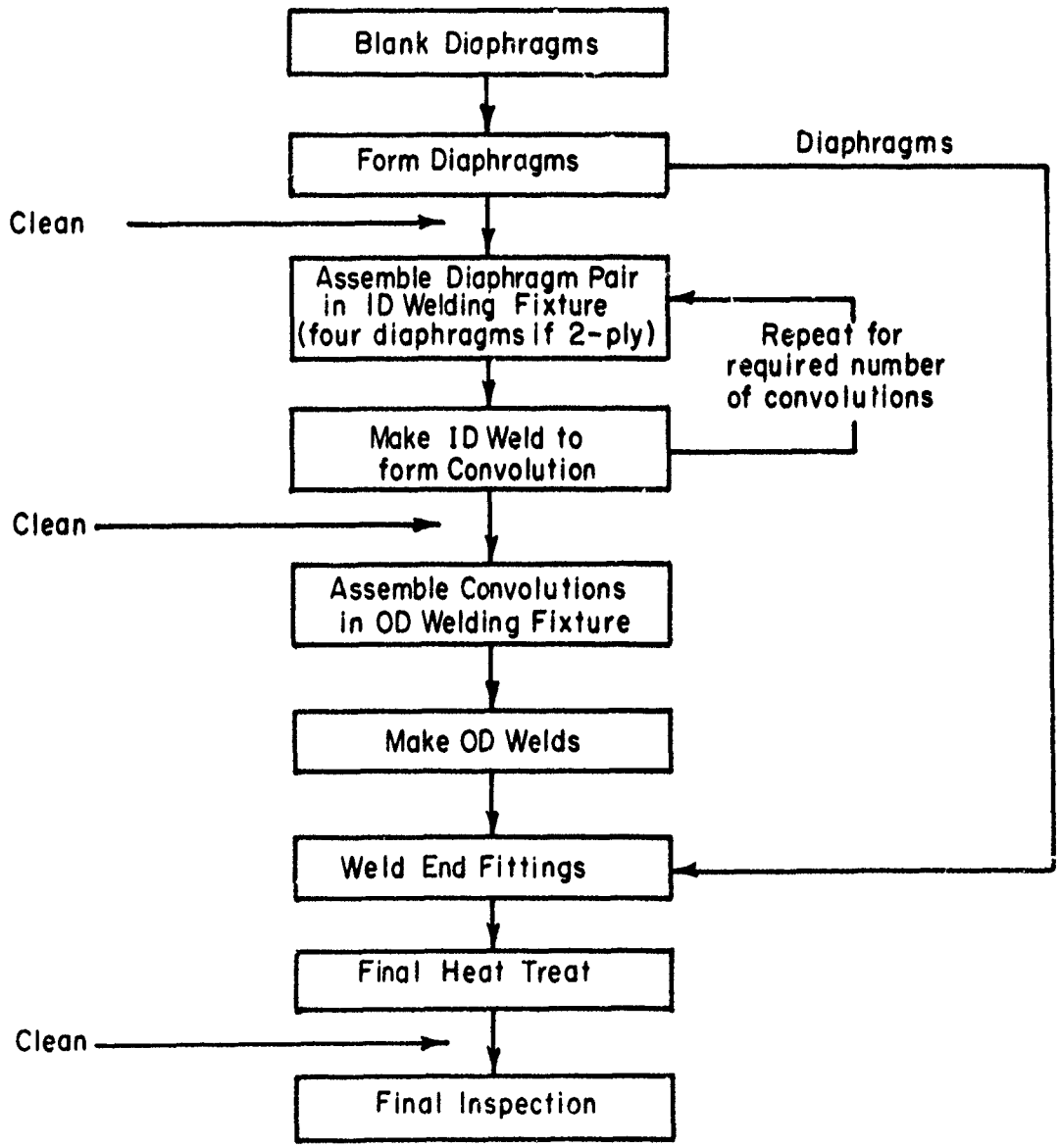

FIGURE 3. MANUFACTURING FLOW SHEET FOR WELDED BELLOWS AND DIAPHRAGMS

In the hydrostatic process, a metal blank is clamped against a corrugated die and hydraulic pressure or pressure from steel-backed rubber forces the blank against the die. Small bleed holes relieve the pressure between the blank and the die.

The material may be annealed prior to forming to make it more easily worked. After formation, the diaphragm may be heat treated to reduce the residual stresses created by the forming operation, and, for some materials, to increase the strength. The type of heat treatment required before and after forming is a function of the material and of the diaphragm shape.

Inner-Diameter Welding

A pair of diaphragms are placed in a welding jig with the inner diameters in contact and clamped with chill blocks on either side of the joint. An edge weld is then made around the inner circumference. This operation is usually accomplished with the gas-tungsten-arc process (GTA or TIG), but some manufacturers claim more uniform welds with the electron-beam process. The welded pair of diaphragms is referred to as a convolution. The welding operation is repeated for the number of convolutions desired in the bellows.

In the case of diaphragms, the end fittings can be attached at this point by arc or resistance welding. If end fittings are to be attached by soldering, the diaphragms must be heat treated first.

Outer-Diameter Welding

The convolutions are stacked in another welding fixture with the outer diameters of adjacent convolutions in contact, split chill rings being used between the mated pairs of surfaces, and the outer diameters are welded in the same manner as the inner diameters.

Most welded-bellows manufacturers use a semiautomatic form of the GTA welding process in which the material to be welded is rotated beneath a stationary torch. Upon completion of a weld, the fixture is moved to the next weld position and the process is repeated. Some manufacturers now use electron-beam welding, at least for the outer-diameter welds. Small-scale plasma-arc welding equipment has recently become commercially available. Both of these latter processes are less sensitive to slight changes in power or arc length than the GTA process for welding thin metals. Electron-beam welding is particularly attractive for making the outer-diameter welds when diaphragms are joined to make aneroid capsules, since welding and evacuation can be done simultaneously.

Many of the welding difficulties that occur in welded bellows are related to the bellows materials, some of which are not as weldable as the alloys used for formed bellows. Heat-resistant alloys, most of which are vacuum melted, typically contain two or more phases and undergo various solid-solution and precipitation reactions during the thermal cycle associated with welding. In some alloys, these reactions may result in loss of ductility or strength in the weld heat-affected zone. These materials problems will not be entirely eliminated regardless of which welding process is used.

Multi-Ply Welded Bellows

An increasing number of two-ply welded bellows are being produced. Techniques for their manufacture are analogous to those for single-ply bellows except that pairs of diaphragms are used. Extreme care must be taken to see that diaphragm surfaces are clean, so that no contaminants are trapped between plies. The weld beads in two-ply bellows will be proportionately larger than for single-ply bellows, and will thus require melting of more metal and use of higher welding cements. There may be difficulty in making the outer-diameter welds due to blowout of the weld pool by gas from between plies. If this condition occurs, electron-beam welding of the outer-diameter seams should be considered.

Heat Treating

The final heat treating required in a completed bellows is dictated by the material. Best strengths in the welds are usually obtained by going through a complete solution and aging treatment rather than by using an aging treatment only. Care must be taken to avoid grain growth in the material during heat treatment. Since the heat-treating temperatures are typically rather high, approaching 2000 F in some cases, bellows must be heat treated in jigs to maintain the desired convolution shapes and free lengths. Because of the thin cross sections of bellows and diaphragms, heat treatments that sometimes differ from those recommended in handbooks have had to be worked out by manufacturers. They usually differ in requiring shorter times and/or lower temperatures, but details are often considered proprietary by each manufacturer.

Deposited Bellows

Deposited bellows are produced, as outlined in Figure 4, either by electroplating or by chemical deposition. Both of these processes offer freedom from several of the restrictions on formed or welded bellows. Very thin walls (0.0003 inch) can be achieved, thus resulting in bellows that have extremely low spring rates. Also, deposited bellows need not be axisymmetric and may be of variable cross section along their length. Although the base material for deposited bellows is usually nickel, it is possible to produce chemically deposited bellows of at least one proprietary nickel alloy, and it is possible to use composite wall structures in electrodeposited bellows by plating successive layers of different metals, such as nickel and copper.

Deposited bellows are made on mandrels that have been machined to the precise shape desired, and apparently 6061 aluminum alloy is universally used as the mandrel material. A separate mandrel must be used for each bellows, and imperfections in the surface of the mandrel will be reflected in the structure of the bellows. The expense of machining and finishing the mandrels to the rigid quality requirements necessary is a major cost item in the manufacture of deposited bellows.

After the bellows have been deposited on the mandrels, the mandrels are dissolved away, presumably in an alkaline solution in order not to damage the bellows. The bellows may then be gold plated, although this is not essential, and end fittings are soldered in place. Soldering is often used because of the thinness of the bellows walls. Welded end fittings can be used for thicker-walled deposited bellows. A limited number of diaphragms have also been made by this process.

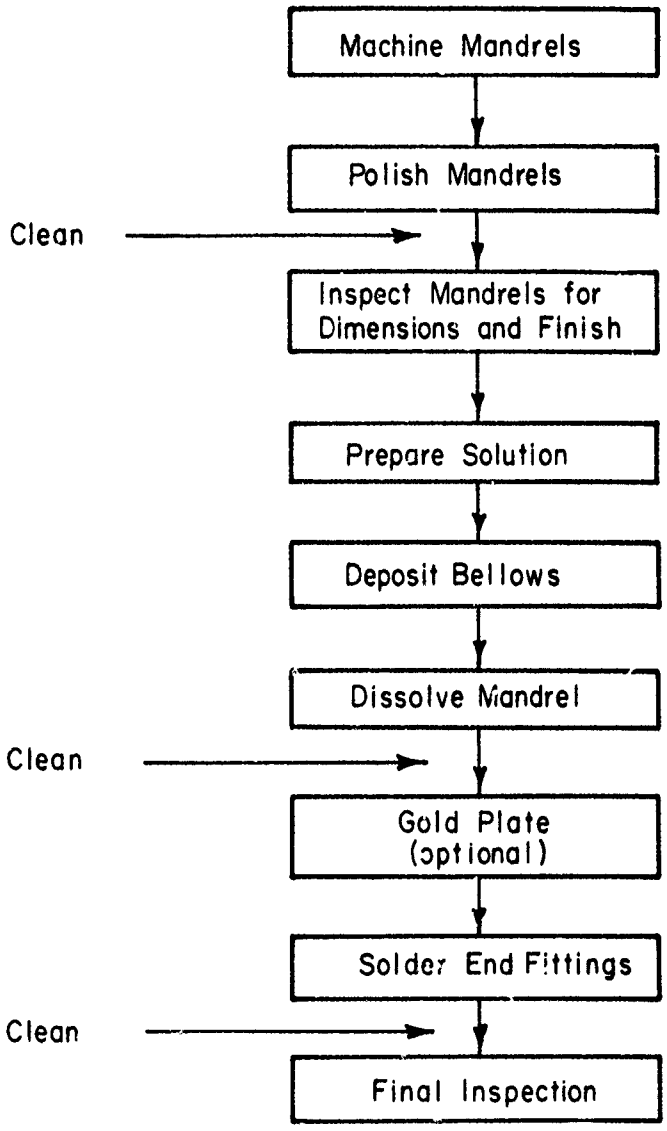

FIGURE 4. MANUFACTURING FLOW SHEET FOR DEPOSITED BELLOWS

End-Fitting Design

The design and attachment of end fittings is influenced by the system in which the bellows is to be used. Seam welding, either arc, electron beam, or electric resistance, is the preferred joining method for end-fitting attachment. The use of welded end fittings results in the lightest construction and gives better high-temperature-service capability than that provided by other joining methods.

Brazing and soldering require the use of fluxes that may cause corrosion if not completely removed. They also introduce a foreign metal into the joint which may present galvanic corrosion problems. However, soldering is the only practical end-fitting-attachment method for extremely thin-walled deposited bellows. There may be cases where heat-treatment requirements of the support structure dictate the use of soldering or brazing in preference to welding.

The most difficult end-fitting-attachment problems are those where small bellows must be installed in a severely cramped space in a device. Access and fixturing requirements for making the attachment joints should be considered during the early stages of the device design and should be kept in mind through its evolution to the final design.

Figure 5 shows typical end-fitting-joint configurations. Three of the joints shown can be made with gas-tungsten-arc, plasma-arc, or electron-beam equipment. The fourth is a design for electric-resistance-seam welding and is particularly adapted for ducting applications. The corner-flange weld is widely used on both formed and welded bellows.

End-fitting materials that are metallurgically compatible with the bellows material must be chosen if welding is to be the joining method.

The flanges shown in the corner-flange and arc-seam joint designs (a and d in Figure 5) should not exceed two or three times the thickness of the bellows material. The flange of the corner-flange joint should have a straight section about four times the bellows wall thickness. The bottom radius of the flange groove in the end fitting should be constant and about four times the bellows wall thickness. The smooth curvature helps maintain adequate gas shielding during welding by minimizing turbulence. Best welding practice includes the use of shielding gas introduced to the back side of the weld as well as gas from the welding torch.

For applications involving corrosive fluids, end-fitting-joint designs that result in crevices in which fluid can be trapped, such as Designs b and c in Figure 5, must not be used.

If soldered or brazed end-fitting joints are to be used, they should be of the lap or slip type and should have sufficient bond area to take the required loading in shear.

Sample joints should always be examined metallographically to insure that the welding conditions give the desired depth of penetration.

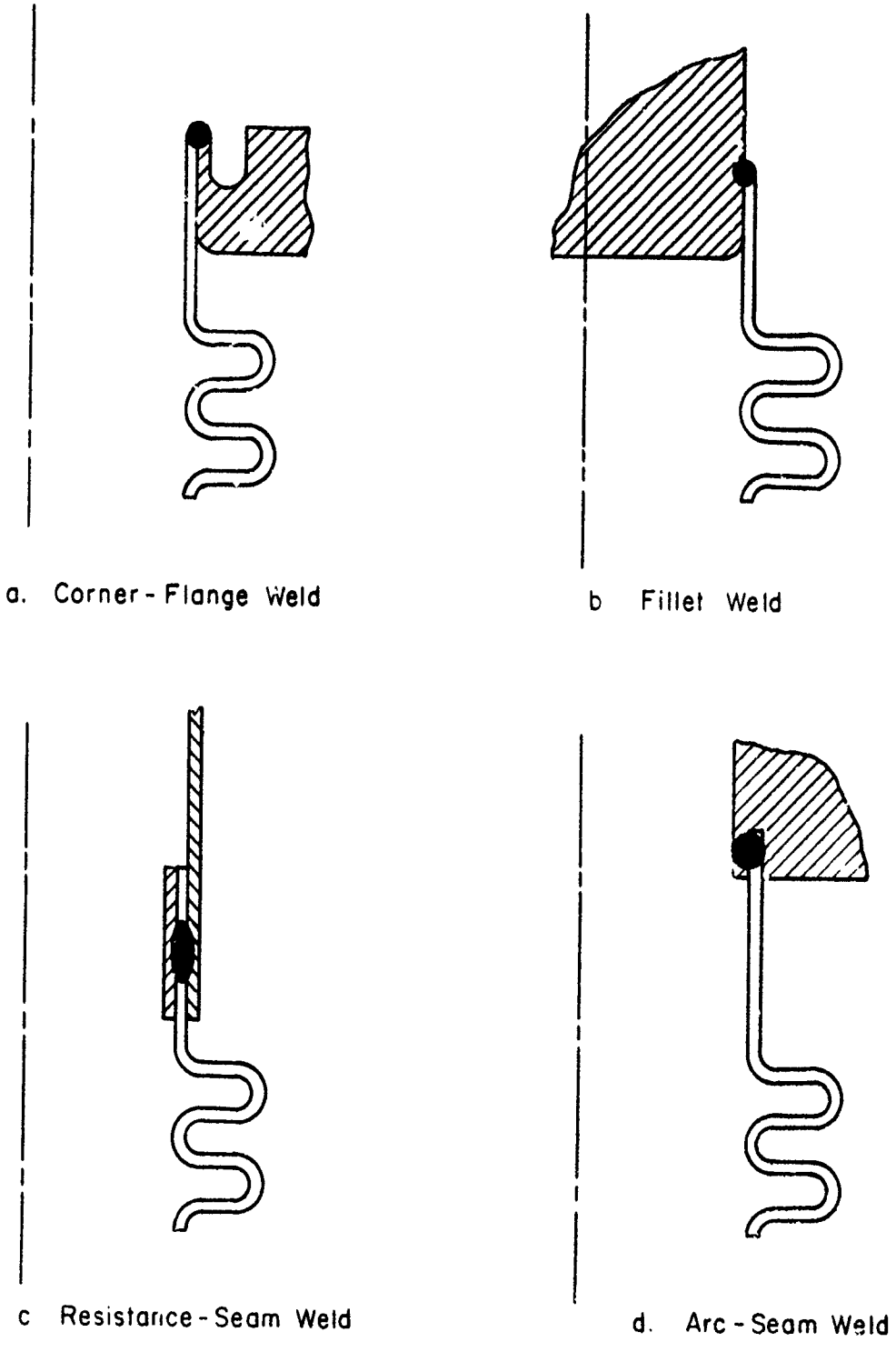

FIGURE 5. TYPICAL BELLOWS END-FITTING JOINTS

Surface Irregularities

Surface irregularities, such as scratches, dents, nicks, bulges, and die marks, should be avoided as far as possible. This is especially true in the root and crown portions of the convolutions, which are likely to be the regions of highest stress. Large bulges or dents may alter the stress distribution sufficiently to change the magnitude and location of maximum stress and affect bellows life. Sharp scratches and die marks may act as notches and concentrate stresses. Irregularities also may initiate instability failures such as buckling and squirm.

Unfortunately, the severity of a surface irregularity with respect to the service performance of a bellows cannot be determined in advance, and its estimation is largely a subjective judgment made by the inspector. In the research program on which this report is based, there was no case in which a surface irregularity was observed to have had any influence on fatigue-crack propagation or initiation. Slight irregularities in convolution alignment, however, had a large effect on the pressure at which the bellows squirmed.

Cleanliness

Cleanliness of bellows materials before, during, and after manufacture is extremely important. Many of the high-performance aerospace metals are much less tolerant of improper manufacturing procedures than are the more common metals.

Hydraulic forming oils, soap solutions, dye penetrants, and other fluids should be thoroughly removed as soon as possible after forming and inspection are completed. Even fingerprints can cause corrosion of some of the high-quality surfaces desired in bellows. In no case should bellows be heat treated without prior cleaning to remove such materials.

It is recommended that in-process bellows be stored in a dry atmosphere.

Employment of LOX cleaning procedures prior to longitudinal seam welding, assembly of plies, end welding, and heat treating will pay dividends in the quality of the resulting bellows. Awareness on the part of the manufacturing personnel of the importance of maintaining these standards of cleanliness is essential and may decrease the number of cleaning operations that are necessary.

In-Process Inspection

Bellows and diaphragms should be inspected during and after fabrication. In-process inspection is intended to detect faulty material, faulty welding, improper convolution formation, handling damage, and lack of cleanliness.

Materials Inspection

As described previously, materials for bellows and diaphragms must be very uniform and free from defects. When material is received, its thickness must be measured and it must be inspected carefully to make sure that there are no large irregularities such as thinning, bulges, wrinkles, and dents and no surface damage such as nicks, scratches, and pits. Specimens from each sheet should be used to determine the yield strength, ultimate strength, hardness, and chemical composition of the material. Sample cross sectioning to inspect grain size and physical and metallurgical structure is necessary for adequate quality control.

Weld Inspection

Many manufacturers of formed bellows consider the forming process itself to be an adequate check on the quality of the seam weld. This is particularly true of bellows formed by hydraulic or rubber pressure. Welded bellows are not subjected to any analogous proof test during their manufacture, so weld quality in these items must be assessed by different means.

Visual inspection, if carefully done, is a useful method of checking weld quality. If inspection is performed immediately after welding and before any planishing, pickling, or heat treatment has been done, the presence of an oxide film covering the weld may be informative. Thin, multicolored interference films of oxide are not usually harmful, even in oxygen-sensitive metals such as titanium, but the presence of a thick brown, gray, or black oxide indicates poor gas shielding, and is in titanium a warning of probable weld-metal contamination. Weld beads should be generally smooth and regular. TIG beads often tend to have a striated appearance which results from tiny surface ripples caused by stepwise solidification of the weld pool. These ripples are not harmful. However, variations in bead size and shape along a weld are danger signs. They indicate lack of control in the welding power supply, poor fitup, variable heat sinking, or a changing arc length. The bead diameter in welded bellows should be between two-and-one-half and three times the material thickness. A smaller bead is an indication of inadequate burndown and the weld is likely to fail prematurely in service by fracture through the bead. The size of the weld beads in welded bellows could be measured rather easily by using a rigidly mounted pair of indicator heads arranged to contact opposite sides of a bead as a weld is rotated between them. Output signals could be summed and recorded or visually displayed. Acceptance could be on a go-no-go basis. Such a system is not presently being used, to Battelle's knowledge. The presence of unusual isolated lumps or depressions on weld beads is suspicious, since they may indicate subsurface inclusions or voids. Visual inspection of inner-diameter welds in welded bellows is difficult at best, and in small bellows it is nearly impossible. The inspection is relatively easy, however, if it is done on individual convolutions before they are laid up for outer-diameter welding. Such inspection should be done with the same care as a final bellows inspection, and convolutions that are rejected should be immediately destroyed so that they do not find their way into a bellows at a later date.

Dye-penetrant testing is a useful method of detecting cracks and gross porosity extending to the surface, but care must be taken to remove all traces of the penetrant materials after use and before any heat treatment. Dye-penetrant testing is chiefly of use with longitudinal seams in formed bellows and for locating leaks and fatigue failures that cannot be detected visually.

Radiography has proved useful for examining longitudinal seam welds and detecting ruptured internal plies in multi-ply formed bellows, but it lacks the sensitivity to detect small flaws in welded bellows.

Eddy-current testing using special miniaturized detection coils is a promising method for making subsurface-weld inspections in bellows. As far as is known, it is not presently being used for this purpose.

Ultrasonic-inspection techniques do not appear promising because of the small size of the welds, with the resultant likelihood of masking of indications of internal flaws by reflections from the surface.

Convolution and Corrugation Formation

Visual and shadowgraph inspections can be used to verify at least some of the critical shape parameters, but occasional cross sectioning of a bellows is necessary to assure control of all dimensions.

Handling Damage

Extreme care must be taken to assure that the thin bellows and diaphragm material is not damaged during manufacture. Inspection for such damage is done visually. In general, it appears that manufacturers should use much better packaging procedures than those currently in use to prevent damage in shipping and to impress upon the user the susceptibility of very thin materials to handling damage.

Leak Testing

The presence of a leak in a bellows is cause for rejection. It should not be assumed by the bellows purchaser that leak tests will be performed by the bellows manufacturer unless they are specifically requested. For the many formed bellows used in aircraft ducting, the satisfactory performance of one of the first bellows of a production run is usually taken as evidence that the entire run of similar bellows will also be free from leaks. If the run is large, leak tests may be made on a spot-check basis during the production.

For bellows intended for space hardware, manufacturing procedures normally require the leak testing and certification of each bellows. This adds to the cost of the bellows, but provides an added degree of quality assurance.

The helium mass spectrometer is the standard method of verifying bellows leak tightness. Most bellows manufacturers now have helium leak-test equipment or have access to commercial leak-testing services. The helium mass spectrometer is capable of detecting leaks in the range of 10^{-9} atm cc of He/sec.

As an in-process leak test, many bellows manufacturers pressurize and immerse their bellows in deaerated water for about 15 minutes. Formation of bubbles is taken as an indication of a leak. The immersion test is simple and useful, although it is not as sensitive as the more expensive helium-mass-spectrometer leak test. The immersion

test can detect leaks as small as about 10^{-3} atm cc/sec. Bellows should be thoroughly cleaned and dried following an immersion test to remove any oil and water entrained in the pressurizing gas and the carryout from the immersion tank.

The use of soap or detergent solution as an alternative to the immersion tank is not recommended, since detergents may cause stress corrosion of many aerospace alloys. Such a case was encountered during this program (Appendix P). If soap or detergent solution is used, it should be thoroughly removed immediately upon completion of the leak test.

CONCLUSIONS AND RECOMMENDATIONS

Many conclusions, suggestions, and recommendations have been incorporated in the different parts of the report body and the appendixes. These have been so numerous and diverse that it is not practical to repeat all of them here. Only the major conclusions and recommendations affecting the future manufacture and use of bellows and diaphragms in aerospace applications are listed below.

Conclusions

Formed Bellows

(1) There are many capable and conscientious manufacturers of formed bellows When such a manufacturer has produced a number of bellows of a given material and configuration and has accumulated test results for several such bellows operated under the particular operating conditions of interest to the user, then this particular bellows can be purchased from the manufacturer with a high degree of confidence. Any departure from such known conditions significantly increases the risk of bellows failure. The risk can be reduced only by obtaining statistical evidence of manufacturing consistency, if the configuration is different, or by obtaining statistical evidence of satisfactory performance, if the operating conditions are different. The stress-analysis procedure developed during this program can be used to reduce the amount of statistical data required.

(2) There are four primary reasons for the premature failure of formed bellows in aerospace applications: (a) manufacturing variations, (b) user negligence, (c) unexpected operating conditions, and (d) general lack of understanding of low-cycle fatigue.

(a) Almost every bellows configuration made for an aerospace application must be tested satisfactorily by the manufacturer in a simulated system. However, such tests have an appreciable effect on overall cost and it is not usually practical for a manufacturer to obtain statistical data concerning the effect of normal manufacturing variations on the performance characteristics of the configuration. Consequently, an unevaluated combination of normal manufacturing variations can cause premature failure. Manufacturing variations beyond expected limits are a primary cause of premature failure.

(b) During this research program there was considerable evidence that the average bellows user considers a formed bellows to be a rather simple, rugged device. In reality, many formed bellows can be plastically deformed by hand and their operating characteristics can be extremely complex. It is believed that bellows users must learn to treat bellows with a great deal more care, in order to prevent premature bellows failure because of damage due to handling, improper installation, and poor system simulation resulting from incomplete system analysis.

(c) Even when the operating characteristics of a system have been analyzed carefully, the complexity of an aerospace system can result in an unexpected, possibly transient operating condition that can cause premature failure. The most likely sources are unexpectedly high deflections, pressures, or temperatures, and the unexpected introduction of corrosive elements. In addition, as described in the report body, there are some performance characteristics of bellows that are not generally understood.

(d) There is a widespread lack of understanding of the statistics of low-cycle fatigue. Both the manufacturers and the users generally accept a life test of 100 to 150 percent of the required life as being evidence of a satisfactory fatigue test. The fatigue life of identical coupon specimens can vary as much as three to one. The fatigue life of "identical" bellows can vary even more. Premature fatigue failure will continue to occur in formed bellows until more sophisticated test-analysis methods are used, and until a fatigue-analysis procedure similar to the one described in Appendixes L and M is used.

(3) It is believed that the stress-analysis procedure developed during this program is of such fundamental importance to the design, fabrication, and application of formed bellows, that it is expected to become a basic tool for the industry. The many ways that the analysis procedures can be used are difficult to envision. These procedures may prove to be particularly beneficial in

(a) The design of new bellows and the investigation of the effect of new operating conditions on existing bellows

(b) The selection of critical parameters whose control may result in more uniformly operating bellows

(c) The analysis by bellows users of competing designs to provide a more rational basis for design selection

(d) The evaluation of the effects of manufacturing variations to determine whether production bellows should be accepted or rejected

(e) The reduction of the amount of empirical data required to determine various performance characteristics. This would be accomplished through the use of the analysis procedures with statistically based test procedures.

Welded Bellows

(1) There are several capable and conscientious manufacturers of welded bellows. The comments made for formed bellows in Item (1) above apply to welded bellows with the exception that many welded-bellows characteristics are much less predictable than formed-bellows characteristics. In fact, it is the opinion of the research staff that a standard welded bellows should not be used in a highly critical system without redundance. This is particularly true for a required fatigue life greater than 500,000 cycles.

(2) The four primary reasons for premature fatigue failure of formed bellows described in Item (2) above apply also to welded bellows. An insufficient number of test samples is a particular problem with welded bellows because the cost per bellows is so much higher than that of formed bellows. Leaf interference in compression was also found to be a possible cause for premature failure.

(3) The stress-analysis procedure will be useful in determining which of a manufacturer's welded-bellows designs would be best for a particular application. However, it is believed that this use of the analysis procedure will result in welded bellows which have only nominally better operating characteristics. More striking improvements may be made if the analysis procedure is utilized to evaluate unconventional designs. For example, the tilt-edge concept described in Appendix D is so promising for reducing the stresses at the welds to nominal values that the successful development of optimized configurations could make the present standard configurations obsolete in a relatively short time. For tilt-edge bellows, the five uses of the stress-analysis theory as listed under Item (3) above would be equally applicable.

Diaphragms

Very few manufacturers offer diaphragms for sale and the selection is very limited. Most diaphragms are manufactured for use in a component by the manufacturing company. Thus, the use of the stress-analysis procedure for diaphragm design and manufacture will be determined by the needs of each company. However, since deformation behavior of diaphragms is complex and nonlinear, it is believed that the analysis procedure should also become a basic tool of diaphragm manufacturers.

Recommendations

(1) It is recommended that the following types of organizations should establish groups having the capability of using the stress-analysis procedure:

(a) Bellows and diaphragm manufacturers wishing to develop designs to meet operating conditions different from those for which their standard product lines were designed

(b) Large users of bellows and diaphragms who must select from several potential configurations

(c) Government facilities that must select from among a number of bidders and that must determine a basis for bellows or diaphragm rejection.

(2) The Air Force should initiate, in behalf of the government agencies, a standardized purchasing procedure requiring stress-analysis procedures similar to the one described in Appendix B.

(3) A research program should be initiated to determine the potential of the tilt-edge configuration for improving the fatigue life and reliability of welded bellows.

(4) A program should be initiated to develop manufacturing methods capable of producing more consistent formed bellows. As part of such a program, consideration should be given by large-volume bellows users (such as the Air Force) to the quantity purchase of bellows materials to obtain improved metallurgical and dimensional control of starting materials.

(5) A program should be undertaken to investigate alternative methods of manufacturing welded bellows, such as diffusion bonding.

(6) A program should be undertaken to investigate unconventional diaphragm configurations for the purpose of increasing the deflection and pressure capability of diaphragms. Composite configurations, similar to automobile leaf springs, should be included in the investigation.

REFERENCES

(1) Newell, F. B., Diaphragm Characteristics, Design and Terminology, A. S. M. E., New York, New York (1958).

(2) Wildhack, W. A., et al., "Investigations of the Properties of Corrugated Diaphragms", ASME Trans., 79 (1), 65-82 (January, 1957).

(3) Pressure Transducing and Instrumentation Techniques, I, Bk I, Giannini Controls Corp., Duarte, California (August 1, 1960) (AD 251111).

(4) Marcal, P. V., and Turner, C. E., "Elastic Solution to the Limit Analysis of Shells of Revolution With Special Reference to Expansion Bellows", J. Mech. Eng. Sci., 3 (3), 252-257 (September 1961).

(5) Newland, D. E., "Buckling of Double Bellows Expansion Joints Under Internal Pressure", J. Mech. Eng. Sci., 6 (3) (1964).

(6) Lestingi, J. F., "Nonlinear Stability Analysis of Thin Elastic Shells of Revolution", Dissertation, Yale University (June 1966).

(7) Daniels, V. R., "Dynamic Aspects of Metal Bellows", The Shock and Vibration Bulletin (January, 1966), Bulletin 35, Part 3, USNRL, Washington, D. C.

(8) Timoshenko, S. P., Vibration Problems in Engineering, 3rd Edition, D. Van Nostrand Co., Inc., p 329 (1955).

(9) Akasaka, T., and Takagishi, T., "Vibration of Corrugated Diaphragms", Bulletin of JSME, 1 (3), 215-221 (1958).

(10) Haringx, J. A., "The Rigidity of Corrugated Diaphragms", Applied Scientific Research, Series A, 2, 299-325 (1950).

(11) Jackson, J. D., and Boyd, W. K., "The Compatibility of Materials in LEM Vehicle Tank with N_2O_4 During Vibrational Attack", Battelle Memorial Institute Final Report to Grumman Aircraft Engineering Corp., Contact NAS 9-1100, P. O. No. 2-24455-c (October, 1964). [See also "Impact Studies for the Lunar Excursion Module Oxidizer Tank", Materials Protection, 5, 65-67 (April, 1966)].

Note: For a more comprehensive bibliography, the reader is referred to Technical Report No. AFRPL-TR-65-215, "State-of-the-Art Survey of Metallic Bellows and Diaphragms for Aerospace Applications", by Battelle Memorial Institute, dated November, 1965 (AD 479046).

APPENDIX A

THEORETICAL ANALYSIS OF ELASTIC DEFORMATIONS OF BELLOWS AND DIAPHRAGMS

ABBREVIATIONS AND SYMBOLS

ϕ^*	Angle between normal and axis of revolution, deg
μ	Parameter for toroidal shell analysis, $\mu = \sqrt{12\ (1 - \nu^2)}\ r_1^2/ah$
r_1	Local radius of curvature of torus, in.
a	Radial distance from bellows axis to point of torus, in.
ν	Poisson's ratio
h	Bellows thickness, in.
Q	Effective shear resultant force in direction normal to the shell, lb/in.
N_φ, N_θ	Membrane resultant forces in meridional and circumferential directions, respectively, lb/in.
M_φ, M_θ	Bending moment resultants in meridional and circumferential directions, respectively, in-lb/in.

*The symbol ϕ appearing in this and subsequent appendixes is a variation of the symbol φ, which will also be found in the appendixes.

APPENDIX A

THEORETICAL ANALYSIS OF ELASTIC DEFORMATIONS OF BELLOWS AND DIAPHRAGMS

Bellows and diaphragms belong to a class of structures usually designated as "thin shells of revolution" or as "axisymmetric shells". The main theoretical developments in the investigation of these shells have taken place in the past half century since the derivation of the H. Reissner-Meissner equations for the linear elastic deformations of the shell of revolution. Prior to the development of computers, investigations were limited to attempts to derive approximate formulas for stresses and deflections in axisymmetric shells of special shapes. However, the development of digital computers and the accompanying development of numerical methods have made it possible to obtain direct numerical solutions for deflections and stresses in axisymmetric shells of arbitrary meridional shape.

This appendix gives a description of approaches that have been used for obtaining solutions to the elastic deformation of bellows and diaphragms as well as a discussion of the selection of the computer program used in this research study. The approaches that have been used may be divided into three major categories: (1) approximate formulas for simple shell geometries, (2) finite-difference approximations to the differential equations, and (3) direct numerical integration of the differential equations. The direct-integration approach will be discussed in some detail here and in Appendixes B and C, since it was the basis of the computing program used in the research study.

Approximate Formulas for Simple Shell Geometries

The general equation for shells of revolution with axisymmetric loading is a complicated differential equation of the sixth order. Until the development of digital computers, there was no practical way of integrating this differential equation directly. However, most corrugated diaphragms and bellows may be considered as aggregates of much simpler structural elements such as plates and shells of constant curvature. Therefore, until recently the major emphasis in the theoretical analysis of diaphragm and bellows deformation was directed toward obtaining relatively simple closed-form approximations to the solutions for these plates and shells. It was the apparent intent of the investigators that if such solutions could be obtained, they would suitably combine sets of solutions to obtain solutions for actual diaphragms and bellows. Actually, the combination of sets of solutions to synthesize a diaphragm requires extensive calculations. Apparently, only one such synthesis was ever performed without the aid of a digital computer. Although formed bellows can be synthesized from as few as two semitoroidal sections or two toroidal sections and a conical or flat-plate section, the application of these formulas has been made to only a few formed bellows without using computers. Computer programs have now been developed to use these formulas so that it is appropriate to describe the development of some of the most useful formulas.

As noted, the simplified shell formulas have been developed primarily for shells of constant curvature. The theory for the conical shell was worked out by Dubois in 1917 in a thesis at Zurich. The first theory for toroidal shells was presented by Wissler, also in a Zurich thesis, in 1916. In 1917 Lorenz published a theory for stress in Bourdon tubes.

A somewhat simpler form of the theory for toroidal shells was produced by Schwerin in 1929. Then a solution was developed by Stange in 1931 in the form of a power series in the angle ϕ.[A-1]* This solution was limited to arc-shaped segments of the shell for which ϕ is not near $\pi/2$. In addition to this limitation, Stange's power series solution was rather cumbersome to evaluate.

An improvement in the theory for the analysis of toroidal shells was achieved almost simultaneously in 1950 by Clark[A-2] and by Haringx[A-3]. Both used some newly tabulated Hankel functions of order one-third. In 1951 Novozhilov obtained an approximate solution in terms of the same functions.[A-4] Subsequent refinements in the asymptotic solution were made by Clark.[A-5, A-6] Tumarkin also developed higher order approximations in the asymptotic series similar to Clark's development.[A-7]

Another approach to the toroidal shell was presented in a paper by Dahl.[A-8] In this paper Dahl obtains a strain-energy solution to toroidal shells in terms of a power series in $\mu = \sqrt{12(1-\gamma^2)}\, r_1^2/ah$, where a is the center-line radius of the torus. Dahl's solution is applicable to regions of small μ, but it is interesting to note that his solution checked with Clark's over the approximate range of from 8 to 40[A-2].

In the past 10 years, problems involving toroidal shells have been extensively studied in Russia. The bulk of the investigations have been based on the use of either asymptotic expansions or power-series expansions to solve specific problems involving the omega joint or simple bellows with one to three corrugations. Many of the papers describing these investigations were reviewed in a monograph by Chernykh and Shamina in 1963. The authors indicated that the monograph was to be the initial effort in an extensive program of investigations of toroidal shells at Leningrad University.[A-9] The monograph, which is an extensive review of the state of the art of theory of toroidal shells to about 1961, included references to both Western and Russian literature. Another extensive monograph on the theory of toroidal shells was written by Bulgakov in 1962.[A-10] Bulgakov discussed the various approaches used to obtain approximate solutions. He also discussed solutions for toroidal shells that he obtained on the computer "URAL I" at Kiev using both the Runge-Kutta and the finite-difference techniques. This seems to be the first attempt in Russia to use computers for the calculation of axisymmetric shells. This lag would appear to be a result of the slow development of the computer industry in Russia.

Although approximate formulas have been developed for shells of relatively simple shapes, they can be combined to predict stresses and deflections of corrugated bellows or diaphragms. Two well-known applications of this approach are the analysis by Grover and Bell of a corrugated diaphragm[A-11] and the analysis by Laupa and Weil of a U-shaped bellows.[A-12] This approach involves extensive numerical computations (except for toroidal bellows). Consequently, for practical application to bellows and diaphragm analysis, it is desirable to carry out the calculations on a digital computer.

A number of computer programs have been developed utilizing combinations of the various formulas to solve bellows problems. Some such programs were obtained by computerizing the formulas used by Laupa and Weil. In a recent study[A-13/A-16] Atomics International Division of North American Aviation, Inc., developed a computer program incorporating several of the approximate formulas which permitted the analysis of a single-ply toroidal and convoluted bellows with and without reinforcing rings and of single-sweep welded bellows.

References for Appendix A are listed on p A-8

The chief disadvantage of this approach is that it is limited to bellows or diaphragm configurations that can be made up of sections that can be solved analytically. Each section, in addition to having constant meridional curvature, must also have constant thickness and must be isotropic and homogeneous. These parameters can be allowed to vary from segment to segment to account for the nonuniform thickness or variation in the elastic properties of the bellows. However, unless the bellows is broken into a fairly large number of segments, this may not be a satisfactory way to approximate shells with varying thickness or varying elastic properties.

One approach which is being exploited widely at the present time for many types of problems is the finite-element technique. The application of this technique to shells of revolution consists of approximating the actual shell by large numbers of small shell elements (usually conical shell elements). The behavior of the individual shell elements is described by one or the other of the approximate formulas mentioned above. Because the approach leads to the generation of a large matrix equation describing the behavior of the entire bellows or diaphragm, the technique requires the use of a computer.

Finite-Difference Approximations to the Differential Equations

The finite-difference approach involves choosing a set of grid points along the bellows and approximating the differential equations by finite-difference equations defined at the grid points. This approach has been used as the basis for a number of computer solutions for problems involving shells of revolution.[A-17/A-20] The technique is quite general and may be applied to the solution of arbitrarily shaped thin shells of revolution with both varying thickness and varying elastic parameters.* Considerable progress has been made in solving the large matrices of the type that are encountered in this technique. These matrices are quasidiagonal and can be solved by successive elimination and the back-substitution technique. As a result, bellows problems can be solved by finite-difference codes such as the AVCO code[A-18] or the CEGB code[A-17] in a matter of 1 or 2 minutes on computer machines of the IBM 7090 class.[A-21]

Finite-difference programs have been written with the capability of analyzing a variety of bellows configurations and loading conditions. For example, the AVCO code permits the analysis of bellows with both axisymmetric and nonsymmetric loading in the linear elastic range. It also permits the analysis of multilayer shells in which the layers are completely bonded together along the entire length of the shell. The code developed at Bell Aerosystems Company[A-22] permits the analysis of linear and nonlinear axisymmetric elastic deformations of bellows, while the computer code recently developed at MIT[A-23] apparently permits the analysis of axisymmetric elastic and plastic deformations of shells.

The chief disadvantage of the finite-difference techniques is that the accuracy of the solution depends on the choice of the mesh-point spacing. Since this dependence is not known beforehand for a given problem, the user will either have to choose a mesh spacing finer than necessary or risk having to run the problem over again if his original choice of mesh spacing is not fine enough. This dilemma is even more serious when an iterative

*The capability of taking varying thickness and elastic parameters into account includes accounting for discontinuous changes in these quantities. This permits analysis of end fittings, circumferential weld beads, etc.

solution must be obtained for nonlinear problems. The direct-integration approach provides a way of overcoming this difficulty.

Direct Numerical Integration of the Differential Equations

A number of direct numerical-integration techniques have been developed for the solution of ordinary differential equations. Since many problems involving axisymmetric shells can be reduced to one-dimensional problems involving ordinary differential equations, numerical-integration techniques can be used to solve them. The problems mentioned above that have been solved by finite-difference techniques may also be solved by direct-integration techniques. One of the first computer solutions to a convoluted-diaphragm problem[A-24] employed the Runge-Kutta integration approach. Subsequent to this work, a number of computer solutions were obtained with the Runge-Kutta technique.[A-25] However, it soon became apparent that the direct-integration techniques became inaccurate if applied to some shell problems. This phenomenon is discussed in a paper by Sepetoski, et al.[A-20] Briefly, the difficulty stems from the fact that self-equilibrating boundary loads on shells give rise to stresses only in a narrow "edge-effect" zone near the boundary. In solving a shell problem, it is necessary to take into account the boundary loads at both ends of the shell. In the direct-integration approach, the set of first-order differential equations are integrated directly to obtain the coefficient matrix of a system of equations relating the values of the fundamental variables at each end of the shell. The magnitudes of the elements in the fundamental matrix are proportional to the length of the shell. Thus, the longer the shell, the larger the elements. If the shell is sufficiently long, the elements become very large and nearly proportional so that the matrix is very nearly singular. When this system of equations is solved for the values of the variables, the round-off error is so great that the inversion procedure yields meaningless results.

As a result of this deficiency in the direct-integration technique, many investigators turned to the finite-difference technique discussed above. An indication of this was that most of the general computer programs discovered in the literature search at the beginning of this research study were based on the finite-difference approach rather than on the direct-integration approach.

Kalnins[A-27] extended the technique suggested by Collatz[A-26] to the solution of the differential equations governing the static linear response of thin elastic shells of revolution and developed a computer program which permits the analysis of a shell of any length. Similar techniques were derived by Goldberg and Bogdanoff,[A-28] Mirabal and Dight,[A-29] and by Cohen[A-30]. Since the technique consists in dividing the shell into a number of segments, it is referred to as the multisegment method. Numerical integration of the differential equations over one of these segments yields a set of equations with small elements. To solve the shell problem, the sets of equations obtained from the integration of the differential equations over each of the segments are combined with the continuity conditions at the junctions of the segments and with the boundary conditions at the edges of the shell to form a single large matrix equation. This matrix equation ordinarily is well conditioned and can be solved by a Gaussian elimination procedure.

Whether a segment is sufficiently small can be determined by using an approximate formula for the decay length of a shell. Also, an automatic check on the validity of the analysis can be carried out in the following way. First, the solutions at the ends of the segments are obtained from the Gaussian elimination. Second, the governing differential equations are integrated again over each segment using the results of the Gaussian elimination as the initial values at the initial edge of the segment. If the values of the variables obtained by integrating over the segments agree with the values obtained from the Gaussian elimination procedure, the solution is exact. Any errors in the solution are easily indicated by this check.

It was mentioned earlier that the direct-integration technique has a wide range of applicability to the solution of bellows problems. The computer program MOLSA (Multilayer Orthotropic Linear Shell Analysis)*, which was used extensively in the early phases of this research study permits the analysis of symmetric and nonsymmetric deformations of isotropic or orthotropic single or multilayer shells of revolution. (Here, as in the AVCO code, a multilayer shell is considered to have layers completely bonded together along the entire length of the shell.) Arbitrary variations in thickness and elastic properties, including discontinuous variation, are easily accounted for. Thus, the effects of end fittings and weldments may be considered. Cohen[A-30] has also developed a computer program that permits the linear elastic analysis of orthotropic shells subject to either symmetric or nonsymmetric loads.

The capability of Program MOLSA for the analysis of multilayer shells was utilized in an attempt to develop a simple theoretical model of multiple-ply bellows. However, as described in Appendix G, this model proved to be inadequate to predict all of the observed characteristics of two-ply bellows. With this exception, the bellows models analyzed in this research study were single ply and of isotropic materials.

Program NONLIN was used for most of the bellows analyses performed in this research study. This program was developed by Dr. J. F. Lestingi[A-31] utilizing the multisegment numerical-integration technique. The method of solution and the governing differential equations are described in Appendix C, together with a listing of Program NONLIN. This program permits the analysis of linear elastic axisymmetric and nonsymmetric deformations and of nonlinear axisymmetric deformations of bellows. It is believed that these capabilities will be of most benefit to bellows designers.

The remainder of this appendix will give a comparison of solutions for certain bellows problems obtained with the methods outlined above.

Comparison of Computer Programs

One of the first tasks performed in the research study was the selection and evaluation of the thin-shell computer program to be used as a major tool in the research. As described in earlier sections of this appendix, the most general computer programs used are based on two techniques — the multisegment direct-integration technique and the finite-difference technique. A decision was made to obtain two programs, one representing each approach.

*Program MOLSA is a modification of the computer program developed by Dr. A. Kalnins.[A-27]

The computer code developed by Dr. P. P. Radkowski and others of the AVCO Corporation[A-18] was selected as being representative of the finite-difference approach. The program developed by Dr. A. Kalnins[A-27] was selected as being the best program using the multisegment direct-integration technique. (As mentioned earlier, this program was modified extensively. The modified program was called MOLSA.) The AVCO code and the MOLSA code were compiled on the Battelle computer and applied to an analysis of an omega-joint bellows.

Using the AVCO code, two solutions were obtained for the omega bellows. In the first, a finite-difference mesh was used with 80 points over half the torus. For the second, 400 points were used.

Table A-1 shows the stresses given by these two solutions at a few points of the torus as well as the solution obtained with the MOLSA code. It is apparent from an examination of this table that the results of the AVCO code converged toward the MOLSA code results as the mesh was refined. The AVCO code results with the fine mesh were almost everywhere within 1 percent of the MOLSA code results.

These results pointed up one of the advantages of the MOLSA code over the AVCO code, namely, that the accuracy of the MOLSA code could be preselected, while the accuracy of the AVCO code could be determined only by running a problem with several mesh sizes.

As a further step in the evaluation of the MOLSA code, calculations were made of the stresses in two semitoroidal bellows studied by Turner and Ford.[A-32] The specimens studied were Bellows A and Bellows D of their paper. Figure A-1 shows the dimensions of these bellows. Figures A-2 through A-5 show the results that Battelle obtained, as well as the experimental and theoretical results that Turner and Ford obtained for a 1-ton axial load. Although they used a simplified theoretical model that was approximately valid only over a certain range of parameters, both their theoretical and experimental results agreed fairly well with the results obtained with the MOLSA code.

The results obtained with the MOLSA code were also compared with data published by Laupa and Weil.[A-12] They reported the stresses calculated at four points of a U-shaped bellows under axial loading and under internal pressure. Battelle used the MOLSA code to investigate the same configuration. Figures A-6 through A-9 give the membrane and bending-stress resultants in meridional and circumferential directions for both the axially loaded and the pressurized U-shaped bellows. The solid curves are the results of Battelle's calculations; the results obtained by Laupa and Weil at the four points reported are also shown. To convert the stress resultants shown in Figures A-7 through A-9 to the stresses reported by Laupa and Weil, it was necessary to multiply the membrane stress resultants in Figures A-6 and A-8 by $1/t$ and the bending stress resultants in Figures A-7 and A-9 by $6/t^2$, where $t = 0.05$ inch, the thickness of the bellows. Battelle's results obtained with the MOLSA code were in excellent agreement with those of Laupa and Weil.

A limited study of computer programs was made by Dr. H. Kraus of United Aircraft for the Pressure Vessel Research Committee of the Welding Research Council.[A-21] Kraus studied four computer programs including the AVCO code, Kalnins' code, and the SEAL SHELL II code.[A-33] In addition, he obtained a finite-difference code written by Dr. R. K. Penny of England.[17] He applied the four programs to the analysis

of a spherical shell segment and a cylindrical pressure vessel with a hemispherical head. In addition, he applied Kalnins' code and the SEAL SHELL II code to a segment of a pressurized semitoroidal bellows restrained against axial movement.

As a result of his study, Kraus concluded that Kalnins' code and the AVCO code were of roughly equal speed and accuracy and were superior to the other two codes on one or the other of these counts. Kraus did not compare the AVCO code with Kalnins' code for the bellows problem since the problems with specified axial displacement could not be solved directly with the AVCO code. Kraus outlined a procedure by which the AVCO code could be used to solve these problems. However, it involved two applications of the code plus some hand computations and he did not feel that it was worthwhile.

A comparison of the results obtained with the MOLSA code was made with a theoretical analysis made by Hetenyi and Timms for a welded bellows.[A-34] Their approach was to analyze a half corrugation of the bellows using shallow-shell theory. The MOLSA code was used to solve the problem corresponding to Case 1 of their numerical results. A comparison of the meridional and circumferential surface stresses is presented in Figures A-10 through A-13.

To determine whether the MOLSA code was capable of analyzing corrugated diaphragms, the Grover-Bell diaphragm was analyzed. The solutions obtained were compared with the results of Dressler, who solved the problem of the Grover-Bell diaphragm with clamped edges.[A-35] Figures A-14 through A-17 show the comparison of the results obtained by Dressler with those obtained with the MOLSA code for surface stresses in the meridional and circumferential directions.

In addition to the comparison of the solutions obtained by the different programs to specific problems, the programs were compared on the basis of simplicity of input, machine running time, and the inherent accuracy of the approach used. In each of these points, Program MOLSA was superior to the AVCO code. In addition, it was determined that Program MOLSA could be modified to simplify the input further so it could be used by a bellows designer with little computing-machine experience. This would be difficult to do with the AVCO code. On the basis of the comparisons made between the different programs, Program MOLSA was chosen as the best available computer program for the analysis of bellows and diaphragms.

Although the input format of the MOLSA code was quite simple, considerable modifications of the program were made to further simplify the input, to permit machine plotting of the stress results, and to extend the range of applicability of the program. The resulting computing program was used for most of the calculations performed in the earlier stages of the research program, including the analysis of multilayer shells. Program MOLSA was eventually replaced by Program NONLIN for carrying out the theoretical analyses of bellows and diaphragms.

Program NONLIN is fully described in Appendixes B and C. This program, developed by Dr. J. F. Lestingi of Battelle, permits the analysis of both linear and nonlinear axisymmetric deformations of bellows and diaphragms and linear nonsymmetric deformations of bellows and diaphragms.

REFERENCES

(A-1) Stange, K., "Strains in an Annularly Corrugated Diaphragm", Ing.-Archiv, 2, 47-91 (1931) (in German).

(A-2) Clark, R. A., "On the Theory of Thin Elastic Toroidal Shells", J. Math. Phys., 29, 146-178 (October, 1950).

(A-3) Haringx, J. A., "The Rigidity of Corrugated Diaphragms", Appl. Sci. Res., Sect. (a), 2, 299-325 (1950).

(A-4) Novozhilov, V. V., Thin Shell Theory, Translation of 2nd Edition, P. Noordhoff, Ltd., Groningen, The Netherlands (1964).

(A-5) Clark, R. A., "Asymptotic Solutions of a Nonhomogeneous Differential Equation With a Turning Point", Archive Rational Mech. Anal., 12, 34-51 (1963).

(A-6) Clark, R. A., "Asymptotic Solutions of Toroidal Shell Problems", Quart. Appl. Math., 16, 47-59 (April, 1958).

(A-7) Tumarkin, S. A., "Asymptotic Solution of a Linear Nonhomogeneous Second Order Differential Equation With a Transition Point and its Application to the Computations of Toroidal Shells and Propeller Blades", Appl. Math. Mech., 23, 1549-1565 (1959).

(A-8) Dahl, N. C., "Toroidal-Shell Expansion Joints", J. Appl. Mech., 20 (4), 497-503 (December, 1953).

(A-9) Chernykh, K. F., and Shamina, V. A., "Calculation of Toroidal Shells, I", Investigations on Elasticity and Plasticity, 2, So. (3) of the Leningrad Univ. (1963), pp 247. 346 (in Russian).

(A-10) Bulgakov, V. N., Statics of Toroidal Shells, Kiev, Akad, Nauk UKrSSS (1962) (in Russian).

(A-11) Grover, H. J., and Bell, J. C., "Some Evaluations of Stresses in Aneroid Capsules", Proc. of Soc. Exptl. Stress Anal., 5, 125-131 (1948).

(A-12) Laupa, A., and Weil, N. A., "Analysis of U-Shaped Expansion Joints", J. Appl. Mech., ASME Trans., 84, 115-123 (March, 1962).

(A-13) Anderson, W. F., "Analysis of Stresses in Bellows", Part I: Design Criteria and Test Results, Atomics International Rept. NAA-SR-4527 (October 15, 1964).

(A-14) Anderson, W. F., "Analysis of Stresses in Bellows", Part II, Mathematical, Atomics International Report NAA-SR-4527 (May 27, 1965).

(A-15) Winborne, R. A., "Simplified Formulas and Curves for Bellows Analysis", Atomics International Rept. NAA-SR-9849 (August 1, 1964).

(A-16) Sinborne, R. A., "Stress and Elevated Temperature Fatigue Characteristics of Large Bellows", Atomics International (September 15, 1964) (N64-29352).

(A-17) Penny, R. K., "Symmetric Bending of the General Shell of Revolution by Finite Difference Method", J. Mech. Eng. Sci., 3, 369-377 (1961).

(A-18) Budiansky, B., and Radkowski, P. P., "Numerical Analysis of Unsymmetrical Bending of Shells of Revolution", AIAA Journal, 1 (8) (August, 1963).

(A-19) Greenbaum, G. A., "Comments on 'Numerical Analysis of Unsymmetrical Bending of Shells of Revolution'", AIAA Journal, 2 (3), 590-592 (March, 1964).

(A-20) Sepetoski, W. K., et al., "A Digital Computer Program for the General Axially Symmetric Thin-Shell Problem", ASME Trans., 84, 655-661 (1962).

(A-21) Kraus, H., "A Review and Evaluation of Computer Programs for the Analysis of Stress in Pressure Vessels", Welding Research Council Bulletin 119 (January, 1967).

(A-22) Bell Aerosystems Co., "A Study of Zero Gravity Positive Expulsion Techniques", Rept. No. 8230-933004 (June, 1963) (N63-19964).

(A-23) Stricklin, J. A., et al., "Large Elastic, Plastic, and Creep Deflections of Beams and Axisymmetric Shells", AIAA Journal, 2 (9), 1613-1620 (September, 1964).

(A-24) Wildhack, W. A., et al., "Investigations of the Properties of Corrugated Diaphragms", ASME Trans., 79 (1), 65-82 (January, 1957).

(A-25) Galletly, G. D., and Radok, J.R.M., "On the Accuracy of Some Shell Solutions", ASME Trans., 81, 577-583 (December, 1959).

(A-26) Collatz, L., The Numerical Treatment of Differential Equations, Springer Verlag, Berlin, 3rd Edition (1960).

(A-27) Kalnins, A., "Analysis of Shells of Revolution Subjected to Symmetrical and Nonsymmetrical Loads", ASME Trans., 86, 467-476 (September, 1964).

(A-28) Goldberg, J. E., Bogdanoff, J. L., "Static and Dynamic Analysis of Nonuniform Conical Shells Under Symmetrical and Unsymmetrical Conditions", Ballistic Missile and Aerospace Technology, pp 19-238 (August, 1961) Academic Press.

(A-29) Mirabal, J. A., and Dight, D. G., "SOR-II, A Program to Perform Stress Analysis of Shells of Revolution", General Electric Company Rept. KAPL-M-EC-19, UC-32 (June 1, 1962).

(A-30) Cohen, G. A., "Computer Analysis of Asymmetrical Deformation of Orthotropic Shells of Revolution", AIAA Journal, 2 (5), 932-934 (May, 1964).

(A-31) Kalnins, A., and Lestingi, J. F., "On Nonlinear Analysis of Elastic Shells of Revolution", ASME Trans., Vol. 34, Series E, No. 1, 59-64 (March, 1967).

(A-32) Turner, C. E., and Ford, H., "Stress and Deflection Studies of Pipeline Expansion Bellows", Proc. Inst. Mech. Eng., 171 (15), 526-552 (1957).

(A-33) Friedrich, C. M., "Seal-Shell-II – A Computer Program for the Stress Analysis of a Thick Shell of Revolution With Axisymmetric Pressures, Temperatures and Distributed Loads", WAPD-TM-398, December, 1963.

(A-34) Hetenyi, M., and Timms, R. J., "Analysis of Axially Loaded Annular Shells With Applications to Welded Bellows" (J. Bas. Eng.), ASME Trans., 82, 741-753, 753-755 (September, 1960).

TABLE A-1. COMPARISON OF MOLSA CODE RESULTS WITH AVCO CODE RESULTS FOR THE STRESS RESULTANTS IN AN OMEGA-JOINT BELLOWS UNDER AXIAL LOADING

Angle, φ	Transverse Stress Resultants, Q	Meridional Resultants N_φ	Meridional Resultants M_φ	Circumferential Resultants N_θ	Circumferential Resultants M_θ
MOLSA Code					
0	0	4.95	0.163	-142.3	0.049
21	-1.878	6.06	-0.189	-157.9	-0.057
42	-2.510	9.10	-1.089	-115.6	-0.317
63	0.707	10.12	-1.571	100.4	-0.427
85	5.026	3.07	0.447	323.0	-0.053
106	3.493	-7.68	1.350	246.7	0.474
127	-1.575	-11.41	1.711	-9.6	0.536
148	-3.947	-9.18	0.622	-80.6	0.184
169	-5.950	-7.01	-1.159	-2.1	-0.348
AVCO Code, 80 Mesh Points					
0	-2.1×10^{-7}	4.95	0.139	-145.1	0.042
21	-1.919	6.08	-0.224	-157.1	-0.067
42	-2.430	9.03	-1.076	-110.3	-0.312
63	0.785	9.96	-1.483	104.6	-0.400
85	5.050	2.81	0.429	318.3	-0.050
106	3.493	-7.67	1.273	238.1	0.450
127	-1.427	-11.21	1.678	-8.6	0.527
148	-3.925	9.17	0.645	-76.5	0.191
169	-5.972	-7.01	-1.028	-2.1	-0.309
AVCO Code, 400 Mesh Points					
0	2.1×10^{-7}	4.95	0.159	-142.9	0.048
21	-1.888	6.06	-0.196	-157.8	-0.059
42	-2.496	9.09	-1.086	-114.5	-0.316
63	0.723	10.08	-1.554	101.3	-0.421
85	5.031	3.01	-0.443	322.2	-0.052
106	3.492	-7.68	1.335	245.0	0.469
127	-1.547	-11.37	1.705	-9.5	0.534
148	-3.943	-9.18	0.627	-79.9	0.185
169	-5.952	-7.01	-1.133	-2.1	-0.340

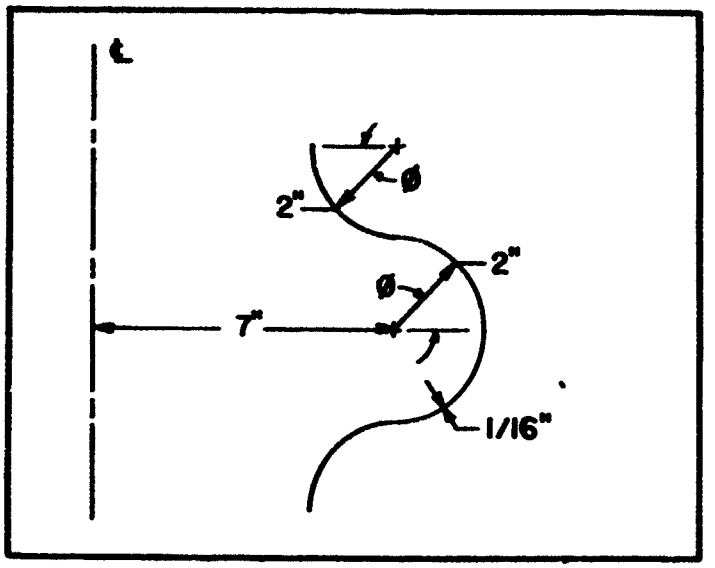

Bellows A

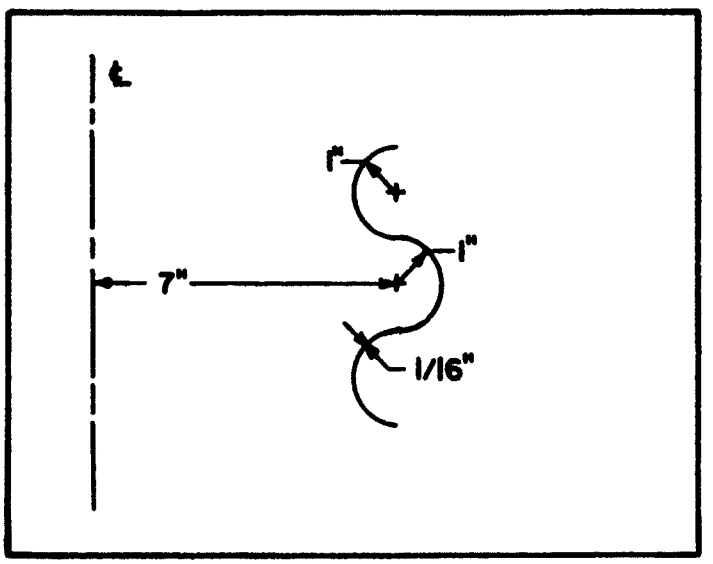

Bellows D

FIGURE A-1. CROSS SECTION OF BELLOWS A AND BELLOWS D CONSIDERED BY TURNER AND FORD

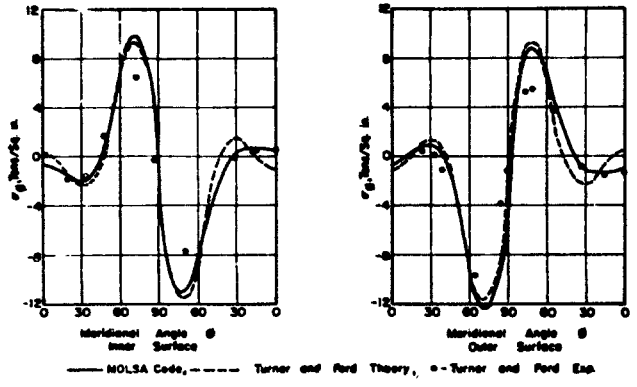

FIGURE A-2. COMPARISON OF MOLSA CODE RESULTS WITH THEORETICAL AND EXPERIMENTAL RESULTS OF TURNER AND FORD FOR MERIDIONAL SURFACE STRESSES IN BELLOWS A FOR A 1-TON AXIAL LOAD

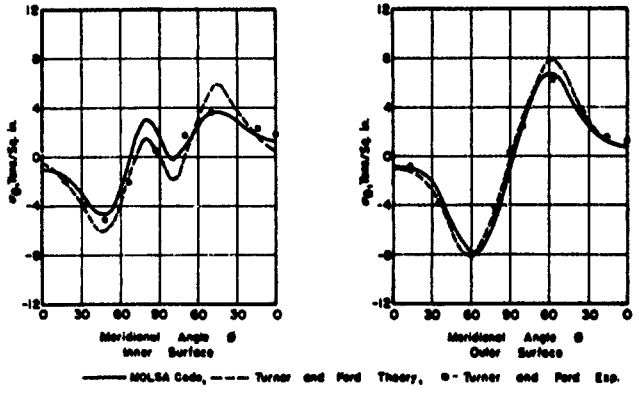

FIGURE A-3. COMPARISON OF MOLSA CODE RESULTS WITH THEORETICAL AND EXPERIMENTAL RESULTS OF TURNER AND FORD FOR CIRCUMFERENTIAL SURFACE STRESSES IN BELLOWS A FOR A 1-TON AXIAL LOAD

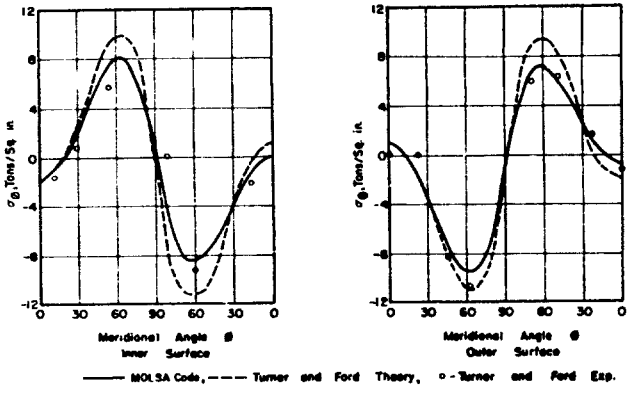

FIGURE A-4. COMPARISON OF MOLSA CODE RESULTS WITH THEORETICAL AND EXPERIMENTAL RESULTS OF TURNER AND FORD FOR MERIDIONAL SURFACE STRESSES IN BELLOWS D FOR A 1-TON AXIAL LOAD

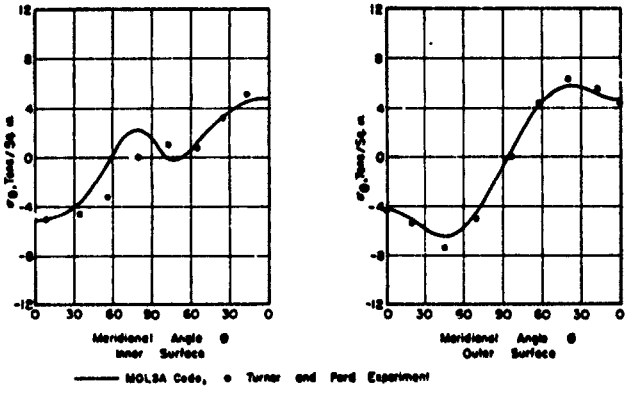

FIGURE A-5. COMPARISON OF MOLSA CODE RESULTS WITH EXPERIMENTAL RESULTS OF TURNER AND FORD FOR CIRCUMFERENTIAL SURFACE STRESSES IN BELLOWS D FOR A 1-TON AXIAL LOAD

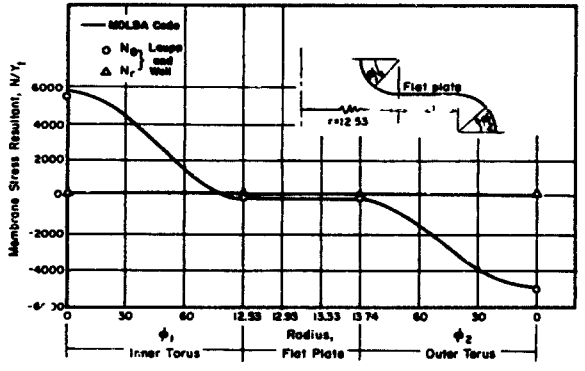

FIGURE A-6. MEMBRANE STRESS RESULTANTS FOR U-SHAPED BELLOWS UNDER AXIAL TENSILE FORCE

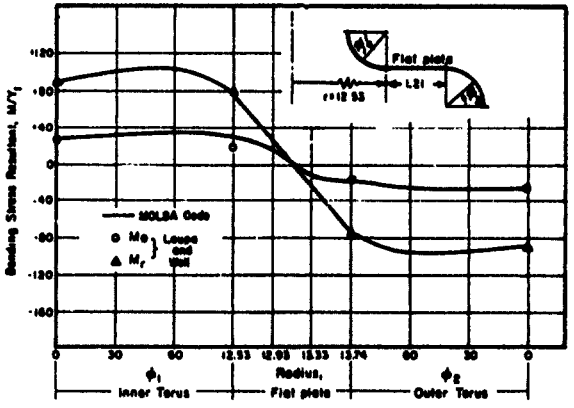

FIGURE A-7. BENDING STRESS RESULTANTS FOR U-SHAPED BELLOWS UNDER AXIAL TENSILE FORCE

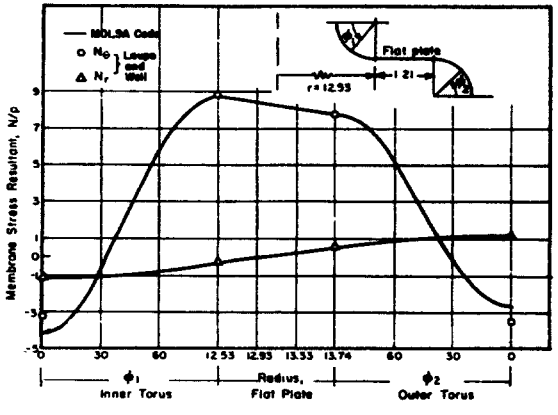

FIGURE A-8. MEMBRANE STRESS RESULTANTS FOR U-SHAPED BELLOWS UNDER INTERNAL PRESSURE

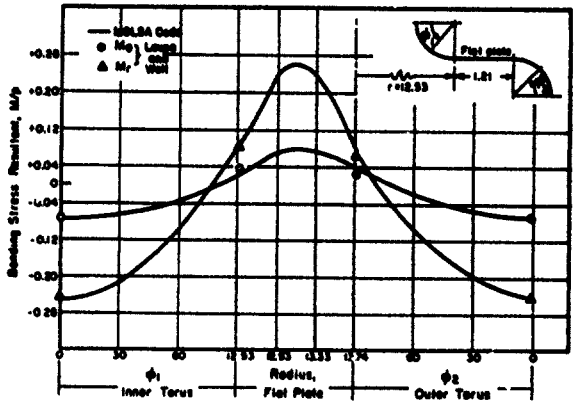

FIGURE A-9. BENDING STRESS RESULTANTS FOR U-SHAPED BELLOWS UNDER INTERNAL PRESSURE

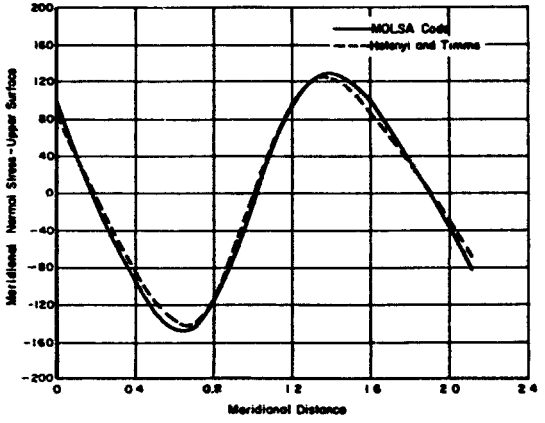

FIGURE A-10. COMPARISON OF MOLSA CODE RESULTS WITH RESULTS FROM HETENYI AND TIMMS CASE 1; MERIDIONAL STRESS ON UPPER SURFACE

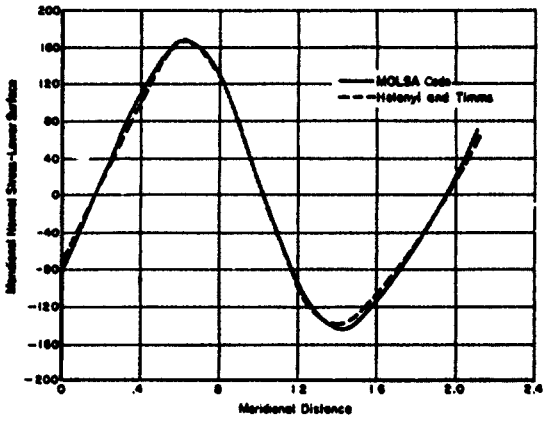

FIGURE A-11. COMPARISON OF MOLSA CODE RESULTS WITH RESULTS FROM HETENYI AND TIMMS CASE 1; MERIDIONAL STRESS ON LOWER SURFACE

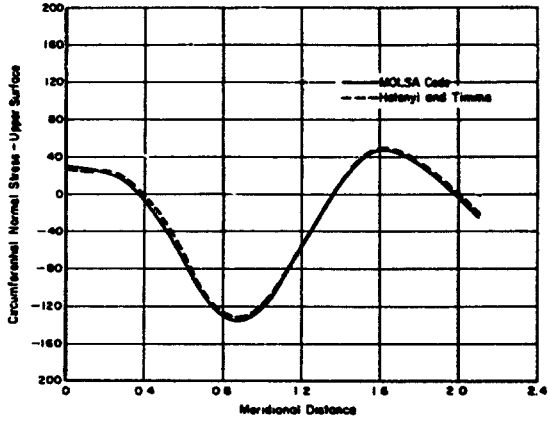

FIGURE A-12. COMPARISON OF MOLSA CODE RESULTS WITH RESULTS FROM HETENYI AND TIMMS CASE 1; CIRCUMFERENTIAL STRESS ON UPPER SURFACE

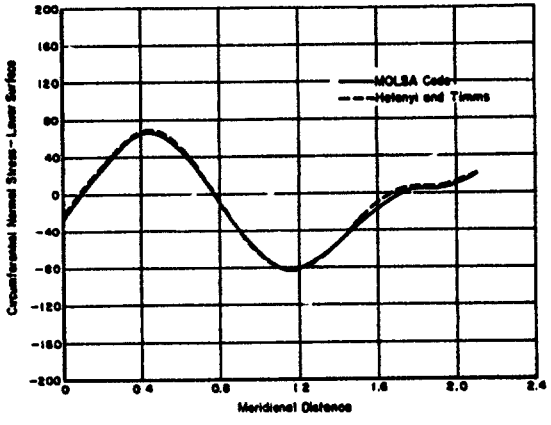

FIGURE A-13. COMPARISON OF MOLSA CODE RESULTS WITH RESULTS FROM HETENYI AND TIMMS CASE 1; CIRCUMFERENTIAL STRESS ON LOWER SURFACE

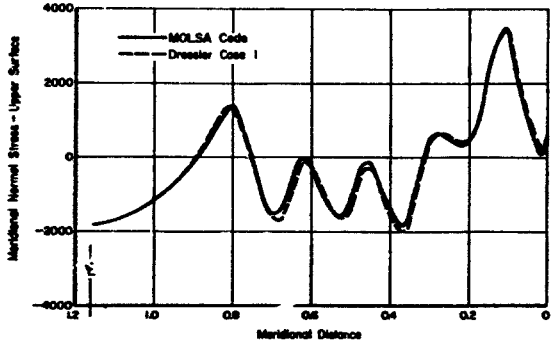

FIGURE A-14. COMPARISON OF MOLSA CODE RESULTS WITH RESULTS FROM DRESSLER CASE 1; MERIDIONAL STRESS ON UPPER SURFACE

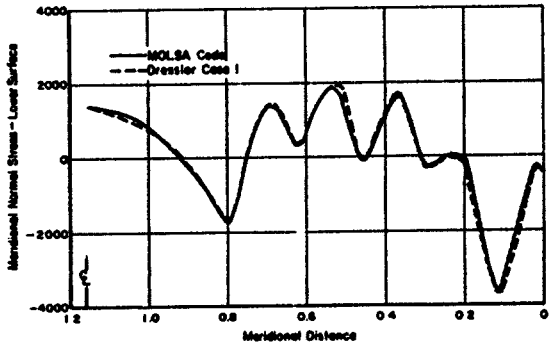

FIGURE A-15. COMPARISON OF MOLSA CODE RESULTS WITH RESULTS FROM DRESSLER CASE 1; MERIDIONAL STRESS ON LOWER SURFACE

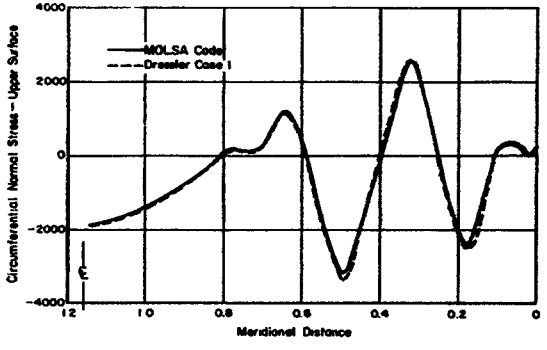

FIGURE A-16. COMPARISON OF MOLSA CODE RESULTS WITH RESULTS FROM DRESSLER CASE 1; CIRCUMFERENTIAL STRESS ON UPPER SURFACE

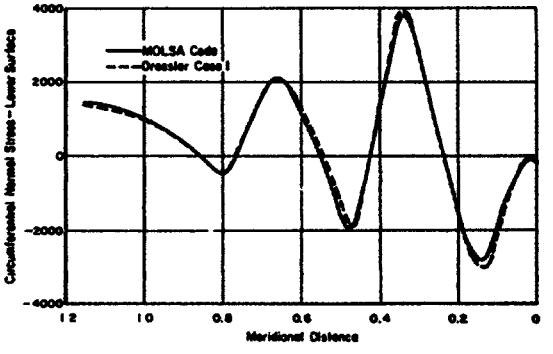

FIGURE A-17. COMPARISON OF MOLSA CODE RESULTS WITH RESULTS FROM DRESSLER CASE 1; CIRCUMFERENTIAL STRESS ON LOWER SURFACE

APPENDIX B

DESCRIPTION OF COMPUTING PROGRAM NONLIN

ABBREVIATIONS AND SYMBOLS

T	Average minimum radius of curvature, in.
h	Bellows thickness, in.
w	Displacement in direction of normal to shell midsurface, in.
Q	Effective shear resultant force in direction normal to the shell, lb/in.
u_ϕ	Displacement in meridional direction, in.
N_ϕ	Meridional membrane resultant force, lb/in.
β_ϕ	Angle of rotation of the bellows normal in the meridional direction, deg
M_ϕ	Meridional bending moment resultant, in-lb/in.
u_θ	Displacement in the circumferential direction, in.
N	Effective shear resultant in circumferential direction, lb/in.
α	Angle of rotation between the coordinate directions "one" and "two" and the meridional and normal directions at the end of the bellows, deg
u_1, u_2	Boundary displacements in the 1 and 2 directions, in.
Q_1, Q_2	Boundary resultant forces in the 1 and 2 directions, lb/in.
n	Direction of normal to bellows midsurface
t_ϕ	Tangential direction to bellows midsurface in meridional plane
a, b, c	Dimensional parameters for shell segments
ϕ	Angle between normal to bellows surface and its axis of revolution, deg
S	Meridional arc length along bellows or bellows segment, in.
Δ_m	Deflection imposed on the mathematical model, in.
Δ_t	Deflection imposed on total live length of actual bellows, in.
e_ϕ	Surface strain in the meridional direction, in./in.
e_θ	Surface strain in the circumferential direction, in./in.

APPENDIX B

DESCRIPTION OF COMPUTING PROGRAM NONLIN

This appendix is intended for those who plan to use the computing program NONLIN for the analysis of composite shells of revolution. In this work, a composite shell is defined as a shell composed of a number of distinct parts which may have the following shapes: cylindrical, spheroidal, ellipsoidal, paraboloidal, conical, or toroidal. The procedures to be discussed will be as general as possible so that the bellows designer can make maximum use of the full capability of the program. The appendix is divided into two parts: B-I – NONLIN Manual; B-II – Analysis Procedure for Bellows.

Program NONLIN was written in FORTRAN IV language for the CDC 6400. It is believed that this program should be easily converted to run on any machine with a FORTRAN IV compiler and a 32,000-word storage. By reduction of the size of the dimension statements it may be possible to implement the program on smaller machines.

B-I. NONLIN Manual

a. Shell Parts
b. Shell Segments
c. Loads
d. Sign Convention for Fundamental Variables
e. Boundary Conditions and Boundary Rotation Angles
f. Meridional Coordinate and Integration Direction
g. Variable-Thickness Data.

B-I-a. Shell Parts

In order to describe the composite shell, the user must divide it into a number of parts. Table B-1 shows the distinct shell types that are available in the GOMTRY subroutine to model the parts. Figure B-1 shows a 3-part composite shell. These shapes are described in detail in Figures B-2 through B-8. Since the shell parts are indicated on the input cards by name, the spelling given in the right-hand column of Table B-1 must be used on the input cards.

An incorrect spelling of any of the shell types given in Table B-1 will result in a termination of the reading of the input. The maximum number of parts allowed in this program is 60.

B-I-b. Shell Segments

Since the method used in this program is based on initial-value integration of the governing differential equations over sufficiently short segments of the shell part, the

midsurface of each part must be divided into an appropriate number of equal segments. The number of segments in a part is determined from the following relationship:

$$\text{number of segments} = \frac{\text{arc length of PART}}{3\sqrt{Th}}$$

where

T = the average minimum radius of curvature

h = average wall thickness.

The maximum number of segments allowed in this program is 60. If the number of segments called for in the different parts totals more than 60, no calculations will be performed. The user must then decide on a new mathematical model. However, the cases in which 60 segments are needed are rare.

B-I-c. Loads

The distributed loads allowed for in this program are normal pressure (pounds per square inch), unit weight* of the shell material (pounds per cubic inch), and dead weight* acting on the shell (pounds per square inch). When analysis is made for unit-weight and dead-weight loadings, the shell centerline must be vertical. These quantities must be constant over the entire part.

Boundary loadings can also be specified at the initial and final edge of the composite shell. Forces, displacements, moments, or slopes can be specified at the boundaries. See B-I-e for a complete description regarding the manner in which these quantities must be specified.

B-I-d. Sign Convention for Fundamental Variables

The fundamental variables used in this program are the variables which appear on the boundary of the rotationally symmetric shell. These variables are

w = displacement along normal to middle surface, in.

Q = effective shear resultant in w direction, lb/in.

u_ϕ = meridional displacement of middle surface, in.

N_ϕ = meridional membrane resultant, lb/in.

β_ϕ = angle of rotation of the normal in meridional direction, radians

M_ϕ = meridional moment resultant, in-lb/in.

u_θ = circumferential displacement of middle surface, in.

N = effective shear resultant in u_θ direction, lb/in.

*In general, the unit weight and dead weight for bellows and diaphragms can be specified as zero.

The positive directions of these quantities are shown in Figure B-9 for a shell segment which has a normal pointing away from the center of curvature. Figure B-10 gives the positive directions of the fundamental variables for a shell segment which has a normal pointing toward the center of curvature.

B-I-e. Boundary Conditions and Boundary Rotation Angles

Boundary Conditions. Boundary conditions at the initial and final ends of the shell are prescribed by specifying the type of boundary condition by name and specifying its numerical value. For axisymmetric deformation, three boundary conditions must be given; for nonsymmetric deformation, four boundary conditions are required. When the prescribed boundary forces or displacements are directed along the normal and tangent to the shell surface at the boundary, the variables that must be considered are the fundamental variables, w, Q, u_ϕ, N_ϕ, β_ϕ, M_ϕ, u_θ, N. In some cases, it may be necessary to specify the boundary conditions in terms of displacements and forces which are not directed along the normal and tangent to the shell at the boundary but along some other directions (designated the 1 and 2 axes). When this case occurs, the variables which must be considered are: u_1, Q_1, u_2, Q_2, β_ϕ, M_ϕ, u_θ, and N. These boundary variables, along with the names used to designate them on the input cards, are given in Table B-2.

Specification and Boundary Conditions. In order to accurately specify the boundary conditions for a shell of revolution, only certain combinations of the boundary variables may be used. Table B-3 shows the boundary variables separated into two columns according to whether they relate to displacements or forces.

The specification of the boundary conditions requires that only one quantity be chosen from each row. For an axisymmetrically loaded shell, Row 4 need not be considered. Examples of common-type boundary conditions are given in Figure B-11 along with the variables which must be prescribed.

Boundary Rotation Angle. When the prescribed variables are along the normal and tangent to the shell surface at the boundary, the boundary rotation angle is zero. For example, see Figure B-11(a), (b), (d), and (f). To determine the boundary rotation angle when the prescribed variables are not along the normal and tangent to the shell surface, but along the 1-2 axes [see Figure B-11(c) and (e)], the following procedure can be used. Assume that the boundary condition at the initial edge of the shell is that shown in Figure B-12(a). The support allows movement of the composite shell edge along the A-A axis but does not allow any movement along the B-B axis. The support is not capable of supporting any meridional bending moment. The first step in determining the proper angle is to sketch a boundary support in which the boundary rotation angle is zero. One such possibility is shown on the left side of Figure B-12(b). Note that the normal and tangential directions have also been indicated by n and t_ϕ. These directions are fixed by the choice of the direction of integration. Next, associate the 1 axis with the n direction and the 2 axis with the t_ϕ direction. Then rotate the support to the position actually required as shown in Figure B-12(a). At the same time, allow the 1-2 axes to rotate with the support. By doing this, the final position of the 1-2 axes will be as shown in Figure B-12(b). The boundary rotation angle is α_i and it is

defined to be negative since the direction of rotation is in the same direction as the integration. It is now necessary to determine which boundary variables are known. An examination of Figure B-12(b) shows that the displacement in the 1 direction is zero, so $u_1 = 0$ while the force in the 2 direction is zero, so $Q_2 = 0$.

The support shown in Figure B-12(a) can be obtained from a second boundary support which is shown on the left side of Figure B-12(c). The normal, tangent, and 1-2 directions are again indicated. The rotation of the support must now be made in a counterclockwise direction until the 1 axis is coincident with the A-A axis. The sign convention makes this angle α_i positive. Now, however, the force in the 1 direction is zero, thus $Q_1 = 0$, while the displacement in the 2 direction is zero, thus $u_2 = 0$.

In considering the final edge of the shell, the same sign convention introduced above is used. In order to show the latitude one has in defining boundary rotation angles, the boundary condition shown in Figure B-13(a) will be considered in detail. The support shown in Figure B-13(a) is skewed with respect to the n-t_ϕ axes. Figure B-13(b) indicates one possibility of rotating a zero-degree boundary angle to the desired position. The angle is negative since the rotation in this case is in the same direction as the integration, the displacement $u_1 = 0$, and the force $Q_2 = 0$. A second possibility for obtaining the correct boundary condition is shown in Figure B-13(c). Note that the angle is negative but $Q_1 = 0$ and $u_2 = 0$. The third possibility makes use of the same support shown in Figure B-13(c). However, in this case the rotation is counterclockwise. This produces a positive boundary rotation angle. Although the support shown on the right-hand side of Figure B-13(d) is pictorially different from that shown in Figure B-13(a), it has the same support characteristics.

Restrictions on Specification of Boundary Conditions. For axisymmetric loadings (i.e., when the Fourier harmonic n = 0), the displacement parallel to the shell centerline must be prescribed at the initial edge.

For nonsymmetric deformations (Fourier harmonic n = 1), the displacement perpendicular to the shell centerline must be prescribed at the initial edge.

B-I-f. Meridional Coordinate and Integration Direction

The independent coordinate used in this program is either the distance s shown in Figures B-2, B-6, and B-8 which is measured along the meridion or the angle ϕ which is measured between the normal and the axis of symmetry of the composite shell. The s coordinate is used only for the CYLINDRICAL, CONICAL, and VARCYLINDER parts. All other parts are described by the angle ϕ.

After the shape of the mathematical model is set up, the initial and final coordinates and radii* of each part must be obtained. These quantities depend on the choice of the direction of the positive normal as well as the direction of integration. The basic concept used in determining these quantities is that within any one part, the normal to the shell middle surface must be continuously turning. This implies that the angle which the normal makes with the axis of symmetry of the shell can increase, decrease, or

*Definitions of those parameters for each type of part are given in Figures B-2 through B-8. To simplify the input, the length of the cylindrical and conical shell parts has been identified as "b" and is thus referred to as a "radius".

remain constant at any point in the shell part. On moving from part to part, the only restriction is that the middle surface be continuous. It is not necessary, however, that the tangent to the shell middle surface be continuous.

Several examples will be shown to demonstrate the manner in which the radii and coordinates are obtained. A composite shell which is composed of 5 parts is shown in Figure B-14. In most cases* the user has the option to choose either end of the shell as the initial edge. In this example, the initial edge is chosen at point A so that the direction of the 0-90-180-270 axes are as shown in Figure B-14. The normal on the first shell part must be chosen to point away from the shell axis of revolution. For Part 1 (VARCYLINDER), the angle which the normal makes with the centerline of the shell is 90.0 degrees. The radius "a" for a VARCYLINDER part is always positive and is GA in this case. The length of the shell is AB and is indicated as "b" in the table in the lower part of Figure B-14.

On proceeding to Part 2 (CØNICAL), the concept of the continuously turning tangent must now be used to determine the angle which the normal makes with the centerline of the shell. Note that at B the shell surface is continuous, but that the tangent to the shell surface is discontinuous. In this case, the continuously turning tangent can best be understood if one imagines that Parts 1 and 2 are connected by a small radius part (auxiliary part) which provides a continuous tangent to the shell surface in going from Part 1 to 2. Then as the normal moves across this auxiliary part, the motion will be in a counterclockwise direction, which in this case means that the angle is decreasing. Eventually, the normal would move from Part 1 across the auxiliary part and on to Part 2. At this time the angle would be 50.0 degrees as noted in Figure B-14. For a CØNICAL part, only one angle is necessary, as indicated in Figure B-6. The radius "a" for Part 2 is HB, the distance from the centerline of the shell to the initial edge of the part. This value is always positive. The length of the part BC is indicated as radius "b" in Figure B-14.

On moving to Part 3 (SPHERØIDAL), the normal makes an angle of 50.0 degrees with the centerline at Point C since the slope of the shell surface at C is continuous. As the normal is moved along Part 3, it begins to rotate in a clockwise direction, which indicates that the angle is increasing. It finally reaches Point D where the magnitude of the angle is 75.0 degrees. The radius of this part is +JC since the normal points away from the Center of Curvature J.

On entering Part 4 (TØRØIDAL), the normal starts to rotate counterclockwise. On reaching Point E (end of Part 4), the normal makes an angle of 20.0 degrees with the horizontal. Thus, for Part 4, the initial coordinate is 75.0 degrees and the final coordinate is 20.0 degrees. The radius "a" for Part 4 is the vertical distance ML. The radius "b" is -KD since the normal is pointing toward the Center of Curvature K.

In order to move from Part 4 to Part 5 (CØNICAL), imagine that an auxiliary part connects the two parts such that the normal is continuously turning. This would show that the normal would be rotating in a clockwise direction across the auxiliary part, with the angle at the beginning of the auxiliary part being 20.0 degrees and that at the end being 130.0 degrees. Thus, the initial coordinate for Part 5 would be 130.0 degrees. Since Part 5 is CØNICAL, the distance "a" is measured from the initial edge of the part to the centerline of the composite shell. This distance is ON. The length, "b", of the part is EF.

*See restrictions in B-I-e

As mentioned previously, the user can usually specify either end of the shell as the initial edge. To demonstrate the differences in describing the mathematical model when the initial edge is at Point A, which is now at the right-hand side of the shell, Figure B-15 has been prepared. The initial and final coordinates and radii are given in the lower portion of Figure B-15.

A six-part composite shell is shown in Figure B-16. The initial edge of the shell is taken at A so that the integration is from A to G. The coordinates and radii for this shell are given in Figure B-16. The angle for Part 1 is 180.0 degrees since the integration is toward the centerline of the shell. The "a" distance is JK since Point A represents the initial edge of the part.

The initial angle for Part 2 is 220.0 degrees since the auxiliary part which connects Parts 1 and 2 would cause the normal to rotate in a clockwise direction. In going from B to C, the angle would start to decrease. The angle in fact becomes 120.0 at Point C. The radius BI is negative since the normal points towards the Center of Curvature I.

The angle for Part 3 becomes 150.0 degrees since the normal rotates 30.0 degrees clockwise in going from C on Part 2 to C on Part 3. The "a" dimension for Part 3 is NO.

To determine the angle for Part 4, imagine that the normal "turns the corner" in a counterclockwise direction at Point D. This causes the angle to decrease to its value of 20.0 degrees on Part 4. The radius "a" for Part 4 is DP while the length "b" is DE.

In going from Point E on Part 4 to Point E on Part 5, the normal turns counterclockwise, which indicates that the angle is decreasing. The angle passes through 0.0 degrees to its value of -30.0* at Point E on Part 5. As the normal moves along Part 5 from E to F, it executes a clockwise movement. Thus, the angle is increasing. It reaches the value of 120.0 degrees at Point F on Part 5. The radius "a" for Part 5 is QR while the radius "b" is +EH since the normal is pointing away from the Center of Curvature H.

In going from Point F on Part 5 to Point F on Part 6, the normal turns counterclockwise. The angle for Part 6 is 0.0 degrees. The "a" distance is ST, while the length "b" is FG.

Figure B-17 shows the same shell discussed in Figure B-16. The initial edge is taken on the right side of the shell. The initial and final coordinates and radii are given in the table in the lower portion of Figure B-17.

B-I-g. Variable-Thickness Data

When a shell part has a variable-thickness distribution, data must be prescribed in one of two ways, depending on the shell type. For the VARCYLINDER and CØNICAL types, imagine that the thickness distribution for the part is that shown in Figure B-18. The shell part is assumed to have b = 0.6 inch. For example, this part can be either the VARCYLINDER, Part 1 in Figure B-14, or the CØNICAL, Part 3 in Figure B-16. Notice that even though these parts are described by giving their lengths b, it is necessary to prescribe one s coordinate for every thickness value. When specifying variable-thickness data, the first point is always s = 0 and the last point s = b.

*Note that the angle must have continuous variation except at points of discontinuity. Thus, the angle is allowed to become negative here after passing through zero instead of being incremented by 2π.

Figure B-19 shows variable-thickness data for the TØRØIDAL Part 5 of Figure B-16. For all shell parts which use ϕ as the independent coordinate, the variable-thickness data must be prescribed as shown in the tabulation in Figure B-19. Notice that the first thickness value is given at $\phi_{initial}$ = -30.0 degrees and the last thickness value is given at ϕ_{final} = 120.0 degrees.

The present program allows 10 values to be prescribed per part.

B-II. Analysis Procedure for Bellows

This part of Appendix B is intended to give the bellows designer a nontechnical description of the procedure for analyzing formed and welded bellows and diaphragms. A prior knowledge of the contents of Appendixes A and C and the first part of Appendix B is not needed to understand this section. However, a reading of Appendix A, for a general background of bellows and diaphragm analysis, and of the first part of this appendix is recommended to obtain a greater understanding of the multisegment-analysis approach.

This discussion of the analysis procedure is divided into the following parts:

a. Preparation of Bellows Cross Section
b. Measurement of x-y Coordinates and Thicknesses
c. Preparation of the Mathematical Model
d. Input Preparation for Program NONLIN
e. Description of Computer-Output Sheets
f. Item-by-Item Description of Input Data
g. Item-by-Item Description of Output Data.

The descriptions are related to the analysis of formed bellows. In particular the preparation of the input data and the output data obtained for the analysis of the 3-inch formed bellows JL68 is described. The results of the analysis of this bellows were reported in Appendix E.

Although the discussion is primarily related to formed bellows, it is believed that much of the discussion is applicable to the preparation of input data for welded bellows and diaphragms. The differences between the usual description of boundary conditions for welded and formed bellows are discussed.

B-II-a. Preparation of Bellows Cross Section

To obtain geometric measurements for use in preparing the mathematical model of a fabricated bellows, the procedure developed in the research program requires encapsulation of the specimen in a hard plastic, cross sectioning the block after curing, and polishing one-half of the cross-sectioned block. The details of this procedure are given in Appendix P.

B-II-b. Measurement of x-y Coordinates and Thicknesses

According to the assumptions of thin-shell theory, a bellows can be completely described by finding the exact shape of the midsurface of the bellows wall and the wall thickness at each point of the bellows. The first step of the procedure developed for determining both bellows shape and the thickness involves making hardness impressions along the bellows convolutions with a Tukon microhardness tester or similar instrument. These indentations, which are carefully made in the center of the bellows wall, provide benchmarks for measuring the cross-section shape of the bellows. Appendix P describes the method of making these impressions and of making precision measurements of the x-y coordinates of each benchmark. The thickness of the specimen wall is also measured at each benchmark.

The number of convolutions which should be measured depends on the uniformity of the bellows. If the bellows convolutions are as uniform as those shown in Figure E-2 for bellows JD68, then measurements need be made only for one-half of one convolution. Since this bellows was one of the first analyzed in this program, measurements of the x-y coordinates and of the thickness were made for the entire convolution to check the symmetry of the convolution. In this case, the convolution was very nearly symmetrica so that the measurements were averaged and dimensions for only "one-half" of the convolution were considered in the mathematical model. Table E-1 gives the x-y coordinates for each benchmark for JD68 with respect to a fixed reference point (see Appendix E for details) and the thickness measured at each benchmark.

If the bellows has nonuniform convolutions such as those shown in Figure B-20, then it is necessary to measure a sufficient number of convolutions to represent the bellows. In the analysis of this bellows, three convolutions were measured and considered in the mathematical model.

For a welded bellows, at least two leaves must be measured since the upper and lower leaves of a convolution do not have the same shape. Figure B-21 shows the cross section of a 3-inch single-ply AM-350 welded bellows. In this case two complete convolutions were indented and measured. The results for the upper leaves were averaged as were the results for the lower leaves. Note that the outermost and innermost impressions were approximately in the center of the weld bead. The placing of the impressions at these points facilitates the construction of the mathematical model.

In general, the spacing of the benchmarks should be adjusted to the shape being measured. A sufficient number of points are required to describe the convolution shape Generally, the spacing should be about 0.010 inch. In curved areas, the spacing may be as small as 0.002 inch, while in flat areas it may be as large as 0.030 inch. The thickness should be measured within ±0.00001 with a Vickers image-splitting measuring eyepiece mounted in a conventional compound microscope. Any equivalent measuring apparatus can be used for the thickness measurements. Experience during this program indicates that a filar eyepiece can also be used. However, the accuracy obtained with this eyepiece depends on the ability of the operator to align the cross hair along the edge of the specimen wall.

In addition to the measurements described above, the distance from the axis of the bellows to the origin of the x-y coordinate system is required.

B-II-c. Preparation of the Mathematical Model

Once the measurements for the convolution have been made and tabulated, for example, as in Table E-1 (3-inch single-ply formed bellows), Table F-1 (1-inch single-ply formed bellows), and Table H-1 (3-1/2-inch single-ply welded bellows), the mathematical model can be prepared.

The measurements are first plotted on standard graph paper. For bellows of the size considered in this program, it was found that the scale should be approximately 0.010 inch per inch. This scale sometimes requires sheets 11 by 17 in. or larger. After the points are plotted, a continuous curve is drawn through the points with a French curve.

The next step is to divide this curve into a number of distinct parts of the type listed in Table B-1 and described in Figures B-2 through B-8. This procedure requires some judgment on the part of the analyst. It has been found that toroidal and conical parts are sufficient to represent even the most irregular bellows shapes. Accurate determination of the radii of the toroidal parts usually requires a trial-and-error procedure in which overlays of different radii are fitted to each part. Examples of some mathematical models obtained in this way are shown in Figures E-3, F-4, H-3, and H-4. These figures were plotted after the coordinates and radii were obtained from much larger drawings.

The initial and final coordinates, $\phi_{initial}$ and ϕ_{final}, and the radii "a" and "b" described in Figures B-2 through B-8 must then be measured from the mathematical model. Linear and angular measurements should be made within ±0.0005 inch and ±0.50 degree, respectively. This information should then be tabulated in a manner similar to that shown in Tables E-2, F-2, and H-2.

Variable-Thickness Data. To determine the input quantites for the variable thickness, the thickness is plotted as shown in Figure E-3 for the 3-inch single-ply bellows JD68. The independent variable in this figure is the radial distance from the root to the crown. However, this dimension cannot be used as input data. As outlined in B-I-g, VARCYLINDER and CØNICAL parts require the specification of the thickness as a function of the distance s, which is the meridional arc length measured from the beginning point of the part, and the angle ϕ is used as the independent coordinate of other parts (see B-I-g).

If the thickness varies linearly over the meridional length of a part, then it is necessary to specify the thickness only at the end points of the part since the computer program automatically interpolates linearly for the thickness between any two data points. In this case the independent coordinates of the thickness-data points are s = 0 and s = b for the CØNICAL and VARCYLINDER parts where b is the shell length of the part. The independent coordinates for the thickness-data points for TØRØIDAL parts would be $\phi_{initial}$ and ϕ_{final} for the case where the thickness varies linearly along the TØRØIDAL part.

In some instances, the measured thickness variation along the part cannot be represented accurately with a linear variation of distance over the full length of the part. In such cases it is necessary to represent the thickness variation as a piecewise linear function within the part. This requires establishing thickness-data points at intermediate points of the part as well as at the end points of the part. While the thickness

values are obtained directly from a thickness plot such as Figure E-4, the related values of s or ϕ must be established for the data points. This determination may be done graphically by plotting the points on the cross section of the bellows. Then for an intermediate point of a conical part, the value of s is obtained by measuring the distance of the point from the initial point of the part (remembering that s = 0 at the initial point of the cone or cylinder). For a TØRØIDAL or other type part for which ϕ is used as the independent coordinate, the angle of the normal to the shell at the plotted point may be carefully measured with a protractor. A second way of determining the appropriate values of s or ϕ would be to substitute the value of the radius of the point measured from the bellows axis into the equation of the part and to solve for the value of s or ϕ. For instance, the equation for the cylindrical radius at any point of a TØRØIDAL part is

$$r = a + b\cos\phi \qquad \text{(B-1}$$

By substituting the values of a, b, and r in the equation, it is possible to find the value of ϕ using tables of the cosine function.

Continuity of Parts. In the preparation of the mathematical model, care must be taken to insure that the information describing the bellows convolution results in a shape which is continuous. To aid the analyst in achieving this goal, an internal program check has been included. This check amounts to calculating the distance from the center line of the specimen to the beginning and end of the part. This is done for all parts and a check is made to see that adjacent parts do not have values, which describe the same point, differing by more than 0.0025 inch. For example, for the shell shown in Figure B-22, the radial distance from the centerline of the shell to Point B on Part 1, denoted by r^1_B (and given by the relation in the lower half of the figure), must be within 0.0025 inch of the radial distance from the centerline of the shell to the initial point on Part 2, denoted by $r^2_B = a_2$. Errors in measuring distances and angles as well as specification of the incorrect signs of the radius "b" will result in subroutine INPUT rejecting the data. An error message will indicate which part has been incorrectly dimensioned.

To determine the correct signs of the angles and radii for formed bellows and diaphragms, it is recommended that the examples in Figures B-14 and B-15 be studied. For welded bellows, Figures B-16 and B-17 give all the details needed to correctly describe the shape.

B-II-d. Input Preparation for Program NONLIN

The input data for Program NONLIN is composed of 12 different data sets:

1. Title cards (3 cards)
2. Boundary-value data at initial edge of shell (1 card)
3. Boundary-value data at final edge of shell (1 card)
4. Rotation angle between shell supports and shell centerline at initial and final edges of shell (1 card)
5. Control set (1 card)

6. **Young's modulus and Poisson's ratio (1 card)**
7. **Loading parameters – pressure, unit weight, and dead weight (1 card)**
8. **Shell type and control information for each part (1 card per part)**
9. **Shell geometrical parameters for each part (1 card per part)**
10. **Variable elastic parameters (1 card per part when the elastic parameters are variable)**
11. **Variable loading parameters (1 card per part when there are different loads on the different parts)**
12. **Variable thickness data (2 to 4 cards per part when the thickness is variable).**

The preparation of these data sets is relatively simple once the mathematical model has been properly prepared and the parameters described in tabular form. Data sheets showing the proper format for the various data sets are shown in Tables B-4 through B-7 for all of the data sets except Sets 10 and 11*. Preparation of these data sheets will be described in sufficient detail in this section so that the bellows designer can learn to prepare these forms for all standard types of bellows and diaphragms. However, it is emphasized that a real understanding of the procedure will usually be acquired only after a number of bellows have been analyzed. A more complete item-by-item discussion of the input data is presented in Section B-II-f for those who must analyze nonstandard shells and those who desire a deeper understanding of the input data.

The data sets will not be discussed here in numerical order but will be considered in certain related groups in the following way. Data Set 1 which allows a 3-card title for each problem is discussed first. Then Data Sets 5, 6, 8, 9, 10, and 12, which determine the shell geometry and elastic constants, will be discussed. Finally, Data Sets 2, 3, 4, 7, and 11, which relate to the loading parameters, will be described.

Each of the input data will be illustrated by giving the input data prepared for the analysis of the 3-inch formed bellows JD68 which was described in Appendix E. The mathematical model prepared for this bellows consisted of six shell parts which modeled one-half of one convolution. This model is illustrated in Figure B-23 which was transposed from Figure E-3 so that the orientation of the axes would be consistent with those in Figure B-22. The integration for this bellows was carried out from the root to the crown for the 3-inch bellows so that the first part is at the root and the sixth part is at the crown of the convolution as shown. The problem for which the input data will be illustrated involves axial compression of the 10-convolution bellows by 0.060 inch.

Data Set 1. Title Cards. Three free-field title cards have been incorporated in the program input to permit identification of each problem. Any combination of alphanumeric characters acceptable to a given machine system is permitted. Three cards must be read in for every problem, but any part of all three cards may be left blank if desired. The information punched on the cards is printed at the top of the output data sheets in the same format that is punched on the cards. A sample title for the 3-inch bellows is shown entered in the data sheets in Table B-11.

*Data Sets 10 and 11, which ar seldom used, will not be discussed here. For a discussion of these data sets, see Section B-II-f.

Input Data Sets, 5, 6, 8, 9, 10, and 12. Geometrical and Elastic Parameters. Once the mathematical model has been properly prepared and described in tabular form it is relatively simple to translate the information to the data sheets. Table B-8, which is a reproduction of Table E-2, illustrates the geometrical parameters derived from the mathematical model of the 3-inch formed bellows. Table B-9 gives the thickness variation obtained from Figures E-3 and E-4. The data in Tables B-8 and B-9 are used to make up Data Sets 5, 8, 9, and 12. Data Set 6 is used to enter the elastic constants.

Data Set 5 contains control information. For the analysis of the linear deflection of the formed bellows, only the number of parts and the number of the Fourier harmonics must be entered in this set. From Table B-8 it is seen that there are six parts. Since only axisymmetric deformation was considered, only one Fourier harmonic was called for and this was the o-th harmonic. These entries are shown in Table B-11. Note that when the "error control" is left blank, the truncation error in the integration is automatically taken to be 1×10^{-5}. The remaining entries in Data Set 5 are used primarily for nonlinear deformations. These are described in Section B-II-f.

Data Set 6 gives the values of Young's modulus and Poisson's ratio. For uniform materials with constant elastic properties, the first entry under "Constant?" is "YES" and the values of the constants are entered as indicated. The values shown in Table B-11 indicate that Young's modulus was taken to be 0.3×10^8 and Poisson's ratio was 0.3. If the bellows assembly is constructed of two or more materials with different elastic constants, the first entry would be "NO" and the values of the different elastic constants for each part would be entered as Data Set 10. This situation is expected to occur very rarely and will not be discussed here. However, it is discussed in Section B-II-f.

Data Set 8 is used to enter the geometric parameters for each shell part. There is one card for each part. Thus, for the 3-inch formed bellows there were 6 cards and 6 lines in the data sheet in Figure B-12. A comparison of Tables B-8 and B-12 shows how the geometrical data are transferred*. Note that the names of the shell types must start in Column 5. The number of the segments per part (Columns 43 and 44) are calculated from the formula

$$\text{Number of segments} \geq \frac{\text{arc length of PART}}{3\sqrt{\text{Th}}} \quad . \tag{B-2}$$

However, it is not critical to choose exactly the right number for every part and it is easy to estimate the number after some practice. In making such estimates it is better to take too many parts than not enough. The maximum allowable number of segments for the entire bellows is 60.

The number of print points per segment controls the number of points at which the program will print stresses and displacements. This is left to the discretion of the designer.

The specification of the shell wall thickness is controlled by the last three entries in Data Set 8. If the thickness is constant in each part, then "YES" is entered in Columns 52 through 54 and the thickness in Columns 57 through 64 under the heading "VALUE". If the thickness varies within a PART, then "NO" is entered in Columns 53

*The radius b_1 is entered within a minus sign since the normal to the shell points toward the center of curvature. This is illustrated in Figure B-7.

and 54 and the "VALUE" field is left blank. The number of points within each part at which the thickness was measured is inserted in Columns 68 and 69. (This latter field is left blank if the thickness is constant in each part.) The data for the thickness variation of the 3-inch bellows are given in Table B-9 where the independent coordinate has been given in terms of the angle ϕ or the meridional distance s. The description of the conversion from radial coordinates to ϕ or s-coordinates was described in the Section B-II-c on preparation of the mathematical model.

The thickness data for each part are entered in Data Set 12. Note that the independent coordinates of all the points in a given part are read in first and the corresponding values of the thickness are then read in on the next card. With the indicated format it is possible to read in 8 data points on any one pair of cards for each part. When 9 or 10 data points are necessary for specifying the thickness variation in any one part, the 10 independent coordinates are written on two lines and the 10 thickness values are then written on the next two lines.

Input-Data Sets for Boundary and Loading Conditions. Data Sets 2, 3, 4, and 7 are utilized to fix the boundary and loading conditions. Data Set 2 gives the boundary conditions at the initial edge of the shell, while Data Set 3 gives the boundary conditions at the final edge of the shell. As shown in Figure B-4, these data permit a specification of up to four different boundary conditions at either end of the shell. However, for axisymmetric deformation, only three boundary conditions are used. In both Data Sets 2 and 3, the boundary conditions are specified in the following order:

a. Transverse "FØRCE" (Q) or "DISPLACEMENT" (w) is called for by inserting the proper word under "type" beginning in Column 1. Its value is then given in Columns 13 through 20.

b. Meridional "FØRCE" (N_ϕ) or "DISPLACEMENT" (u_ϕ) is called for by inserting the proper word in Columns 21 through 32 with the value inserted in Columns 33 through 40.

c. Meridional "MØMENT" (M_ϕ) or "SLØPE" (β_ϕ) is called for by inserting the proper word in Columns 41 through 52 with the value inserted in Columns 53 through 60.

The choice of the appropriate boundary conditions for the formed bellows is arrived at in the following way. An inspection of the cross section of the bellows illustrated in Figures E-1 and E-2 shows that the ends of the half convolution illustrated in Figure B-23 lie on planes of symmetry. This means that the transverse shear force Q and the angle of rotation of the normal in the meridional direction β_ϕ are zero at both edges of the shell. In the meridional direction it is desirable to specify the displacement at both ends of the convolution. Thus, the type descriptions on Data Sets 2 and 3 would be FØRCE, DISPLACEMENT, SLØPE for both axial deflection and pressure loading. When the bellows is subjected to an internal or external pressure loading with no axial deflection, the values for the boundary conditions are all zero. When the bellows is subjected to an axial deflection loading, the magnitude of the displacement is given in Columns 33 through 40 either on Data Set 2 or Data Set 3. The magnitude of the displacement Δ_m imposed on the mathematical model is related to the displacement Δ_b, imposed on the bellows by the following equation:

$$\Delta_m = \frac{\text{Number of convolutions in mathematical model}}{\text{Number of convolutions in actual bellows}} \times \Delta_b \quad . \qquad \text{(B-3)}$$

Thus, for example, if a bellows has 10 convolutions and the mathematical model is one-half of one convolution, the deflection imposed on the mathematical model would be 1/20 of the deflection imposed on the actual bellows. Thus Δ_m for the 3-inch bellows is taken to be 0.003 inch.

If the displacement Δ_m is imposed at the final edge, an extension of the formed bellows would be read in as a positive value while a compression of the formed bellows would be read in as a negative value as shown in Data Set 3 in Table B-11. The signs are reversed if the deflection is imposed at the initial edge.

Data Set 4 is used to specify the angle between the directions in which the end conditions are applied and the directions of the normal and tangent to the shell meridion at each end of the shell. The angles are zero as shown in Table B-4 for both ends of the shell since the w and u_ϕ are specified in the direction of the normal and in the meridional direction, respectively, for the formed bellows. It will be seen later that nonzero rotation angles are necessary when fixing the boundary conditions for welded bellows.

Data Set 7 is utilized when the shell is subjected to a pressure load or a unit-weight or dead-weight loading. When these parameters are constant (including zero) over the entire bellows, "YES" is entered under "Constant?" in Columns 3 through 5 and the appropriate values are inserted in the other parts of the table. When there is no pressure, unit weight, or dead weight, zeros are to be inserted in the fields as shown in Table B-11, but "YES" is inserted in the first field. It is believed that the capability of the program to analyze problems with variable pressure or weight loads will be rarely used. For such a problem, "NO" is inserted in the first field of Data Set 7 and the variable loads are inserted in Data Set 11. This procedure is described in Section B-II-f.

Finally, in order to solve the problem of linear deformation of the 3-inch formed bellows under internal pressure with end restraints, the only required changes in the input data are that the displacement value in Columns 34 through 39 of Data Set 3 be set to zero and the pressure value in Columns 9 through 19 of Data Set 7 be set equal to the desired pressure.

For additional guidance the actual cards used for the input data for the 3-inch bellows are reproduced in Figures B-24 through B-26.

Welded Bellows Boundary Conditions. The input data for welded bellows are more complicated than for formed bellows for two reasons. The first reason is that the upper and lower leaves are not symmetric so that the mathematical model cannot be applied to only one-half convolution. In practice, it is usually desirable to model at least two full convolutions The stresses and strains of the middle leaves are then taken to be representative of the behavior of the internal convolutions of the actual welded bellows.

The second complicating factor in the analysis of welded bellows is that the mid-surface of the bellows is often inclined with respect to the bellows axis at the bellows root or crown. An example of this is shown in Figure B-21. Further, the advanced-design welded bellows developed in the research program has flat sections which are deliberately inclined to the bellows axis. For the analysis of these bellows, it is necessary to utilize the boundary-rotation capability of Data Set 4. The specification of the boundary conditions and rotation angles was described in detail in Section B-I-e. However, this section was written to cover all possible situations and thus is somewhat complicated. For the routine analysis of welded bellows it is suggested that the following procedure be followed.

As noted above, one or more complete convolutions must be analyzed for the welded bellows. It is recommended that the initial edge of the bellows be at the crown of the upper diaphragm of the upper convolution and the final edge be at the crown of the lower diaphragm of the last convolution. The numerical integration is carried out from the crown to the root of the upper diaphragm of the first convolution, then from the root to the crown of the lower diaphragm of the first convolution; this procedure is followed until the crown of the lower diaphragm of the last convolution is reached. With this convention the rotation angles at the edges of the shell can be standardized as shown in Figure B-27. When the bellows flat is perpendicular to the centerline as shown by the middle drawing for both edges, then the rotation angles of Data Set 4 are zero and the three boundary condition types for both Data Sets 2 and 3 are in the order "DISPLACEMENT", "FØRCE", "SLØPE". When the bellows flats are inclined from the horizontal one way or the other, then for the different orientations indicated in Figure B-27, the rotation angles to be entered in Data Set 4 are given in Table B-10. The boundary condition types are still in the order "DISPLACEMENT", "FØRCE", and "SLØPE". For a pressure-loaded bellows with end restraint, all of the values are set to zero. For axial displacement the desired value of the total displacement for the number of convolutions included in the mathematical model is entered in Columns 13 through 20 of Data Set 3. This displacement can be found by multiplying the deformation for the entire bellows by the ratio of the number of convolutions in the mathematical model to the number of convolutions in the full bellows. A positive value of the displacement is used in this case for compression and a negative value for extension.

B-II-e. Description of Computer-Output Sheets

The interpretation of the output of the computer program is quite straightforward. The output sheets obtained from the analysis of the 3-inch formed bellows are reproduced in Tables B-15 through B-20. The title page is printed out of an array permanently stored in Subroutine INPUT. This may, of course, be changed for each company's purpose. Tables B-16 through B-18 give the input data that were entered. This may be checked visually to insure that the proper input data were key punched. Tables B-19 and B-20 give the values of the stress resultants and moments, the displacements and strains, and the surface stresses at each of the print points requested. An item-by-item description of the output is given in Section B-II-g to aid in interpretation of any unfamiliar quantities.

Finally, it is noted that many checks have been incorporated in the program to insure that the rules governing the specification of the data are followed. However, the data concerning the specification of the variable thickness are not checked internally. Consequently, these should be checked by the analyst when he reviews his output. It is important that when variable-thickness data are prescribed for parts described by the independent coordinate ϕ, the initial and final independent coordinates describing the thickness variation be the same as the initial and final coordinates of the part. When the part is prescribed by the distance s, the initial coordinate must be s = 0 and the final coordinate s = b for thickness-variation input.

The boundary conditions at the final edge of the shell should be checked. When the boundary-rotation angle at the end of the shell is 0 degrees, the three fundamental variables that were prescribed at the boundary should agree closely with the last entries in

the appropriate columns of the stress-resultant and displacement table which is similar to Figure B-19. If a large discrepancy is found, then a check should be made of whether the number of segments selected for the parts is sufficient and if all the input is correct.

When the boundary-rotation angle is not zero, the boundary-input quantities will not appear explicitly for the axial-loading case. A simple check on the correctness of the solution can be obtained by using the following equations:

$$u_1 = w \cos\phi - u_\phi \sin\phi \quad ; \tag{B-4}$$

$$N_2 = Q_\phi \sin\phi + N_\phi \sin\phi \quad . \tag{B-5}$$

The displacement u_1 should equal the deflection imposed on the bellows, while the force N_2 should be zero.

For a bellows analysis the quantity that is usually of most importance is the meridional strain. This is denoted as EPS PHI on the output. The maximum strain for axial loading is related to the fatigue life as explained in Appendix K.

B-II-f. Item-by-Item Description of Input Data

The computer input cards which are necessary to perform an analysis using NONLIN will be described in this section. The special INPUT DATA sheets discussed earlier conform with the indicated FORMATS in each data set.

Data Set 1 Job Identification

READ (5, 500) TITLE 1, TITLE 2, TITLE 3

500 FØRMAT (80 A1)

Any information can be placed on these three cards. It is necessary to have three cards, although any can be left blank.

Data Set 2 Boundary Data at Initial Edge

READ (5, 530) (BØUNDI (I), GA (I), I = 1, 4)

530 FØRMAT (4 (A6, 6X, F8.2))

BØUNDI (1) is either DISPLACEMENT or FØRCE in w or 1 direction
GA (1) is its value

BØUNDI (2) is either DISPLACEMENT or FØRCE in u_ϕ or 2 direction
GA (2) is its value

BØUNDI (3) is either SLØPE or MØMENT
GA (3) is its value

BØUNDI (4) is either DISPLACEMENT or FØRCE in u_θ direction
GA (4) is its value

For an axisymmetrically loaded shell BØUNDI (4) and GA (4) need not be specified.

Data Set 3. Boundary Data at Final Edge

READ (5, 530) (BØUNDF (I), GB (I), I = 5, 8)

530 FØRMAT (4 (A6, 6X, F8.2))

BØUNDF (5) is either DISPLACEMENT or FØRCE in w or 1 direction
GB (5) is its value

BØUNDF (6) is either DISPLACEMENT or FORCE in u_ϕ or 2 direction
GB (6) is its value

BØUNDF (7) is either SLØPE or MØMENT
GB (7) is its value

BØUNDF (8) is either DISPLACEMENT or FØRCE in u_θ direction
GB (8) is its value

For an axisymmetrically loaded shell BØUNDF (8) and GB (8) need not be specified.

Data Set 4 Boundary Rotation Angles

READ (5, 565) ALXL, ALXR

565 FØRMAT (8 F10.5)

ALXL is the boundary rotation angle at the initial edge of the shell

ALXR is the boundary rotation angle at the final edge of the shell

Data Set 5 Control Card

READ (5, 561) IBRM, ITER, NDUMMY, PLØT, INTPRN, INTVAL, LEVEL1, LEVEL2, ERP, CØNVER, NUMHAR, (NFØURA (I), I = 1, 8)

561 FØRMAT (815, 2E10.3, 10I2)

IBRM = number of parts in composite shell

ITER = number of iterations at a load level for nonlinear calculations. ITER = 0 for linear analysis

NDUMMY = not presently used

INTPRN = 0 indicates that intermediate results from the nonlinear analysis, i.e., values of parameters and slopes, will not be printed out. Use 1 to obtain values.

INTVAL = 0 indicates that intermediate results from the initial value integrations will not be printed out. Use 1 to obtain values.

LEVEL1 = number of increments into which the loading is divided for nonlinear analysis.

LEVEL2 = not presently used

ERP = accuracy for integration subroutine. If left blank, it is internally set to 1.0 E-05.

CØNVER = convergence criteria for use in nonlinear analysis.

NUMHAR = number of FØURIER harmonics in the analysis. For a nonlinear analysis, NUMHAR = 1. For a linear analysis, NUMHAR must not be greater than 8. If the shell is axisymmetrically loaded, NUMHAR = 1. For a nonsymetrically loaded shell which has the same boundary conditions for all harmonics, NUMHAR can have any value up to 8.

NFØURA (I) = FØURIER harmonic value. For an axisymmetric deformation, NFOURA (1) = 0

Data Set 6 Elastic Parameters

READ (5, 563) NELAS, YØUNG, PØISØN

563 FØRMAT (2X, A2, 4X, E11.4, 4X, F6.4)

NELAS is either YES or NØ. YES indicates that the elastic parameters are the same for each part in the composite shell. If YES, then the values of Young's modulus and Poisson's ratio are read in on the same card. If NØ, the values for each part are read in as Data Set 10.

YØUNG Young's modulus (lb/in.^{2})

PØISØN Poisson's ratio (in./in.)

Data Set 7 Loading Parameters

READ (5, 680) NPRES, PRESS, DENSTY, DEAD

680 FØRMAT (2X, A2, 4X, 3F 14.5)

NPRES is either YES or NØ. YES indicates that the distributed loadings are the same for each part in the composite shell. If YES, then the values of the normal pressure, the weight density of the material, and the dead loading on the shell are given on the same card. If NØ, then the values for each part are read in as Data Set 11.

Data Set 8 Shell Type

(One card is needed for each part)

READ (5, 512) (NAME2 (L), SI (L), SX (L), IPAR (L), INT (L), TDIST (L), VN(I, L), VARTIK (L), L = 1, IBRM)

512 FØRMAT (4X, A6, 6X, F 11.5, F 12.5, 2I5, 2X, A2, 1X, F 10.5, I5)

NAME2 (L) indicate the shell type by name. Use the spellings in Table B-1.

SI (L) initial coordinate of part.

SX (L) final coordinate of part.

IPAR (L) number of segments in part. See formula in B-I-b to determine the number of segments (maximum of 60).

INT (L) number of print points per segment.

TIDST (L) either YES or NØ. YES if thickness is constant throughout the part.

VN(1, L) if TDIST (L) is YES, then give part thickness; if NØ, then leave blank.

VARTIK (L) If TDIST (L) is YES, then leave blank. If TDIST (L) is NØ, then give number of points which specify the distribution. VARTIK (L) cannot be greater than 10 or less than 2.

Data Set 9 Shell Geometry

(One card is needed for each part)

READ (5, 562) (VN(2, L), VN(3, L), VN(4, L), L = 1, IBRM)

562 FØRMAT (3X, 3 F12.5)

VN (2, L) Radius a
VN (3, L) Radius b
VN (4, L) Radius c.

Data Set 10 Variable Elastic Parameters

(Read only when NELAS = NØ on Data Set 6.
One card is needed for each part)

READ (5, 564) (EYM (L), PSR (L), L = 1, IBRM)

564 FØRMAT (8X, E 11.4, 4X, F6.4)

EYM(L) Young's modulus

PSR(L) Poisson's ratio

Data Set 11 Variable Loading Parameters

(Read only when NPRES = NØ on Data Set 7.
One card is needed for each part)

READ (5, 566) (VN (5, L), VN (6, L), VN (7, L), L = 1, IBRM

566 FØRMAT (5X, 3 F15.5)

VN (5, L) is the normal pressure acting on the shell ($lb/in.^2$)

VN (6, L) is the weight density of the material ($lb/in.^3$)

VN (7, L) is the dead loading acting on the shell ($lb/in.^2$).
The sign of the above loadings depends on the direction of the normal.

Data Set 12 Variable Thickness

(These data are read only for a part when VARTIK (L)
is 2 or greater on Data Set 8.)

READ (5, 565) (XP (I, L), I = 1, NPNT)

READ (5, 565) (YP (I, L), I = 1, NPNT)

565 FØRMAT (8 F10.5)

NPNT is internally set to VARTIK (L)

XP (I, L) is the independent coordinate at which the thickness value is specified. For all shell types except the VARCYLINDER and CØNICAL, the independent coordinate is an angle in degrees. For the VARCYLINDER and CØNICAL, the independent coordinate is the arc length "s" measured along the meridion. The first point XP (1, L) must be zero for the VARCYLINDER and CØNICAL shell types, while the last point XP (NPNT, L) must be equal to the length of the shell part, b.

YP (I, L) is the thickness at the point corresponding to XP (I, L).

Note that the 565 FØRMAT allows only 8 entries per card. Thus, if a part has VARTIK (L) equal to 9 or 10, two cards must be used to describe XP (I, L) and two cards must be used to describe YP (I, L). The sequence of cards for a part which has VARTIK (L) = 10 would be as follows:

Card 1 would have 8 values of XP;
Card 2 would have 2 values of XP;
Card 3 would have 8 values of YP;
Card 4 would have 2 values of YP.

B-II-g. Item-by-Item Description of Output Data

The output presently available from Program NONLIN is outlined below:

(a) Header page which gives name of company. Any title appropriate to a given company can be obtained by modifying FØRMAT statement Numbers 534, 535, 536, 537, 539 in subroutine input.

(b) (1) First three printed lines are the Job Identification cards supplied by user.

(2) Boundary conditions are then listed along with boundary rotation angles.

(3) If elastic parameters are the same for every part in the shell, their values are given.

(4) If loading parameters are the same for every part in the shell, their values are given.

(c) (1) First three printed lines are the Job Identification cards.

(2) Geometry of shell is now listed. The following items are given: Part number, type of part, number of segments, coordinates, radii a, b, and c, and thickness data. If thickness is constant, a YES is printed along with the value. If thickness is variable, a NØ is printed and entry under value is left blank. If there are more than 40 parts in the composite shell, the numbers over 40 are listed on the next page.

(d) If NELAS on Data Set 6 is YES, then following is printed out. Otherwise go to (e).

(1) First three printed lines are the Job Identification cards.

(2) The part number, type, Young's modulus, and Poisson's ratio are then given.

If there are more than 40 parts in the composite shell, the numbers over 40 are listed on the next page.

(e) If NPRES on Data Set 7 is YES, then the following is printed out. Otherwise go to (f).

(1) First three printed lines are the Job Identification cards.

(2) The part number, type, normal pressure, weight density and dead loading are then given.

If there are more than 40 parts in the composite shell, the numbers over 40 are listed on the next page.

(f) If at least one of the parts has variable thickness, then the following is printed out. Otherwise go to (g).

(1) First three printed lines are the Job Identification cards.

(2) The part number, independent coordinates and thickness for each part which has variable thickness are then listed.

(g) The next portion of the output is concerned with the results of the computations. The results are divided into two parts. The first part gives the fundamental variables, w, Q, u_ϕ, β_ϕ and M_ϕ along with the auxiliary variables, N_θ and M_θ at every print point. The maximum surface strains e_θ and e_ϕ are also given at every print point.

The second portion of the computed results is concerned with the stresses. The meridional and circumferential stresses have been calculated for the following conditions: membrane, bending, and inner and outer surface. The membrane stress is the membrane force, N_θ or N_ϕ, divided by the thickness. The bending stress is $6M_\phi/h^2$ (meridional) and $6M_\theta/h^2$ (circumferential). The inner and outer surface depend on the choice of the direction of the normal. See Figure B-28 to determine the meaning of inner and outer surface. The maximum shearing stress in the w direction is also given. This is determined from 1.5 Q/h.

Note: The strains e_θ and e_ϕ do not necessarily refer to the same surface. The strains e_θ and e_ϕ are internally calculated for the inner and outer surface at every print point. Because of space restrictions, only two quantities could be printed out. Thus, the value given for the strains e_θ and e_ϕ is the larger of the strains for the inner and outer surface.

TABLE B-1. SHELL PARTS IN GOMTRY SUBROUTINE

Part	Spelling Used on Input Cards
Cylindrical constant thickness	CYLINDRICAL
Spheroidal	SPHERØIDAL
Ellipsoidal	ELLIPSØIDAL
Paraboloidal	PARABØLØIDAL
Conical	CØNICAL
Toroidal	TØRØIDAL
Cylindrical variable thickness	VARCYLINDER

TABLE B-2. BOUNDARY VARIABLES AND NAMES USED ON INPUT CARDS

Boundary Variable	Name
$w\ (u_1)$	DISPLACEMENT
$Q\ (Q_1)$	FØRCE
$u_\varphi\ (u_2)$	DISPLACEMENT
$N_\varphi\ (Q_2)$	FØRCE
β_φ	SLØPE
M_φ	MØMENT
u_θ	DISPLACEMENT
N	FØRCE

TABLE B-3. BOUNDARY QUANTITIES USED IN THE SPECIFICATION OF THE BOUNDARY CONDITIONS

Row	Displacements	Forces
1	$w\ (u_1)$	$Q\ (Q_1)$
2	$u_\varphi\ (u_2)$	$N_\varphi\ (Q_2)$
3	β_φ	M_φ
4	u_θ	N

TABLE B-4. INPUT SHEET FOR DATA SETS 1-7 FOR PROGRAM NONLIN

DATA SET 1 (three title cards)

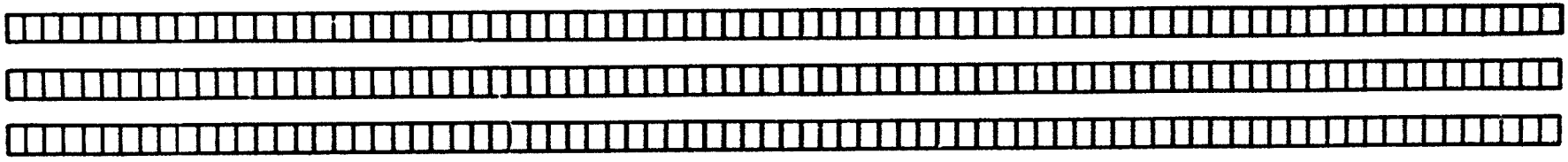

DATA SET 2 (boundary data at initial edge)

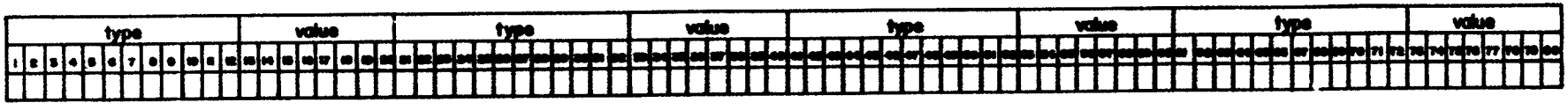

DATA SET 3 (boundary data at final edge)

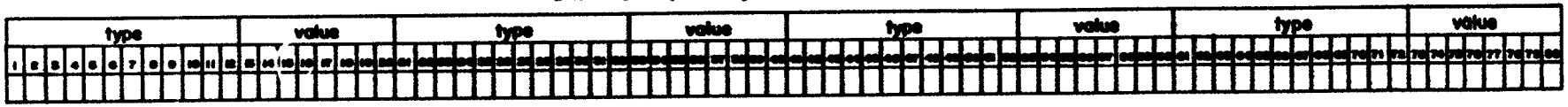

DATA SET 4 (angle between support and shell)

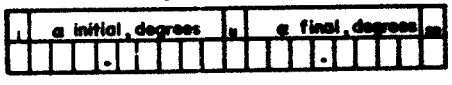

DATA SET 5 (control set)

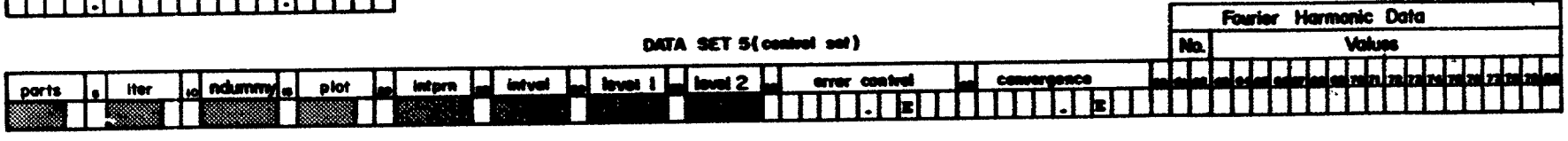

DATA SET 6 (Young's Modulus and Poisson's Ratio)

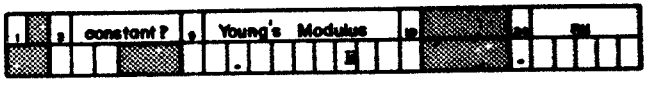

DATA SET 7 (loading parameters)

TABLE B-5. INPUT SHEET FOR DATA SET 8 FOR PROGRAM NONLIN

DATA SET 8

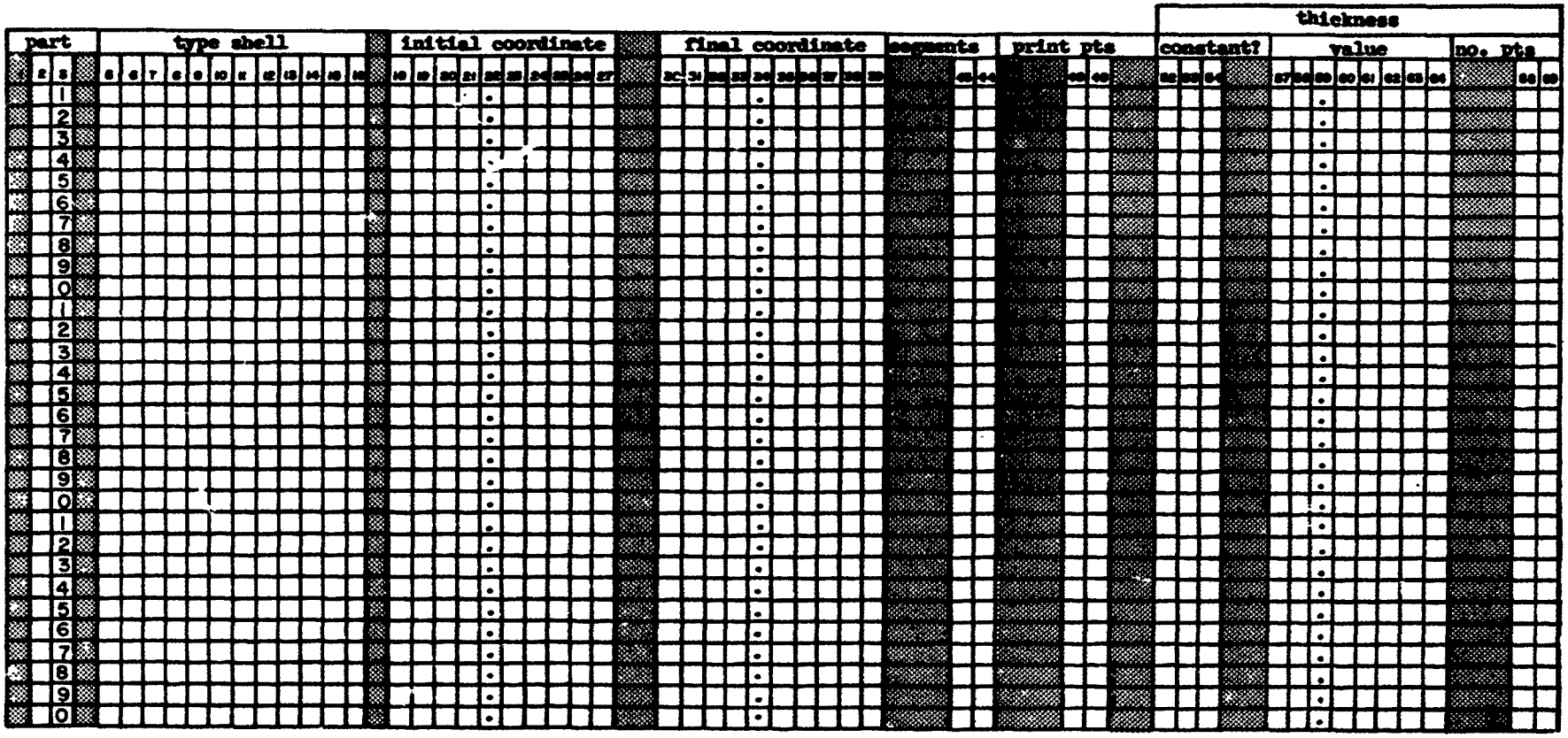

TABLE B-6. INPUT SHEET FOR DATA SET 9 FOR PROGRAM NONLIN

DATA SET 9

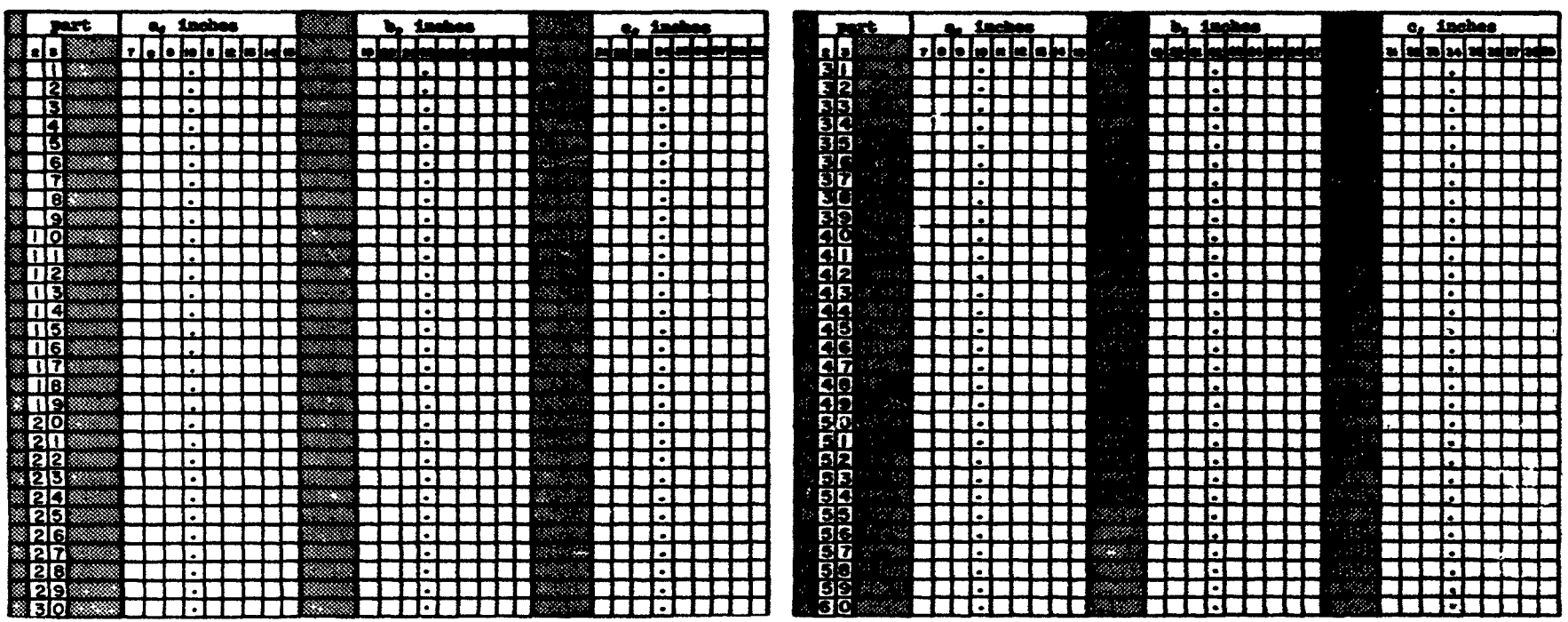

TABLE B-7. INPUT SHEET FOR DATA SET 12 FOR PROGRAM NONLIN

DATA SET 12 (variable thickness)

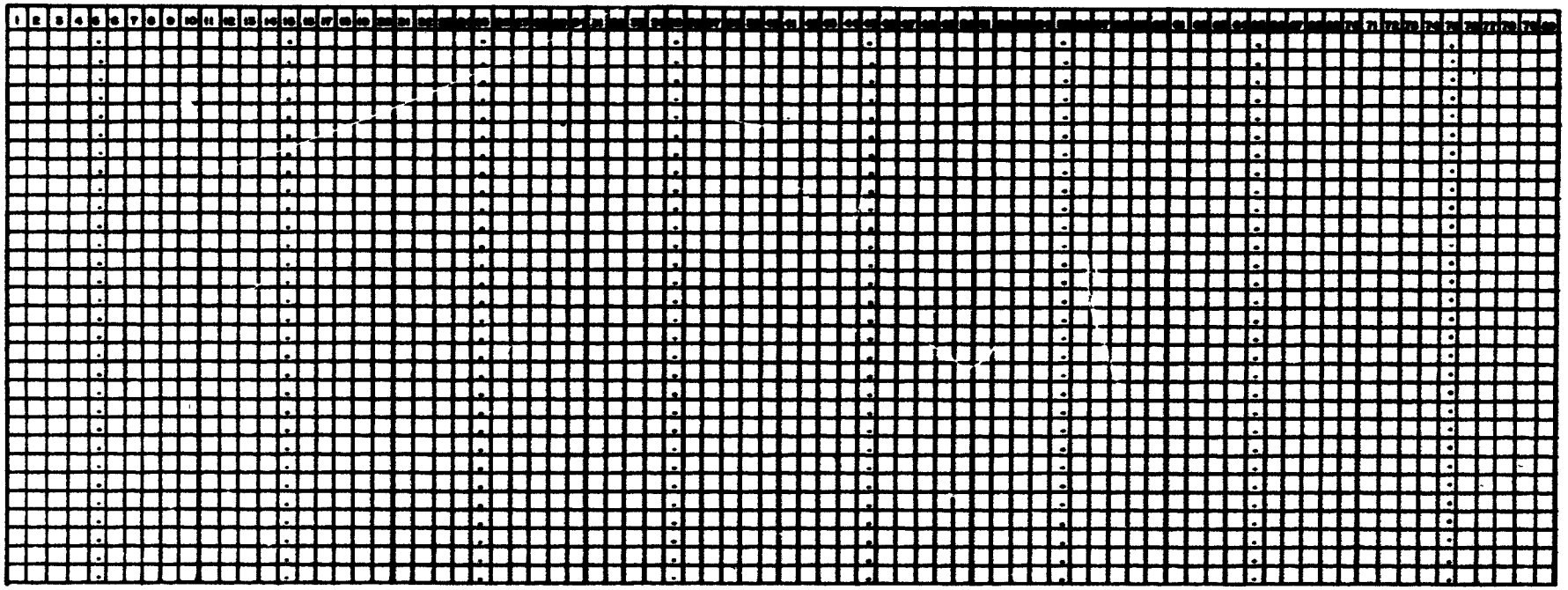

TABLE B-8. DIMENSIONS OF MATHEMATICAL MODEL OF 3-INCH SINGLE-PLY FORMED BELLOWS JD68

Part No.	Shell Type	Coordinates, degrees		Radii, inches	
		Initial	Final	a	b
1	Toroidal	90.0	2.0	1.5295	-0.0267
2	Conical	2.0	-	1.5286	0.0633
3	Toroidal	2.0	6.5	1.5668	0.7630
4	Conical	6.5	-	1.6508	0.0900
5	Toroidal	6.5	24.0	1.7198	0.1875
6	Toroidal	24.0	90.0	1.7753	0.0455

TABLE B-9. THICKNESS VARIATION OF 3-INCH SINGLE-PLY FORMED BELLOWS JD68

Part	φ or s	Thickness, in.	Part	φ or s	Thickness, in.
1	90.0	0.00757	4	0.0	0.00709
	2.0	0.00745		0.0900	0.00690
2	0.0	0.00745	5	6.5	0.00690
	0.0345	0.00728		24.0	0.00678
	0.0633	0.00722			
			6	24.0	0.00678
3	2.0	0.00722		34.0	0.00676
	6.5	0.00709		90.0	0.00661

TABLE B-10. BOUNDARY ROTATION ANGLES FOR INITIAL AND FINAL EDGES

Case	Edge	φ	Boundary Rotation Angle
1		< 180	$\varphi - 180^{(a)}$
2	Initial	= 180	0
3		> 180	$\varphi - 180$
4		< 0	$\varphi^{(a)}$
5	Final	= 0	0
6		> 0	φ

(a) Note that for these cases the angles will be negative.

TABLE B-11. INPUT FOR 3-INCH STAINLESS STEEL BELLOWS JD68

DATA SET 1(three title cards)

3 - INCH STAINLESS STEEL BELLOWS JD68

AXIAL COMPRESSION = 0.060 INCH ON 10 CONVOLUTION SELL=S

MAY 31, 1967

DATA SET 2(boundary data at initial edge)

type	value	type	value	type	value	type	value
FORCE	0.0	DISPLACEMENT	0.0	SLOPE	0.0		

DATA SET 3(boundary data at final edge)

type	value	type	value	type	value	type	value
FORCE	0.0	DISPLACEMENT	-0.0005	SLOPE	0.0		

DATA SET 4(angle between support and shell)

α initial, degrees	α final, degrees
0.0	0.0

DATA SET 5(control set)

parts	iter	ndummy	plot	intprn	intval	level 1	level 2	error control	convergence	Fourier Harmonic Data: No.	Fourier Harmonic Data: Values
6								.E	.E	1	0

DATA SET 6(Young's Modulus and Poisson's Ratio)

constant?	Young's Modulus		
YES	.3	29+06	.3

DATA SET 7(loading parameters)

constant?	pressure, psi	unit weight, lb./in.³	dead weight, psi
YES	0.0	0.0	0.0

TABLE B-12. INPUT FOR 3-INCH STAINLESS STEEL BELLOWS JD68

DATA SET 8

part	type shell	initial coordinate	final coordinate	segments	print pts	thickness: constant?	thickness: value	thickness: no. pts
1	TOROIDAL	90.	2.	4	5	NO	.	2
2	CONICAL	2.	.	1	5	NO	.	2
3	TOROIDAL	2.	6.5	1	10	NO	.	2
4	CONICAL	6.5	.	1	6	NO	.	2
5	TOROIDAL	6.5	24.	1	5	NO	.	2
6	TOROIDAL	24.	90.	3	5	NO	.	3
7		.	.				.	
8		.	.				.	
9		.	.				.	
0		.	.				.	
1		.	.				.	
2		.	.				.	
3		.	.				.	
4		.	.				.	
5		.	.				.	
6		.	.				.	
7		.	.				.	
8		.	.				.	
9		.	.				.	
0		.	.				.	
1		.	.				.	
2		.	.				.	
3		.	.				.	
4		.	.				.	
5		.	.				.	
6		.	.				.	
7		.	.				.	
8		.	.				.	
9		.	.				.	
0		.	.				.	

TABLE B-13. INPUT FOR 3-INCH STAINLESS STEEL BELLOWS JD68

DATA SET 9

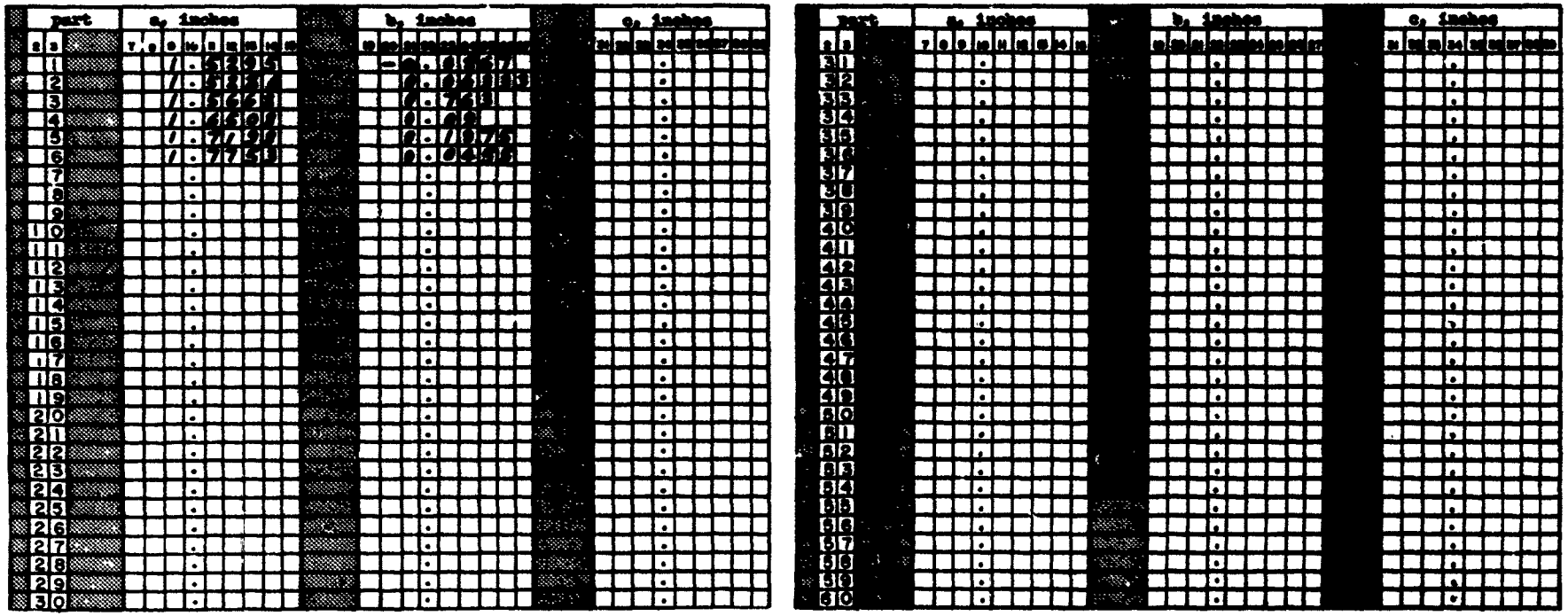

TABLE B-14. INPUT FOR 3-INCH STAINLESS STEEL BELLOWS JD68

DATA SET 12 (variable thickness)

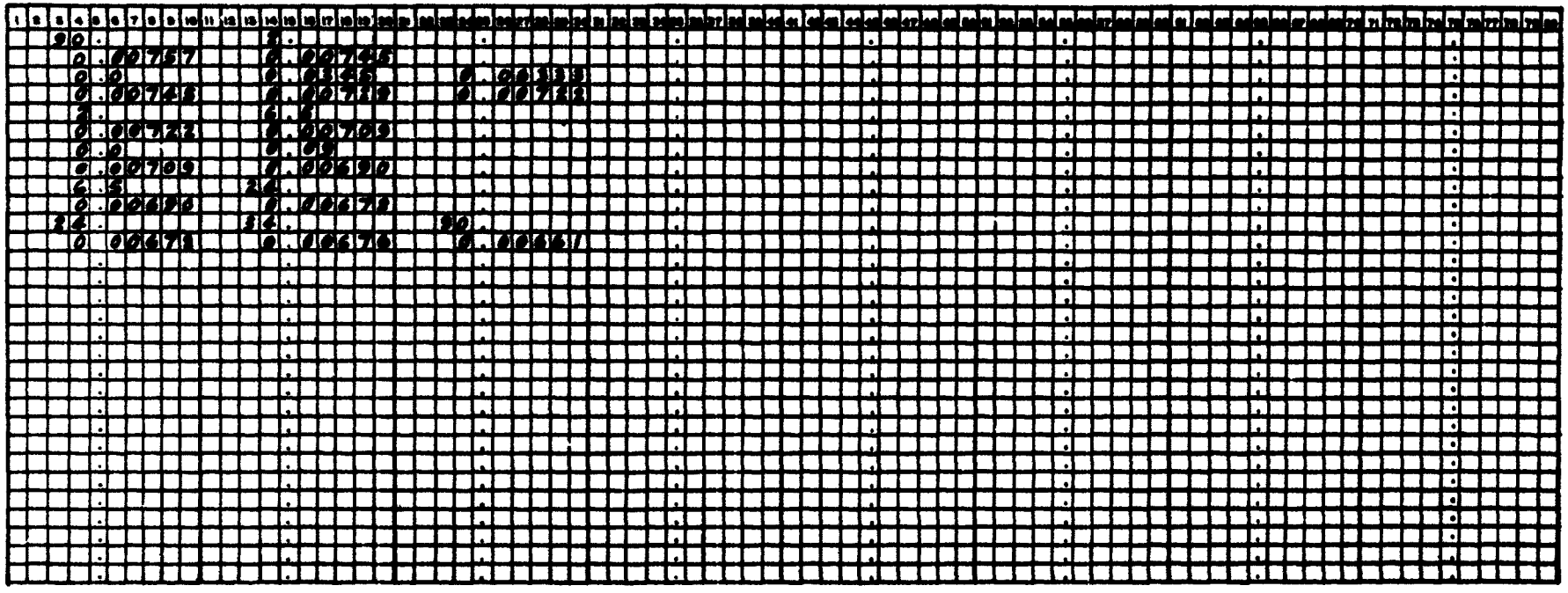

TABLE B-15. OUTPUT FOR 3-INCH SINGLE-PLY BELLOWS JD68

BATTELLE MEMORIAL INSTITUTE

COLUMBUS, OHIO

STRESS ANALYSIS OF A SHELL OF REVOLUTION

ADVANCED SOLID MECHANICS DIVISION

MECHANICAL ENGINEERING DEPARTMENT

TABLE B-16. OUTPUT FOR 3-INCH SINGLE-PLY BELLOWS JD68

3 - INCH STAINLESS STEEL BELLOWS JD 68

AXIAL COMPRESSION = 0.040 INCH ON 10 CONVOLUTION BELLOWS

MAY 31, 1967

* * * PRINTOUT OF INPUT DATA * * *

* BOUNDARY DATA *

INITIAL EDGE		FINAL EDGE	
FORCE =	0.00000	FORCE =	0.00000
DISPLACEMENT =	0.00000	DISPLACEMENT =	-.00200
SLOPE =	0.00000	SLOPE =	0.00000
BOUNDARY ANGLE =	0.00000	BOUNDARY ANGLE =	0.00000

ELASTIC PARAMETERS ARE THE SAME FOR EVERY PART IN THIS SHELL. THEIR VALUES ARE
YOUNGS MODULUS = 0.30000E+08 POUNDS PER SQUARE INCH
POISSONS RATIO = .30000

LOADING PARAMETERS ARE THE SAME FOR EVERY PART IN THIS SHELL. THEIR VALUES ARE
PRESSURE = 0.00000 POUNDS PER SQUARE INCH
UNIT WEIGHT OF MATERIAL = 0.00000 POUNDS PER CUBIC INCH
DEAD WEIGHT = 0.00000 POUNDS PER SQUARE INCH

TABLE B-17. OUTPUT FOR 3-INCH SINGLE-PLY BELLOWS JD68

3 - INCH STAINLESS STEEL BELLOWS JD 68

AXIAL COMPRESSION = 0.060 INCH ON 10 CONVOLUTION BELLOWS

MAY 31, 1967

* GEOMETRY *

PART	TYPE	NO. OF SEGMENTS	COORDINATES INITIAL	COORDINATES FINAL	DIMENSIONS	A, INCHES	B, INCHES	C, INCHES	THICKNESS, INCHES CONSTANT	THICKNESS, INCHES VALUE
1	TOROIDAL	4	90.00000	2.00000	DEGREES	1.52950	-.02670		NO	
2	CONICAL	1	2.00000		DEGREES	1.52860	.06330		NO	
3	TOROIDAL	1	2.00000	6.50000	DEGREES	1.56680	.76300		NO	
4	CONICAL	1	6.50000		DEGREES	1.65080	.09000		NO	
5	TOROIDAL	1	6.50000	24.00000	DEGREES	1.71980	.18750		NO	
6	TOROIDAL	3	24.00000	90.00000	DEGREES	1.77530	.04550		NO	

TABLE B-18. OUTPUT FOR 3-INCH SINGLE-PLY BELLOWS JD68

3 - INCH STAINLESS STEEL BELLOWS JD 68

AXIAL COMPRESSION = 0.060 INCH ON 10 CONVOLUTION BELLOWS

MAY 31, 1967

* VARIABLE THICKNESS *

PART 1			
COORDINATE	90.00000	2.00000	
THICKNESS	.00757	.00745	
PART 2			
COORDINATE	0.00000	.03450	.06330
THICKNESS	.00745	.00728	.00722
PART 3			
COORDINATE	2.00000	6.50000	
THICKNESS	.00722	.00709	
PART 4			
COORDINATE	0.00000	.09000	
THICKNESS	.00709	.00690	
PART 5			
COORDINATE	6.50000	24.00000	
THICKNESS	.00690	.00678	
PART 6			
COORDINATE	24.00000	34.00000	90.00000
THICKNESS	.00678	.00676	.00661

TABLE B-19. OUTPUT FOR 3-INCH SINGLE-PLY BELLOWS JD68

SOUT	W	Q PHI	U PHI	N PHI	BETA PHI	M PHI	N THETA	M THETA	EPS THETA	EPS PHI
RESULTS FOR MAIN SHELL 1 TOROIDAL										
90.0000000	-0.1141E-03	0.	0.	-0.7075E+00	0.	-0.1022E+00	-0.1746E+02	-0.3066E-01	-0.7593E-04	0.3446E-03
84.5000000	-0.1133E-03	0.3821E-01	-0.1088E-04	-0.7070E+00	-0.2201E-03	-0.1022E+00	-0.1740E+02	-0.3066E-01	-0.7579E-04	0.3450E-03
79.0000000	-0.1109E-03	0.7677E-01	-0.2160E-04	-0.7056E+00	-0.4406E-03	-0.1020E+00	-0.1725E+02	-0.3066E-01	-0.7537E-04	0.3449E-03
73.5000000	-0.1069E-03	0.1160E+00	-0.3202E-04	-0.7030E+00	-0.6613E-03	-0.1017E+00	-0.1701E+02	-0.3065E-01	-0.7468E-04	0.3443E-03
68.0000000	-0.1014E-03	0.1561E+00	-0.4198E-04	-0.6990E+00	-0.8818E-03	-0.1013E+00	-0.1670E+02	-0.3064E-01	-0.7375E-04	0.3432E-03
68.0000000	-0.1014E-03	0.1561E+00	-0.4198E-04	-0.6990E+00	-0.8818E-03	-0.1013E+00	-0.1670E+02	-0.3064E-01	-0.7375E-04	0.3432E-03
62.5000000	-0.9435E-04	0.1973E+00	-0.5134E-04	-0.6933E+00	-0.1102E-02	-0.1008E+00	-0.1632E+02	-0.3061E-01	-0.7259E-04	0.3417E-03
57.0000000	-0.8590E-04	0.2396E+00	-0.5995E-04	-0.6856E+00	-0.1321E-02	-0.1002E+00	-0.1589E+02	-0.3057E-01	-0.7126E-04	0.3396E-03
51.5000000	-0.7610E-04	0.2831E+00	-0.6769E-04	-0.6753E+00	-0.1540E-02	-0.9947E-01	-0.1541E+02	-0.3052E-01	-0.6980E-04	0.3371E-03
46.0000000	-0.6504E-04	0.3276E+00	-0.7443E-04	-0.6622E+00	-0.1757E-02	-0.9861E-01	-0.1489E+02	-0.3044E-01	-0.6825E-04	0.3342E-03
46.0000000	-0.6504E-04	0.3276E+00	-0.7443E-04	-0.6622E+00	-0.1757E-02	-0.9861E-01	-0.1489E+02	-0.3044E-01	-0.6825E-04	0.3342E-03
40.5000000	-0.5284E-04	0.3730E+00	-0.8006E-04	-0.6459E+00	-0.1973E-02	-0.9763E-01	-0.1436E+02	-0.3034E-01	-0.6667E-04	0.3308E-03
35.0000000	-0.3960E-04	0.4189E+00	-0.8446E-04	-0.6259E+00	-0.2187E-02	-0.9653E-01	-0.1383E+02	-0.3020E-01	-0.6513E-04	0.3271E-03
29.5000000	-0.2546E-04	0.4650E+00	-0.8755E-04	-0.6020E+00	-0.2399E-02	-0.9530E-01	-0.1333E+02	-0.3004E-01	-0.6367E-04	0.3230E-03
24.0000000	-0.1054E-04	0.5108E+00	-0.8924E-04	-0.5740E+00	-0.2608E-02	-0.9395E-01	-0.1285E+02	-0.2983E-01	-0.6238E-04	0.3185E-03
24.0000000	-0.1054E-04	0.5108E+00	-0.8924E-04	-0.5740E+00	-0.2608E-02	-0.9395E-01	-0.1285E+02	-0.2983E-01	-0.6238E-04	0.3185E-03
18.5000000	0.4998E-05	0.5558E+00	-0.8948E-04	-0.5417E+00	-0.2815E-02	-0.9249E-01	-0.1243E+02	-0.2958E-01	-0.6130E-04	0.3137E-03
13.0000000	0.2102E-04	0.5996E+00	-0.8820E-04	-0.5053E+00	-0.3019E-02	-0.9090E-01	-0.1209E+02	-0.2928E-01	-0.6051E-04	0.3087E-03
7.5000000	0.3735E-04	0.6416E+00	-0.8536E-04	-0.4647E+00	-0.3220E-02	-0.8921E-01	-0.1183E+02	-0.2893E-01	-0.6006E-04	0.3034E-03
2.0000000	0.5386E-04	0.6813E+00	-0.8095E-04	-0.4200E+00	-0.3417E-02	-0.8742E-01	-0.1168E+02	-0.2853E-01	-0.6002E-04	0.2980E-03
RESULTS FOR MAIN SHELL 2 CONICAL										
0.0000000	0.5386E-04	0.6813E+00	-0.8095E-04	-0.4200E+00	-0.3417E-02	-0.8742E-01	-0.1168E+02	-0.2853E-01	-0.6002E-04	0.2980E-03
.0158250	0.1172E-03	0.6702E+00	-0.8074E-04	-0.5326E+00	-0.4562E-02	-0.7616E-01	-0.1113E+02	-0.2580E-01	-0.6048E-04	0.2645E-03
.0316500	0.1976E-03	0.6596E+00	-0.8055E-04	-0.6369E+00	-0.5578E-02	-0.6517E-01	-0.1051E+02	-0.2302E-01	-0.6021E-04	0.2305E-03
.0474750	0.2930E-03	0.6494E+00	-0.8038E-04	-0.7329E+00	-0.6455E-02	-0.5443E-01	-0.9898E+01	-0.2023E-01	-0.5932E-04	0.1941E-03
.0633000	0.4011E-03	0.6397E+00	-0.8022E-04	-0.8208E+00	-0.7182E-02	-0.4392E-01	-0.9251E+01	-0.1742E-01	-0.5788E-04	0.1575E-03
RESULTS FOR MAIN SHELL 3 TOROIDAL										
2.0000000	0.4011E-03	0.6397E+00	-0.8022E-04	-0.8208E+00	-0.7182E-02	-0.4392E-01	-0.9242E+01	-0.1742E-01	-0.5779E-04	0.1575E-03
2.5000000	0.4491E-03	0.6282E+00	-0.8387E-04	-0.8607E+00	-0.7442E-02	-0.3960E-01	-0.8932E+01	-0.1623E-01	-0.5687E-04	0.1422E-03
3.0000000	0.4987E-03	0.6162E+00	-0.8795E-04	-0.8988E+00	-0.7677E-02	-0.3536E-01	-0.8559E+01	-0.1505E-01	-0.5558E-04	0.1271E-03
3.5000000	0.5497E-03	0.6037E+00	-0.9248E-04	-0.9348E+00	-0.7885E-02	-0.3123E-01	-0.8120E+01	-0.1388E-01	-0.5392E-04	0.1121E-03
4.0000000	0.6020E-03	0.5908E+00	-0.9746E-04	-0.9685E+00	-0.8067E-02	-0.2718E-01	-0.7616E+01	-0.1272E-01	-0.5188E-04	0.9723E-04
4.5000000	0.6554E-03	0.5776E+00	-0.1029E-03	-0.9995E+00	-0.8223E-02	-0.2324E-01	-0.7045E+01	-0.1157E-01	-0.4947E-04	0.8298E-04
5.0000000	0.7096E-03	0.5642E+00	-0.1088E-03	-0.1028E+01	-0.8355E-02	-0.1940E-01	-0.6410E+01	-0.1044E-01	-0.4669E-04	0.6810E-04
5.5000000	0.7647E-03	0.5506E+00	-0.1152E-03	-0.1053E+01	-0.8462E-02	-0.1565E-01	-0.5710E+01	-0.9329E-02	-0.4354E-04	0.5302E-04
6.0000000	0.8203E-03	0.5369E+00	-0.1221E-03	-0.1075E+01	-0.8545E-02	-0.1201E-01	-0.4947E+01	-0.8231E-02	-0.4003E-04	0.3974E-04
6.5000000	0.8763E-03	0.5233E+00	-0.1295E-03	-0.1093E+01	-0.8604E-02	-0.8473E-02	-0.4124E+01	-0.7149E-02	-0.3618E-04	0.2585E-04
RESULTS FOR MAIN SHELL 4 CONICAL										
0.0000000	0.8763E-03	0.5233E+00	-0.1295E-03	-0.1093E+01	-0.8604E-02	-0.8473E-02	-0.4129E+01	-0.7196E-02	-0.3623E-04	0.2585E-04

TABLE B-19. (CONTINUED)

SOUT	W	Q PHI	U PHI	N PHI	BETA PHI	M PHI	N THETA	M THETA	EPS THETA	EPS PHI
.0100000	0.9626E-03	0.5178E+00	-0.1295E-03	-0.1108E+01	-0.8649E-02	-0.3271E-02	-0.2852E+01	-0.5550E-02	-0.3017E-04	-0.7616E-05
.0200000	0.1049E-02	0.5133E+00	-0.1296E-03	-0.1114E+01	-0.8640E-02	0.1860E-02	-0.1595E+01	-0.3939E-02	-0.2407E-04	-0.1525E-04
.0300000	0.1135E-02	0.5096E+00	-0.1296E-03	-0.1114E+01	-0.8579E-02	0.6929E-02	-0.3654E+00	-0.2321E-02	-0.1797E-04	-0.3505E-04
.0400000	0.1220E-02	0.5067E+00	-0.1296E-03	-0.1106E+01	-0.8465E-02	0.1194E-01	0.8302E+00	-0.6926E-03	0.2295E-04	-0.5597E-04
.0500000	0.1304E-02	0.5047E+00	-0.1297E-03	-0.1091E+01	-0.8296E-02	0.1692E-01	0.1985E+01	0.9462E-03	0.2796E-04	-0.7624E-04
.0600000	0.1386E-02	0.5035E+00	-0.1298E-03	-0.1070E+01	-0.8074E-02	0.2185E-01	0.3093E+01	0.2598E-02	0.3267E-04	-0.9649E-04
.0700000	0.1466E-02	0.5029E+00	-0.1299E-03	-0.1043E+01	-0.7797E-02	0.2677E-01	0.4147E+01	0.4263E-02	0.3704E-04	-0.1167E-03
.0800000	0.1542E-02	0.5031E+00	-0.1300E-03	-0.1010E+01	-0.7464E-02	0.3166E-01	0.5141E+01	0.5944E-02	0.4105E-04	-0.1370E-03
.0900000	0.1615E-02	0.5039E+00	-0.1302E-03	-0.9723E+00	-0.7076E-02	0.3653E-01	0.6069E+01	0.7642E-02	0.4466E-04	-0.1573E-03
RESULTS FOR MAIN SHELL 5 TOROIDAL										
6.5000000	0.1615E-02	0.5039E+00	-0.1302E-03	-0.9723E+00	-0.7076E-02	0.3653E-01	0.6066E+01	0.7644E-02	0.4464E-04	-0.1573E-03
10.8750000	0.1697E-02	0.4353E+00	-0.2569E-03	-0.9452E+00	-0.6423E-02	0.4300E-01	0.7680E+01	0.9986E-02	0.5098E-04	-0.1853E-03
15.2500000	0.1759E-02	0.3776E+00	-0.3892E-03	-0.8998E+00	-0.5667E-02	0.4852E-01	0.9032E+01	0.1208E-01	0.5980E-04	-0.2107E-03
19.6250000	0.1799E-02	0.3353E+00	-0.5255E-03	-0.8354E+00	-0.4819E-02	0.5331E-01	0.1227E+02	0.1398E-01	0.6996E-04	-0.2339E-03
24.0000000	0.1816E-02	0.3124E+00	-0.6640E-03	-0.7538E+00	-0.3887E-02	0.5762E-01	0.1473E+02	0.1575E-01	0.8023E-04	-0.2556E-03
RESULTS FOR MAIN SHELL 6 TOROIDAL										
24.0000000	0.1816E-02	0.3124E+00	-0.6640E-03	-0.7538E+00	-0.3887E-02	0.5762E-01	0.1475E+02	0.1574E-01	0.8033E-04	-0.2556E-03
29.5000000	0.1760E-02	0.2563E+00	-0.8359E-03	-0.7466E+00	-0.3587E-02	0.5877E-01	0.1551E+02	0.1629E-01	0.8336E-04	-0.2618E-03
35.0000000	0.1687E-02	0.2053E+00	-0.1002E-02	-0.7346E+00	-0.3281E-02	0.5969E-01	0.1634E+02	0.1676E-01	0.8674E-04	-0.2672E-03
40.5000000	0.1597E-02	0.1600E+00	-0.1160E-02	-0.7186E+00	-0.2968E-02	0.6040E-01	0.1720E+02	0.1716E-01	0.9033E-04	-0.2721E-03
46.0000000	0.1491E-02	0.1209E+00	-0.1308E-02	-0.6997E+00	-0.2651E-02	0.6094E-01	0.1807E+02	0.1751E-01	0.9398E-04	-0.2764E-03
46.0000000	0.1491E-02	0.1209E+00	-0.1308E-02	-0.6997E+00	-0.2651E-02	0.6094E-01	0.1807E+02	0.1751E-01	0.9398E-04	-0.2764E-03
51.5000000	0.1369E-02	0.8811E-01	-0.1445E-02	-0.6792E+00	-0.2330E-02	0.6132E-01	0.1890E+02	0.1779E-01	0.9756E-04	-0.2800E-03
57.0000000	0.1234E-02	0.6156E-01	-0.1571E-02	-0.6582E+00	-0.2005E-02	0.6159E-01	0.1968E+02	0.1802E-01	0.1009E-03	-0.2831E-03
62.5000000	0.1086E-02	0.4095E-01	-0.1682E-02	-0.6380E+00	-0.1677E-02	0.6176E-01	0.2038E+02	0.1821E-01	0.1040E-03	-0.2857E-03
68.0000000	0.9261E-03	0.2571E-01	-0.1779E-02	-0.6198E+00	-0.1346E-02	0.6186E-01	0.2097E+02	0.1835E-01	0.1067E-03	-0.2879E-03
68.0000000	0.9261E-03	0.2571E-01	-0.1779E-02	-0.6198E+00	-0.1346E-02	0.6186E-01	0.2097E+02	0.1835E-01	0.1067E-03	-0.2879E-03
73.5000000	0.7564E-03	0.1507E-01	-0.1860E-02	-0.6044E+00	-0.1013E-02	0.6191E-01	0.2144E+02	0.1846E-01	0.1088E-03	-0.2899E-03
79.0000000	0.5783E-03	0.8015E-02	-0.1926E-02	-0.5928E+00	-0.6775E-03	0.6193E-01	0.2177E+02	0.1853E-01	0.1104E-03	-0.2915E-03
84.5000000	0.3935E-03	0.3412E-02	-0.1971E-02	-0.5856E+00	-0.3399E-03	0.6194E-01	0.2195E+02	0.1857E-01	0.1114E-03	-0.2930E-03
90.0000000	0.2035E-03	0.1411E-06	-0.2000E-02	-0.5832E+00	-0.3949E-10	0.6195E-01	0.2198E+02	0.1858E-01	0.1117E-03	-0.2942E-03

TABLE B-20. OUTPUT FOR 3-INCH SINGLE-PLY BELLOWS JD68

	MERIDIONAL STRESSES				CIRCUMFERENTIAL STRESSES				SHEAR STRESS
SOUT	MEMBRANE	BENDING	INNER	OUTER	MEMBRANE	BENDING	INNER	OUTER	
RESULTS FOR MAIN SHELL 1 TOROIDAL									
90.0000000	-0.93458E+02	-0.10702E+05	0.10609E+05	-0.10796E+05	-0.23061E+04	-0.32107E+04	0.90465E+03	-0.55168E+04	0.
84.5000000	-0.93489E+02	-0.10718E+05	0.10624E+05	-0.10811E+05	-0.23002E+04	-0.32170E+04	0.91673E+03	-0.55172E+04	0.75788E+01
79.0000000	-0.93390E+02	-0.10722E+05	0.10628E+05	-0.10815E+05	-0.22828E+04	-0.32229E+04	0.94010E+03	-0.55057E+04	0.15242E+02
73.5000000	-0.93139E+02	-0.10714E+05	0.10621E+05	-0.10807E+05	-0.22542E+04	-0.32284E+04	0.97414E+03	-0.54826E+04	0.23050E+02
68.0000000	-0.92704E+02	-0.10694E+05	0.10602E+05	-0.10787E+05	-0.22154E+04	-0.32332E+04	0.10178E+04	-0.54485E+04	0.31052E+02
68.0000000	-0.92704E+02	-0.10694E+05	0.10602E+05	-0.10787E+05	-0.22154E+04	-0.32332E+04	0.10178E+04	-0.54485E+04	0.31052E+02
62.5000000	-0.92042E+02	-0.10663E+05	0.10571E+05	-0.10755E+05	-0.21673E+04	-0.32370E+04	0.10697E+04	-0.54042E+04	0.39283E+02
57.0000000	-0.91104E+02	-0.10618E+05	0.10527E+05	-0.10709E+05	-0.21113E+04	-0.32394E+04	0.11280E+04	-0.53507E+04	0.47762E+02
51.5000000	-0.89835E+02	-0.10561E+05	0.10471E+05	-0.10651E+05	-0.20492E+04	-0.32400E+04	0.11907E+04	-0.52892E+04	0.56498E+02
46.0000000	-0.88180E+02	-0.10491E+05	0.10403E+05	-0.10579E+05	-0.19829E+04	-0.32383E+04	0.12554E+04	-0.52212E+04	0.65441E+02
46.0000000	-0.88180E+02	-0.10491E+05	0.10403E+05	-0.10579E+05	-0.19829E+04	-0.32383E+04	0.12554E+04	-0.52212E+04	0.65441E+02
40.5000000	-0.86085E+02	-0.10407E+05	0.10321E+05	-0.10493E+05	-0.19143E+04	-0.32338E+04	0.13195E+04	-0.51481E+04	0.74580E+02
35.0000000	-0.83504E+02	-0.10310E+05	0.10227E+05	-0.10394E+05	-0.18458E+04	-0.32260E+04	0.13802E+04	-0.50718E+04	0.83844E+02
29.5000000	-0.80397E+02	-0.10199E+05	0.10119E+05	-0.10280E+05	-0.17797E+04	-0.32145E+04	0.14348E+04	-0.49941E+04	0.93159E+02
24.0000000	-0.76734E+02	-0.10075E+05	0.99985E+04	-0.10152E+05	-0.17183E+04	-0.31986E+04	0.14803E+04	-0.49169E+04	0.10243E+03
24.0000000	-0.76734E+02	-0.10075E+05	0.99985E+04	-0.10152E+05	-0.17183E+04	-0.31986E+04	0.14803E+04	-0.49169E+04	0.10243E+03
18.5000000	-0.72498E+02	-0.99379E+04	0.98654E+04	-0.10010E+05	-0.16641E+04	-0.31781E+04	0.15140E+04	-0.48422E+04	0.11157E+03
13.0000000	-0.67686E+02	-0.97875E+04	0.97198E+04	-0.98552E+04	-0.16194E+04	-0.31525E+04	0.15330E+04	-0.47719E+04	0.12048E+03
7.5000000	-0.62307E+02	-0.96247E+04	0.95624E+04	-0.96870E+04	-0.15866E+04	-0.31214E+04	0.15348E+04	-0.47080E+04	0.12904E+03
2.0000000	-0.56381E+02	-0.94500E+04	0.93936E+04	-0.95064E+04	-0.15678E+04	-0.30847E+04	0.15169E+04	-0.46525E+04	0.13718E+03
RESULTS FOR MAIN SHELL 2 CONICAL									
0.0000000	-0.56381E+02	-0.94500E+04	0.93936E+04	-0.95064E+04	-0.15678E+04	-0.30847E+04	0.15169E+04	-0.46524E+04	0.13718E+03
.0158250	-0.72244E+02	-0.84083E+04	0.83361E+04	-0.84806E+04	-0.15096E+04	-0.28489E+04	0.13393E+04	-0.43586E+04	0.13638E+03
.0316500	-0.87322E+02	-0.73493E+04	0.72620E+04	-0.74367E+04	-0.14415E+04	-0.25957E+04	0.11542E+04	-0.40372E+04	0.13505E+03
.0474750	-0.10105E+03	-0.62076E+04	0.61065E+04	-0.63087E+04	-0.13647E+04	-0.23076E+04	0.94291E+03	-0.36723E+04	0.13431E+03
.0633000	-0.11369E+03	-0.50556E+04	0.49419E+04	-0.51693E+04	-0.12813E+04	-0.20050E+04	0.72373E+03	-0.32863E+04	0.13289E+03
RESULTS FOR MAIN SHELL 3 TOROIDAL									
2.0000000	-0.11369E+03	-0.50556E+04	0.49419E+04	-0.51693E+04	-0.12800E+04	-0.20045E+04	0.72448E+03	-0.32846E+04	0.13289E+03
2.5000000	-0.11945E+03	-0.45761E+04	0.44566E+04	-0.46955E+04	-0.12396E+04	-0.18751E+04	0.63545E+03	-0.31147E+04	0.13077E+03
3.0000000	-0.12499E+03	-0.41033E+04	0.39783E+04	-0.42283E+04	-0.11902E+04	-0.17456E+04	0.55546E+03	-0.29358E+04	0.12853E+03
3.5000000	-0.13026E+03	-0.36376E+04	0.35073E+04	-0.37679E+04	-0.11315E+04	-0.16164E+04	0.48493E+03	-0.27478E+04	0.12618E+03
4.0000000	-0.13522E+03	-0.31795E+04	0.30443E+04	-0.33147E+04	-0.10633E+04	-0.14875E+04	0.42418E+03	-0.25508E+04	0.12374E+03
4.5000000	-0.13984E+03	-0.27292E+04	0.25894E+04	-0.28690E+04	-0.98566E+03	-0.13591E+04	0.37345E+03	-0.23448E+04	0.12122E+03
5.0000000	-0.14409E+03	-0.22871E+04	0.21430E+04	-0.24312E+04	-0.89855E+03	-0.12314E+04	0.33285E+03	-0.21300E+04	0.11863E+03
5.5000000	-0.14792E+03	-0.18533E+04	0.17054E+04	-0.20012E+04	-0.80205E+03	-0.11045E+04	0.30242E+03	-0.19065E+04	0.11601E+03
6.0000000	-0.15131E+03	-0.14281E+04	0.12767E+04	-0.15794E+04	-0.69633E+03	-0.97843E+03	0.28211E+03	-0.16748E+04	0.11337E+03
6.5000000	-0.15423E+03	-0.10113E+04	0.85711E+03	-0.11656E+04	-0.58162E+03	-0.85335E+03	0.27174E+03	-0.14350E+04	0.11072E+03
RESULTS FOR MAIN SHELL 4 CONICAL									

TABLE B-20. (CONTINUED)

	MERIDIONAL STRESSES				CIRCUMFERENTIAL STRESSES				SHEAR STRESS
SOUT	MEMBRANE	BENDING	INNER	OUTER	MEMBRANE	BENDING	INNER	OUTER	
0.0000000	-0.15423E+03	-0.10113E+04	0.85711E+03	-0.11656E+04	-0.58239E+03	-0.85415E+03	0.27176E+03	-0.14365E+04	0.11072E+03
.0100000	-0.15672E+03	-0.39273E+03	0.23602E+03	-0.54945E+03	-0.40348E+03	-0.66647E+03	0.26299E+03	-0.10699E+04	0.10908E+03
.0200000	-0.15813E+03	0.22466E+03	-0.38278E+03	0.66532E+02	-0.22634E+03	-0.47584E+03	0.24950E+03	-0.70218E+03	0.10924E+03
.0300000	-0.15849E+03	0.84197E+03	-0.10005E+04	0.68348E+03	-0.52007E+02	-0.28200E+03	0.22999E+03	-0.33400E+03	0.10878E+03
.0400000	-0.15783E+03	0.14603E+04	-0.16181E+04	0.13025E+04	0.11851E+03	-0.84678E+02	0.20319E+03	0.33832E+02	0.10850E+03
.0500000	-0.15620E+03	0.20808E+04	-0.22370E+04	0.19246E+04	0.28422E+03	0.11638E+03	0.16784E+03	0.40060E+03	0.10839E+03
.0600000	-0.15365E+03	0.27044E+04	-0.28580E+04	0.25507E+04	0.44413E+03	0.32144E+03	0.12269E+03	0.76557E+03	0.10845E+03
.0700000	-0.15021E+03	0.33322E+04	-0.34824E+04	0.31820E+04	0.59729E+03	0.53075E+03	0.66539E+02	0.11280E+04	0.10867E+03
.0800000	-0.14594E+03	0.39651E+04	-0.41111E+04	0.38192E+04	0.74273E+03	0.74457E+03	-0.18378E+01	0.14873E+04	0.10903E+03
.0900000	-0.14091E+03	0.46042E+04	-0.47451E+04	0.44632E+04	0.87950E+03	0.96313E+03	-0.83627E+02	0.18426E+04	0.10954E+03
RESULTS FOR MAIN SHELL 5 TOROIDAL									
6.5000000	-0.14091E+03	0.46042E+04	-0.47451E+04	0.44632E+04	0.87908E+03	0.96332E+03	-0.84246E+02	0.18424E+04	0.10954E+03
10.8750000	-0.13758E+03	0.54659E+04	-0.56034E+04	0.53283E+04	0.11179E+04	0.12694E+04	-0.15157E+03	0.23873E+04	0.95036E+02
15.2500000	-0.13155E+03	0.62229E+04	-0.63544E+04	0.60913E+04	0.14374E+04	0.15498E+04	-0.11240E+03	0.29872E+04	0.82809E+02
19.6250000	-0.12267E+03	0.68977E+04	-0.70203E+04	0.67750E+04	0.18018E+04	0.18092E+04	-0.74460E+01	0.36110E+04	0.73850E+02
24.0000000	-0.11118E+03	0.75213E+04	-0.76325E+04	0.74101E+04	0.21723E+04	0.20553E+04	0.11704E+03	0.42276E+04	0.69109E+02
RESULTS FOR MAIN SHELL 6 TOROIDAL									
24.0000000	-0.11118E+03	0.75213E+04	-0.76325E+04	0.74101E+04	0.21751E+04	0.20551E+04	0.12007E+03	0.42302E+04	0.69109E+02
29.5000000	-0.11030E+03	0.76962E+04	-0.78065E+04	0.75859E+04	0.22913E+04	0.21325E+04	0.15882E+03	0.44238E+04	0.56786E+02
35.0000000	-0.10871E+03	0.78435E+04	-0.79522E+04	0.77347E+04	0.24185E+04	0.22018E+04	0.21665E+03	0.46203E+04	0.45559E+02
40.5000000	-0.10657E+03	0.79719E+04	-0.80784E+04	0.78653E+04	0.25515E+04	0.22651E+04	0.28641E+03	0.48166E+04	0.35603E+02
46.0000000	-0.10400E+03	0.80777E+04	-0.81817E+04	0.79737E+04	0.26855E+04	0.23205E+04	0.36497E+03	0.50060E+04	0.26959E+02
46.0000000	-0.10400E+03	0.80777E+04	-0.81817E+04	0.79737E+04	0.26855E+04	0.23205E+04	0.36497E+03	0.50060E+04	0.26959E+02
51.5000000	-0.10117E+03	0.81645E+04	-0.82657E+04	0.80633E+04	0.28159E+04	0.23687E+04	0.44717E+03	0.51846E+04	0.19608E+02
57.0000000	-0.98266E+02	0.82357E+04	-0.83339E+04	0.81374E+04	0.29383E+04	0.24102E+04	0.52813E+03	0.53485E+04	0.13785E+02
62.5000000	-0.95462E+02	0.82947E+04	-0.83902E+04	0.81992E+04	0.30490E+04	0.24457E+04	0.60334E+03	0.54947E+04	0.91896E+01
68.0000000	-0.92932E+02	0.83449E+04	-0.84378E+04	0.82519E+04	0.31445E+04	0.24757E+04	0.66877E+03	0.56202E+04	0.57835E+01
68.0000000	-0.92932E+02	0.83449E+04	-0.84378E+04	0.82519E+04	0.31445E+04	0.24757E+04	0.66877E+03	0.56202E+04	0.57835E+01
73.5000000	-0.90832E+02	0.83891E+04	-0.84799E+04	0.82982E+04	0.32219E+04	0.25009E+04	0.72097E+03	0.57228E+04	0.33952E+01
79.0000000	-0.89289E+02	0.84297E+04	-0.85190E+04	0.83404E+04	0.32790E+04	0.25218E+04	0.75713E+03	0.58008E+04	0.18109E+01
84.5000000	-0.88402E+02	0.84685E+04	-0.85569E+04	0.83801E+04	0.33139E+04	0.25388E+04	0.77515E+03	0.58527E+04	0.77264E+00
90.0000000	-0.88230E+02	0.85066E+04	-0.85948E+04	0.84184E+04	0.33257E+04	0.25520E+04	0.77370E+03	0.58777E+04	0.32014E-04

DETERMINANT OF FLEXIBILITY MATRIX FOR LINEAR ANALYSIS WAS 0.13714226E+01

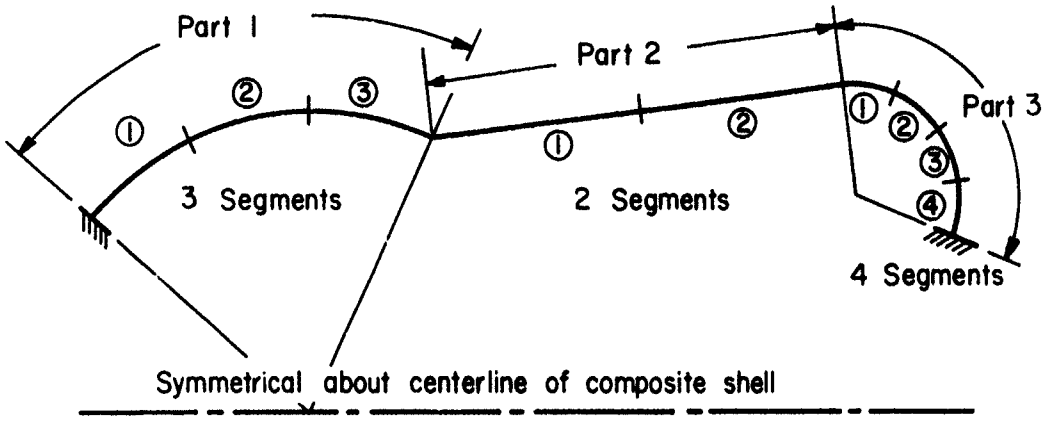

FIGURE B-1. THREE-PART COMPOSITE SHELL SHOWING SEGMENTS

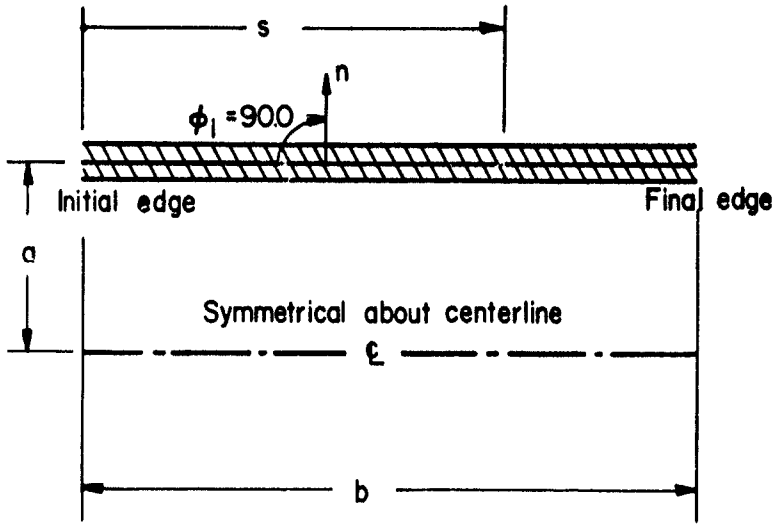

a = radius (inches) of cylinder midsurface
b = length (inches) of cylinder
c - not used for this type part
$\varphi_{initial}$ = 90.0, -90.0, or 270.0 degrees, depending on direction of normal and position of cylindrical part in a composite shell
φ_{final} - not used for this type part.

Special requirements:

(1) Spelling on data card must be CYLINDRICAL
(2) 'a' and 'b' are always positive
(3) This shell type can only be used if it has constant thickness, constant meridional properties, and is subjected to constant loadings. If any of these are variable, then the VARCYLINDER part must be used.

FIGURE B-2. CYLINDRICAL SHELL PART

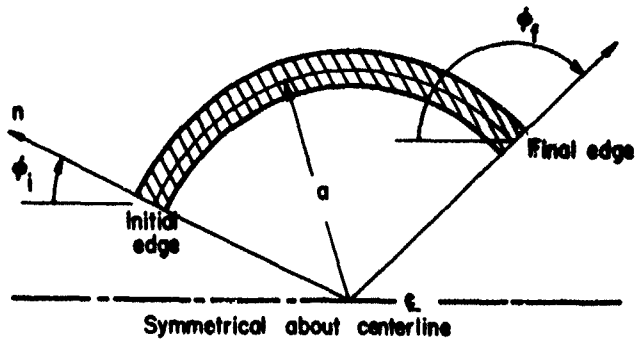

a = radius (inches) of sphere midsurface
b - not used for this type part
c - not used for this type part
$\varphi_{initial}$ = angle (degrees) at initial edge of part
φ_{final} = angle (degrees) at final edge of part.

Special requirements:

(1) 'a' is positive when normal n points away from the centerline; 'a' is negative when normal n points toward the centerline.
(2) The angle φ must not be 0 or 180 degrees.
(3) Spelling on data card must be SPHERØIDAL.

FIGURE B-3. SPHERØIDAL SHELL PART

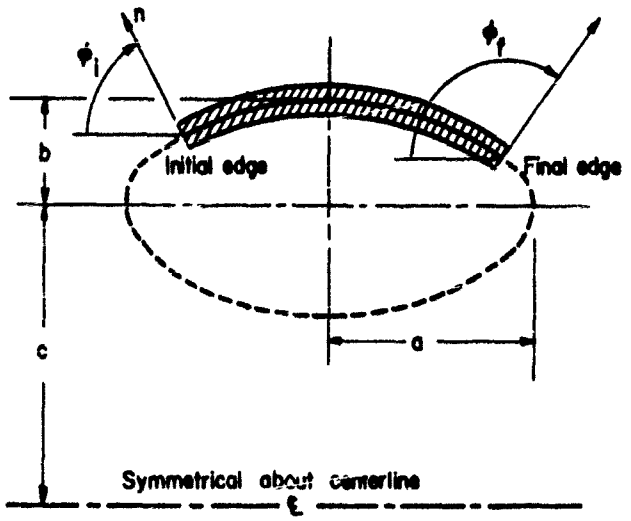

a = semi-axis (inches) of ellipse midsurface parallel to centerline of part
b = semi-axis (inches) of ellipse midsurface perpendicular to centerline of part
c = distance (inches from centerline of composite shell to centerline of ellipse.
$\varphi_{initial}$ = angle (degrees) at the initial edge of part
φ_{final} = angle (degrees) at the final edge of part.

Special requirements:

(1) When c = 0, this represents an ellipsoidal shell part. The angle φ cannot pass through 0 or 180 degrees.
(2) 'a' and 'b' are both positive for the case shown. When the normal points toward the interior of the shell part both 'a' and 'b' are negative.
(3) For $c>0$, the shell part is a toroidal shell of elliptical cross section. If $c \geq |b|$, then φ can have any value. If $c<|b|$, the midsurface of the ellipse cannot intersect the centerline of the composite shell.
(4) Spelling on data card must be ELLIPSØIDAL.

FIGURE B-4. ELLIPSOIDAL SHELL PART

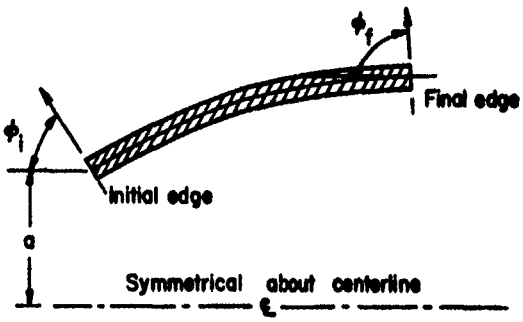

a = vertical distance (inches) from initial edge of part to centerline of the composite shell
b - not used for this type part
c - not used for this type part
$\varphi_{initial}$ = angle (degrees) at the initial edge of the part
φ_{final} = angle (degrees) at the final edge of the part

See B-I-e for instructions when normal points toward center of part.

Special requirements:

(1) The angle φ cannot be zero
(2) 'a' is always positive
(3) Spelling on data card must be PARABØLØIDAL

FIGURE B-5. PARABOLOIDAL SHELL PART

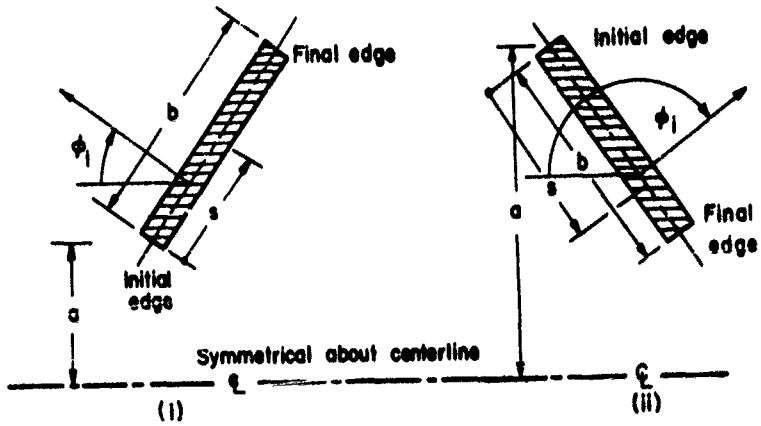

a = vertical distance (inches) from initial edge of part to centerline of the composite shell
b = slant length (inches) of shell part
c - not used for this type part
$\varphi_{initial}$ = angle (degrees) which the normal makes with the centerline of the composite shell
φ_{final} - not used for this type part.

Special requirements:

(1) 'a' and 'b' are always positive for a conical shell.
(2) Shell part cannot begin or end on axis of composite shell, that is, in (i), 'a' cannot be zero and in (ii) the final edge of the shell cannot touch the centerline of the composite shell.
(3) The angle $\varphi_{initial}$ can have <u>any</u> value. When it is 0.0, 180.0. -180.0, the shape part becomes a flat plate. 'a' and 'b' are still positive. The angle can also be 90.0, 270.0, or -90.00 deg. In this case the shell part would be cylindrical. However, it is not recommended that the CONICAL part be used to describe a cylindrical shell since additional calculations would have to be performed in the GOMTRY subroutine, thus making the calculation time somewhat longer.
(4) Spelling on data card must be CØNICAL.

FIGURE B-6. CONICAL SHELL PART

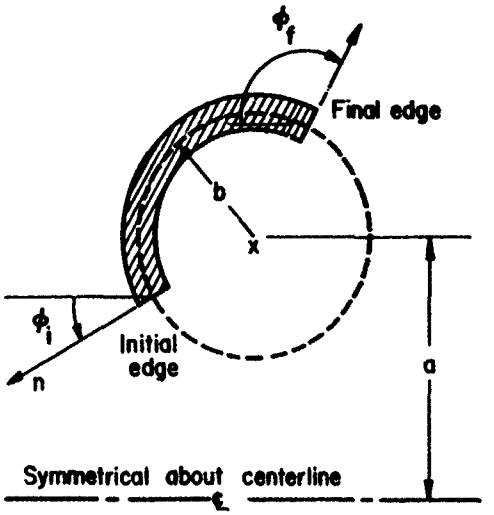

a = distance (inches) from centerline of composite shell to center of tube
b = radius (inches) of tube midsurface
c - not used for this type part
$\varphi_{initial}$ = angle (degrees) at initial edge of part
φ_{final} = angle (degrees) at final edge of part
See B-I-e for instructions for determining $\varphi_{initial}$ and φ_{final} when normal points toward center of tube.

Special requirements:

(1) 'a' is always positive
(b) 'b' is positive when normal n points away from x (shown above); 'b' is negative when normal n points toward x
(3) The angle φ can have any value provided $a > |b|$.
(4) Spelling on data card must be TØRØIDAL.

FIGURE B-7. TOROIDAL SHELL PART

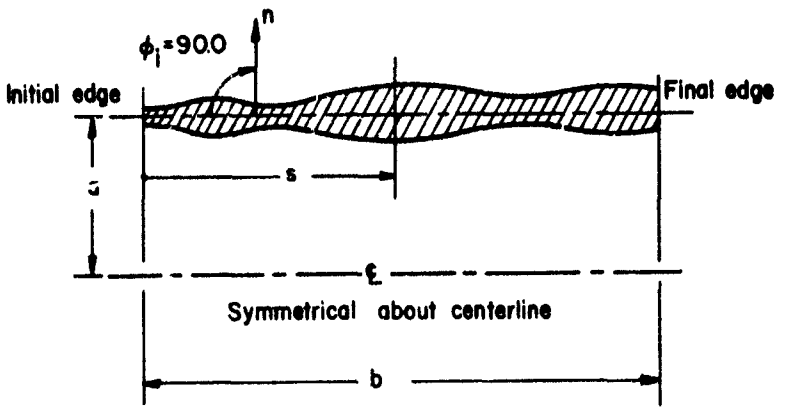

a = radius (inches) of cylinder midsurface
b = length (inches) of cylinder
c - not used for this part
$\varphi_{initial}$ = 90.0, -90.0, 270.0 deg., depending on direction of normal and position of cylindrical part in composite shell
φ_{final} - not used for this part.

Special requirements:

(1) 'a' and 'b' are always positive
(2) Spelling on data card must be VARCYLINDER.

FIGURE B-8. VARCYLINDER SHELL PART

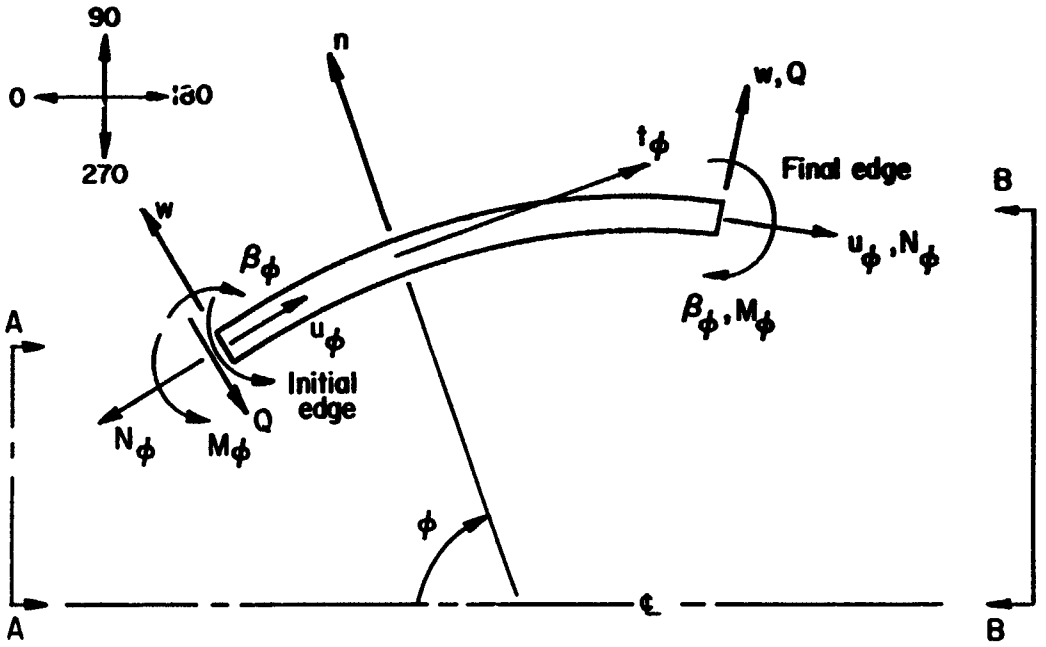

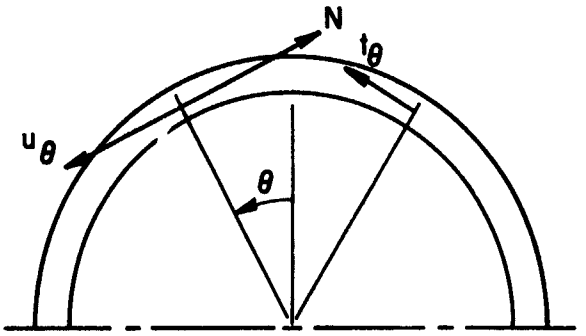

Section AA

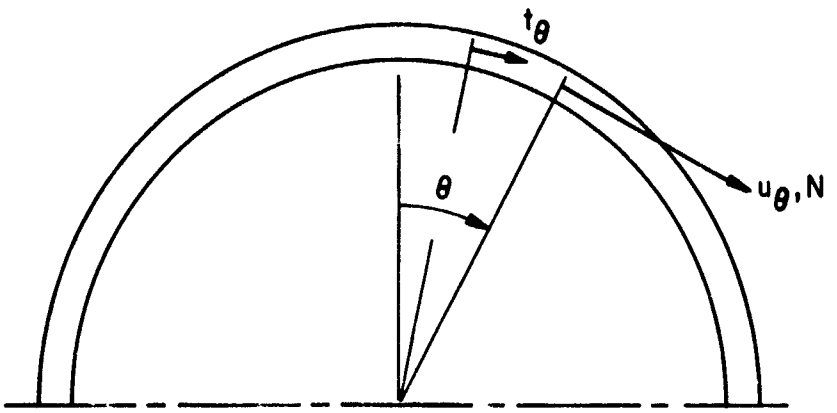

Section BB

FIGURE B-9. POSITIVE VALUES OF FUNDAMENTAL VARIABLES FOR A NORMAL POINTING AWAY FROM THE CENTER OF CURVATURE

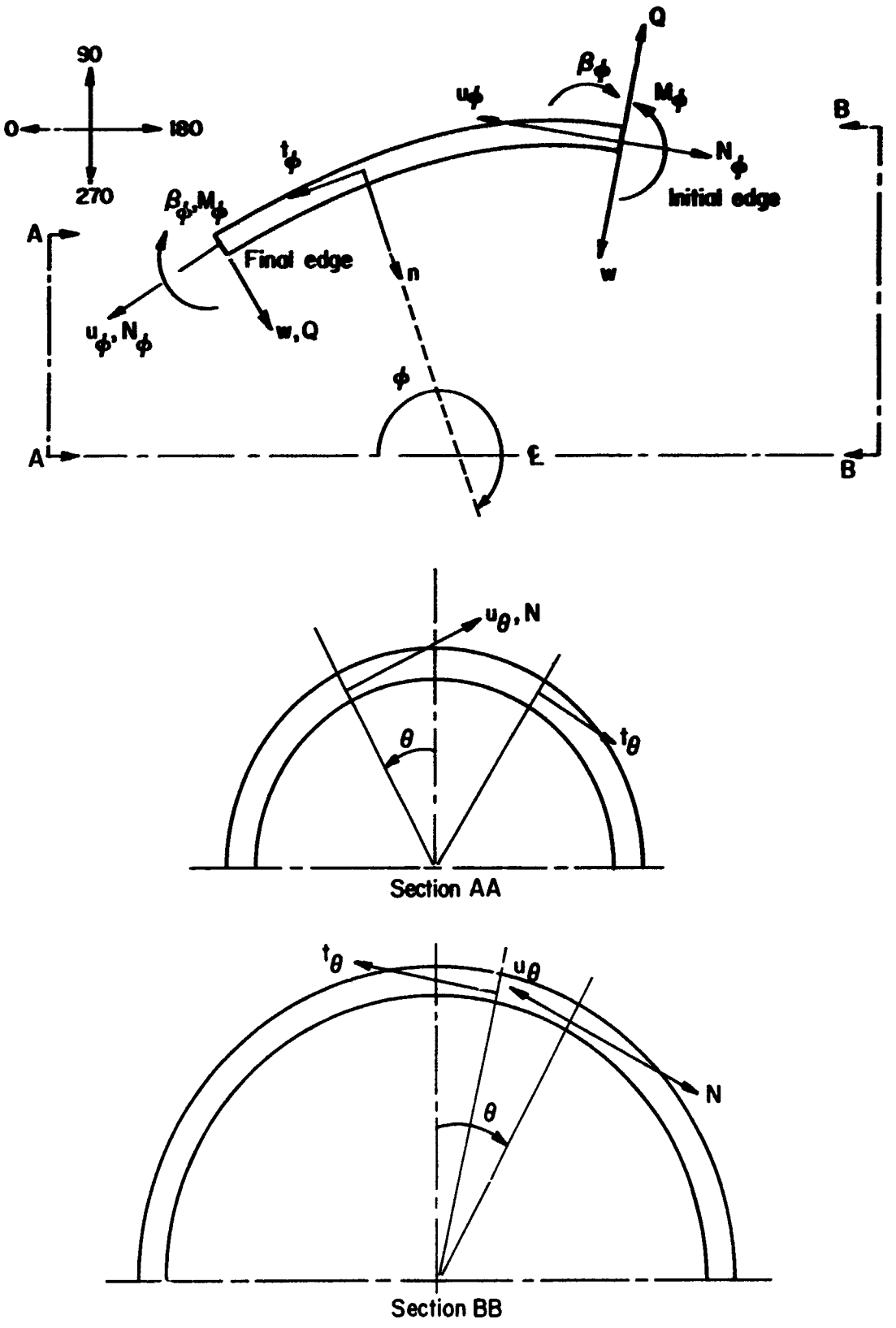

FIGURE B-10. POSITIVE VALUES OF FUNDAMENTAL VARIABLES FOR A NORMAL POINTING TOWARD THE CENTER OF CURVATURE

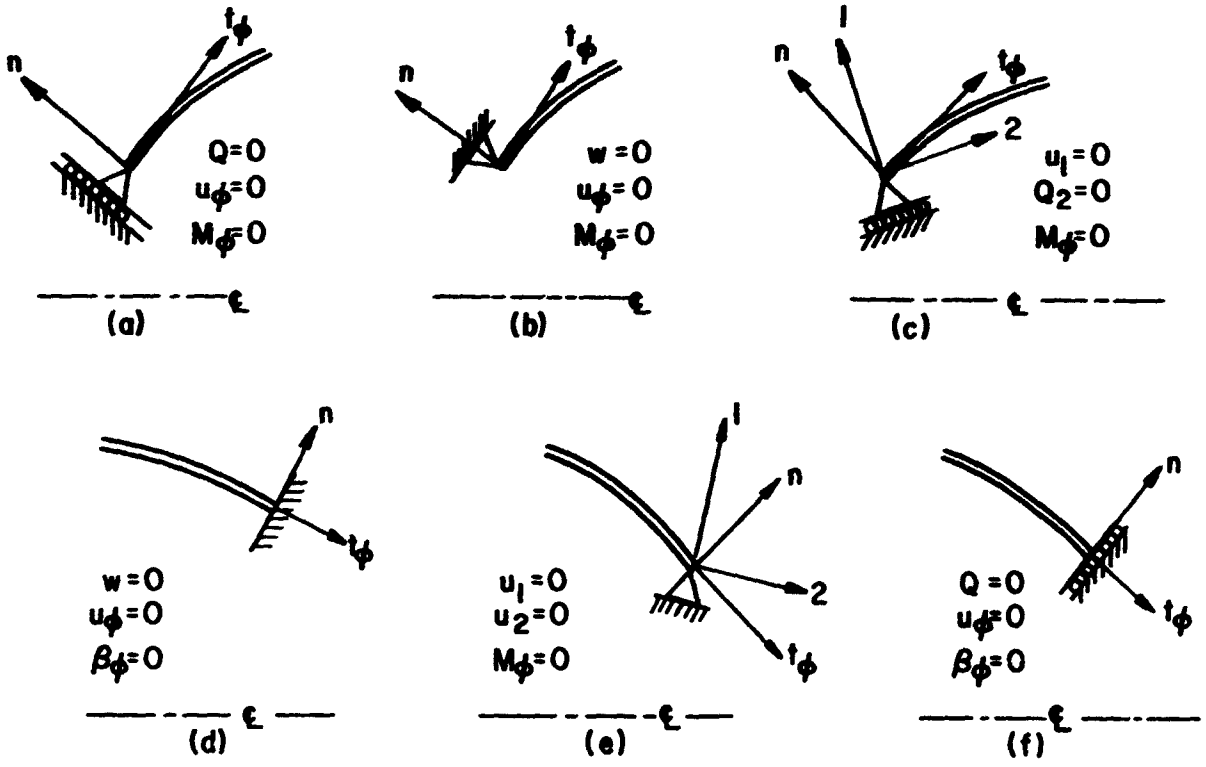

FIGURE B-11. EXAMPLES OF COMMON TYPES BOUNDARY CONDITIONS

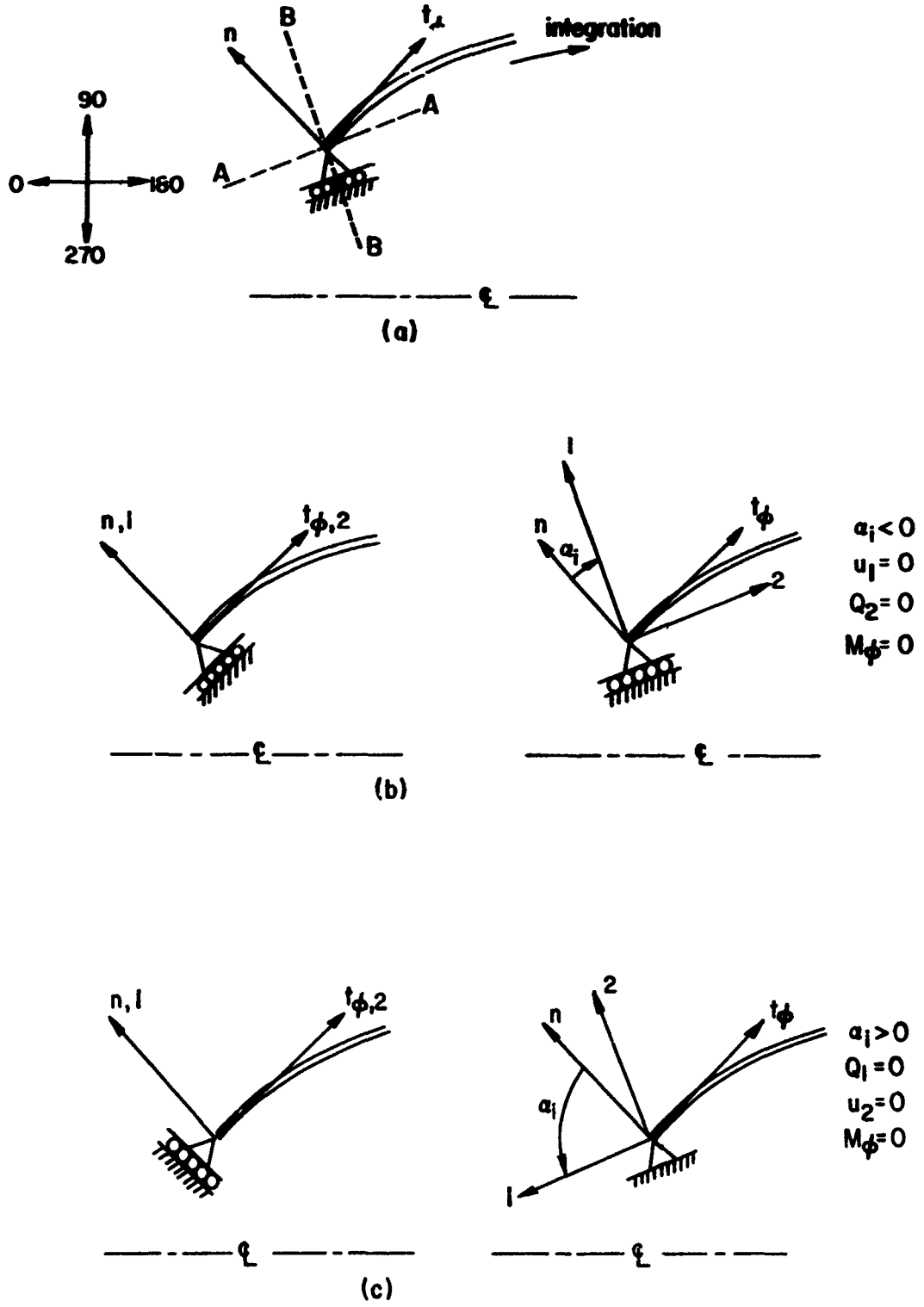

FIGURE B-12. SKETCHES SHOWING MANNER IN WHICH BOUNDARY ROTATION ANGLE IS OBTAINED AT INITIAL EDGE OF SHELL

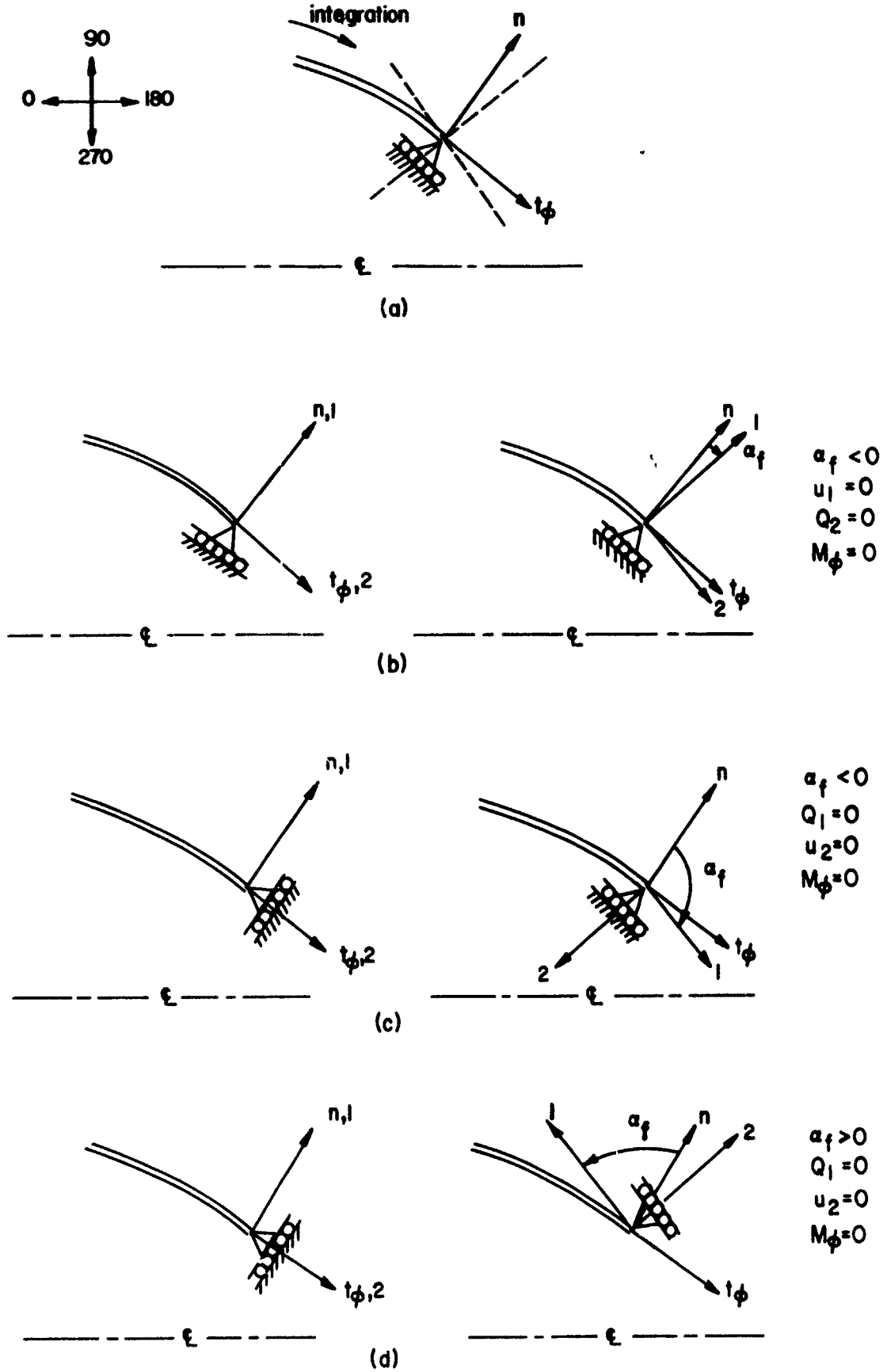

FIGURE B-13. SKETCHES SHOWING MANNER IN WHICH BOUNDARY ROTATION ANGLE IS DETERMINED AT FINAL EDGE OF SHELL

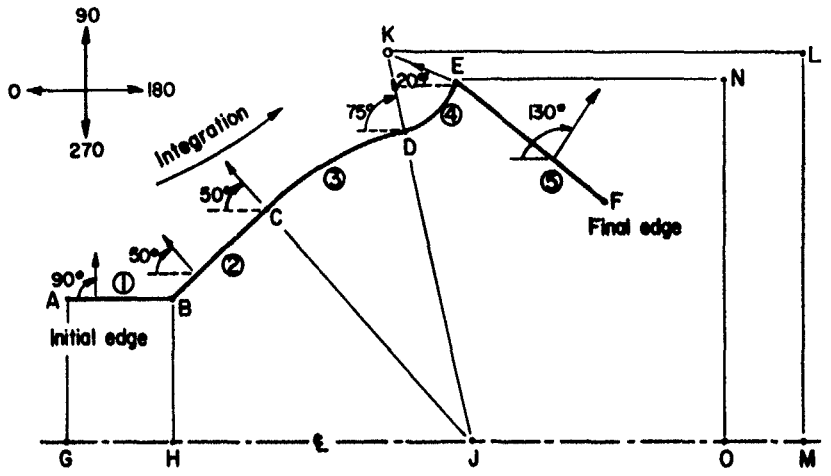

Part	Type	Coordinates, Degrees Initial	Final	Radii, inches a	b*	Reference Figures
1	VARCYLINDER	90.0	-	GA	AB	B-8
2	CØNICAL	50.0	-	HB	BC	B-6
3	SPHERØIDAL	50.0	75.0	JC	-	B-3
4	TØRØIDAL	75.0	20.0	ML	-KD	B-7
5	CØNICAL	130.0	-	ON	EF	B-6

* For the VARCYLINDER, CØNICAL and CYLINDRICAL shell parts, the 'b' distance is the length of the part.

FIGURE B-14. FIVE-PART COMPOSITE SHELL SHOWING INITIAL AND FINAL COORDINATES AND RADII a AND b WHEN INITIAL EDGE IS ON LEFT OF SHELL

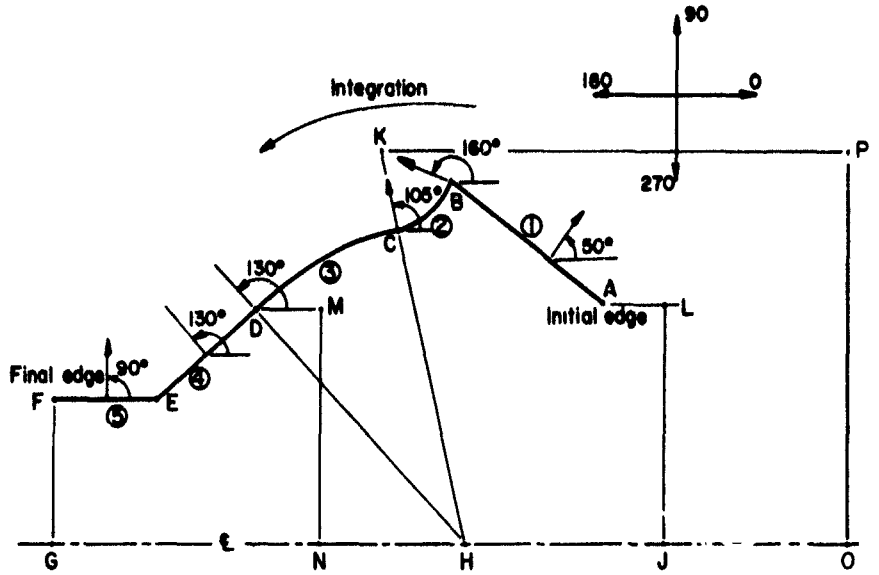

Part	Type	Coordinates, Degrees Initial	Final	Radii, inches a	b*	Reference Figures
1	CØNICAL	50.0	-	JL	AB	B-6
2	TØRØIDAL	160.0	105.0	OP	-BK	B-7
3	SPHERØIDAL	105.0	130.0	HC	-	B-3
4	CØNICAL	130.0	-	MN	DE	B-6
5	VARCYLINDER	90.0	-	FG	EF	B-8

* For the VARCYLINDER, CØNICAL and CYLINDRICAL shell parts, the 'b' distance is the length of the part.

FIGURE B-15. FIVE-PART COMPOSITE SHELL SHOWING INITIAL AND FINAL COORDINATES AND RADII a AND b WHEN INITIAL EDGE IS ON RIGHT OF SHELL

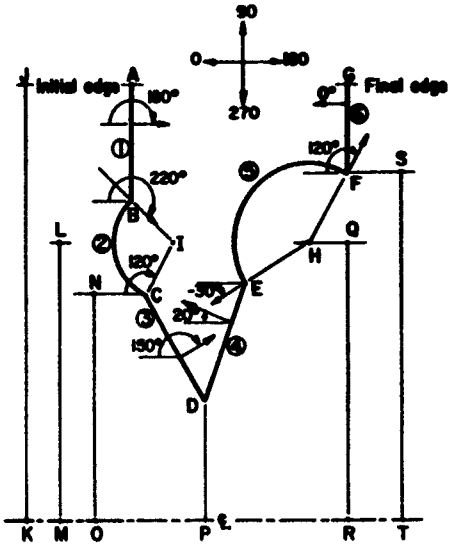

Part	Type	Coordinates, Degrees Initial	Final	Radii, inches a	b*	Reference Figures
1	CONICAL	180.0	-	JK	AB	B-6
2	TOROIDAL	220.0	120.0	LM	-EI	B-7
3	CONICAL	150.0	-	NO	CD	B-6
4	CONICAL	20.0	-	DP	DE	B-6
5	TOROIDAL	-30.0	120.0	QR	EH	B-7
6	CONICAL	0.0	-	TS	FG	B-6

* For the CONICAL shell parts, the 'b' distance is the length of the part.

FIGURE B-16. SIX-PART COMPOSITE SHELL SHOWING INITIAL AND FINAL COORDINATES AND RADII a AND b WHEN INITIAL EDGE IS ON LEFT OF SHELL

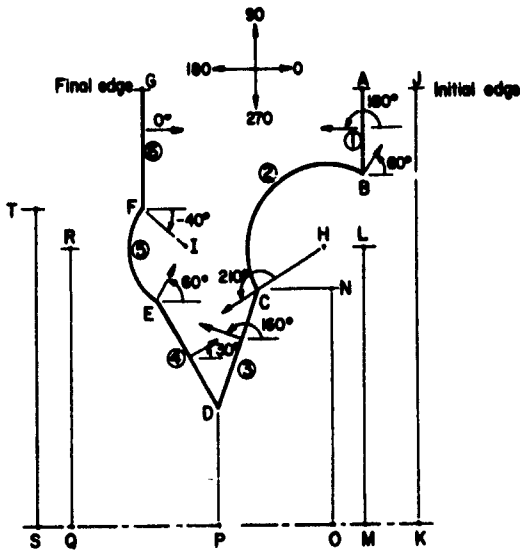

Part	Type	Coordinates, degrees Initial	Final	Radii, inches a	b*	Reference Figures
1	CONICAL	180.0	-	JK	AB	B-6
2	TOROIDAL	60.0	210.0	LM	HC	B-7
3	CONICAL	160.0	-	NO	CD	B-6
4	CONICAL	30.0	-	DP	DE	B-6
5	TOROIDAL	60.0	-40.0	QR	-EI	B-7
6	CONICAL	0.0	-	ST	FG	B-6

* For the CONICAL shell parts, the 'b' distance is the length of the part.

FIGURE B-17. SIX-PART COMPOSITE SHELL SHOWING INITIAL AND FINAL COORDINATES AND RADII a AND b WHEN INITIAL EDGE IS ON RIGHT OF SHELL

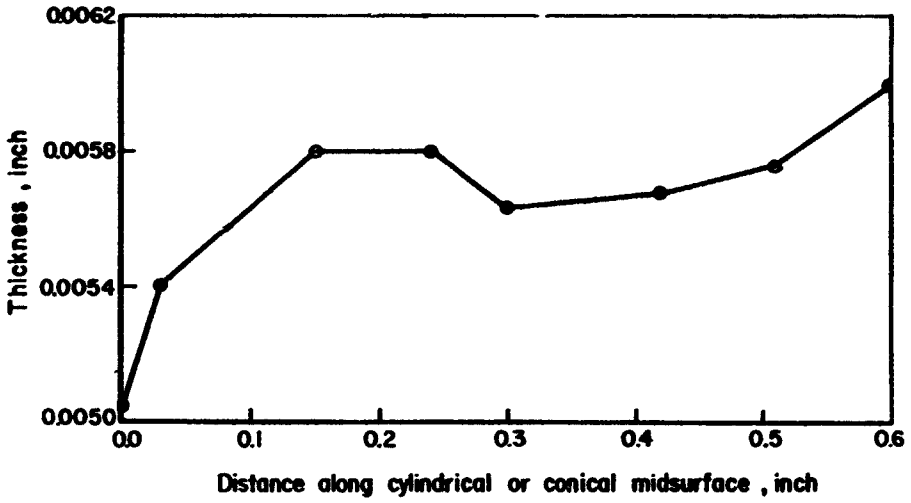

s, inches	Thickness, inches
0.0	0.00504
0.03	0.00540
0.15	0.00580
0.24	0.00580
0.30	0.00564
0.42	0.00568
0.52	0.00576
0.60	0.00600

FIGURE B-18. TYPICAL REPRESENTATION OF THICKNESS DISTRIBUTION FOR VARCYLINDER OF CONICAL PARTS

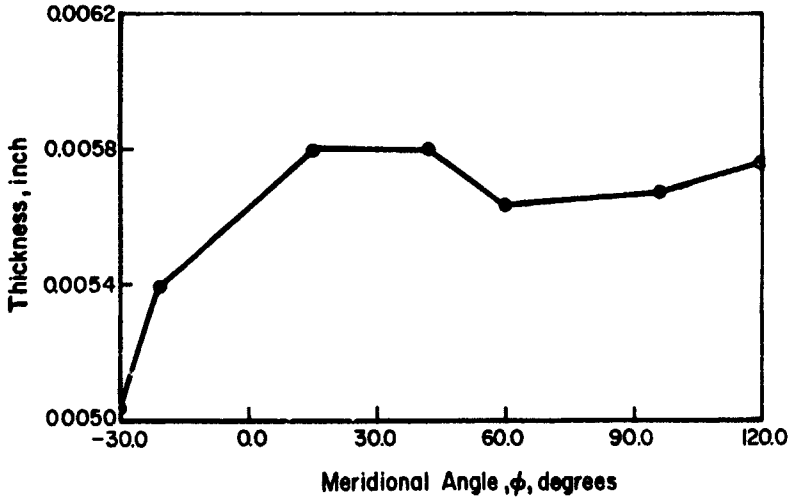

Angle, Degrees	Thickness, inches
-30.0	0.00504
-21.0	0.00540
15.0	0.00580
42.0	0.00580
60.0	0.00564
96.0	0.00568
120.0	0.00576

FIGURE B-19. THICKNESS DISTRIBUTION FOR TOROIDAL PART 5 SHOWN IN FIGURE B-16

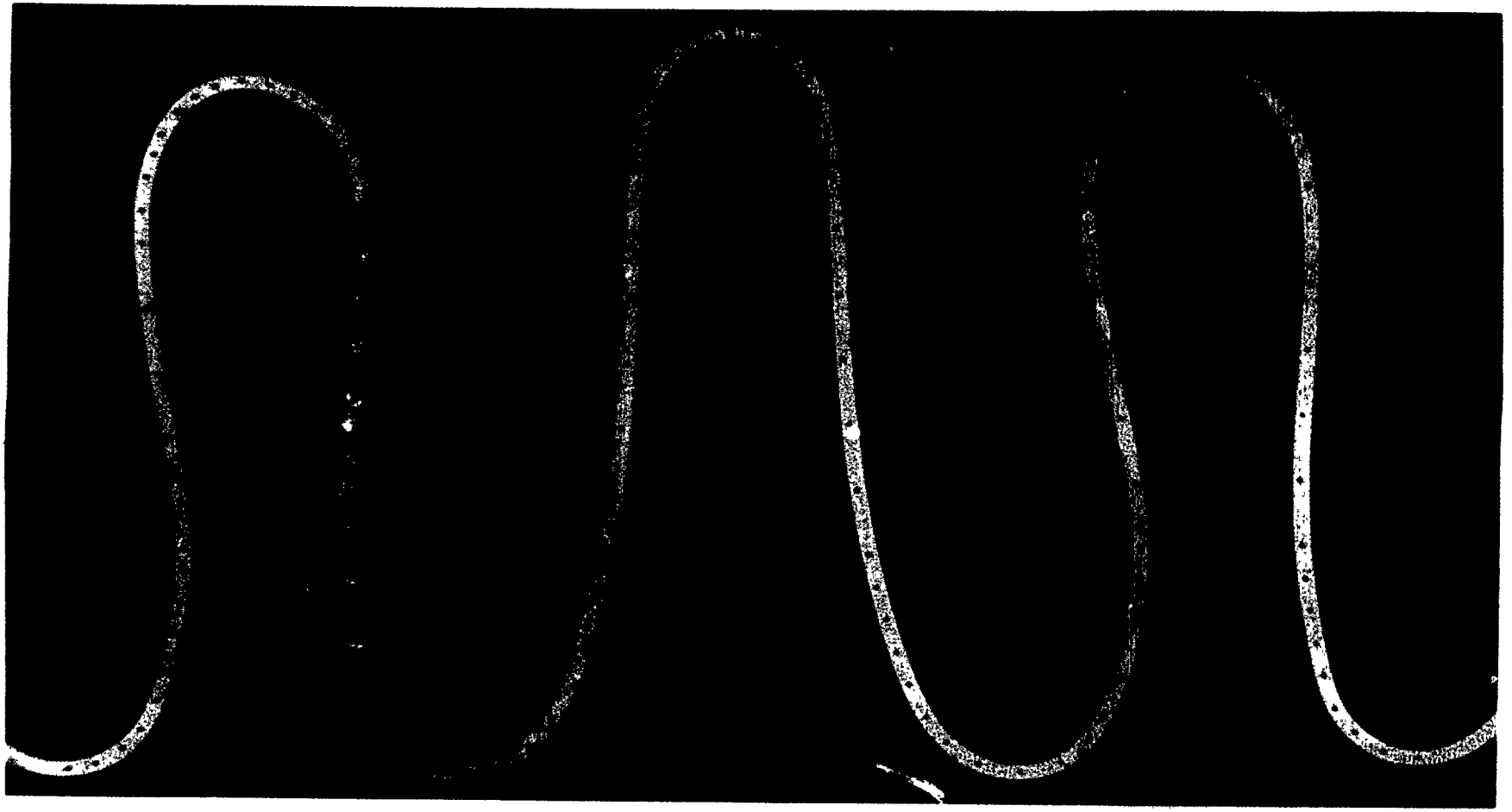

20X

9A164

FIGURE B-20. CONVOLUTIONS OF CROSS-SECTIONED 3-INCH ONE-PLY INCONEL 718 BELLOWS

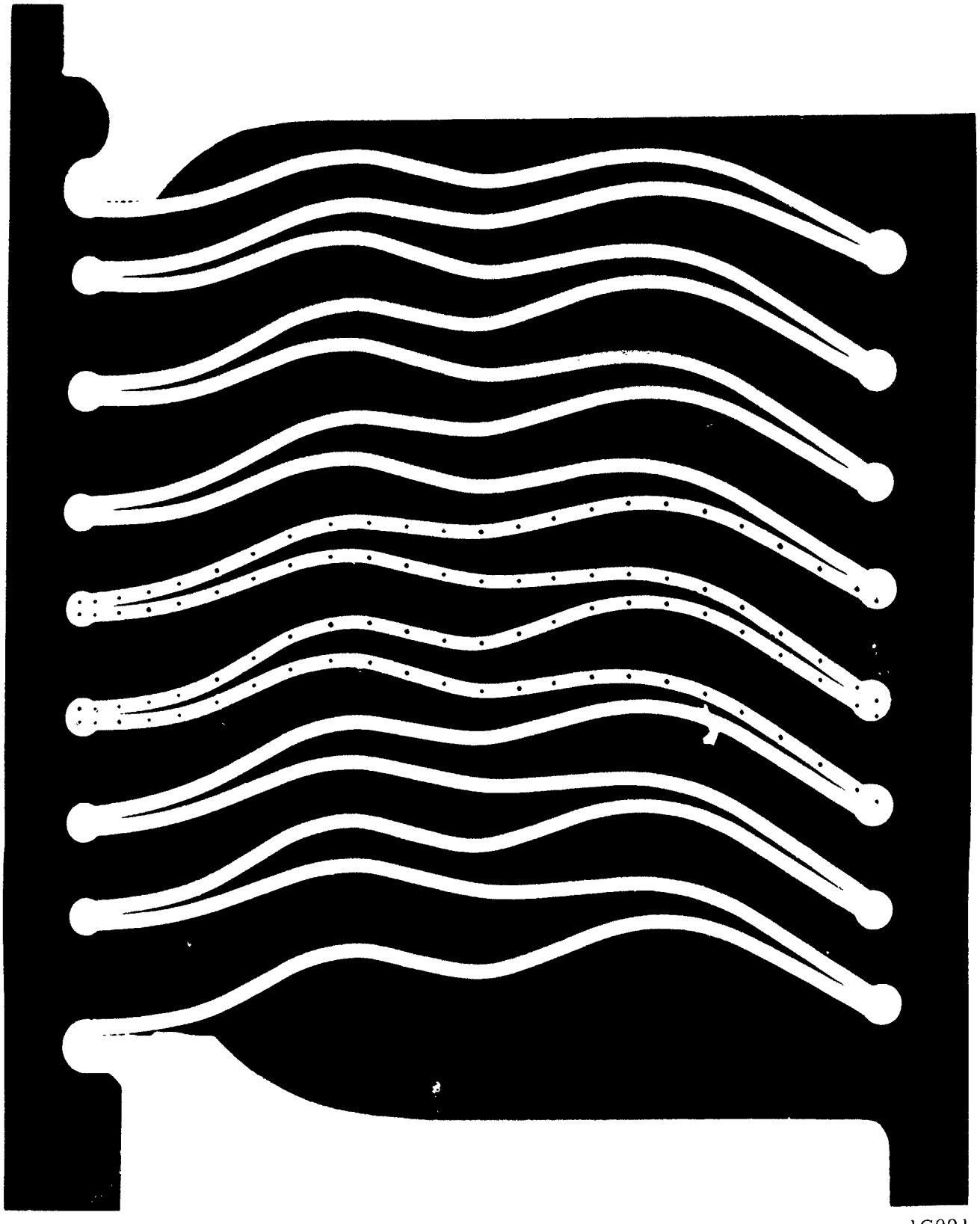

20X 1C991

FIGURE B-21 CONVOLUTIONS OF CROSS-SECTIONED 3-INCH SINGLE-PLY AM 350 WELDED BELLOWS

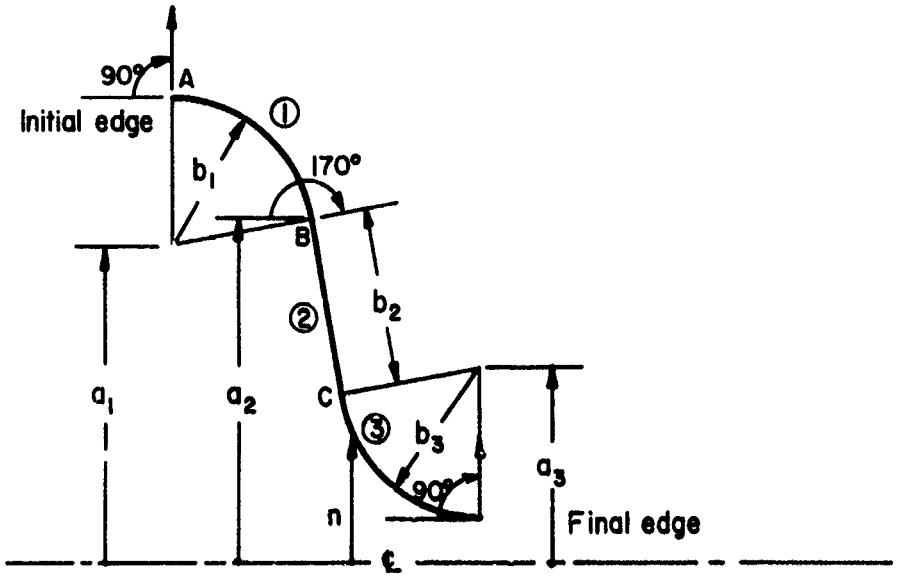

For Part 1: $r_B^1 = a_1 + b_1 \sin \varphi_i$

For Part 2: $r_B^2 = a_2$; $r_C^2 = a_2 + b_2 \cos\varphi_i$

For Part 3: $r_C^3 = a_3 + b_3 \sin \varphi_i$

FIGURE B-22. RELATIONSHIP BETWEEN THE POINTS B AND C ON THE CONVOLUTION OF A FORMED BELLOWS

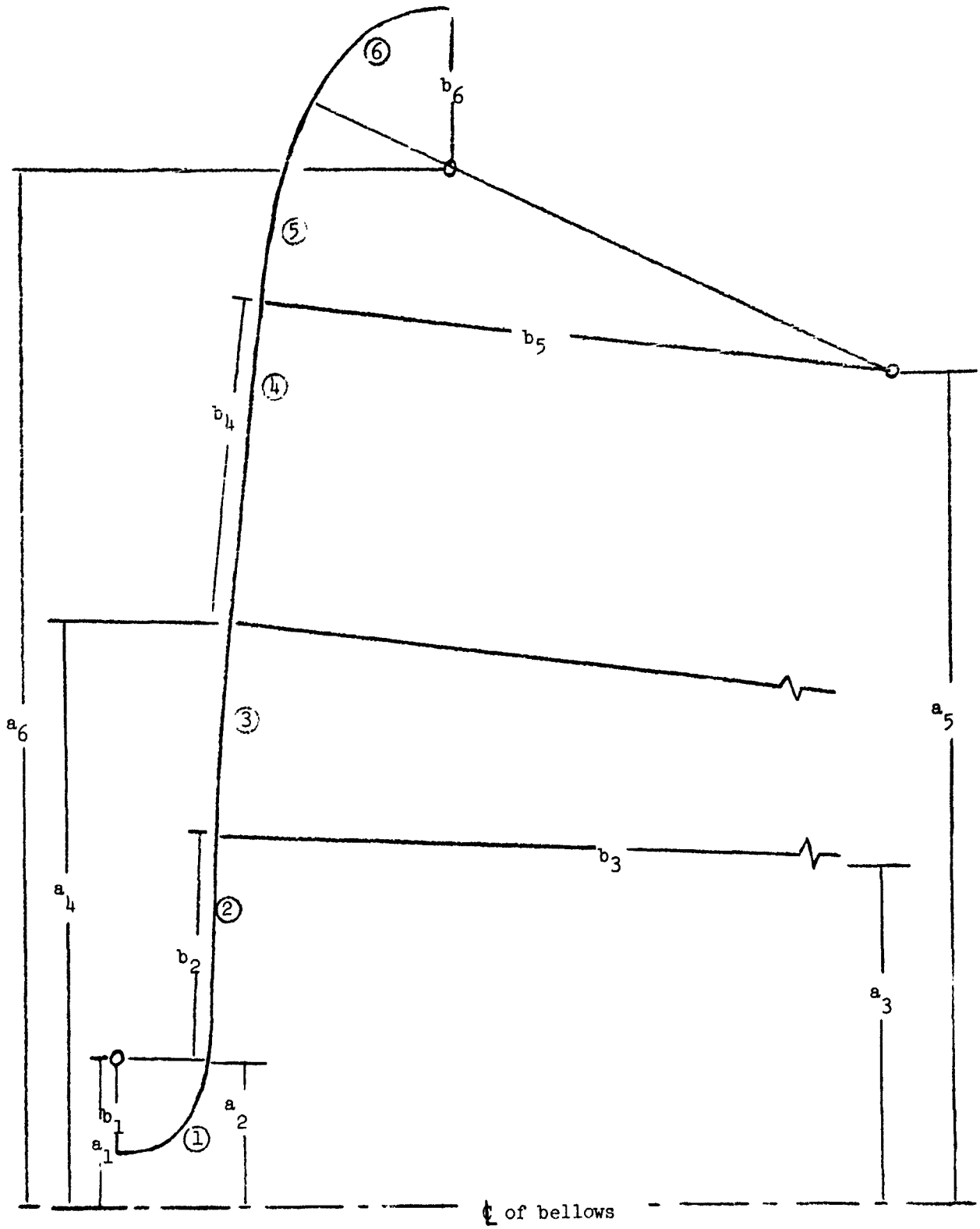

FIGURE B-23. MATHEMATICAL MODEL OF 3-INCH BELLOWS

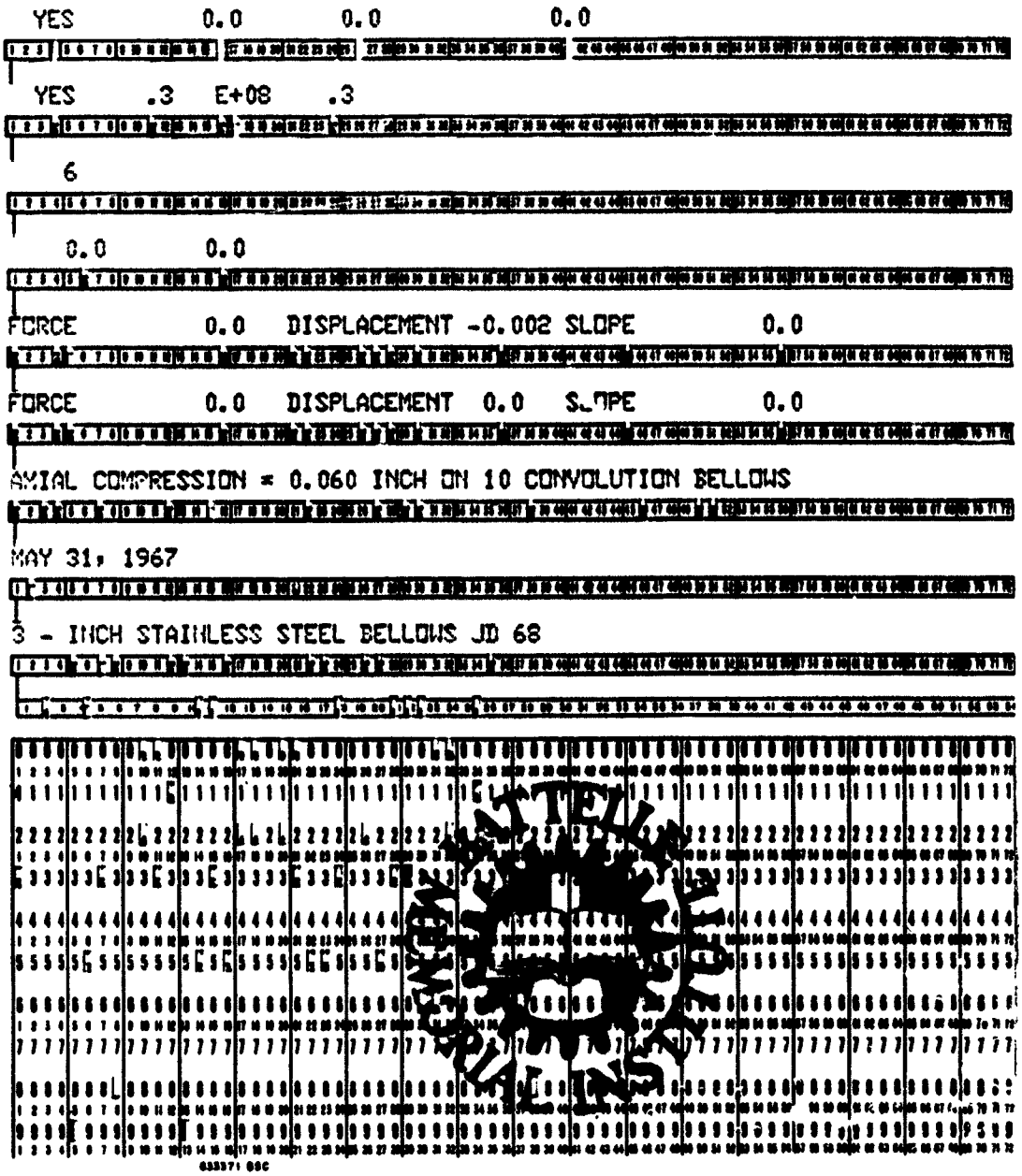

FIGURE B-24. PUNCHED INPUT CARDS FOR DATA SETS 1-7 FOR 3-INCH SINGLE PLY FORMED BELLOWS JD68 (READ FROM BOTTOM OF PAGE TO TOP)

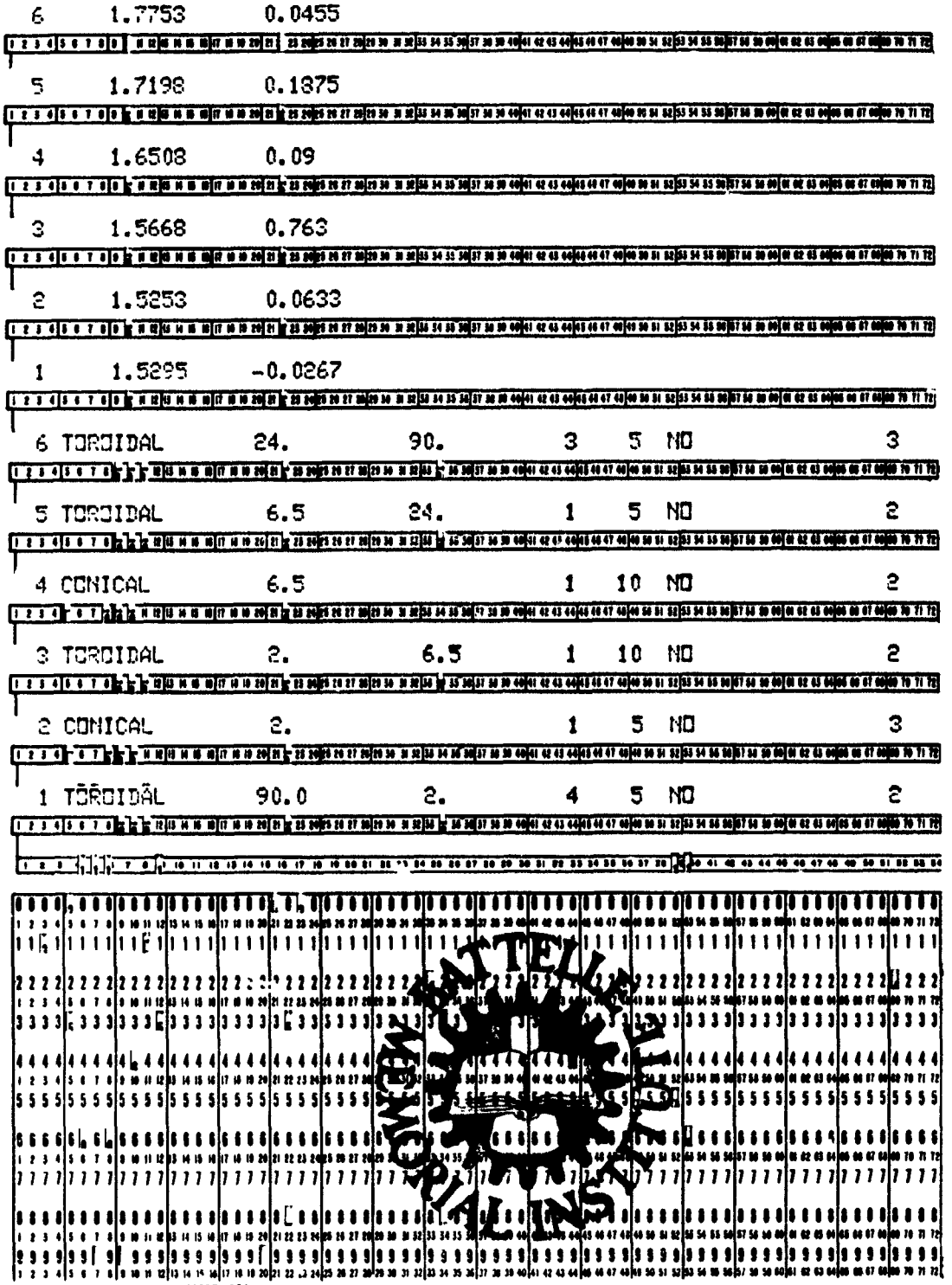

FIGURE B-25. PUNCHED INPUT CARDS FOR DATA SETS 8 AND 9 FOR 3-INCH SINGLE PLY FORMED BELLOWS JD 68 (READ FROM BOTTOM OF PAGE TO TOP)

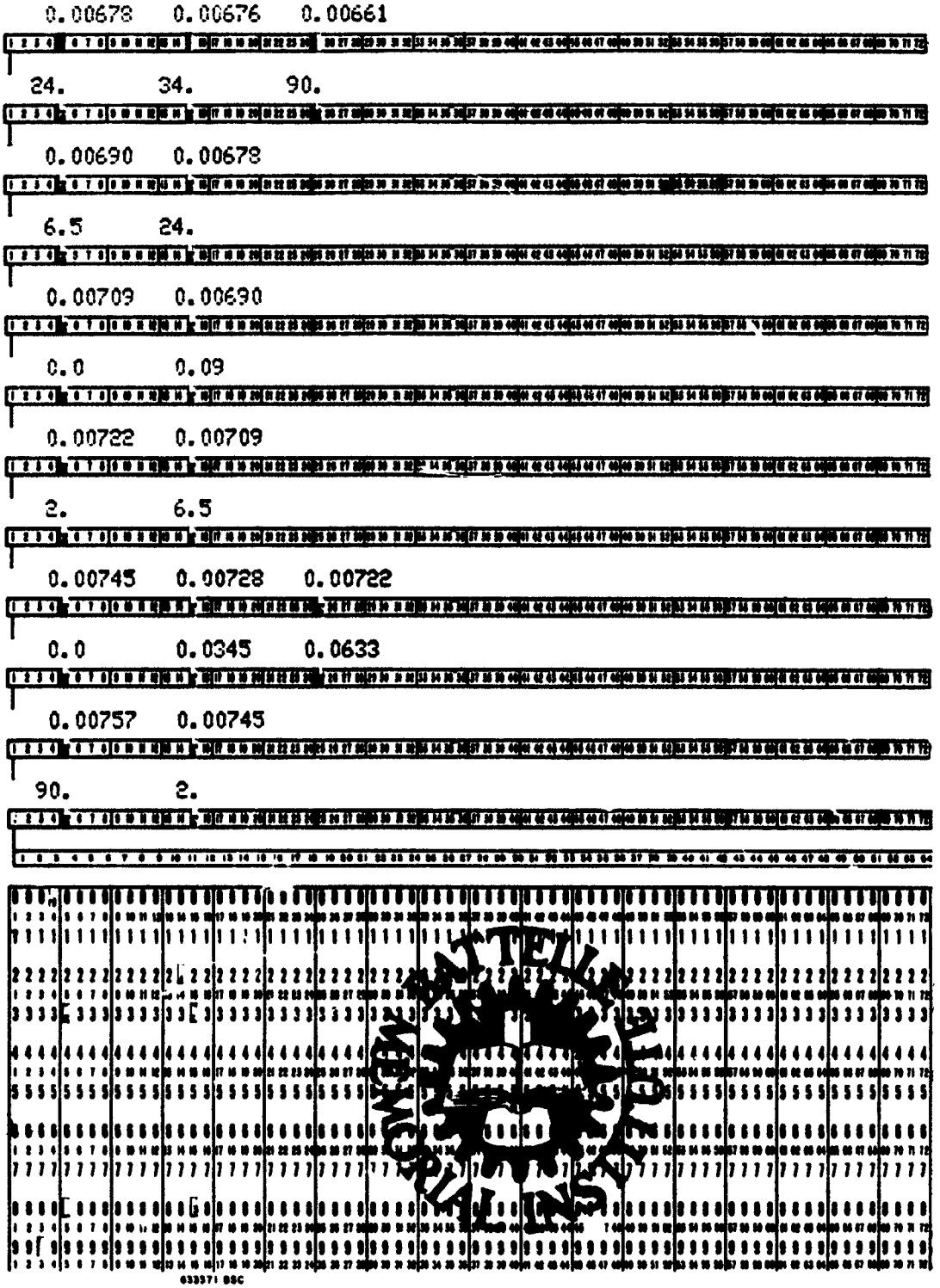

FIGURE B-26. PUNCHED INPUT CARDS FOR DATA SET 12 FOR 3-INCH SINGLE PLY FORMED BELLOWS JD68 (READ FROM BOTTOM OF PAGE TO TOP)

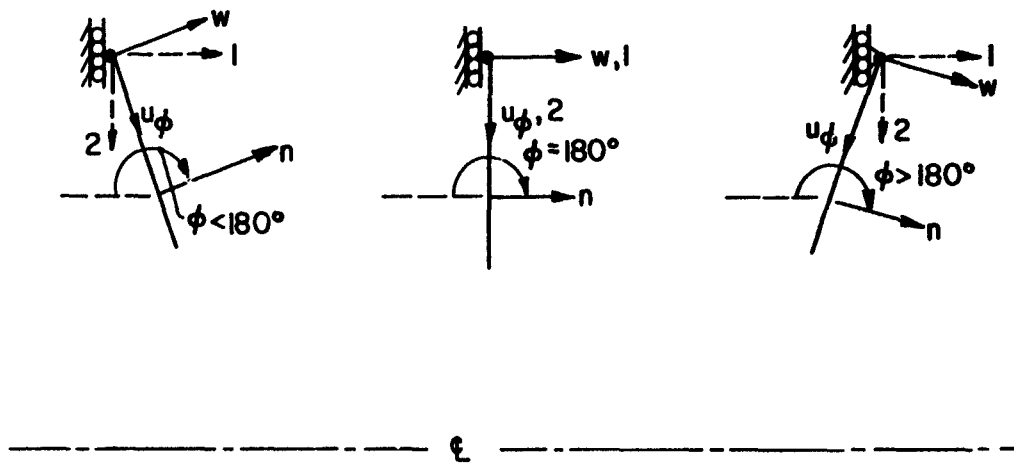

FIGURE B-27. VARIOUS POSSIBILITIES FOR BOUNDARY CONDITIONS ON WELDED BELLOWS AT INITIAL AND FINAL EDGES

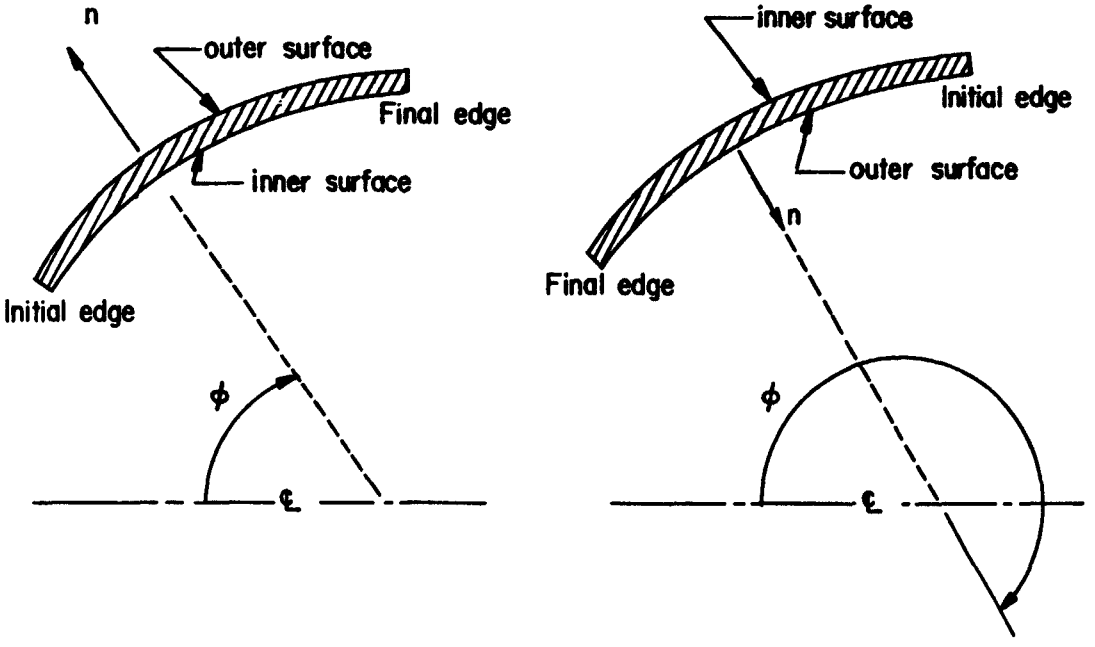

FIGURE B-28. DEFINITION OF INNER AND OUTER SURFACE FOR STRESSES

APPENDIX C

THEORETICAL DEVELOPMENT AND LISTING OF COMPUTER PROGRAM

ABBREVIATIONS AND SYMBOLS

x	Independent variable, in.
$y(x)$	n-fold vector with elements $y^j(x)$, J = 1, 2, ... n
$Y(x)$	n by n matrix
$[Y(x)]^j$	j-th column of Y(x)
T	Transformation vector
$u(a)$, $u(b)$	Boundary condition vectors at x = a and x = b
S_i	i-th subinterval in the interval $a \leq x \leq b$, in.
$\delta[y^j(x)]$	A small change in the vector y
I	n by n unit matrix
r	Radial distance from bellows axis to a point on the bellows, in.
R_ϕ	Meridional radius of curvature, in.
ϕ	Angle between normal to the bellows surface and its axis of revolution, deg
θ	Angle measured in circumferential direction, deg
Q_ϕ	Effective shear resultant force in direction normal to shell, lb/in.
N_ϕ, N_θ	Membrane resultant forces in the meridional and circumferential directions, respectively, lb/in.
M_ϕ, M_θ	Bending moment resultants in the meridional and circumferential directions, respectively, in-lb/in.
ϵ_ϕ, ϵ_θ	Midsurface membrane strains in the meridional and circumferential directions, respectively, in./in.
β_ϕ	Angle of rotation of the normal in the meridional direction, deg
p_ϕ, p	Components of the pressure or body force loading in the meridional or normal directions, respectively, psi
η_ϕ, η_θ	Bending strains in the meridional and circumferential directions, respectively
κ	Poisson's ratio
E	Modulus of elasticity, psi
h	Bellows thickness, in.
D	$Eh^3/12(1 - \nu^2)$, bending rigidity, in-lb
K	$Eh/(1 - \nu^2)$, membrane stiffness, lb/in.
w	Displacement in direction of normal to the shell midsurface, in.
u_ϕ	Displacement in meridional direction, in.

APPENDIX C

THEORETICAL DEVELOPMENT AND LISTING OF COMPUTER PROGRAM

This appendix is intended for those who desire a thorough understanding of the mathematical techniques and equations used in the theoretical portion of the research program, as well as a detailed account of the computation program.

The first portion of this appendix gives a description of the method of solution and a derivation of the governing fundamental set of differential equations.

The second portion consists of a listing of the computer program.

Preliminaries

Since some items involving matrix algebra, and initial-value and boundary-value problems are used in the following, a brief description of points pertinent to the theoretical development will be given here.

Initial-Value Problem. The two distinguishing characteristics of an initial-value problem are (1) the problem can be formulated in terms of n simultaneous first-order differential equations relating the n independent variables to a single independent variable on the open interval $a \leq x$. The equations may be linear or nonlinear. (2) A specific solution is determined when n independent relations between the dependent variables are given at $x = a$.

One-Dimensional Boundary-Value Problem (Single Independent Variable). The two distinguishing characteristics of a one-dimensional boundary-value problem are: (1) The problem can be formulated in terms of n simultaneous first-order differential equations relating the n independent variables to a single independent variable on the closed interval $a \leq x \leq b$. (2) A specific solution is determined when n/2 independent relations between the dependent variables are given at $x = a$ and n/2 independent relations are given at $x = b$.

From the above descriptions it is noted that the only difference between the initial-value problem and the boundary-value problem is the manner in which the fundamental variables are prescribed at the boundaries. In the initial-value problem, all the fundamental variables are prescribed at one point, $x = a$. In the boundary-value problem, half the fundamental variables are specified at a and half at b.

Matrix Notation. In the development of the basic equations, standard matrix notation will be used. A vector will be referred to by the small letter, y(x). This vector will have n elements denoted by $y^j(x)$, $j = 1, 2, \ldots, n$. A square matrix will be denoted by a capital letter, Y(x), which will have n x n elements. The jth column of Y(x) will be denoted by $[Y(x)]^j$. When the vector y(x) is partitioned into two subvectors $y_1(x)$ and $y_2(x)$, it means that the upper n/2 elements of y(x) are contained in $y_1(x)$ and the lower n/2 elements of y(x) are contained in $y_2(x)$. When Y(x) is partitioned into four

submatrices $Y^1(x)$, $Y^2(x)$, $Y^3(x)$, and $Y^4(x)$, this amounts to placing the upper left-hand quadrant of Y(x) in $Y^1(x)$, the upper right-hand quadrant of Y(x) in $Y^2(x)$, the lower left-hand quadrant of Y(x) in $Y^3(x)$ and the lower right-hand quadrant of Y(x) into $Y^4(x)$. Thus, each submatrix $Y^m(x)$, m = 1, 2, ..., 4 contains (n/2) x (n/2) elements.

Elementary Transformation Matrices. An elementary transformation matrix T is defined as one which operates on a vector y(x) such that the elements of y(x) are rearranged. An elementary transformation matrix is obtained from the unit matrix by elementary transformation(C-1)*. In the present application, the elementary transformations used are those associated with the interchange of two or more rows or two or more columns.

Segmentation of Interval. The multisegment numerical integration technique requires that the interval $I(a \leq x \leq b)$ be divided into M segments, as shown in Figure C-1. The initial point of the interval is defined as $x = x_1 = a$, and the final point of the interval is defined as $x = x_{M+1} = b$. The M segments need not be of the same length. The ith segment is denoted by S_i and is bounded by $x_i < x < x_{i+1}$.

Method of Solution

The method of solution developed here is applicable to any boundary-value problem governed in the interval $I(a \leq x \leq b)$ by a system of n first-order ordinary differential equations

$$\frac{dy(x)}{dx} = f\left[x,\ y^1(x),\ y^2(x),\ \ldots,\ y^n(x),\ h(x)\right] \quad , \tag{C-1a}$$

where h(x) denotes the nonhomogeneous terms.

It is assumed that values of n/2 elements of each vector y(a) and y(b) are known. Then the boundary conditions are written in the form

$$T_1 y(a) = u(a) \tag{C-1b}$$

$$T_{M+1} y(b) = u(b) \quad ,$$

where T_1 and T_{M+1} are elementary boundary-transformation matrices which are chosen so that the first n/2 elements of $T_1 y(a)$ and the last n/2 elements of $T_{M+1} y(b)$ contain the specified boundary values of the variables. Thus, the first n/2 elements of u(a) and the last n/2 elements of u(b) contain the known boundary values.

The application of numerical integration techniques to boundary-value problems is not quite as straightforward as their application to initial-value problems. In initial-value problems, as noted earlier, values of all of the variables are known at the initial point. Beginning with these values the differential equations are integrated numerically to find the variables at any other value of x. However, for a boundary-value problem only n/2 values are known at x = a. One possible way of solving this problem would be to

*References for Appendix C are listed on p C-11.

guess the remaining n/2 values at x = a, integrate from x = a to x = b, and compare the values obtained at x = b with the prescribed values. If the values at x = b obtained through integration agree with the prescribed values, then the problem is solved. If not, a new estimate can be made of the trial values of x = a and another integration of the equations can be carried out. By observing the variation of the solution at x = b as the initial values of x = a are changed, it would be possible to eventually choose the correct initial values for the solution. This procedure, although feasible, is not efficient, and a more direct approach to the solution of a boundary-value problem governed by a system of n first-order ordinary differential equations will now be described.

Derivation of Basic Relationships Used in the Linear and Nonlinear Multisegment Numerical Integration Analysis

Assuming that an initial-value solution of (C-1a) exists and is unique everywhere in S_i (Figure C-1), it is concluded that a given set of initial values at x_i uniquely determines, through (C-1a), a corresponding set y(x) at any x in S_i. This can be expressed as

$$y(x) = g\left[y^1(x_i),\ y^2(x_i),\ \ldots,\ y^n(x_i)\right] \quad , \tag{C-2}$$

where the function g is uniquely dependent on x and the System of Equations (C-1a).

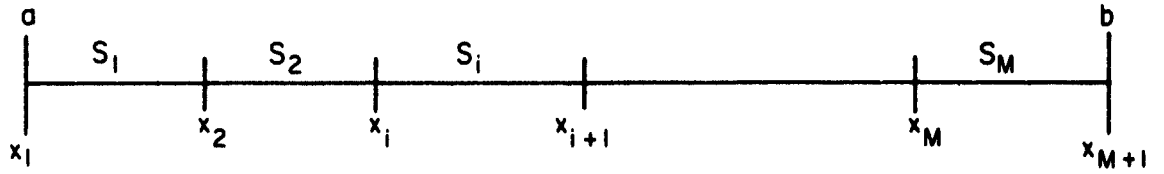

FIGURE C-1. NOTATION FOR SEGMENTS OF SHELL

Small changes in $y^j(x_i)$, denoted by $\delta y^j(x_i)$, j = 1, 2, ..., n, produce changes in the variables $y^j(x)$, denoted by $\delta y^j(x)$, j = 1, 2, ..., n. The relationship between these changes can be obtained by using Taylor's series and the chain rule of differentiation. This results in

$$\delta y^j(x) = \sum_{s=1}^{n} \frac{\partial y^j(x)}{\partial y^s(x_i)}\, \delta y^s(x_i) \qquad j = 1,\ 2,\ \ldots,\ n \ . \tag{C-3}$$

$\delta y^j(x_i)$ can be regarded as the difference between two different sets of variables at x_i, namely, $y(x_i)^*$ and $y(x_i)$, while $\delta y^j(x)$ can be regarded as the difference between the two sets of variables, $y(x)^*$ and y(x), obtained at x by integrating (C-1a) from x_i to x with $y(x_i)^*$ and $y(x_i)$ as the initial values. With these definitions, (C-3) can be rewritten as

$$y(x)^* - y(x) = Y_i(x)\left[y(x_i)^* - y(x_i)\right] \quad , \tag{C-4}$$

where the (n, n) matrix $Y_i(x)$ is defined by

$$Y_i(x) = \begin{bmatrix} \frac{\partial y^1(x)}{\partial y^1(x_i)} & \frac{\partial y^1(x)}{\partial y^2(x_i)} & \cdots & \frac{\partial y^1(x)}{\partial y^j(x_i)} & \cdots & \frac{\partial y^1(x)}{\partial y^n(x_i)} \\ \frac{\partial y^2(x)}{\partial y^1(x_i)} & \frac{\partial y^2(x)}{\partial y^2(x_i)} & \cdots & \frac{\partial y^2(x)}{\partial y^j(x_i)} & \cdots & \frac{\partial y^2(x)}{\partial y^n(x_i)} \\ \vdots & \vdots & & \vdots & & \vdots \\ \frac{\partial y^n(x)}{\partial y^1(x_i)} & \frac{\partial y^n(x)}{\partial y^2(x_i)} & \cdots & \frac{\partial y^n(x)}{\partial y^j(x_i)} & \cdots & \frac{\partial y^n(x)}{\partial y^n(x_i)} \end{bmatrix} . \qquad \text{(C-5)}$$

The j^{th} column of $Y_i(x)$ can be regarded as a set of new variables. In order to obtain numerical values of these variables at particular values of x, say x_{i+1}, it is only necessary to have a set of n simultaneous first-order differential equations relating these new variables. This set of equations can then be integrated from x_i to x_{i+1} n times, thus forming the matrix $Y_i(x_{i+1})$.

The set of equations needed to form the matrix $Y_i(x)$ can be easily obtained by differentiating (C-1a) with respect to $y^j(x_i)$; thus,

$$\frac{d}{dx}\left[\frac{dy(x)}{dy^j(x_i)}\right] = \frac{d}{dy^j(x_i)} f\left[x, y^1(x), y^2(x), \ldots, y^n(x), h(x)\right]. \qquad \text{(C-6)}$$

The initial values of the columns of $Y_i(x)$ can be easily determined from the inspection of (C-5). At $x = x_i$, the j^{th} column of $Y_i(x)$ contains all zeros except for the j^{th} row, and that element is one. Thus, the columns of the matrix $Y_i(x)$ are obtained as the solutions of the n initial-value problems governed in S_i by (C-6) (with $j = 1, 2, \ldots, n$), with the initial values specified by

$$Y_i(x_i) = I \ , \qquad \text{(C-7)}$$

where I denotes the (n, n) unit matrix.

If the Equations (C-1a) are linear, then Equations (C-6) simply reduce to (C-1a), with the nonhomogeneous terms h(x) deleted. In the event that (C-1a) are nonlinear, then the right-hand side of (C-6) contains not only the elements of $Y_i(x)$, but also some of the variables of the y(x) solution state. Suitable values of these variables can be obtained as part of the procedure for solving the nonlinear problem which is discussed next.

The solution to the nonlinear problem is obtained as the limit of a sequence of solution states which are obtained by an iteration procedure. The initial trial-solution state can be chosen in some arbitrary manner, although it has been found that using the solution of the linearized problem as the initial trial-solution state enhances the convergence of the iteration procedure. The application of Newton's rule as given by

Fox(C-2) to find the iterated solution state from the trial solution state can be accomplished using Equations (C-4), in which x is set equal to x_{i+1}. In Equations (C-4), the variables $y(x_i)$ will be identified with the trial-solution state $y^t(x)$ evaluated at x_i. The variables obtained by integrating (C-1a) from x_i to x_{i+1} with the initial values $y^t(x_i)$ will be denoted as $y^c(x_{i+1})$. These values replace $y(x_{i+1})$ in (C-4). The values of the iterated solution state $y^a(x)$, evaluated at x_i and x_{i+1} are substituted for the corresponding starred variables. With these substitutions, Equations (C-4) become, after rearranging:

$$Y_i(x_{i+1})\, y^a(x_i) - y^a(x_{i+1}) = -z_i(x_{i+1}) \quad , \tag{C-8a}$$

where

$$z_i(x_{i+1}) = y^c(x_{i+1}) - Y_i(x_{i+1})\, y^t(x_i) \quad . \tag{C-8b}$$

When evaluated at the end of every segment S_i, i = 1, 2, ..., M, (C-8) represent a system of M matrix equations which contain M + 1 unknown vectors: $y^a(x_i)$, (i = 1, 2, ..., M + 1). However, recalling that exactly n boundary conditions are specified by (C-1b), the number of unknowns becomes the same as the number of equations and, consequently, the combined system of Equations (C-8a) for all i can be solved uniquely for $y^a(x_i)$, using the Gaussian elimination technique.

The iterated solution state $y^a(x_i)$, when integrated by means of (C-1a) from x_i to x_{i+1} in every segment, may not necessarily satisfy the required continuity and boundary conditions because Equations C-4 are approximate. By repeating the iteration with $y^a(x_i)$ as the new trial solution $y^t(x_i)$, the iterated sequence of $y^a(x_i)$ will converge to the solution of the nonlinear boundary value problem as rapidly as in any Newton-type method.

By way of recapitulation, the solution of the boundary-value problem defined by (C-1) is obtained by means of the multisegment method given in this section in the following way: (1) an assumed trial solution $y^t(x_i)$ is integrated by means of (C-1a) from x_i to x_{i+1} in every segment to obtain all of the values of $y^c(x_{i+1})$ i = 1, 2, ..., M, as well as all of the values of those variables which appear in the nonlinear terms of f; (2) initial-value integrations of (C-6), starting with (C-7), are performed from x_i to x_{i+1} in every segment to obtain the elements of $Y_i(x_{i+1})$, i = 1, 2, ..., M; (3) the data obtained in Steps (1) and (2) are substituted in Equations (C-8). The system of Equations (C-8) for all different i are then solved by means of the standard Gaussian elimination technique for $y^a(x_i)$; (4) using $y^a(x_i)$ as the initial value, (C-1a) is integrated from x_i to x_{i+1} in every segment and the integration results at x_{i+1} are compared to the elements of $y^a(x_{i+1})$ as obtained from (C-8). This comparison serves as a convenient check on the degree of accuracy of every trial solution state. If the corresponding variables at the ends of consecutive segments agree (including the M^{th} segment, where the solution must agree with the specified boundary conditions) within a desired number of significant figures, then the solution state is accepted as the solution of the boundary-value problem as defined by (C-1) If not, then $y^a(x_i)$ is taken as the next trial solution $y^t(x_i)$, and the process is repeated by returning to (1).

When the functions f in (C-1a) are linear, the multisegment method developed in this section is identical to the one given in Reference (C-3) for the solution of linear boundary-value problems. For the linear case, the trial solution can be conveniently assumed as $y^t(x_i) = 0$ [this choice simplifies (C-8b)], and the iterated solution state,

obtained from (C-8) after one "iteration cycle", represents the solution of the linear problem.

Gaussian Elimination Procedure. Since the nonlinearities in (C-1a) make some changes necessary in the solution of (C-8), a brief outline of the required Gaussian elimination procedure is given in the following section. [More details can be found in References (C-3) and (C-4)].

Because the variables at the end points of the interval i are connected by the boundary condition relations (C-1b), (C-8) must be investigated for i = 1 and i = M separately. From (C-8) there results*

$$Y_1(x_2)\, y(x_1) - y(x_2) = - z_1(x_2) \tag{C-9a}$$

$$Y_M(x_{M+1})\, y(x_M) - y(x_{M+1}) = - z_M(x_{M+1}) \ . \tag{C-9b}$$

It is convenient to use the transformed variables $u(x_1)$ and $u(x_{M+1})$ in (C-8) instead of $y(x_1)$ and $y(x_{M+1})$. Using (C-1b) in (C-9) yields

$$Y_1(x_2)\, T_1^{-1}\, u(x_1) - y(x_2) = - z_1(x_2) \tag{C-10a}$$

$$T_{M+1}\, Y_M(x_{M+1}) - u(x_{M+1}) = - T_{M+1}\, z_M(x_{M+1}) \ . \tag{C-10b}$$

By defining

$$U_1(x_2) = Y_1(x_2)\, T_1^{-1} \tag{C-11a}$$

$$U_M(x_{M+1}) = T_{M+1}\, Y_M(x_{M+1}) \tag{C-11b}$$

$$d_M(x_{M+1}) = T_{M+1}\, z_M(x_{M+1}) \ , \tag{C-11c}$$

the form of (C-8) can be retained if the coefficient matrices $Y_1(x_2)$, $Y_M(x_{M+1})$, $z_M(x_{M+1})$, occurring in (C-8) for i = 1 and i = M are replaced before Gaussian elimination by their transformed expressions as given by (C-11), remembering that the variables at $x = x_i$ and $x = x_{M+1}$ are the transformed variables $u(x_1)$ and $u(x_{M+1})$ as given by (C-1b).

After the transformations required by (C-11) are carried out, (C-8) is partitioned in the form

$$\left[\begin{array}{c|c} Y_i^1(x_{i+1}) & Y_i^2(x_{i+1}) \\ \hline Y_i^3(x_{i+1}) & Y_i^4(x_{i+1}) \end{array}\right] \left\{\begin{array}{c} y_1(x_i) \\ \hline y_2(x_i) \end{array}\right\} - \left\{\begin{array}{c} y_1(x_{i+1}) \\ \hline y_2(x_{i+1}) \end{array}\right\} = - \left\{\begin{array}{c} z_i^1(x_{i+1}) \\ \hline z_i^2(x_{i+1}) \end{array}\right\}, \quad i = 1, 2, \ldots, M. \tag{C-12}$$

*Throughout the remainder of this section, the superscript a on y(x) will be omitted.

Note that, due to the definition of T_1 and T_{M+1}, the vectors $y_1(x_1)$ and $y_2(x_{M+1})$ are known through the boundary conditions.

The system of equations (C-12) can be solved conveniently by the standard Gaussian elimination procedure in the same way as the linear problem treated in Reference (C-3). This procedure requires, for the purpose of triangularization of (C-8), the calculation of intermediate matrices E_i, C_i, a_i, b_i, defined by

$$E_i = Y_i^2 + Y_i^1 C_{i-1}^{-1} \tag{C-13a}$$

$$C_i = (Y_i^4 + Y_i^3 C_{i-1}^{-1}) E_i^{-1} \tag{C-13b}$$

$$a_i = - z_i^1 - Y_i^1 C_{i-1}^{-1} b_{i-1} \tag{C-13c}$$

$$b_i = - z_i^2 - Y_i^3 C_{i-1}^{-1} b_{i-1} - C_i a_i \tag{C-13d}$$

where C_o^{-1} and b_o are taken as null matrices and the calculation is carried out in succession over all values of i, starting with i = 1 and ending with i = M. The unknown variables, $y_1(x_i)$ (i = 2, 3, ..., M+1) and $y_2(x_i)$ (i = 1, 2, ... M), are obtained from

$$y_1(x_{M-i+2}) = C_{M-i+1}^{-1} [y_2(x_{M-i+2}) + b_{M-i+1}] \tag{C-14a}$$

$$y_2(x_{M-i+1}) = E_{M-i+1}^{-1} [y_1(x_{M-i+2}) + a_{M-i+1}] \tag{C-14b}$$

Again, the calculation of (C-14) is carried out in succession, starting with i = 1 and ending with i = M, by taking in (C-14a) $y_2(x_{M+1}) = 0$. Of course, the vectors $y_2(x_1)$ and $y_1(x_{M+1})$ which result from (C-14), together with the known vectors $y_1(x_1)$ and $y_2(x_{M+1})$ which are prescribed in (C-1b), are really the transformed variables $u(x_1)$ and $u(x_{M+1})$, and, if desired, they may be transformed back into the regular fundamental variables by (C-1b).

Derivation of the Fundamental Equations for Nonlinear Thin-Elastic-Shell Analysis

In this section the fundamental equations for the nonlinear thin-elastic-shell analysis will be derived. The equations describing the linear axisymmetric response of thin elastic shells can be obtained from the equations to be derived by simply deleting all nonlinear terms, i.e., terms which contain the product of two fundamental variables. The equations describing the nonsymmetric linear response of thin elastic shells can be obtained from Reference (C-3).

The application of the multisegment numerical integration technique to the nonlinear thin-elastic-shell equations is the same regardless of the theory used. The equations given by Sanders(C-5) for small strain but moderately large rotation will be reduced to those required for a shell of revolution. The governing equations can be

obtained from Equations (A1), (A3), (A5), (A7), (A8), and (A9) in Reference (C-5), by making the following substitutions

$$\begin{aligned} \alpha_1 &= r \\ \alpha_2 &= R_\phi \\ \alpha_{1,2} &= R_\phi \cos\phi \\ \alpha_{2,1} &= 0 \\ r &= R_\theta \sin\phi \ , \end{aligned} \tag{C-15}$$

where the 1 coordinate has been related to θ and the 2 coordinate to ϕ. Using (C-15) in Sanders' equations yields:

Equilibrium Equations

$$N_{\phi,s} + \frac{\cos\phi}{r}(N_\phi - N_\theta) + \frac{1}{R_\phi}(Q_\phi - \beta_\phi N_\phi) + p_\phi = 0 \tag{C-16a}$$

$$Q_{\phi,s} + \frac{\cos\phi}{r} Q_\phi - \left(\kappa_\theta + \frac{\sin\phi}{r}\right) N_\theta + \frac{1}{R_\phi} Q_\phi \beta_\phi$$

$$- \left[\beta_{\phi,s} + \frac{1}{R_\phi}\left(1 + \beta_\phi^2\right)\right] N_\phi + p = o \tag{C-16b}$$

$$M_{\varphi,s} + \frac{\cos\phi}{r}(M_\phi - M_\theta) - Q_\phi = 0 \ . \tag{C-16c}$$

Stress-Strain Relations

$$N_\theta = K(\epsilon_\theta + \nu\epsilon_\phi) \tag{C-17a}$$

$$N_\phi = K(\epsilon_\phi + \nu\epsilon_\theta) \tag{C-17b}$$

$$M_\theta = D(\kappa_\theta + \nu\kappa_\phi) \tag{C-17c}$$

$$M_\phi = D(\kappa_\phi + \nu_\theta) \tag{C-17d}$$

where

$$K = \frac{Eh}{(1 - \nu^2)} \tag{C-18a}$$

$$D = \frac{Eh^3}{12(1 - \nu^2)} \ . \tag{C-18b}$$

Strain-Displacement Relations

$$\epsilon_\theta = \frac{1}{r}(u_\phi \cos\phi + w \sin\phi) \tag{C-19a}$$

$$\epsilon_\phi = u_{\phi,s} + \frac{w}{R_\phi} + \frac{1}{2}\beta_\phi^2 \tag{C-19b}$$

$$\beta_\phi = \frac{1}{R_\phi} u_\phi - w_{,s} \tag{C-19c}$$

$$\kappa_\theta = \frac{1}{r}\beta_\phi \cos\phi \tag{C-19d}$$

$$\kappa_\phi = \beta_{\phi,s} \ . \tag{C-19e}$$

In the above, use has been made of the expression

$$\frac{\partial}{\partial\phi}(\ ) = R_\phi \frac{\partial}{\partial s}(\ ) \ . \tag{C-20}$$

Now that the equations for the axisymmetrically loaded shell of revolution have been tabulated, the fundamental set of equations which describe the nonlinear bending of a symmetrically loaded shell of revolution can be derived. In particular, this set will be expressed as a system of six first-order nonlinear ordinary differential equations such that they can be used in the formulation of the multisegment method previously described.

The fundamental set of equations is derived and listed in a manner such that digital computation is kept to a minimum. In this set, the fundamental variables are defined as those quantities which appear as natural boundary conditions. They are w, Q_ϕ, u_ϕ, N_ϕ, β_ϕ, M_ϕ.

Define as auxiliary quantities

$$\epsilon_\theta = (u_\phi \cos\phi + w \sin\phi)/r \tag{C-21a}$$

$$\kappa_\theta = \cos\phi\, \beta_\phi / r \ . \tag{C-21b}$$

Eliminating ϵ_ϕ from (C-17a) and C-17b) yields a third auxiliary quantity

$$N_\theta = \nu N_\phi + Eh\epsilon_\theta \ . \tag{C-21c}$$

Similarly, elimination of κ_ϕ from Equations (C-17c) and (C-17d) yields the final auxiliary quantity

$$M_\theta = \nu M_\phi + \frac{Eh^3}{12}\kappa_\theta \ . \tag{C-21d}$$

Rearranging Equation (C-19c) gives

$$w_{,s} = \frac{u_\phi}{R_\phi} - \beta_\phi \quad . \tag{C-22a}$$

Equations (C-17d) and (C-19e) give

$$\beta_{\phi,s} = \frac{12(1-\nu^2)}{Eh^3} M_\phi - \nu\kappa_\theta \quad . \tag{C-22b}$$

The last equilibrium equation, Equation (C-16c), can be expressed as

$$M_{\phi,s} = \frac{\cos\phi}{r}(M_\theta - M_\phi) + Q_\phi \quad . \tag{C-22c}$$

Use of Equations (C-17b) and (C-18b) gives

$$u_{\phi,s} = \frac{(1-\nu^2)}{Eh} N_\phi - \frac{w}{R_\phi} - \nu\epsilon_\theta - \frac{1}{2}\beta_\phi^2 \quad . \tag{C-22d}$$

The second equilibrium equation, Equation (C-16b), is solved to give

$$Q_{\phi,s} = N_\theta\left(\frac{\sin\phi}{r} + \kappa_\theta\right) + N_\phi\left[\frac{1}{R_\phi}\left(1+\beta_\phi^2\right) + \beta_{\phi,s}\right] - Q_\phi\left(\frac{\cos\phi}{r} + \frac{1}{R_\phi}\beta_\phi\right) - p. \tag{C-22e}$$

Equation (C-16a) provides the last equation of the fundamental set:

$$Q_{\phi,s} = \left(\frac{\sin\phi}{r} + \kappa_\theta\right) N_\theta - \frac{\cos\phi}{r} Q_\phi + \left(\beta_{\phi,s} + \frac{1}{R_\phi}\right) N_\phi - p \, . \tag{C-22f}$$

Now that the fundamental set of equations has been obtained, it is necessary to derive a system of equations corresponding to (C-6). This is obtained by differentiating (C-21)-(C-22) in succession with respect to each of the fundamental variables. Since (C-6) has the same form with any value of j, the system of equations (C-6) is recorded here by indicating derivatives with respect to any one of the six fundamental variables by a prime:

$$\epsilon_\theta' = (u_\phi' \cos\phi + w' \sin\phi)/r \tag{C-23a}$$

$$\kappa_\theta' = \cos\phi \, \beta_\phi'/r \tag{C-23b}$$

$$N_\theta' = \nu N_\phi' + Eh\epsilon_\theta' \tag{C-23c}$$

$$M_\theta' = \nu M_\phi' + \frac{Eh^3}{12}\kappa_\theta' \tag{C-23d}$$

$$w'_{,s} = \frac{u'_\phi}{R_\phi} - \beta'_\phi \tag{C-23e}$$

$$\beta'_{\phi,s} = \frac{12\,(1-\nu^2)}{Eh^3} M'_\phi - \nu\kappa'_\theta \tag{C-23f}$$

$$M'_{\phi,s} = \frac{\cos\phi}{r}\,(M'_\theta - M'_\phi) + Q'_\phi \tag{C-23g}$$

$$u'_{\phi,s} = \frac{(1-\nu^2)}{Eh} N'_\phi - \nu\epsilon'_\theta - \frac{w'}{R_\phi} - \beta_\phi\beta'_\phi \tag{C-23h}$$

$$Q'_{\phi,s} = N'_\theta\left(\frac{\sin\phi}{r} + \kappa_\theta\right) + N_\theta\,\kappa'_\theta + N'_\phi\left[\frac{1}{R_\phi}\left(1+\beta_\phi^2\right) + \beta_{\phi,s}\right] \tag{C-23i}$$

$$+ N_\phi\left(\frac{2}{R_\phi}\beta_\phi\beta'_\phi + \beta'_{\phi,s}\right) - Q'_\phi\left(\frac{\cos\phi}{r} + \frac{1}{R_\phi}\beta_\phi\right) - \frac{Q_\phi}{R_\phi}\beta'_\phi$$

$$N'_{\phi,s} = \frac{\cos\phi}{r}\left(N'_\theta - N'_\phi\right) - \frac{1}{R_\phi}Q'_\phi + \frac{1}{R_\phi}\left(\beta'_\phi N_\phi + \beta_\phi N'_\phi\right). \tag{C-23j}$$

REFERENCES

(C-1) Wade, T. L., The Algebra of Vectors and Matrices, Addison-Wesley Publishing Company, Incorporated, Cambridge, Massachusetts (1951).

(C-2) Fox, L., Numerical Solution of Ordinary and Partial Differential Equations, Addison-Wesley Publishing Company, Incorporated, Reading, Massachusetts (1962).

(C-3) Kalnins, A., "Analysis of Shells of Revolution Subjected to Symmetrical and Non-symmetrical Loads", ASME Trans., 86, 467-476 (September, 1964).

(C-4) Kalnins, A., and Lestingi, J. F., "On Nonlinear Analysis of Elastic Shells of Revolution", ASME Trans., 89, 59-64 (March, 1967).

(C-5) Sanders, J. L., "Nonlinear Theories of Thin Shells", Quarterly of Applied Mathematics, 21 (1) (April, 1963).

Listing of Computer Program

The multisegment numerical integration procedure for the analysis of nonlinear elastic thin shells of revolution described in the first portion of this appendix has been incorporated into the computer program NONLIN, which is presented in the following pages.

The program is written in FORTRAN IV and is operational on the CDC 6400 at Battelle-Columbus. The program is self-contained, except, of course, for the standard library functions COS (X), SIN (X), TAN (X). The program uses Logical Input Tape 5 and Logical Output Tape 6.

The program has been coded such that a maximum of ten arrays can be stored and consequently placed on a magnetic tape for use by a digital-plot subroutine. This subroutine, which is available at Battelle-Columbus and is called PLTXYI, has not been included in this listing since it would not, in most cases, be compatible with other systems. However, a dummy subroutine, PLTXYI (this appears as the last program in the listing), has been added so that the coding in the subroutine CALCUL did not have to be changed. In the event a user has the capability of calling a plot subroutine, he would only have to provide the proper call to his subroutine, since the coding necessary to generate the arrays is included in CALCUL.

```
 PROGRAM NONLIN(INPUT,OUTPUT,TAPE5=INPUT,TAPE6=OUTPUT,PUNCH)
 DIMENSION      IA(8)          , SI(60)         , IPAR(60)      ,
*               IB(8)          , SX(60)         , INT(60)       ,
*               GA(8)          , PRNT(8)        , ISS(60)       ,
*               GB(8)          , ERR(8)         , PSR(60)       ,
*               Y(8)           , DM(8,61)       , EYM(60)       ,
*               DY(8)          , TL(8,8)        , A(8,9)        ,
*               TR(8,8)        , TLI(8,8)       , JOBPLT(10)    ,
*               TRI(8,8)       , TRY(8,61)      , TR2(8,8)      ,
*               SOUT(275)      , D(8,9,60)      , P(5,275)      ,
*               SLOPE(5,275)   , TR1(8,8)       , E(9,60)
 DIMENSION      V3(8)          , VN(7,60)       , YAM(72)       ,
*               DYAM(72)       , ABC(21)        , EAM(10)       ,
*               BACK(60)       , YSAVE(8)       , DETERM(10)    ,
*               IPLOT(10)      , XPLOT(350)     , YPLOT(350,10),
*               STROUT(350)    , SIGNPH(350)    , SIGMPH(350)   ,
*               SIGPHT(350)    , SIGPHB(350)    , SIGNTH(350)   ,
*               SIGMTH(350)    , SIGTHT(350)    , SIGTHB(350)   ,
*               TAUPHI(350)    , VARTIK(60)     , POINT(60)     ,
*               DMSAVE(6,61)
 COMMON / BLOCKA / NU, P1, XLD, NTYPE, INDEX, IBR, PN, NPOINT,
1                  ISH, TT, T1, T2, HTT, INTC
 COMMON / BLOCKB / H, R1, R2, R3, SXN, CXS
 COMMON / BLOCKC / DM, GA, GB, NF, NFP, NPL, NH, NN, IRY
 COMMON / BLOCKD / TL, TR, TLI, TRI, ALFL, ALFR
 COMMON / BLOCKF / NFF, SMXX, SZERO, GO, ERP, ISS, E,
*                  MAX, INTPRN, INTVAL, NPP
 COMMON / BLOCKG / NPARTS, PHI1, V3, KIND, NT, MI, SPRINT, VN, EYM,
1                  BACK, NBACK
 COMMON / BLOCKH / NDE
 COMMON / BLOCKJ / DELX, PDELX, ABC, EAM
 COMMON / BLOCKK / PIN, PMIN, HO, XO, EMIN, EMAX
 COMMON / BLOCKL / YAM, DYAM
 COMMON / BLOCKM / YSAVE
 COMMON / BLOCKN / DETERM
 COMMON / BLOCKP / PLOT, PLTIME, SPLOT, PLOTPT, IPLOT, YMOD, KST,
*                  HGAMMA, DEAD, NFH
 COMMON / BLOCKQ / TIME, VARTIK, NVARTK
 COMMON / BLOCKS / JOBPLT, ALXL, ALXR, IA, IB, NOPUNC, INPUN,
*                  CONVER, SI, SX, INT, IPAR, PSR, ITER, NTRY,
*                  NERROR, IBRM, TRYIN, IBRMAX
 COMMON / BLOCKX / LEVEL1, LEVEL2
 COMMON / PLXY1C / IEX(8), DUM(4)
 COMMON             SLOPE, P, SOUT, D, A
 EQUIVALENCE   (Y(1), PRNT(1)), (Y(1), YAM(2)), (DY(1), DYAM(2)),
1              (S, YAM(1)), (VARTIK(1), POINT(1))
 EQUIVALENCE    (SLOPE(1)  ,  YPLOT(1)   ),
*               (D(476)    ,  XPLOT(1)   ),
*               (D(826)    ,  STROUT(1)  ),
*               (D(1176)   ,  SIGNPH(1)  ),
*               (D(1526)   ,  SIGMPH(1)  ),
*               (D(1876)   ,  SIGPHT(1)  ),
*               (D(2226)   ,  SIGPHB(1)  ),
*               (D(2576)   ,  SIGNTH(1)  ),
*               (D(2926)   ,  SIGMTH(1)  ),
```

```
*                (U(3276)   ,  SIGTHT(1)   ),
*                (U(3626)   ,  SIGTHB(1)   ),
*                (U(3976)   ,  TAUPHI(1)   )
      INTEGER   GO, TRYIN, PASS, SPACE, ADMSCT, FINIS, PLOT,
     *          PLOTPT, PLTIME, TIME, VARTIK, POINT
      DATA(RPD) = 0.17453292520E-01)
      REAL      NU, NT, MT, NBACK, NFH


C         ************************************************
C         *                                              *
C         *                SUMMARY OF COMMON             *
C         *                                              *
C         ************************************************
C         * PROGRAM *A*B*C*D*E*F*G*H*J*K*L*M*N*O*P*Q*S*X*1* *
C         ************************************************
C         * ADMINT  * * * * * * * * *Y*Y*Y*Y* * *Y* * * * * *
C         ************************************************
C         * ADMRES  * * * * * * * * *Y*Y*Y*Y* * *Y* * * * * *
C         ************************************************
C         * BCOND   * * * *Y* * * *Y* * * * * * * * * * * *
C         ************************************************
C         * CALCUL  *Y*Y*Y*Y* *Y*Y*Y*Y*Y*Y*Y*Y* *Y*Y*Y* *Y*Y*
C         ************************************************
C         * DIFFEQ  *Y*Y* * * * * *Y* * *Y* * * *Y* * * * *Y*
C         ************************************************
C         * GOMTRY  *Y*Y*Y* * *Y*Y* * * *Y* * * *Y*Y* * * *Y*
C         ************************************************
C         * INPUT   *Y* *Y* *Y*Y*Y*Y* * * * *Y* *Y*Y*Y*Y* * *
C         ************************************************
C         * INTEG   *Y*Y*Y* * *Y* *Y*Y*Y*Y* * * *Y* * * * *Y*
C         ************************************************
C         * INVERT  * * * * * * * * * * * * * * * * * * * * *
C         ************************************************
C         * MATML   * * * * * * * * * * * * * * * * * * * * *
C         ************************************************
C         * NONLIN  *Y*Y*Y*Y* *Y*Y*Y*Y*Y*Y*Y*Y* *Y*Y*Y*Y*Y*Y*
C         ************************************************
C         * PLTXY1  * * * * * * * * * * * * * * * * * * *Y* *
C         ************************************************
C         * PRINT   *Y*Y*Y*Y* *Y*Y*Y*Y*Y*Y*Y*Y* *Y*Y*Y* *Y*Y*
C         ************************************************
C         * THICK   *Y*Y* * *Y* *Y* * * *Y* * * * *Y* * * * *
C         ************************************************
C         * TRIANG  * * *Y* * *Y* *Y* * * * *Y* * * * * *Y*
C         ************************************************

999   CALL INPUT
      PLTIME = 0
      IF(INTVAL .EQ. 0) GO TO 415
      WRITE  (6,403)
415   ALFL = ALXL*RPD
      ALFR = ALXR*RPD
      CALL BCOND
      DO 250 I = 1, 8
      DO 250 J = 1, 8
```

```
      TLI(I,J) = 0.0
      TRI(I,J) = 0.0
250   CONTINUE
      DO 20 J=1,NDE
      DO 20 I=1,NDE
      K=IA(I)
      L=IB(I)
      DM(I,J)=TL(K,J)
   20 A (I,J)=TR(L,J)
      DO 23 I=1,NDE
      DO 23 J=1,NDE
      TL(I,J)=DM(I,J)
   23 TR(I,J)=A (I,J)
      DO 21 I=1,NDE
      DO 21 J=1,NDE
      TLI(I,J)=TL(I,J)
   21 TRI(I,J)=TR(I,J)
      CALL INVERT (TLI,NDE,8,DET,ISCAL)
      CALL INVERT (TRI,NDE,8,DET,ISCAL)
      IF(INTVAL .EQ. 0) GO TO 410
      WRITE(6,22)  ((TL(I,J), J = 1, 8),   (TR(I,J), J = 1, 8),
     1             I = 1, NDE)
      WRITE  (6,24 )
      WRITE(6,22)  ((TLI(I,J), J = 1, 8),   (TRI(I,J), J = 1, 8),
     1             I = 1, NDE)
410   NFP = NPARTS + 1
      DO 859 I = 1, IBRM
      BACK(I) = 1.0
859   CONTINUE
      DO 770 IBR = 1, IBRM
      ISH = ISS(IBR)
      GO TO (770, 770, 7703, 7703, 7703, 770, 7703, 770),  ISH
7703  IF(SX(IBR) .GT. SI(IBR))  GO TO 7710
      BACK(IBR) = - 1.0
      SI(IBR) = 180.0 - SI(IBR)
      SX(IBR) = 180.0 - SX(IBR)
7710  SX(IBR) = SX(IBR)*RPD
      SI(IBR) = SI(IBR)*RPD
770   CONTINUE
      IF(ISS(IBRM) .EQ. 1) GO TO 855
      IBRMAX = IBRM
      GO TO 856
855   IBRMAX = IBRM - 1
856   DO 1100 J = 1, NFP
      DO 1100 I = 1, 8
      TRY(I,J) = 0.0
1100  CONTINUE
      DO 1103 L = 1, IBRMAX
      DO 1103 I = 1, 8
      DM(I,L) = 0.0
1103  CONTINUE
      NN = 1
      NTYPE = 1
      CALL CALCUL
      CALL PRINT
      WRITE(6,693)  DETERM(1)
```

```
      IF(ITER .EQ. 0)  GO TO 999
      WRITE(6,601)  PN, GA(1), GA(2), GB(4), GB(5)
      FACTOR = 1.0/FLOAT(LEVEL1)
      DO 420 L = 1, NFP
      DO 420 I = 1, 6
      TRY(I,L) = DM(I,L)*FACTOR
  420 CONTINUE
      NN = 0
      NFAIL = 0
      NTYPE = 2
      NNNMAX = LEVEL1
      PNMAX = VN(5,1)
      DEMAX1 = GA(1)
      DEMAX2 = GA(2)
      DEMAX3 = GB(4)
      DEMAX4 = GB(5)
      GA(1) = 0.0
      GA(2) = 0.0
      GB(4) = 0.0
      GB(5) = 0.0
      PNINCR = PNMAX/FLOAT(NNNMAX)
      DEINC1 = DEMAX1/FLOAT(NNNMAX)
      DEINC2 = DEMAX2/FLOAT(NNNMAX)
      DEINC3 = DEMAX3/FLOAT(NNNMAX)
      DEINC4 = DEMAX4/FLOAT(NNNMAX)
      TEMP = 0.0
      DO 105 L = 1, NFP
      DO 105 I = 1, 6
      DMSAVE(I,L) = 0.0
  105 CONTINUE
      DO 400 NNN = 1, NNNMAX
      TEMP = TEMP + PNINCR
      DO 397 L = 1, IBRM
      VN(5,L) = TEMP
  397 CONTINUE
      GA(1) = GA(1) + DEINC1
      GA(2) = GA(2) + DEINC2
      GB(4) = GB(4) + DEINC3
      GB(5) = GB(5) + DEINC4
      ITERCT = 0
  810 NN = NN + 1
      CALL CALCUL

COMMENT   CHECK CONVERGENCE

      ITERCT = ITERCT + 1
      MAXXX = NPARTS - 1
      DO 811 L = 2, MAXXX
      DO 811 I = 1, 6
      IF(TRY(I,L) .EQ. 0.0)  GO TO 811
      IF(DM(I,L) .EQ. 0.0)  GO TO 811
      IF(ABS((DM(I,L) - TRY(I,L))/DM(I,L)) .GT. CONVER)  GO TO 850
  811 CONTINUE
      DO 110 L = 1, NFP
      DO 110 I = 1, 6
      TRY(I,L) = 2.0*DM(I,L) - DMSAVE(I,L)
```

```
  110 CONTINUE
      DO 112 L = 1, NFP
      DO 112 I = 1, 6
      DMSAVE(I,L) = DM(I,L)
  112 CONTINUE
      GO TO 815
  850 IF(ITERCT .EQ. ITER)  GO TO 8115
      DO 100 L = 1, NPARTS
      DO 100 I = 1, 6
      TRY(I,L) = DM(I,L)
  100 CONTINUE
      GO TO 810
 8115 NFAIL = 1
  815 CALL PRINT
      WRITE(6,601)  PN, GA(1), GA(2), GB(4), GB(5)
      IF(NFAIL .EQ. 0)  GO TO 3951
      WRITE(6,692) ITER
      GO TO 396
 3951 WRITE(6,689)  ITERCT
      ITERCT = 0
  396 WRITE(6,690)
      DO 425 I = 1, NN
      WRITE(6,691)  I, DETERM(I)
  425 CONTINUE
      IF(NFAIL .EQ. 1)  GO TO 999
      NN = 0
  400 CONTINUE
      GO TO 999
403   FORMAT (1H0,22X, 20HT MATRIX AT LEFT END,44X, 21HT MATRIX AT RIGHT
     1 END)
22    FORMAT(1H , 8F8.4, 2X, 8F8.4)
24    FORMAT(1H0)
693   FORMAT(1H0, 58HDETERMINANT OF FLEXIBILITY MATRIX FOR LINEAR ANALYS
     1IS WAS E15.8)
  601 FORMAT(1H0, 32HLOADINGS FOR THIS ANALYSIS WERE /
     $              6H PN = E14.7 /
     $              9H GA(1) = E14.7 /
     $              9H GA(2) = E14.7 /
     $              9H GB(4) = E14.7 /
     $              9H GB(5) = E14.7 )
692   FORMAT(1H0, 28HCONVERGENCE NOT OBTAINED IN 11, 11H ITERATIONS)
689   FORMAT(1H0, 34HCONVERGENCE OBTAINED ON ITERATION 11)
690   FORMAT(1H0, 57HDETERMINANTS OF FLEXIBILITY MATRIX FOR THIS LOADING
     $ WERE    )
  691 FORMAT(1H , 10HITERATION I1, 3X, E15.8)
      END
```

```
      SUBROUTINE AUMINT
      DIMENSION     Y(72),  YP(72),  ABC(21),  E(10),  PRNT(8)
      COMMON / BLOCKH / N
      COMMON / BLOCKJ / DELX, PDELX, ABC, E
      COMMON / BLOCKK / PI, PMIN, H0, X0, EMIN, EMAX
      COMMON / BLOCKL / Y, YP
      COMMON / BLOCKO / NN
      EQUIVALENCE  (PRNT(1), Y(2))
C N = NDE
C E = EAM
C Y = YAM
C YD = DYAM
C THIS SUBROUTINE IS A MODIFICATION OF SUBROUTINE AMI(BATTELLE
C MEMORIAL INSTITUTE PROBLEM NO. 64 - 64 DECK NO. 4064A). MAJOR
C DIFFERENCES ARE THAT PARAMETER LIST HAS BEEN REPLACED BY COMMON
C AND SUBROUTINE PROGRAM WHICH CALCULATES DERIVATIVES MUST NOW BE
C CALLED DIFFEQ.
C SUBROUTINE SUBPROGRAM FOR THE ADAMS-MOULTON AND/OR RUNGE-KUTTA-    AMI    3
C   GILL INTEGRATION OF A SYSTEM OF SIMULTANEOUS FIRST ORDER         AMI    4
C   DIFFERENTIAL EQUATIONS. THE ADAMS-MOULTON METHOD USES RUNGE-     AMI    5
C   KUTTA-GILL AS A STARTER.
C                                          ADAMS-MOULTON INTEGRATION
C                                  WITH AUTOMATIC LOCAL ERROR CONTROL,AMI   11
C                                  VARIABLE STEP SIZE.ALL COUNTERS ANDAMI   12
C                                  TABLES ARE UPDATED AT EACH        AMI   13
C                                  INTEGRATION STEP.                 AMI   14
C         NN = N + 1
C         N       = NUMBER OF EQUATIONS IN THE SYSTEM                AMI   34
C         DELX    = (TRIAL) STEP SIZE IN THE INDEPENDENT VARIABLE.   AMI   35
C                   IAMI INITIALIZES DELX. INTEGRATION MODES 2,3 ANDAMI   36
C                   4 RESULT IN AN INTEGRATION STEP OF THIS SIZE,    AMI   37
C                   AND DO NOT ALTER DELX. INTEGRATION MODE 1 MAY    AMI   38
C                   RESULT IN A SMALLER STEP OF THE FORM DELX/2.**K.AMI   39
C                   INTEGRATION MODE 1 MAY ALTER DELX, BUT ALWAYS    AMI   40
C                   LEAVES IT PROPERLY SET FOR THE NEXT CALL ( AS    AMI   41
C                   EITHER THE ACTUAL STEP SIZE OR TWICE THIS). THUSAMI   42
C                   ONLY IN INTEGRATION MODE 4 NEED THE USER ADJUST AMI   43
C                   DELX BETWEEN CALLS.                              AMI   44
C         PDELX   = THE ACTUAL STEP SIZE TAKEN, AN OUTPUT IN ALL FOURAMI   45
C                   INTEGRATION MODES, EQUAL TO DELX EXCEPT POSSIBLYAMI   46
C                   IN MODE 1.                                       AMI   47
C         Y       = A ONE DIMENSIONAL ARRAY CONSISTING OF 7*(N+1)    AMI   48
C                   ELEMENTS WHICH CONTAINS THE VALUES OF            AMI   49
C                   INDEPENDENT AND DEPENDENT VARIABLES. THE FIRST   AMI   50
C                   N+1 ELEMENTS CONTAIN THE VALUES OF THE PRESENT   AMI   51
C                   INTEGRATION STEP. THE NEXT N+1 ELEMENTS CONTAIN  AMI   52
C                   THE VALUES OF THE LAST PREVIOUS INTEGRATION STEPAMI   53
C                   AND SO ON. THE FIRST ELEMENT IN EACH GROUP OF    AMI   54
C                   N+1 ELEMENTS CONTAINS THE VALUE OF THE           AMI   55
C                   INDEPENDENT VARIABLE.INTEGRATION MODES 1,2 AND 3AMI   56
C                   SLIDE THE FIRST SIX GROUPS DOWN ONE GROUP BEFOREAMI   57
C                   PERFORMING EACH INTEGRATION STEP. INTEGRATION    AMI   58
C                   MODE 4 DOES NOT ALTER THE ARRAY EXCEPT TO PLACE  AMI   59
C                   THE PRESENT VALUES IN THE FIRST N+1 ELEMENTS.    AMI   60
C         YP      = A ONE DIMENSIONAL ARRAY CONSISTING OF 7*(N+1)    AMI   61
```

```
C                ELEMENTS WHICH CONTAINS THE VALUES OF THE          AMI   62
C                DERIVATIVES OF THE INDEPENDENT AND DEPENDENT       AMI   63
C                VARIABLES. THE STRUCTURE AND PROCESSING OF THIS    AMI   64
C                ARRAY IS EXACTLY THE SAME AS DESCRIBED FOR THE YAMI   65
C                ARRAY. THE FIRST ELEMENT IN EACH GROUP OF N+1      AMI   66
C                ELEMENTS CONTAINS THE VALUE OF THE DERIVATIVE      AMI   67
C                OF THE INDEPENDENT VARIABLE,ONE.                   AMI   68
C       DIFFEQ   = NAME OF A SUBROUTINE SUBPROGRAM WHICH CALCULATES AMI   69
C                THE VALUES OF THE DERIVATIVES.                     AMI   70
C          ABC   = A ONE DIMENSIONAL ARRAY CONSISTING OF N+13       AMI   71
C                ELEMENTS. THE FIRST N+1 ELEMENTS ARE THE RUNGE-    AMI   72
C                KUTTA-GILL Q VECTOR. THESE ELEMENTS ARE MODIFIEDAMI   73
C                EACH TIME AN INTEGRATION STEP IS TAKEN,            AMI   74
C                REGARDLESS   OF THE INTEGRATION MODE. THE LAST     AMI   75
C                TWELVE ELEMENTS OF THIS ARRAY ARE CONSTANTS        AMI   76
C                NEEDED BY THE RUNGE-KUTTA-GILL INTEGRATION         AMI   77
C                METHOD. THESE CONSTANTS ARE LOADED INTO ABC BY     AMI   78
C                IAM1. THE CONSTANTS ARE*                           AMI   79
C                 ABC(N+2)=.5                                       AMI   80
C                 ABC(N+3)=.292893218814                            AMI   81
C                 ABC(N+4)=1.707106781186                           AMI   82
C                 ABC(N+5)=.1666666666667                           AMI   83
C                 ABC(N+6)=2.                                       AMI   84
C                 ABC(N+7)=1.                                       AMI   85
C                 ABC(N+8)=1.                                       AMI   86
C                 ABC(N+9)=2.                                       AMI   87
C                 ABC(N+10)=.5                                      AMI   88
C                 ABC(N+11)=.292893218814                           AMI   89
C                 ABC(N+12)=1.707106781186                          AMI   90
C                 ABC(N+13)=.5                                      AMI   91
C          E     = A ONE DIMENSIONAL ARRAY CONSISTING OF TEN        AMI   97
C                ELEMENTS WHICH CONTAIN  VARIOUS COUNTERS AND       AMI   98
C                CONTROL VARIABLES. EACH ELEMENT WILL BE            AMI   99
C                DISCUSSED SEPARATELY*                              AMI  100
C                 E(1)  = MINIMUM ALLOWABLE LOCAL ERROR. THIS       AMI  101
C                         VALUE IS IGNORED BY INTEGRATION MODES     AMI  102
C                         2,3 AND 4. WHEN IN INTEGRATION MODE 1     AMI  103
C                         IF FIVE CONSECUTIVE INTEGRATION STEPS     AMI  104
C                         HAVE A MAXIMUM LOCAL ERROR LESS THAN      AMI  105
C                         E(1) THAN AN ATTEMPT IS MADE TO DOUBLEAMI  106
C                         THE STEPSIZE ON THE NEXT CALL OF AM1.     AMI  107
C                 E(2)  = MAXIMUM ALLOWABLE LOCAL ERROR. THIS       AMI  108
C                         VALUE IS IGNORED BY INTEGRATION MODES     AMI  109
C                         2,3 AND 4. WHEN IN INTEGRATION MODE 1     AMI  110
C                         IF THE MAXIMUM LOCAL ERROR ON ANY ONE     AMI  111
C                         INTEGRATION STEP EXCEEDS E(2) THEN AN     AMI  112
C                         ATTEMPT IS MADE TO HALVE THE STEP SIZEAMI  113
C                         AND INITIATE A RESTART.                   AMI  114
C                 E(3)  = MINIMUM ALLOWABLE STEP SIZE. THIS VALUEAMI  115
C                         IS IGNORED BY INTEGRATION MODES 2,3       AMI  116
C                         AND 4. IN INTEGRATION MODE 1 NO STEP      AMI  117
C                         SIZE SMALLER THAN E(3) WILL BE USED.      AMI  118
C                 E(4)  = MAXIMUM ALLOWABLE STEP SIZE. THIS VALUEAMI  119
C                         IS IGNORED BY INTEGRATION MODES 2,3       AMI  120
C                         AND 4. IN INTEGRATION MODE 1 NO STEP      AMI  121
C                         SIZE LARGER THAN E(4) WILL BE USED.       AMI  122
```

```
C                    E(5)  = DOUBLE STEP SIZE COUNTER. IN                AMI 123
C                            INTEGRATION MODES 2,3 E(5) ALWAYS          AMI 124
C                            EQUALS ZERO. IN INTEGRATION MODE 4         AMI 125
C                            E(5) REMAINS UNCHANGED. IN INTEGRATIONAMI 126
C                            MODE 1 E(5) COUNTS THE NUMBER OF           AMI 127
C                            SUCCESSIVE ADAMS-MOULTON STEPS IN          AMI 128
C                            WHICH THE MAXIMUM LOCAL ERROR IS LESS AMI 129
C                            THAN E(1). WHEN E(5) BECOMES FIVE          AMI 130
C                            DOUBLING THE STEP SIZE IS ATTEMPTED.  AMI 131
C                            E(5) IS RESET TO ZERO EACH TIME A STEPAMI 132
C                            IS TAKEN IN WHICH THE MAXIMUM LOCAL        AMI 133
C                            ERROR IS GREATER THAN OR EQUAL TO E(1)AMI 134
C                    E(6)  = PAST HISTORY COUNTER. IN INTEGRATION       AMI 135
C                            MODES 1,2 AND 3 E(6) INDICATES THE         AMI 136
C                            NUMBER OF GROUPS OF N+1 VALUES             AMI 137
C                            AVAILABLE IN THE Y AND YP ARRAYS. THE AMI 138
C                            VALUE OF E(6) IS ALWAYS ONE TO SEVEN       AMI 139
C                            INCLUSIVE. IN INTEGRATION MODE 4 E(6) AMI 140
C                            REMAINS UNCHANGED.                         AMI 141
C                    E(7)  = RUNGE-KUTTA-GILL LAST POINT INDICATOR. AMI 142
C                            IN INTEGRATION MODE 3 E(7) IS ALWAYS AMI 143
C                            EQUAL TO ZERO. IN INTEGRATION 4 E(7)       AMI 144
C                            REMAINS UNCHANGED. IN INTEGRATION          AMI 145
C                            MODES 1 AND 2 IF THE STEP JUST TAKEN AMI 146
C                            WAS A RUNGE-KUTTA-GILL STEP THEN           AMI 147
C                            E(7) = 1.,OTHERWISE E(7) = 0.              AMI 148
C                    E(8)  = BASE POINT COUNTER. IN INTEGRATION         AMI 149
C                            MODES 1,2 AND 3 A BASE POINT IS            AMI 150
C                            ESTABLISHED EACH TIME THE INDEPENDENT AMI 151
C                            VARIABLE IS ADVANCED AN INTEGRAL           AMI 152
C                            NUMBER OF E(4) FROM THE INITIAL            AMI 153
C                            STARTING POINT. AT EACH BASE POINT THEAMI 154
C                            INDEPENDENT VARIABLE IS RECALCULATED AMI 155
C                            AS E(8)*E(4)+E(10) THUS REDUCING THE AMI 156
C                            ACCUMULATED ROUNDOFF ERROR. IN             AMI 157
C                            INTEGRATION MODE 4 E(8) REMAINS            AMI 158
C                            UNCHANGED.                                 AMI 159
C                    E(9)  = STEP COUNTER TO THE NEXT BASE POINT. INAMI 160
C                            INTEGRATION MODES 1,2 AND 3 E(9)           AMI 161
C                            INDICATES THE NUMBER OF DELX STEPS         AMI 162
C                            REQUIRED TO REACH THE NEXT BASE POINT.AMI 163
C                            E(9) HAS ONLY INTEGRAL VALUES. IN          AMI 164
C                            INTEGRATION MODE 4 E(9) REMAINS            AMI 165
C                            UNCHANGED.                                 AMI 166
C                    E(10) = INITIAL VALUE OF THE INDEPENDENT           AMI 167
C                            VARIABLE AS ESTABLISHED IN IAM1.           AMI 168
C  THE SUBROUTINE IAM1 MUST BE CALLED PRIOR TO THE FIRST CALL TO AM1.AMI 169
C   IAM1 INITIALIZES THE ARRAYS YP,ABC AND E AS WELL AS THE VARIABLESAMI 170
C   DELX,PDELA AND Y(1). PRIOR TO THE CALL TO IAM1 THE USER MUST      AMI 171
C                                 PLACE THE INITIAL VALUES OF THEAMI 172
C   DEPENDENT VARIABLES INTO Y(2) THROUGH Y(N+1). THE USER MUST ALSO AMI 173
C   PROVIDE A SUBROUTINE SUBPROGRAM FOR THE EVALUATION OF THE         AMI 174
C   DERIVATIVES. THIS SUBPROGRAM IS CALLED BY BOTH AM1 AND IAM1 USINGAMI 175
C   THE STATEMENT CALL DIF(Y,YP) WHERE DIF,Y AND YP ARE AS DEFINED AMI 176
C   ABOVE. THE SUBPROGRAM OBTAINS THE VALUE OF THE INDEPENDENT         AMI 177
C   VARIABLE FROM Y(1) AND THE VALUES OF THE DEPENDENT VARIABLE FROM AMI 178
```

```
C      Y(2) THROUGH Y(N+1). THE SUBPROGRAM MUST PLACE THE VALUES OF THE AMI 179
C      DERIVATIVES OF THE DEPENDENT VARIABLES INTO YP(2) THROUGH YP(N+1)AMI 180
C     *** CAUTION *** IF THE USER DESIRES TO CHANGE INTEGRATION MODE    AMI 181
C                     (EXCEPTION INTMOD = 4),SYSTEM OF EQUATIONS OR STEPAMI 182
C                     SIZE HE SHOULD RESTART THE INTEGRATION WITH A CALLAMI 183
C                     TO IAM1.                                          AMI 184
C     THE QUANTITY REFERED TO ABOVE AS MAXIMUM LOCAL ERROR,COMPUTED AND AMI 185
C      USED IN MODE 1 TO CONTROL HALVING AND DOUBLING OF THE INTEGRATIONAMI 186
C      STEP SIZE,IS DEFINED AS THE MAXIMUM OVER I=1,2,...,N  OF         AMI 187
C                                                                       AMI 188
C              MIN1F(ABSF(P(I)-C(I)),ABSF((P(I)-C(I))/C(I)))            AMI 189
C                                                                       AMI 190
C      WHERE P(I), C(I)                                                 AMI 191
C      DENOTE,RESPECTIVELY,THE ADAMS-MOULTON PREDICTED AND CORRECTED    AMI 192
C      VALUES OF THE DEPENDENT VARIABLE Y(I+1). THIS ERROR IS THUS A    AMI 193
C      WEIGHTED MAXIMUM OVER ALL DEPENDENT VARIABLES OF THE DISCREPANCY AMI 194
C      BETWEEN PREDICTED AND CORRECTED VALUES OF EACH VARIABLE. FOR     AMI 195
C      EACH VARIABLE THIS DISCREPANCY IS RECKONED AS THE SMALLER OF THE AMI 196
C      ABSOLUTE AND THE RELATIVE DIFFERENCES BETWEEN PREDICTED AND      AMI 197
C      CORRECTED VALUES. THUS THE ABSOLUTE DIFFERENCE CONTROLS WHEN     AMI 198
C      ABSF(C(I)) IS LESS THAN ONE#OTHERWISE,THE RELATIVE DIFFERENCE    AMI 199
C      DOES. THIS PROVIDES A PARTLY RELATIVE ERROR CONTROL,WHILE        AMI 200
C      AVOIDING THE DIFFICULTY A PURELY RELATIVE CONTROL MIGHT          AMI 201
C      EXPERIENCE IN THE VICINITY OF A ZERO OF A DEPENDENT VARIABLE.    AMI 202
       PDELX=DELX                                                       AMI 204
       IF (E(9))47,2,47                                                 AMI 206
C      THIS IS A BASEPOINT - RECALCULATE E(9)                           AMI 207
    2  II=E(4)/DELX+.5                                                  AMI 208
       E(9)=II                                                          AMI 209
47     IF (E(6)-4.)46,4,4                                               AMI 211
C      ENOUGH PAST HISTORY IS AVAILABLE                                 AMI 212
    4  TEMP=DELX/24.                                                    AMI 213
       ICON=1                                                           AMI 214
C      SLIDE THE Y AND YP VECTORS DOWN ONE BLOCK EACH                   AMI 215
    5  IIII=E(6)                                                        AMI 216
       IF (IIII-7)7,6,7                                                 AMI 217
    6  IIII=IIII-1                                                      AMI 218
    7  IIII=IIII*NN                                                     AMI 219
       DO 8 I=1,IIII                                                    AMI 220
       III=IIII+1-I                                                     AMI 221
       II=III+NN                                                        AMI 222
       Y(II)=Y(III)                                                     AMI 223
    8  YP(II)=YP(III)                                                   AMI 224
       GO TO ( 9,35),ICON                                               AMI 225
C      CALCULATE PREDICATED Y                                           AMI 226
    9  K=NN+2                                                           AMI 227
       L=NN+NN                                                          AMI 228
       DO 10 I=K,L                                                      AMI 229
       KKKK=I-NN                                                        AMI 230
       II=I+NN                                                          AMI 231
       III=II+NN                                                        AMI 232
       IIII=III+NN                                                      AMI 233
   10  Y(KKKK)=Y(I)+TEMP*(55.*YP(I)-59.*YP(II)+37.*YP(III)-9.*YP(IIII)) AMI 234
       Y(1)=Y(NN+1)+DELX                                                AMI 235
C      CALCULATE PREDICATED YP                                          AMI 236
       CALL DIFFEQ
```

```
      DO 11 I=1,NN                                                      AMI 238
   11 ABC(I)=Y(I)                                                       AMI 239
C     CALCULATE CORRECTED Y                                            AMI 240
      DO 12 I=2,NN                                                      AMI 241
      II=I+NN                                                           AMI 242
      III=II+NN                                                         AMI 243
      IIII=III+NN                                                       AMI 244
   12 Y(I)=Y(II)+TEMP*(9.*YP(I)+19.*YP(II)-5.*YP(III)+YP(IIII))         AMI 245
C     CALCULATE CORRECTED YP                                           AMI 246
      CALL DIFFEQ
C     AUTOMATIC ERROR CHECKING                                         AMI 249
C     DETERMINE MAXIMUM LOCAL ERROR                                    AMI 250
      TEMP=0.                                                           AMI 251
      DO 16 I=2,NN                                                      AMI 252
      IF (Y(I))15,14,15                                                 AMI 253
   14 TEMP1=1.                                                          AMI 254
      GO TO 16                                                          AMI 255
   15 TEMP1=ABC(I)/Y(I)                                                 AMI 256
16    TEMP = MAXIF(TEMP, MINIF(ABS(ABC(I) - Y(I)), ABS(TEMP1 - 1.0)))
      IF (TEMP-E(1))17,38,24                                            AMI 259
C     THE ERROR IS LESS THAN THE MINIMUM ALLOWABLE ERROR               AMI 260
   17 IF (E(5)-4.)18,19,19                                              AMI 261
C     NOT ENOUGH SMALL ERRORS TO DOUBLE                                AMI 262
   18 E(5)=E(5)+1.                                                      AMI 263
      ICON=2                                                            AMI 264
      GO TO 38                                                          AMI 265
C     ENOUGH SMALL ERRORS TO DOUBLE                                    AMI 266
   19 II=(E(9)-1.)/2.                                                   AMI 267
      TEMP=II                                                           AMI 268
      IF (TEMP*2.+1.-E(9))18,20,18                                      AMI 269
C     WE ARE PROPERLY POSITIONED TO DOUBLE                             AMI 270
   20 TEMP1=2.*DELX                                                     AMI 271
      IF (E(4)-TEMP1)38,21, 21                                          AMI 272
C     STEP SIZE CAN BE DOUBLED                                         AMI 273
   21 E(9)=TEMP+1.                                                      AMI 274
      DELX=TEMP1                                                        AMI 275
      E(6)=3                                                            AMI 276
      DO 23 I=1,NN                                                      AMI 277
      II=I+NN                                                           AMI 278
      III=II+NN                                                         AMI 279
      DO 22 IIII=1,3                                                    AMI 280
      Y(II)=Y(III)                                                      AMI 281
      YP(II)=YP(III)                                                    AMI 282
      II=II+NN                                                          AMI 283
   22 III=III+NN+NN                                                     AMI 284
   23 CONTINUE                                                          AMI 285
      GO TO 38                                                          A . 286
C     ERROR IS OK AT LOWER BOUND CHECK UPPER BOUND                     AMI 287
   24 IF (TEMP-E(2))38,38,25                                            AMI 288
C     ERROR IS GREATER THAN THE MAXIMUM ALLOWABLE ERROR                AMI 289
   25 TEMP=.5*DELX                                                      AMI 290
      IF (TEMP-E(3))38,26,26                                            AMI 291
C     STEP SIZE CAN BE HALVED                                          AMI 292
   26 DELX=TEMP                                                         AMI 293
      PDELX=DELX                                                        AMI 294
      IF (E(7))31,31,27                                                 AMI 295
```

```
C       LAST POINT IS A RKG POINT-GO BACK TO INITIAL CONDITIONS          AMI 296
   27   DO 28 I=1,NN                                                    AMI 297
        II=I+NN                                                         AMI 298
        III=II+3*NN                                                     AMI 299
        Y(II)=Y(III)                                                    AMI 300
   28   YP(II)=YP(III)                                                  AMI 301
        E(9)=E(9)+3.                                                    AMI 302
        II=.5*E(4)/DELX+.5                                              AMI 303
        TEMP=II                                                         AMI 304
   29   IF (E(9)-TEMP)31,31,30                                          AMI 305
   30   E(9)=E(9)-TEMP                                                  AMI 306
        E(8)=E(8)-1.                                                    AMI 307
        GO TO 29                                                        AMI 308
C       COMPLETELY RESET AND EXECUTE RKG STEP                           AMI 309
   31   DO 32 I=1,NN                                                    AMI 310
        II=I+NN                                                         AMI 311
        Y(I)=Y(II)                                                      AMI 312
   32   YP(I)=YP(II)                                                    AMI 313
        E(9)=2.*E(9)                                                    AMI 314
        E(6)=1.                                                         AMI 315
   33   DO 34 I=1,NN                                                    AMI 316
   34   ABC(I)=0.                                                       AMI 317
   35   II=NN+3                                                         AMI 318
        DO 37 III=NN,II                                                 AMI 319
        DO 36 I=1,NN                                                    AMI 320
        TEMP=ABC(III+1)*(YP(I)-ABC(III+5)*ABC(I))                       AMI 321
        Y(I)=Y(I)+DELX*TEMP                                             AMI 322
   36   ABC(I)=ABC(I)+3.*TEMP-ABC(III+9)*YP(I)                          AMI 323
        CALL DIFFEQ
   37   CONTINUE                                                        AMI 325
        GO TO 39                                                        AMI 326
C       LAST POINT NOT RKG                                              AMI 327
   38   E(7)=0.                                                         AMI 328
        GO TO (40,41),ICON                                              AMI 329
   39   E(7)=1.                                                         AMI 330
   40   E(5)=0.                                                         AMI 331
   41   IF (E(6)-7.)42,43,43                                            AMI 332
   42   E(6)=E(6)+1.                                                    AMI 333
   43   E(9)=E(9)-1.                                                    AMI 334
        IF (E(9))45,44,45                                               AMI 335
   44   Y(1)=E(10)+E(8)-E(4)                                            AMI 336
        E(8)=E(8)+1.                                                    AMI 337
   45   RETURN                                                          AMI 338
C       NOT ENOUGH PAST HISTORY OR INTEGRATION MODE 3                   AMI 339
   46   ICON=2                                                          AMI 340
        GO TO 5                                                         AMI 341
        END                                                             AMI 342
```

```
      SUBROUTINE ADMRES
      DIMENSION      Y(72),  YP(72),  ABC(21),  E(10),  PRNT(8)
      COMMON / BLOCKH / N
      COMMON / BLOCKJ / DELX, PDELX, ABC, E
      COMMON / BLOCKK / PI, PMIN, HO, XO, EMIN, EMAX
      COMMON / BLOCKL / Y, YP
      COMMON / BLOCKO / NN
      EQUIVALENCE  (PRNT(1), Y(2))
C     N = NDE
C     E = EAM
C     Y = YAM
C     YP = DYAM
C     SUBROUTINE SUBPROGRAM FOR INITIALIZING ADMINT
C        *HERE    N      = SEE ADMINT
C                 DELX   = SEE ADMINT
C                 PDELX  = SEE ADMINT
C                 Y      = SEE ADMINT
C                 YP     = SEE ADMINT
C                 DIR    = SEE ADMINT
C                 ABC    = SEE ADMINT
C                 E      = SEE ADMINT
C                 PI     = INITIAL STEP SIZE IS HO*2.**(-PI)                IAM1 15
C                 PMIN   = MINIMUM ALLOWABLE STEP SIZE IS HO*2.**(-PMIN).   IAM1 16
C                            ALSO SEE E(3) OF ADMINT
C                 HO     = MAXIMUM ALLOWABLE STEP SIZE. ALSO SEE E(4) OF    IAM1 18
C                            ADMINT
C                 XO     = INITIAL VALUE OF THE INDEPENDENT VARIABLE. ALSO  IAM1 20
C                            SEE E(10) OF ADMINT
C                 EMIN   = MINIMUM ALLOWABLE LOCAL ERROR. ALSO SEE E(1) OF  IAM1 22
C                            ADMINT
C                 EMAX   = MAXIMUM ALLOWABLE LOCAL ERROR. ALSO SEE E(2) OF  IAM1 24
C                            ADMINT
C ADMINT INITIALIZES THE ARRAYS YP,ABC AND E AS WELL AS THE VARIABLES
C    DELX,PDELX AND Y(1). PRIOR TO THE CALL TO ADMRES
C                                          PLACE THE INITIAL VALUES OF THE  IAM1 28
C    DEPENDENT VARIABLES INTO Y(2) THROUGH Y(N+1).                          IAM1 29
      Y(1)=XO                                                               IAM1 30
      YP(1)=1.                                                              IAM1 31
      CALL DIFFEQ
      NN=N+1                                                                IAM1 33
      DO 1 I=1,NN                                                           IAM1 34
    1 ABC(I)=0.                                                             IAM1 35
      ABC(NN+1)=.5                                                          IAM1 36
      ABC(NN+2)=.292893218814                                               IAM1 37
      ABC(NN+3)=1.707106781186                                              IAM1 38
      ABC(NN+4)=.1666666666667                                              IAM1 39
      ABC(NN+5)=2.                                                          IAM1 40
      ABC(NN+6)=1.                                                          IAM1 41
      ABC(NN+7)=1.                                                          IAM1 42
      ABC(NN+8)=2.                                                          IAM1 43
      ABC(NN+9)=.5                                                          IAM1 44
      ABC(NN+10)=.292893218814                                              IAM1 45
      ABC(NN+11)=1.707106781186                                             IAM1 46
      ABC(NN+12)=.5                                                         IAM1 47
      E(1)=EMIN                                                             IAM1 48
```

```
      E(2)=EMAX                                                    IAM1 49
      E(4)=H0                                                      IAM1 50
      E(5)=0.                                                      IAM1 51
      E(6)=1.                                                      IAM1 52
      E(7)=0.                                                      IAM1 53
      E(8)=1.                                                      IAM1 54
      E(9)=0.                                                      IAM1 55
      E(10)=X0                                                     IAM1 56
      PDELX=0.                                                     IAM1 57
      TEMP=H0                                                      IAM1 58
      IF (PI)4,4,2                                                 IAM1 59
    2 J=PI+.4                                                      IAM1 60
      DO 3 I=1,J                                                   IAM1 61
    3 TEMP=TEMP/2.                                                 IAM1 62
    4 DELX=TEMP                                                    IAM1 63
      J=PMIN-PI+.4                                                 IAM1 64
      IF (J)7,7,5                                                  IAM1 65
    5 DO 6 I=1,J                                                   IAM1 66
    6 TEMP=TEMP/2.                                                 IAM1 67
    7 E(3)=TEMP                                                    IAM1 68
      RETURN                                                       IAM1 69
      END                                                          IAM1 70
```

```
      SUBROUTINE BCOND
      DIMENSION      TL(8,8),  TR(8,8),  TLI(8,8), TRI(8,8)
      COMMON / BLOCKD / TL, TR, TLI, TRI, ALFL, ALFR
      COMMON / BLOCKH / NDE
      DO 2 I = 1, 8
      DO 2 J = 1, 8
      TL (I,J)=0.0
    2 TR (I,J)=0.0
      DO 3 I = 5, NDE
      TL (I,I)=1.0
    3 TR (I,I)=1.0
      SIL=SIN (ALFL)
      COL=COS (ALFL)
      SIR=SIN (ALFR)
      COR=COS (ALFR)
      TL(1,1)= COL
      TR(1,1)= COR
      TL(1,3)=-SIL
      TR(1,3)=-SIR
      TL(2,2)= COL
      TR(2,2)= COR
      TL(2,4)=-SIL
      TR(2,4)=-SIR
      TL(3,1)= SIL
      TR(3,1)= SIR
      TL(3,3)= COL
      TR(3,3)= COR
      TL(4,2)= SIL
      TR(4,2)= SIR
      TL(4,4)= COL
      TR(4,4)= COR
    5 RETURN
      END
```

```
      SUBROUTINE CALCUL
      DIMENSION       IA(8)          , SI(60)         , IPAR(60)       ,
     *                IB(8)          , SX(60)         , INT(60)        ,
     *                GA(8)          , PRNT(8)        , ISS(60)        ,
     *                GB(8)          , ERR(8)         , PSR(60)        ,
     *                Y(8)           , DM(8,61)       , EYM(60)        ,
     *                DY(8)          , TL(8,8)        , A(8,9)         ,
     *                TR(8,8)        , TLI(8,8)       , JOBPLT(10)     ,
     *                TRI(8,8)       , TRY(8,61)      , TR2(8,8)       ,
     *                SOUT(275)      , D(8,9,60)      , P(5,275)       ,
     *                SLOPE(5,275)   , TRI(8,8)       , E(9,60)
      DIMENSION       V3(8)          , VN(7,60)       , YAM(72)        ,
     *                DYAM(72)       , ABC(21)        , EAM(10)        ,
     *                BACK(60)       , YSAVE(8)       , DETERM(10)     ,
     *                IPLOT(10)      , XPLOT(350)     , YPLOT(350,10)  ,
     *                STROUT(350)    , SIGNPH(350)    , SIGMPH(350)    ,
     *                SIGPHT(350)    , SIGPHB(350)    , SIGNTH(350)    ,
     *                SIGMTH(350)    , SIGTHT(350)    , SIGTHB(350)    ,
     *                TAUPHI(350)    , VARTIK(60)     , POINT(60)
      COMMON / BLOCKA / NU, P1, XLO, NTYPE, INDEX, IBK, PN, NPOINT,
     1                  ISH, TT, T1, T2, HTT, INTC
      COMMON / BLOCKB / H, R1, R2, R3, SXN, CXS
      COMMON / BLOCKC / DM, GA, GB, NF, NFP, NPL, NH, NN, IRY
      COMMON / BLOCKD / TL, TR, TLI, TRI, ALFL, ALFR
      COMMON / BLOCKF / NFF, SMXX, SZERO, GO, ERP, ISS, E,
     *                  MAX, INTPRN, INTVAL, NPP
      COMMON / BLOCKG / NPARTS, PHI1, V3, KIND, NT, MT, SPRINT, VN, EYM,
     1                  BACK, NBACK
      COMMON / BLOCKH / NDE
      COMMON / BLOCKJ / DELX, PDELX, ABC, EAM
      COMMON / BLOCKK / PIN, PMIN, HO, XO, EMIN, EMAX
      COMMON / BLOCKL / YAM, DYAM
      COMMON / BLOCKM / YSAVE
      COMMON / BLOCKN / DETERM
      COMMON / BLOCKP / PLOT, PLTIME, SPLOT, PLOTPT, IPLOT, YMOD, KST,
     1                  HGAMMA, DEAD, NFH
      COMMON / BLOCKQ / TIME, VARTIK, NVARTK
      COMMON / BLOCKS / JOBPLT, ALXL, ALXR, IA, IB, NOPUNC, INPUN,
     *                  CONVER, SI, SX, INT, IPAR, PSR, ITER, NTRY,
     *                  NERROR, IBRM, TRYIN, IBRMAX
      COMMON            SLOPE, P, SOUT, D, A
      COMMON / PLXYIC / IEX(8), DUM(4)
      EQUIVALENCE  (Y(1), PRNT(1)), (Y(1), YAM(2)), (DY(1), DYAM(2)),
     1            (S, YAM(1)), (VARTIK(1), POINT(1))
      EQUIVALENCE   (SLOPE(1)  ,  YPLOT(1)   ),
     *              (D(476)    ,  XPLOT(1)   ),
     *              (D(826)    ,  STROUT(1)  ),
     *              (D(1176)   ,  SIGNPH(1)  ),
     *              (D(1526)   ,  SIGMPH(1)  ),
     *              (D(1876)   ,  SIGPHT(1)  ),
     *              (D(2226)   ,  SIGPHB(1)  ),
     *              (D(2576)   ,  SIGNTH(1)  ),
     *              (D(2926)   ,  SIGMTH(1)  ),
     *              (D(3276)   ,  SIGTHT(1)  ),
     *              (D(3626)   ,  SIGTHB(1)  ),
```

```
     *                (D(39/6)   ,  TAUPHI(1)   )
      INTEGER  GO, TRYIN, PASS, SPACE, ADMSCT, FINIS, PLOT,
     1         PLOTPT, PLTIME, TIME, VARTIK, POINT
      DATA(RPD = 0.1745329252E-01)
      REAL           NU, NT, MT, NBACK, NFM
      NF = 0
      DO 10 I = 1, 8
      DO 10 L = 1, 8
      TR1(I,L) = 0.0
      TR2(I,L) = 0.0
10    CONTINUE
      DO 11 I = 5, 8
      TR1(I,I) = 1.0
      TR2(I,I) = 1.0
11    CONTINUE
      DO 4340 IBR = 1, IBRMAX
      NBACK = BACK(IBR)
      NVARTK = POINT(IBR)
      ISH = ISS(IBR)
      YMOD = EYM(IBR)
      NU = PSR(IBR)
      P1 = (1.0 - NU*NU)/YMOD
      INDEX = 1
      CALL GOMTRY
      TT = H*H/12.0
      T1 = P1/H
      T2 = T1/TT
      HTT = H*TT
      NFF = IPAR(IBR)
      NPP = INT(IBR)
      SMXX = (SX(IBR) - SI(IBR))/FLOAT(NFF)
      SZERO = SI(IBR)

C     GO IS SET TO 1 IN INTEG IF THE DIMENSION(275) OF SOUT IS EXCEEDED.
C     CALCULATIONS ARE STOPPED.

      GO = 0
      CALL INTEG
      IF(GO .EQ. 1) GO TO 205
      IF(IBR .EQ. IBRMAX) GO TO 501
      S=SX(IBR)
      ISH = ISS(IBR)
      NBACK = BACK(IBR)
      INDEX = 3
      CALL GOMTRY
      TR1(1,1) = CXS
      TR1(1,3)= -SXN
      TR1(2,2)=  CXS
      TR1(2,4)= -SXN
      TR1(3,1)=  SXN
      TR1(3,3)=  CXS
      TR1(4,2)=  SXN
      TR1(4,4)=  CXS
      IF(INTVAL .EQ. 0) GO TO 778
      WRITE(6,678)
      WRITE(6,676)  ((TR1(I,J), J = 1, 8), I = 1, NDE)
```

```
778   IBRSAV = IBR
      IBR = IBR + 1
      S = SI(IBR)
      ISH = ISS(IBR)
      NBACK = BACK(IBR)
      INDEX = 3
      CALL GOMTRY
      IBR = IBRSAV
      TR2(1,1) = CXS
      TR2(1,3)=  SXN
      TR2(2,2)=  CXS
      TR2(2,4)=  SXN
      TR2(3,1)= -SXN
      TR2(3,3)=  CXS
      TR2(4,2)= -SXN
      TR2(4,4)=  CXS
      IF(INTVAL .EQ. 0) GO TO 779
      WRITE(6,679)
      WRITE(6,676)  ((TR2(I,J), J = 1, 8), I = 1, 8)

C     FORM PRODUCT OF TR2 AND TR1
C     PUT RESULT IN TR1.

779   CALL MATML(TR2(1,1), 8, 8, 1, 1, NDE, NDE,
     *           TR1(1,1), 8, 8, 1, 1, NDE,
     *           TR1(1,1), 8, 8, 1, 1, A)
      IF(INTVAL .EQ. 0) GO TO 780
      WRITE(6,680)
      WRITE(6,676)  ((TR1(I,J), J = 1, 8), I = 1, NDE)

C     FORM PRODUCT OF (TR2*TR1) AND D(I,J,NF). D(I,J,NF) CONTAINS THE
C     COMPLEMENTARY AND PARTICULAR SOLNS FOR THE LAST PART OF THE BRANCH
C     PUT RESULT IN D(I,J,NF)

780   CALL MATML(TR1(1,1), 8, 8, 1, 1, NDE, NDE,
     *           D(1,1,NF), 8, 9, 1, 1, NPL,
     *           D(1,1,NF), 8, 9, 1, 1, A)
4340  CONTINUE
501   IF(ISS(IBRM) .GT. 1) GO TO 5028
      INDEX = 1
      KIND = 0
      ISH = 1
      IBR = IBRM
      YMOD = EYM(IBR)
      NU = PSR(IBR)
      IF(NTYPE .NE. 1)  GO TO 518
      XLO = 0.0
      GO TO 519
518   XLO = 1.0
519   CALL GOMTRY

C     MODIFY COMPLEMENTARY SOLNS FOR THE FIRST PART OF THE FIRST BRANCH.
C     STORE RESULT IN D(1,I,J)
5028  CALL MATML(D(1,1,1), 8, 9, 1, 1, NDE, NDE,
     *           TLI(1,1), 8, 8, 1, 1, NDE,
     *           D(1,1,1), 8, 9, 1, 1, A)
```

```
C     IF THERE IS A CROWN, NO MODIFICATION OF COMPLEMENTARY AND
C     PARTICULAR SOLUTIONS IS NECESSARY SINCE THERE IS CONTINUITY AND
C     ELEMENTS HAVE BEEN CORRECTLY POSITIONED.

      IF(ISS(IBRM) .EQ. 1) GO TO 706

C     MODIFY COMPLEMENTARY AND PARTICULAR SOLNS FOR THE LAST PART OF THE
C     LAST BRANCH.
C     STORE RESULTS IN D(I,J,NF)

      CALL MATML(TR(1,1), 8, 8, 1, 1, NDE, NDE,
     *           D(1,1,NF), 8, 9, 1, 1, NPL,
     *           D(1,1,NF), 8, 9, 1, 1, A)

C     MODIFY TRY(I,J) FOR LINEAR COMBINATIONS AND ARRANGE ELEMENTS
C     SO THAT UPPER THREE ARE THOSE PRESCRIBED ON BOUNDARY.
C     STORE RESULT IN TRY(I,1)

706   CALL MATML(TL(1,1), 8, 8, 1, 1, NDE, NDE,
     *           TRY(1,1), 8, 1, 1, 1, 1,
     *           TRY(1,1), 8, 1, 1, 1, A)
      IF(ISS(IBRM) .GT. 1) GO TO 4675
      DO 4676 I = 1, 8
      TRY(I,NPARTS) = 0.0
4676  CONTINUE
4675  IF(INTVAL .EQ. 0) GO TO 4680
      WRITE(6,670) NN
      WRITE(6,671) ((TRY(I,J), I = 1, 8), J = 1, NTRY)
4680  NF = NPARTS
      CALL TRIANG
      IF(ISS(IBRM) .GT. 1) GO TO 4685
      DO 4690 I = 1, 6
      TRY(I,NFP) = DM(I,NFP)
4690  CONTINUE

C     MODIFY DM(I,1) FOR LINEAR COMBINATIONS AND ARRANGE ELEMENTS INTO
C     CORRECT POSITIONS.
C     STORE RESULT IN DM(I,1)

4685  CALL MATML(TLI(1,1), 8, 8, 1, 1, NDE, NDE,
     *           DM(1,1), 8, 1, 1, 1, 1,
     *           DM(1,1), 8, 1, 1, 1, A)
C     MODIFY DM(I,NFP) FOR LINEAR COMBINATIONS AND ARRANGE ELEMENTS INTO
C     CORRECT POSITIONS.
C     STORE RESULTS IN DM(I,NFP)
      CALL MATML(TRI(1,1), 8, 8, 1, 1, NDE, NDE,
     *           DM(1,NFP), 8, 1, 1, 1, 1,
     *           DM(1,NFP), 8, 1, 1, 1, A)
      WRITE(6,24 )
      IF(INTVAL .EQ. 0)  RETURN
      WRITE(6,671) ((DM(J,I), J = 1, 8), I = 1, NFP)
      RETURN
  205 WRITE(6,667)
      CALL EXIT
678   FORMAT(1H1, 8HTR1(I,J))
```

```
676   FORMAT(1H0, 8E16.7)
679   FORMAT(1H0, /, 1H0, 8HTR2(I,J))
680   FORMAT(1H0, /, 1H0, 22HPRODUCT OF TR2 AND TR1)
670   FORMAT(1H1, 31HTHIS IS TRY(I,J) FOR ITERATION I2, /, 1H0)
671   FORMAT(1H , 8E16.7)
24    FORMAT(1H0)
  667 FORMAT(1H0, 26HDIMENSION OF SOUT EXCEEDED)
      END
```

```
      SUBROUTINE DIFFEQ
      DIMENSION     Y(8)          , DY(8)         , P(5,275)     ,
     *              SOUT(275)     , SLOPE(5,275)  , YAM(72)      ,
     *              DYAM(72)      , PRNT(8)       , XPLOT(350)   ,
     *              YPLOT(350,10) , STROUT(350)   , SIGNPH(350)  ,
     *              SIGMPH(350)   , SIGPHT(350)   , SIGPHB(350)  ,
     *              SIGNTH(350)   , SIGMTH(350)   , SIGTHT(350)  ,
     *              SIGTHB(350)   , TAUPHI(350)   , D(8,9,60)    ,
     *              IPLOT(10)     , A(8,9)
      COMMON / BLOCKA / NU, P1, XLD, NTYPE, INDEX, IBR, PN, NPOINT,
     1                  ISH, TT, T1, T2, HTT, INTC
      COMMON / BLOCKB / H, R1, R2, R3, SXN, CXS
      COMMON / BLOCKH / NDE
      COMMON / BLOCKL / YAM, DYAM
      COMMON / BLOCKP / PLOT, PLTIME, SPLOT, PLOTPT, IPLOT, YMOD, KST,
     1                  HGAMMA, DEAD, NFH
      COMMON            SLOPE, P, SOUT, D, A
      EQUIVALENCE   (Y(1), YAM(2)), (DY(1), DYAM(2)), (S, YAM(1)),
     *              (PRNT(1), YAM(2))
      EQUIVALENCE   (SLOPE(1) , YPLOT(1)   ),
     *              (D(476)   , XPLOT(1)   ),
     *              (D(826)   , STROUT(1)  ),
     *              (D(1176)  , SIGNPH(1)  ),
     *              (D(1526)  , SIGMPH(1)  ),
     *              (D(1876)  , SIGPHT(1)  ),
     *              (D(2226)  , SIGPHB(1)  ),
     *              (D(2576)  , SIGNTH(1)  ),
     *              (D(2926)  , SIGMTH(1)  ),
     *              (D(3276)  , SIGTHT(1)  ),
     *              (D(3626)  , SIGTHB(1)  ),
     *              (D(3976)  , TAUPHI(1)  )
      REAL      NU, KT, NI, MT, NR2, NFH, MTP

C     ET = EPSILON THETA
C     KT = KAPPA THETA
C     NT = N SUB THETA
C     MT = M SUB THETA
C     NU = POISSON*S RATIO
C     P1 = (1.0 - NU*NU)/YMOD
C     TT = H*H/12.0
C     T1 = P1/H
C     T2 = T1/TT
C     HTT = H*TT
C     NFH = FOURIER HARMONIC
C     NR2 = NFH*R2
C     MTP = M THETA PHI
C     PN  = NORMAL SURFACE LOADING
C     PL  = LONGITUDINAL SURFACE LOADING
C     PC  = CIRCUMFERENTIAL SURFACE LOADING
C     BT  = BETA THETA
C     NTYPE = 1     LINEAR
C     NTYPE = 2     NONLINEAR
C     NTYPE = 3     AUXILIARY EQUATIONS FOR NONLINEAR  ANALYSIS.

      INIC = INTC + 1
```

```
      CALL GOMTRY
      R2COSS = R2*CXS
      R2SINS = R2*SXN
      IF(NDE .EQ. 8)  GO TO 65
      ET = R2COSS*Y(3) + R2SINS*Y(1)
      KT = R2COSS*Y(5)
      NT = NU*Y(4) + H*ET*YMOD
      MT = NU*Y(6) + HTT*KT*YMOD
      DY(1) = R1*Y(3) - Y(5)
      DY(5) = T2*Y(6) - NU*KT
      DY(6) = R2COSS*(MT - Y(6)) + Y(2)
      GO TO (10, 20, 30), NTYPE

C     THIS SECTION COMPLETES LINEAR EQUATIONS.

10    DY(2) = R2SINS*NT - R2COSS*Y(2) + R1*Y(4) -
     1        (PN + (HGAMMA + DEAD)*CXS)*XLD
      DY(3) = T1*Y(4) - R1*Y(1) - NU*ET
      DY(4) = R2COSS*(NT - Y(4)) - R1*Y(2) + (HGAMMA + DEAD)*SXN*XLD
      GO TO 59

C     THIS SECTION COMPLETES NONLINEAR EQUATIONS.

20    DY(3) = T1*Y(4) - R1*Y(1) - NU*ET - 0.5*Y(5)*Y(5)
      DY(2) = NT*(R2SINS + R2COSS*Y(5)) +
     *        Y(4)*(DY(5) + (1.0 +Y(5)*Y(5))*R1) -
     *        Y(2)*(R2COSS + R1*Y(5)) - PN - (HGAMMA + DEAD)*CXS
      DY(4) = R2COSS*(NT - Y(4)) + R1*(Y(5)*Y(4) - Y(2)) +
     *        (HGAMMA + DEAD)*SXN
      GO TO 59

C     THIS SECTION COMPLETES AUXILIARY EQUATIONS FOR NONLINEAR ANALYSIS.


C     PAR1 = Q PHI
C     PAR2 = N PHI
C     PAR3 = BETA PHI
C     PAR4 = BETA PHI COMMA S
C     PAR5 = N THETA

30    I = NPOINT
      IF(SOUT(I) - S) 38, 38, 32
32    IL = 1
      IU = NPOINT
33    IF(IU - IL - 1) 37, 37, 34
34    I = (IL + IU)/2
      IF(S - SOUT(I)) 35, 38, 36
35    IU = I
      GO TO 33
36    IL = I
      GO TO 33
37    I = IU
38    DO 49 J = 1, 5
      SUM = SLOPE(J,I - 1)*S + P(J,I - 1)
      GO TO (41, 42, 43, 44, 45), J
41    PAR1 = SUM
```

```
      GO TO 49
42    PAR2 = SUM
      GO TO 49
43    PAR3 = SUM
      GO TO 49
44    PAR4 = SUM
      GO TO 49
45    PAR5 = SUM
      GO TO 55
49    CONTINUE
55    DY(3) = T1*Y(4) - NU*ET - R1*Y(1) - PAR3*Y(5)
      DY(2) = NT*(R2SINS + R2COSS*PAR3) + KT*PAR5 - R1*Y(5)*PAR1 +
     *        Y(4)*(R1*(1.0 + PAR3*PAR3) + PAR4) +
     *        PAR2*(2.0*R1*PAR3*Y(5) + DY(5)) - Y(2)*(R2COSS + R1*PAR3)
      DY(4) = R2COSS*(NT - Y(4)) + R1*(PAR2*Y(5) + PAR3*Y(4) - Y(2))
59    IF(R3 .EQ. 1.0) RETURN
      DO 60 I = 1, 6
      DY(I) = DY(I)/R3
60    CONTINUE
      RETURN
65    NR2 = NFH*R2
      ET = R2COSS*Y(3) + R2SINS*Y(1) + NR2*Y(7)
      BT = R2SINS*Y(7) + NR2*Y(1)
      KT = R2COSS*Y(5) + NR2*BT
      NT = NU*Y(4) + H*YMOD*ET
      MT = NU*Y(6) + HTT*YMOD*KT
      DY(1) = R1*Y(3) - Y(5)
      DY(3) = T1*Y(4) - NU*ET - R1*Y(1)
      DY(5) = T2*Y(6) - NU*KT
      DY(7) = R2COSS*Y(7) + NR2*Y(3) + 2.0*(Y(8)*(1.0 + NU)/(YMOD*H) +
     $        R2SINS*TT*(NR2*Y(5) + BT*R2COSS))
      MTP = 0.5*(1.0 - NU)*(R2COSS*(R1*Y(7) - 2.0*BT) +
     $                      NR2*(R1*Y(3) - 2.0*Y(5)) +
     $                      R2SINS*DY(7))/T2
      DY(2) = R2SINS*NT + R1*Y(4) - R2COSS*Y(2) + NR2*(NR2*MT - 2.0*
     *        R2COSS*MTP) - PN*XLD
      DY(4) = R2COSS*(NT - Y(4)) - R1*Y(2) + NR2*(MTP*(R1 + R2SINS) -
     *        Y(8))
      DY(6) = (MT - Y(6))*R2COSS + Y(2) - 2.0*NR2*MTP
      DY(8) = R2COSS*(MTP*(R1 - R2SINS) - 2.0*Y(8)) +
     *        NR2*(NT + R2SINS*MT)
      IF(R3 .EQ. 1.0)  RETURN
      DO 70 I = 1, 8
      DY(I) = DY(I)/R3
70    CONTINUE
      RETURN
      END
```

```
      SUBROUTINE GOMTRY
      DIMENSION      VN(7,60)       , DM(8,61)       , GA(8)          ,
     *               GB(8)          , TRY(8,61)      , SOUT(275)      ,
     *               V1(4,4)        , V2(4,4)        , V3(8)          ,
     *               D(8,9,60)      , V4(4,4)        , V5(4,4)        ,
     *               PRNT(8)        , ISS(60)        , E(9,60)        ,
     *               YAM(72)        , DYAM(72)       , VARTIK(60)     ,
     *               P(5,275)       , SLOPE(5,275)   , STROUT(350)    ,
     *               SIGNPH(350)    , SIGMPH(350)    , SIGPHT(350)    ,
     *               SIGPHB(350)    , SIGNTH(350)    , SIGMTH(350)    ,
     *               SIGTHT(350)    , SIGTHB(350)    , TAUPHI(350)    ,
     *               XPLOT(350)     , YPLOT(350,10)  , POINT(60)      ,
     *               EYM(60)        , IPLOT(10)      , BACK(60)       ,
     *               A(8,9)
      COMMON / BLOCKA / NU, P1, XLD, NTYPE, INDEX, IBR, PN, NPOINT,
     1                  ISH, TT, T1, T2, HTT, INTC
      COMMON / BLOCKB / H, R1, R2, R3, SXN, CXS
      COMMON / BLOCKC / DM, GA, GB, NF, NFP, NPL, NH, NN, IRY
      COMMON / BLOCKF / NFF, SMXX, SZERO, GO, ERP, ISS, E,
     *                  MAX, INTPRN, INTVAL, NPP
      COMMON / BLOCKG / NPARTS, PHI1, V3, KIND, NT, MT, SPRINT, VN, EYM,
     1                  BACK, NBACK
      COMMON / BLOCKL / YAM, DYAM
      COMMON / BLOCKP / PLOT, PLTIME, SPLOT, PLOTPT, IPLOT, YMOD, KST,
     1                  HGAMMA, DEAD, NFH
      COMMON / BLOCKQ / TIME, VARTIK, NVARTK
      COMMON            SLOPE, P, SOUT, D, A
      EQUIVALENCE  (S, YAM(1)), (PRNT(1), YAM(2)), (VARTIK(1), POINT(1))
      EQUIVALENCE   (SLOPE(1) ,  YPLOT(1)   ),
     *              (D(476)   ,  XPLOT(1)   ),
     *              (D(826)   ,  STROUT(1)  ),
     *              (D(1176)  ,  SIGNPH(1)  ),
     *              (D(1526)  ,  SIGMPH(1)  ),
     *              (D(1876)  ,  SIGPHT(1)  ),
     *              (D(2226)  ,  SIGPHB(1)  ),
     *              (D(2576)  ,  SIGNTH(1)  ),
     *              (D(2926)  ,  SIGMTH(1)  ),
     *              (D(3276)  ,  SIGTHT(1)  ),
     *              (D(3626)  ,  SIGTHB(1)  ),
     *              (D(3976)  ,  TAUPHI(1)  )
      REAL  NU, N0, M0, N1, M1, NT, MT, NBACK, NFH
      INTEGER GO, VARTIK, TIME, POINT
      DATA( RPU = 0.1745329252E-01 )
      GO TO (1, 2, 3, 4, 5, 6, 7, 8), ISH

C     THIS SECTION IS FOR THE CROWN.

1     GO TO (13, 14), INDEX
13    H = VN(1,IBR)
      R1 = 1.0/VN(2,IBR)
      PN = VN(5,IBR)
      GAMMA = VN(6,IBR)
      DEAD  = VN(7,IBR)
      HGAMMA = H*GAMMA
      PM1 = (1.0 - NU)/YMOD
```

```
      P2M1 = (1.0 - NU*NU)/YMOD
      PP3 = 3.0 + NU
      R1H = 1.0/(R1*H)
      R1H3 = 1.0/(R1*H*H*H)
      IF(KIND .EQ. 4) GO TO 180
      PHI1 = 0.02
      PHI2 = 0.0004
      W0 = TRY(1,NFP)
      N0 = TRY(2,NFP)
      M0 = TRY(3,NFP)
      GO TO 190
180   PHI2 = PHI1**2
      W0 = DM(1,NFP)
      N0 = DM(4,NFP)
      M0 = DM(6,NFP)
190   U0 = PM1*N0*R1H - W0
      B0 = 12.0*PM1*R1H3*M0
      B01 = 1.0 + B0*XLD
      Q0 = N0*B01 - 0.5*(PN - HGAMMA - DEAD)/R1
      W1 = 0.5*(U0 - B0/R1)
      M1 = 0.125*(PP3*Q0/R1 - PM1*M0*YMOD)
      B1 = 0.5*R1H3*(3.0*P2M1*Q0/R1 - (1.0 - 3.0*NU)*PM1*M0)
      N1 = - 0.5*(3.0*R1H*PM1*(1.0 + 0.5*B0*XLD)*M0*YMOD/H +
     1       0.25*PP3*B01*Q0) - 0.125*(HGAMMA + DEAD)*PP3/R1
      U1 = - W1/3.0 - 0.125*P2M1*B01*Q0*R1H
     1     - (3.0 - NU)*B0*B0*XLD/(16.0*R1)
     2     - 0.5*PM1*(1.0 - 3.0*NU)*R1H3*M0/R1
     3     - 0.125*P2M1*(HGAMMA + DEAD)/(R1*R1*H)
      Q1 = 0.25*Q0*(B01*B01 + 1.0/3.0) + B01*N1 + N0*(B1 - B0/12.0)*XLD
     1     + 0.125*(HGAMMA + DEAD)*(1.0 + 2.0*B0*XLD)/R1
      V3(1) = W0 + W1*PHI2
      V3(4) = N0 + N1*PHI2
      V3(6) = M0 + M1*PHI2
      V3(2) = - (Q0 + Q1*PHI2)*PHI1
      V3(3) = - (U0 + U1*PHI2)*PHI1
      V3(5) = - (B0 + B1*PHI2)*PHI1
      IF(KIND .EQ. 5) GO TO 195
      NT = N0 + (3.0*N1 + B01*Q0)*PHI2
      MT = M0 + (3.0*M1 - Q0/R1)*PHI2
      RETURN
195   DO 200 I = 1, 3
      DO 200 J = 1, 3
      V1(I,J) = 0.0
      V2(I,J) = 0.0
      V4(I,J) = 0.0
      V5(I,J) = 0.0
200   CONTINUE
      V5(1,2) = 1.0
      V5(2,3) = 12.0*PM1*R1H3
      V5(3,3) = 1.0
      V4(1,1) = 1.0
      V4(2,2) = B01
      V4(2,3) = N0*V5(2,3)
      V4(3,1) = - 1.0
      V4(3,2) = PM1*R1H
      V2(1,2) = - 0.125*PP3*B01*V4(2,2)
```

```
      V2(1,3) = - 1.5*PM1*R1H*(1.0 + 0.5*B0)*YMOD/H -
     1          ( 0.75*PM1*R1H*N0*V5(2,3)*YMOD/H
     2          + 0.125*PP3*(B01*V4(2,3) + Q0*V5(2,3)))*XLD
      V2(2,2) = 1.5*P2M1*R1H3*V4(2,2)/R1
      V2(2,3) = 0.5*R1H3*(3.0*P2M1*V4(2,3)/R1 -
     1          (1.0 - 3.0*NU)*PM1*V5(3,3))
      V2(3,2) = 0.125*PP3*V4(2,2)/R1
      V2(3,3) = 0.125*(PP3*V4(2,3)/R1 - PM1*YMOD)
      V1(1,1) = 0.5*V4(3,1)
      V1(1,2) = 0.5*V4(3,2)
      V1(1,3) = - 0.5*V5(2,3)/R1
      V1(2,2) = 0.25*V4(2,2)*(B01*B01 + 1.0/3.0) + B01*V2(1,2) +
     1          ((B1 - B0/12.0)*V5(1,2) + N0*V2(2,2))*XLD
      V1(2,3) = 0.25*V4(2,3)*(B01*B01 + 1.0/3.0) + B01*V2(1,3) +
     1          N0*(V2(2,3) - V5(2,3)/12.0) +
     2          V5(2,3)*(0.5*Q0*B01 + N1)*XLD
      V1(3,1) = - V1(1,1)/3.0
      V1(3,2) = - V1(1,2)/3.0 - 0.125*P2M1*R1H*B01*V4(2,2)
      V1(3,3) = - V1(1,3)/3.0 - 0.5*PM1*(1.0 - 3.0*NU)*R1H3/R1
     1          - 0.125*P2M1*B01*R1H*V4(2,3)
     2          - 0.125*(P2M1*Q0/H + (3.0 - NU)*B0)*V5(2,3)*XLD/R1
      V1(1,1) = V4(1,1) + V1(1,1)*PHI2
      V1(1,2) = V4(1,2) + V1(1,2)*PHI2
      V1(1,3) = V4(1,3) + V1(1,3)*PHI2
      V2(1,1) = V5(1,1) + V2(1,1)*PHI2
      V2(1,2) = V5(1,2) + V2(1,2)*PHI2
      V2(1,3) = V5(1,3) + V2(1,3)*PHI2
      V2(3,1) = V5(3,1) + V2(3,1)*PHI2
      V2(3,2) = V5(3,2) + V2(3,2)*PHI2
      V2(3,3) = V5(3,3) + V2(3,3)*PHI2
      V1(2,1) = - (V4(2,1) + V1(2,1)*PHI2)*PHI1
      V1(2,2) = - (V4(2,2) + V1(2,2)*PHI2)*PHI1
      V1(2,3) = - (V4(2,3) + V1(2,3)*PHI2)*PHI1
      V1(3,1) = - (V4(3,1) + V1(3,1)*PHI2)*PHI1
      V1(3,2) = - (V4(3,2) + V1(3,2)*PHI2)*PHI1
      V1(3,3) = - (V4(3,3) + V1(3,3)*PHI2)*PHI1
      V2(2,1) = - (V5(2,1) + V2(2,1)*PHI2)*PHI1
      V2(2,2) = - (V5(2,2) + V2(2,2)*PHI2)*PHI1
      V2(2,3) = - (V5(2,3) + V2(2,3)*PHI2)*PHI1
      IF(INTVAL .EQ. 0) GO TO 166
      WRITE(6,603)
      WRITE(6,602) ((V1(I,J), J = 1, 3), V3(I), I = 1, 3)
      WRITE(6,604)
      DO 165 I = 1, 3
      M = I + 3
      WRITE(6,602) (V2(I,J), J = 1, 3), V3(M)
  165 CONTINUE
  166 CALL INVERT(V1, 3, 4, DET, ISCAL)
      DO 100 I = 1, 3
      DO 100 J = 1, 3
      D(I,J,NPARTS) = V1(I,J)
  100 CONTINUE
      CALL MATML (V2(1,1), 4, 4, 1, 1, NH, NH,
     *            V1(1,1), 4, 4, 1, 1, NH,
     *            D(1,1,NPARTS), 8, 9, NH + 1, 1, A)
      DO 115 I = 1, 6
```

```
      DO 115 J = 4, 7
      D(I,J,NPARTS) = 0.0
115   CONTINUE
      DO 120 I = 4, 6
      D(I,I,NPARTS) = - 1.0
120   CONTINUE
      DO 130 J = 1, 3
      SUM = 0.0
      DO 125 I = 1, 3
      SUM = SUM + D(J,I,NPARTS)*V3(I)
125   CONTINUE
      D(J,7,NPARTS) = - SUM
130   CONTINUE
      DO 135 I = 1, 3
      D(I,7,NPARTS) = D(I,7,NPARTS) + TRY(I,NFP)
135   CONTINUE
      DO 145 J = 4, 6
      SUM = 0.0
      DO 140 I = 1, 3
      SUM = SUM + D(J,I,NPARTS)*V3(I)
140   CONTINUE
      D(J,7,NPARTS) = - SUM
145   CONTINUE
      DO 150 I = 4, 6
      D(I,7,NPARTS) = D(I,7,NPARTS) + V3(I)
150   CONTINUE
      IF(INTVAL .EQ. 0) RETURN
      WRITE(6,607)
      WRITE(6,606)  ((D(I,J,NPARTS), J = 1, 7), I = 1, 6)
      WRITE(6,604)
      WRITE(6,605) DET
      WRITE(6,604)
14    RETURN

C     THIS SECTION IS FOR THE CYLINDER(CONSTANT THICKNESS)

2     GO TO (23, 24, 23), INDEX
23    H = VN(1,IBR)
      R1 = 0.0
      R2 = 1.0/VN(2,IBR)
      R3 = 1.0
      CXS = 0.0
      SXN = 1.0
      PN = VN(5,IBR)
      GAMMA = VN(6,IBR)
      DEAD  = VN(7,IBR)
      HGAMMA = H*GAMMA
      INDEX = 2
      IF(VN(3,IBR) .NE. 90.0)  SXN = - 1.0
24    RETURN

C     THIS SECTION IS FOR THE SPHERE.

3     GO TO (33, 34, 345), INDEX
33    H = VN(1,IBR)
      R1 = 1.0/VN(2,IBR)
```

```
      R3 = NBACK*R1
      PN = VN(5,IBR)
      GAMMA = VN(6,IBR)
      DEAD  = VN(7,IBR)
      HGAMMA = H*GAMMA
      INDEX = 2
      IF(NVARTK .EQ. 0) INDEX = 3
      RETURN
34    CALL THICK
      TT = H*H/12.0
      T1 = P1/H
      T2 = T1/TT
      HTT = H*TT
      HGAMMA = H*GAMMA
345   SXN = SIN(S)
      CXS = COS(S)
      IF(NBACK .EQ. - 1.0)  CXS = - CXS
      R2 = R1/SXN
      RETURN

C     THIS SECTION IS FOR A PARABOLOIDAL SHELL.

4     GO TO (43, 44, 445), INDEX
43    H = VN(1,IBR)
      PN = VN(5,IBR)
      GAMMA = VN(6,IBR)
      DEAD  = VN(7,IBR)
      HGAMMA = H*GAMMA
      A = 1.0/VN(2,IBR)
      INDEX = 2
      IF(NVARTK .EQ. 0) INDEX = 3
      RETURN
44    CALL THICK
      TT = H*H/12.0
      T1 = P1/H
      T2 = T1/TT
      HTT = H*TT
      HGAMMA = H*GAMMA
445   CXS = COS(S)
      SXN = SIN(S)
      IF(NBACK .EQ. - 1.0)  CXS = - CXS
      R2 = A*CXS/SXN
      R1 = A*CXS**3
      R3 = NBACK*R1
      RETURN

C     THIS SECTION IS FOR AN ELLIPSOIDAL SHELL.

5     GO TO (53, 54, 545), INDEX
53    H = VN(1,IBR)
      A = VN(2,IBR)
      B = VN(3,IBR)
      C = VN(4,IBR)
      AOVERB = (A/B)**2
      FACTOR = 1.0 - AOVERB
      PN = VN(5,IBR)
```

```
      GAMMA = VN(6,IBR)
      DEAU  = VN(7,IBR)
      HGAMMA = H*GAMMA
      INDEX = 2
      IF(NVARTK .EQ. 0) INDEX = 3
      RETURN
54    CALL THICK
      TT = H*H/12.0
      T1 = P1/H
      T2 = T1/TT
      HTT = H*TT
      HGAMMA = H*GAMMA
545   SXN = SIN(S)
      CXS = COS(S)
      IF(NBACK .EQ. -1.0)  CXS = -CXS
      R = SQRT(AOVERB + FACTOR*SXN*SXN)
      R1 = R*R*R/(B*AOVERB)
      R2 = 1.0/(C + B*SXN/R)
      R3 = NBACK*R1
      RETURN

C     THIS SECTION IS FOR A CONICAL SHELL.

6     GO TO (63, 64, 63, 645), INDEX
63    H = VN(1,IBR)
      R1 = 0.0
      R3 = 1.0
      ALFA = VN(2,IBR)*RPD
      SXN = SIN(ALFA)
      CXS = COS(ALFA)
      A = VN(3,IBR)
      PN = VN(5,IBR)
      GAMMA = VN(6,IBR)
      DEAU  = VN(7,IBR)
      HGAMMA = H*GAMMA
      INDEX = 2
      IF(NVARTK .EQ. 0) INDEX = 4
      RETURN
64    CALL THICK
      TT = H*H/12.0
      T1 = P1/H
      T2 = T1/TT
      HTT = H*TT
      HGAMMA = H*GAMMA
645   R2 = 1.0/(A + S*CXS)
      RETURN

C     THIS SECTION IS FOR THE TORUS.

7     GO TO (73, 74, 745), INDEX
73    H = VN(1,IBR)
      R1 = 1.0/VN(3,IBR)
      R3 = NBACK*R1
      A = VN(2,IBR)
      BTORUS = VN(3,IBR)
      PN = VN(5,IBR)
```

```
      GAMMA = VN(6,IBR)
      DEAD  = VN(7,IBR)
      HGAMMA = H*GAMMA
      INDEX = 2
      IF(NVARTK .EQ. 0)  INDEX = 3
      RETURN
74    CALL THICK
      TT = H*H/12.0
      T1 = P1/H
      T2 = T1/TT
      HTT = H*TT
      HGAMMA = H*GAMMA
745   SXN = SIN(S)
      CXS = COS(S)
      IF(NBACK .EQ. - 1.0)  CXS = - CXS
      R2 = 1.0/(A + BTORUS*SXN)
      RETURN

C     THIS SECTION FOR VARIABLE THICKNESS CYLINDRICAL SHELL.

8     GO TO (83, 84, 83), INDEX
83    H = VN(1,IBR)
      R1 = 0.0
      R2 = 1.0/VN(2,IBR)
      R3 = 1.0
      SXN = 1.0
      CXS = 0.0
      PN = VN(5,IBR)
      GAMMA = VN(6,IBR)
      DEAD  = VN(7,IBR)
      HGAMMA = H*GAMMA
      INDEX = 2
      IF(VN(3,IBR) .NE. 90.0)  SXN = - 1.0
      RETURN
84    CALL THICK
      TT = H*H/12.0
      T1 = P1/H
      T2 = T1/TT
      HTT = H*TT
      HGAMMA = H*GAMMA
      RETURN
603   FORMAT(1H1, 25HSERIES SOLUTION FOR CROWN)
602   FORMAT(1H0, 3E20.8, 10X, E20.8)
604   FORMAT(1H0, /, 1H0)
607   FORMAT(1H0, 13HD(I,J,NPARTS))
606   FORMAT(1H0, 6E17.7, 10X, E17.7)
605   FORMAT(1H0, 14HDETERMINANT = E15.8)
      END
```

```
      SUBROUTINE INPUT
      DIMENSION       TITLE1(20)    , BOUNDI(8)     , GA(8)         ,
     *                TITLE2(20)    , BOUNDF(8)     , GB(8)         ,
     *                TITLE3(20)    , SI(60)        , IA(8)         ,
     *                NAMEBI(6)     , SX(60)        , IB(8)         ,
     *                NAME2(60)     , IPAR(60)      , INT(60)       ,
     *                TDIST(60)     , VN(7,60)      , VARTIK(60)    ,
     *                NAMES1(8)     , EYM(60)       , XP(10,60)     ,
     *                NAMES2(8)     , PSR(60)       , YP(10,60)     ,
     *                ISS(60)       , IPLOT(10)     , TRY(8,61)     ,
     *                SL(9,60)      , DM(8,61)      , V3(8)         ,
     *                BACK(60)      , POINT(60)     , UNITI(2)      ,
     *                UNITD(2)      , JOBPLT(10)    , DETERM(10)    ,
     *                E(9,60)       , NFOURA(9)
      COMMON / BLOCKA / NU, PI, ALD, NTYPE, INDEX, IBR, PN, NPOINT,
     1                  ISH, TT, T1, T2, HTT, INTC
      COMMON / BLOCKC / DM, GA, GB, NF, NFP, NPL, NH, NN, TRY
      COMMON / BLOCKE / XP, YP, SL
      COMMON / BLOCKF / NFF, SMXX, SZERO, GO, ERP, ISS, E,
     *                  MAX, INTPRN, INTVAL, NPP
      COMMON / BLOCKG / NPARTS, PHI1, V3, KIND, NT, MT, SPRINT, VN, EYM,
     1                  BACK, NBACK
      COMMON / BLOCKH / NDE
      COMMON / BLOCKN / DETERM
      COMMON / BLOCKP / PLOT, PLTIME, SPLOT, PLOTPT, IPLOT, YMOD, KST,
     1                  HGAMMA, DEAD, NFH
      COMMON / BLOCKQ / TIME, VARTIK, NVARTK
      COMMON / BLOCKS / JOBPLT, ALXL, ALXR, IA, IB, NOPUNC, INPUN,
     *                  CONVER, SI, SX, INT, IPAR, PSR, ITER, NTRY,
     *                  NERROR, IBRM, TRYIN, IBRMAX
      COMMON / BLOCKX / LEVEL1, LEVEL2
      EQUIVALENCE  (VARTIK(1), POINT(1))
      DATA( RPD = 0.1745329252E-01 )
      DATA  (NAMEBI(1) = 6HDISPLA) , (NAMEBI(5) = 6HCEMENT) ,
     *      (NAMEBI(2) = 6HFORCE ) ,
     *      (NAMEBI(3) = 6HSLOPE ) , (NAMEBI(6) = 6H      ) ,
     *      (NAMEBI(4) = 6HMOMENT)
      DATA  (MARKC = 2HYE), (MARKD = 2HNO), (MARKE = 1HS),
     *      (MARKN = 3HNO ), (MARKY = 3HYES)
      DATA ((NAMES1(I), I = 1, 8) = 6HCROWN , 6HCYLIND, 6HSPHERO,
     *                              6HPARABO, 6HELLIPS, 6HCONICA,
     *                              6HTOROID, 6HVARCYL),
     *     ((NAMES2(I), I = 1, 8) = 6H      , 6HRICAL , 6HIDAL  ,
     *                              6HLOIDAL, 6HOIDAL , 6HL     ,
     *                              6HAL    , 6HINDER )
      DATA    (UNITI(1) = 6HINCHES),
     *        (UNITI(2) = 1H      ),
     *        (UNITD(1) = 6HDEGREE),
     *        (UNITD(2) = 1HS     )
      INTEGER  VARTIK, POINT, GO, TRYIN, PLOT, PLTIME, TIME, BOUNDI,
     *         BOUNDF, TDIST
      REAL           NU, NT, MT, NBACK, NFH

C     FOR PLOTTING USE THE FOLLOWING CODE NUMBERS TO INDICATE THE VARIABLE
```

```
C     DESIRED.
C
C                          CODE NUMBER        VARIABLE
C
C                               1             W
C                               2             Q PHI
C                               3             U PHI
C                               4             N PHI
C                               5             BETA PHI
C                               6             M PHI
C                               7             N THETA
C                               8             M THETA
C                               9             EPSILON THETA
C                              10             EPSILON PHI
C                              11             SIGMA N PHI
C                              12             SIGMA M PHI
C                              13             SIGMA PHI OUTER
C                              14             SIGMA PHI INNER
C                              15             SIGMA N THETA
C                              16             SIGMA M THETA
C                              17             SIGMA THETA OUTER
C                              18             SIGMA THETA INNER
C                              19             TAU PHI

C     TRYIN = 0 INDICATES THAT LINEAR PROBLEM WILL BE SOLVED.
C     TRYIN = 1 INDICATES THAT LINEAR PROBLEM AND POSSIBLY ONE OR MORE
C     ITERATIONS HAVE BEEN DONE AND THE LAST RESULT IS TO BE READ IN.

C     INTPRN = 0 INDICATES THAT INTERMEDIATE RESULTS FROM THE NONLINEAR
C     ANALYSIS, I.E., VALUES OF PARAMETERS AND SLOPES, WILL NOT BE
C     PRINTED OUT.

C     INTVAL = 0 INDICATES THAT INTERMEDIATE RESULTS FROM INITIAL VALUE
C     INTEGRATIONS WILL NOT BE PRINTED OUT.

C      NOPUNC = 0 INDICATES THAT SOLUTIONS, DM(I,NF) AND E(I,JJ) WILL
C     NOT BE PUNCHED.
C     NOPUNCH = 1 INDICATES THAT THEY WILL BE PUNCHED.

C     PLOT = NUMBER OF COLUMNS OF VARIABLES TO BE PUT ON PLOT TAPE TO
C     BE MACHINE PLOTTED AT LATER TIME.

COMMENT   SET NUMBER 1        ( CARDS = 3 )

      READ(5,500)  TITLE1
      IF(EOF,5) 998, 997
997   CONTINUE
      READ(5,500)  TITLE2, TITLE3
      WRITE(6,534)
```

```
      WRITE(6,535)
      WRITE(6,536)
      WRITE(6,537)
      WRITE(6,539)
      NTIME = 1
350   WRITE(6,501)  TITLE1, TITLE2, TITLE3
      GO TO (355, 360, 365, 370,375), NTIME

COMMENT   SET NUMBER 2        ( CARDS = 1 )
COMMENT   BOUNDARY DATA AT INITIAL EDGE

355   READ(5,530)  (BOUNDI(I), GA(I), I = 1, 4)

COMMENT   SET NUMBER 3        ( CARDS = 1 )
COMMENT   BOUNDARY DATA AT FINAL EDGE

      READ(5,530)  (BOUNDF(I), GB(I), I = 5, 8)

COMMENT   SET NUMBER 4        ( CARDS = 1 )
COMMENT   ANGLE IN DEGREES AT INITIAL AND FINAL BOUNDARIES

      READ(5,565)  ALXL, ALXR
      IF(BOUNDI(1) .EQ. NAMEBI(1) .OR. BOUNDI(1) .EQ. NAMEBI(2)) 815,800
815   IF(BOUNDI(2) .EQ. NAMEBI(1) .OR. BOUNDI(2) .EQ. NAMEBI(2)) 816,800
816   IF(BOUNDI(3) .EQ. NAMEBI(3) .OR. BOUNDI(3) .EQ. NAMEBI(4)) 817,800
817   IF(BOUNDI(4) .EQ. NAMEBI(1) .OR. BOUNDI(4) .EQ. NAMEBI(2)
     *                            .OR. BOUNDI(4) .EQ. NAMES2(1)) 818,800
818   IF(BOUNDF(5) .EQ. NAMEBI(1) .OR. BOUNDF(5) .EQ. NAMEBI(2)) 819,800
819   IF(BOUNDF(6) .EQ. NAMEBI(1) .OR. BOUNDF(6) .EQ. NAMEBI(2)) 820,800
820   IF(BOUNDF(7) .EQ. NAMEBI(3) .OR. BOUNDF(7) .EQ. NAMEBI(4)) 821,800
821   IF(BOUNDF(8) .EQ. NAMEBI(1) .OR. BOUNDF(8) .EQ. NAMEBI(2)
     *                            .OR. BOUNDF(8) .EQ. NAMES2(1)) 822,800
822   CONTINUE

COMMENT   CONTROL CARD
COMMENT   SET NUMBER 5        ( CARDS = 1 )

      READ(5,561)  IBRM, ITER, NDUMMY, PLOT, INTPRN, INTVAL,
     *             LEVEL1, LEVEL2, ERP, CONVER, NUMHAR, (NFOURA(I),
     *             I = 1, 8)
      NOPUNC = 0
      INPUN = 0
      TRYIN = 0
      NDE = 6
      IF(NFOURA(1) .GT. 0)  NDE = 8
      NPL = NDE + 1
      NFH = FLOAT(NFOURA(1))
      IF(ABS(ERP) .EQ. 0.0)  ERP = 1.E - 05
      IF(IBRM) 802, 802, 990
990   IF(IBRM .GT. 60)  GO TO 802
      IF(PLOT .GT. 10)  GO TO 803

COMMENT   SET NUMBER 6        ( CARDS = 1 )
COMMENT   INDICATE BY YES OR NO WHETHER ELASTIC PARAMETERS ARE SAME
COMMENT   FOR EACH PART. IF YES, ON SAME CARD, GIVE VALUES. IF NO, READ
COMMENT   THEM IN AFTER SET NUMBER 9.
```

```
      READ(5,563) NELAS, YOUNG, POISON
      IF(NELAS .EQ. MARKC .OR. NELAS .EQ. MARKD)  8215, 809
8215  CONTINUE

COMMENT   SET NUMBER 7        ( CARDS = 1 )
COMMENT   INDICATE BY YES OR NO WHETHER PRESSURE LOADING, DENSITY OF MATERIAL,
COMMENT   OR DEAD LOAD ON SHELL IS THE SAME FOR EACH PART. IF YES, ON SAME
COMMENT   CARD, GIVE VALUES. IF NO, READ THEM IN AFTER SET NUMBER 10.

      READ(5,680)  NPRES, PRESS, DENSTY, DEAD
      IF(NPRES .EQ. MARKC .OR. NPRES .EQ. MARKD)  8225, 810
8225  CONTINUE

COMMENT   SET NUMBER 8        ( CARDS = NUMBER OF PARTS )
COMMENT   TYPE OF SHELL, INITIAL AND FINAL COORDINATES, NUMBER OF SEGMENTS,
COMMENT   NUMBER OF PRINT POINTS, YES OR NO FOR THICKNESS DISTRIBUTION, IF
COMMENT   YES, THEN SPECIFY VALUE. IF NO, SPECIFY NUMBER OF POINTS WHICH
COMMENT   SPECIFIES DISTRIBUTION.

COMMENT   FOR CYLINDER SI(L) IS EITHER 90.0 DEGREES (NORMAL OUT) OR
COMMENT   270.0 DEGREES (NORMAL IN). SX(L) IS LEFT BLANK.

COMMENT   FOR CONE SI(L) IS THE ANGLE (DEGREES) WHICH THE NORMAL MAKES WITH
COMMENT   THE AXIS OF THE SHELL. SX(L) IS LEFT BLANK.

      READ(5,512) (NAME2(L), SI(L), SX(L), IPAR(L), INI(L),
     *             IDIST(L), VN(1,L), VARTIK(L), L = 1, IBRM)

COMMENT   DETERMINE IF SPELLING OF SHELL PARTS IS CORRECT.

      DO 325 L = 1, IBRM
      IF(NAME2(L) .EQ. NAMES1(1) .OR.
     *   NAME2(L) .EQ. NAMES1(2) .OR.
     *   NAME2(L) .EQ. NAMES1(3) .OR.
     *   NAME2(L) .EQ. NAMES1(4) .OR.
     *   NAME2(L) .EQ. NAMES1(5) .OR.
     *   NAME2(L) .EQ. NAMES1(6) .OR.
     *   NAME2(L) .EQ. NAMES1(7) .OR.
     *   NAME2(L) .EQ. NAMES1(8))   325, 801
325   CONTINUE

COMMENT   DETERMINE IF IDIST(L) CONTAINS CORRECT SPELLING.

      DO 326 L = 1, IBRM
      IF(IDIST(L) .EQ. MARKC .OR. IDIST(L) .EQ. MARKD)  326, 804
326   CONTINUE
      PLOTPT = 0
      DO 1234 I = 1, IBRM
      PLOTPT = PLOTPT + IPAR(I)*INT(I)
1234  CONTINUE
      IF(PLOTPT .GT. 380)  GO TO 805
      NPARTS = 0
      DO 85 I = 1, IBRM
      NPARTS = NPARTS + IPAR(I)
85    CONTINUE
```

```
      IF(NPARTS .GT. 60)  GO TO 806
      DO 327 L = 1, IBRM
      VARTIK(L) = IABS(VARTIK(L))
327   CONTINUE
      DO 300 L = 1, IBRM
      IF(IDIST(L) .EQ. MARKC)  GO TO 329
      IF(VARTIK(L) .LT. 2 .OR. VARTIK(L) .GT. 10)  GO TO 807
      GO TO 300
329   IF(VARTIK(L) .NE. 0)  GO TO 808
300   CONTINUE

COMMENT   SET ISS(L) MATRIX. THIS SPECIFES CODE NUMBER FOR SHELL TYPES.

COMMENT   CROWN          = 1
COMMENT   CYLINDRICAL    = 2
COMMENT   SPHEROIDAL     = 3
COMMENT   PARABOLOIDAL   = 4
COMMENT   ELLIPSOIDAL    = 5
COMMENT   CONICAL        = 6
COMMENT   TOROIDAL       = 7
COMMENT   VARCYLINDER    = 8

      DO 150 L = 1, IBRM
      DO 150 I = 1, 8
      IF(NAME2(L) .NE. NAMES1(I))  GO TO 150
      ISS(L) = I
150   CONTINUE

COMMENT   DETERMINE IF CYLINDRICAL SHELL 2 HAS VARTIK(L) .EQ. 0 AND IF
COMMENT   VARCYLINDER SHELL 8 HAS VARTIK(L) .NE. 0.

      DO 994 L = 1, IBRM
      ISH = ISS(L)
      GO TO (994, 995, 994, 994, 994, 994, 994, 996), ISH
995   IF(VARTIK(L) .NE. 0)  GO TO 808
      GO TO 994
996   IF(VARTIK(L) .EQ. 0)  GO TO 807
994   CONTINUE


COMMENT   SET NUMBER 9        ( CARDS = NUMBER OF PARTS )
COMMENT   READ IN A, B, C

COMMENT   FOR CROWN AND SPHERE ONLY SPECIFY A

COMMENT   FOR CYLINDER A IS RADIUS, B IS LENGTH

COMMENT   FOR CONE A IS RADIUS AT INITIAL, B IS SLANT LENGTH

COMMENT   FOR ELLIPSE C .GT. 0.0 INDICATES TOROIDAL SHELL OF ELLIPTICAL CROSS
COMMENT        SECTION PROVIDED A .NE. B.

      READ(5,562)  (VN(2,L), VN(3,L), VN(4,L), L = 1, IBRM)

COMMENT   DETERMINE IF SHELL PARTS ARE CONTINUOUS.
```

```
      NTIME=0
      L=0
    3 L=L+1
      IF(L.GT.IBRM) GO TO 13
      ISH=ISS(L)
      ALFAI = SI(L)*RPD
      ALFAF = SX(L)*RPD
      A = VN(2,L)
      B = VN(3,L)
      GO TO (3, 4, 5, 6, 7, 8, 9, 4), ISH
    4 RI = A
      RF = RI
      GO TO 10
    5 RI = A*SIN(ALFAI)
      RF = A*SIN(ALFAF)
      GO TO 10
    6 RI = A
      RF = A*TAN(ALFAF)/TAN(ALFAI)
      GO TO 10
    7 DO 75 I = 1, 2
      IF(I .EQ. 2)  GO TO 76
      SXN = SIN(ALFAI)
      GO TO 77
   76 SXN = SIN(ALFAF)
   77 R = VN(4,L) + B*SXN/((A/B)**2 + (1.0 - (A/B)**2)*SXN*SXN)
      IF(I .EQ. 2)  GO TO 78
      RI = R
      GO TO 75
   78 RF = R
   75 CONTINUE
      GO TO 10
    8 RI = A
      RF = A + B*COS(ALFAI)
      GO TO 10
    9 RI = A + B*SIN(ALFAI)
      RF = A + B*SIN(ALFAF)
   10 IF (NTIME.EQ.1) GO TO 11
      RI1=RI
      RF1=RF
      NTIME=1
      GO TO 3
   11 RI2=RI
      RF2=RF
      IF(ABS(RF1 - RI2) .GT. 0.0025)  GO TO 812
      RF1=RF2
      RI1=RI2
      GO TO 3
   13 CONTINUE

COMMENT    SET NUMBER 10
COMMENT    READ IN YOUNG*S MODULUS AND POISSON*S RATIO ONLY IF
COMMENT    NOT THE SAME FOR EACH PART.

      IF(NELAS .EQ. MARKC)  GO TO 400
      READ(5,564)  (EYM(L), PSR(L), L = 1, IBRM)
      GO TO 402
```

```
400   DO 401 L = 1, IBRM
      EYM(L) = YOUNG
      PSR(L) = POISON
401   CONTINUE

COMMENT   SET NUMBER 11
COMMENT   READ IN PRESSURE LOADING, DENSITY OF MATERIAL, AND DEAD WEIGHT
COMMENT   ONLY IF THEY ARE NOT THE SAME FOR EACH PART.

402   IF(NPRES .EQ. MARKC)  GO TO 4025
      READ(5,566)  (VN(5,L), VN(6,L), VN(7,L), L = 1, IBRM)
      GO TO 4026
 4025 DO 963 L = 1, IBRM
      VN(5,L) = PRESS
      VN(6,L) = DENSTY
      VN(7,L) = DEAD
963   CONTINUE
COMMENT   SET NUMBER 12
COMMENT   READ IN VARIABLE THICKNESSES

 4026 DO 403 L = 1, IBRM
      IF(VARTIK(L) .EQ. 0)  GO TO 403
      NPNT = VARTIK(L)
      READ(5,565)  (XP(I,L), I = 1, NPNT)
      READ(5,565)  (YP(I,L), I = 1, NPNT)
403   CONTINUE
      IF(ISS(IBRM) .GT. 1) GO TO 86
      NTRY = NPARTS + 1
      NERROR = NPARTS - 1
      GO TO 87
86    NTRY = NPARTS
      NERROR = NPARTS
COMMENT   SET NUMBER 13

   87 IF(PLOT .EQ. 0) GO TO 1238
      READ(5,525) (IPLOT(I), I = 1, PLOT)
      READ(5,526) (JOBPLT(I), I = 1, PLOT)
1238  CONTINUE
      IA(1) = 1
      IA(2) = 3
      IA(3) = 5
      IA(4) = 7
      IB(5) = 1
      IB(6) = 3
      IB(7) = 5
      IB(8) = 7
      IF(BOUNDI(1) .NE. NAMEBI(1))  IA(1) = 2
      IF(BOUNDI(2) .NE. NAMEBI(1))  IA(2) = 4
      IF(BOUNDI(3) .NE. NAMEBI(3))  IA(3) = 6
      IF(BOUNDI(4) .NE. NAMEBI(1))  IA(4) = 8
      IF(BOUNDF(5) .NE. NAMEBI(1))  IB(5) = 2
      IF(BOUNDF(6) .NE. NAMEBI(1))  IB(6) = 4
      IF(BOUNDF(7) .NE. NAMEBI(3))  IB(7) = 6
      IF(BOUNDF(8) .NE. NAMEBI(1))  IB(8) = 8
      WRITE(6,503)
      WRITE(6,504)
```

```
      WRITE(6,505)
      IF(IA(1) .EQ. 1 .AND. IB(5) .EQ. 1)  GO TO 121
      IF(IA(1) .EQ. 1 .AND. IB(5) .EQ. 2)  GO TO 122
      IF(IA(1) .EQ. 2 .AND. IB(5) .EQ. 1)  GO TO 123
      IF(IA(1) .EQ. 2 .AND. IB(5) .EQ. 2)  GO TO 124
121   WRITE(6,551)   GA(1), GB(5)
      GO TO 125
122   WRITE(6,552)   GA(1), GB(5)
      GO TO 125
123   WRITE(6,553)   GA(1), GB(5)
      GO TO 125
124   WRITE(6,554)   GA(1), GB(5)
125   IF(IA(2) .EQ. 3 .AND. IB(6) .EQ. 3)  GO TO 126
      IF(IA(2) .EQ. 3 .AND. IB(6) .EQ. 4)  GO TO 127
      IF(IA(2) .EQ. 4 .AND. IB(6) .EQ. 3)  GO TO 128
      IF(IA(2) .EQ. 4 .AND. IB(6) .EQ. 4)  GO TO 129
126   WRITE(6,551)   GA(2), GB(6)
      GO TO 130
127   WRITE(6,552)   GA(2), GB(6)
      GO TO 130
128   WRITE(6,553)   GA(2), GB(6)
      GO TO 130
129   WRITE(6,554)   GA(2), GB(6)
130   IF(IA(3) .EQ. 5 .AND. IB(7) .EQ. 5)  GO TO 131
      IF(IA(3) .EQ. 5 .AND. IB(7) .EQ. 6)  GO TO 132
      IF(IA(3) .EQ. 6 .AND. IB(7) .EQ. 5)  GO TO 133
      IF(IA(3) .EQ. 6 .AND. IB(7) .EQ. 6)  GO TO 134
131   WRITE(6,555)   GA(3), GB(7)
      GO TO 135
132   WRITE(6,556)   GA(3), GB(7)
      GO TO 135
133   WRITE(6,557)   GA(3), GB(7)
      GO TO 135
134   WRITE(6,558)   GA(3), GB(7)
135   IF(NDE .EQ. 6)  GO TO 140
      IF(IA(4) .EQ. 7 .AND. IB(8) .EQ. 7)  GO TO 136
      IF(IA(4) .EQ. 7 .AND. IB(8) .EQ. 8)  GO TO 137
      IF(IA(4) .EQ. 8 .AND. IB(8) .EQ. 7)  GO TO 138
      IF(IA(4) .EQ. 8 .AND. IB(8) .EQ. 8)  GO TO 139
136   WRITE(6,551)  GA(4), GB(8)
      GO TO 140
137   WRITE(6,552)  GA(4), GB(8)
      GO TO 140
138   WRITE(6,553)  GA(4), GB(8)
      GO TO 140
139   WRITE(6,554)  GA(4), GB(8)
140   WRITE(6,559)   ALXL, ALXR
      IF(NDE .EQ. 8)  GO TO 100
      IB(4) = IB(5)
      IB(5) = IB(6)
      IB(6) = IB(7)
      GB(4) = GB(5)
      GB(5) = GB(6)
      GB(6) = GB(7)
100   NH = NDE/2
COMMENT   THIS LOOP SETS UP IA(4), IA(5), IA(6) FOR NDE = 6 AND
```

```
COMMENT   IA(5), IA(6), IA(7), IA(8) FOR NDE = 8.
      M = NH + 1
      L = 1
      DO 104 IK = M, NDE
      DO 102 N = L, NDE
      DO 101 J = 1, NH
      IF(IA(J) .EQ. N)  GO TO 102
101   CONTINUE
      GO TO 103
102   CONTINUE
103   L = N + 1
      IA(IK) = N
104   CONTINUE
COMMENT   THIS LOOP SETS UP IB(4), IB(5), IB(6) FOR NDE = 6 AND
COMMENT   IB(5), IB(6), IB(7), IB(8) FOR NDE = 8.
      L = 1
      DO 108 IK = 1, NH
      DO 106 N = L, NDE
      DO 105 J = M, NDE
      IF(IB(J) .EQ. N)  GO TO 106
105   CONTINUE
      GO TO 107
106   CONTINUE
107   L = N + 1
      IB(IK) = N
108   CONTINUE
COMMENT   IF ELASTIC PARAMETERS ARE SAME FOR EACH PART, THEN WRITE THEM RIGHT
COMMENT        UNDER BOUNDARY DATA. IF THEY ARE NOT THE SAME FOR EACH PART,
COMMENT        THEN SKIP TO NEXT PAGE , WRITE GEOMETRY, SKIP PAGE, WRITE
COMMENT        ELASTIC PARAMETERS, SKIP PAGE, WRITE VARIABLE THICKNESSES.
      IF(NELAS .EQ. MARKD)  GO TO 475
      WRITE(6,575)   YOUNG, POISON
475   IF(NPRES .EQ. MARKD)  GO TO 4755
      WRITE(6,682)  PRESS, DENSTY, DEAD
4755  DO 478 II = 1, 2
      IF(II .EQ. 1)  GO TO 476
      IF(IBRM .LT. 41)  GO TO 479
476   NTIME = 2
      GO TO 350
360   WRITE(6,513)
      WRITE(6,514)
      GO TO (3605, 3606), II
3605  IMIN = 1
      IMAX = IBRM
      IF(IBRM .GT. 40)  IMAX = 40
      GO TO 3607
3606  IMIN = 41
      IMAX = IBRM
3607  DO 385 L = IMIN, IMAX
      ISH = ISS(L)
      GO TO (881, 882, 881, 883, 884, 882, 883, 882), ISH
881   IF(VARTIK(L) .EQ. 0)  GO TO 8815
      WRITE(6,776) L, NAMES1(ISH), NAMES2(ISH), IPAR(L), SI(L), SX(L),
     *             UNITD(1), UNITD(2), VN(2,L), MARKN
      GO TO 385
8815  WRITE(6,777) L, NAMES1(ISH), NAMES2(ISH), IPAR(L), SI(L), SX(L),
```

```
     *              UNITD(1), UNITD(2), VN(2,L), MARKY, VN(1,L)
      GO TO 385
882   IF(VARTIK(L) .EQ. 0)  GO TO 8825
      WRITE(6,778) L, NAMES1(ISH), NAMES2(ISH), IPAR(L), SI(L),
     *              UNITD(1), UNITD(2), VN(2,L), VN(3,L), MARKN
      GO TO 385
8825  WRITE(6,779) L, NAMES1(ISH), NAMES2(ISH), IPAR(L), SI(L),
     *              UNITD(1), UNITD(2), VN(2,L), VN(3,L), MARKY, VN(1,L)
      GO TO 385
883   IF(VARTIK(L) .EQ. 0)  GO TO 8835
      WRITE(6,780) L, NAMES1(ISH), NAMES2(ISH), IPAR(L), SI(L), SX(L),
     *              UNITD(1), UNITD(2), VN(2,L), VN(3,L), MARKN
      GO TO 385
8835  WRITE(6,781) L, NAMES1(ISH), NAMES2(ISH), IPAR(L), SI(L), SX(L),
     *              UNITD(1), UNITD(2), VN(2,L), VN(3,L), MARKY, VN(1,L)
      GO TO 385
884   IF(VARTIK(L) .EQ. 0)  GO TO 8845
      WRITE(6,782) L, NAMES1(ISH), NAMES2(ISH), IPAR(L), SI(L), SX(L),
     *              UNITD(1), UNITD(2), VN(2,L), VN(3,L), VN(4,L),
     *              MARKN
      GO TO 385
8845  WRITE(6,783) L, NAMES1(ISH), NAMES2(ISH), IPAR(L), SI(L), SX(L),
     *              UNITD(1), UNITD(2), VN(2,L), VN(3,L), VN(4,L),
     *              MARKY, VN(L,1)
385   CONTINUE
478   CONTINUE
479   IF(NELAS .EQ. MARKC)  GO TO 480
      DO 482 II = 1, 2
      IF(II .EQ. 1)  GO TO 483
      IF(IBRM .LT. 41)  GO TO 480
483   NTIME = 3
      GO TO 350
365   WRITE(6,508)
      WRITE(6,577)
      GO TO (3608, 3609), II
3608  IMIN = 1
      IMAX = IBRM
      IF(IBRM .GT. 40)  IMAX = 40
      GO TO 3610
3609  IMIN = 41
      IMAX = IBRM
3610  DO 386 L = IMIN, IMAX
      ISH = ISS(L)
      WRITE(6,576)  L, NAMES1(ISH), NAMES2(ISH), EYM(L), PSR(L)
386   CONTINUE
482   CONTINUE
480   IF(NPRES .EQ. MARKC)  GO TO 4805
      DO 1782 II = 1, 2
      IF(II .EQ. 1)  GO TO 1783
      IF(IBRM .LT. 41)  GO TO 4805
1783  NTIME = 4
      GO TO 350
370   WRITE(6,683)
      WRITE(6,684)
      GO TO (7830, 7831), II
7830  IMIN = 1
```

```
      IMAX = IBRM
      IF(IBRM .GT. 40)  IMAX = 40
      GO TO 7832
7831  IMIN = 41
      IMAX = IBRM
7832  DO 786 L = IMIN, IMAX
      ISH = ISS(L)
      WRITE(6,685)  L, NAMES1(ISH), NAMES2(ISH), (VN(I,L), I = 5, 7)
  786 CONTINUE
1782  CONTINUE

COMMENT   PUT YP(1,L) IN VN(1,L)

4805  DO 950 L = 1, IBRM
      IF(VARTIK(L) .EQ. 0)  GO TO 950
      VN(1,L) = YP(1,L)
950   CONTINUE

COMMENT   NVARC = INDICATES NO VARIABLE THICKNESS

      NVARC = 0
      DO 974 L = 1, IBRM
      NVARC = NVARC + VARTIK(L)
974   CONTINUE
      IF(NVARC .EQ. 0)  GO TO 978

COMMENT   WRITE OUT VARIABLE THICKNESS DATA

      NTIME = 5
      GO TO 350
375   WRITE(6,686)
      DO 975 L = 1, IBRM
      NPNT = VARTIK(L)
      IF(NPNT .EQ. 0)  GO TO 975
      WRITE(6,687)  L
      WRITE(6,688) (XP(I,L), I = 1, NPNT)
      WRITE(6,689) (YP(I,L), I = 1, NPNT)
      WRITE(6,690)
975   CONTINUE

COMMENT   FOLLOWING REPLACEMENTS MUST BE MADE TO MAKE ARRAYS COMPATIBLE
COMMENT   FOR USE IN GOMTRY

978   DO 955 L = 1, IBRM
      ISH = ISS(L)
      GO TO (955, 953, 955, 955, 955, 954, 955, 953), ISH
953   SX(L) = VN(3,L)
      VN(3,L) = SI(L)
      SI(L) =  0.0
      GO TO 955
954   SX(L) = VN(3,L)
      VN(3,L) = VN(2,L)
      VN(2,L) = SI(L)
      SI(L) = 0.0
955   CONTINUE
```

```
COMMENT   CHANGE XP(I,L) TO RADIANS AND ADJUST IF FINAL COORDINATE IS
COMMENT         LESS THAN INITIAL COORDINATE

      DO 404 L = 1, IBRM
      IF(VARTIK(L) .EQ. 0)  GO TO 404
      NPNT = VARTIK(L)
      ISH  = ISS(L)
      GO TO (404, 404, 2505, 2505, 2505, 404, 2505, 404), ISH
2505  IF(XP(NPNT,L) .GT. XP(1,L))  GO TO 2605
      DO 255 I = 1, NPNT
      XP(I,L) = 180.0 - XP(I,L)
255   CONTINUE
2605  DO 265 I = 1, NPNT
      XP(I,L) = XP(I,L)*RPD
265   CONTINUE
404   CONTINUE
      DO 405 L = 1, IBRM
      IF(VARTIK(L) .EQ. 0)  GO TO 405
      NPNT = VARTIK(L)
      DO 384 I = 2, NPNT
      SL(I - 1,L) = (YP(I,L) - YP(I - 1,L))/
     *              (XP(I,L) - XP(I - 1,L))
      YP(I - 1,L) = YP(I - 1,L) - SL(I - 1,L)*XP(I - 1,L)
384   CONTINUE
405   CONTINUE
      RETURN
800   WRITE(6,670)
      GO TO 9980
801   WRITE(6,671)  L
      GO TO 9980
802   WRITE(6,666)
      GO TO 9980
803   WRITE(6,664)  PLOT
      GO TO 9980
804   WRITE(6,672)  L
      GO TO 9980
805   WRITE(6,663)  PLOTPT
      GO TO 9980
806   WRITE(6,665)  NPARTS
      GO TO 9980
807   WRITE(6,673)  L, VARTIK(L)
      GO TO 9980
808   WRITE(6,674)  L, VARTIK(L)
      GO TO 9980
809   WRITE(6,675)
      GO TO 9980
810   WRITE(6,676)
      GO TO 9980
811   WRITE(6,677)
      GO TO 9980
  812 WRITE(6,691)  L
9980  WRITE(6,669)
      GO TO 998
500   FORMAT(20A4)
534   FORMAT(1H1, ////////////////54X, 27HBATTELLE MEMORIAL INSTITUTE)
535   FORMAT(//60X, 14HCOLUMBUS, OHIO)
```

```
536   FORMAT(// 47X, 40HSTRESS ANALYSIS OF A SHELL OF REVOLUTION)
537   FORMAT(// 50X, 33HADVANCED SOLID MECHANICS DIVISION)
539   FORMAT(// 50X, 33HMECHANICAL ENGINEERING DEPARTMENT)
501   FORMAT(1H1, 20A4/(1H0, 20A4))
530   FORMAT(A6, 6X, F8.2, A6, 6X, F8.2, A6, 6X, F8.2, A6, 6X, F8.2)
565   FORMAT(8F10.5)
561   FORMAT(8I5, 2E10.3, 10I2)
563   FORMAT(2X, A2, 4X, E11.4, 4X, F6.4)
680   FORMAT(2X, A2, 4X, 3F14.5)
512   FORMAT(4X, A6, 6X, F11.5, F12.5, 2I5, 2X, A2, 1X, F10.5, I5)
562   FORMAT(3X, 3F12.5)
564   FORMAT(8X, E11.4, 4X, F6.4)
  566 FORMAT(5X, 3F15.5)
525   FORMAT(10I5)
526   FORMAT(10A8)
503   FORMAT(   ///// 49X, 36H* * *  PRINTOUT OF INPUT DATA  * * *//// )
504   FORMAT(1H0, 57X, 19H*  BOUNDARY DATA  * /// )
505   FORMAT(1H , 34X, 12HINITIAL EDGE, 36X, 10HFINAL EDGE, / )
551   FORMAT(1H , 27X, 15HDISPLACEMENT = F10.5,
     *             20X, 15HDISPLACEMENT = F10.5)
552   FORMAT(1H , 27X, 15HDISPLACEMENT = F10.5,
     *             20X, 15H       FORCE = F10.5)
553   FORMAT(1H , 27X, 15H       FORCE = F10.5,
     *             20X, 15HDISPLACEMENT = F10.5)
554   FORMAT(1H , 27X, 15H       FORCE = F10.5,
     *             20X, 15H       FORCE = F10.5)
555   FORMAT(1H , 27X, 15H       SLOPE = F10.5,
     *             20X, 15H       SLOPE = F10.5)
556   FORMAT(1H , 27X, 15H       SLOPE = F10.5,
     *             20X, 15H      MOMENT = F10.5)
557   FORMAT(1H , 27X, 15H      MOMENT = F10.5,
     *             20X, 15H    ROTATION = F10.5)
558   FORMAT(1H , 27X, 15H      MOMENT = F10.5,
     *             20X, 15H      MOMENT = F10.5)
559   FORMAT(1H0, 25X, 17HBOUNDARY ANGLE = F10.5,
     *             18X, 17HBOUNDARY ANGLE = F10.5)
575   FORMAT(1H0, /// 24X, 42HELASTIC PARAMETERS ARE THE SAME FOR EVERY
     *                  36HPART IN THIS SHELL. THEIR VALUES ARE , /
     *       1H ,     38X, 16HYOUNGS MODULUS = E12.5,
     *                 1X, 22HPOUNDS PER SQUARE INCH,  /
     *       1H ,     38X, 16HPOISSONS RATIO = F8.5)
682   FORMAT(1H0, ///  24X, 42HLOADING PARAMETERS ARE THE SAME FOR EVERY
     *                ,   36HPART IN THIS SHELL. THEIR VALUES ARE , /
     *             1H , 38X, 11HPRESSURE = F11.5,
     *                   1X, 22HPOUNDS PER SQUARE INCH,  /
     *             1H ,     38X, 25HUNIT WEIGHT OF MATERIAL = F11.5,
     :                   1X, 21HPOUNDS PER CUBIC INCH  /
                   1H , 38X, 13HDEAD WEIGHT = F11.5,
                         1X, 22HPOUNDS PER SQUARE INCH)
513   FORMAT(//// 62X, 14H*  GEOMETRY  * //,
     *       1H , 25X, 6HNO. OF, 10X, 21HC O O R D I N A T E S, 46X,
     *            17HTHICKNESS, INCHES)
514   FORMAT(1H , 5X,
     *            4HPART, 6X, 4HTYPE, 5X, 8HSEGMENTS, 4X, /HINITIAL, 5X,
     *            5HFINAL, 4X, 10HDIMENSIONS, 3X, 8HA,INCHES, 5X,
     *            8HB,INCHES, 5X, 8HC,INCHES, 4X, 17HCONSTANT    VALUE)
```

```
776   FORMAT(1H , I8, 3X, 2A6, I5, 4X, 2F12.5, 2X, A6, A1,  F13.5,
     *                    32X, A3          )
777   FORMAT(1H , I8, 3X, 2A6, I5, 4X, 2F12.5, 2X, A6, A1,  F13.5,
     *                    32X, A3, F13.5  )
778   FORMAT(1H , I8, 3X, 2A6, I5, 4X,  F12.5,14X, A6, A1, 2F13.5,
     *                    19X, A3          )
779   FORMAT(1H , I8, 3X, 2A6, I5, 4X,  F12.5,14X, A6, A1, 2F13.5,
     *                    19X, A3, F13.5 )
780   FORMAT(1H , I8, 3X, 2A6, I5, 4X, 2F12.5, 2X, A6, A1, 2F13.5,
     *                    19X, A3          )
781   FORMAT(1H , I8, 3X, 2A6, I5, 4X, 2F12.5, 2X, A6, A1, 2F13.5,
     *                    19X, A3, F13.5 )
782   FORMAT(1H , I8, 3X, 2A6, I5, 4X, 2F12.5, 2X, A6, A1, 2F13.5,
     *                F13.5,  6X, A3          )
783   FORMAT(1H , I8, 3X, 2A6, I5, 4X, 2F12.5, 2X, A6, A1, 2F13.5,
     *                F13.5,  6X, A3, F13.5 )
508   FORMAT(////, 59X, 16H*  PROPERTIES  * ///,
     *       1H , 44X, 43HE = YOUNGS MODULUS (POUNDS PER SQUARE INCH), /
     *       1H , 44X, 19HNU = POISSONS RATIO   / )
577   FORMAT(1H , 44X, 4HPART, 6X, 4HTYPE, 13X, 1HE, 12X, 2HNU)
576   FORMAT(1H , 45X, I2, 3X, 2A6, 3X, E12.5, 3X, F8.5)
683   FORMAT(//// , 57X, 16H*   LOADINGS   *///,
     *        1H , 46X, 39HP = PRESSURE (POUNDS PER SQUARE INCH)   ,/
     *        1H , 46X, 39Hw = UNIT WEIGHT (POUNDS PER CUBIC INCH) ,/
     *        1H , 46X, 40HD = DEAD WEIGHT (POUNDS PER SQUARE INCH)  )
684   FORMAT(1H0, 34X, 4HPART, 6X, 4HTYPE, 13X, 1HP, 13X, 1Hw, 13X, 1HD)
685   FORMAT(1H , 35X, I2, 3X, 2A6, 3F14.5)
686   FORMAT(////, 50X, 22H* VARIABLE THICKNESS * ///)
687   FORMAT(1H , 4HPART I3)
688   FORMAT(1H , 10HCOORDINATE 10F12.5)
689   FORMAT(1H , 10HTHICKNESS  10F12.5)
690   FORMAT(1H )
670   FORMAT(1H0, 39HSPELLING ON BOUNDARY CARD IS INCORRECT.)
671   FORMAT(1H0, 17HSPELLING OF PART I2, 14H IS INCORRECT.)
666   FORMAT(1H0, 50HNUMBER OF PARTS IS EITHER ZERO OR GREATER THAN 60.)
664   FORMAT(1H0, 30HNUMBER OF PLOTS REQUESTED WAS I4,
     *            26H. ONLY 10 CAN BE OBTAINED.)
672   FORMAT(1H0, 44HSPELLING OF YES OR NO IS INCORRECT FOR PART I2,1H.)
663   FORMAT(1H0, 37HNUMBER OF PRINT POINTS REQUESTED WAS I5,
     *            34H. ONLY 380 POINTS CAN BE OBTAINED.)
665   FORMAT(1H0, 22HNUMBER OF SEGMENTS IS I3,
     *            35H. ONLY 60 SEGMENTS CAN BE ANALYZED.)
673   FORMAT(1H0,  5HPART I2, 24H HAS VARIABLE THICKNESS.
     *           29HNUMBER OF POINTS READ IN WAS I3,
     *           48H. THIS CANNOT BE LESS THAN 2 OR GREATER THAN 10.)
674   FORMAT(1H0,  5HPART I2, 24H HAS CONSTANT THICKNESS.
     *           29HNUMBER OF POINTS READ IN WAS I3,
     *           19H. THIS SHOULD BE 0.)
675   FORMAT(1H0, 45HSPELLING INCORRECT ON ELASTIC PARAMETER CARD.)
676   FORMAT(1H0, 44HSPELLING INCORRECT ON DISTRIBUTED LOAD CARD.)
677   FORMAT(1H0, 34HSPELLING INCORRECT ON CONTROL CARD.)
691   FORMAT(1H0, 35HTWO SHELL PARTS ARE NOT CONTINUOUS.
     $           47H CHECK INITIAL AND FINAL COORDINATES AND RADII
     $            9HFOR PART I2, 19H AND PREVIOUS PART.)
669   FORMAT(1H0, 33HPROCESSING OF INPUT DATA STOPPED.)
998   CALL EXIT

      END
```

```
      SUBROUTINE INTEG
      DIMENSION     DY(8)          , Y(8)           , IRY(8,61)     ,
     *              ERR(8)         , SOUT(275)      , P(5,275)      ,
     *              PRNT(8)        , D(8,9,60)      , SLOPE(5,275)  ,
     *              DM(8,61)       , GA(8)          , GB(8)         ,
     *              ISS(60)        , E(9,60)        , DYAM(72)      ,
     *              YAM(72)        , ABC(21)        , EAM(10)       ,
     *              WAM(8)         , XSAVE(3)       , YSAVE(8,3)    ,
     *              FSAVE(8)       , XPLOT(350)     , YPLOT(350,10),
     *              STROUT(350)    , SIGNPH(350)    , SIGMPH(350)   ,
     *              SIGPHT(350)    , SIGPHB(350)    , SIGNTH(350)   ,
     *              SIGMTH(350)    , SIGTHT(350)    , SIGTHB(350)   ,
     *              TAUPHI(350)    , IPLOT(10)      , A(8,9)
      COMMON / BLOCKA / NU, P1, XLO, NTYPE, INDEX, IBR, PN, NPOINT,
     1                  ISW, TT, T1, T2, HTT, INTC
      COMMON / BLOCKB / H, R1, R2, R3, SXN, CXS
      COMMON / BLOCKC / DM, GA, GB, NF, NFP, NPL, NH, NN, IRY
      COMMON / BLOCKF / NFF, SMXX, SZERO, GO, ERP, ISS, E,
     *                  MAX, INTPRN, INTVAL, NPP
      COMMON / BLOCKH / NDE
      COMMON / BLOCKJ / DELX, PDELX, ABC, EAM
      COMMON / BLOCKK / PIN, PMIN, HO, XO, EMIN, EMAX
      COMMON / BLOCKL / YAM, DYAM
      COMMON / BLOCKP / PLOT, PLTIME, SPLOT, PLOTPT, IPLOT, YMOD, KST,
     1                  HGAMMA, DEAD, NFH
      COMMON            SLOPE, P, SOUT, D, A
      EQUIVALENCE  (Y(1), PRNT(1)), (Y(1), YAM(2)), (DY(1), DYAM(2)),
     1             (S, YAM(1))
      EQUIVALENCE   (SLOPE(1) ,  YPLOT(1)   ),
     *              (D(476)   ,  XPLOT(1)   ),
     *              (D(826)   ,  STROUT(1)  ),
     *              (D(1176)  ,  SIGNPH(1)  ),
     *              (D(1526)  ,  SIGMPH(1)  ),
     *              (D(1876)  ,  SIGPHT(1)  ),
     *              (D(2226)  ,  SIGPHB(1)  ),
     *              (D(2576)  ,  SIGNTH(1)  ),
     *              (D(2926)  ,  SIGMTH(1)  ),
     *              (D(3276)  ,  SIGTHT(1)  ),
     *              (D(3626)  ,  SIGTHB(1)  ),
     *              (D(3976)  ,  TAUPHI(1)  )
      INTEGER GO, PASS, EXTRA, ADMSCT, FINAL
      REAL          NU, NT, MT, NBACK, NFH
      PIN = 4.0
      PMIN = 8.0
      DO 4330 L = 1, NFF
      IF(INTPRN .EQ. 0) GO TO 4210
      WRITE(6,697) L, IBR
4210  NF = NF + 1
      DO 4320 JJ = 1, NPL

C     FINAL = 0 IF OUTPUT FROM ADMINT IS AN ADAMS MOULTON POINT AT
C     SFINAL.
C     FINAL = 1 IF OUTPUT FROM ADMINT IS A RUNGE KUTTA POINT AT SFINAL.

      FINAL = 0
```

```
      NOSAVE = 0
      DO 4310 I = 1, NUE
      Y(I) = 0.0
4310  CONTINUE
      SFINAL = SZERO + SMXX

C     INIC COUNTS NUMBER OF TIMES DIFFEQ IS CALLED.

      INIC = 0

C     ADMSCT COUNTS NUMBER OF TIMES ADMINT IS CALLED.

      ADMSCT = 0
      IF(PN .NE. 0.0 .OR. HGAMMA .NE. 0.0 .OR. DEAD .NE. 0.0) GO TO 4200
      IF(NTYPE .EQ. 1 .AND. JJ .EQ. 1)  GO TO 777
4200  IF(JJ .GT. 1) GO TO 4526
      DO 4390 I = 1, NUE
      Y(I) = TRY(I,NF)
4390  CONTINUE

C     NOSAVE = 0 IF NTYPE = 1 (LINEAR ANALYSIS) OR IF JJ IS GREATER
C     THAN 1 (COMPLEMENTARY SOLUTIONS BEING OBTAINED). OTHERWISE
C     NOSAVE = 1.

      NOSAVE = 1
      GO TO 4527
4526  Y(JJ - 1) = 1.0
      NOSAVE = 0
4527  IF(NTYPE .NE. 1) GO TO 4531
      NOSAVE = 0
      IF(L .GT. 1) GO TO 1310
      IF(JJ .GT. 1) GO TO 4530
      XLU = 1.0
      ERROR = ERP
      GO TO 1308
4530  XLU = 0.0
      ERROR = ERP
      GO TO 1308
1310  IF(JJ .GT. 1) GO TO 1315
      XLU = 1.0
      ERROR = E(JJ,NF - 1)*ERP
      GO TO 1308
1315  XLU = 0.0
      ERROR = E(JJ,NF - 1)*ERP
      GO TO 1308
4531  IF(JJ .GT. 1) GO TO 4533
      NTYPE = 2
      S = SZERO
      CALL GOMTRY

C     P(1,NPR) = Q PHI
C     P(2,NPR) = N PHI
C     P(3,NPR) = BETA PHI
C     P(4,NPR) = BETA PHI COMMA S
C     P(5,NPR) = N THETA
```

```
      P(1,1) = Y(2)
      P(2,1) = Y(4)
      P(3,1) = Y(5)
      P(4,1) = T2*Y(6) - NU*R2*CXS*Y(5)
      P(5,1) = NU*Y(4) + H*(R2*CXS*Y(3) + R2*SXN*Y(1))*YMOD
      SOUT(1) = S
      ERROR = E(JJ,NF)*ERP
      GO TO 1308
4533  NTYPE = 3
      ERROR = E(JJ,NF)*ERP
1308  EMAX = ERROR
      EMIN = ERROR*0.01
      IF(INTPRN .EQ. 0) GO TO 4220
      DO 1102 I = 1, NDE
      ERR(I) = ERROR
1102  CONTINUE
      WRITE(6,696) (ERR(I), I = 1, NDE)
      WRITE(6,675) SZERO, (Y(I), I = 1, NDE)
4220  HO = SMXX
      XO = SZERO
      CALL AUMRES
      NPR = 0
      PASS = 0
      EXTRA = 0
80    ADMSCT = ADMSCT + 1
      CALL ADMINT
      IF(NOSAVE .EQ. 0) GO TO 138

C     THE SOUT(I) AND P(I,NPR), J = 1, 5 HAVE THE INDEPENDENT VARIABLE
C     AND THE CORRESPONDING PARAMETERS WHICH ARE USED IN THE AUXILIARY
C     EQNS (TYPE 3) FOR THE NONLINEAR ANALYSIS.

      IF(EAM(7) .EQ. 0.0) GO TO 375
      EXTRA = 1
      IF(PASS .EQ. 3) GO TO 310
      PASS = PASS + 1
      GO TO 315
310   PASS = 1
315   DO 350 I = 1, NDE
      YSAVE(I,PASS) = Y(I.
350   CONTINUE
      XSAVE(PASS) = S
      GO TO 80
375   IF(EXTRA .EQ. 0) GO TO 400
      SSAVE = S
      DO 390 M = 1, 3
      NPR = NPR + 1
      S = XSAVE(M)
      CALL GOMTRY
      P(1,NPR + 1) = YSAVE(2,M)
      P(2,NPR + 1) = YSAVE(4,M)
      P(3,NPR + 1) = YSAVE(5,M)
      P(4,NPR + 1) = T2*YSAVE(6,M) - NU*R2*CXS*YSAVE(5,M)
      P(5,NPR + 1) = NU*YSAVE(4,M) + H*(R2*CXS*YSAVE(3,M) +
                     R2*SXN*YSAVE(1,M))*YMOD
      SOUT(NPR + 1) = S
```

```
390   CONTINUE
      S = SSAVE
      EXTRA = 0
400   NPR = NPR + 1
      IF(EXTRA .EQ. 0) GO TO 410
      CALL GOMTRY
410   P(1,NPR + 1) = Y(2)
      P(2,NPR + 1) = Y(4)
      P(3,NPR + 1) = Y(5)
      P(4,NPR + 1) = T2*Y(6) - NU*R2*CXS*Y(5)
      P(5,NPR + 1) = NU*Y(4) + H*(R2*CXS*Y(3) + R2*SXN*Y(1))*YMOD
      SOUT(NPR + 1) = S
      IF(NPR .LT. 276)  GO TO 138
      WRITE(6,686) JJ
      WRITE(6,678)
      WRITE(6,676)  (SOUT(N), (P(I,N), I = 1, 5), N = 1, 275)
      GO = 1
      RETURN
138   IF(S .LT. SFINAL) GO TO 80
      IF(EAM(7) .EQ. 0.0) GO TO 830
      IF(FINAL .EQ. 1) GO TO 80
      DO 825 I = 1, NDE
      FSAVE(I) = Y(I)
825   CONTINUE
      FINAL = 1
      GO TO 80
830   IF(FINAL .EQ. 0) GO TO 840
      DO 835 I = 1, NDE
      PRNT(I) = FSAVE(I)
835   CONTINUE
840   TERM1 = MAX1F(ABS(PRNT(1)), ABS(PRNT(2)), ABS(PRNT(3)),
     1              ABS(PRNT(4)), ABS(PRNT(5)), ABS(PRNT(6)))
      IF(NDE .EQ. 6)  GO TO 8406
      TERM1 = MAX1F(TERM1, ABS(PRNT(7)), ABS(PRNT(8)))
8406  E(JJ,NF) = TERM1
      IF(JJ .GT. 1) GO TO 4540
777   JJJ = NPL
      GO TO 1491
4540  JJJ = JJ - 1
1491  DO 4542 I = 1, NDE
      C(I,JJJ,NF) = PRNT(I)
4542  CONTINUE
      IF(INTPRN .EQ. 0) GO TO 4240
      WRITE(6,675) YAM(1), (PRNT(I), I = 1, NDE)
      WRITE(6,605) ADMSCT, INTC
4240  IF(NOSAVE .EQ. 0) GO TO 4320
      NPOINT = NPR + 1
      IF(INTPRN .EQ. 0) GO TO 1490
      WRITE(6,677)
      WRITE(6,676) (SOUT(N), (P(I,N), I = 1, 5), N = 1, NPOINT)
1490  DO 5035 N = 2, NPOINT
      DELTA = 1.0/(SOUT(N) - SOUT(N - 1))
      DO 5030 I = 1, 5
      SLOPE(I,N - 1) = (P(I,N) - P(I,N - 1))*DELTA
      P(I,N - 1) = P(I,N - 1) - SLOPE(I,N - 1)*SOUT(N - 1)
5030  CONTINUE
```

```
5035  CONTINUE
      IF(INTPRN .EQ. 0) GO TO 4320
      WRITE(6,637)
      MPOINT = NPOINT - 1
      WRITE(6,679) (M, (SLOPE(I,M), I = 1, 5), M = 1, MPOINT)
4320  CONTINUE
      IF(ISH .EQ. 2 .AND. NTYPE .EQ. 1)  GO TO 4536
      SZERO = SFINAL
4330  CONTINUE
      RETURN
4536  NPARTC = NFF + NF - 2
      DO 4375 JJ = NF, NPARTC
      DO 4381 I = 1, NDE
      DO 4381 J = 1, NPL
      D(I,J,JJ + 1) = D(I,J,JJ)
4381  CONTINUE
4375  CONTINUE
      NF = NPARTC + 1
      RETURN
697   FORMAT(1H0, 39H****************************************,
     1             27HTHESE RESULTS ARE FOR PART I2, 11H OF BRANCH I2,
     2             39H****************************************)
696   FORMAT(1H , 15H***** ERR(I) = 2H** E16.8, 2H** E16.8, 2H** E16.8,
     1                              2H** E16.8, 2H** E16.8, 2H** E16.8)
675   FORMAT(1H , F10.5, 8E15.6)
686   FORMAT(1H1, 47HDIMENSION OF SOUT EXCEEDED FOR INTEGRATION NO. I1,
     1             23H. CALCULATIONS STOPPED.)
678   FORMAT(1H0, 11X, 4HSOUT, 16X, 4HQPHI, 16X, 4HNPHI, 16X, 4HBPHI,
     1             14X, 8HDBPHI/DS, 15X, 2HNT)
676   FORMAT(1H , 6E20.8)
605   FORMAT(1H , 14HADMINT CALLED I3, 6H TIMES, 5X,
     1             14HDIFFEQ CALLED I3, 6H TIMES)
677   FORMAT(1H1, 11X, 4HSOUT, 16X, 4HQPHI, 16X, 4HNPHI, 16X, 4HBPHI,
     1             14X, 8HDBPHI/DS, 15X, 2HNT)
637   FORMAT(1H1, 69HVALUES FOR SLOPES IN FOLLOWING ORDER - QPHI, NPHI,
     1BPHI, DBPHI/DS, NT)
679   FORMAT(1H , 13, 6X, 5E20.8)
      END
```

```
      SUBROUTINE INVERT (BA,MAX,NAX,DETERM,ISCAL)
      DIMENSION  DP(8,8), M(8), C(8), BA(64)
      DO 310 J=1,MAX
      K=(J-1)*NAX+1
      DO 305 I=1,MAX
      DP(I,J)=BA(K)
  305 K=K+1
  310 CONTINUE
      DETERM = 1.

C     INITIALIZE BOOK-KEEPING ARRAY

      DO 90 I = 1, MAX
      M(I) = - I
90    CONTINUE
      DO 140 II = 1, MAX

C     LOCATE LARGEST ELEMENT

      D = 0.0
      DO 112 K = 1, MAX
      IF (M(K)) 100,100,112
100   DO 110 L = 1, MAX
      IF (M(L)) 103,103,110
103   IF(ABS(D) - ABS(DP(K,L))) 105, 105, 110
  105 LD = L
      KD = K
      D = DP(K,L)
110   CONTINUE
112   CONTINUE

C     CALCULATE DETERMINANT

      IF(KD - LD) 900, 901, 900
900   DETERM = - DETERM
901   DETERM = D*DETERM

C     INTERCHANGE COLUMNS AND SUBSTITUTE IDENTITY ELEMENTS

      NEMP = -M(LD)
      M(LD)=M(KD)
      M(KD)= NEMP
      DO 114 I = 1, MAX
      C(I) = DP(I,LD)
      DP(I,LD) = DP(I,KD)
      DP(I,KD) = 0.0
114   CONTINUE
      DP(KD,KD) = 1.

C     DIVIDE ROW BY LARGEST ELEMENT

      DO 115 J = 1, MAX
      DP(KD,J) = DP(KD,J)/D
115   CONTINUE
```

```
C       REDUCE REMAINING ROWS AND COLUMNS

        DO 135 I = 1, MAX
        IF (I-KD) 130,135,130
130     DO 134 J = 1, MAX
        DP(I,J) = DP(I,J) - C(I)*DP(KD,J)
134     CONTINUE
135     CONTINUE
140     CONTINUE

C       INTERCHANGE ROWS

        DO 200 I = 1, MAX
        L = 0
150     L = L + 1
        IF (M(L)-I) 150,160,150
160     M(L)=M(I)
        M(I)=I
        DO 200 J = 1, MAX
        TEMP = DP(L,J)
        DP(L,J) = DP(I,J)
        DP(I,J) = TEMP
200     CONTINUE
        DO 330 J=1,MAX
        K=(J-1)*NAX+1
        DO 325 I=1,MAX
        BA(K)=DP(I,J)
  325   K=K+1
  330   CONTINUE
        RETURN
        END
```

```
      SUBROUTINE MATML(A, NRA, NCA, IRA, ICA, NRSA, NCSA,
     *                 B, NRB, NCB, IRB, ICB, NCSB,
     *                 C, NRC, NCC, IRC, ICC, DUMMY)
      DIMENSION A(NRA,NCA), B(NRB,NCB), C(NRC,NCC), DUMMY(NRC,NCC)
COMMENT   IF A IS DOUBLY SUBSCRIPTED, THEN WRITE A(1,1).
COMMENT   IF A IS TRIPLY SUBSCRIPTED, THEN WRITE A(1,1,K) WHERE K
COMMENT   INDICATES THE K - TH A ARRAY.
COMMENT   IF B IS VECTOR, I.E., SINGLY SUBSCRIPTED, THEN WRITE B(1).
COMMENT   IF B IS DOUBLY SUBSCRIPTED, THEN WRITE B(1,1), IF B IS
COMMENT   SQUARE. OTHERWISE IF B IS RECTANGULAR, THEN WRITE B(1,K),
COMMENT   WHERE K IS THE K - TH COLUMN IN B.
COMMENT   IF B IS TRIPLY SUBSCRIPTED, THEN WRITE B(1,1,K) WHERE K
COMMENT   INDICATES THE K - TH B ARRAY.
COMMENT   IF C IS VECTOR, I.E., SINGLY SUBSCRIPTED, THEN WRITE C(1).
COMMENT   IF C IS DOUBLY SUBSCRIPTED, THEN WRITE C(1,1).
COMMENT   IF C IS TRIPLY SUBSCRIPTED, THEN WRITE C(1,1,K) WHERE K
COMMENT   INDICATES THE K - TH C ARRAY.
COMMENT   NRA = NUMBER OF ROWS IN A.
COMMENT   NCA = NUMBER OF COLUMNS IN A.
COMMENT   NRSA = NUMBER OF ROWS IN SUB MATRIX OF A WHICH WILL BE
COMMENT   MULTIPLIED.
COMMENT   NCSA = NUMBER OF COLUMNS IN SUB MATRIX OF A WHICH WILL BE
COMMENT          MULTIPLIED.
COMMENT   IRA = NUMBER OF THE ROW IN WHICH THE SUBMATRIX STARTS.
COMMENT   ICA = NUMBER OF THE COLUMN IN WHICH THE SUBMATRIX STARTS.
COMMENT   SIMILAR DEFINITIONS FOR OTHER QUANTITIES.

COMMENT   CALLING PROGRAM MUST PROVIDE TEMPORARY STORAGE OF NRC*NCC
COMMENT   DECIMAL WORDS.
      IMAX = IRA + NRSA - 1
      JMAX = ICB + NCSB - 1
      LMAX = ICA + NCSA - 1
      MMAX = IRC + NRSA - 1
      NMAX = ICC + NCSB - 1
      M = 1
      DO 110 I = IRA, IMAX
      N = 1
      DO 105 J = ICB, JMAX
      SUM = 0.0
      K = IRB
      DO 100 L = ICA, LMAX
      SUM = SUM + A(I,L)*B(K,J)
      K = K + 1
100   CONTINUE
      DUMMY(M,N) = SUM
      N = N + 1
105   CONTINUE
      M = M + 1
110   CONTINUE
      MM = 1
      DO 120 M = IRC, MMAX
      NN = 1
      DO 115 N = ICC, NMAX
      C(M,N) = DUMMY(MM,NN)
      NN = NN + 1
```

```
115   CONTINUE
      MM = MM + 1
120   CONTINUE
      RETURN
      END
```

```
      SUBROUTINE PRINT
      DIMENSION      IA(8)          , SI(60)         , IPAR(60)       ,
     *               IB(8)          , SX(60)         , INT(60)        ,
     *               GA(8)          , PRNT(8)        , ISS(60)        ,
     *               GB(8)          , ERR(8)         , PSR(60)        ,
     *               Y(8)           , DM(8,61)       , EYM(60)        ,
     *               DY(8)          , TL(8,8)        , A(8,9)         ,
     *               IR(8,8)        , TLI(8,8)       , JOBPLT(10)     ,
     *               TRI(8,8)       , TRY(8,61)      , TR2(8,8)       ,
     *               SOUT(275)      , D(8,9,60)      , P(5,275)       ,
     *               SLOPE(5,275)   , TR1(8,8)       , E(9,60)
      DIMENSION      V3(8)          , VN(7,60)       , YAM(72)        ,
     *               DYAM(72)       , ABC(21)        , EAM(10)        ,
     *               BACK(60)       , YSAVE(8)       , DETERM(10)     ,
     *               IPLOT(10)      , XPLOT(350)     , YPLOT(350,10)  ,
     *               STROUT(350)    , SIGNPH(350)    , SIGMPH(350)    ,
     *               SIGPHT(350)    , SIGPHB(350)    , SIGNTH(350)    ,
     *               SIGMTH(350)    , SIGTHT(350)    , SIGTHB(350)    ,
     *               TAUPHI(350)    , VARTIK(60)     , POINT(60)
      COMMON / BLOCKA / NU, PI, XLD, NTYPE, INDEX, IBR, PN, NPOINT,
     1                  ISH, TT, T1, T2, HTT, INTC
      COMMON / BLOCKB / H, R1, R2, R3, SXN, CXS
      COMMON / BLOCKC / DM, GA, GB, NF, NFP, NPL, NH, NN, IRY
      COMMON / BLOCKD / TL, TR, TLI, TRI, ALFL, ALFR
      COMMON / BLOCKF / NFF, SMXX, SZERO, GO, ERP, ISS, E,
     *                  MAX, INTPRN, INTVAL, NPP
      COMMON / BLOCKG / NPARTS, PHI1, V3, KIND, NT, MT, SPRINT, VN, EYM,
     1                  BACK, NBACK
      COMMON / BLOCKH / NDE
      COMMON / BLOCKJ / DELX, PDELX, ABC, EAM
      COMMON / BLOCKK / PIN, PMIN, H0, X0, EMIN, EMAX
      COMMON / BLOCKL / YAM, DYAM
      COMMON / BLOCKM / YSAVE
      COMMON / BLOCKN / DETERM
      COMMON / BLOCKP / PLOT, PLTIME, SPLOT, PLOTPT, IPLOT, YMOD, KST,
     1                  HGAMMA, DEAD, NFH
      COMMON / BLOCKQ / TIME, VARTIK, NVARTK
      COMMON / BLOCKS / JOBPLT, ALXL, ALXR, IA, IB, NOPUNC, INPUT,
     *                  CONVER, SI, SX, INT, IPAR, PSR, ITER, NTRY,
     *                  NERROR, IBRM, TRYIN, IBRMAX
      COMMON            SLOPE, P, SOUT, D, A
      COMMON / PLXY1C / IEX(8), DUM(4)
      EQUIVALENCE   (Y(1), PRNT(1)), (Y(1), YAM(2)), (DY(1), DYAM(2)),
     1              (S, YAM(1)), (VARTIK(1), POINT(1))
      EQUIVALENCE    (SLOPE(1)  ,  YPLOT(1)    ),
     *               (D(476)    ,  XPLOT(1)    ),
     *               (D(826)    ,  STROUT(1)   ),
     *               (D(1176)   ,  SIGNPH(1)   ),
     *               (D(1526)   ,  SIGMPH(1)   ),
     *               (D(1876)   ,  SIGPHT(1)   ),
     *               (D(2226)   ,  SIGPHB(1)   ),
     *               (D(2576)   ,  SIGNTH(1)   ),
     *               (D(2926)   ,  SIGMTH(1)   ),
     *               (D(3276)   ,  SIGTHT(1)   ),
     *               (D(3626)   ,  SIGTHB(1)   ),
```

```
*                (D(3976)  ,  TAUPHI(1)  )
      INTEGER  GO, IRYIN, PASS, SPACE, ADMSCT, FINIS, PLOT,
     1         PLOTPT, PLTIME, TIME, VARTIK, POINT, COLUMN
      DATA(RPD = 0.17453292525-01), (DPR = 57.29577951)
      REAL     NU, NT, MT, NBACK, NFH, NR2
      IF(NDE .EQ. 8)  GO TO 105
      DO 100 I = 7, 8
      YSAVE(I) = 0.0
      PRNT(I) = 0.0
      V3(I) = 0.0
  100 CONTINUE
  105 NF = 0
      PIN = 1.0
      PMIN = 5.0
      PLOTPT = 1
      SPLOT = 0.0
      KST = 0
      NPLACE = 1
  106 WRITE(6,355)
      KOUNT = 1
      GO TO (107, 109, 161, 166, 234, 246, 576), NPLACE
  107 DO 245 IBR = 1, IBRMAX
      NVARTK = POINT(IBR)
      NBACK = BACK(IBR)
      ISH = ISS(IBR)
      INDEX = ISH - 1
      KOUNT = KOUNT + 2
      IF(KOUNT .LT. 53)  GO TO 109
      NPLACE = 2
      GO TO 106
  109 WRITE(6,345)
      GO TO (110, 115, 120, 125, 130, 135, 140), INDEX
  110 WRITE(6,365) IBR
      GO TO 145
  115 WRITE(6,370) IBR
      GO TO 145
  120 WRITE(6,375) IBR
      GO TO 145
  125 WRITE(6,380) IBR
      GO TO 145
  130 WRITE(6,385) IBR
      GO TO 145
  135 WRITE(6,390) IBR
      GO TO 145
  140 WRITE(6,365) IBR
  145 INDEX = 1
      CALL GOMTRY
      YMOD = EYM(IBR)
      NU = PSR(IBR)
      P1 = (1.0 - NU*NU)/YMOD
      TT = H*H/12.0
      T1 = P1/H
      T2 = T1/TT
      HT1 = H*TT
      NFF = IPAR(IBR)
      SMAX = (SX(IBR) - SI(IBR))/FLOAT(NFF)
```

```
      NPP = INT(IBR)
      PPR = SMXX/FLOAT(NPP - 1)
      SZERO = SI(IBR)
      DO 240 L = 1, NFF
      SFINAL = SZERO + SMXX
      NF = NF + 1
      IF(NTYPE .NE. 1)  GO TO 155
      IF(L .EQ. NFF) GO TO 160
      TERM1 = MAX1F(ABS(DM(1,NF + 1)), ABS(DM(2,NF + 1)),
     1              ABS(DM(3,NF + 1)), ABS(DM(4,NF + 1)),
     2              ABS(DM(5,NF + 1)), ABS(DM(6,NF + 1)))
      IF(NDE .EQ. 6)  GO TO 150
      TERM1 = MAX1F(TERM1, ABS(DM(7,NF + 1)), ABS(DM(8,NF + 1)))
  150 ERROR = TERM1*ERP
      GO TO 160
  155 ERROR = E(1,NF)*ERP
  160 EMAX = ERROR
      EMIN = ERROR*0.01
      KOUNT = KOUNT + 1
      IF(KOUNT .LT. 53)  GO TO 161
      NPLACE = 3
      GO TO 106
  161 WRITE(6,345)
      IF(INTVAL .EQ. 0) GO TO 170
      DO 165 I = 1, NDE
      ERR(I) = ERROR
  165 CONTINUE
      KOUNT = KOUNT + 1
      IF(KOUNT .LT. 53)  GO TO 166
      NPLACE = 4
      GO TO 106
  166 WRITE(6,400) (ERR(I), I = 1, 6)
  170 DO 175 I = 1, NDE
      Y(I) = DM(I,NF)
  175 CONTINUE
      HO = PPR
      XO = SZERO
      IF(NTYPE .NE. 1)  GO TO 180
      XLO = 1.0
      GO TO 185
  180 NTYPE = 2


C     KIND = 1 INDICATES FUNDAMENTAL VARIABLES ARE FROM THE BEGINNING
C     OF A PART, THAT IS, DM(I,NF).
C     KIND = 2 INDICATES FUNDAMENTAL VARIABLES ARE ADAMS-MOULTON POINTS,
C     THAT IS, PRNT(I).
C     KIND = 3 INDICATES FUNDAMENTAL VARIABLES ARE FROM THE YSAVE(I),
C     WHICH MEANS THEY ARE PERMANENT RUNGE KUTTA POINTS.
C     KIND = 4 INDICATES FUNDAMENTAL VARIABLES ARE FROM CROWN CALCULA-
C     TIONS.


  185 CALL ADMRES
      S = SZERO
      SPRINT = SZERO
```

```
      KIND = 1
      LPLACE = 1
      GO TO 495
  186 PASS = 0
      INIC = 0
      SPACE = 1
      ADMSCT = 0
  190 ADMSCT = ADMSCT + 1
      CALL ADMINT
      IF(PASS .EQ. 2 .AND. EAM(9) .EQ. 0.0) GO TO 225
      IF(PASS .EQ. 0) GO TO 195
      IF(SPACE .EQ. XFIXF(EAM(8))) GO TO 200
      IF(PASS .EQ. 3) GO TO 205
      PASS = PASS + 1
      GO TO 190
  195 IF(EAM(9) .EQ. 0.0) GO TO 210
      GO TO 190
  200 PASS = 0
      GO TO 190
  205 PASS = 0
      KIND = 3
      SSAVE = S
      SPRINT = XSAVE
      S = XSAVE
      SPLOT = SPLOT + PPR
      PLOTPT = PLOTPT + 1
      LPLACE = 2
      GO TO 495
  206 S = SSAVE
      SPACE = SPACE + 1
      IF(SPACE .LT. NPP) GO TO 190
      GO TO 230
  210 IF(EAM(7) .EQ. 0.0) GO TO 220
      DO 215 I = 1, NDE
      YSAVE(I) = Y(I)
  215 CONTINUE
      XSAVE = S
      PASS = 1
      GO TO 190
  220 KIND = 2
      SPRINT = S
      SPLOT = SPLOT + PPR
      PLOTPT = PLOTPT + 1
      LPLACE = 3
      GO TO 495
  221 SPACE = SPACE + 1
      IF(SPACE .LT. NPP) GO TO 190
      GO TO 230
  225 PASS = 0
      KIND = 3
      SSAVE = S
      S = XSAVE
      SPRINT = XSAVE
      SPLOT = SPLOT + PPR
      PLOTPT = PLOTPT + 1
      LPLACE = 4
```

```
      GO TO 495
  226 SPACE = SPACE + 1
      S = SSAVE
      IF(S .GT. 1.00001*SFINAL)  GO TO 230
      KIND = 2
      SPRINT = S
      SPLOT = SPLOT + PPR
      PLOTPT = PLOTPT + 1
      LPLACE = 5
      GO TO 495
  227 SPACE = SPACE + 1
      IF(SPACE .LT. NPP) GO TO 190
  230 IF(INIVAL .EQ. 0) GO TO 235
      KOUNT = KOUNT + 1
      IF(KOUNT .LT. 53)  GO TO 234
      NPLACE = 5
      GO TO 106
  234 WRITE(6,350) ADMSCT, INTC
  235 TERM3 = MAXIF(ABS(PRNT(1)), ABS(PRNT(2)), ABS(PRNT(3)),
     1              ABS(PRNT(4)), ABS(PRNT(5)), ABS(PRNT(6)))
      E(1,NF) = TERM3
      SZERO = SFINAL
  240 CONTINUE
  245 CONTINUE
      IF(ISS(IBRM) .GT. 1) GO TO 280
      KOUNT = KOUNT + 5
      IF(KOUNT .LT. 53)  GO TO 246
      NPLACE = 6
      GO TO 106
  246 WRITE(6,345)
      WRITE(6,360)
      WRITE(6,345)
      ISM = 1
      IBR = IBRM
      YMOD = EYM(IBR)
      NU = PSR(IBR)
      KIND = 4
      INDEX = 1
      IF(NTYPE .NE. 1)  GO TO 250
      XLO = 0.0
      GO TO 255
  250 XLO = 1.0
  255 DO 275 M = 1, 2
      GO TO (260, 265), M
  260 PHI1 = 0.02
      GO TO 270
  265 PHI1 = 0.0
      SPLOT = SPLOT + 0.02
      PLOTPT = PLOTPT + 1
  270 CALL GOMTRY
      LPLACE = 6
      GO TO 495
  271 CONTINUE
  275 CONTINUE
      GO TO 280
  495 IF(KIND .EQ. 4) GO TO 535
```

```
      CALL GOMTRY
      GO TO (500, 510, 520), KIND
  500 DO 505 I = 1, NDE
      V3(I) = DM(I,NF)
  505 CONTINUE
      GO TO 530
  510 DO 515 I = 1, NDE
      V3(I) = PRNT(I)
  515 CONTINUE
      GO TO 530
  520 DO 525 I = 1, NDE
      V3(I) = YSAVE(I)
  525 CONTINUE
  530 NR2 = NFH*R2
      NT = NU*V3(4) + H*(R2*CXS*V3(3) + R2*SXN*V3(1) + NR2*V3(7))*YMOD
      MT = NU*V3(6) + HTT*(R2*CXS*V3(5) + NR2*(R2*SXN*V3(7) +
     1     NR2*V3(1)))*YMOD
  535 DO 575 J = 1, 2
      GO TO (540, 545), J
  540 TERM1 = (NT - NU*V3(4))/H
      TERM2 = 0.5*(MT - NU*V3(6))/TT
      GO TO 550
  545 TERM1 = (V3(4) - NU*NT)/H
      TERM2 = 0.5*(V3(6) - NU*MT)/TT
  550 IF(TERM1 .GT. 0.0) GO TO 555
      SIGN = - 1.0
      GO TO 560
  555 SIGN = 1.0
  560 TERM3 = SIGN*MAX1F(ABS(TERM1 + TERM2), ABS(TERM1 - TERM2))/YMOD
      GO TO (565, 570), J
  565 EPI = TERM3
      GO TO 575
  570 EPP = TERM3
  575 CONTINUE
      KOUNT = KOUNT + 1
      IF(KOUNT .LT. 53)  GO TO 577
      NPLACE = 7
      GO TO 106
  576 WRITE(6,345)
      KOUNT = KOUNT + 1
  577 GO TO (580, 590, 585, 585, 585, 590, 585, 590),  ISH
  580 SPRINT = (3.14159265 - PHI1)*DPR
      GO TO 590
  585 SPRINT = SPRINT*DPR
      IF(NBACK .EQ. - 1.0)  SPRINT = 180.0 - SPRINT
  590 WRITE(6,670) SPRINT, (V3(I), I = 1, 6), NT, MT, EPI, EPP
      TERM1 = V3(4)/H
      TERM2 = 0.5*V3(6)/TT
      TERM3 = NT/H
      TERM4 = 0.5*MT/TT
      KST = KST + 1
      STROUT(KST) = SPRINT
      SIGNPH(KST) = TERM1
      SIGMPH(KST) = TERM2
      SIGPHT(KST) = TERM1 - TERM2
      SIGPHB(KST) = TERM1 + TERM2
```

```
      SIGNTH(KST) = TERM3
      SIGMTH(KST) = TERM4
      SIGTHT(KST) = TERM3 - TERM4
      SIGTHB(KST) = TERM3 + TERM4
      TAUPHI(KST) = 1.5*V3(2)/H
      IF(PLTIME .EQ. 0)  GO TO 666
      XPLOT(PLOTPT) = SPLOT
      DO 665 I = 1, PLOT
      COLUMN = IPLOT(I)
      IF(COLUMN .GT. 6) GO TO 595
      YPLOT(PLOTPT,I) = V3(COLUMN)
      GO TO 665
  595 KOLUMN = COLUMN - 6
      GO TO (600, 605, 610, 615, 620, 625,
     1       630, 635, 640, 645, 650, 655, 660), KOLUMN
  600 YPLOT(PLOTPT,I) = NT
      GO TO 665
  605 YPLOT(PLOTPT,I) = MT
      GO TO 665
  610 YPLOT(PLOTPT,I) = EPT
      GO TO 665
  615 YPLOT(PLOTPT,I) = EPP
      GO TO 665
  620 YPLOT(PLOTPT,I) = SIGNPH(KST)
      GO TO 665
  625 YPLOT(PLOTPT,I) = SIGMPH(KST)
      GO TO 665
  630 YPLOT(PLOTPT,I) = SIGPHT(KST)
      GO TO 665
  635 YPLOT(PLOTPT,I) = SIGPHB(KST)
      GO TO 665
  640 YPLOT(PLOTPT,I) = SIGNTH(KST)
      GO TO 665
  645 YPLOT(PLOTPT,I) = SIGMTH(KST)
      GO TO 665
  650 YPLOT(PLOTPT,I) = SIGTHT(KST)
      GO TO 665
  655 YPLOT(PLOTPT,I) = SIGTHB(KST)
      GO TO 665
  660 YPLOT(PLOTPT,I) = TAUPHI(KST)
  665 CONTINUE
  666 GO TO (186, 206, 221, 226, 227, 271), LPLACE

C     WRITE OUT STRESSES.

  280 KST = 0
      NPLACE = 1
  281 WRITE(6,405)
      KOUNT = 3
      GO TO (282, 283, 321, 322, 336), NPLACE
  282 DO 335 IBR = 1, IBRMAX
      NFF = IPAR(IBR)
      NPP = INT(IBR)
      ISH = ISS(IBR)
      INDEX = ISH - 1
      KOUNT = KOUNT + 2
```

```
      IF(KOUNT .LT. 53)  GO TO 283
      NPLACE = 2
      GO TO 281
  283 WRITE(6,345)
      GO TO (285, 290, 295, 300, 305, 310, 315), INDEX
  285 WRITE(6,365) IBR
      GO TO 320
  290 WRITE(6,370) IBR
      GO TO 320
  295 WRITE(6,375) IBR
      GO TO 320
  300 WRITE(6,380) IBR
      GO TO 320
  305 WRITE(6,385) IBR
      GO TO 320
  310 WRITE(6,390) IBR
      GO TO 320
  315 WRITE(6,365) IBR
  320 DO 330 L = 1, NFF
      KOUNT = KOUNT + 1
      IF(KOUNT .LT. 53)  GO TO 321
      NPLACE = 3
      GO TO 281
  321 WRITE(6,345)
      DO 325 N = 1, NPP
      KOUNT = KOUNT + 1
      IF(KOUNT .LT. 53)  GO TO 323
      NPLACE = 4
      GO TO 281
  322 WRITE(6,345)
      KOUNT = KOUNT + 1
  323 KST = KST + 1
      WRITE(6,415) STHOUT(KST), SIGNPH(KST), SIGMPH(KST), SIGPHT(KST),
     1             SIGPHB(KST), SIGNTH(KST), SIGMTH(KST), SIGTHT(KST),
     2             SIGTHB(KST), TAUPHI(KST)
  325 CONTINUE
  330 CONTINUE
  335 CONTINUE
      IF(ISS(IBRM) .GT. 1)  RETURN
      KOUNT = KOUNT + 5
      IF(KOUNT .LT. 53)  GO TO 336
      NPLACE = 5
      GO TO 281
  336 WRITE(6,345)
      WRITE(6,360)
      WRITE(6, 345)
      DO 340 M = 1, 2
      KST = KST + 1
      WRITE(6,415) STHOUT(KST), SIGNPH(KST), SIGMPH(KST), SIGPHT(KST),
     1             SIGPHB(KST), SIGNTH(KST), SIGMTH(KST), SIGTHT(KST),
     2             SIGTHB(KST), TAUPHI(KST)
  340 CONTINUE
      RETURN
  395 FORMAT(1H1, 3X, 4HSOUT, 10X, 1HW, 9X, 5HQ PHI, 7X, 5HU PHI,
     1           7X, 5HN PHI, 6X, 8HBETA PHI, 5X, 5HM PHI,
     2           6X, 7HN THETA, 5X, 7HM THETA, 4X, 9HEPS THETA,
```

```
   3             4X, 7HEPS PHI)
345 FORMAT(1H )
365 FORMAT(1H , 23HRESULTS FOR MAIN SHELL I2, 12H CYLINDRICAL)
370 FORMAT(1H , 23HRESULTS FOR MAIN SHELL I2, 10H SPHERICAL)
375 FORMAT(1H , 23HRESULTS FOR MAIN SHELL I2, 13H PARABOLOIDAL)
380 FORMAT(1H , 23HRESULTS FOR MAIN SHELL I2, 12H ELLIPSOIDAL)
385 FORMAT(1H , 23HRESULTS FOR MAIN SHELL I2,  8H CONICAL)
390 FORMAT(1H , 23HRESULTS FOR MAIN SHELL I2,  9H TOROIDAL)
400 FORMAT(1H ,11H**ERR(I) =     1H*E11.4, 1H*E11.4, 1H*E11.4,
   1                             1H*E11.4, 1H*E11.4, 1H*E11.4)
350 FORMAT(1H , 14HADMINT CALLED I3, 6H TIMES, 5X,
   1            14HDIFFEQ CALLED I3, 6H TIMES)
360 FORMAT(1H , 17HRESULTS FOR CROWN)
670 FORMAT(1H , F11.7, 10E12.4,
405 FORMAT(1H1, 31X, 19HMERIDIONAL STRESSES,
   1            29X, 24HCIRCUMFERENTIAL STRESSES,
   2            16X, 12HSHEAR STRESS    //
   3       5X, 4HSOUT,  8X, 8HMEMBRANE, 6X, 7HBENDING, 7X, 5HINNER,
   4       8X, 5HOUTER, 6X, 8HMEMBRANE, 6X, 7HBENDING, 7X, 5HINNER,
   5       8X, 5HOUTER)
415 FORMAT(1H , F12.7, 2X, 9E13.5)
    END
```

```
      SUBROUTINE THICK
      DIMENSION     XP(10,60),      POINT(60),      YAM(72),
     *              YP(10,60),      DYAM(72),       PRNT(8),
     *              SL( 9,60),      VARTIK(60),     V3(8),
     *              VN(7,60),       EYM(60),        BACK(60)
      COMMON / BLOCKA / NU, P1, XLD, NTYPE, INDEX, IBR, PN, NPOINT,
     1                  ISH, TT, T1, T2, HTT, INTC
      COMMON / BLOCKB / H, R1, R2, R3, SXN, CXS
      COMMON / BLOCKE / XP, YP, SL
      COMMON / BLOCKG / NPARTS, PHI1, V3, KIND, NT, MT, SPRINT, VN, EYM,
     1                  BACK, NBACK
      COMMON / BLOCKL / YAM, DYAM
      COMMON / BLOCKQ / TIME, VARTIK, NVARTK
      EQUIVALENCE  (X, YAM(1)), (PRNT(1), YAM(2)), (VARTIK(1), POINT(1))
      INTEGER  TIME, POINT, VARTIK
      REAL          NU, NT, MT, NBACK, NFH
      I = NVARTK
      IF(XP(I,IBR) - X)  38, 38, 32
32    IL = 1
      IU = NVARTK
33    IF(IU - IL - 1)    37, 37, 34
34    I = (IL + IU)/2
      IF(X - XP(I,IBR))  35, 38, 36
35    IU = I
      GO TO 33
36    IL = I
      GO TO 33
37    I = IU
38    H = SL(I - 1,IBR)*X + YP(I - 1,IBR)
      RETURN
      END
```

```
      SUBROUTINE TRIANG
      DIMENSION      UC(4,4,60)    , UE(4,4,60)    , D(8,9,60)     ,
     *               DETE(60)      , DETC(60)      , ZA(4,60)      ,
     *               ZB(4,60)      , GA(8)         , GB(8)         ,
     *               TRY(8,61)     , P(5,275)      , SLOPE(5,275)  ,
     *               UU(4,4)       , DM(8,61)      , DETERM(10)    ,
     *               E(9,60)       , ISS(60)       , SOUT(275)     ,
     *               STROUT(350)   , SIGNPH(350)   , SIGMPH(350)   ,
     *               SIGPHT(350)   , SIGPHB(350)   , SIGNTH(350)   ,
     *               SIGMTH(350)   , SIGTHT(350)   , SIGTHB(350)   ,
     *               TAUPHI(350)   , XPLOT(350)    , YPLOT(350,10),
     *               A(8,9)
      COMMON / BLOCKC / DM, GA, GB, NF, NFP, NPL, NH, NN, IRY
      COMMON / BLOCKF / NFF, SMXX, SZERO, GO, ERP, ISS, E,
     *                  MAX, INTPHN, INTVAL, NPP
      COMMON / BLOCKH / NDE
      COMMON / BLOCKN / DETERM
      COMMON            SLOPE, P, SOUT, D, A
      EQUIVALENCE    (SLOPE(1) ,  YPLOT(1)   ),
     *               (D(476)   ,  XPLOT(1)   ),
     *               (D(826)   ,  STROUT(1)  ),
     *               (D(1176)  ,  SIGNPH(1)  ),
     *               (D(1526)  ,  SIGMPH(1)  ),
     *               (D(1876)  ,  SIGPHT(1)  ),
     *               (D(2226)  ,  SIGPHB(1)  ),
     *               (D(2576)  ,  SIGNTH(1)  ),
     *               (D(2926)  ,  SIGMTH(1)  ),
     *               (D(3276)  ,  SIGTHT(1)  ),
     *               (D(3626)  ,  SIGTHB(1)  ),
     *               (D(3976)  ,  TAUPHI(1)  )

C     NF COUNTS NUMBER OF PARTS. THUS AT THIS POINT IN PROGRAM IT EQUALS
C     THE TOTAL NUMBER OF PARTS.

C     D(I,J,K) CONTAINS THE COMPLEMENTARY AND PARTICULAR SOLNS AT THE
C     ENDS OF SEGMENTS. K REFERS TO THE SEGMENT NUMBER. I = 1, NDE AND
C     J = 1, NDE ARE THE COMPLEMENTARY SOLNS. I = 1, NDE AND J = NDE + 1
C     IS THE PARTICULAR SOLN.


C     NPL = NDE + 1
C     NFP = NF + 1

      DO 67 I=1,NH
      DO 67 J=1,NH
      JJ=J+NH
      UE(I,J,1) = D(I,JJ,1)
67    CONTINUE
      CALL INVERT(UE(1,1,1),NH,4,DET,ISCAL)
      CALL MATML (D(1,1,1), 8, 9, NH + 1, NH + 1, NH, NH,
     *            UE(1,1,1), 4, 4, 1, 1, NH,
     *            UC(1,1,1), 4, 4, 1, 1, A)
      DETE(1) = DET
      DO 10 I=1,NH
      II=I+NH
```

```
      SUMA = - D(I,NPL,1)
      SUMB = - D(II,NPL,1)
      DO 9 J = 1, NH
      JJ = J + NH
      SUMA = SUMA - D(I,J,1)*(GA(J) - TRY(J,1)) + D(I,JJ,1)*
     1           TRY(JJ,1)
      SUMB = SUMB - D(II,J,1)*(GA(J) - TRY(J,1)) + D(II,JJ,1)*
     1           TRY(JJ,1)
9     CONTINUE
      ZA(I,1) = SUMA
      ZB(I,1) = SUMB
10    CONTINUE
      DO 11 I=1,NH
      SUM = ZB(I,1)
      DO 12 J = 1, NH
      SUM = SUM - UC(I,J,1)*ZA(J,1)
12    CONTINUE
      ZB(I,1) = SUM
11    CONTINUE
      IF(NF .EQ. 1) GO TO 59
      DO 56 K = 2, NF
      CALL INVERT(UC(1,1,K - 1), NH, 4, DET, ISCAL)
      DETC(K - 1) = DET
      CALL MATML (D(1,1,K), 8, 9, 1, 1, NH, NH,
     *            UC(1,1,K - 1), 4, 4, 1, 1, NH,
     *            UD(1,1), 4, 4, 1, 1, A)
      DO 721 I = 1, NH
      DO 721 J = 1, NH
      JJ = J + NH
      UE(I,J,K) = D(I,JJ,K) + UD(I,J)
721   CONTINUE
      CALL INVERT(UE(1,1,K),NH,4,DET,ISCAL)
      DETE(K) = DET
      DO 73 I=1,NH
      SUM = - D(I,NPL,K)
      DO 74 J = 1, NH
      JJ = J + NH
      SUM = SUM - UD(I,J)*ZB(J,K - 1) + D(I,J,K)*TRY(J,K) +
     *      D(I,JJ,K)*TRY(JJ,K)
74    CONTINUE
      ZA(I,K) = SUM
73    CONTINUE
      CALL MATML (D(1,1,K), 8, 9, NH + 1, 1, NH, NH,
     *            UC(1,1,K - 1), 4, 4, 1, 1, NH,
     *            UD(1,1), 4, 4, 1, 1, A)
      DO 76 I=1,NH
      II=I+NH
      SUM = - D(II,NPL,K)
      DO 761 J = 1, NH
      SUM = SUM - UD(I,J)*ZB(J,K - 1)
761   CONTINUE
      ZB(I,K) = SUM
76    CONTINUE
      DO 77 I=1,NH
      II=I+NH
      DO 77 J=1,NH
```

```
      JJ=J+NH
      UD(I,J) = D(II,JJ,K) + UD(I,J)
77    CONTINUE
      CALL MATML (UD(1,1), 4, 4, 1, 1, NH, NH,
     *            UE(1,1,K), 4, 4, 1, 1, NH,
     *            UC(1,1,K), 4, 4, 1, 1, A)
      DO 54 I=1, 4
      II = I + NH
      SUM = ZB(I,K)
      DO 55 J = 1, NH
      JJ = J + NH
      SUM = SUM - UC(I,J,K)*ZA(J,K) + D(II,J,K)*TRY(J,K) +
     *      D(II,JJ,K)*TRY(JJ,K)
55    CONTINUE
      ZB(I,K) = SUM
54    CONTINUE
56    CONTINUE
59    DO 57 I=1,NH
      II=I+NH
      ZB(I,NF) = ZB(I,NF) + GB(II)
57    CONTINUE
      DIAG=UC(1,1,NF )*UC(2,2,NF )*UC(3,3,NF )
      IF(NDE .EQ. 6) GO TO 575
      DIAG = DIAG*UC(4,4,NF)
575   CONTINUE
      IF(INTVAL .EQ. 0) GO TO 500
      WRITE (6,424)
      WRITE(6,9118)  ((UC(I,J,NF), J = 1, 4), I = 1, NH)
500   CALL INVERT (UC(1,1,NF ),NH,4,DET,ISCAL)
      IF(INTVAL .EQ. 0) GO TO 505
      WRITE (6,302) DET,DIAG
505   DETC(NF) = DET
      IF(INTVAL .EQ. 0) GO TO 510
      WRITE(6,425) (DETE(I), I = 1, NF)
      WRITE(6,426) (DETC(I), I = 1, NF)

C     AT THIS POINT UM CONTAINS THE FUNDAMENTAL VARIABLES AT THE END OF
C     EACH PART AND THE BEGINNING OF THE FIRST PART.

510   DETERM(NN) = DET
      DO 79 I=1,NH
      II=I+NH
      UM(II,NFP) = 0.0
79    CONTINUE
      DO 810 J = 1, NF
      K=NFP-J
      DO 84 I=1,NH
      II=I+NH
      ZB(I,K) = ZB(I,K) + UM(II,K + 1)
84    CONTINUE
      CALL MATML (UC(1,1,K), 4, 4, 1, 1, NH, NH,
     *            ZB(1,K), 4, 1, 1, 1, 1,
     *            UM(1,K + 1), 8, 1, 1, 1, A)
      DO 85 I=1,NH
      ZA(I,K) = ZA(I,K) + UM(I,K + 1)
85    CONTINUE
```

```
      CALL MATML (UE(1,1,K), 4, 4, 1, 1, NH, NH,
     *            ZA(1,K), 4, 1, 1, 1, 1,
     *            DM(1,K), 8, 1, NH + 1, 1, A)
810   CONTINUE
      DO 98 I=1,NH
      II=I+NH
      DM(II,NFP1) = GB(II)
      DM(I,1) = GA(I)
98    CONTINUE
  424 FORMAT (1H0,40X,45HSOLUTION IS BASED ON FOLLOWING C-SUB-M MATRIX)
9118  FORMAT(1H0, 13X, 4E18.8)
302   FORMAT(1H0, 14HDETERMINANT = E15.8, 10X, 16HDIAGONAL TERM = E15.8)
  425 FORMAT(1H0,8HDET(UE)= 8E15.7)
  426 FORMAT(1H0,8HDET(UC)= 8E15.7)
      RETURN
      END
```

```
      SUBROUTINE PLTXY1(X,Y,M,N)
      RETURN
      END
```

APPENDIX D

PARAMETER ANALYSES

ABBREVIATIONS AND SYMBOLS

t	Thickness of U-shaped bellows, in.
c	One-half of the convolution depth of U-shaped bellows, in.
b	Local radius of torus segment, in.
$\bar{R}$	Average bellows radius, in.
L	Live length of bellows, in.
δ	Amount of axial compression imposed on bellows, in.
E	Modulus of elasticity, psi
k	Axial spring constant, lb/in.
p	Internal pressure, psi
r	Radial distance from axis of revolution to point on bellows or diaphragm, in.
σ_ϕ	Meridional surface stress, psi
σ_θ	Circumferential surface stress, psi
γ	Chord angle of welded bellows, deg
ψ	Angle of tilt for welded bellows convolution ends, deg

APPENDIX D

PARAMETER ANALYSES

During the research program, analyses were made of the changes in stress caused by variations in selected parameters of formed bellows, diaphragms, and welded bellows. The results of much of this work are presented in this appendix.

The results are described in four sections: D-I – Parametric Analysis of One-Ply Formed Bellows; D-II – Analysis of Effects of Small Variations in the Formed Bellows Convolution Dimensions; D-III – Parametric Analysis of Corrugated Diaphragms; D-IV – Parametric Analysis of Welded Bellows.

D-I. Parametric Analysis of One-Ply Formed Bellows

The computing program MOLSA (described in Appendix A) was used to carry out theoretical analyses of stresses in single-ply formed bellows of different configurations subjected to internal pressure or to axial extension. It was decided to limit the parameter study to U-shaped bellows and semitoroidal bellows with equal inner and outer torus radii. The U-shaped bellows had flat annular sections (normal to the bellow axis) which connected the toroidal segments. Shapes with unequal inner and outer torus radii or conical segments instead of flat-plate segments were not considered, although it was recognized that actual bellows may have such variations in convolution shape. To be practicable, the parametric study was restricted to a study of the effects of variation in only a few major parameters.

The convolution shape of the U-shaped bellows may be specified by the four parameters shown in Figure D-1. These parameters are the thickness t, convolution depth 2c, torus radius b, and the average bellows radius $\bar{R}$. When the number of convolutions or the overall free length of the bellows is specified in addition to the four parameters, the bellows is completely dimensioned.

It is possible to group the parameters so that the shape of the bellows may be determined by three dimensionless ratios. The ratios chosen for this study were $c/\bar{R}$, $t/\bar{R}$, anb b/c. The first of these ratios, together with the value of $\bar{R}$ and the bellows length L, establishes the envelope of the bellows. The second ratio describes the relative thickness of the bellows, and the third ratio establishes the shape of the convolution.

It is noted that the absolute values of $\bar{R}$ and L must be specified in addition to the values of the three ratios in order to fix the absolute size of a given bellows. However, results were determined in the form of dimensionless ratios and it is possible to calculate relative values of the stresses in the bellows configurations for arbitrary values of $\bar{R}$ and L.

It was noted earlier that analyses were made for two loading conditions – axial extension and internal pressure. For a bellows with some given total axial extension, δ, the relative stresses are reported as $\sigma L/\delta E$, where σ is some stress component and E is

Young's Modulus. A relative spring rate was determined from the results of the axial extension calculations in the form $kL/\bar{R}E$ where k is the actual spring rate. For the case of an internal pressure load, p, with no axial deflection, the stresses are given as σ/p. These ratios are used in plotting the various results of the parametric studies given below. The spring rates and stresses for actual bellows can be easily calculated from these quantities when L, E, δ, $\bar{R}$, and p are known.

It was decided to perform the calculations for configurations given by three values of the parametric ratios. The values chosen were: $c/\bar{R} = 0.075, 0.150, 0.225$; $b/c = 0.2, 0.6, 1.0$; $t/\bar{R} = 0.004, 0.0067, 0.02$. Figure D-2 shows the convolution shapes corresponding to the three values of b/c. For certain combinations of the parameters, the torus-radius-to-shell-thickness ratio, b/t, is much smaller than the ratios for which thin-shell theory is generally considered to be applicable. Therefore, three of the bellows with the smallest b/t were omitted from the calculations. The remaining 24 bellows were analyzed using program MOLSA.

Table D-1 summarizes in tabular form the geometric ratios for the different cases considered.

The results of the analyses are presented in different ways. First, the stress distributions were machine plotted and are presented in Figures D-3 through D-50. Second, the relative spring rates were determined from the axial extension calculations and plotted in Figures D-51 through D-53 to show the variation in spring rate with variation in geometrical parameters. Finally, the values of the maximum stresses for axial extension and for internal pressure loading are plotted against the geometrical parameters in Figures D-54 through D-69.

Stress Distributions

The stress distributions are plotted in Figures D-3 through D-50 as a function of angle in the torus sections and a function of radius in the flat-plate sections.

Results for each separate bellows configuration are described by a pair of graphs with the meridional surface stresses for both axial extension and internal pressure loading on the first graph and the corresponding circumferential stresses on the second graph. The ordinate for the axial extension is on the left side in each figure and the ordinate for the internal pressure is on the right.

The four curves in each figure are distinguished in the following manner: ao refers to the stress on the outer surface caused by the axial extension and ai to stress on the inner surface caused by the axial extension, while the po and pi refer to the stresses on the outer and inner surfaces, respectively, caused by the internal pressure. If the results are needed for axial compression or external pressure, the signs of the corresponding stresses must be changed.

Although these figures are accurate for the cases considered, they are useful primarily as a guide in the selection of a satisfactory shape for a particular loading condition and material. The stresses for any bellows finally selected should be analyzed as a particular case unless it conforms exactly to one of the 24 cases considered.

The variation of maximum stresses with the geometrical parameters is discussed later.

Spring Rates

An examination of Figures D-51 through D-53 shows that the bellows stiffness is most affected by a change in convolution shape (Figure D-2) and decreases as the shape is changed from the semitoroidal (Shape 3, b/c = 1) to the U-shaped bellows. A reduction in convolution depth decreases the stiffness of the semitoroidal bellows (except for small $c/\bar{R}$ in Figure D-53), while the stiffness of the U-shaped bellows increases slightly as the convolution depth decreases.

It was noted above that for some of the cases b/t was smaller than that allowed by thin-shell theory. The top half of Figures D-51 through D-53 shows the values of b/t for each of the bellows configurations. The dashed line at b/t = 10 represents the minimum value of b/t usually taken to be the limit of thin-shell theory. It is seen that b/t is smaller than 10 for a number of the bellows. However, the calculated spring rates seem to be reasonable except perhaps for the semitoroidal bellows with $t/\bar{R} = 0.02$ and $c/\bar{R} = 0.075$, Shape 3 in Figure D-53.

Maximum Stresses

As shown in Figures D-54 through D-56, the maximum stresses in the bellows under axial loading also decrease with convolution depth for the semitoroidal bellows and tend to increase slightly with decreasing convolution depth for the U shaped bellows. The maximum stress for the semitoroidal bellows for $t/\bar{R} = 0.02$ and $c/\bar{R} = 0.075$ corresponding to small b/t may also be too high.

The maximum stress calculated for each of the bellows under axial loading occurred in the meridional direction and was found on the inner bellows surface. This can be confirmed by an examination of Figures D-3 through D-50. In contrast, the maximum stress for some of the bellows configurations under internal pressure, plotted in Figures D-57 to D-59, was found to occur in the circumferential direction.

Because of this difference in the direction of the maximum stresses, for the different pressurized bellows, in addition to the plots of maximum stress given in Figures D-57 through D-59, the maximum stresses are summarized in Table D-2. This table gives the actual maximum surface stresses with proper sign on both inner and outer surfaces and in both meridional and curcumferential directions.

An examination of Table D-2 shows that pressure in the deep U-shaped bellows (Shape 1) results in significant bending stresses in the circumferential direction. This can be seen from the different signs for the stresses on the inner and outer surfaces. In the intermediate bellows and the semitoroidal bellows (Shapes 2 and 3), the predominant stresses in the circumferential direction are membrane stresses. In the meridional direction the bending stresses predominate for all of the cases.

The maximum absolute value of the stress for each of the cases is denoted by an asterisk in Table D-2. It can be seen from this table that absolute maximum stresses for all of the bellows of Shape 1 are negative meridional stresses on the outer surface of the

bellows. For all but two of the bellows of Shape 2, the absolute maximum stresses are positive meridional stresses on the outer surface. For every bellows of Shape 3, the maximum stresses are positive circumferential stresses on the outer surface.

The reason for the two exceptional cases for bellows Shape 2 can be explained by referring to the figures giving the meridional stress distributions for Shape 2 (Figures D-5, D-11, D-17, etc.). From these figures it is seen that in most of the bellows of Shape 2, the pressure stress on the outer surface at the root of the bellows is negative and very nearly as large as the positive maximum stress on the outer surface near the center of the bellows. In the two exceptional cases (shown in Figures D-21 and D-41), the stresses at the root were slightly larger in magnitude than the stresses at the center of the bellows.

Figures D-57 through D-59 show the effect of the convolution depth on the absolute value of maximum stress for the different shapes and thickness. It is interesting to note that the absolute value of stress increases almost linearly with the convolution depth in the range of values considered.

D-II. Analysis of Effects of Small Variations in the Formed-Bellows Convolution Dimensions

One of the major objectives of the research program was the development of an approach to the theoretical analysis of bellows that would give accurate predictions of the stresses and deformations of bellows of any type. In developing this approach, it was necessary to determine how closely the actual bellows had to be modeled mathematically both as to cross-sectional shape and thickness variation in order to obtain accurate predictions of the bellows characteristics. As a part of this investigation, theoretical analyses were made to determine variations in the stresses in a 5-inch bellows due to small variations in the cross-sectional shape. The effect of thickness variation on the stress state in a 3-inch formed bellows was also investigated. Although the analysis of the 3-inch bellows is described later in Appendix E, the results of the analyses in both the 5-inch bellows and the 3-inch bellows are discussed together in this Appendix.

Specimens of both the 5-inch and 3-inch formed bellows were encapsulated, cross sectioned and microscopically measured following the procedures outlined in Appendix P. These measurements were used to construct mathematical models which were then analyzed with the computing program NONLIN (described in Appendix C).

Using measurements from several convolutions of the encapsulated and sectioned 5-inch bellows, four mathematical models were chosen to represent typical variations in the convolution shapes. In addition, two mathematical models were considered which had the shape of the actual bellows. For one of these models, a constant thickness of 0.010 inch was assumed. In the other model, the thickness was taken to be the actual variable thickness measured in the bellows.

The following paragraphs describe the different mathematical models and the theoretically calculated stresses obtained for each 5-inch bellows model. Poisson's ratio was assumed to be 0.3 and Young's Modulus was assumed to be 29×10^6 psi.

Convolution Variation No. 1

Since the radii of the convolution roots were fairly uniform, a root radius of 0.063 inch was used in all four convolution variations. The angles of the conical sections varied, however, and the curvature of the convolution crowns was somewhat elliptical. Consequently, in Variations 1-5 the modeling of these irregular features constituted the differences in the selected variations. In these variations, a constant thickness of 0.010 inch was assumed. Finally in Variation No. 6, the variable thicknesses were also included.

For Convolution Variation No. 1, the smallest average angle, 5 degrees, was selected for the conical section. A crown radius of 0.071 inch was selected because this was judged to approximate the centerline of the outermost curvature of the elliptical shape, as shown in Figure D-60.

Convolution Variation No. 2

For Convolution Variation No. 2, the 5-degree conical angle was combined with a convolution crown radius of 0.085 inch. This radius was chosen to approximate the centerline of the entire elliptical section, as shown in Figure D-61.

Convolution Variation No. 3

Convolution Variation No. 3 (Figure D-62) is the same as No. 2 except that the cone angle was increased to 7° 10′. The convolution root radius of 0.063 inch and the convolution crown radius of 0.085 inch were used with the number of convolutions and the length of the bellows to calculate the average cone angle of 7° 10′. Except for modeling the actual shape of the convolution crown, this approach was thought to be the most representative of an average bellows.

Convolution Variation No. 4

For Convolution Variation No. 4 (Figure D-63), the largest average cone angle of 8 degrees was combined with a convolution crown radius of 0.085 inch.

Convolution Variation No. 5

For Convolution Variation No. 5, the exact cross-sectional shape was modeled. This shape is shown as the solid line in Figures D-60 through D-63.

Convolution Variation No. 6

For Convolution Variation No. 6 the mathematical model used both the exact shape and the exact thickness variation. The measured thickness varied from 0.0099 inch at the convolution root to 0.0093 inch at the convolution crown.

Effects on Stresses of the Convolution Variations

In each of the 5-inch models considered, the maximum meridional stresses for both pressure and deflection loading occurred at the convolution roots and crowns. The locations of the maximum circumferential stresses were sometimes at the root and crown and sometimes displaced from these points. However, since the meridional stresses were always significantly larger than the circumferential stresses, the convolution roots and crowns were selected as the most critical stress locations.

Tables D-3 and D-4 show the stresses calculated at the crowns and roots for the different 5-inch models of JD92 using the computing program NONLIN. An examination of these results shows that the deflection stresses are sensitive to changes in shape, while the pressure stresses are sensitive to changes in thickness but relatively insensitive to small changes in shape. For the deflection stresses, two specific effects were noted:

(1) An increase in the convolution crown radius (see Convolution Variations Nos. 1 and 2) results primarily in an increase in the meridional deflection stress at the convolution root, and a decrease in the meridional pressure stress at the convolution crown.

(2) An increase in the cone angle increases the meridional deflection stresses at both the convolution root and the convolution crown.

Comparison of Stresses in the 5-Inch Bellows With the Parametric Models

Strictly speaking, the parametric analyses of the formed bellows described earlier were applicable only to semitoroidal and U-shaped bellows with flat-plate sections. However, the usefulness of these parametric curves would be considerably enhanced if they could be used to obtain the approximate magnitude and distribution of the stresses in other formed bellows without the cost of a bellows analysis. Therefore, a check was made to determine whether the parametric curves could be used to obtain approximate values of the stresses in the 5-inch bellows.

Table D-5 shows the nominal dimensions of the 5-inch bellows which were supplied by the manufacturer and the values of the bellows parameters t, C, $\bar{R}$, and b. Table D-6 shows the parametric ratios of this bellows as well as the ratios of the most similar parametric model. The stresses for this parametric model are plotted in Figures D-5 and D-6. Comparing these figures with the results given in Tables D-3 and D-4 shows that while the pressure stresses predicted by the parametric model are reasonably close to the stresses for the actual bellows, the deflection stresses are considerably underestimated. This is another indication of the significant effect of shape on the deflection stresses in bellows.

For further comparison, the meridional and circumferential stress distributions for Convolution Variation No. 3 are plotted in Figures D-64 and D-65 in the same format used for the parametric models. A comparison of these figures with Figures D-5 and D-6 shows that the parametric curves approximated from the nominal bellows dimensions show a fairly good agreement with the location and magnitude of the meridional pressure stresses in the variation. While the distribution of the meridional deflection stresses

was similar in both configurations, the stresses were significantly higher in Variation No. 3 than in the parametric model. Although a comparison of Figures D-5 and D-6 with D-64 and D-65 shows some points of similarity for the circumferential stresses, in general, there is little agreement between the stresses for the two models.

Appendix E gives a comparison of the stresses calculated from the exact mathematical model of the 3-inch bellows (including varying thickness) and three models with the same cross-sectional shape but with three different constant thickness values. Figures E-5 through E-20 show parts of the stress distributions calculated in the bellows. These figures indicate that small variations in thickness have a significant effect, particularly on the pressure stresses.

As a result of the analyses of the 3-inch and 5-inch bellows, it is clear that in order to obtain a reliable prediction of the stresses and deformations of a given bellows, the bellows cross section must be accurately modeled. This, of course, requires that the actual thickness variation must be used. These conclusions were strengthened by the results of the theoretical and experimental analyses performed on all of the bellows and diaphragms in this program. The procedures for measuring the cross-sectional shape and thickness variations of the bellows are described in Appendix P. The computer program for performing the theoretical analyses is described in Appendixes B and C.

D-III. Parametric Analysis of Corrugated Diaphragms

The primary objective of this analysis was to obtain a detailed picture of the stress distribution and the displacement characteristics for several possible diaphragm shapes. In this way, possible improvements in the design of diaphragms could be envisioned.

Since an infinite number of variations in the corrugation shapes could have been tried, the decision was made to limit the study to shapes which were representative of possible types of configurations. In addition, in order to isolate the effect of changes in the corrugation shapes, a single corrugation was used for each model. The four shapes chosen for study and the related stress distributions are shown in Figures D-66 through D-73.

The diaphragms had the same shape from the centerline to a radius of 0.85 inch. The shape from 0.85 inch to 1.0 inch was designed such that it consisted of two toroidal sections which were tangent to the flat plate section at r = 0.85 inch, and tangent to the outer corrugation at r = 1.00 inch. Because the four shapes of outer corrugations had different tangents at r = 1.00 inch, this restriction necessarily produced different configurations for the diaphragms in the range $0.85 \leq r \leq 1.00$. In order to have a basic configuration with which to compare these diaphragms, a flat plate diaphragm (Figures D-74 and D-75) was also studied. The thickness of all diaphragms was 0.005 inch except for the center pad which was 0.10 inch. Poisson's ratio was taken as 0.3 and the modulus of elasticity as 30×10^6 psi. The direction of the pressure is shown in Figure D-66.

To determine if a nonstandard shape had better characteristics than a standard shape, a semitoroidal corrugation (Figure D-66) commonly used in diaphragm design

was chosen for study and comparison with the somewhat nonstandard shapes shown in Figures D-68 through D-72.

Since many diaphragms respond nonlinearly with increasing pressure, calculations were performed with both Program MOLSA and Program NONLIN.

Table D-7 summarizes the results for the relative deflection of the center of the diaphragms for the linear and nonlinear calculations for p = 1.75 psi. The results show that an accurate estimate of diaphragm behavior requires a nonlinear calculation procedure.

The center deflection caused by an increasing pressure is shown in Figure D-76. The numbers on each line correspond to the five diaphragms. For lower pressures, the flat-plate diaphragm (Line No. 5 in Figure D-76) produced more deflection, but for larger pressures its advantage quickly disappeared. The limited effectiveness of the flat-plate diaphragm is further evidenced by examining Figure D-75 in which the outer-surface normal stress is shown for the region $0.85 \leq r \leq 1.25$. The solid line gives the relative stress, σ_ϕ/p, obtained from the nonlinear calculations for p = 1.75 psi. The broken line gives the relative stress, σ_ϕ/p, for the linear calculations. Note the high stress at the outer boundary. This condition only occurs for the flat-plate diaphragm. Figures D-67, D-69, D-71, and D-73 show the relative surface stresses for the different diaphragm shapes. These stresses are superposed on the shape of the diaphragm so that the diaphragm cross section corresponds to a zero stress level with tensile values being plotted above the line and compressive stresses below. Diaphragms Nos. 1 through 4 produce relative stresses of 5000 or less at the outer boundary, whereas Diaphragm No. 5 shows a value of 18,000.

Figure D-76 indicates that the most promising corrugation shape, based on a deflection comparison, is Diaphragm No. 4. Diaphragms Nos. 1 and 3 show some promise since the slopes of the deflection-pressure curves are changing gradually. The decreasing slope of the curve for Diaphragm No. 2 shows that less deflection will be produced with increasing pressure. Thus, on the basis of Figure D-76, the diaphragms which should be considered are Nos. 1, 3, and 4. It is noted that Diaphragm No. 4 (Figure D-73) also offers the best stress profile.

An examination of the stress distribution shows that there is a stress reversal in the outer convolutions at the middle of the convolution. In No. 4, this occurs at the intersection of the cone segments as shown in Figure D-73. Thus, the corner does not act as a stress raiser. The introduction of the flat-plate sections in Nos. 2 and 3 moves the corners to regions where there are significant bending stresses.

Thus, it appears that although the conical-segment convolution has abrupt changes in slope, these discontinuities are located at regions of zero stress. This may be the reason for good fatigue life reported in the literature for some aneroid capsules made of conical segments.

On the basis of this study it appears that a diaphragm incorporating conical segments shows promise of giving increased deflection capabilities.

D-IV. Parametric Analysis of Welded Bellows

A thorough parametric analysis of welded bellows could be a monumental task since the number of parameters which would have to be investigated is significantly greater than that required for the formed bellows study. In addition to this, a limited parametric study performed by Bell Aerosystems(D-1, D-2)* shows that there is so much interaction between parameters that the author concluded, "the strong influence of various individual geometric parameters and their apparent complex coupling effects on the stress-deflection relationships of welded bellows has been demonstrated. The folly of using approximate formulas, such as bending of flat plates, to calculate these relationships is clearly indicated."

The approach taken during the Battelle research program was to attempt to find, through selected theoretical analyses, a welded bellows configuration which would reduce the stress in the vicinity of the convolution root and crown.

A survey of the manufacturers' literature and technical reports on welded bellows indicated that in the majority of designs, the flat portion of the diaphragm was perpendicular to the bellows axis and the area in the vicinity of the weld bead was the most highly stressed region of the diaphragm. Exploratory theoretical analyses showed that these zones were indeed regions of maximum stress for both deflection and pressure loading. The regions near the welds include possible heat-affected zones in which the characteristics of the bellows material may have been changed by the welding process. Further, the notch at the inner surface of the weld can act as a stress raiser. Thus it would appear desirable to alter the design of welded bellows to reduce the stresses in the vicinity of both the root and crown welds.

Since there appeared to be no manufacturing reason why the flat portion of the diaphragm has to be perpendicular to the bellows axis, the welded-bellows study was directed toward determining whether a tilted flat section would provide a better stress pattern than a bellows which had a flat section perpendicular to the bellows axis. (This direction of research was suggested in part by the results of the diaphragm analyses where conical shapes show advantage over flat plates.)

The study progressed in three steps. First, a number of single-sweep bellows were analyzed to investigate gross changes in the stress pattern for different tilt angles. Next, a series of three-sweep bellows were studied to determine the effect of tilting the flats of a more realistic bellows. Since the results proved very promising, the third step was to investigate the possibility of obtaining an "optimum" bellows, at least for the size being studied. The remainder of the appendix describes these three steps in detail.

Variations in Tilt Angle of a Single-Sweep Welded Bellows

Initially the study was concerned with the effect of tilt-angle changes on the stress distribution throughout the leaves for a single-sweep bellows which had an inside radius of 1.5 inches and a span of 0.5 inch. The nomenclature used in describing the mathematical models is shown in Figure D-77. The four variations investigated are shown in

* References for Appendix D are listed on page D-15.

Figures D-78 through D-81. The mathematical model of each bellows consisted of six leaves so that the stresses in the third and fourth leaves would not be affected by the rotational restraint at the boundaries. Table D-8 gives the dimensions of the mathematical models. As indicated in Table D-9, each model had an upper chord angle of $\gamma = 15$ degrees. The lower-leaf chord angle varied from 15 to 0 degrees. The tangent angle Ψ is also given in Table D-9, along with the tilt angle which is the mean of the upper- and lower-leaf tangent angles.

In order to assess the effect of the rigidity of the weld bead at the junction of the leaves, a second mathematical model was considered. The model in this case consisted of the same bellows described above with the addition of cylindrical rings representing the weld bead at the inner and outer leaf junctions. This model did not include the stress concentration effect at the root of the weld. The length of the cylinder was taken equal to the thickness of the ply (0.006 in.). In all cases, the bellows were subjected to an axial load of 2 lb/in. on the outside circumference, shown as P in Figures D-78 through D-81.

The meridional inner surface stresses for the third and fourth leaves are shown in Figures D-82 through D-85. These stresses are superposed on the shape of the leaf so that the leaf cross section corresponds to a zero stress level. The solid lines give the results for the calculations in which no weld bead was considered, while the dotted line indicates the stress state when the weld bead was included in the mathematical model.

An examination of Figures D-82 through D-85 shows that the weld-bead effects are greater for the larger angle openings, i.e., lower chord angles of 15 and 10 degrees, but are not significant for the smaller openings (5 and 0 degrees). A careful examination of the stress changes in the bellows leaves shows that as the lower chord angle is decreased, the stress at the inside radius decreases, while the stress at the outside radius remains essentially constant. Thus it appears that a decrease in the tilt angle at the inside diameter produces a more favorable stress condition. The change in tilt angle at the outside diameter has apparently little effect, at least for the single-sweep bellows investigated, on the stress state at the outside diameter.

These results on single-sweep bellows demonstrate the possibility that an optimum tilt angle might exist, giving a low stress state near the weld bead. However, only one simple mathematical model was used in this investigation. In welded-bellows models such as the single-sweep bellows, many parameters are interdependent so that a variation in one parameter necessitates variation in other parameters as well. Thus, in varying the tilt angle for the weld juncture in the above model, it was necessary to vary not only the chord angle of the lower leaf, but also the radius of curvature of the lower leaf. (However, note from Table D-8 that the radius of curvature b varied by only 3.5 percent.) To obtain more information on the effect of angle changes when a flat is included in the bellows leaf, it was decided to investigate another mathematical model which consisted of three large sweeps, two small sweeps, and two flats per leaf.

Variations in the Tilt Angle of the Flats of a Three-Sweep Welded Bellows

Most welded bellows are formed with flat sections which are perpendicular to the bellows' axis at the root and crown of each leaf. These flat sections allow intimate contact between the bellows and the chill-block rings which act as heat sinks to keep the

bellows material cool during the welding process. One example of bellows of this type is represented by the 3-inch stainless steel welded bellows discussed in Appendix H. Figure H-2 shows the cross section of this bellows. A study of Figure H-2 shows that the leaves of this relatively "standard" bellows can be characterized as having interior regions composed of four toroidal segments joined at the root and crown to flat sections. At both the root and crown there is a relatively sharp bend in each leaf at the junction of the flat with the first toroidal segment. The theoretically calculated stress distributions for this bellows are shown in Figures H-7 through H-14 of Appendix H. Note that the maximum stresses for both axial deflection and internal pressure occur at the weld bead. It is believed that this is the most undesirable location for the maximum stresses to occur in welded bellows because of the notch effect at the weld and because of the possibility of weakened metal in the heat-affected zone. As shown in Figure H-2 the flat sections of the 3-inch bellows are horizontal (i.e., normal to the bellows' axis).

The results of the study of the single-sweep bellows discussed in the previous section indicated that tilting the flat sections of the bellows at an angle other than 90 degrees to the bellows axis might lead to a reduction in the stresses in the neighborhood of the weld. Consequently, a parametric study was performed to determine the effects of tilting the bellows flats.

Two basic models, similar to a "standard" three-sweep welded bellows, were chosen for the parametric study. The principal difference between the two basic models was in the chord angles of the bellows leaves. In the first model (designated Model No. 1) the upper and lower leaves had +5-degree and -5-degree chord angles respectively. In the second model (designated Model No. 2), the upper leaf had a +10-degree chord angle, and the lower leaf had a 0-degree chord angle. The bodies of both models had three major toroidal segments and two small toroidal segments. The small segments joined the major toroidal segments to the flats of the convolution roots and crowns. Nine cases were analyzed for each model in which the flats at the root or the crown were either normal to the bellows axis or tilted ±10 degrees.

Table D-10 lists the tilt angles assumed for the flat sections at the root and crown for each of the nine cases of Models No. 1 and 2. (The same tilt angles were assumed for the flats of both models.) Figure D-86 illustrates the configuration of Case 1 for Model No. 1, while Figure D-87 shows the cross section of Case 9 for Model No. 2.

Because the objective of this study was to isolate the effects of changing the tilt angles of the flats, the three main toroidal sections were made identical in the nine cases of each model. Furthermore, the lengths of the flat sections of the upper leaves were kept constant. To maintain continuity of the bellows sections, the included angle of the minor toroidal segments joining the flats to the main toroidal sections was changed as the tilt angles of the flat were changed. The lengths of the flats of the lower leaves were also changed slightly to maintain continuity with the upper leaves at the root and crown.

Tables D-11 and D-12 list the dimensions of the mathematical models of Cases 1, 5, and 9 for the two models. The main toroidal sections are Parts 3 through 5 for the upper leaf, and Parts 10 through 12 for the lower leaf. Parts 1, 2, 13, and 14 represent the flats and minor torus sections at the root, while Parts 6 through 9 represent the flats and minor toroidal sections at the crown. The mathematical models for the remaining cases were obtained from these cases by appropriately interchanging the

specifications of the minor torus sections and the flats at the root and crowns to obtain the appropriate flat angles.

The nine cases were analyzed for both axial compression and internal pressure. A unit axial deflection per unit length of bellows was assumed for axial compression, while the pressure load was assumed to be 1 psi. In order to reduce the effect of the end conditions on the stresses, two complete convolutions (four leaves) were analyzed, and only the stresses on the middle two leaves were considered. All calculations were made according to linear elastic shell theory.

Table D-13 gives the outer surface meridional and circumferential stresses at the root and crown for the axial compressive loading and internal pressure in Model No. 1. Table D-14 shows the same stresses for Model No. 2.

An examination of Table D-13 shows that as the angle of tilt of Parts 8 and 14 was reduced, that is, as Part 8 slanted down to the left and Part 14 slanted down to the right, a significant reduction in both the meridional and circumferential stresses was achieved. Similar reductions for the internal pressure loading are also shown in Table D-13.

Table D-14, which gives the stresses in Model No. 2, shows a similar reduction in the stresses for a change on the tilting of Parts 8 and 14. However, the optimum configuration was no longer Case 9 but Case 7. The reason for this was that a change in the tilt angle of the flats at the root had a significant effect on the stresses at the bellows crown for Model No. 2. For Model No. 1, there was almost no interaction. This is shown in Table D-13, by comparing Cases 1, 2, and 3, or 4, 5, and 6, or 7, 8, and 9 for the crown stresses. For example, the tilt angle at the crown was constant at 10 degrees for Cases 1, 2, and 3, and the crown stresses were nearly constant as the tilt angle varied at the root from -10 degrees to +10 degrees.

In Figures D-88 through D-99 the linear meridional circumferential outer surface stresses due to both axial loading and internal pressure are shown for the upper and lower leaves of Model No. 1. Figures D-100 through D-111 show the same stresses for Model No. 2.

The stresses in Figures D-88 through D-111 are superimposed on the shape of the leaf so that the leaf cross section corresponds to a zero stress level. The figures have been arranged in the following manner. Of Figures D-88 through D-99 which give results for Model No. 1, Figures D-88 through D-93 show stresses arising from axial loading, and Figures D-94 through D-99 are concerned with internal pressure. Further, Figures D-88 through D-90 give the stresses for the upper leaves, while Figures D-91 through D-93 give the stresses for the lower leaves. This sequence is followed for Model No. 2 in Figures D-100 through D-111.

An examination of Figures D-88 through D-93 clearly shows that, for Model No. 1, the angle which the flat-plate portions make with the bellows centerline has a significant effect on the stress level in the vicinity of the weld bead. The stresses due to internal pressure are similarly dependent on the tilt angle of the flat-plate segments of the bellows.

Model No. 2 was studied to assess the effect of changes in the chord angle. The individual leaves of Model No. 2 have the same shape as the leaves of Model No. 1, but

they are rotated 5 degrees in a counterclockwise direction: the 10-degree angle between the chords of the upper and lower leaves was maintained. The stress results for Model No. 2 are shown in detail for Cases 1, 5, and 9 in Figures D-100 through D-111. A similar reduction in the stresses for a change in the tilt angle of the flat segment is noted. However, the optimum case for this model occurred when the inside flat segment was sloped 10 degrees up to the left while the outside flat was sloped 10 degrees down to the right (Case 7).

In Table D-15, the spring rates for the two convolution models are shown for each study. Model No. 2 was generally stiffer. Case 1 gave the lowest spring rate in both models. Model No. 1, Case 5, which approximated a "standard" bellows (the flat-plate segments were horizontal at the inside and outside), was 13 percent more flexible than Case 9, which gave the best stress distribution for Model No. 1. However, for Model No. 2, the optimum shape, Case 7, was 7 percent more flexible than the standard shape, Case 5.

Investigation of an Optimum Shape for a Three-Sweep Welded Bellows

Since the results of the preceding section showed that significant differences in the stress distribution can be obtained by tilting the flats, it was decided to attempt to find an "optimum" shape for the two bellows just considered. In this study, an "optimum" shape was defined as one which had a negligible stress in the vicinity of the weld beads.

To accomplish this task, the models shown in Figures D-86 and D-87 were modified such that the flats at the roots and crown were tangent to the adjacent major torus sections and the minor toroidal sections were deleted from the configuration. The resulting shapes are shown in Figures D-112 and D-113. The dimensions of the mathematical models are given in Tables D-16 and D-17. As before, the model used in the computer calculations consisted of two convolutions so that the boundary conditions would not be a factor on the stress distribution on the middle two leaves.

The two models were analyzed according to linear-shell bending theory for both an axial compression and internal pressure loading. The relative meridional outer surface stresses for the upper and lower leaves for these loading conditions are shown in Figures D-114 through D-117. The leaf cross section corresponds to a zero stress state.

Compared with the stresses in Figures D-88 through D-111, Figures D-114 and D-115 show a dramatic decrease in the stress level at both the convolution root and crown for both types of loading. Thus, it appears that the shape, Figure D-112, chosen for study can be considered optimum. Of course, the lower stress level near the weld beads is not achieved without increasing the stiffness of the bellows. However, the spring rate for this bellows was 137 lb/in. which is only 15 percent stiffer than Case 9 for the Model No. 1 and 30 percent stiffer than Case 5 for the Model No. 2 (standard bellows).

For the second model shown in Figure D-113, the decrease in the stress level produced by the new arrangement of flats is significant although the stresses are not quite as small as those in the first model shown in Figure D-112. Figures D-116 and D-117 show the relative meridional outer surface stresses for axial compressive and internal pressure loading, respectively. The stress level at the convolution crown of this model could undoubtedly be reduced still further by additional modification of the tilt angle of the

flat. At the convolution root, it appears that the optimum tilt angle has been surpassed, although the stresses are low. It is recalled that according to the study described in the preceding section the most efficient model for the 0-degree to 10-degree bellows was not Case 9, from which the bellows in Figure D-113 was designed, but Case 7. A careful comparison of these stress figures shows that there is a significant amount of interaction between the tilting of the bellows flat, the cone angle, and the size of the minor toroidal sections. However, it is apparent from these studies that with a careful choice of the flat angles at both root and crown, a welded bellows can be designed with negligible stress levels in the vicinity of the weld beads to increase the operating life many fold. The slight increase in stiffness, which usually results from the tilting of the bellows flats can be compensated for in the design. Since the designer will have all of the information in this report, he can make the choice of parameters which will give him a bellows with the appropriate stiffness for a required number of operating cycles.

REFERENCES

D-1. Bell Aerosystems Company, "Study of Zero-Gravity Positive Expulsion Techniques", Report No. 8230-933004, June 1963, (N63-19964), (U).

D-2. Bell Aerosystems Company, "Study of Zero-Gravity Positive Expulsion Techniques", Report No. 8230-933007, April 1964, (U).

TABLE D-1. VALUES OF $t/\bar{R}$, $c/\bar{R}$, AND b/c USED IN DIFFERENT CASES OF PARAMETRIC ANALYSIS

Shape	Case	$t/\bar{R}$	$c/\bar{R}$	b/c
1	1.1	0.004	0.075	0.2
2	1.2		0.075	0.6
3	1.3		0.075	1.0
1	1.4		0.150	0.2
2	1.5		0.150	0.6
3	1.6		0.150	1.0
1	1.7		0.225	0.2
2	1.8		0.225	0.6
3	1.9		0.225	1.0
2	2.2	0.0067	0.075	0.6
3	2.3		0.075	1.0
1	2.4		0.150	0.2
2	2.5		0.150	0.6
3	2.6		0.150	1.0
1	2.7		0.225	0.2
2	2.8		0.225	0.6
3	2.9		0.225	1.0
3	3.3	0.02	0.075	1.0
1	3.4		0.150	0.2
2	3.5		0.150	0.6
3	3.6		0.150	1.0
1	3.7		0.225	0.2
2	3.8		0.225	0.6
3	3.9		0.225	1.0

TABLE D-2. MAXIMUM MERIDIONAL AND CIRCUMFERENTIAL STRESSES FOR OUTER AND INNER SURFACES DUE TO INTERNAL PRESSURE OF p = 1 psi FOR ALL CASES ANALYZED

Shape	Case	Meridional		Circumferential	
		Outer	Inner	Outer	Inner
1	1.1	-641*	606	-174	199
2	1.2	395*	-395	298	164
3	1.3	284	-283	330*	201
1	1.4	-2340*	2260	-1160	610
2	1.5	975*	-974	687	465
3	1.6	448	-443	549*	354
1	1.7	-4170*	3960	-2950	1630
2	1.8	1620*	-1620	1070	839
3	1.9	590	-580	721*	471
2	2.2	-163*	152	124	91
3	2.3	125	-124	157*	109
1	2.4	-917*	869	-359	229
2	2.5	440*	-439	307	191
3	2.6	232	-227	279*	180
1	2.7	-1750*	1670	-1060	559
2	2.8	700*	-696	483	368
3	2.9	302	-294	365*	242
3	3.3	-17	19	38*	37
1	3.4	-111*	99	29	35
2	3.5	-75*	-65	49	33
3	3.6	52	-50	60*	40
1	3.7	-248*	222	-87	66
2	3.8	124*	-122	85	56
3	3.9	73	-70	84*	57

* Indicates maximum stress.

TABLE D-3. MAXIMUM MERIDIONAL CONVOLUTION STRESSES FOR FOUR APPROXIMATE CONVOLUTION VARIATIONS AND TWO IMPROVED VARIATIONS OF 5-INCH SINGLE-PLY FORMED BELLOWS JD92

Mathematical Model	Relative Membrane Stress[a]	Relative Bending Stress[a], Outer Surface	Relative Stress[a], Inner Surface	Relative Stress[a], Outer Surface
Compression-Deflection Stresses				
Convolution Crown				
Variation No. 1	+7,463.79	-677,252	+684,716	-669,788
Variation No. 2	+8,088.53	-671,013	+679,102	-662,925
Variation No. 3	+8,898.54	-700,932	+709,830	-692,033
Variation No. 4	+9,258.62	-713,698	+722,956	-704,439
Variation No. 5	+7,510.31	-644.062	+651,572	-636,552
Variation No. 6	+7,451.85	-644,955	+652,406	-637,503
Convolution Root				
Variation No. 1	+8,509.98	+755,499	-746,989	+764,009
Variation No. 2	+9,222.28	+813,516	-804,294	+822,738
Variation No. 3	+10,145.4	+852,666	-842,521	+862,812
Variation No. 4	+10,556.4	+869,253	-858,697	+879,810
Variation No. 5	+8,594.92	+792,853	-784,258	+801,448
Variation No. 6	+8,014.38	+776,503	-768,489	+784,518
Internal Pressure Stresses				
Convolution Crown				
Variation No. 1	+17.0907	-413.204	+430.29	-396.11
Variation No. 2	+17.2103	-374.033	+391.24	-356.82
Variation No. 3	+17.2433	-375.927	+393.17	-358.68
Variation No. 4	+17.2557	-376.571	+393.83	-359.32
Variation No. 5	+17.8211	-426.070	+443.89	-408.25
Variation No. 6	+19.0537	-457.496	+476.55	-438.44
Convolution Root				
Variation No. 1	-17.9668	-459.961	+441.99	-477.93
Variation No. 2	-17.8302	-458.764	+440.93	-476.59
Variation No. 3	-17.7927	-458.449	+440.66	-476.24
Variation No. 4	-17.7780	-458.253	+440.48	-476.03
Variation No. 5	-18.1549	-501.969	+483.81	-520.12
Variation No. 6	-18.6447	-533.292	+514.65	-551.94

(a) To obtain stresses (in psi) due to deflection, multiply value by deflection in inches, divide by live length of bellows in inches (see page D-2).
To obtain stresses (in psi) due to pressure, multiply value by pressure in psi.
Plus values are tensile stresses; minus values are compressive stresses.

TABLE D-4. CIRCUMFERENTIAL CONVOLUTION STRESSES FOR FOUR APPROXIMATE VARIATIONS AND TWO IMPROVED VARIATIONS OF 5-INCH SINGLE-PLY FORMED BELLOWS JD92

Mathematical Model	Relative Membrane Stress[a]	Relative Bending Stress[a], Outer Surface	Relative Stress[a], Inner Surface	Relative Stress[a], Outer Surface
Compression-Deflection Stresses				
Convolution Crown				
Variation No. 1	-170,788	-203,176	+32,388	-373,963
Variation No. 2	-212,145	-201,304	-10,842	-413,449
Variation No. 3	-247,034	-210,280	-36,755	-457,314
Variation No. 4	-261,694	-214,109	-47,585	-475,804
Variation No. 5	-201,128	-193,219	-7,909	-394,347
Variation No. 6	-211,554	-193,485	-18,068	-405,041
Convolution Root				
Variation No. 1	+182,951	+226,650	-43,699	+409,601
Variation No. 2	+207,616	+244,055	-36,439	+451,671
Variation No. 3	+247,829	+255,800	-7,917	+503,629
Variation No. 4	+264,651	+260,776	+3,875	+525,427
Variation No. 5	+183,595	+237,856	-54,263	+421,449
Variation No. 6	+179,993	+232,951	-52,958	+412,944
Internal Pressure Stresses				
Convolution Crown				
Variation No. 1	+39.8208	-123.961	+163.78	-84.14
Variation No. 2	+33.8562	-112.210	+146.07	-78.35
Variation No. 3	+37.1844	-112.778	+149.96	-75.59
Variation No. 4	+38.3877	-112.971	+151.36	-74.58
Variation No. 5	+21.8896	-127.821	+149.71	-105.93
Variation No. 6	+14.6292	-137.249	+151.88	-122.62
Convolution Root				
Variation No. 1	+46.3967	-137.988	+184.39	-91.59
Variation No. 2	+57.3028	-137.629	+194.93	-80.33
Variation No. 3	+60.8525	-137.535	+198.39	-76.68
Variation No. 4	+62.0356	-137.476	+199.51	-75.44
Variation No. 5	+59.6044	-150.591	+210.20	-90.99
Variation No. 6	+59.0096	-159.988	+219.00	-100.98

(a) To obtain stresses (in psi) due to deflection, multiply value by deflection in inches, divide by live length of bellows in inches (see page D-2).
To obtain stresses (in psi) due to pressure, multiply value by pressure in psi.
Plus values are tensile stresses; minus values are compressive stresses.

TABLE D-5. NOMINAL DIMENSIONS OF SINGLE-PLY 5-INCH BELLOWS AND CALCULATION OF BELLOWS PARAMETERS

Ply thickness (t)	0.010 in.
Convolution root diameter	5.00 in.
Convolution height	0.350 in.
Live Length	4.00 in.
Number of convolutions	12
C (1/2 convolution height = $\frac{0.350}{2}$)	0.175 in.
$\bar{R}$ (1/2 convolution root diameter + C = $\frac{5.00}{2}$ + 0.175)	2.675 in.
b - Torus radius ($\frac{\text{Live length - 2 x No. of conv. x t}}{\text{4 x No. of conv.}}$) = $\frac{4.00 - 2 \times 12 \times 0.010}{4 \times 12}$)	0.078 in.

TABLE D-6. PARAMETRIC VALUES OF NOMINAL 5-INCH BELLOWS AND NEAREST PARAMETRIC MODEL

Parametric Ratios	Nominal 5-inch Bellows	Nearest Parametric Model (Figures D-5 and D-6)
$\frac{b}{c}$	0.445	0.6
$\frac{t}{\bar{R}}$	0.00374	0.004
$\frac{C}{\bar{R}}$	0.0654	0.075

TABLE D-7. RELATIVE DEFLECTION, w/p*, AT CENTER OF DIAPHRAGM BY LINEAR AND NONLINEAR BENDING THEORIES FOR p = 1.75 PSI

Diaphragm	Linear	Nonlinear	% Difference
1	0.01928	0.01134	41.2
2	0.02061	0.01194	42.1
3	0.01973	0.01190	39.7
4	0.02281	0.01323	42.0
5	0.08224	0.00983	88.0

* w = deflection, inches; p = pressure, psi.

TABLE D-8. LEAF CHARACTERISTICS OF WELDED BELLOWS SHOWN IN FIGURES D-78 THROUGH D-81

Model	Leaf	a	b	φ Initial	φ Final
1	upper	1.8660	-0.5176	45	-15
	lower	1.6340	0.5176	135	195
2	upper	1.8660	-0.5176	45	-15
	lower	1.6736	0.5077	140	200
3	upper	1.8660	-0.5176	45	-15
	lower	1.7121	0.5019	145	205
4	upper	1.8660	-0.5176	45	-15
	lower	1.7500	0.5000	150	210

TABLE D-9. CHARACTERISTICS OF BELLOWS JUNCTION FOR SINGLE-SWEEP BELLOWS IN FIGURE D-77

	Chord Angle, γ		Tangent Angle, ψ				Tilt Angle, Degrees*	
			Upper		Lower			
Model	Upper	Lower	ID	OD	ID	OD	ID	OD
1	15	15	45	-75	15	-45	60.0	-60.0
2	15	10	45	-75	70	-50	57.5	-62.5
3	15	5	45	-75	65	-55	55.0	-65.0
4	15	0	45	-75	60	-60	52.5	-67.5

* Tilt angle is the mean of the upper and lower tangent angle.

TABLE D-10. TILT ANGLE OF FLAT SEGMENTS IN MODEL NO. 1 AND MODEL NO. 2 3-SWEEP WELDED BELLOWS

	Tilt Angle, Degrees*	
Case	Root	Crown
1	-10	10
2	0	10
3	10	10
4	-10	0
5	0	0
6	10	0
7	-10	-10
8	0	-10
9	10	-10

* Tilt angle is the mean of the upper and lower tangent angle.

TABLE D-11. DIMENSIONS FOR MATHEMATICAL MODELS OF CASES 1, 5, AND 9 USED IN A STUDY OF THE EFFECT OF FLAT SECTIONS ON THE STRESSES IN WELDED BELLOWS MODEL NO. 1

	Case 1				Case 5				Case 9			
Part	a*	b	φ_i	φ_f	a	b	φ_i	φ_f	a	b	φ_i	φ_f
1	2.1287	0.080000	170	-	2.1146	0.080000	180	-	2.0982	0.080000	190	-
2	2.0346	0.087835	170	205	2.0346	0.087835	180	205	2.0346	0.087835	190	205
3	1.9233	-0.17567	205	145	1.9233	-0.17567	205	145	1.9233	-0.17567	205	145
4	1.7217	0.17567	145	205	1.7217	0.17567	145	205	1.7217	0.17567	145	205
5	1.5733	-0.17567	205	145	1.5733	-0.17567	205	145	1.5733	-0.17567	205	145
6	1.4222	0.087835	145	190	1.4222	0.087835	145	180	1.4222	0.087835	145	170
7	1.4069	0.08000	190	-	1.4222	0.080000	180	-	1.4374	0.080000	170	-
8	1.3281	0.094488	10	-	1.3421	0.093259	0	-	1.3586	0.094488	-10	-
9	1.4354	-0.087835	10	-25	1.4354	-0.087835	0	-25	1.4354	-0.087835	-10	-25
10	1.5467	0.17567	-25	35	1.5467	0.17567	-25	35	1.5467	0.17567	-25	35
11	1.7483	-0.17567	35	-25	1.7483	-0.17567	35	-25	1.7483	-0.17567	35	-25
12	1.8967	0.17567	-25	35	1.8967	0.17567	-25	35	1.8967	0.17567	-25	35
13	2.0479	-0.087835	35	-10	2.0479	-0.087835	35	0	2.0479	-0.087835	35	10
14	2.0631	0.066538	-10	-	2.0479	0.066741	0	-	2.0326	0.06628	10	-

* The dimensions of a and b are inches. The dimensions of φ_i and φ_f are degrees.

TABLE D-12. DIMENSIONS FOR MATHEMATICAL MODELS OF CASES 1, 5, AND 9 USED IN A STUDY OF THE EFFECT OF TILT OF FLAT SECTIONS ON THE STRESSES IN WELDED BELLOWS MODEL NO. 2

	Case 1				Case 5				Case 9			
Part	a*	b	φ_i	φ_f	a	b	φ_i	φ_f	a	b	φ_i	φ_f
1	2.1221	0.08000	170	-	2.1079	0.08000	180	-	2.0912	0.08000	190	-
2	2.0279	0.08885	170	200	2.0279	0.08885	180	200	2.0279	0.08885	190	200
3	1.9367	-0.17777	200	140	1.9367	-0.17777	200	140	1.9367	-0.17777	200	140
4	1.7083	0.17777	140	200	1.7083	0.17777	140	200	1.7083	0.17777	[illegible]	200
5	1.5867	-0.17777	200	140	1.5867	-0.17777	200	140	1.5867	-0.17777	200	140
6	1.4154	0.08885	140	190	1.4154	0.08885	140	180	1.4154	0.08885	140	170
7	1.4000	0.08000	190	-	1.4154	0.08000	180	-	1.4308	0.08000	170	-
8	1.3212	0.09279	10	-	1.3354	0.09336	0	-	1.3520	0.09333	-10	-
9	1.4288	-0.08750	10	-30	1.4288	-0.08750	0	-30	1.4288	-0.08750	-10	-30
10	1.5600	0.17500	-30	30	1.5600	0.17500	-30	30	1.5600	0.17500	-30	30
11	1.7350	-0.17500	30	-30	1.7350	-0.17500	30	-30	1.7350	-0.17500	30	-30
12	1.9100	0.17500	-30	30	1.9100	0.17500	-30	30	1.9100	0.17500	-30	30
13	2.0413	-0.08750	30	-10	2.0413	-0.08750	30	0	2.0413	-0.08750	30	10
14	2.0564	0.06667	-10	-	2.0413	0.06664	0	-	2.0261	0.06619	10	-

* The dimensions of a and b are inches. The dimensions of φ_i and φ_f are degrees.

TABLE D-13. OUTER SURFACE STRESSES AT ROOT (BEGINNING OF PART 8) AND CROWN (END OF PART 14) IN BELLOWS MODEL NO. 1 DUE TO AXIAL COMPRESSIVE LOADING AND INTERNAL PRESSURE

	Compressive Loading				Internal Pressure			
	Meridional		Circumferential		Meridional		Circumferential	
Case*	Root	Crown	Root	Crown	Root	Crown	Root	Crown
1	-95,620	68,610	-46,670	32,380	-11,770	-9,540	-4,670	-3,560
2	-74,900	72,430	-28,300	33,770	-9,220	-8,810	-2,670	-3,240
3	-41,100	76,110	-12,050	35,420	-5,190	-8,200	-1,030	-2,970
4	-97,640	56,130	-47,470	23,680	-11,200	-7,580	-4,420	-2,330
5	-69,820	54,160	-26,330	22,780	-8,800	-6,990	-2,520	-2,090
6	-42,160	62,810	-12,400	26,240	-4,970	-6,480	-970	-1,890
7	-95,490	39,740	-46,320	15,980	-10,680	-5,350	-4,170	-1,380
8	-78,300	44,050	-29,430	17,801	-8,400	-4,910	-2,380	-1,200
9	-43,210	46,810	-12,650	18,730	-4,760	-4,530	-910	-1,060

* Table D-10 gives tilt angles for flat segments.

TABLE D-14. OUTER SURFACE STRESSES AT ROOT (BEGINNING OF PART 8) AND CROWN (END OF PART 14) IN BELLOWS MODEL NO. 2 DUE TO AXIAL COMPRESSIVE LOADING AND INTERNAL PRESSURE

	Compressive Loading				Internal Pressure			
	Meridional		Circumferential		Meridional		Circumferential	
Case*	Root	Crown	Root	Crown	Root	Crown	Root	Crown
1	-86,210	61,760	-38,340	22,750	-11,200	-9,210	-4,080	-3,560
2	-77,330	91,040	-19,240	33,440	-8,220	-8,720	-2,150	-3,280
3	-37,370	117,610	3,560	43,440	-4,260	-8,180	-640	-3,060
4	-64,500	43,400	-28,700	18,550	-10,690	-8,360	-3,860	-2,860
5	-63,760	70,630	-16,050	29,940	-7,890	-7,600	-2,050	-2,560
6	-33,750	99,390	2,790	42,100	-4,110	-7,090	-630	-2,350
7	-46,130	26,850	-20,500	12,630	-10,160	-6,540	-3,630	-2,060
8	-52,350	50,260	-13,250	23,330	-7,540	-5,880	-1,950	-1,780
9	-28,380	72,270	2,140	33,370	-3,980	-5,450	-620	-1,590

* Table D-10 gives tilt angles for flat segments.

TABLE D-15. RELATIVE SPRING RATES FOR TWO WELDED BELLOWS FOR NINE DIFFERENT FLAT CONFIGURATIONS (CALCULATED FOR TWO CONVOLUTIONS)

Case*	Model No. 1	Model No. 2
1	92.5	100.7
2	100.7	112.5
3	101.3	121.0
4	96.5	104.9
5	105.5	116.8
6	113.7	126.9
7	100.3	109.6
8	110.1	123.5
9	119.1	137.9

* Table D-10 gives tilt angles for flat segments.

TABLE D-16. DIMENSIONS OF MATHEMATICAL MODEL SHOWN IN FIGURE D-112

Part No.	Shell Type	Coordinate, degree		Radii, inches	
		Initial	Final	a	b
1	Conical	215.0		2.0896	0.08
2	Toroidal	215.0	145.0	1.9233	-0.1757
3	Toroidal	145.0	205.0	1.7217	0.1757
4	Toroidal	205.0	145.0	1.5733	-0.1757
5	Conical	145.0		1.4725	0.11
6	Conical	-35.0		1.3824	0.0776
7	Toroidal	-35.0	35.0	1.5467	0.1757
8	Toroidal	35.0	-25.0	1.7483	-0.1757
9	Toroidal	-25.0	35.0	1.8967	0.1757
10	Conical	35.0		1.9975	0.1124

Thickness of bellows = 0.005 inch

TABLE D-17. DIMENSIONS OF MATHEMATICAL MODEL SHOWN IN FIGURE D-113

Part No.	Shell Type	Coordinate, degree		Radii, inches	
		Initial	Final	a	b
1	Conical	210.0		2.0949	0.08
2	Toroidal	210.0	140.0	1.9367	-0.1777
3	Toroidal	140.0	200.0	1.7083	0.1777
4	Toroidal	200.0	140.0	1.5867	-0.1777
5	Conical	140.0		1.4725	0.11
6	Conical	-40.0		1.4018	0.0774
7	Toroidal	-40.0	30.0	1.5600	0.1750
8	Toroidal	30.0	-30.0	1.7350	-0.1750
9	Toroidal	-30.0	30.0	1.9100	0.1750
10	Conical	30.0		1.9975	0.1124

Thickness of bellows = 0.005 inch

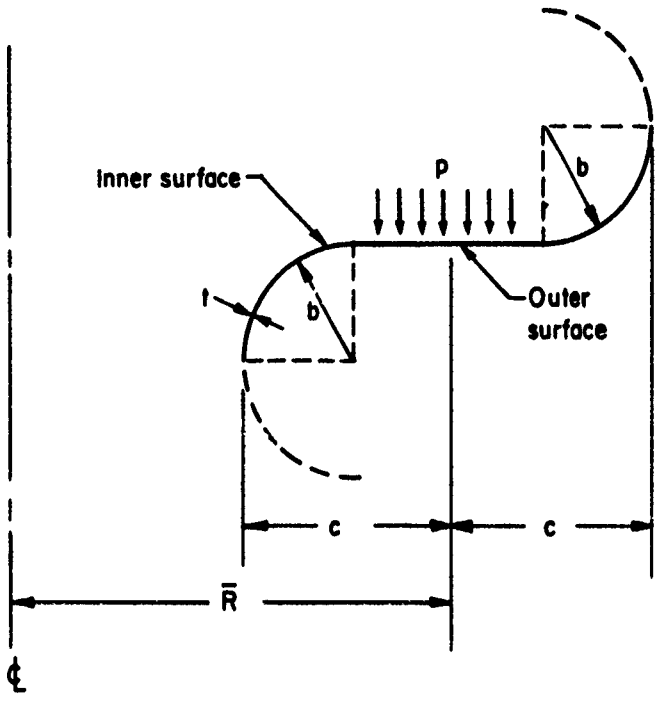

FIGURE D-1. ILLUSTRATION OF NOMENCLATURE USED FOR BELLOWS DIMENSIONS

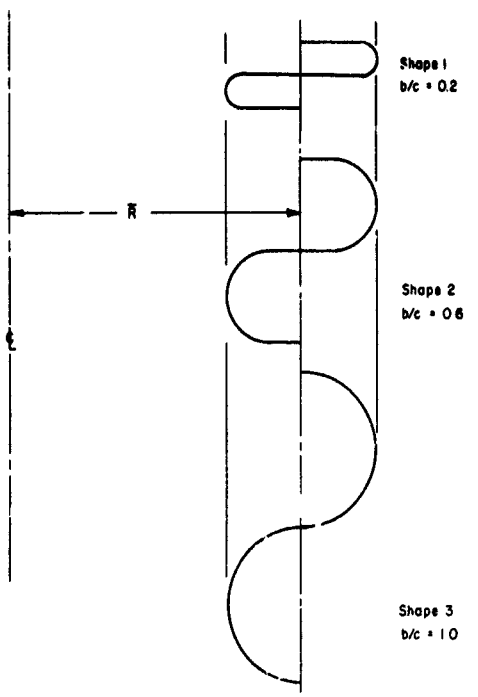

FIGURE D-2. ILLUSTRATION OF CONVOLUTION SHAPES FOR DIFFERENT VALUES OF b/c

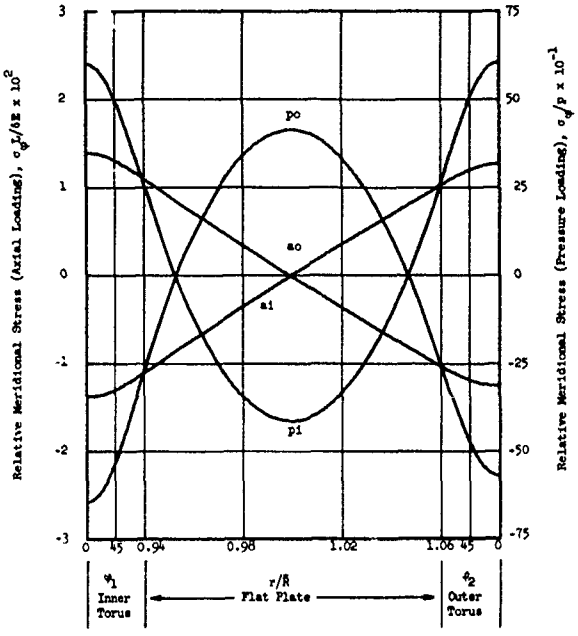

FIGURE D-3. RELATIVE MERIDIONAL SURFACE STRESSES FOR AXIAL LOADING AND INTERNAL PRESSURE IN BELLOWS OF SHAPE 1 WITH $t/\bar{R} = 0.004$ AND $c/\bar{R} = 0.075$

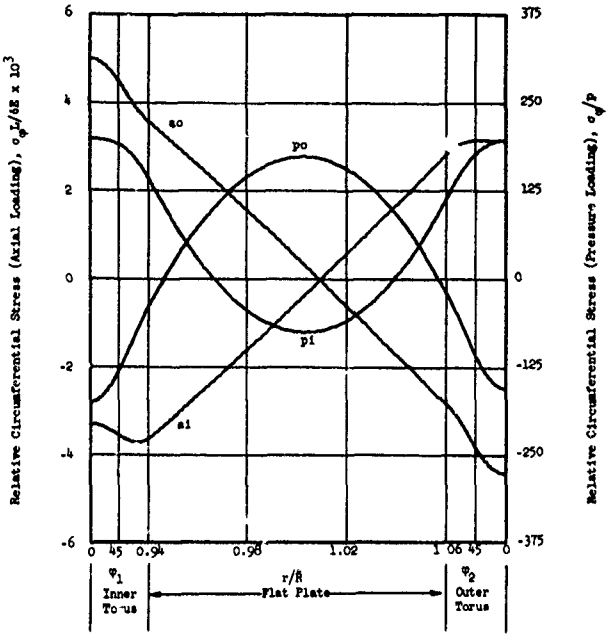

FIGURE D-4. RELATIVE CIRCUMFERENTIAL SURFACE STRESSES FOR AXIAL LOADING AND INTERNAL PRESSURE IN BELLOWS OF SHAPE 1 WITH $t/\bar{R} = 0.004$ AND $c/\bar{R} = 0.075$

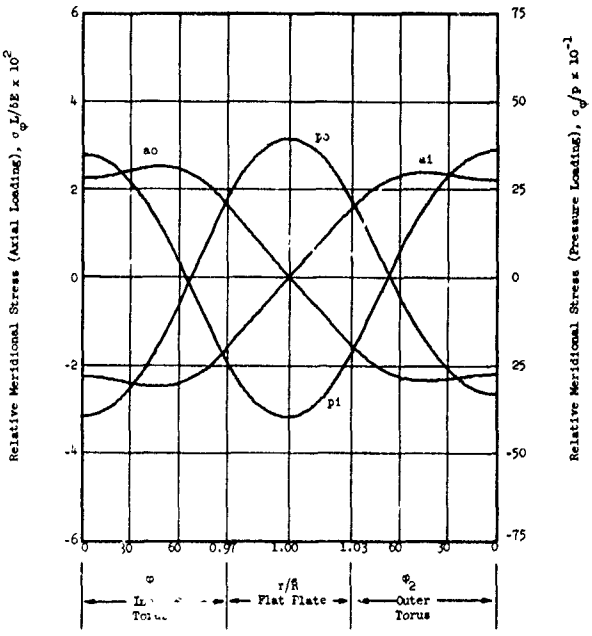

FIGURE D-5. RELATIVE MERIDIONAL SURFACE STRESSES FOR AXIAL LOADING AND INTERNAL PRESSURE IN BELLOWS OF SHAPE 2 WITH $t/\bar{R} = 0.004$ AND $c/\bar{R} = 0.075$

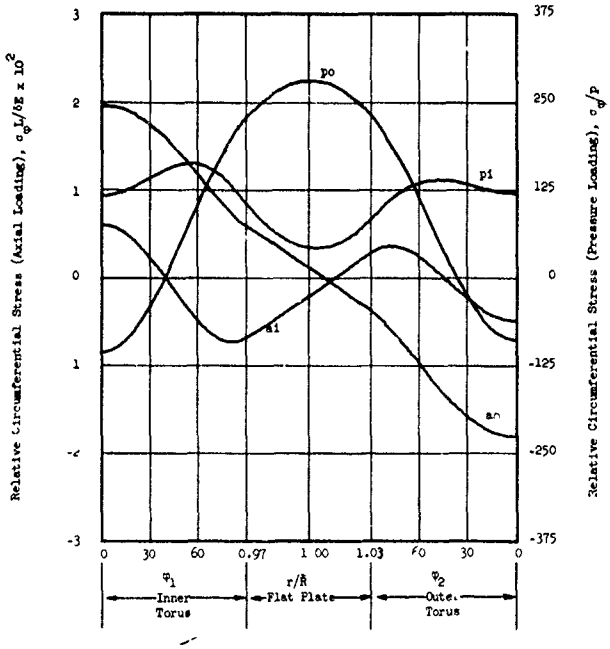

FIGURE D-6. RELATIVE CIRCUMFERENTIAL SURFACE STRESSES FOR AXIAL LOADING AND INTERNAL PRESSURE IN BELLOWS OF SHAPE 2 WITH $t/\bar{R} = 0.004$ AND $c/\bar{R} = 0.075$

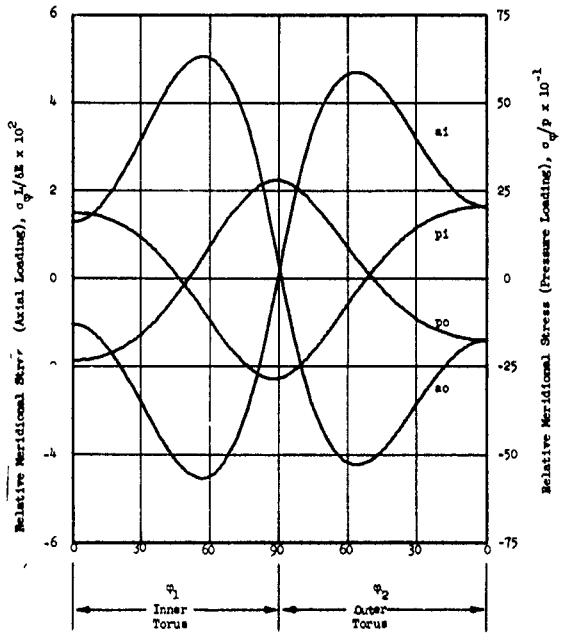

FIGURE D-7. RELATIVE MERIDIONAL SURFACE STRESSES FOR AXIAL LOADING AND INTERNAL PRESSURE IN BELLOWS OF SHAPE 3 WITH $t/\bar{R} = 0.004$ AND $c/\bar{R} = 0.075$

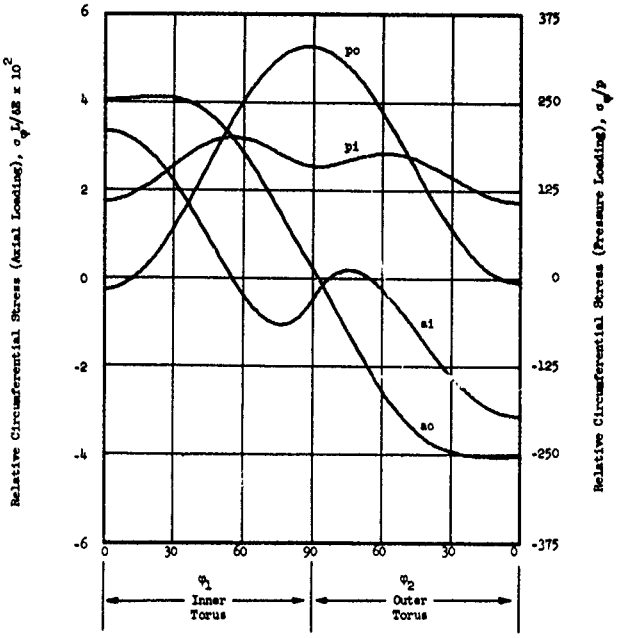

FIGURE D-8. RELATIVE CIRCUMFERENTIAL SURFACE STRESSES FOR AXIAL LOADING AND INTERNAL PRESSURE IN BELLOWS OF SHAPE 3 WITH $t/\bar{R} = 0.004$ AND $c/\bar{R} = 0.075$

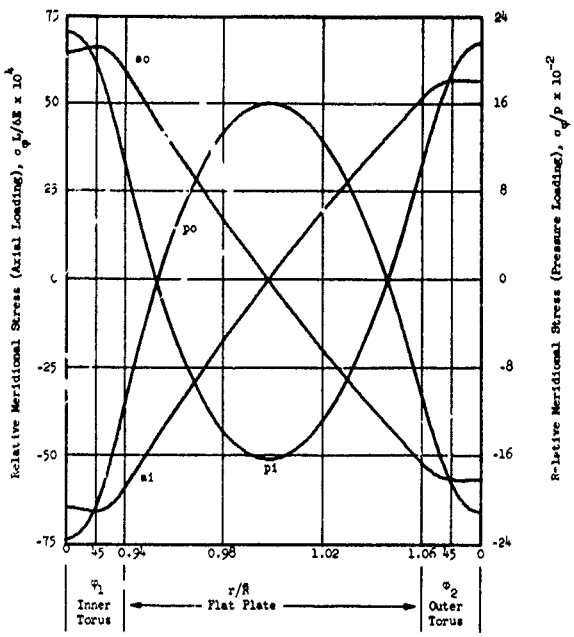

FIGURE D-9. RELATIVE MERIDIONAL SURFACE STRESSES FOR AXIAL LOADING AND INTERNAL PRESSURE IN BELLOWS OF SHAPE 1 WITH $t/\bar{R} = 0.004$ AND $c/\bar{R} = 0.150$

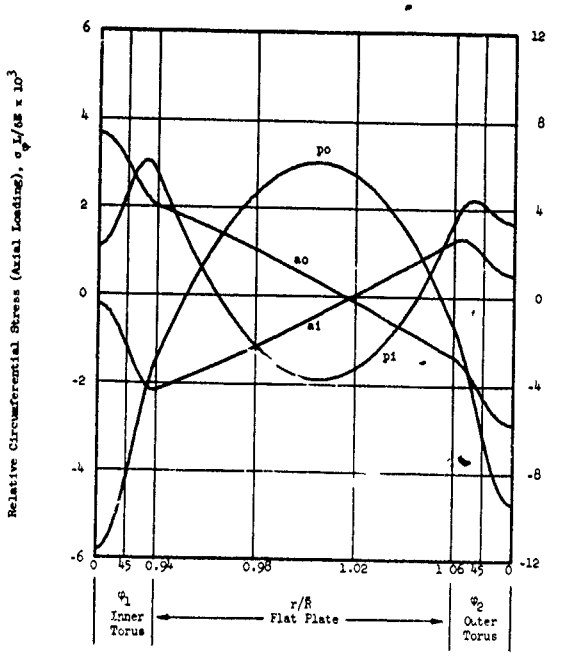

FIGURE D-10. RELATIVE CIRCUMFERENTIAL SURFACE STRESSES FOR AXIAL LOADING AND INTERNAL PRESSURE IN BELLOWS OF SHAPE 1 WITH $t/\bar{R} = 0.004$ AND $c/\bar{R} = 0.150$

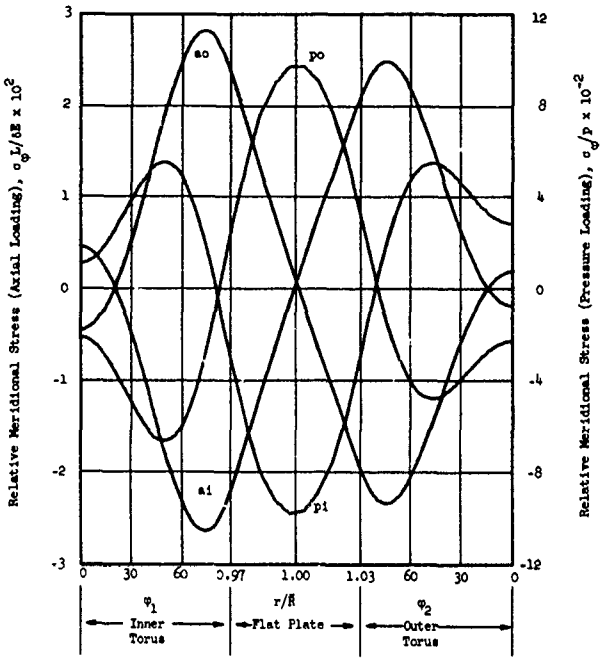

FIGURE D-11. RELATIVE MERIDIONAL SURFACE STRESSES FOR AXIAL LOADING AND INTERNAL PRESSURE IN BELLOWS OF SHAPE 2 WITH $t/\bar{R} = 0.004$ AND $c/\bar{R} = 0.150$

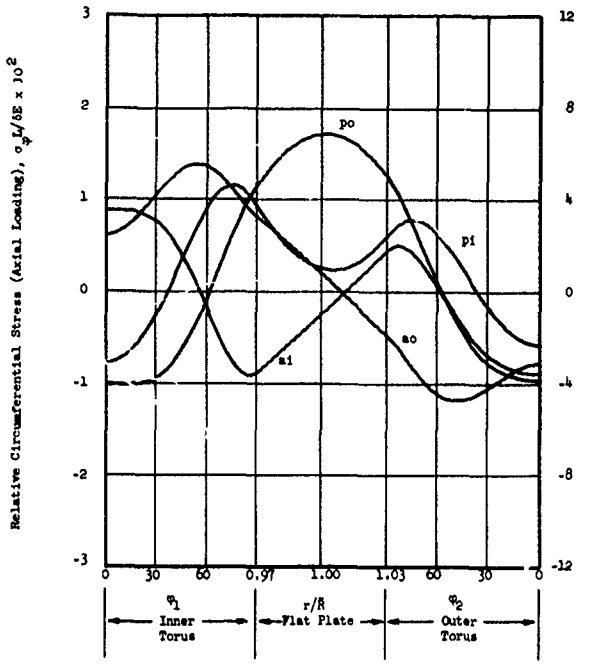

FIGURE D-12. RELATIVE CIRCUMFERENTIAL SURFACE STRESSES FOR AXIAL LOADING AND INTERNAL PRESSURE IN BELLOWS OF SHAPE 2 WITH $t/\bar{R} = 0.004$ AND $c/\bar{R} = 0.150$

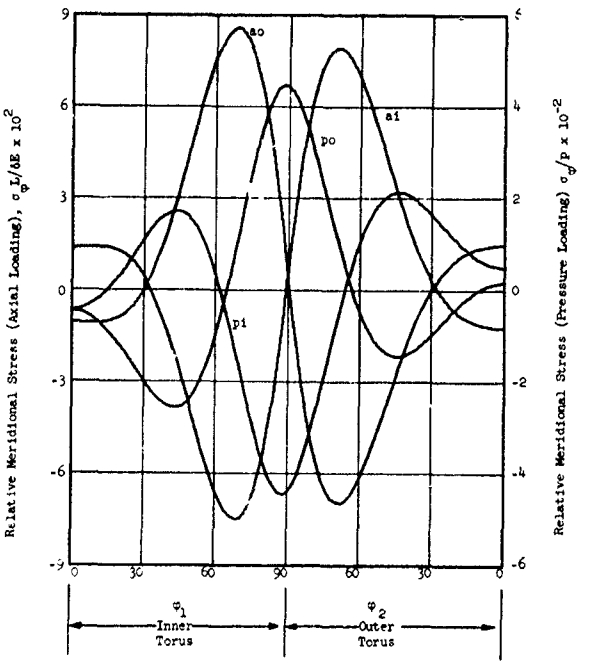

FIGURE D-13. RELATIVE MERIDIONAL SURFACE STRESSES FOR AXIAL LOADING AND INTERNAL PRESSURE IN BELLOWS OF SHAPE 3 WITH $t/\bar{R} = 0.004$ AND $c/\bar{R} = 0.150$

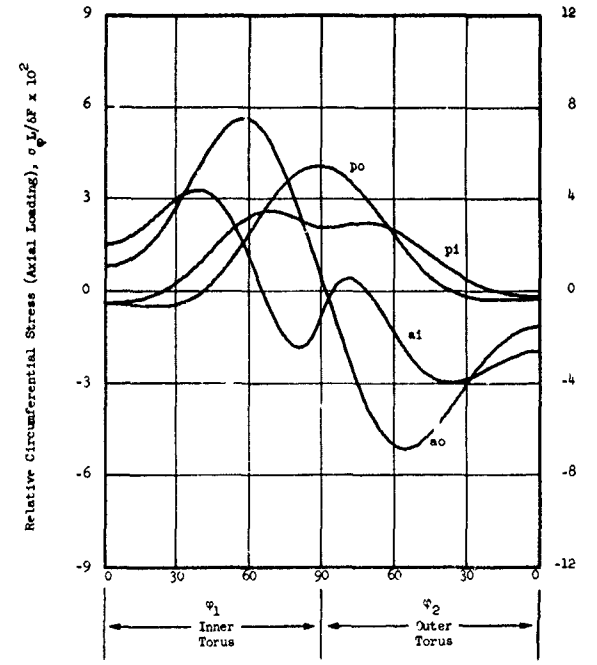

FIGURE D-14. RELATIVE CIRCUMFERENTIAL SURFACE STRESSES FOR AXIAL LOADING AND INTERNAL PRESSURE IN BELLOWS OF SHAPE 3 WITH $t/\bar{R} = 0.004$ AND $c/\bar{R} = 0.150$

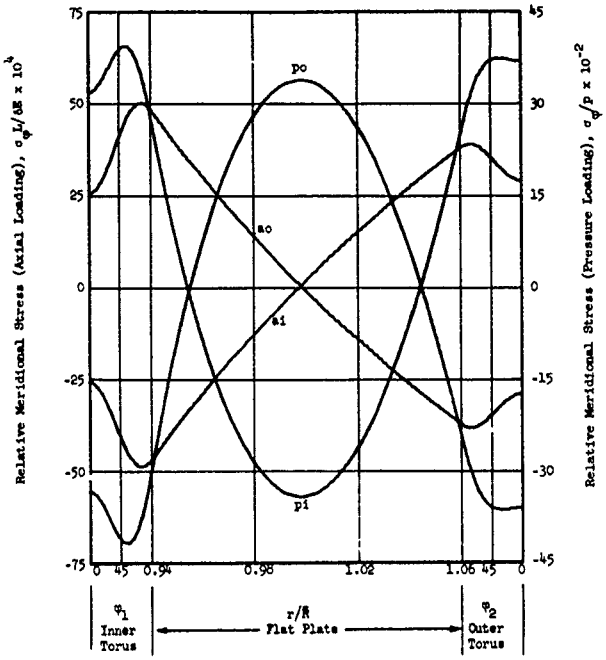

FIGURE D-15. RELATIVE MERIDIONAL SURFACE STRESSES FOR AXIAL LOADINC AND INTERNAL PRESSURE IN BELLOWS OF SHAPE 1 WITH $t/\bar{R} = 0.004$ AND $c/\bar{R} = 0.225$

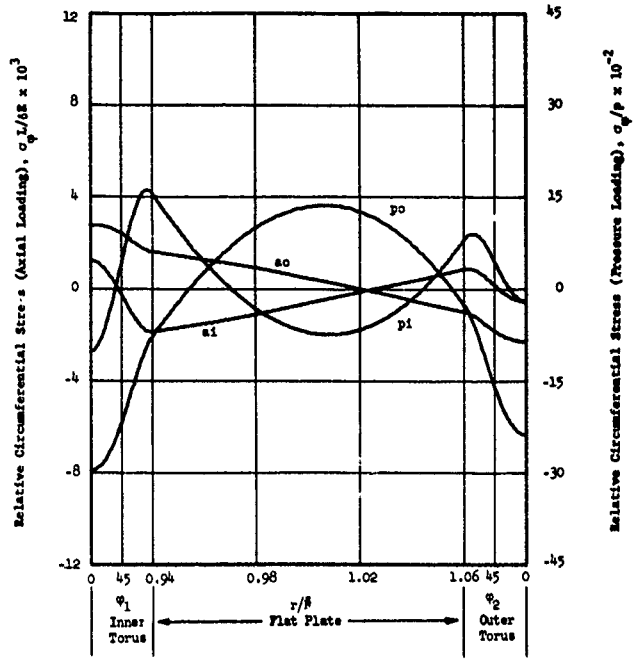

FIGURE D-16. RELATIVE CIRCUMFERENTIAL SURFACE STRESSES FOR AXIAL LOADING AND INTERNAL PRESSURE IN BELLOWS OF SHAPE 1 WITH $t/\bar{R} = 0.004$ AND $c/\bar{R} = 0.225$

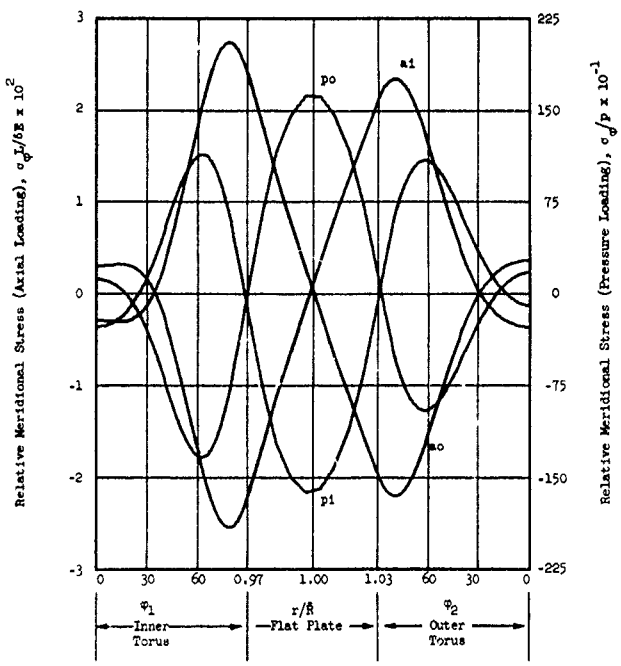

FIGURE D-17. RELATIVE MERIDIONAL SURFACE STRESSES FOR AXIAL LOADING AND INTERNAL PRESSURE IN BELLOWS OF SHAPE 2 WITH $t/\bar{R} = 0.004$ AND $c/\bar{R} = 0.225$

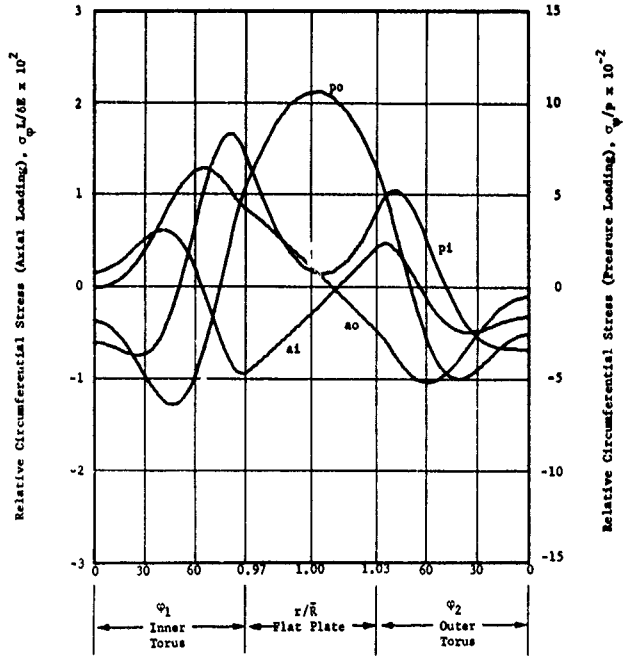

FIGURE D-18. RELATIVE CIRCUMFERENTIAL SURFACE STRESSES FOR AXIAL LOADING AND INTERNAL PRESSURE IN BELLOWS OF SHAPE 2 WITH $t/\bar{R} = 0.004$ AND $c/\bar{R} = 0.225$

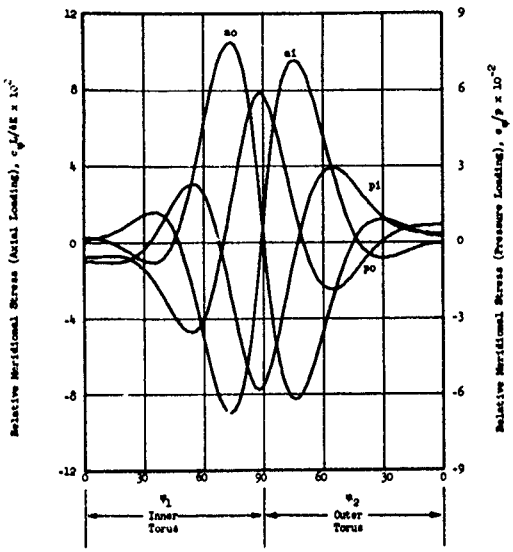

FIGURE D-19. RELATIVE MERIDIONAL SURFACE STRESSES FOR AXIAL LOADING AND INTERNAL PRESSURE IN BELLOWS OF SHAPE 3 WITH $t/\overline{R} = 0.004$ and $c/\overline{R} = 0.225$

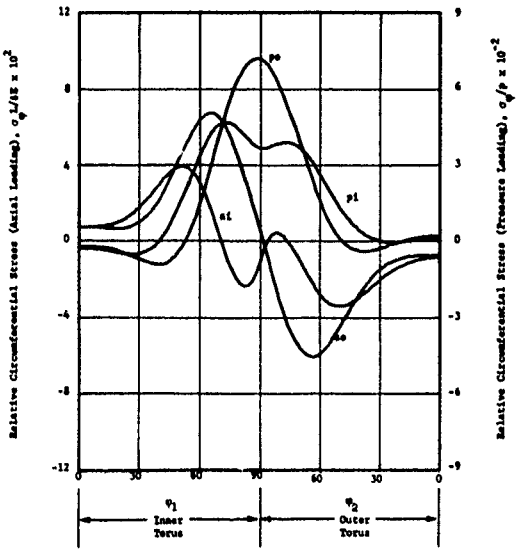

FIGURE D-20. RELATIVE CIRCUMFERENTIAL SURFACE STRESSES FOR AXIAL LOADING AND INTERNAL PRESSURE IN BELLOWS OF SHAPE 3 WITH $t/\overline{R} = 0.004$ AND $c/\overline{R} = 0.225$

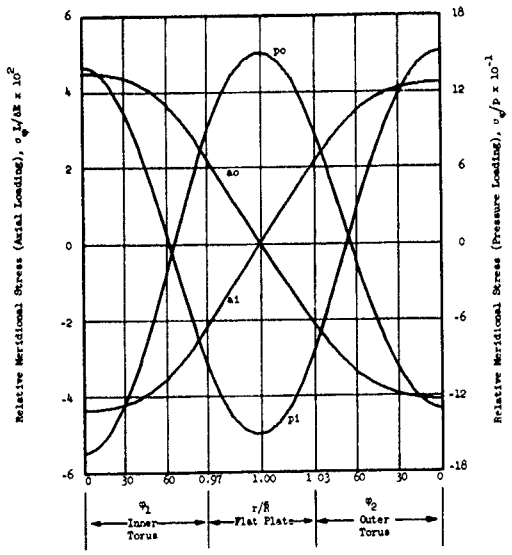

FIGURE D-21. RELATIVE MERIDIONAL SURFACE STRESSES FOR AXIAL LOADING AND INTERNAL PRESSURE IN BELLOWS OF SHAPE 2 WITH $t/\overline{R} = 0.0067$ AND $c/\overline{R} = 0.075$

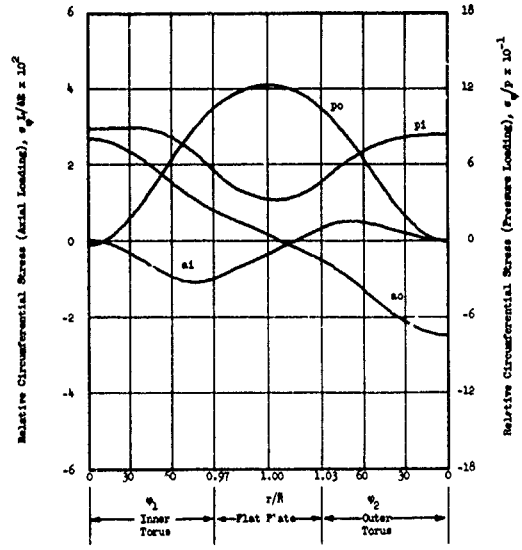

FIGURE D-22. RELATIVE CIRCUMFERENTIAL SURFACE STRESSES FOR AXIAL LOADING AND INTERNAL PRESSURE IN BELLOWS OF SHAPE 2 WITH $t/\overline{R} = 0.0067$ AND $c/\overline{R} = 0.075$

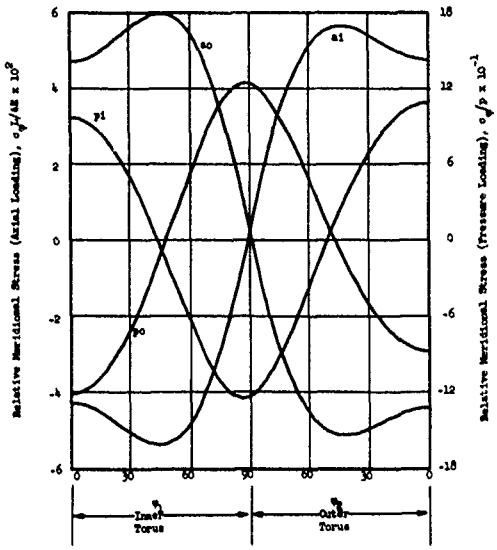

FIGURE D-23. RELATIVE MERIDIONAL SURFACE STRESSES FOR AXIAL LOADING AND INTERNAL PRESSURE IN BELLOWS OF SHAPE 3 WITH $t/\bar{R} = 0.0067$ AND $c/\bar{R} = 0.075$

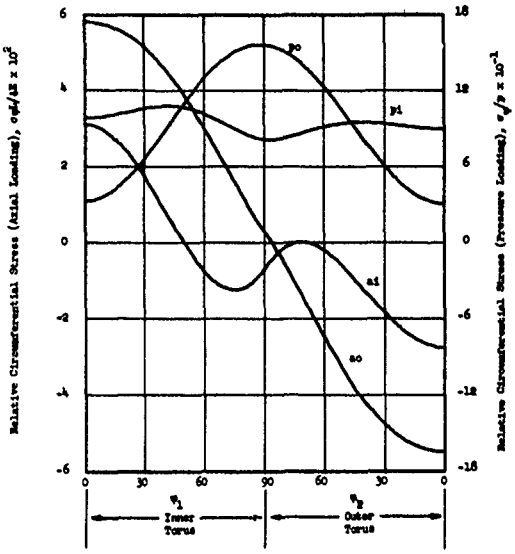

FIGURE D-24. RELATIVE CIRCUMFERENTIAL SURFACE STRESSES FOR AXIAL LOADING AND INTERNAL PRESSURE IN BELLOWS OF SHAPE 3 WITH $t/\bar{R} = 0.0067$ AND $c/\bar{R} = 0.075$

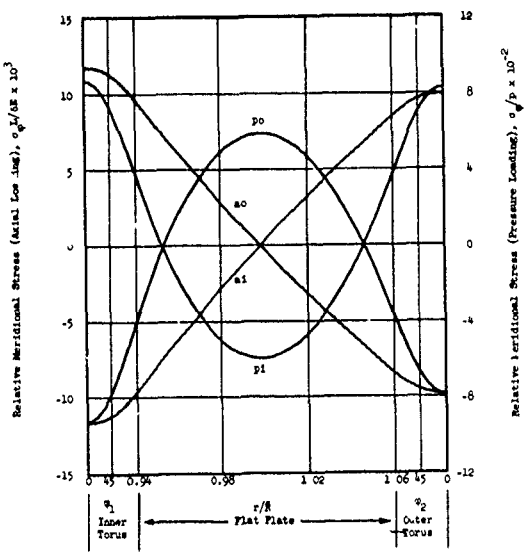

FIGURE D-25. RELATIVE MERIDIONAL SURFACE STRESSES FOR AXIAL LOADING AND INTERNAL PRESSURE IN BELLOWS OF SHAPE 1 WITH $t/\bar{R} = 0.0067$ AND $c/\bar{R} = 0.150$

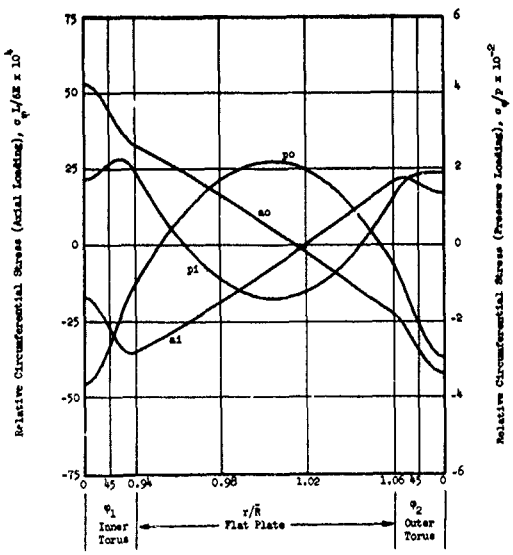

FIGURE D-26. RELATIVE CIRCUMFERENTIAL SURFACE STRESSES FOR AXIAL LOADING AND INTERNAL PRESSURE IN BELLOWS OF SHAPE 1 WITH $t/\bar{R} = 0.0067$ AND $c/\bar{R} = 0.150$

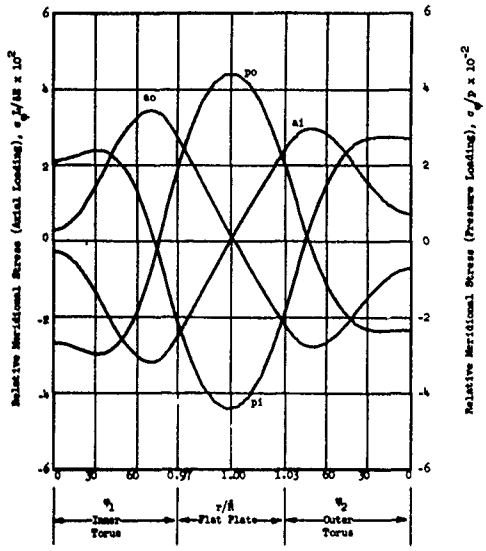

FIGURE D-27. RELATIVE MERIDIONAL SURFACE STRESSES FOR AXIAL LOADING AND INTERNAL PRESSURE IN BELLOWS OF SHAPE 2 WITH $t/\overline{R} = 0.0067$ AND $c/\overline{R} = 0.150$

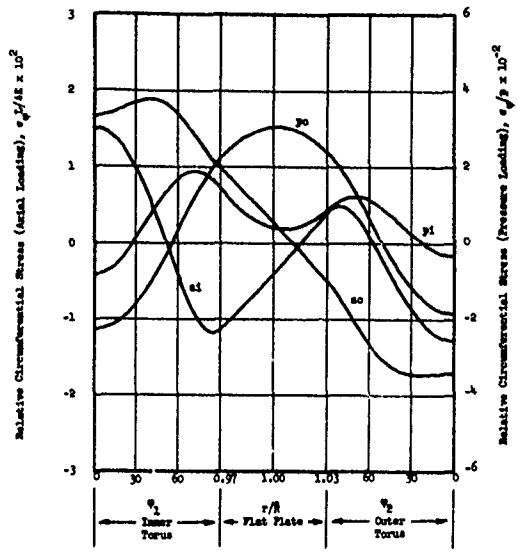

FIGURE D-28. RELATIVE CIRCUMFERENTIAL SURFACE STRESSES FOR AXIAL LOADING AND INTERNAL PRESSURE IN BELLOWS OF SHAPE 2 WITH $t/\overline{R} = 0.0067$ AND $c/\overline{R} = 0.150$

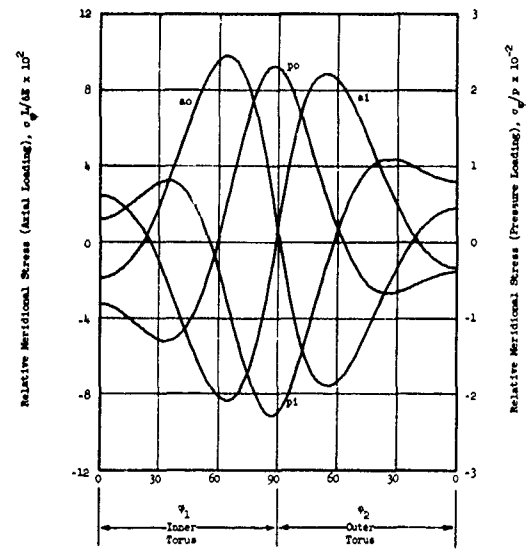

FIGURE D-29. RELATIVE MERIDIONAL SURFACE STRESSES FOR AXIAL LOADING AND INTERNAL PRESSURE IN BELLOWS OF SHAPE 3 WITH $t/\overline{R} = 0.0067$ AND $c/\overline{R} = 0.150$

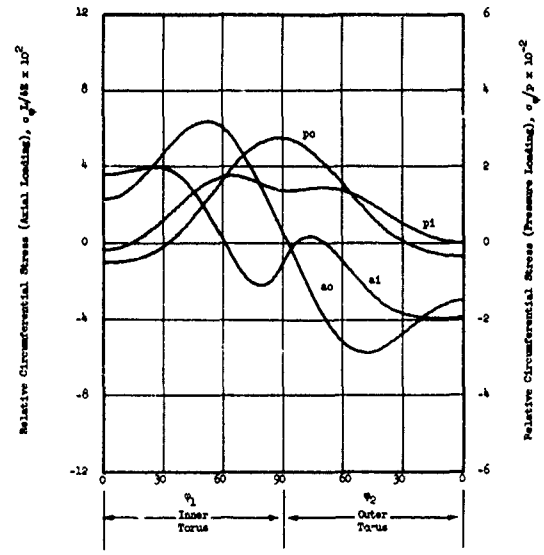

FIGURE D-30. RELATIVE CIRCUMFERENTIAL SURFACE STRESSES FOR AXIAL LOADING AND INTERNAL PRESSURE IN BELLOWS OF SHAPE 3 WITH $t/\overline{R} = 0.0067$ AND $c/\overline{R} = 0.150$

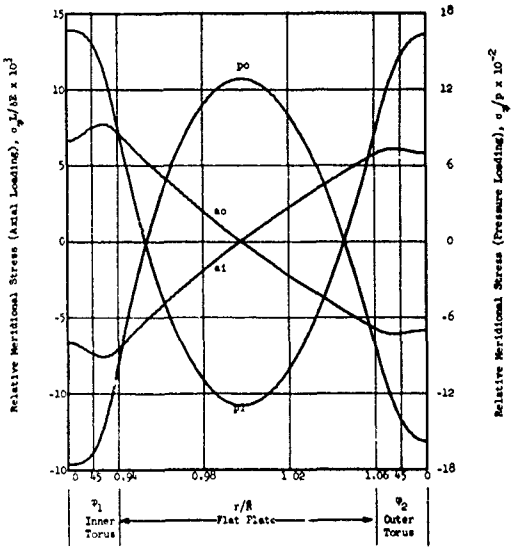

FIGURE D-31. RELATIVE MERIDIONAL SURFACE STRESSES FOR AXIAL LOADING AND INTERNAL PRESSURE IN BELLOWS OF SHAPE 1 WITH $t/\bar{R} = 0.0067$ AND $c/\bar{R} = 0.225$

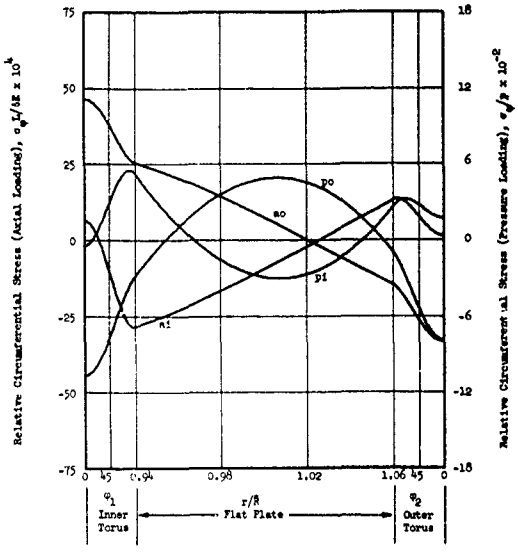

FIGURE D-32. RELATIVE CIRCUMFERENTIAL SURFACE STRESSES FOR AXIAL LOADING AND INTERNAL PRESSURE IN BELLOWS OF SHAPE 1 WITH $t/\bar{R} = 0.0067$ AND $c/\bar{R} = 0.225$

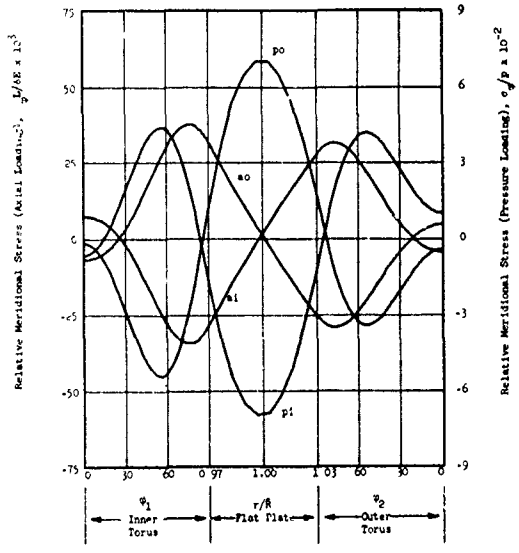

FIGURE D-33. RELATIVE MERIDIONAL SURFACE STRESSES FOR AXIAL LOADING AND INTERNAL PRESSURE IN BELLOWS OF SHAPE 2 WITH $t/\bar{R} = 0.0067$ AND $c/\bar{R} = 0.225$

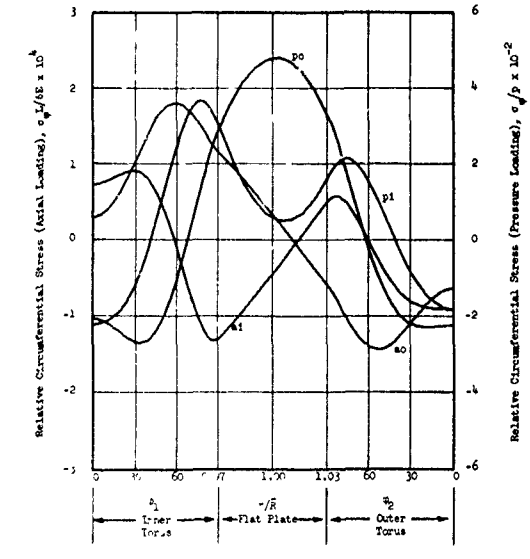

FIGURE D-34. RELATIVE CIRCUMFERENTIAL SURFACE STRESSES FOR AXIAL LOADING AND INTERNAL PRESSURE IN BELLOWS OF SHAPE 2 WITH $t/\bar{R} = 0.0067$ AND $c/\bar{R} = 0.225$

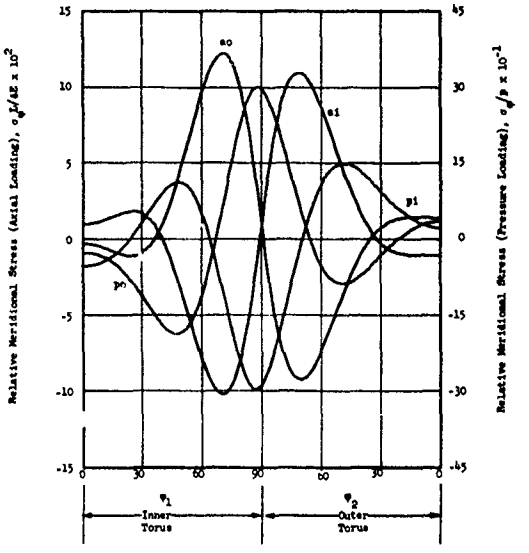

FIGURE D-35. RELATIVE MERIDIONAL SURFACE STRESSES FOR AXIAL LOADING AND INTERNAL PRESSURE IN BELLOWS OF SHAPE 3 WITH $t/\overline{R} = 0.0067$ AND $c/\overline{R} = 0.225$

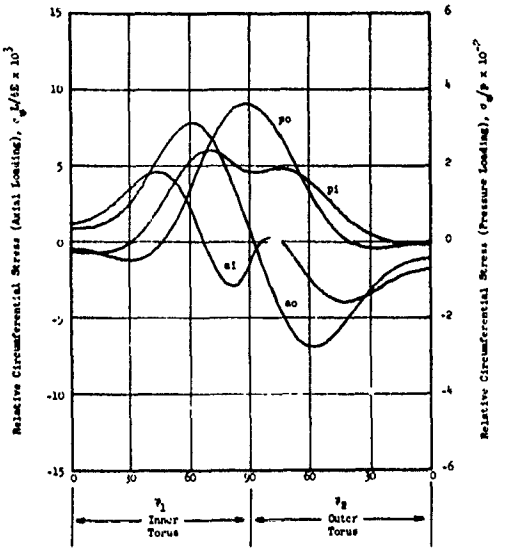

FIGURE D-36. RELATIVE CIRCUMFERENTIAL SURFACE STRESSES FOR AXIAL LOADING AND INTERNAL PRESSURE IN BELLOWS OF SHAPE 3 WITH $t/\overline{R} = 0.0067$ AND $c/\overline{R} = 0.225$

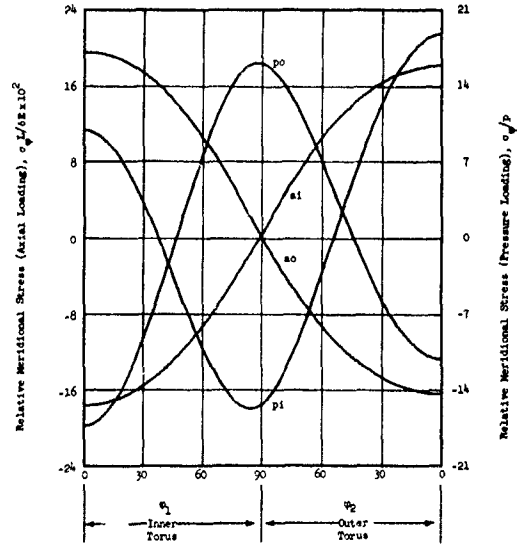

FIGURE D-37. RELATIVE MERIDIONAL SURFACE STRESSES FOR AXIAL LOADING AND INTERNAL PRESSURE IN BELLOWS OF SHAPE 3 WITH $t/\overline{R} = 0.02$ AND $c/\overline{R} = 0.075$

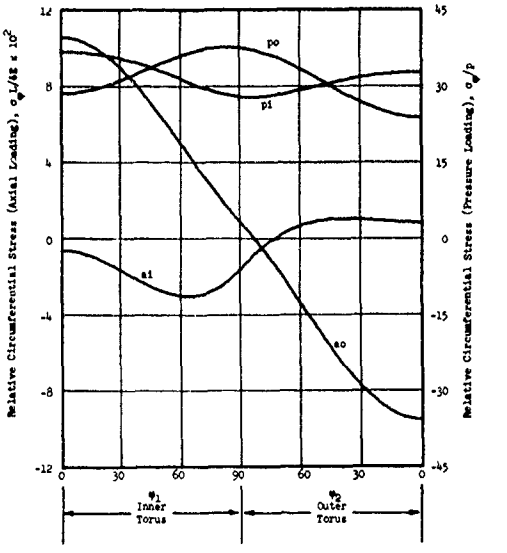

FIGURE D-38. RELATIVE CIRCUMFERENTIAL SURFACE STRESSES FOR AXIAL LOADING AND INTERNAL PRESSURE IN BELLOWS OF SHAPE 3 WITH $t/\overline{R} = 0.02$ AND $c/\overline{R} = 0.075$

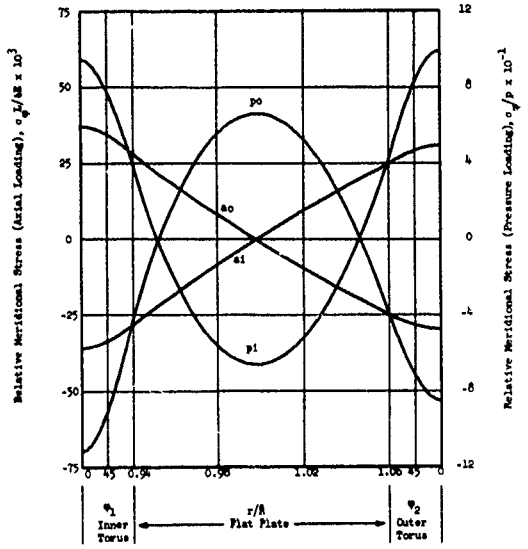

FIGURE D-39. RELATIVE MERIDIONAL SURFACE STRESSES FOR AXIAL LOADING AND INTERNAL PRESSURE IN BELLOWS OF SHAPE 1 WITH $t/\bar{R} = 0.02$ AND $c/\bar{R} = 0.150$

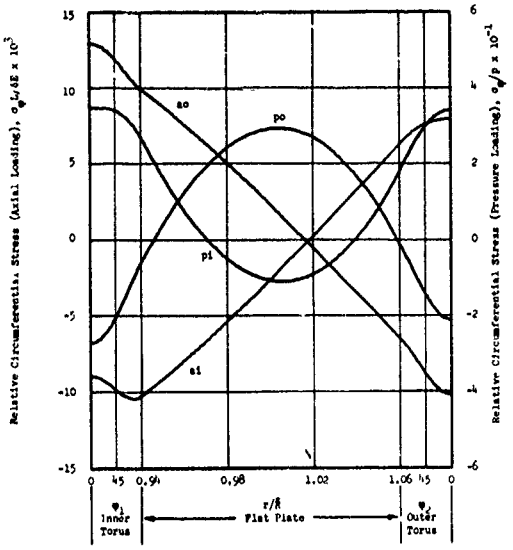

FIGURE D-40. RELATIVE CIRCUMFERENTIAL SURFACE STRESSES FOR AXIAL LOADING AND INTERNAL PRESSURE IN BELLOWS OF SHAPE 1 WITH $t/\bar{R} = 0.02$ AND $c/\bar{R} = 0.150$

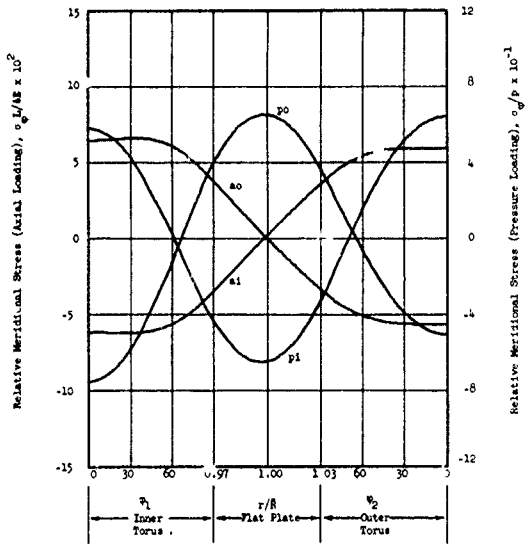

FIGURE D-41. RELATIVE MERIDIONAL SURFACE STRESSES FOR AXIAL LOADING AND INTERNAL PRESSURE IN BELLOWS OF SHAPE 2 WITH $t/\bar{R} = 0.02$ AND $c/\bar{R} = 0.150$

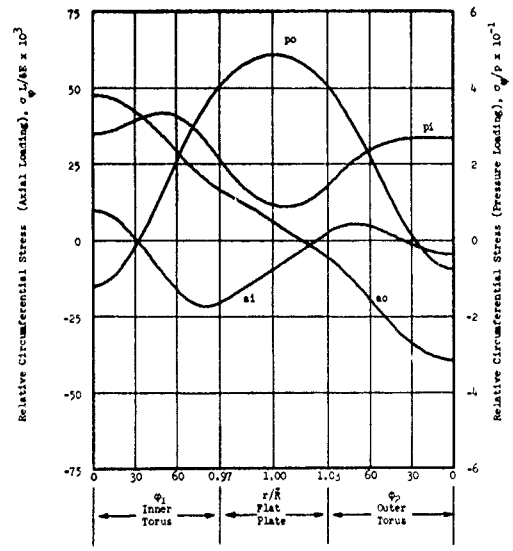

FIGURE D-42. RELATIVE CIRCUMFERENTIAL SURFACE STRESSES FOR AXIAL LOADING AND INTERNAL PRESSURE IN BELLOWS OF SHAPE 2 WITH $t/\bar{R} = 0.02$ AND $c/\bar{R} = 0.150$

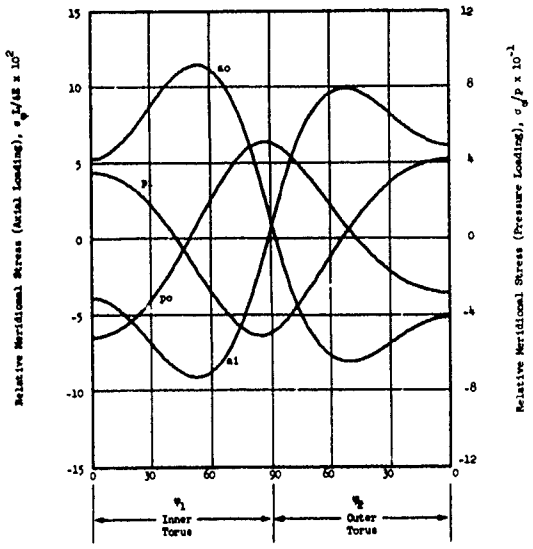

FIGURE D-43. RELATIVE MERIDIONAL SURFACE STRESSES FOR AXIAL LOADING AND INTERNAL PRESSURE IN BELLOWS OF SHAPE 3 WITH $t/\overline{R} = 0.02$ AND $c/\overline{R} = 0.150$

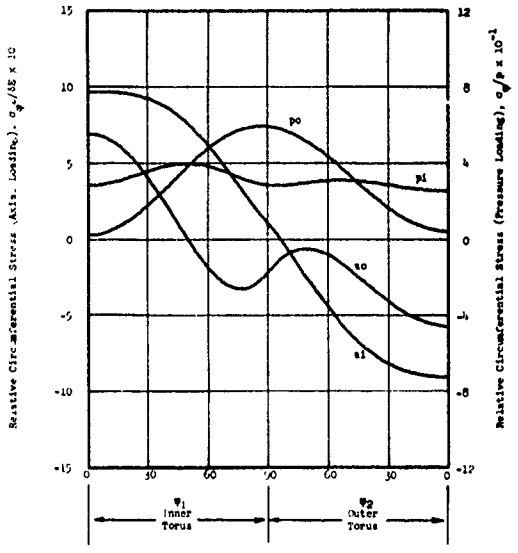

FIGURE D-44. RELATIVE CIRCUMFERENTIAL SURFACE STRESSES FOR AXIAL LOADING AND INTERNAL PRESSURE IN BELLOWS OF SHAPE 3 WITH $t/\overline{R} = 0.02$ AND $c/\overline{R} = 0.150$

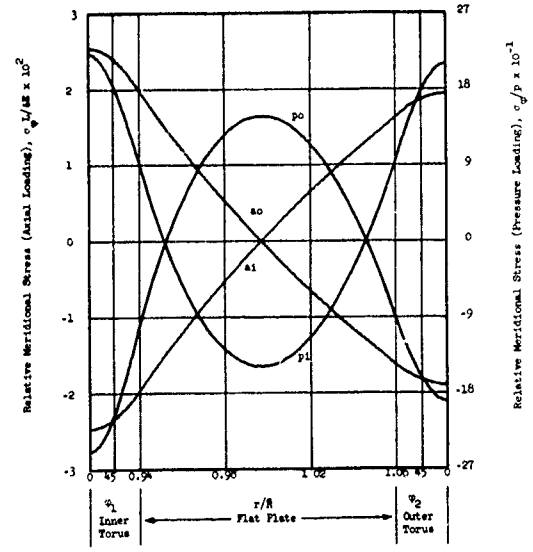

FIGURE D-45. RELATIVE MERIDIONAL SURFACE STRESSES FOR AXIAL LOADING AND INTERNAL PRESSURE IN BELLOWS OF SHAPE 1 WITH $t/\overline{R} = 0.02$ AND $c/\overline{R} = 0.225$

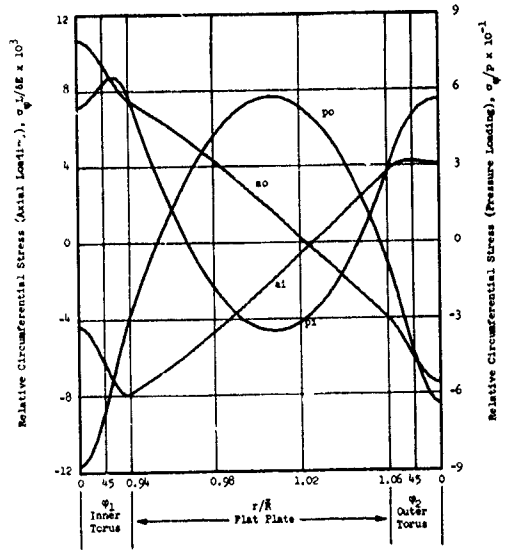

FIGURE D-46. RELATIVE CIRCUMFERENTIAL SURFACE STRESSES FOR AXIAL LOADING AND INTERNAL PRESSURE IN BELLOWS OF SHAPE 1 WITH $t/\overline{R} = 0.02$ AND $c/\overline{R} = 0.225$

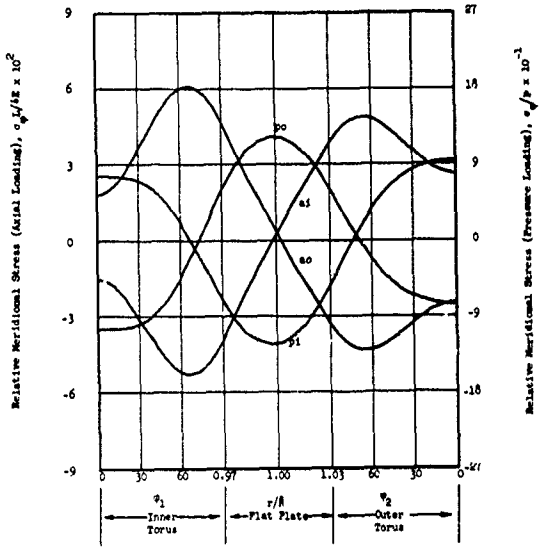

FIGURE D-47. RELATIVE MERIDIONAL SURFACE STRESSES FOR AXIAL LOADING AND INTERNAL PRESSURE IN BELLOWS OF SHAPE 2 WITH $t/\bar{R} = 0.02$ AND $c/\bar{R} = 0.225$

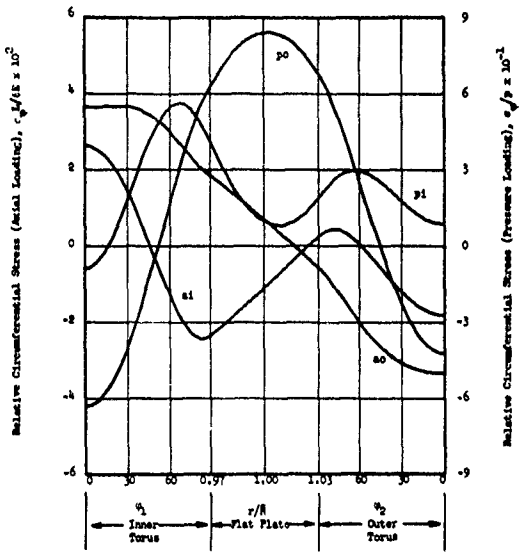

FIGURE D-48. RELATIVE CIRCUMFERFNTIAL SURFACE STRESSES FOR AXIAL LOADING AND INTERNAL PRESSURE IN BELLOWS OF SHAPE 2 WITH $t/\bar{R} = 0.02$ AND $c/\bar{R} = 0.225$

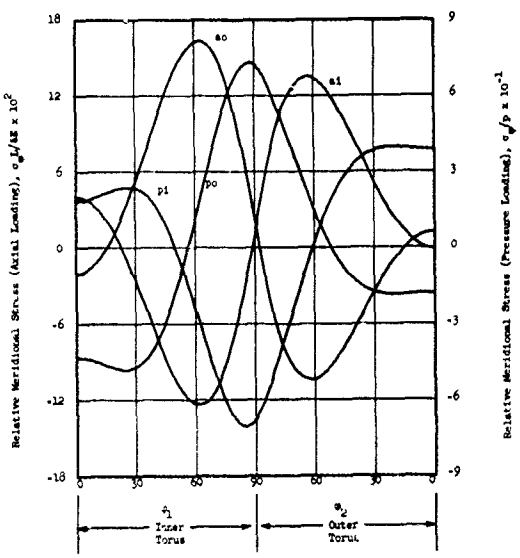

FIGURE D-49. RELATIVE MERIDIONAL SURFACE STRESSES FOR AXIAL LOADING AND INTERNAL PRESSURE IN BELLOWS OF SHAPE 3 WITH $t/\bar{R} = 0.02$ AND $c/\bar{R} = 0.225$

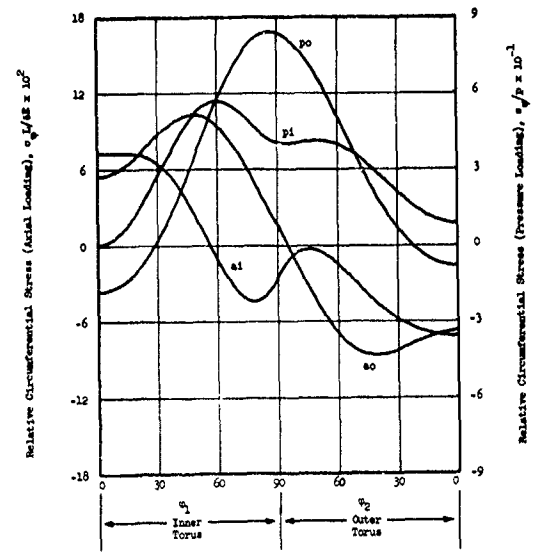

FIGURE D-50. RELATIVE CIRCUMFERENTIAL SURFACE STRESSES FOR AXIAL LOADING AND INTERNAL PRESSURE IN BELLOWS OF SHAPE 3 WITH $t/\bar{R} = 0.02$ AND $c/\bar{R} = 0.225$

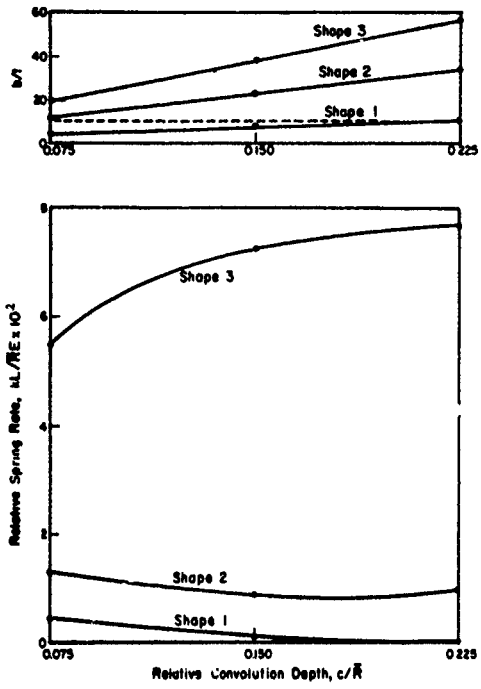

FIGURE D-51. RELATIVE SPRING RATES, $kL/\bar{R}E$, AND THICKNESS RATIOS, b/t, FOR FORMED BELLOWS WITH RELATIVE THICKNESS $t/\bar{R} = 0.004$

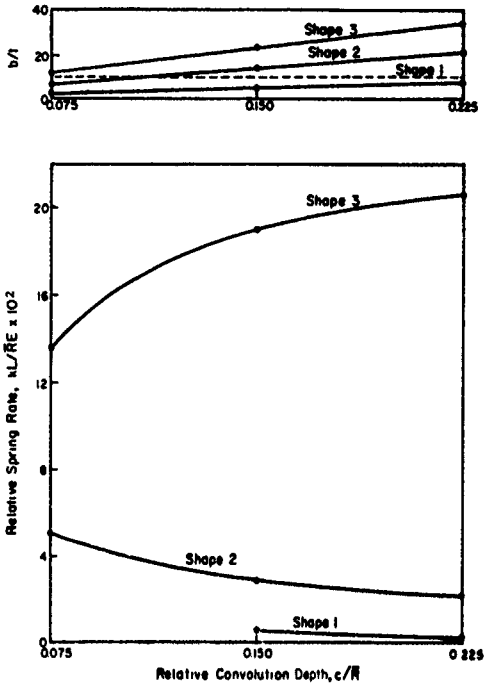

FIGURE D-52. RELATIVE SPRING RATES, $kL/\bar{R}E$, AND THICKNESS RATIOS, b/t, FOR FORMED BELLOWS WITH RELATIVE THICKNESS $t/\bar{R} = 0.0067$

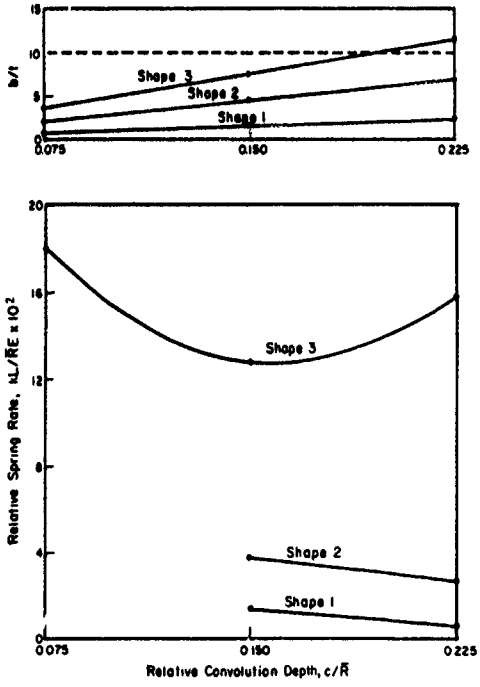

FIGURE D-53. RELATIVE SPRING RATES, $kL/\bar{R}E$, AND THICKNESS RATIOS, b/t, FOR FORMED BELLOWS WITH RELATIVE THICKNESS, $t/\bar{R} = 0.02$

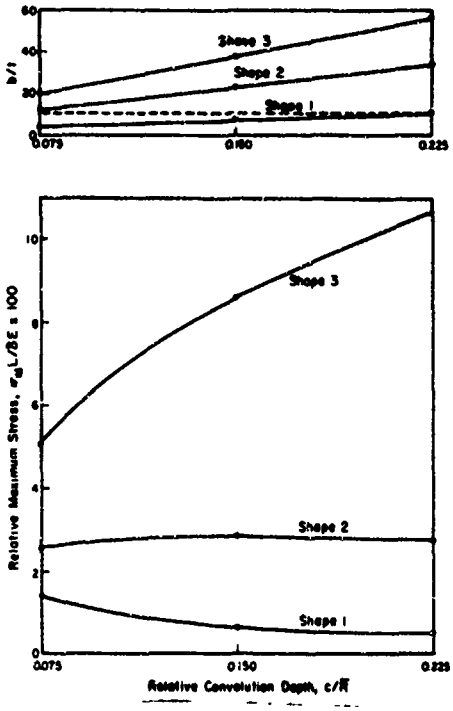

FIGURE D-54. RELATIVE MAXIMUM STRESS, $\sigma_M L/\delta E$, AND THICKNESS RATIOS, b/t, FOR AXIALLY LOADED BELLOWS WITH RELATIVE THICKNESS $t/\bar{R} = 0.004$

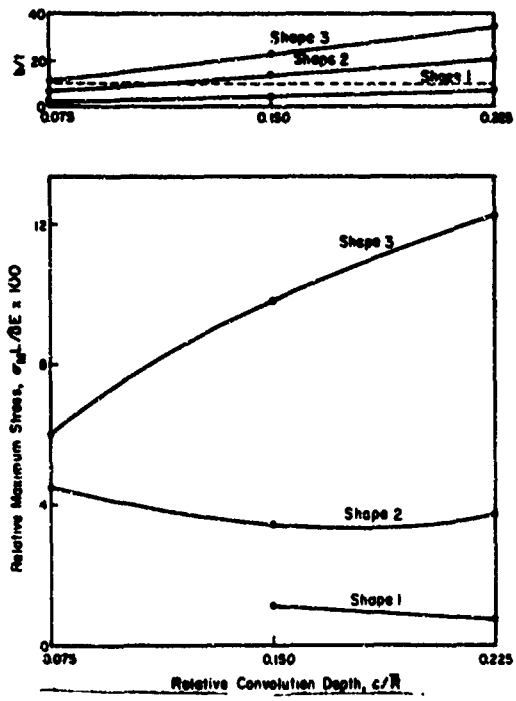

FIGURE D-55. RELATIVE MAXIMUM STRESS, $\sigma_M L/\delta E$, AND THICKNESS RATIOS, b/t, FOR AXIALLY LOADED FORMED BELLOWS WITH RELATIVE THICKNESS $t/\bar{R} = 0.0067$

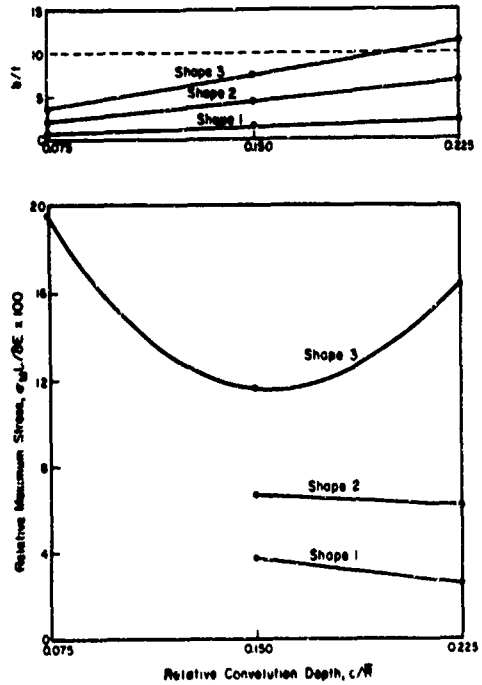

FIGURE D-56. RELATIVE MAXIMUM STRESS, $\sigma_M L/\delta E$, AND THICKNESS RATIOS, b/t, FOR AXIALLY LOADED FORMED BELLOWS WITH RELATIVE THICKNESS $t/\bar{R} = 0.02$

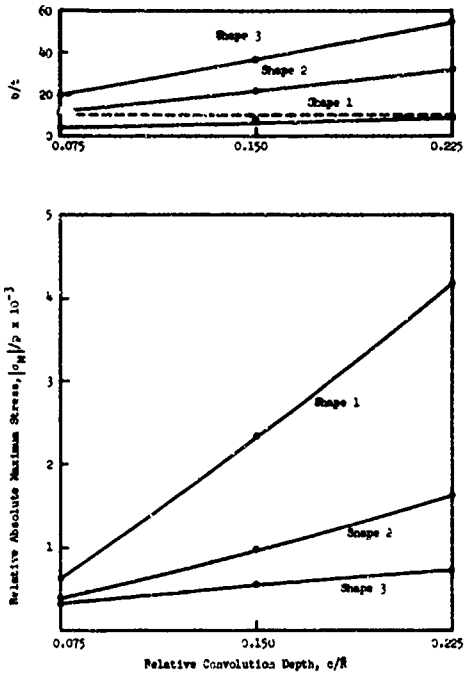

FIGURE D-57. RELATIVE ABSOLUTE MAXIMUM STRESS, $|\sigma_M|/p$, AND THICKNESS RATIOS, b/t, FOR INTERNALLY PRESSURIZED FORMED BELLOWS WITH RELATIVE THICKNESS $t/\bar{R} = 0.004$

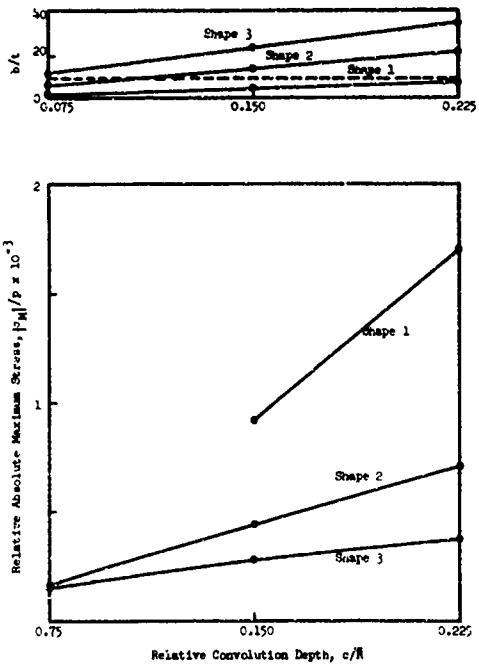

FIGURE D-58. RELATIVE ABSOLUTE MAXIMUM STRESS, $|\sigma_M|/p$, AND THICKNESS RATIOS, b/t, FOR INTERNALLY PRESSURIZED FORMED BELLOWS WITH RELATIVE THICKNESS $t/\bar{R} = 0.0067$

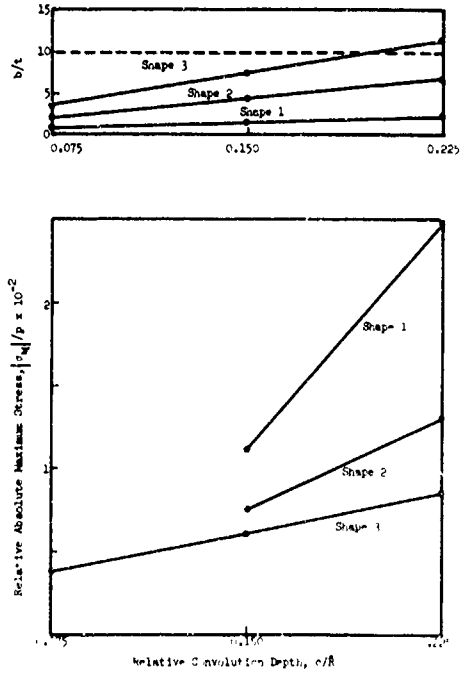

FIGURE D-59 RELATIVE ABSOLUTE MAXIMUM STRESS, $|\sigma_M|/p$, AND THICKNESS RATIOS, b/t, FOR INTERNALLY PRESSURIZED FORMED BELLOWS WITH RELATIVE THICKNESS $t/\bar{R} = 0.02$

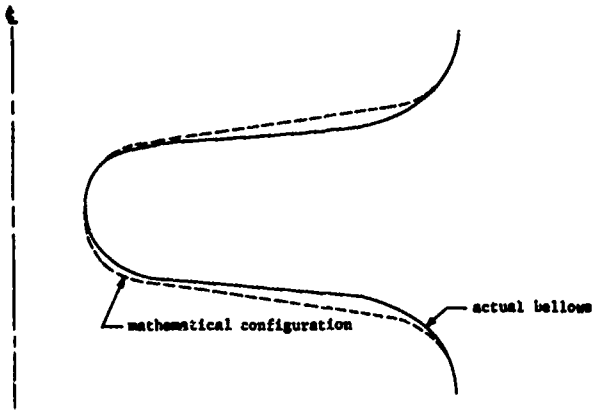

FIGURE D-60. CONVOLUTION VARIATION NO. 1 FOR 5" BELLOWS JD 92. INSIDE TORUS RADIUS = 0.063 INCH, OUTSIDE TORUS RADIUS = 0.071 INCH, CONE ANGLE = 5°

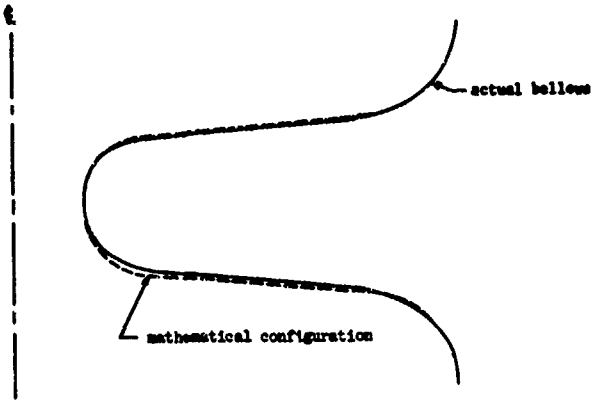

FIGURE D-61. CONVOLUTION VARIATION NO. 2 FOR 5" BELLOWS JD 92. INSIDE TORUS RADIUS = 0.063 INCH, OUTSIDE TORUS RADIUS = 0.085 INCH, CONE ANGLE = 5°

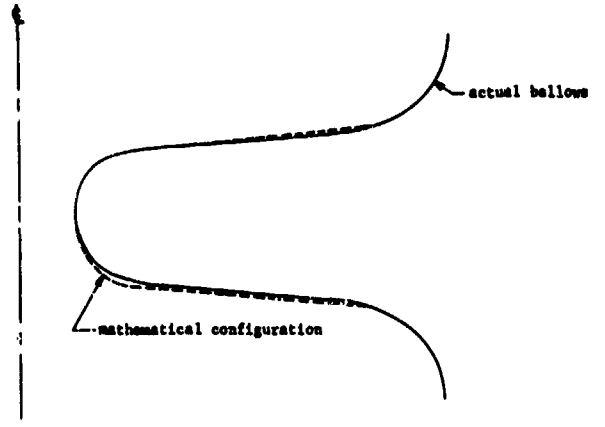

FIGURE D-62. CONVOLUTION VARIATION NO. 3 FOR 5" BELLOWS JD 92. INSIDE TORUS RADIUS = 0.063 INCH, OUTSIDE TORUS RADIUS = 0.085 INCH, CONE ANGLE = 7°10'

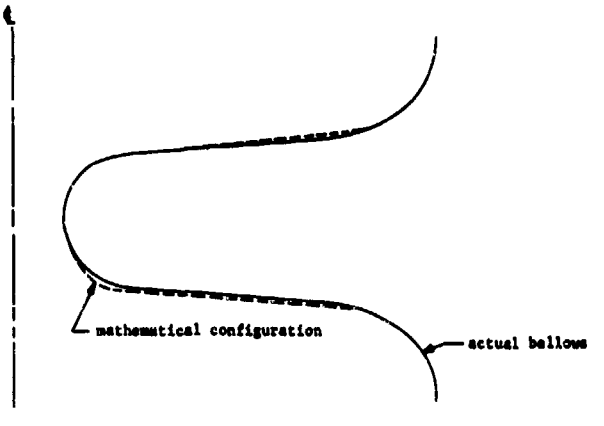

FIGURE D-63. CONVOLUTION VARIATION NO. 4 FOR 5" BELLOWS JD 92. INSIDE TORUS RADIUS = 0.063 INCH, OUTSIDE TORUS RADIUS = 0.085 INCH, CONE ANGLE = 8°

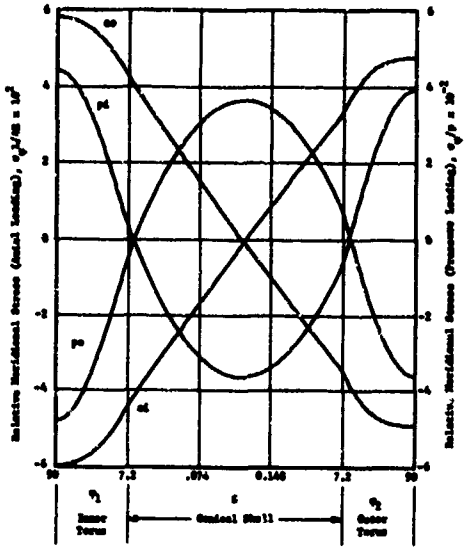

FIGURE D-64. RELATIVE MERIDIONAL SURFACE STRESSES FOR AXIAL LOADING AND INTERNAL PRESSURE IN 5" BELLOWS JD 92 (CONVOLUTION VARIATION NO. 3). $t/\bar{R} = 0.00374$, $c/\bar{R} = 0.0654$

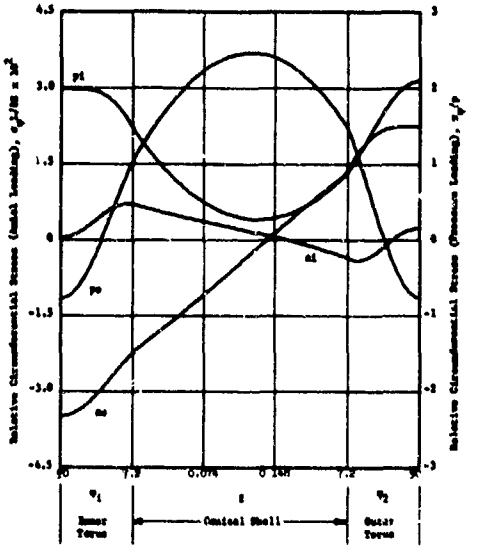

FIGURE D-65. RELATIVE CIRCUMFERENTIAL SURFACE STRESSES FOR AXIAL LOADING AND INTERNAL PRESSURE IN 5" BELLOWS JD 92 (CONVOLUTION VARIATION NO. 3). $t/\bar{R} = 0.00374$, $c/\bar{R} = 0.0654$

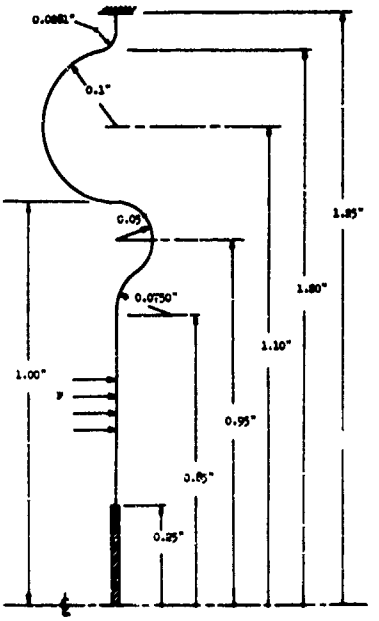

FIGURE D-66. MATHEMATICAL MODEL FOR CORRUGATED DIAPHRAGM NO. 1

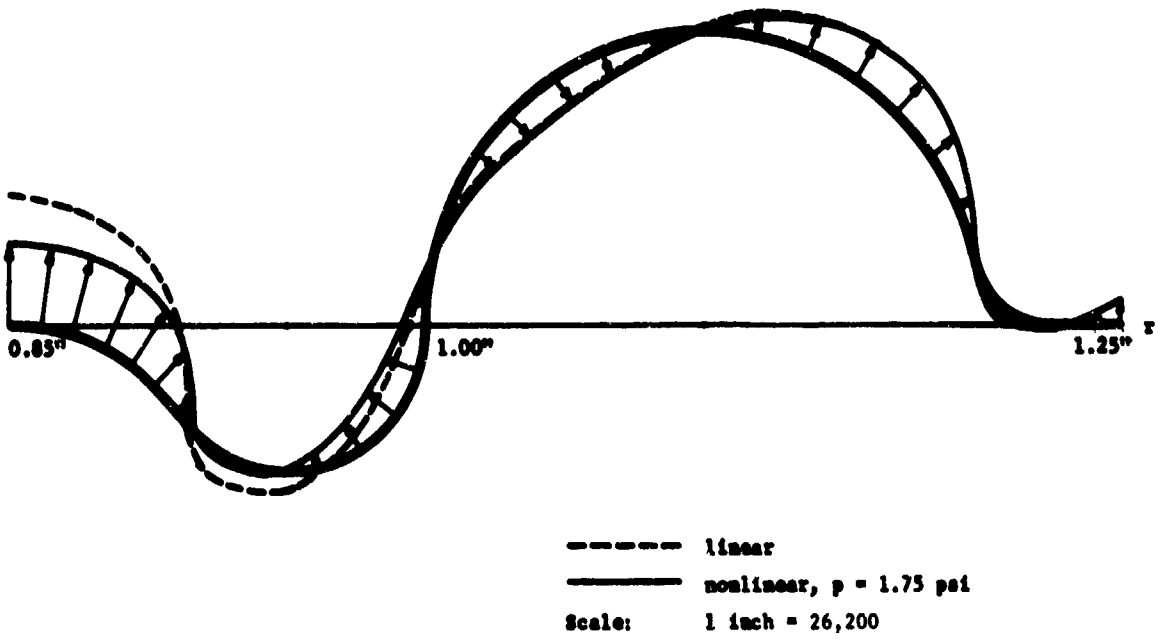

FIGURE D-67. RELATIVE OUTER SURFACE STRESS, σ_ϕ/p, FOR DIAPHRAGM NO. 1

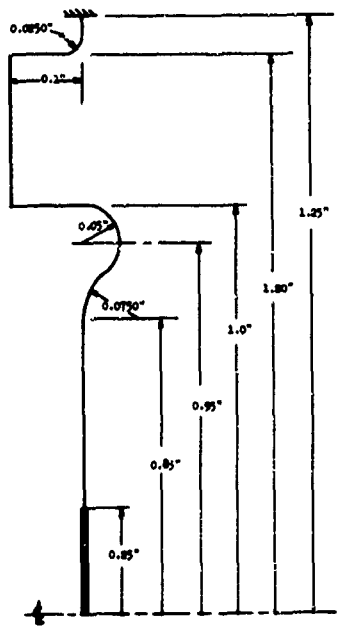

FIGURE D-68. MATHEMATICAL MODEL FOR CORRUGATED DIAPHRAGM NO. 2

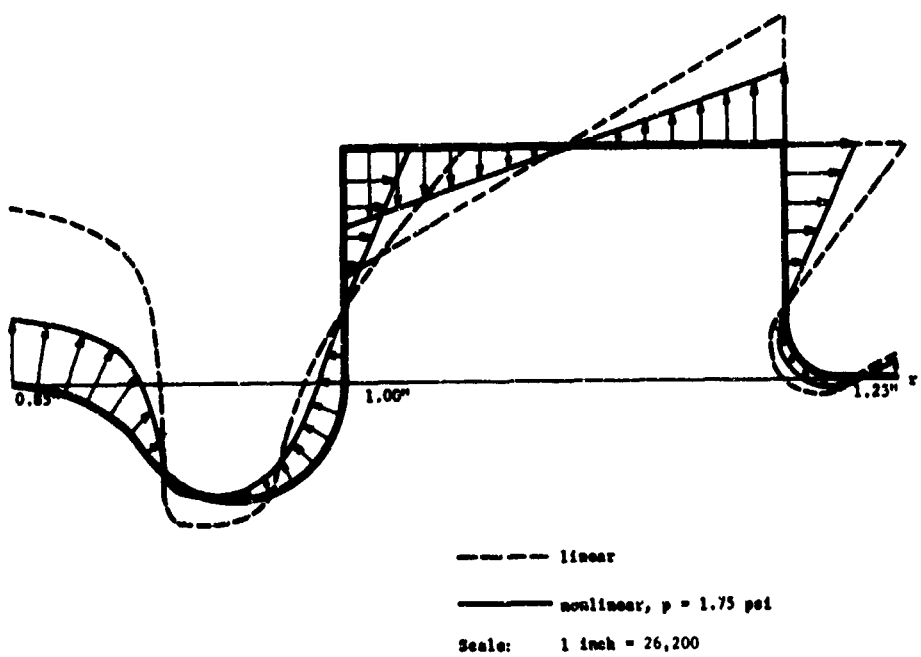

FIGURE D-69. RELATIVE OUTER SURFACE STRESS, σ_ϕ/p, FOR DIAPHRAGM NO. 2

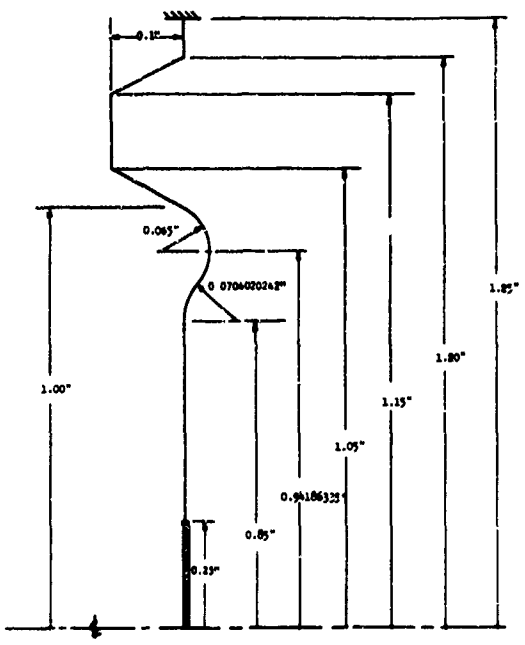

FIGURE D-70. MATHEMATICAL MODEL FOR CORRUGATED DIAPHRAGM NO. 3

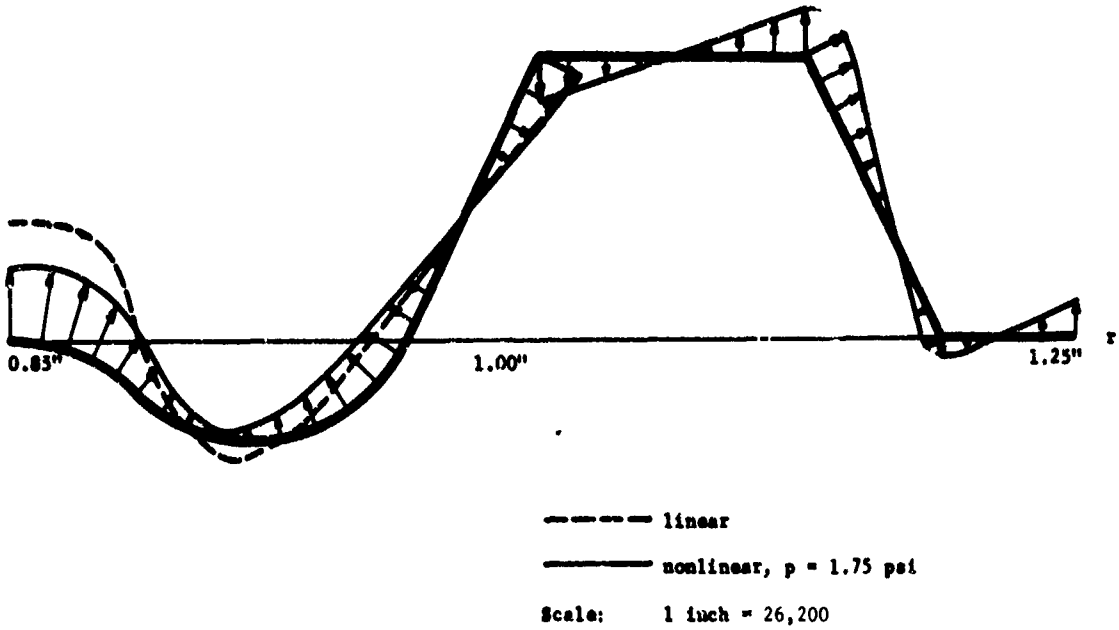

FIGURE D-71. RELATIVE OUTER SURFACE STRESS, σ_ϕ/p, FOR DIAPHRAGM NO. 3

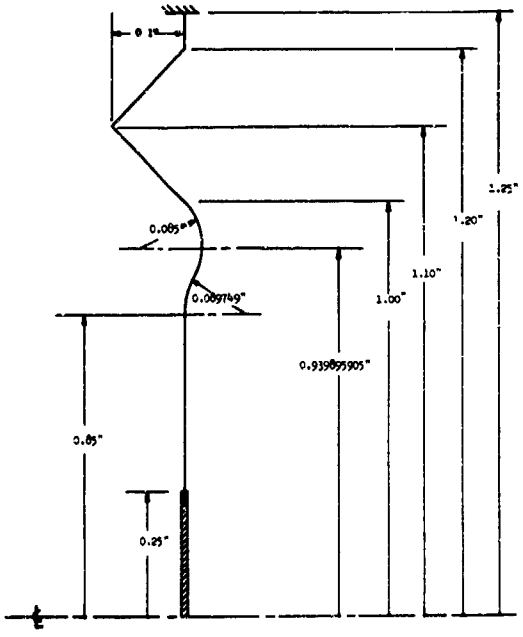

FIGURE D-72. MATHEMATICAL MODEL FOR CORRUGATED DIAPHRAGM NO. 4

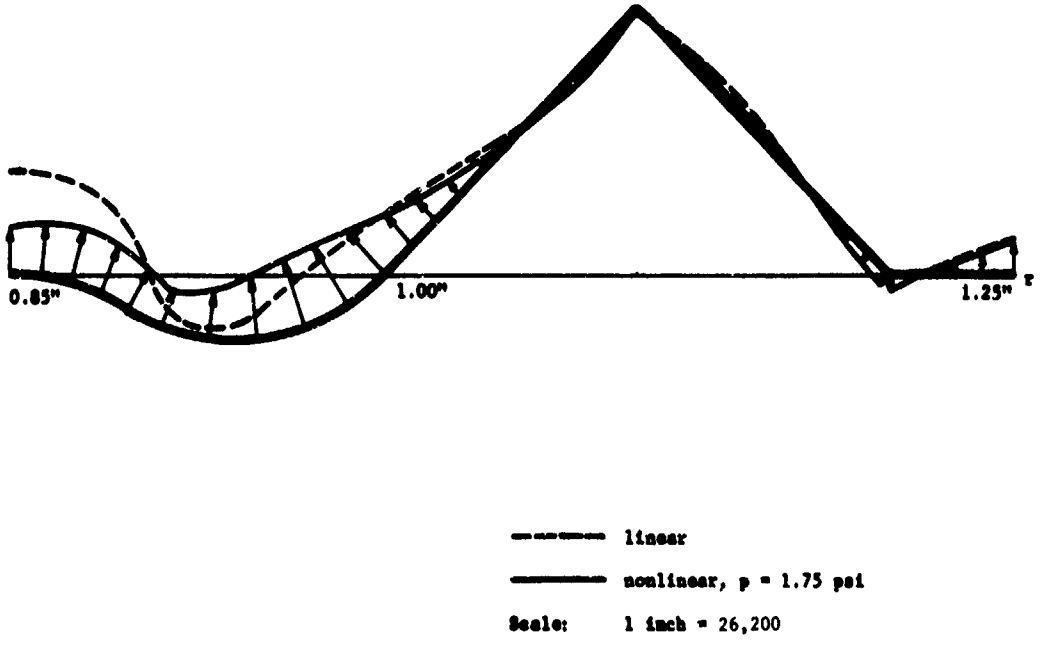

FIGURE D-73. RELATIVE OUTER SURFACE STRESS, σ_ϕ/p, FOR DIAPHRAGM NO. 4

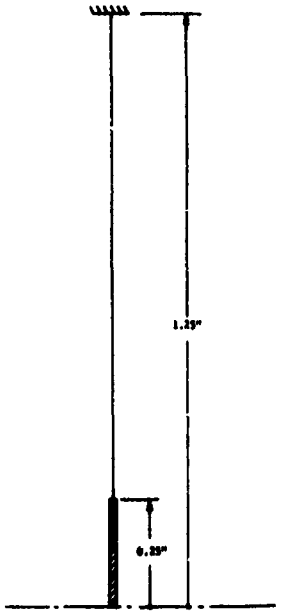

FIGURE D-74. MATHEMATICAL MODEL FOR DIAPHRAGM NO. 5

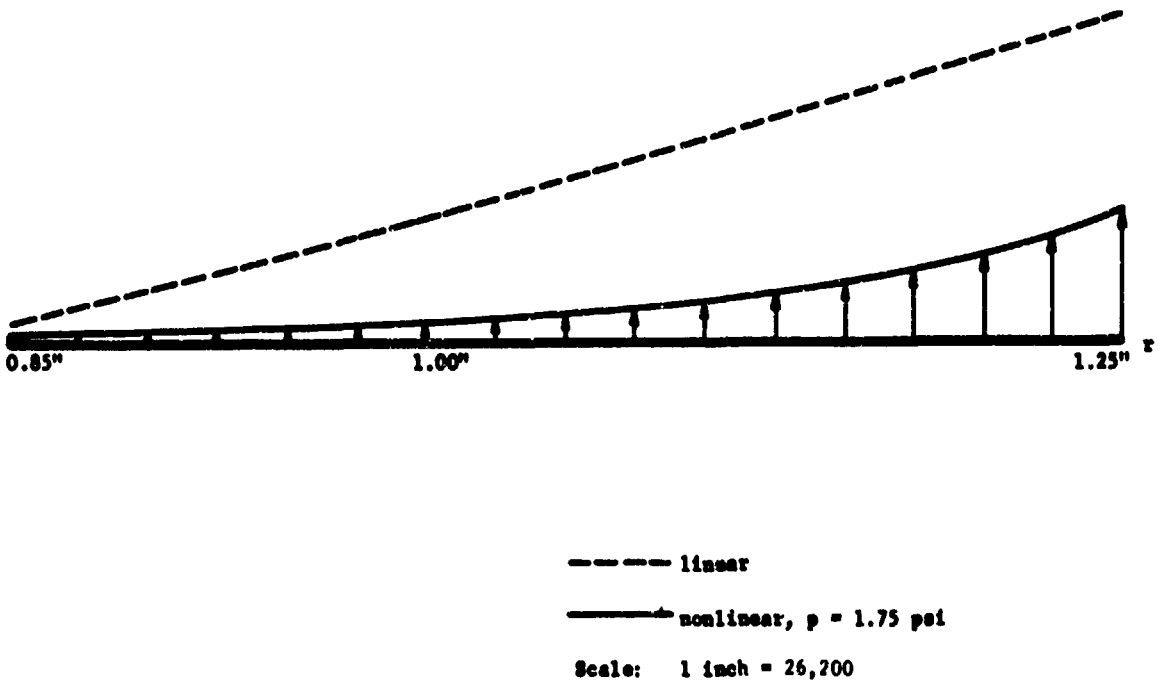

FIGURE D-75. RELATIVE OUTER SURFACE STRESS, σ_ϕ/p, FOR DIAPHRAGM NO. 5

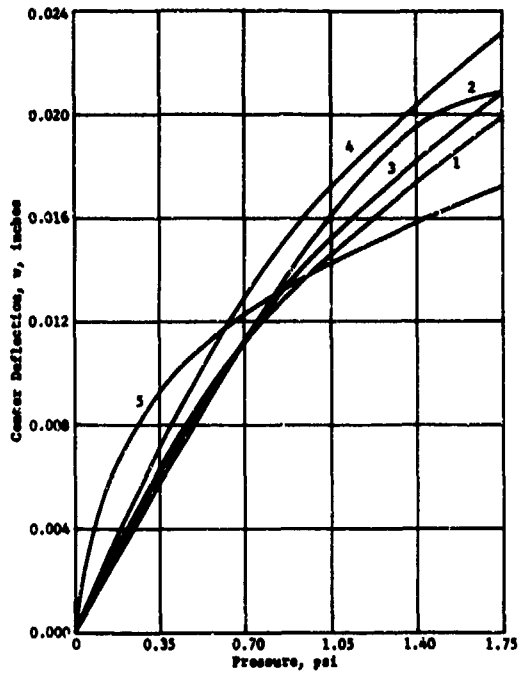

FIGURE D-76. CENTER DEFLECTION, w, FOR DIAPHRAGMS 1-5 FOR INCREASING PRESSURE (NONLINEAR THEORY)

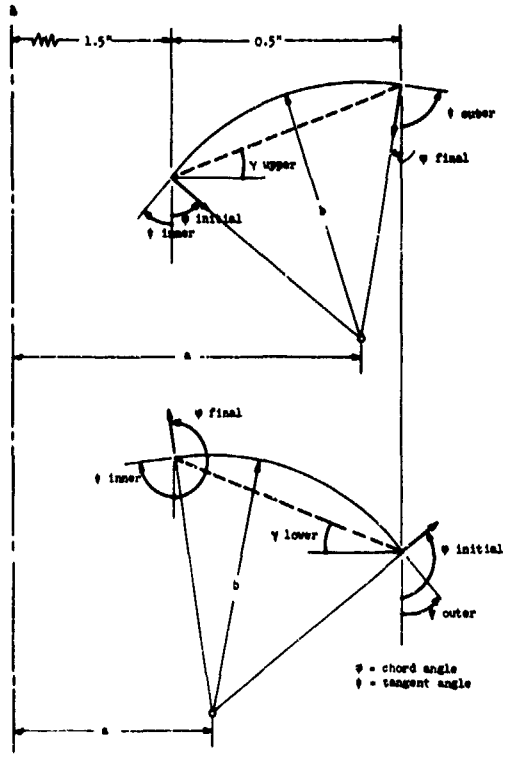

FIGURE D-77. NOMENCLATURE FOR SINGLE-SWEEP UPPER AND LOWER BELLOWS LEAVES

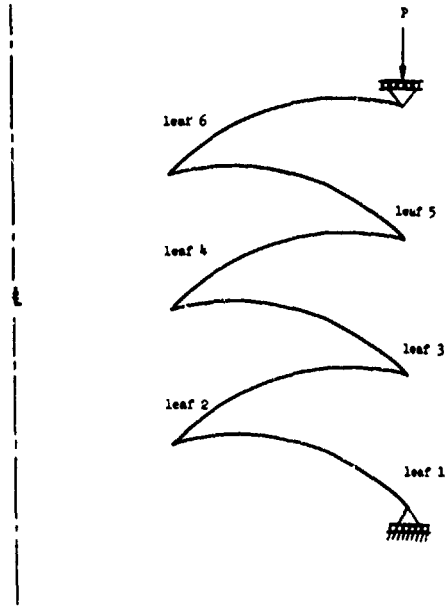

FIGURE D-78. MATHEMATICAL MODEL NO. 1 OF SINGLE-SWEEP WELDED BELLOWS WITH 15° UPPER CHORD ANGLE AND 15° LOWER CHORD ANGLE

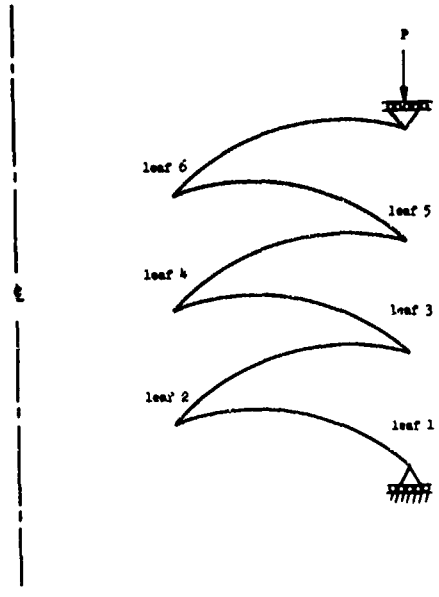

FIGURE D-79. MATHEMATICAL MODEL NO. 2 OF SINGLE-SWEEP WELDED BELLOWS WITH 15° UPPER CHORD ANGLE AND 10° LOWER CHORD ANGLE

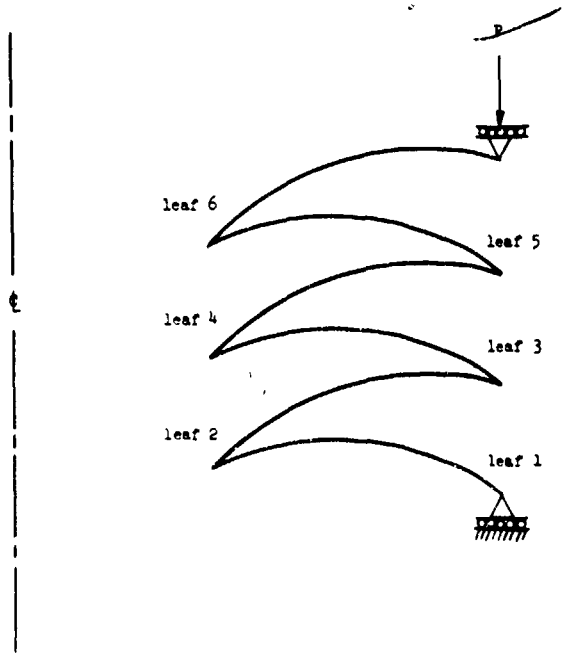

FIGURE D-80. MATHEMATICAL MODEL NO. 3 OF SINGLE-SWEEP WELDED BELLOWS WITH 15° UPPER CHORD ANGLE AND 5° LOWER CHORD ANGLE

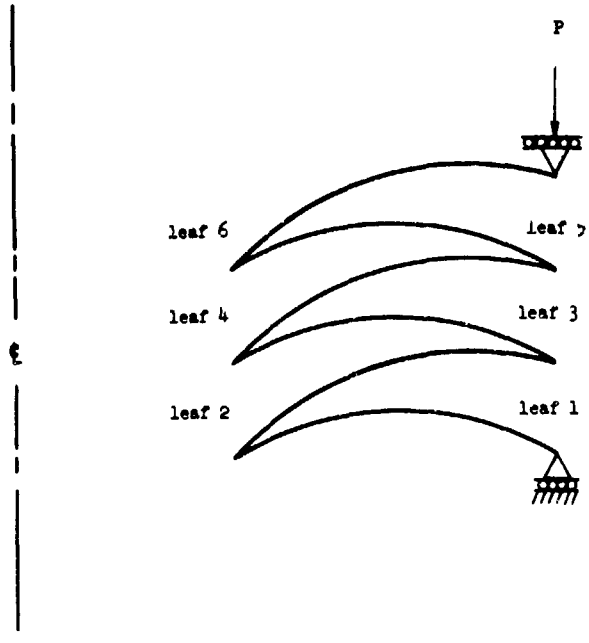

FIGURE D-81. MATHEMATICAL MODEL NO. 4 OF SINGLE-SWEEP WELDED BELLOWS WITH 15° UPPER CHORD ANGLE AND 0° LOWER CHORD ANGLE

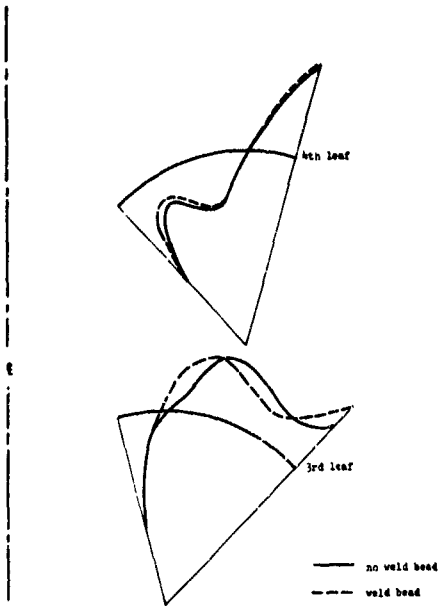

FIGURE D-82. MERIDIONAL INNER SURFACE STRESS DUE TO AXIAL LOADING IN SINGLE-SWEEP BELLOWS WITH 15° UPPER CHORD ANGLE AND 15° LOWER CHORD ANGLE (P = 2 lb/in.)

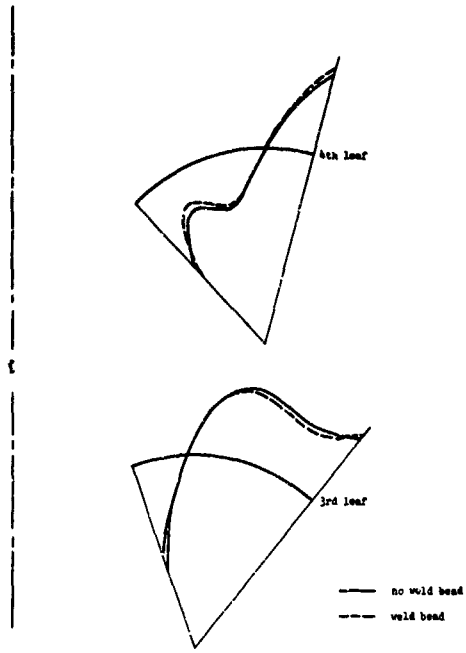

FIGURE D-83. MERIDIONAL INNER SURFACE STRESS DUE TO AXIAL LOADING IN SINGLE-SWEEP WELDED BELLOWS WITH 15° UPPER CHORD ANGLE AND 10° LOWER CHORD ANGLE (P = 2 lb/in.)

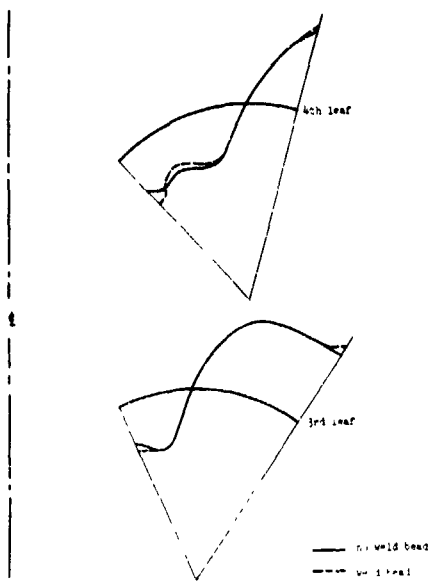

FIGURE D-84. MERIDIONAL INNER SURFACE STRESS DUE TO AXIAL LOADING IN SINGLE-SWEEP WELDED BELLOWS WITH 15° UPPER CHORD ANGLE AND 5° LOWER CHORD ANGLE (P = 2 lb/in.)

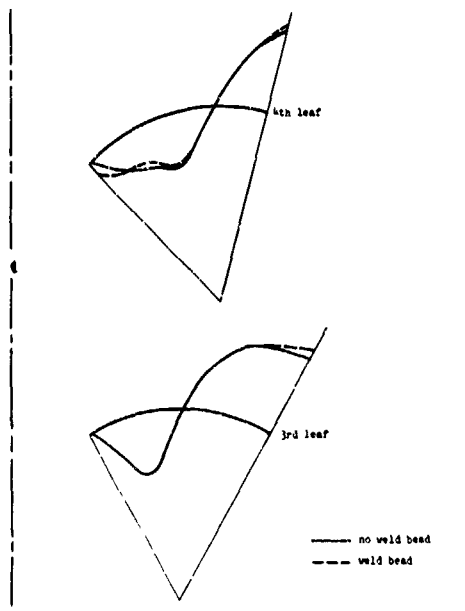

FIGURE D-85. MERIDIONAL INNER SURFACE STRESS DUE TO AXIAL LOADING IN SINGLE-SWEEP WELDED BELLOWS WITH 15° UPPER CHORD ANGLE AND 0° LOWER CHORD ANGLE (P = 2 lb/in.)

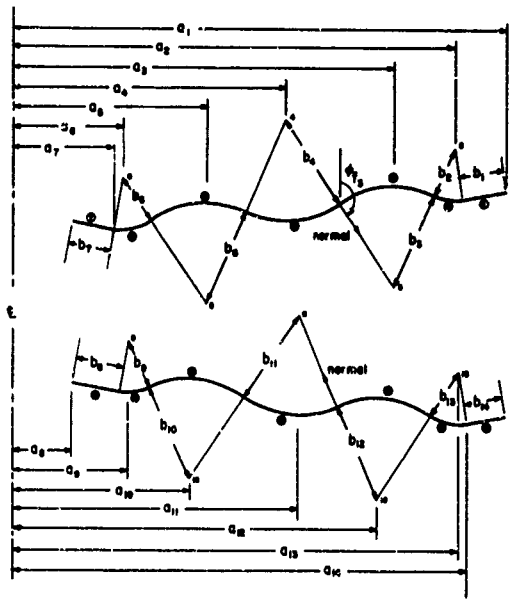

FIGURE D-86. MATHEMATICAL MODEL OF 5°-5° WELDED BELLOWS, MODEL NO. 1, CASE 1

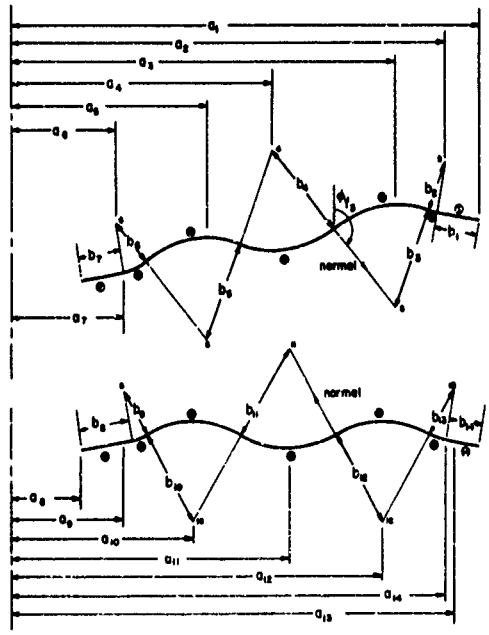

FIGURE D-87. MATHEMATICAL MODEL OF 0°-10° WELDED BELLOWS, MODEL NO. 2, CASE 9

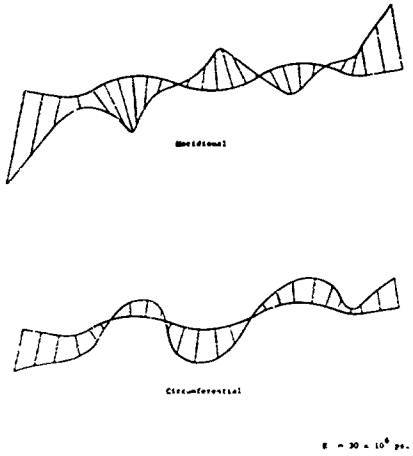

FIGURE D-88 RELATIVE OUTER SURFACE STRESS, $\sigma L/\delta$, ON UPPER LEAF DUE TO AXIAL LOADING ON WELDED BELLOWS, MODEL NO. 1, CASE 1

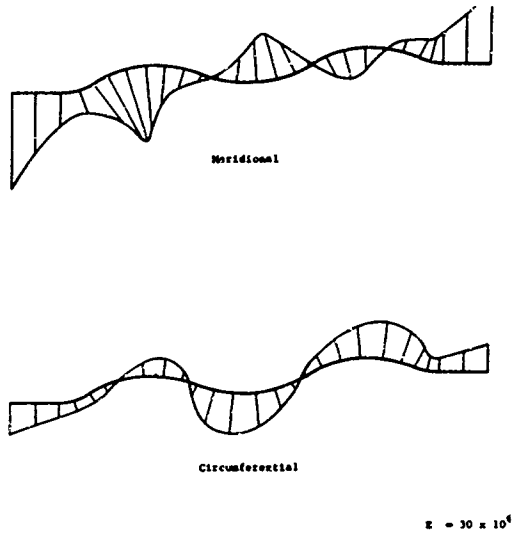

FIGURE D-89. RELATIVE OUTER SURFACE STRESS, $\sigma L/\delta$, ON UPPER LEAF DUE TO AXIAL LOADING ON WELDED BELLOWS, MODEL NO. 1, CASE 5

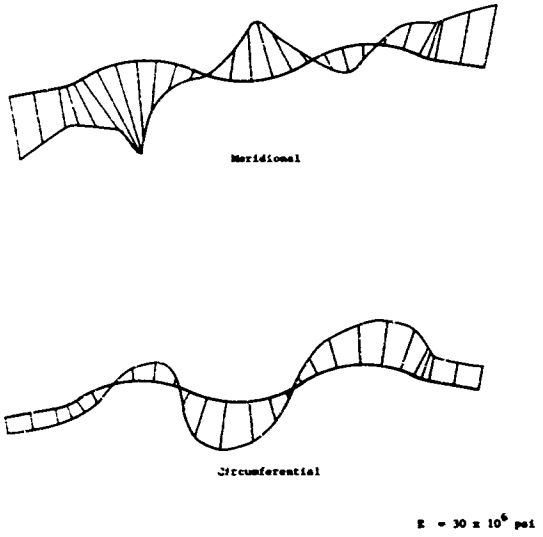

FIGURE D-90. RELATIVE OUTER SURFACE STRESS, $\sigma L/\delta$, ON UPPER LEAF DUE TO AXIAL LOADING ON WELDED BELLOWS, MODEL NO. 1, CASE 9

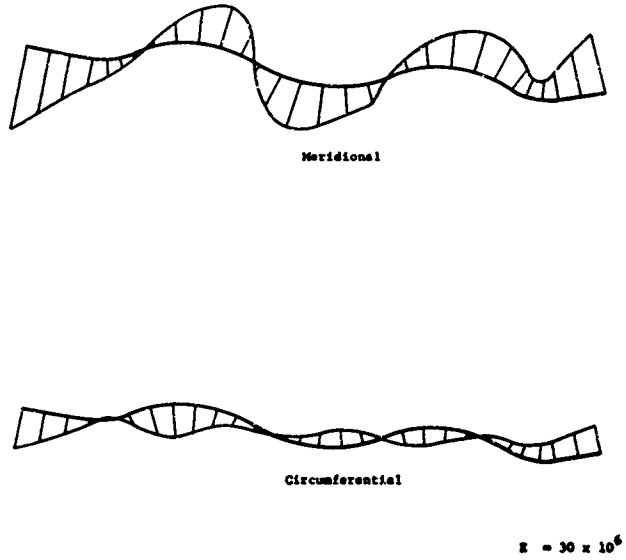

FIGURE D-91. RELATIVE OUTER SURFACE STRESS, $\sigma L/\delta$, ON LOWER LEAF DUE TO AXIAL LOADING ON WELDED BELLOWS, MODEL NO. 1, CASE. 1

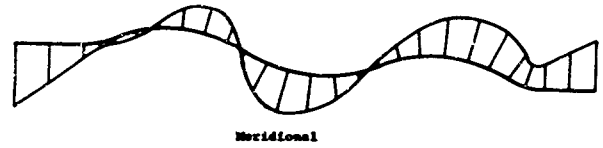

E = 30 x 10^6 psi

FIGURE D-92. RELATIVE OUTER SURFACE STRESS, $\sigma L/\delta$, ON LOWER LEAF DUE TO AXIAL LOADING ON WELDED BELLOWS, MODEL NO. 1, CASE 5

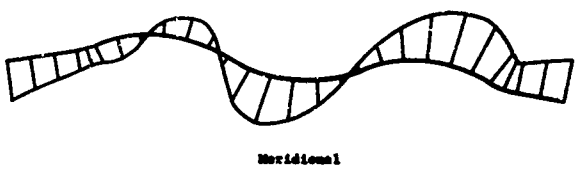

E = 30 x 10^6 psi

FIGURE D-93. RELATIVE OUTER SURFACE STRESS, $\sigma L/\delta$, ON LOWER LEAF DUE TO AXIAL LOADING ON WELDED BELLOWS, MODEL NO. 1, CASE 9

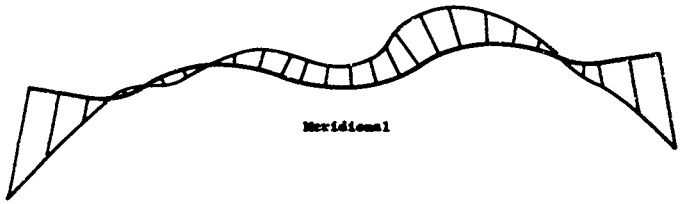

FIGURE D-94. RELATIVE OUTER SURFACE STRESS, σ/p, ON UPPER LEAF DUE TO INTERNAL PRESSURE IN WELDED BELLOWS, MODEL NO. 1, CASE 1

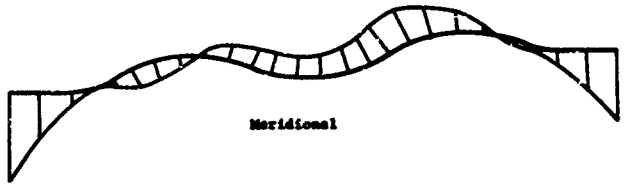

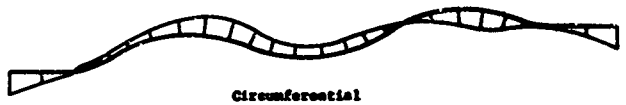

FIGURE D-95. RELATIVE OUTER SURFACE STRESS, σ/p, ON UPPER LEAF DUE TO INTERNAL PRESSURE IN WELDED BELLOWS, MODEL NO. 1, CASE 5

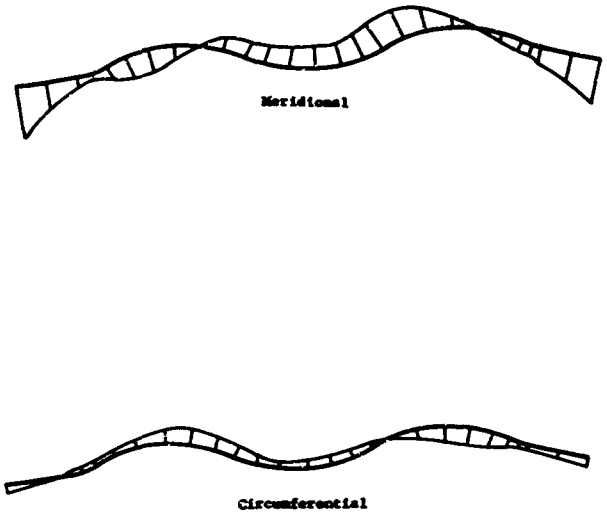

FIGURE D-96. RELATIVE OUTER SURFACE STRESS, σ/p, ON UPPER LEAF DUE TO INTERNAL PRESSURE IN WELDED BELLOWS, MODEL NO. 1, CASE 9

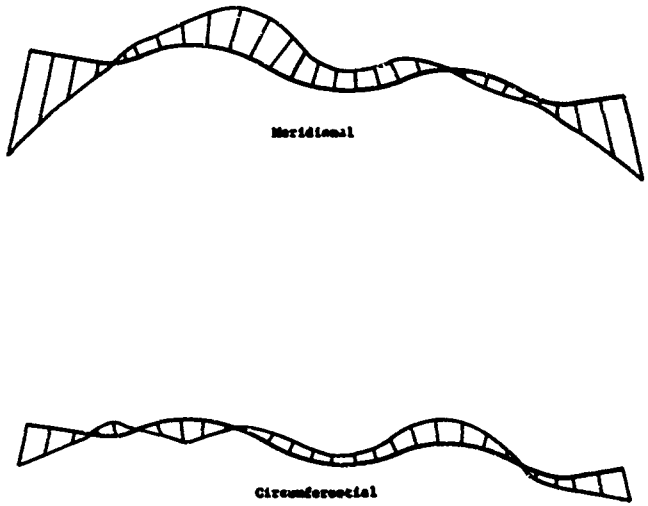

FIGURE D-97. RELATIVE OUTER SURFACE STRESS, σ/p, ON LOWER LEAF DUE TO INTERNAL PRESSURE IN WELDED BELLOWS, MODEL NO. 1, CASE 1

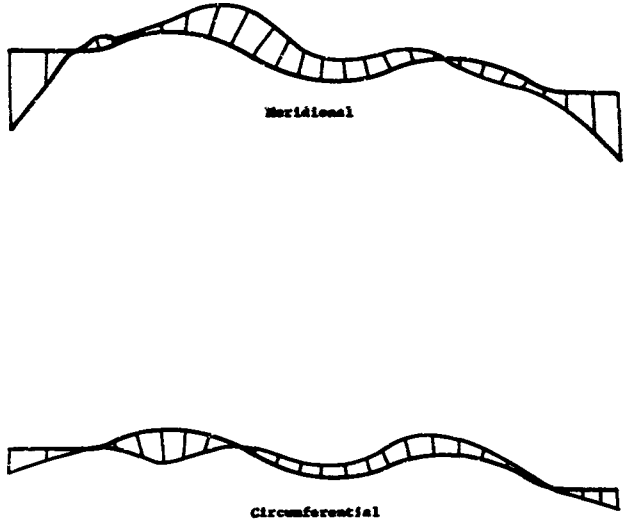

FIGURE D-98. RELATIVE OUTER SURFACE STRESS, σ/p, ON LOWER LEAF DUE TO INTERNAL PRESSURE IN WELDED BELLOWS, MODEL NO. 1, CASE 5

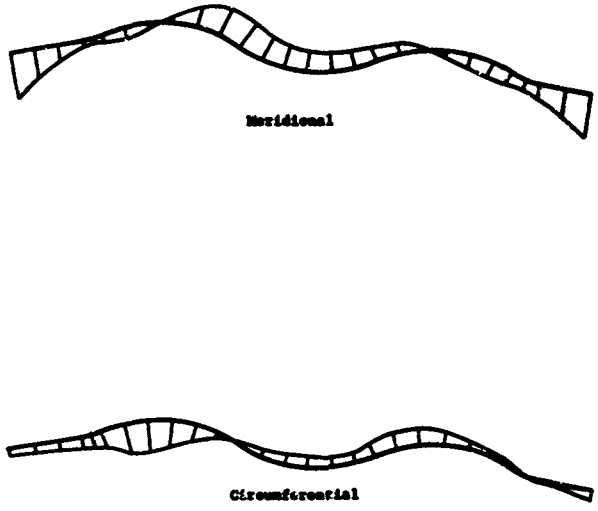

FIGURE D-99. RELATIVE OUTER SURFACE STRESS, σ/p, ON LOWER LEAF DUE TO INTERNAL PRESSURE IN WELDED BELLOWS, MODEL NO. 1, CASE 9

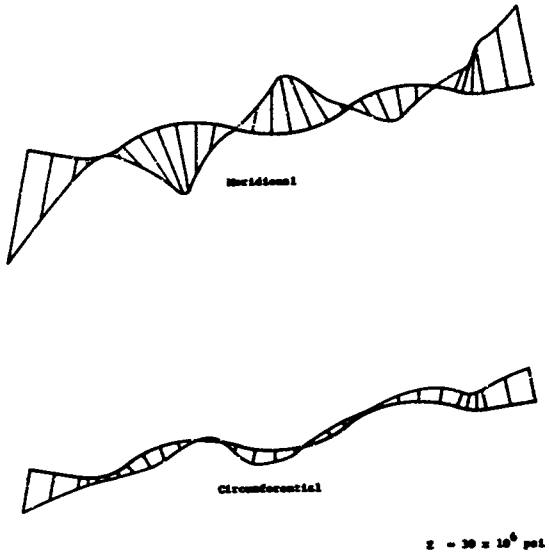

FIGURE D-100. RELATIVE OUTER SURFACE STRESS, $\sigma L/\delta$, ON UPPER LEAF DUE TO AXIAL LOADING ON WELDED BELLOWS, MODEL NO. 2, CASE 1

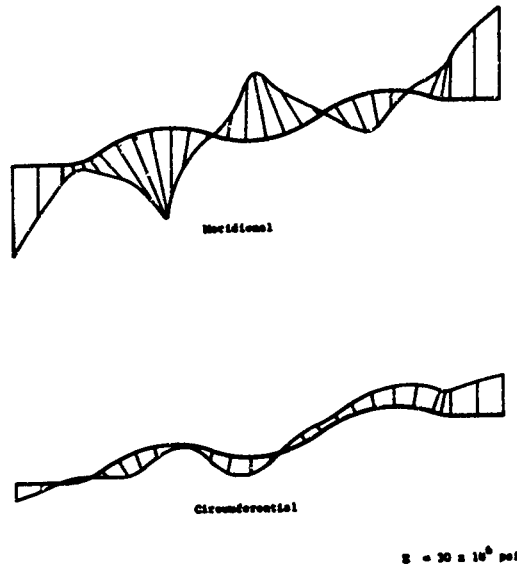

FIGURE D-101. RELATIVE OUTER SURFACE STRESS, $\sigma L/\delta$, ON UPPER LEAF DUE TO AXIAL LOADING ON WELDED BELLOWS, MODEL NO. 2, CASE 5

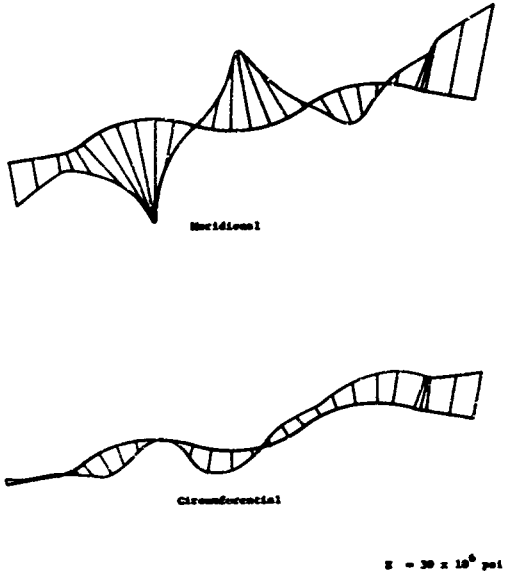

FIGURE D-102. RELATIVE OUTER SURFACE STRESS, $\sigma L/\delta$, ON UPPER LEAF DUE TO AXIAL LOADING ON WELDED BELLOWS, MODEL NO. 2, CASE 9

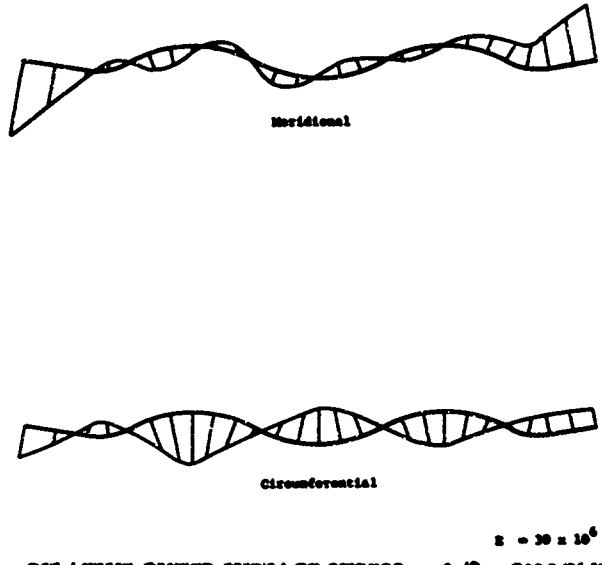

FIGURE D-103. RELATIVE OUTER SURFACE STRESS, $\sigma L/\delta$, ON LOWER LEAF DUE TO AXIAL LOADING ON WELDED BELLOWS, MODEL NO. 2, CASE 1

E = 30 x 10^6 psi

FIGURE D-104. RELATIVE OUTER SURFACE STRESS, $\sigma L/\delta$, ON LOWER LEAF DUE TO AXIAL LOADING ON WELDED BELLOWS MODEL NO. 2, CASE 5

E = 30 x 10^6 psi

FIGURE D-105. RELATIVE OUTER SURFACE STRESS, $\sigma L/\delta$, ON LOWER LEAF DUE TO AXIAL LOADING ON WELDED BELLOWS, MODEL NO. 2, CASE 9

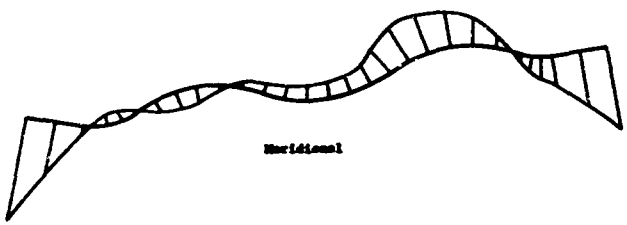

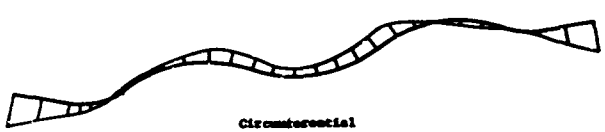

FIGURE D-106. RELATIVE OUTER SURFACE STRESS, σ/p, ON UPPER LEAF DUE TO INTERNAL PRESSURE IN WELDED BELLOWS, MODEL NO. 2, CASE 1

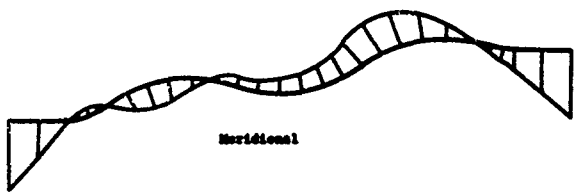

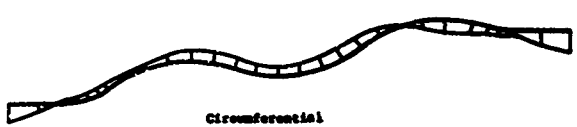

FIGURE D-107. RELATIVE OUTER SURFACE STRESS, σ/p, ON UPPER LEAF DUE TO INTERNAL PRESSURE IN WELDED BELLOWS, MODEL NO. 2, CASE 5

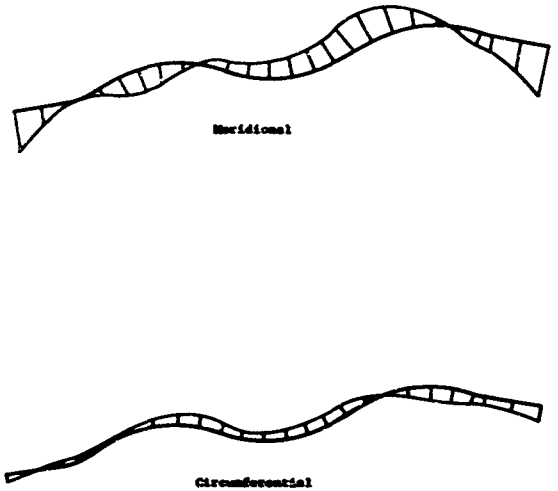

FIGURE D-108. RELATIVE OUTER SURFACE STRESS, σ/p, ON UPPER LEAF DUE TO INTERNAL PRESSURE IN WELDED BELLOWS, MODEL NO. 2, CASE 9

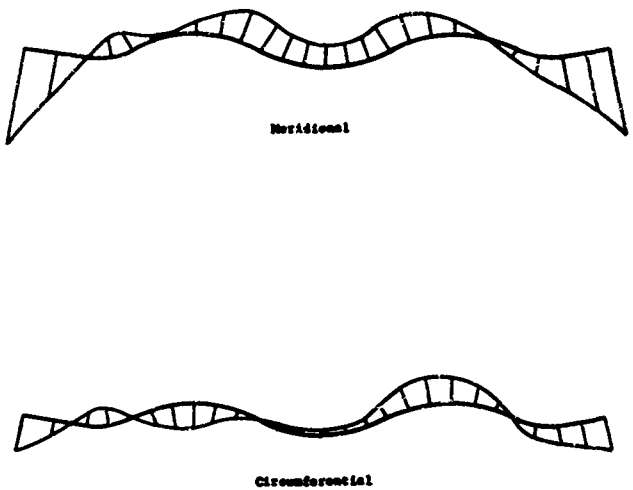

FIGURE D-109. RELATIVE OUTER SURFACE STRESS, σ/p, ON LOWER LEAF DUE TO INTERNAL PRESSURE IN WELDED BELLOWS, MODEL NO. 2, CASE 1

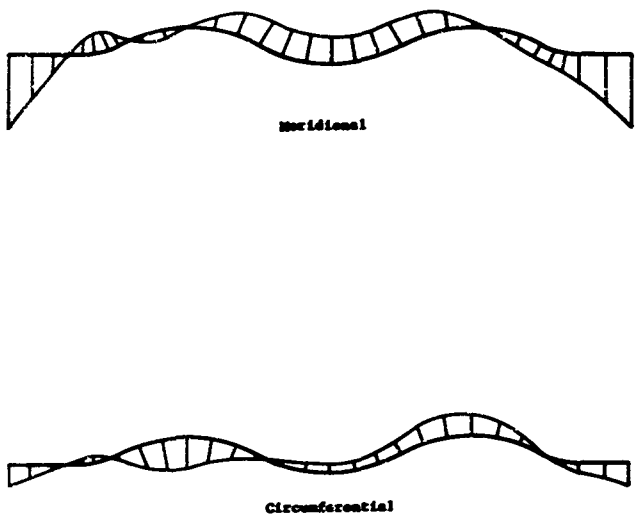

FIGURE D-110. RELATIVE OUTER SURFACE STRESS, σ/p, ON LOWER LEAF DUE TO INTERNAL PRESSURE IN WELDED BELLOWS, MODEL NO. 2 CASE 5

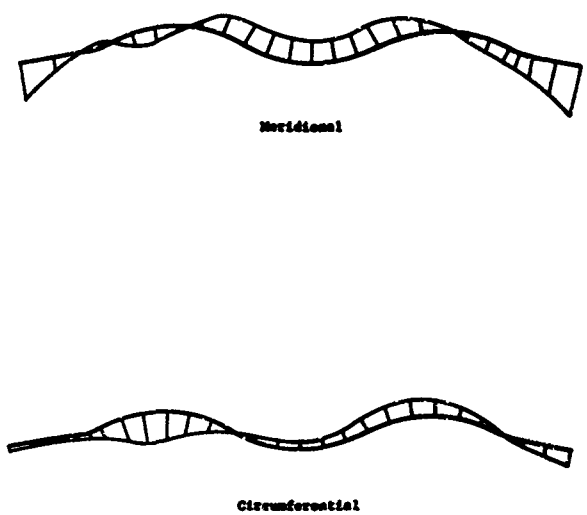

FIGURE D-111. RELATIVE OUTER SURFACE STRESS, σ/p, ON LOWER LEAF DUE TO INTERNAL PRESSURE IN WELDED BELLOWS, MODEL NO. 2, CASE 9

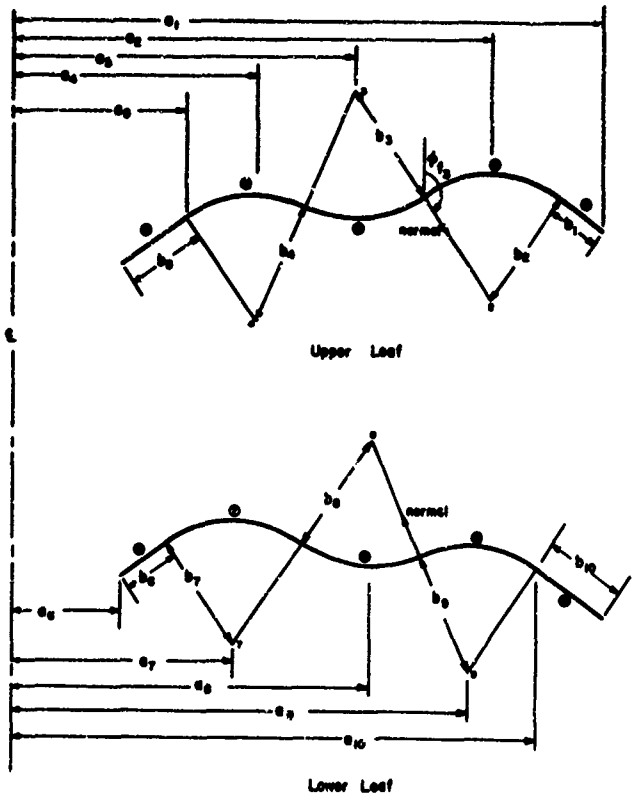

FIGURE D-112. MATHEMATICAL MODEL OF 5°-5° OPTIMUM WELDED BELLOWS

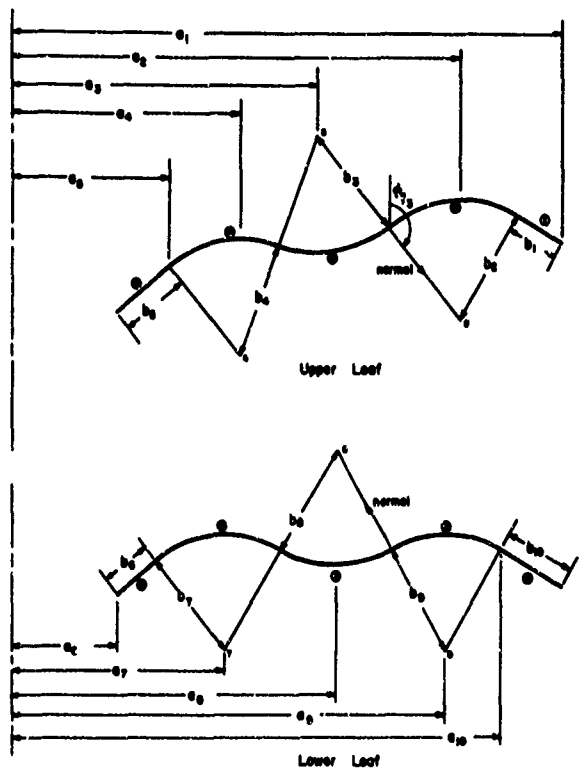

FIGURE D-113. MATHEMATICAL MODEL OF 0°-10° OPTIMUM WELDED BELLOWS

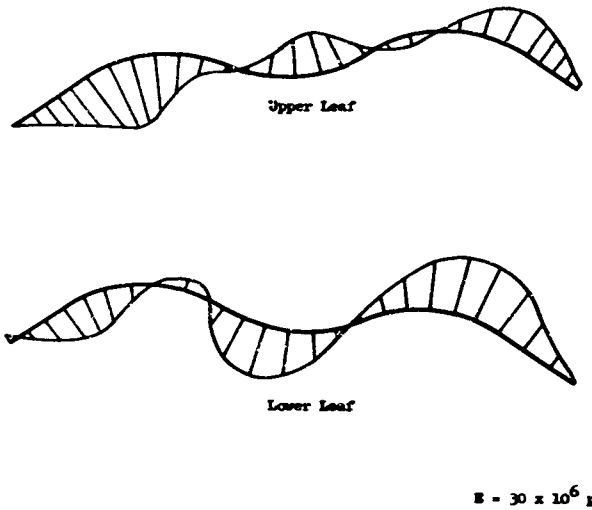

FIGURE D-114. RELATIVE MERIDIONAL OUTER SURFACE STRESS, $\sigma\phi L/\delta$ ON UPPER AND LOWER LEAVES DUE TO AXIAL LOADING ON BELLOWS SHOWN IN FIGURE D-112

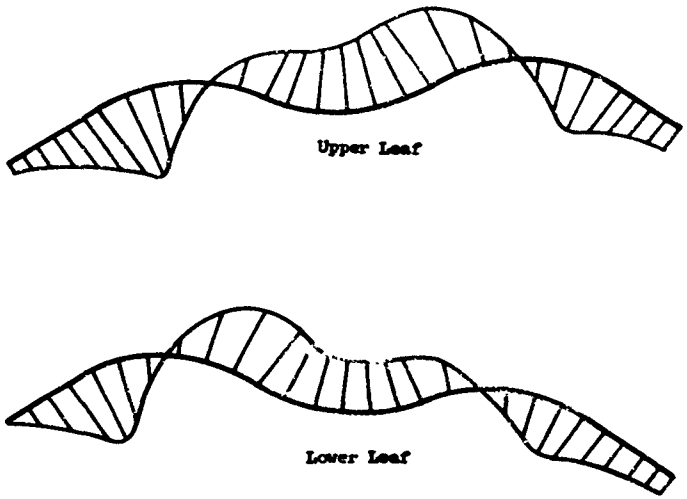

FIGURE D-115. RELATIVE MERIDIONAL OUTER SURFACE STRESS, $\sigma\phi$ /p, δ ON UPPER AND LOWER LEAVES DUE TO INTERNAL PRESSURE IN BELLOWS SHOWN IN FIGURE D-112.

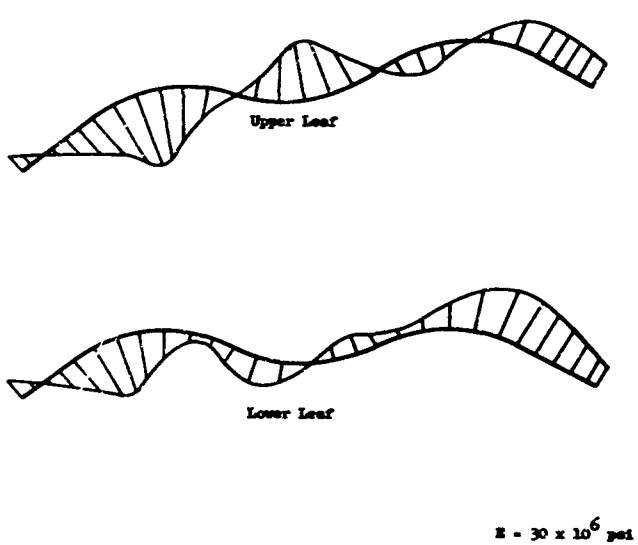

FIGURE D-116. RELATIVE MERIDIONAL OUTER SURFACE STRESS, $\sigma\phi$ L/δ, ON UPPER AND LOWER LEAVES DUE TO AXIAL LOADING ON BELLOWS SHOWN IN FIGURE D-113.

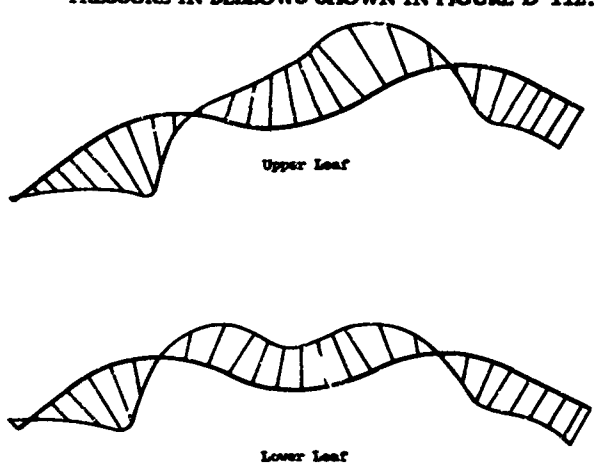

FIGURE D-117. RELATIVE MERIDIONAL OUTER SURFACE STRESS, $\sigma\phi$/p, δ ON UPPER AND LOWER LEAVES DUE TO INTERNAL PRESSURE IN BELLOWS SHOWN IN FIGURE D-113

APPENDIX E

STRESS ANALYSIS OF A 3-INCH, ONE-PLY FORMED BELLOWS - TYPE 321 STAINLESS STEEL

ABBREVIATIONS AND SYMBOLS

S_1, S_2	Measured stresses in bellows, psi
E	Modulus of elasticity, psi
t	Bellows thickness, in.
ϕ	Angle between normal to bellows midsurface and its axis of revolution, deg
p	Internal pressure, psi
δ	Axial deflection imposed on bellows of length L, in.

APPENDIX E

STRESS ANALYSIS OF A 3-INCH, ONE-PLY FORMED BELLOWS - TYPE 321 STAINLESS STEEL

The stress analysis of a 3-inch, one-ply stainless steel bellows was selected for inclusion in the report for three reasons: (1) it is representative of an analysis of a uniform bellows, (2) it was used during the program to determine the need for including thickness variations in mathematical models, and (3) its use facilitates the discussion of the analysis of two-ply bellows in Appendix G. Following the description of the theoretical analysis, the experimental stress analysis of the bellows is described, and theoretically determined and experimentally determined stresses and strains are compared.

Theoretical Stress Analysis

Mathematical Model

A mathematical model was developed using dimensions obtained from the encapsulated cross section of JD68, shown in Figures E-1 and E-2. The inner torus between Convolutions 7 and 8 (measured from the flanged end) was taken as the origin of the rectangular coordinate system. The x-coordinate was in the axial direction with a negative sign indicating measurements taken on Convolution 7. The x- and y-coordinates of points of the midsurface of the convolutions are given in Table E-1. The bellows thicknesses measured at each point normal to the midsurface are also included in Table E-1.

It was believed that the convolution cross section was sufficiently symmetrical about the origin that only one-half a convolution need be considered. To obtain a representative convolution shape, the x-coordinates at symmetric points were averaged. Thus, the x-coordinates of Points 1 and 43, 2 and 42, etc., in Table E-1 were averaged. In addition, the thicknesses at each pair of symmetric points were averaged.

The mathematical model obtained from these measurements is shown in Figure E-3. The actual dimensions of the toroidal and conical sections are given in Table E-2. The thickness variations from the root to the crown are plotted in Figure E-4. The circled points indicate the averaged measurements. The thickness variation selected for the mathematical model is shown by the solid line in Figure E-4.

An examination of Figure E-4 shows that the nominal thickness of 0.008 inch is a poor estimate of the actual thickness of the bellows. It was decided that the variable thickness model should be compared with models having different but constant thicknesses to determine the general necessity for using a mathematical model with thickness variations. Accordingly, stresses were calculated for both internal-pressure loading and axial-compressive loading for three bellows having constant thicknesses of 0.008, 0.00757, and 0.00661 inch as well as for the variable-thickness model. As noted above, 0.008 inch was the nominal thickness. The other two thicknesses were the

maximum and minimum measured thicknesses as shown in Figure E-4. The meridional cross-sectional shape for all the models was taken to be that given in Figure E-3.

Comparison of Stresses From Different Mathematical Models

The bending and membrane stresses in the meridional and circumferential directions calculated for both internal pressure and for axial compression in each of the four models are shown in Figures E-5 through E-12 for the inner torus (Part 1 in Figure E-3) and in Figures E-13 through E-20 for the outer toroidal section (Parts 5 and 6 in Figure E-3).

The stresses at the root and crown for both the axial compressive loading and internal pressure are summarized in Table E-3 for the various thicknesses. The results given in Figures E-5 through E-20 and in Table E-3 show that variations in thickness significantly affect the stresses in the bellows.

Modification of Theoretically Determined Stresses and Strains

It was necessary to modify the theoretical stresses to allow for the thickness of the strain gages before the theoretically determined stresses and strains could be compared with the experimentally determined stresses and strains. Table E-4 shows the theoretical stresses for the variable-thickness model of the 3-inch bellows modified to reflect the thickness of the strain gages (as discussed in Appendix Q). In accordance with the dimensions used for the different mathematical models (see above), a thickness of 0.00757 inch was selected for the inner convolution and a thickness of 0.00661 inch was selected for the outer convolution. To calculate compression stresses, a bellows live length of 2.03 inches was used. This value was obtained by multiplying the measured length for nine convolutions of the JD68 test bellows by the ratio 10/9, since the test bellows had ten convolutions. Strains calculated using the modified theoretical stresses are also shown in Table E-4.

Experimental Stress Analysis

The experimental stress analysis of a 3-inch, formed bellows is described in four parts: (1) strain-gage locations, (2) strains due to axial deflection, (3) strains due to pressure, and (4) stresses calculated from experimentally determined strains.

Strain-Gage Locations

In Appendix Q, a description is given of the type of strain gages used, the techniques of instrumentation, and the philosophy underlying the location of the gages on the bellows. That discussion applies to the strain gages used on the 3-inch bellows. The "middle" convolution chosen for the 3-inch bellows was five convolutions from the bottom. The locations of the gages on the 3-inch formed bellows are shown in Figure E-21.

Strains Due to Axial Deflection

Two types of tests were conducted in which the strains due to axial deflection could be determined. In the first type of test, the bellows was deflected alternately in increments of compression (0.030 inch and 0.060 inch) and extension (0.030 inch and 0.060 inch), and strain-gage readings were taken at each deflection increment and at the intermediate zero deflections. In the second type of test, in which pressure was combined with deflection, the bellows was deflected alternately in increments of compression (0.030 inch and 0.060 inch) and extension (0.030 inch and 0.060 inch), and at each deflection increment, the internal (and subsequently the external) pressure of the bellows was increased in 10-psi increments to 30 psi. By subtracting the readings obtained at each pressure level in the latter type of test, the strain due to deflection could be determined.

Table E-5 shows the results of the deflection tests with no pressure. (None of the tabulated values are corrected for gage thickness.) Despite the apparent flexibility of the 3-inch bellows, the readings of the gages were quite uniform. Table E-6 shows the strains due to deflection when the bellows was pressurized. No significant difference was discernible between the deflection strains for the unpressurized bellows, and the strains for the pressurized bellows.

Strains Due to Pressure

Two types of tests were conducted in which the strains due to pressure could be determined. In the first type of test, the bellows was pressurized at zero deflection: (1) in 10-psi increments of internal pressure to 50 psi and (2) in 10-psi increments of external pressure to 50 psi. The second type of test, combining deflection and pressure, was described above.

Table E-7 shows the primary results of the pressure tests with no deflection. Only two gages were read during the external pressure tests. A similarity of the strains for the last two internal-pressure tests was noted. This probably indicated that the first internal-pressure-test results were less representative, although they were included in the calculation of the average values.

Table E-8 shows the strains due to pressure when the bellows was deflected and pressurized. The results of these tests are given in considerable detail to show the degree of repeatability of the strains due to pressure at different amounts and types of deflection. Not only was the repeatability good, but the average strains in Table E-8 were very similar to those for the unpressurized bellows.

Experimentally Determined Stresses and Strains

The method of calculating stresses from experimentally determined strains is explained in Appendix Q. It is also explained that the strains as given by Gage 18 and the average readings of Gages 11 and 12 and 13 and 17 were used as representative strains in the bellows. Finally, it is explained that the values were selected from tests which did not combine deflection and pressure.

Table E-9 shows the representative compression strains and the representative internal pressure strains as given in Tables E-5 and E-7. To determine the stresses at the convolution roots, where no circumferential gages were used, it was assumed that the ratio of the experimental meridional stress to the experimental circumferential stress was identical to the ratio of the corresponding theoretical meridional and circumferential stresses.

Comparison of Theoretically Determined and Experimentally Determined Stresses and Strains

Table E-10 shows a comparison of the modified theoretical stresses and strains and the experimentally determined stresses and strains. The results are in excellent agreement.

It is noted that the theoretical results shown in Table E-10 were obtained from the mathematical model in which the thickness variations were closely approximated. Because of the importance of thickness (as shown in Figures E-5 through E-20) it is believed that a theoretical analysis of a bellows must incorporate a close approximation to the actual thickness variations of the bellows to provide an accurate prediction of the stresses.

TABLE E-1. COORDINATES AND THICKNESSES FOR MATHEMATICAL MODEL OF 3-INCH BELLOWS JD68 (NOMINAL THICKNESS = 0.008 INCH), 1 UNIT = 0.0005 INCH

Reading	Coordinates x	Coordinates y	Thickness, inches	Reading	Coordinates x	Coordinates y	Thickness, inches
1	-192	641	0.00665	23	13	1	0.00761
2	-176	639	0.00668	24	26	5	0.00761
3	-160	633	0.00668	25	39	16	0.00753
4	-144	622	0.00693	26	49	29	0.00761
5	-128	607	0.00688	27	54	41	0.00738
6	-112	586	0.00685	28	57	53	0.00725
7	-98	560	0.00685	29	59	116	0.00709
8	-90	534	0.00685	30	62	178	0.00705
9	-79	475	0.00696	31	66	237	0.00696
10	-70	415	0.00708	32	71	296	0.00700
11	-64	356	0.00713	33	77	356	0.00693
12	-59	296	0.00717	34	86	415	0.00685
13	-56	237	0.00738	35	94	475	0.00685
14	-54	178	0.00733	36	104	534	0.00677
15	-53	116	0.00750	37	111	560	0.00677
16	-51	53	0.00778	38	123	586	0.00677
17	-49	41	0.00770	39	138	609	0.00656
18	-45	29	0.00753	40	153	626	0.00640
19	-38	16	0.00741	41	169	635	0.00648
20	-26	6	0.00753	42	184	640	0.00660
21	-13	1	0.00753	43	199	641	0.00656
22	0	0	0.00757				

TABLE E-2. DIMENSIONS OF MATHEMATICAL MODEL OF 3-INCH BELLOWS JD68

Part No.	Shell Type	a, inches	b, inches	Coordinates, degree Initial	Final
1	Toroidal	1.5295	-0.0267[a]	90.0	2.0
2	Conical[b]	1.5253	0.0633	2.0	-
3	Toroidal	1.5668	0.763	2.0	6.5
4	Conical	1.6508	0.09	6.5	-
5	Toroidal	1.7198	0.1875	6.5	24.0
6	Toroidal	1.7753	0.0455	24.0	90.0

(a) A negative radius indicates that the normal is pointing toward the center of curvature.

(b) For the conical shell, a is the radial distance from the center of the bellows to the inner edge; b is the slant length of the shell. The initial coordinate is the cone angle.

TABLE E-3. STRESSES DUE TO AXIAL COMPRESSIVE LOADING AND INTERNAL PRESSURE IN 3-INCH BELLOWS JD68 AT THE ROOT AND CROWN AS A FUNCTION OF THE THICKNESS

Thickness, inches	Location	Meridional[a] Membrane	Meridional[a] Bending	Circumferential[a] Membrane	Circumferential[a] Bending
Axial Compression					
0.008	root	-5876.48	-617633	-117301	-185290
	crown	-4843.80	+448685	+150583	+134605
0.00757	root	-5348.06	-586426	-117258	-175928
	crown	-4408.24	+419341	+149899	+125802
variable	root	-4518.20	-517450	-111349	-155235
	crown	-4265.10	+411165	+160782	+123350
0.00661	root	-4271.70	-517093	-117226	-155128
	crown	-3521.03	+352846	+147807	+105854
Internal Pressure					
0.008	root	-20.6477	-727.177	+32.4481	-218.153
	crown	+19.4921	-560.958	-46.9840	-168.287
0.00757	root	-21.7834	-809.540	+31.0523	-242.862
	crown	+20.6299	-621.974	-61.8579	-186.592
variable	root	-22.2870	-881.699	+32.2481	-264.510
	crown	+23.1507	-732.999	-92.3308	-219.900
0.00661	root	-24.8225	-1051.76	+24.6324	-315.527
	crown	+23.7288	-798.477	-111.591	-239.543

(a) Plus values are tensile stresses, minus values are compressive stresses. To obtain stresses in psi due to deflection, multiply value by deflection in inches, divide by live length of bellows in inches. To obtain stresses in psi due to pressure, multiply value by pressure in psi.

TABLE E-4. MODIFIED THEORETICAL COMPRESSION AND INTERNAL PRESSURE STRESSES AND STRAINS FOR THREE-INCH ONE-PLY STAINLESS STEEL FORMED BELLOWS JD68

			Stresses from Table E-3: Membrane Stress	Stresses from Table E-3: Bending Stress, Outer Surface	Modified Bending Stress[a], Outer Surface	Combined Stress at Gage Location	Stress, psi, Calc. for 0.060-in. Compression or 50-psi Int. Pressure	Strain, μin./in. Calc. for 0.060-in. Compression or 50-psi Int. Pressure
Compression Stresses	Outer Convolution	Meridional Stress	-4265.10	+411,165	+578,920	+574,655	+16,987	+484
		Circumferential Stress	+160,782	+123,350	+173,677	+334,459	+9,887	+165
	Inner Convolution	Meridional Stress	-4518.20	-517,450	-702,180	+697,662[b]	+20.623	+681
		Circumferential Stress	-111,349	-155,235	-210,654	+99,305[b]	+2,935	-112
Internal Pressure Stresses	Outer Convolution	Meridional Stress	+23.1507	-732.999	-1032.063	-1008.912	-30,446	-1532
		Circumferential Stress	-92.3308	-219.900	-309.619	-401.950	-20,098	-171
	Inner Convolution	Meridional Stress	-22.2870	-881.699	-1196.466	+1174.179[c]	+58,709	+1822
		Circumferential Stress	+32.2481	-264.510	-358.940	+391.188[c]	+19,559	+67

(a) Bending stresses at outer convolution multiplied by 1.408; bending stresses at inner convolution multiplied by 1.357.
(b) The ratio of these stresses is 7.03.
(c) The ratio of these stresses is 3.00.

TABLE E-5. DEFLECTION STRAINS FOR COMPRESSION AND EXTENSION OF 3-INCH FORMED BELLOWS - NO INTERNAL PRESSURE (c)

Gage No.	Microin. of Strain (a), Bellows in Compression: Test No. 1	Test No. 2	Test No. 3	Test No. 4	Test No. 5	Compression Average	Microinches of Strain (b), Bellows in Extension: Test No. 1	Test No. 2	Test No. 3	Test No. 4	Test No. 5	Extension Average	Combined Average
11	175	177	180	187	182	180	198	195	195	188	195	194	187
12	180	175	180	182	180	179	190	190	190	198	193	192	186
13	375	397	392	395	395	391	388	400	395	405	395	397	394
14	435	435	440	447	442	440	430	430	440	430	438	434	437
15	410	425	397	405	402	408	385	408	418	410	413	407	408
16	395	385	392	387	385	389	398	405	408	408	405	405	397
17	417	400	405	407	405	407	400	400	408	418	415	408	408
18	617	625	622	627	627	624	613	633	630	628	633	627	626
19	512	510	532	525	530	522	585	573	568	565	563	571	547

(a) All measured strains in compression were tensile - deflection was 0.060 inch.

(b) All measured strains in extension were compressive - deflection was 0.060 inch.

(c) Compression and Extension Tests were alternated.

TABLE E-6. DEFLECTION STRAINS FOR 3-INCH FORMED BELLOWS COMPRESSED AND EXTENDED, AND PRESSURIZED INTERNALLY AND EXTERNALLY TO 30 PSI

	Gage No.	Microin. of Strain (a), Bellows in Compression: 0 psi	10 psi	20 psi	30 psi	Compression Average	Microinches of Strain (b), Bellows in Extension: 0 psi	10 psi	20 psi	30 psi	Extension Average	Combined Average
Internal Pressure	11	167	172	180	185	176	188	185	180	175	181	179
	12	180	185	172	180	179	168	180	175	175	177	178
	13	385	380	395	372	383	380	380	378	365	376	380
	14	435	440	430	437	436	400	408	410	390	402	419
	15	405	405	397	407	404	375	388	390	348	375	390
	16	372	387	380	382	380	375	395	378	360	377	379
	17	402	412	390	412	404	373	393	393	375	384	394
	18	645	650	657	657	652	645	648	660	680	661	657
	19	532	532	537	537	535	570	560	563	578	568	552
External Pressure	11	187	182	180	190	185	180	193	180	193	187	186
	13	392	395	390	405	396	385	395	395	403	395	396

(a) All measured strains in compression were tensile - deflection was 0.060 inch.

(b) All measured strains in extension were compressive - deflection was 0.060 inch.

TABLE E-7. PRESSURE STRAINS FOR 3-INCH FORMED BELLOWS PRESSURIZED INTERNALLY AND EXTERNALLY--NO DEFLECTION

Gage	Microinches of Strain[a] Internal Pressure, 50 psi Test No. 1	Test No. 2	Test No. 3	Average	Av. per 10 psi	Microinches of Strain[a] External Pressure, 50 psi Test No. 1	Test No. 2	Test No. 3	Average	Av. per 10 psi
11	-253	-240	-245	-246	-49.2	+267	+267	+267	+267	+53.4
12	-225	-215	-213	-218	-43.6	-	-	-	-	-
13	-1383	-1330	-1328	-1347	-269.4	+1375	+1377	+1377	+1376	+275.2
14	-1348	-1303	-1303	-1318	-263.6	-	-	-	-	-
15	-1180	-1158	-1160	-1166	-233.2	-	-	-	-	-
16	-1603	-1535	-1533	-1557	-311.4	-	-	-	-	-
17	-1248	-1243	-1238	-1243	-248.6	-	-	-	-	-
18	+1885	+1807	+1807	+1833	+366.6	-	-	-	-	-
19	+1147	+1060	+1052	+1086	+217.2	-	-	-	-	-

Plus values indicate measured tensile strain; minus values indicate measured compressive strain.

(a) Tests were run in 10-psi increments ascending and descending--values shown are differences between readings at 50 psi (maximum pressure) and average readings for zero pressure before and after test.

TABLE E-8. PRESSURE STRAINS FOR 3-INCH FORMED BELLOWS COMPRESSED, EXTENDED, AND PRESSURIZED INTERNALLY AND EXTERNALLY TO 30 PSI

		Gage No.	Microinches of Strain[a] for Pressure Increments: Deflection--0.0 in.[b] 0-10 psi	10-20 psi	20-30 psi	Deflection--0.030 in.[b] 0-10 psi	10-20 psi	20-30 psi	Deflection--0.060 in. 0-10 psi	10-20 psi	20-30 psi	Average Change per 10 psi
Compression	Internal Pressure	11	-050	-053	-050	-053	-040	-043	-045	-045	-055	-048
		12	-030	-038	-043	-030	-048	-033	-025	-050	-035	-037
		13	-275	-270	-273	-293	-255	-283	-280	-255	-295	-275
		14	-260	-260	-273	-263	-268	-258	-255	-270	-265	-264
		15	-235	-233	-245	-238	-245	-233	-235	-240	-235	-238
		16	-310	-298	-318	-310	-318	-305	-300	-305	-315	-309
		17	-225	-243	-248	-223	-265	-215	-215	-265	-225	-236
		18	+350	+358	+375	+360	+365	+363	+355	+365	+375	+363
		19	+210	+210	+220	+215	+213	+210	+210	+215	+220	+214
	External Pressure	11	+060	+048	+050	+058	+050	+048	+055	+045	+060	+053
		13	+278	+255	+275	+268	+273	+263	+280	+250	+290	+270
Extension	Internal Pressure	11	-043	-055	-045	-028	-055	-045	-040	-050	-040	-045
		12	-038	-030	-050	-050	-030	-045	-050	-025	-050	-041
		13	-250	-288	-253	-250	-280	-255	-250	-285	-240	-262
		14	-258	-258	-275	-263	-255	-263	-265	-260	-255	-261
		15	-233	-233	-248	-243	-235	-213	-245	-235	-205	-233
		16	-300	-308	-318	-313	-300	-303	-325	-290	-300	-306
		17	-240	-230	-263	-258	-223	-250	-260	-230	-245	-244
		18	+353	+353	+375	+355	+343	+363	+350	+340	+345	+353
		19	+210	+208	+225	+223	+203	+220	+220	+205	+210	+213
	External Pressure	11	+068	+053	+048	+070	+050	+050	+055	+065	+035	+059
		13	+280	+260	+278	+285	+260	+270	+270	+260	+270	+270

( ) Plus values indicate tensile strains; minus values indicate compressive strains.
( ) Average of two readings.

TABLE E-9. EXPERIMENTALLY DETERMINED REPRESENTATIVE STRAINS AND STRESSES IN 3-INCH FORMED BELLOWS

			Gage No. 11	Gage No. 12	Gage No. 13	Gage No. 17	Gage No. 18	Average Representative Strains	Calculated Representative Stresses
Strains for 0.060-in. compression - from Table E-5	Convolu. Crown	Meridional	-	-	+394	+408	-	+401	+14,580
		Circumferential	+187	+186	-	-	-	+187	+ 9,780
	Convolu. Root	Meridional	-	-	-	-	+626	+626	+18,963[a]
		Circumferential	-	-	-	-	-	-	+ 2,697[a]
Strains for 50-psi internal pressure - from Table E-7	Convolu. Crown	Meridional	-	-	-1347	-1243	-	-1295	-43,500
		Circumferential	-246	-218	-	-	-	- 232	-19,800
	Convolu. Root	Meridional	-	-	-	-	+1833	+1833	+59,064[b]
		Circumferential	-	-	-	-	-	-	+19,688[b]

(a) Calculated on the assumption that $S_1/S_2 = 7.03$ (See Table E-4).

(b) Calculated on the assumption that $S_1/S_2 = 3.00$ (See Table E-4).

TABLE E-10. COMPARISON OF THEORETICALLY DETERMINED AND EXPERIMENTALLY DETERMINED STRESSES AND STRAINS FOR 3-INCH ONE-PLY FORMED BELLOWS JD68

			Comparison of Strains[a] microinch/inch		Comparison of Stresses[a] psi	
			Experimental	Theoretical	Experimental	Theoretical
Compression Stresses and Strains	Convolution Crown	Meridional	+401	+484	+14,580	+16,987
		Circumferential	+187	+165	+9,780	+9,887
	Convolution Root	Meridional	+626	+681	+18,963[b]	+20,623
		Circumferential	-	-112	+2,697[b]	+2,935
Internal Pressure Stresses and Strains	Convolution Crown	Meridional	-1295	-1532	-43,500	-50,446
		Circumferential	-232	-171	-19,800	-20,098
	Convolution Root	Meridional	+1833	+1822	+59,064[c]	+58,709
		Circumferential	-	+067	+19,588[c]	+19,559

(a) Calculated and tested for 0.060-in. compression and 50-psi internal pressure.

(b) Calculated on the assumption that $S_1/S_2 = 7.03$ (See Table E-9).

(c) Calculated on the assumption that $S_1/S_2 = 3.00$ (See Table E-9).

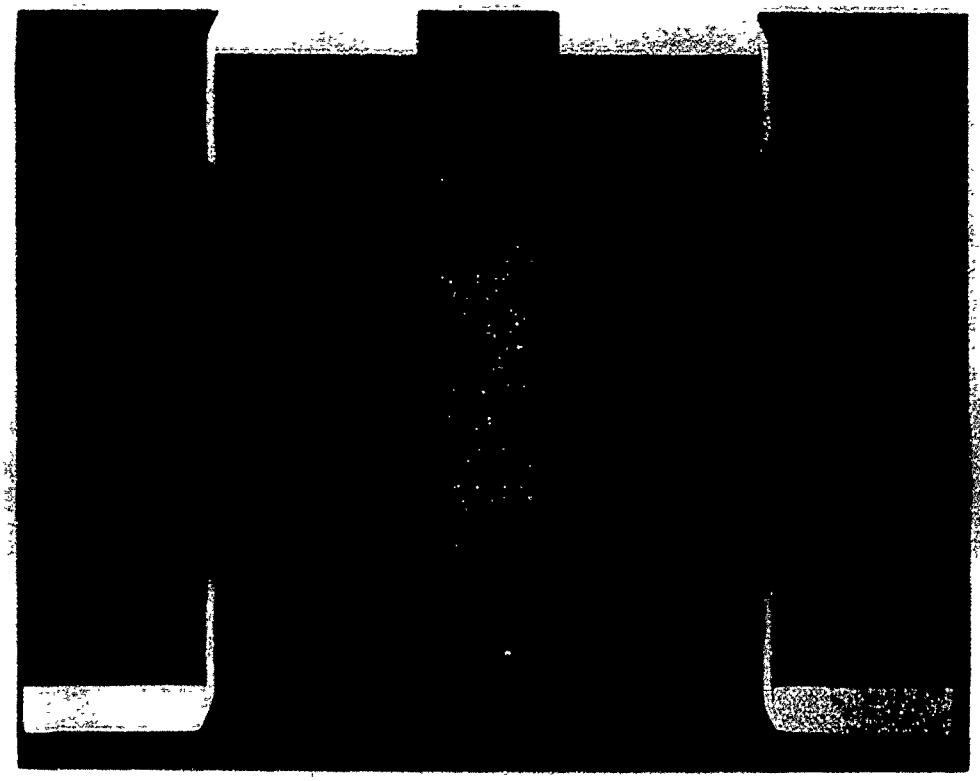

1X As Polished 4A509

FIGURE E-1. CROSS SECTION OF 3-INCH, 1-PLY FORMED BELLOWS JD68 – TYPE 321 STAINLESS STEEL

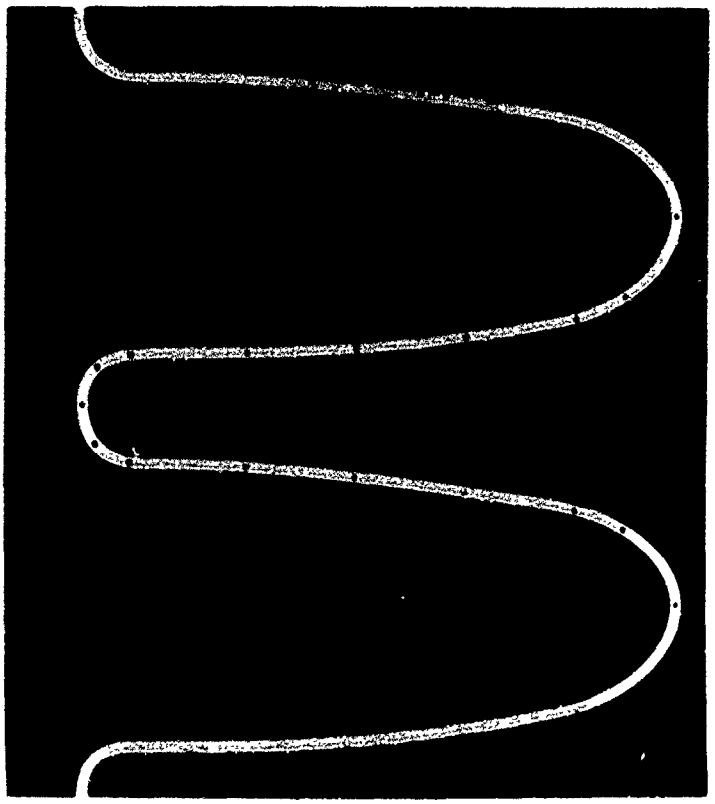

10X As Polished 4A510

FIGURE E-2. ENLARGED VIEW OF CONVOLUTIONS OF CROSS-SECTIONED 3-INCH, 1-PLY FORMED BELLOWS JD68 – TYPE 321 STAINLESS STEEL

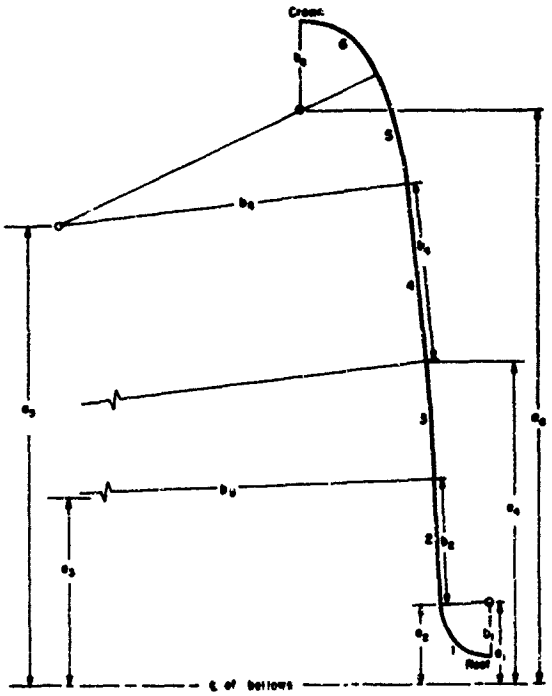

FIGURE E-3. MATHEMATICAL MODEL OF 3-INCH BELLOWS JD68

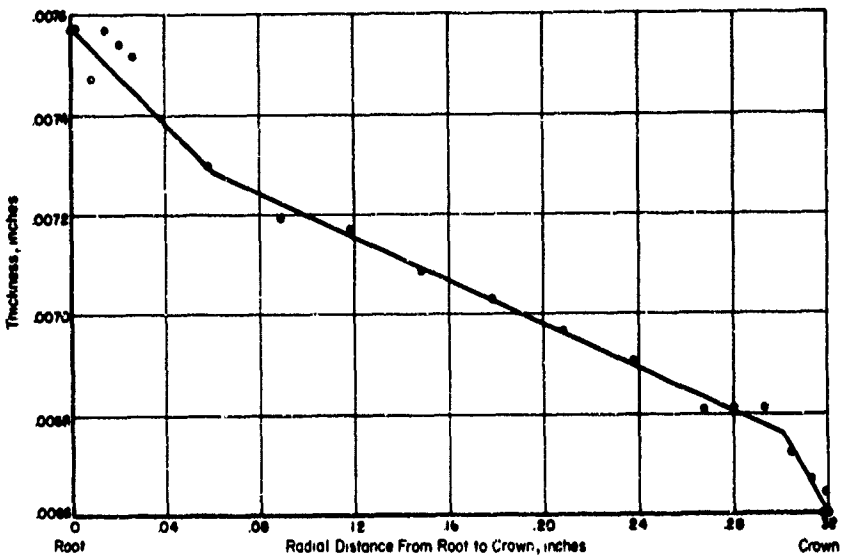

FIGURE E-4. THICKNESS VARIATION IN 3-INCH BELLOWS JD68 (NOMINAL THICKNESS = 0.008 INCH)

Circled points indicate measured thicknesses and solid line is thickness variation used with mathematical model shown in Figure E-3.

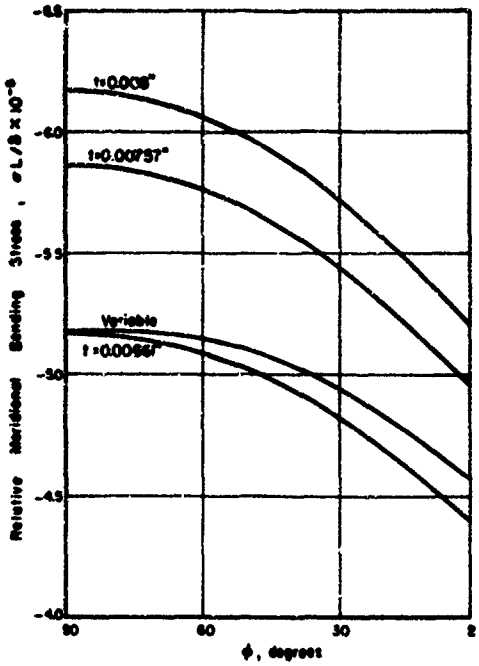

FIGURE E-5. RELATIVE MERIDIONAL BENDING STRESS IN 3-INCH BELLOWS JD68 (PART 1) DUE TO AXIAL COMPRESSIVE LOADING (E = 29 X 10^6 PSI)

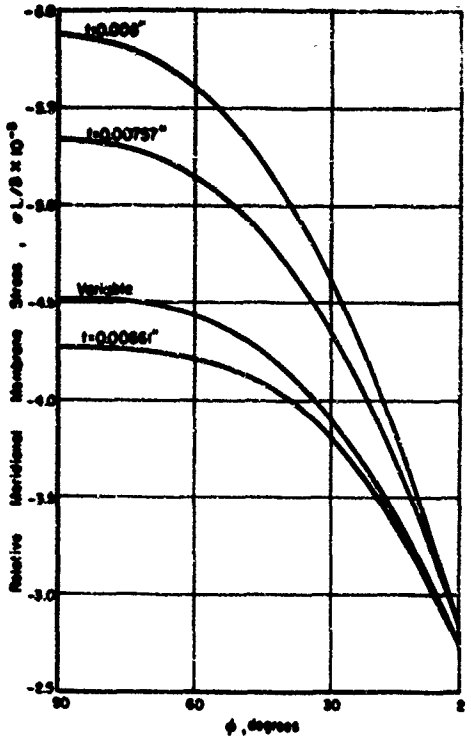

FIGURE E-6. RELATIVE MERIDIONAL MEMBRANE STRESS IN 3-INCH BELLOWS JD68 (PART 1) DUE TO AXIAL COMPRESSIVE LOADING (E = 29 X 10^6 PSI)

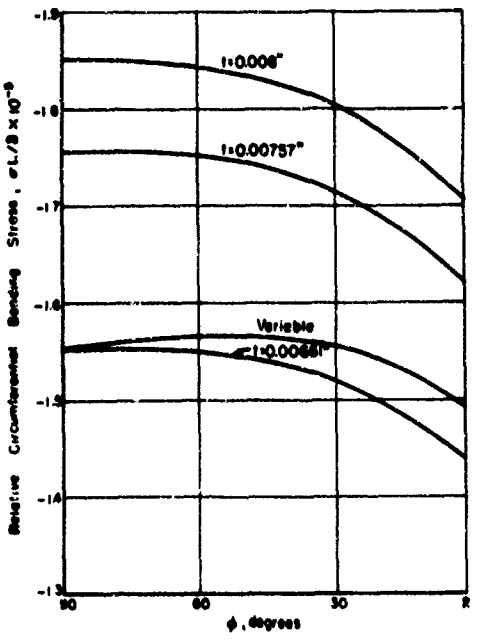

FIGURE E-7. RELATIVE CIRCUMFERENTIAL BENDING STRESS IN 3-INCH BELLOWS JD68 (PART 1) DUE TO AXIAL COMPRESSIVE LOADING (E = 29 X 10^6 PSI)

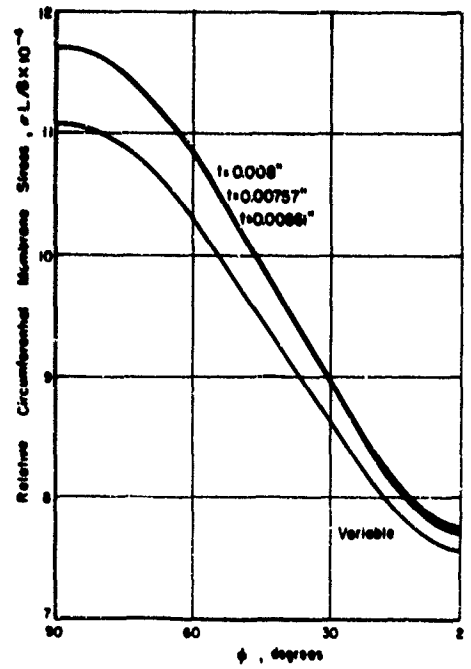

FIGURE E-8. RELATIVE CIRCUMFERENTIAL MEMBRANE STRESS IN 3-INCH BELLOWS JD68 (PART 1) DUE TO AXIAL COMPRESSIVE LOADING (E = 29 X 10^6 PSI)

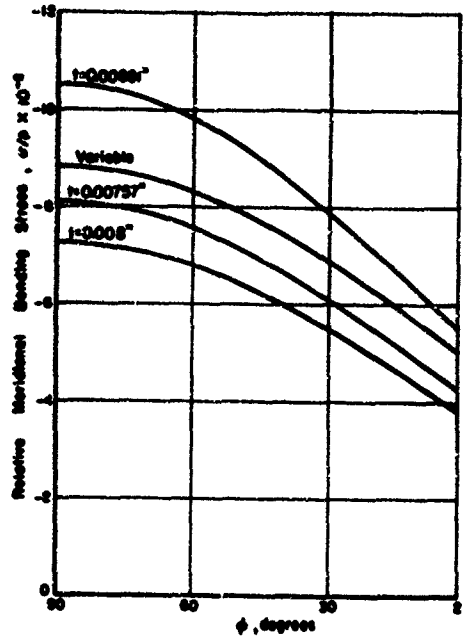

FIGURE E-9. RELATIVE MERIDIONAL BENDING STRESS IN 3-INCH BELLOWS JD68 (PART 1) DUE TO INTERNAL PRESSURE

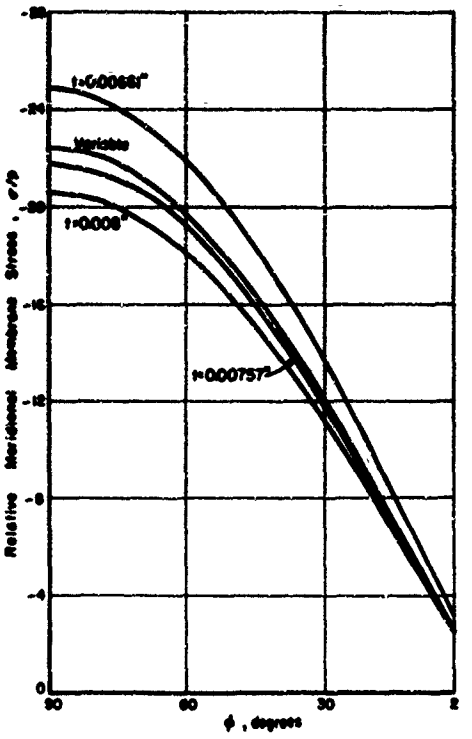

FIGURE E-10. RELATIVE MERIDIONAL MEMBRANE STRESS IN 3-INCH BELLOWS JD68 (PART 1) DUE TO INTERNAL PRESSURE

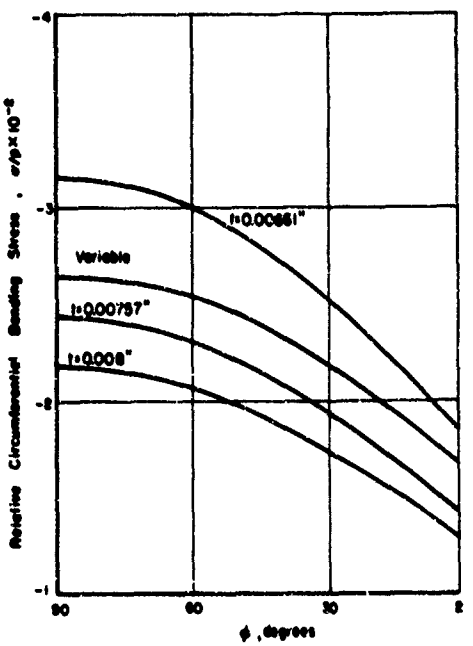

FIGURE E-11. RELATIVE CIRCUMFERENTIAL BENDING STRESS IN 3-INCH BELLOWS JD68 (PART 1) DUE TO INTERNAL PRESSURE

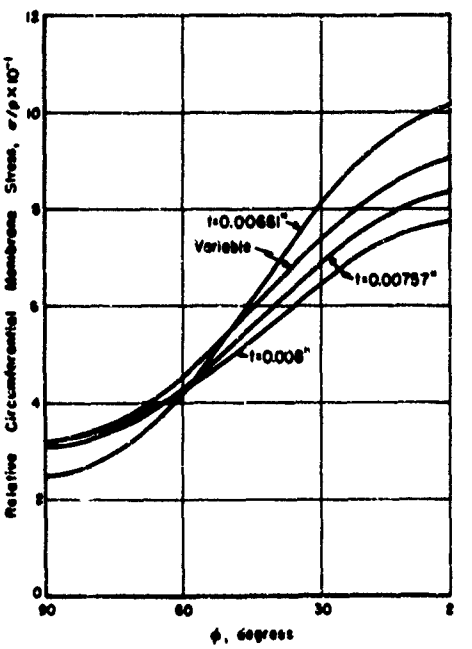

FIGURE E-12. RELATIVE CIRCUMFERENTIAL MEMBRANE STRESS IN 3-INCH BELLOWS JD68 (PART 1) DUE TO INTERNAL PRESSURE

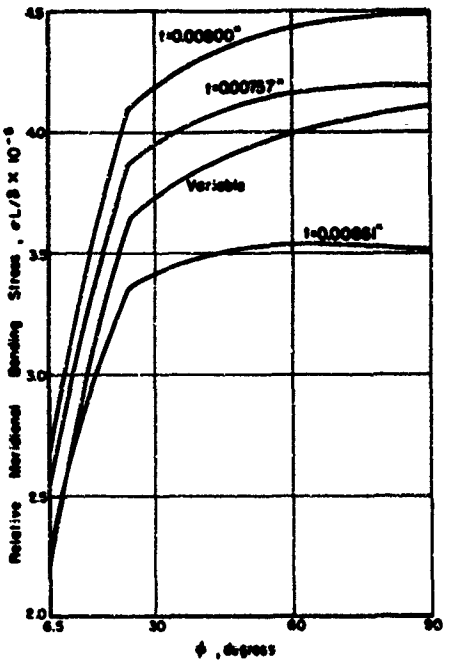

FIGURE E-13. RELATIVE MERIDIONAL BENDING STRESS IN 3-INCH BELLOWS JD68 (PARTS 5, 6) DUE TO AXIAL COMPRESSIVE LOADING (E = 29 X 10^6 PSI)

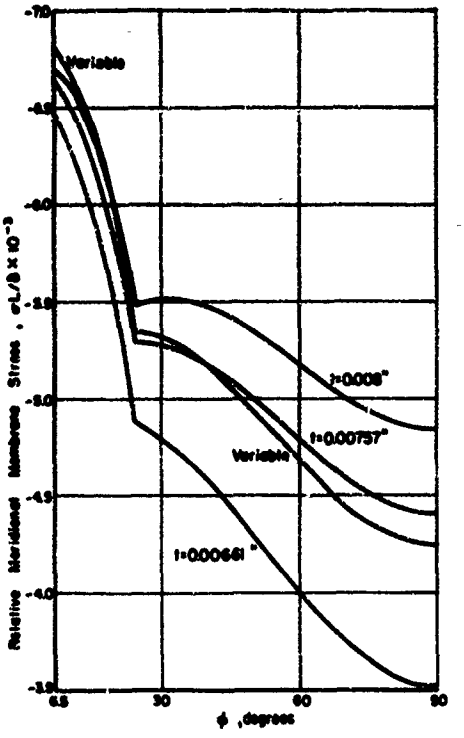

FIGURE E-14. RELATIVE MERIDIONAL MEMBRANE STRESS IN 3-INCH BELLOWS JD68 (PARTS 5, 6) DUE TO AXIAL COMPRESSIVE LOADING (E = 29 X 10^6 PSI)

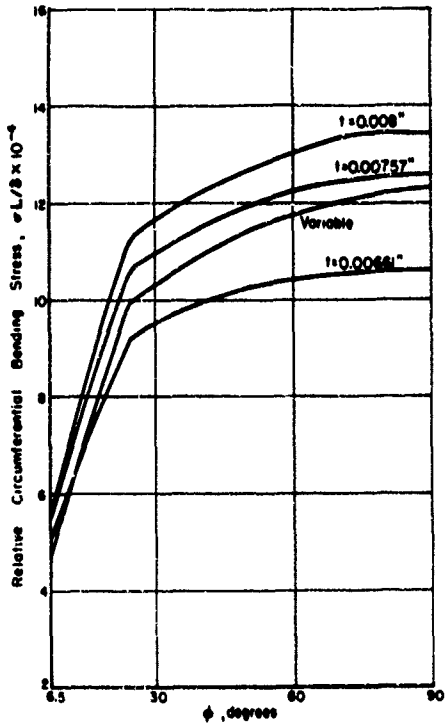

FIGURE E-15. RELATIVE CIRCUMFERENTIAL BENDING STRESS IN 3-INCH BELLOWS JD68 (PARTS 5, 6) DUE TO AXIAL COMPRESSIVE LOADING (E = 29 X 10^6 PSI)

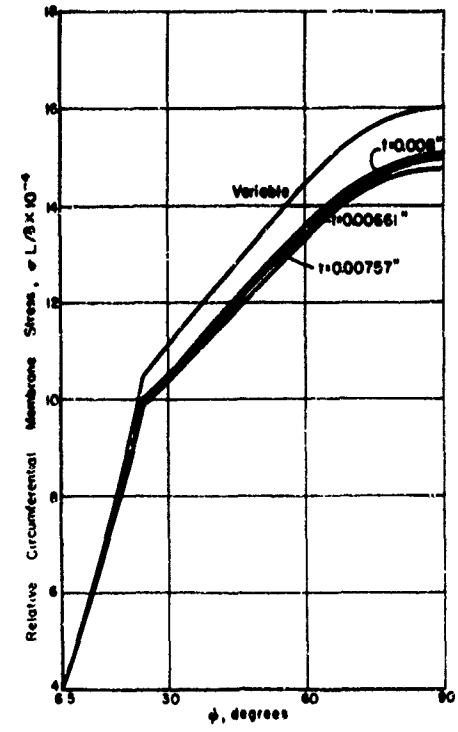

FIGURE E-16. RELATIVE CIRCUMFERENTIAL MEMBRANE STRESS IN 3-INCH BELLOWS JD68 (PARTS 5, 6) DUE TO AXIAL COMPRESSIVE LOADING (E = 29 X 10^6 PSI)

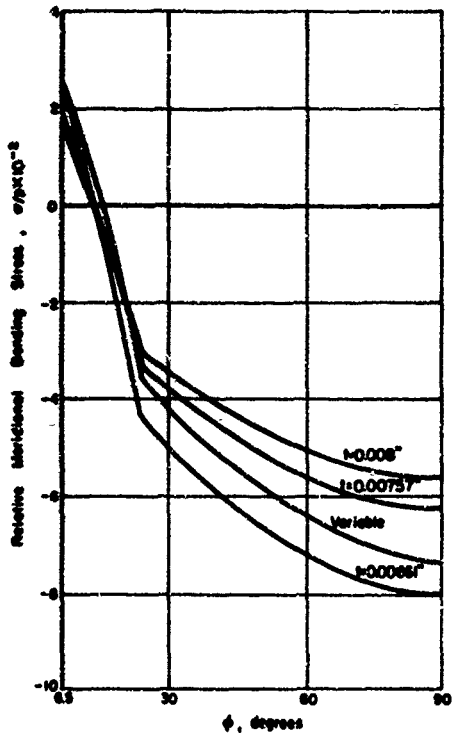

FIGURE E-17. RELATIVE MERIDIONAL BENDING STRESS IN 3-INCH BELLOWS JD68 (PARTS 5, 6) DUE TO INTERNAL PRESSURE

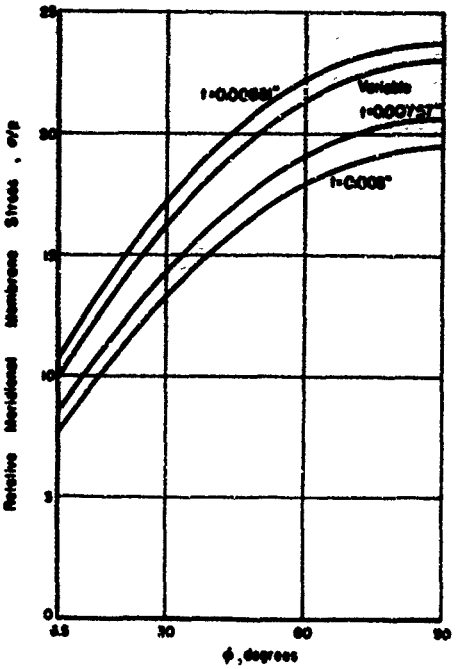

FIGURE E-18. RELATIVE MERIDIONAL MEMBRANE STRESS IN 3-INCH BELLOWS JD68 (PARTS 5, 6) DUE TO INTERNAL PRESSURE

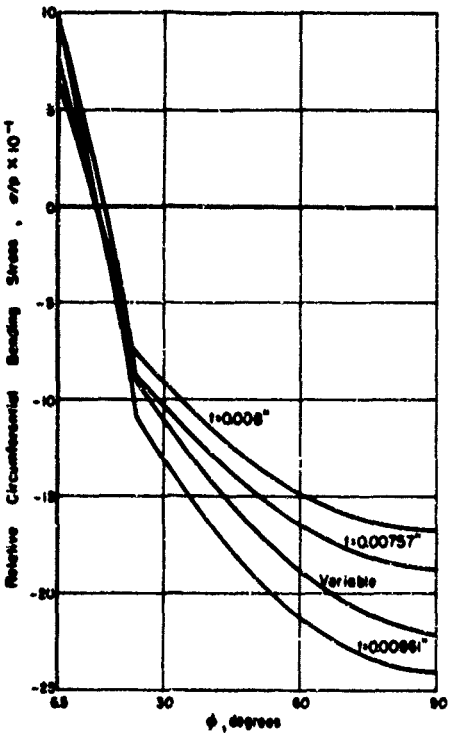

FIGURE E-19. RELATIVE CIRCUMFERENTIAL BENDING STRESS IN 3-INCH BELLOWS JD68 (PARTS 5, 6) DUE TO INTERNAL PRESSURE

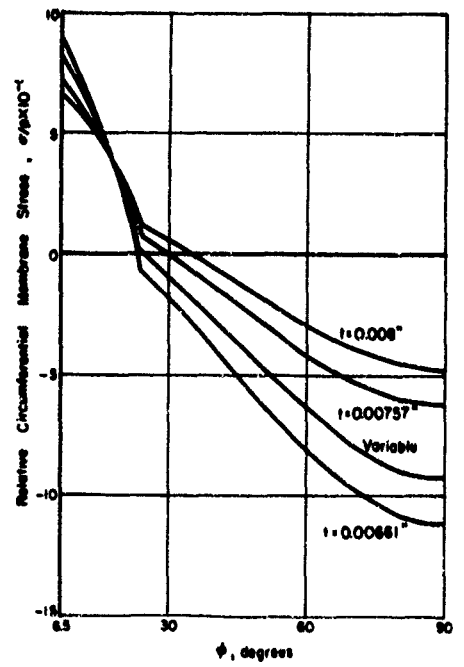

FIGURE E-20. RELATIVE CIRCUMFERENTIAL MEMBRANE STRESS IN 3-INCH BELLOWS JD68 (PARTS 5, 6) DUE TO INTERNAL PRESSURE

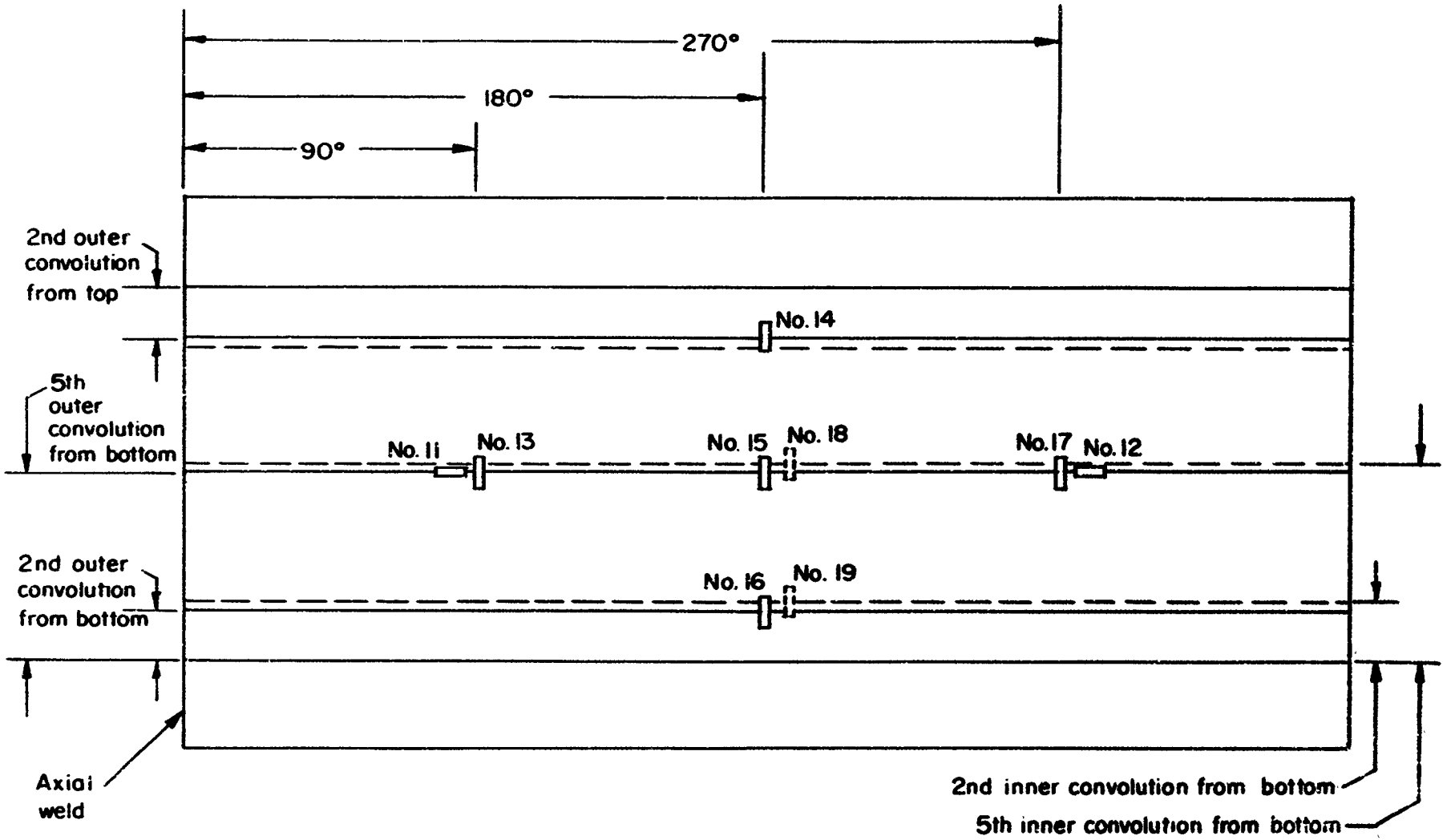

FIGURE E-21. STRAIN-GAGE LOCATIONS FOR 3-INCH, ONE-PLY STAINLESS STEEL FORMED BELLOWS

APPENDIX F

STRESS ANALYSIS OF A 1-INCH ONE-PLY FORMED BELLOWS - TYPE 321 STAINLESS STEEL

APPENDIX F

STRESS ANALYSIS OF A 1-INCH ONE-PLY FORMED BELLOWS - TYPE 321 STAINLESS STEEL

The theoretical stress analysis of a 1-inch, one-ply stainless steel formed bellows was selected for inclusion in the report because (1) it demonstrates an approach to modeling convolutions which are not symmetrical and (2) it facilitates the discussion in Appendix G of the stress analysis of two-ply bellows. Following the theoretical stress analysis, the experimental stress analysis is described, and theoretically determined and experimentally determined stresses and strains are compared.

Theoretical Stress Analysis

Mathematical Model

The theoretical stress analysis of the 1-inch bellows (JD29) proved to be more complex than the analysis of the 3-inch bellows which was described in Appendix E. The irregular shape of the convolutions, as shown in Figures F-1, F-2, and F-3, required a more detailed mathematical model. The data used to construct this model, which is shown in Figure F-4, are given in Tables F-1 and F-2. In the analysis, the mathematical model was taken to be a full convolution since there appeared to be no symmetry with respect to a half convolution either in the shape of the midsurface of the shell, or in the variation of the thickness (as shown in Figures F-5 and F-6). The solid lines in Figures F-5 and F-6 show the thickness variations used in the mathematical model.

Theoretical Stresses

The theoretical stresses at the outer convolution and two inner convolutions of the mathematical model (the locations of highest stress) are shown in Table F-3. Irregularities in the bellows are indicated by the differences in the calculations for each convolution root of the mathematical model. The results of the analysis of the 1-inch bellows by thin-shell theory should eventually be compared with a rigorous theory-of-elasticity solution, since the radius-to-thickness ratio for certain portions of bellows JD29 was as low as 2:1 as compared with the ratio of 10:1 which is generally considered to be the lower limit for which thin-shell theory is accurate.

Modification of Theoretically Determined Stresses and Strains

Table F-4 shows theoretical stresses for the 1-inch bellows modified to reflect the thickness of the strain gages (as described in Appendix Q). In accordance with Figures F-5 and F-6, a thickness of 0.0391 inch was selected for the outer convolution and a thickness of 0.0045 inch was selected for inner convolution Part 1 (for the location of the strain gages, see below). A live length of 1.01 inches was used to determine the deflection stresses. The length of seven convolutions (0.886 inch) was multiplied by 8/7

to estimate the live length of the test bellows. Table F-4 also shows strains calculated using the modified theoretical stresses.

Experimental Stress Analysis

Strain-Gage Locations

Appendix Q gives a description of the type of strain gages used, the techniques of instrumentation, and the philosophy underlying the location of the gages on the bellows. Because the 1-inch bellows had eight convolutions, the "middle" convolution selected was the fourth convolution from the bottom. The strain-gage locations are shown in Figure F-7. Both of the root gages were located on convolution roots corresponding to Part 1 in Figure F-4.

Strains Due to Axial Deflection

The types of tests conducted with the 3-inch one-ply formed bellows (see Appendix E) were conducted with the 1-inch formed bellows. Table F-5 shows the results of the deflection tests with no pressure, while Table F-6 shows the strains due to deflection when the bellows was pressurized. (For simplicity, the readings were not corrected for gage thickness.) No significant differences were noted between the strains shown in Table F-5 and those shown in Table F-6, if allowance is made for the difference in deflection.

Strains Due to Pressure

The types of pressure tests conducted with the 3-inch bellows were conducted with the 1-inch bellows. Table F-7 shows the results of the pressure tests with no deflection, while Table F-8 shows the results of the tests with pressure and deflection. No significant differences were noted between the strains shown in Table F-7 and those shown in Table F-8.

Experimentally Determined Stresses and Strains

Table F-9 shows the representative compression strains and the representative internal pressure strains selected according to the procedures described in Appendix Q. Also shown are stresses calculated using these strains. For the convolution root, where no circumferential strain gage was used, the stresses were calculated with the assumption that the ratio of the experimental meridional stress to the experimental circumferential stress was the same as the ratio of the theoretical meridional stress to the theoretical circumferential stress.

Comparison of Theoretically and Experimentally Determined Stresses and Strains

Table F-10 shows a comparison of the modified theoretical stresses and strains and the experimentally determined stresses and strains. Although the values did not compare as closely as for the 3-inch bellows, the agreement was believed to be good. Further, the compression meridional strains measured by Gages Nos. 15, 16, and 17 (1041, 1073, and 1007 microin./in. in Table F-5) at the convolution crowns agreed closely with the theoretically predicted strain (1004 microin./in.) while the internal-pressure meridional strain at the convolution crowns measured by Gages Nos. 14 and 15 (-195 and -210 microin./in. in Table F-7) agreed closely with the theoretically predicted strain (-209 microin./in.).

It was thought that the greater variation in gage readings for the 1-inch bellows (as compared with the 3-inch bellows) might have been caused by greater nonuniformity in thickness. However, an examination of the thickness in both cross-sectioned bellows did not show greater nonuniformity in the 1-inch bellows than in the 3-inch bellows. Consequently, it was presumed that the greater variations in measured strains were caused at least partially by variations in convolution curvature such as those noted in Figures F-1 through F-3.

TABLE F-1. COORDINATES AND THICKNESSES FOR 1-INCH BELLOWS JD29
Nominal thickness = 0.005 in.; 1 unit = 0.005 in.

Reading	Coordinates x	Coordinates y	Thickness, inch	Reading	Coordinates x	Coordinates y	Thickness, inch
1	0	0	0.00442	52	232	9	0.00438
2	8	2	0.00446	53	241	12	0.00446
3	14	4	0.00446	54	248	17	0.00441
4	20	8	0.00446	55	254	23	0.00450
5	24.5	12	0.00446	56	260	31	0.00450
6	30	17	0.00446	57	265.5	38	0.00450
7	35	23	0.00442	58	270.5	46	0.00441
8	40	31	0.00442	59	274.4	55	0.00446
9	44	38	0.00442	60	278	72	0.00441
10	47	46	0.00442	61	276.5	88	0.00433
11	48	55	0.00437	62	273.5	106	0.00433
12	46	72	0.00437	63	267	134	0.00433
13	44	88	0.00434	64	263	160	0.00425
14	41	106	0.00425	65	260	188	0.00417
15	36	134	0.00425	66	258	215	0.00417
16	32	160	0.00417	67	257	243	0.00397
17	29	188	0.00405	68	258.5	271	0.00397
18	27.5	215	0.00401	69	261	285	0.00405
19	28	243	0.00393	70	264	297	0.00401
20	31	271	0.00385	71	271	310	0.00401
21	35	285	0.00385	72	279	321	0.00401
22	39	297	0.00385	73	289	332	0.00397
23	45	310	0.00385	74	306	344	0.00397
24	54	321	0.00385	75	325	349.5	0.00397
25	64	332	0.00381	76	344	344	0.00401
26	80	344	0.00381	77	362	332	0.00401
27	102	349.5	0.00381	78	371	321	0.00397
28	130	342	0.00368	79	380	310	0.00401
29	144	332	0.00381	80	386	297	0.00401
30	154	321	0.00385	81	390	285	0.00401
31	162	310	0.00385	82	393	271	0.00401
32	168.5	297	0.00381	83	397	243	0.00397
33	172.5	285	0.00377	84	399.5	215	0.00401
34	176	271	0.00381	85	401	188	0.00409
35	178	243	0.00385	86	401	160	0.00413
36	179.5	215	0.00385	87	399	134	0.00417
37	180	188	0.00393	88	397.5	106	0.00433
38	178.5	160	0.00405	89	396	88	0.00437
39	177.5	134	0.00405	90	393.5	72	0.00437
40	175	106	0.00413	91	391	55	0.00446
41	173	88	0.00421	92	390	46	0.00446
42	171	72	0.00425	93	389.5	38	0.00446
43	169	55	0.00433	94	390	31	0.00442
44	168	46	0.00433	95	394	23	0.00458
45	170	38	0.00437	96	399	17	0.00466
46	173.5	31	0.00446	97	405	12	0.00466
47	182.5	23	0.00450	98	410	9	0.00470
48	191	17	0.00470	99	415	6	0.00458
49	200	12	0.00458	100	420	4	0.00458
50	210.5	9	0.00437	101	426	3	0.00454
51	223	8	0.00441	102	433	2	0.00454

TABLE F-2. DIMENSIONS OF MATHEMATICAL MODEL OF 1-INCH BELLOWS JD29

Part	Shell Type	a, inches	b, inches	Coordinates, degrees Initial	Final
1	Toroidal	0.5026	-0.00950	90.0	70.0
2	Toroidal	0.5726	-0.08432	70.0	59.25
3	Toroidal	0.5108	-0.01233	59.25	30.25
4	Toroidal	0.5143	-0.01916	30.25	-7.0
5	Conical[a]	0.5166	0.01667	-7.0	-
6	Toroidal	0.5706	0.30214	-7.0	-3.5
7	Conical	0.5561	0.01600	-3.5	-
8	Toroidal	0.5870	0.23964	-3.5	2.25
9	Conical	0.5968	0.01800	2.25	-
10	Toroidal	0.6120	0.06583	2.25	35.0
11	Toroidal	0.6300	0.03466	35.0	85.25
12	Toroidal	0.6459	0.01833	85.25	121.5
13	Toroidal	0.6128	0.05766	121.5	139.0
14	Toroidal	0.6203	0.04600	139.0	164.75
15	Toroidal	0.6048	0.10716	164.75	176.25
16	Toroidal	0.6001	0.19180	176.25	189.0
17	Conical	0.5690	0.05000	189.0	-
18	Toroidal	0.5110	-0.01700	189.0	162.5
19	Toroidal	0.5223	-0.03550	162.5	114.0
20	Toroidal	0.4990	-0.01000	114.0	90.0

(a) a is the radial distance from the center of the bellows to the inner edge for Shells 5, 7, and 9 and to the outer edge for Shell 17. b is the slant length of the conical shell. The initial coordinate is the cone angle.

TABLE F-3. STRESSES DUE TO AXIAL COMPRESSIVE LOADING AND INTERNAL PRESSURE IN 1-INCH BELLOWS JD29 AT THE CROWN AND EACH ROOT OF THE MATHEMATICAL MODEL

	Location	Meridional Stresses[a] Membrane	Meridional Stresses[a] Bending	Circumferential Stresses[a] Membrane	Circumferential Stresses[a] Bending
Axial Loading	Root (Part No. 1)	-5305.79	-519,640	-95,843.8	-155,892
	Crown	-4575.00	+352,630	+155,462	+105,778
	Root (Part No. 20)	(-5458.67)	(-583,078)	(-58,007.0)	(-174,923)
Pressure Loading	Root (Part No. 1)	-19.2756	-565.000	+1.19862	-169.500
	Crown	+20.6420	-436.388	-150.044	-130.910
	Root (Part No. 20)	(-21.9054)	(-736.986)	(-29.9186)	(-221.096)

(a) Plus values are tensile stresses, minus values are compressive stresses. To determine stresses in psi due to deflection, multiply value by deflection in inches, divide by live length of bellows in inches. To obtain stresses in psi due to pressure, multiply value by pressure in psi.

TABLE F-4. MODIFIED THEORETICAL DEFLECTION AND PRESSURE STRESSES AND STRAINS FOR 1-INCH SINGLE-PLY STAINLESS STEEL FORMED BELLOWS

			Stresses From Table F-3		Modified Bending Stress[a] Outer Surface	Combined Stress at Gage Location	Stress, psi, Calculated for 0.060-in. Compression, or 10-psi Internal Pressure	Strain, μin/in, Calc. for 0.060-in. Compression, or 10-psi Internal Pressure
			Membrane Stress	Bending Stress, Outer Surface				
Compression Stresses	Outer Convolution	Meridional Stress	-4,575.00	+352,630	+596,297	+591,722	+35,048	+1004
		Circumferential Stress	+155,462	+105,778	+178,871	+334,333	+19,803	+320
	Inner Convolution	Meridional Stress	-5,305.79	-519,640	-831,424	+826,118[b]	+48,931	+1593
		Circumferential Stress	-95,843.8	-155,892	-249,427	+153,583[b]	+9,097	-192
Internal Pressure Stresses	Outer Convolution	Meridional Stress	+20.6420	-436.388	-737.932	-717.290	-7,173	-209
		Circumferential Stress	-150.044	-130.910	-221.369	-371.413	-3,714	-054
	Inner Convolution	Meridional Stress	-19.2756	-565.000	-904.000	+884.724[c]	+8,847	+277
		Circumferential Stress	+1.19862	-169.500	-271.200	+272.399[c]	+2,724	+003

(a) Bending Stresses at outer convolution multiplied by 1.691; bending stresses at inner convolution multiplied by 1.600.
(b) The ratio of these stresses is 5.38.
(c) The ratio of these stresses is 3.25.

TABLE F-5. DEFLECTION STRAINS FOR COMPRESSION AND EXTENSION OF 1-INCH FORMED BELLOWS - NO INTERNAL PRESSURE[a]

Gage No.	Microinches of Strain[b], Bellows in Compression: Test No. 1	Test No. 2	Test No. 3	Test No. 4	Test No. 5	Compression Average	Microinches of Strain[c] Bellows in Extension: Test No. 1	Test No. 2	Test No. 3	Test No. 4	Test No. 5	Extension Average	Combined Average
11	490	480	487	490	480	485	510	505	503	498	503	504	495
12	390	375	365	370	380	376	448	433	440	440	443	441	409
13	805	775	832	792	765	794	695	673	675	693	645	676	735
14	815	802	805	807	802	806	703	703	708	700	708	704	755
15	1127	1122	1125	1125	1117	1123	958	960	955	953	965	958	1041
16	1140	1135	1135	1147	1137	1137	1018	1013	1003	1005	1008	1009	1073
17	1052	1047	1047	1042	1030	1044	970	965	973	965	970	969	1007
18	1372	1360	1372	1370	1360	1367	1350	1345	1348	1350	1345	1348	1358
19	1372	1360	1375	1372	1365	1369	1420	1415	1415	1415	1418	1417	1393

(a) Compression and extension tests were alternated.
(b) All measured strains in compression were tensile--deflection was 0.060 inch.
(c) All measured strains in extension were compressive--deflection was 0.060 inch.

TABLE F-6. DEFLECTION STRAINS FOR 1-INCH FORMED BELLOWS COMPRESSED AND EXTENDED, AND PRESSURIZED INTERNALLY AND EXTERNALLY TO 50 PSI

	Gage No.	Microinches of Strain[a], Bellows in Compression: 0 psi	10 psi	20 psi	30 psi	40 psi	50 psi	Compression Average	Microinches of Strain[b] Bellows in Extension: 0 psi	10 psi	20 psi	30 psi	40 psi	50 psi	Extension Average	Combined Average
Internal Pressure	11	253	250	248	243	249	234	246	251	255	247	246	252	247	250	248
	12	210	200	191	185	184	179	192	212	208	197	203	198	193	202	197
	13	360	365	361	359	328	340	352	330	319	327	340	330	322	328	340
	14	386	370	349	383	400	377	378	347	344	377	370	361	365	361	370
	15	554	549	540	530	525	532	538	498	487	497	507	504	508	500	519
	16	577	560	549	546	536	543	552	524	518	537	532	534	530	529	541
	17	534	523	525	528	534	509	526	509	505	508	483	499	507	502	514
	18	684	690	696	686	698	705	693	684	692	683	693	693	693	690	692
	19	688	696	695	689	690	694	692	719	719	708	715	718	712	715	704
External Pressure	11	251	243	246	248	250	251	248	265	267	272	280	273	267	271	260
	13	291	271	279	285	302	315	291	284	277	297	305	288	298	292	292

(a) All measured strains in compression were tensile - deflection was 0.030 inch - average of two tests.
(b) All measured strains in extension were compressive - deflection was 0.030 inch - average of two tests.

TABLE F-7. PRESSURE STRAINS FOR 1-INCH FORMED BELLOWS PRESSURIZED INTERNALLY AND EXTERNALLY--NO DEFLECTION

Gage No.	Microin. of Strain[a], 50-psi Internal Pressure: Test No. 1	Test No. 2	Test No. 3	Test No. 4	Test No. 5	Test No. 6[b]	Test No. 7[b]	Average	Av per 10 psi	Microin. of Strain[a], 50-psi External Pres.: Test No. 1	Test No. 2	Test No. 3	Test No. 4	Test No. 5	Average	Av per 10 psi
11	-310	-323	-310	-313	-310	-304	-309	-311	-062	+332	+345	+335	+360	+360	+346	+069
12	-228	-263	-258	-270	-280	-238	-242	-253	-051	-	-	-	-	-	-	-
13	-800	-810	-790	-810	-820	-763	-732	-789	-158	+807	+810	+807	+832	+835	+818	+164
14	-988	-965	-970	-1003	-995	-950	-950	-974	-195	-	-	-	-	-	-	-
15	-1055	-1050	-1033	-1060	-1070	-1035	-1040	-1049	-210	-	-	-	-	-	-	-
16	-848	-848	-843	-865	-865	-840	-835	-849	-170	-	-	-	-	-	-	-
17	-795	-755	-783	-813	-815	-823	-842	-804	-161	-	-	-	-	-	-	-
18	+960	+970	+972	+997	+1005	+950	+960	+973	+195	-	-	-	-	-	-	-
19	+950	+945	+955	+977	+985	+935	+945	+956	+191	-	-	-	-	-	-	-

(a) Tests were run in 10-psi increments, ascending and descending - values shown are differences between readings at 50 psi (maximum pressure) and average readings for zero pressure.

(b) These tests were run to 60 psi, values proportioned for 50 psi.

Plus values indicate measured tensile strain; minus values indicate measured compression strain.

TABLE F-8. PRESSURE STRAINS FOR 1-INCH FORMED BELLOWS COMPRESSED AND EXTENDED, AND PRESSURIZED INTERNALLY AND EXTERNALLY TO 50 PSI

		Gage No.	Microinches of Strain[a] for 10-psi Pressure Increments: First Test 0-10 psi	10-20 psi	20-30 psi	30-40 psi	40-50 psi	Average	Second Test 0-10 psi	10-20 psi	20-30 psi	30-40 psi	40-50 psi	Average	Combined Average
Compression - 0.030 in.	Internal Pressure	11	-070	-060	-070	-055	-090	-069	-065	-065	-065	-060	-070	-065	-067
		12	-075	-045	-065	-030	-045	-052	-070	-040	-070	-030	-070	-056	-054
		13	-200	-135	-190	-160	-165	-170	-200	-120	-145	-200	-160	-165	-168
		14	-210	-215	-160	-180	-220	-197	-220	-190	-180	-195	-205	-198	-198
		15	-220	-235	-205	-220	-200	-216	-230	-205	-210	-225	-195	-213	-215
		16	-180	-190	-175	-185	-140	-174	-195	-165	-175	-180	-160	-175	-175
		17	-130	-210	-130	-170	-175	-163	-150	-190	-165	-170	-145	-164	-164
		18	+200	+205	+185	+210	+195	+199	+210	+180	+205	+200	+210	+201	+200
		19	+205	+195	+180	+205	+185	+194	+210	+175	+200	+185	+200	+194	+194
	External Pressure	11	+070	+070	+080	+060	+050	+066	+095	+080	+065	+055	+060	+071	+069
		13	+155	+170	+170	+170	+160	+165	+190	+180	+165	+155	+155	+169	+167
Extension - 0.030 inch	Internal Pressure	11	-065	-055	-060	-070	-060	-062	-070	-050	-060	-070	-060	-062	-062
		12	-065	-025	-060	-030	-060	-048	-055	-030	-070	-025	-060	-048	-048
		13	-185	-155	-140	-125	-190	-159	-180	-130	-165	-155	-155	-161	-160
		14	-210	-210	-175	-195	-210	-200	-195	-215	-195	-200	-200	-201	-201
		15	-205	-220	-190	-210	-225	-210	-210	-230	-210	-215	-215	-216	-213
		16	-155	-180	-160	-170	-180	-169	-170	-190	-170	-175	-175	-176	-173
		17	-130	-200	-115	-195	-140	-156	-130	-210	-125	-205	-130	-160	-158
		18	+200	+200	+185	+185	+210	+196	+190	+205	+185	+200	+195	+195	+196
		19	+200	+200	+175	+185	+215	+195	+190	+200	+190	+190	+200	+194	+195
	External Pressure	11	+100	+060	+065	+065	+060	+070	+095	+075	+060	+060	+060	+070	+070
		13	+215	+140	+150	+170	+135	+162	+200	+160	+155	+155	+135	+161	+162

(a) Plus values indicate tensile strains; minus values indicate compressive strains. Compression and extension tests were alternated.

TABLE F-9. EXPERIMENTALLY DETERMINED REPRESENTATIVE STRAINS AND STRESSES IN 1-INCH SINGLE-PLY FORMED BELLOWS

			Gage No. 11	Gage No. 12	Gage No. 13	Gage No. 17	Gage No. 18	Average Representative Strains	Calculated Representative Stresses
Strains for 0.060-inch Compression (Table F-5)	Convolution Crown	Meridional	-	-	+735	+1007	-	+871	+32,075
		Circumferential	+495	+409	-	-	-	+452	+22,750
	Convolution Root	Meridional	-	-	-	- -	+1358	+1358	+41,695 (a)
		Circumferential	-	-	-	-	-	-	+7,750 (a)
Strains for 10-psi Internal Pres. (Table F-7)	Convolution Crown	Meridional	-	-	-158	-161	-	-160	- 5,155
		Circumferential	-062	-051	-	-	-	-057	- 1,710
	Convolution Root	Meridional	-	-	-	-	+195	+195	+6,230 (b)
		Circumferential	-	-	-	-	-	-	+1,917 (b)

(a) Calculated on the assumption that $S_1/S_2 = 5.38$ (see Table F-4).
(b) Calculated on the assumption that $S_1/S_2 = 3.25$ (see Table F-4).

TABLE F-10. COMPARISON OF THEORETICALLY DETERMINED AND EXPERIMENTALLY DETERMINED STRESSES AND STRAINS FOR 1-INCH SINGLE-PLY FORMED BELLOWS JD29

			Strains (a), μin/in.		Stresses (a), psi	
			Experimental	Theoretical	Experimental	Theoretical
Deflection Stresses and Strains	Convolution Crown	Meridional	+871	+1004	+32,075	+35,048
		Circumferential	+452	+320	+22,750	+19,803
	Convolution Root	Meridional	+1358	+1593	+41,695 (b)	+48,931
		Circumferential	-	-192	+7,750 (b)	+9,097
Pressure Stresses and Strains	Convolution Crown	Meridional	-160	-209	-5,155	-7,173
		Circumferential	-057	-054	-1,710	-3,714
	Convolution Root	Meridional	+195	+277	+6,230 (c)	+8,847
		Circumferential	-	+003	+1,917 (c)	+2,724

(a) Calculated and tested for 0.060-in. compression and 10-psi internal pressure.
(b) Calculated on the assumption that $S_1/S_2 = 5.38$ (see Table F-4).
(c) Calculated on the assumption that $S_1/S_2 = 3.25$ (see Table F-4).

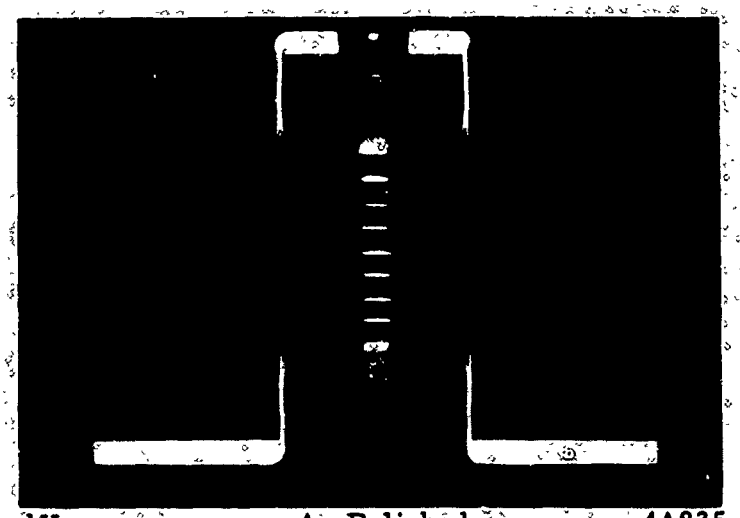

FIGURE F-1. CROSS SECTION OF 1-INCH, 1-PLY FORMED BELLOWS JD29 - TYPE 321 STAINLESS STEEL

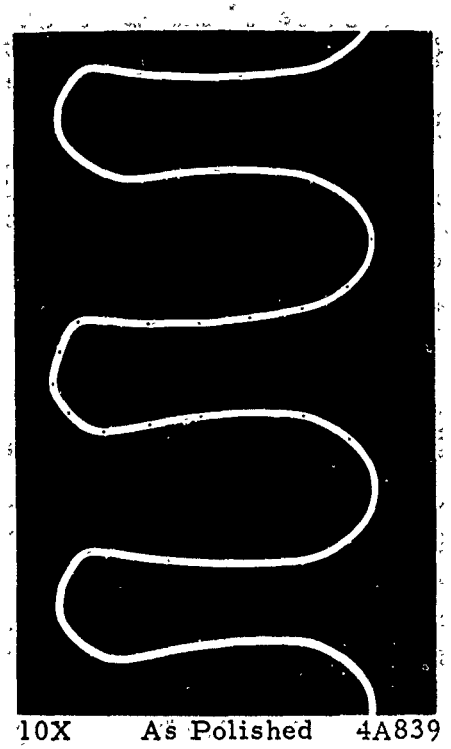

FIGURE F-2. ENLARGED VIEW OF CONVOLUTIONS OF CROSS SECTIONED 1-INCH, 1-PLY FORMED BELLOWS JD29 - TYPE 321 STAINLESS STEEL

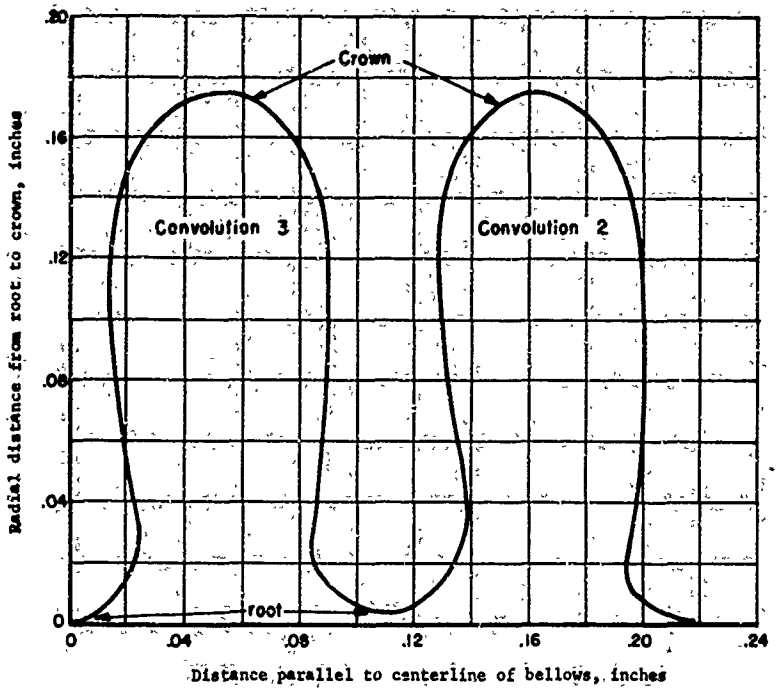

FIGURE F-3. SHAPE OF CONVOLUTIONS 2 AND 3 OF 1-INCH BELLOWS JD29

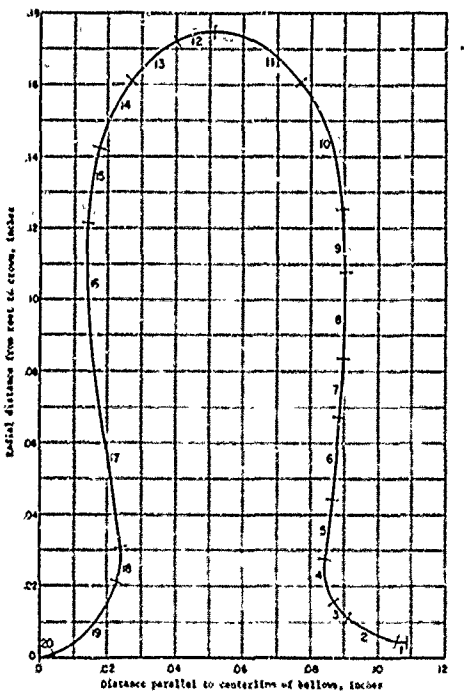

FIGURE F-4. MATHEMATICAL MODEL OF CONVOLUTION NO. 3 OF 1-INCH BELLOWS JD29

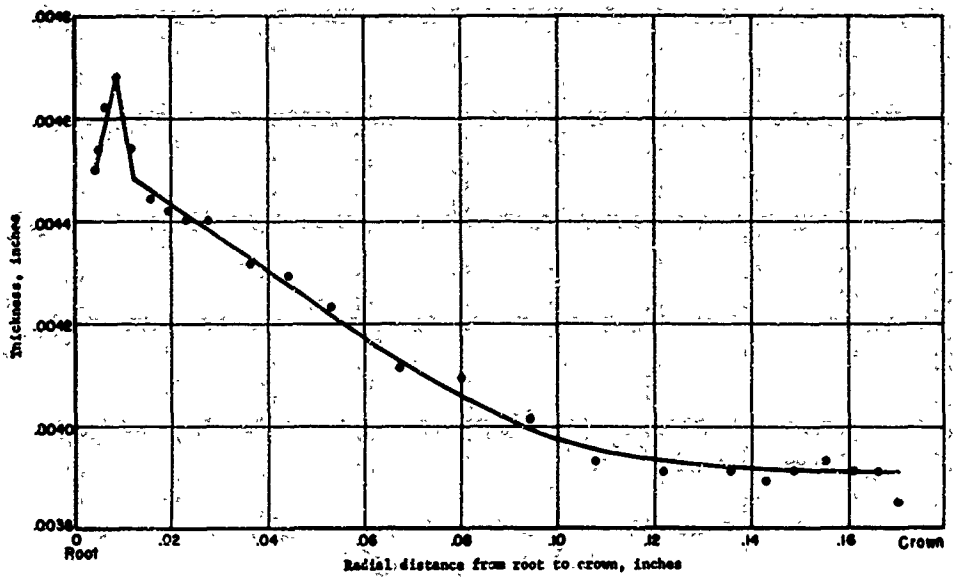

FIGURE F-5. THICKNESS VARIATION FOR PARTS 1-11 FOR 1-INCH BELLOWS JD29 (nominal thickness = 0 005 inch)

Circled points indicate measured thicknesses and solid line is thickness variation used for parts 1-11 in mathematical model shown in Figure F-4.

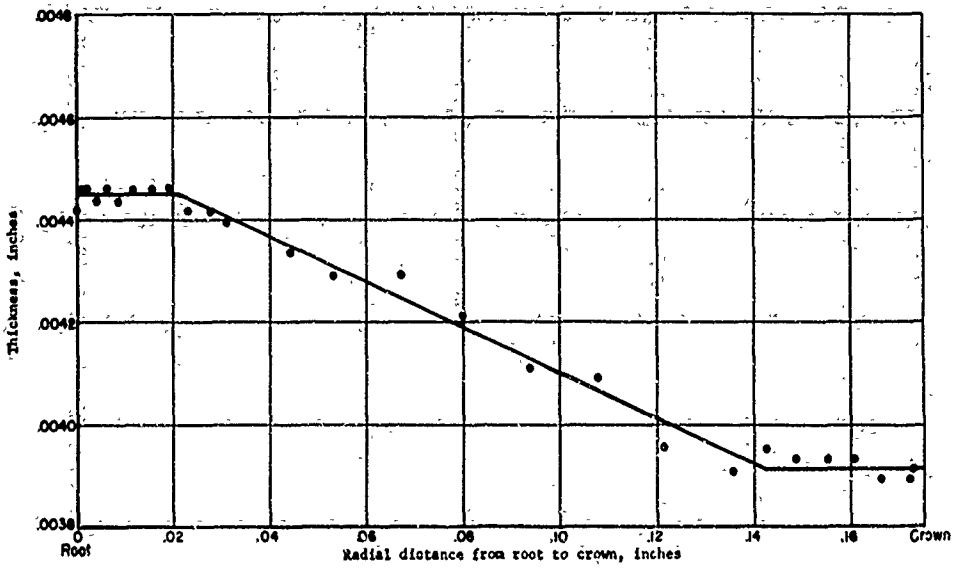

FIGURE F-6. THICKNESS VARIATION FOR PARTS 12-20 FOR 1-INCH BELLOWS JD29 (nominal thickness = 0.005 inch)

Circled points indicate measured thicknesses and solid line is thickness variation used for parts 12-20 in mathematical model shown in Figure F-4.

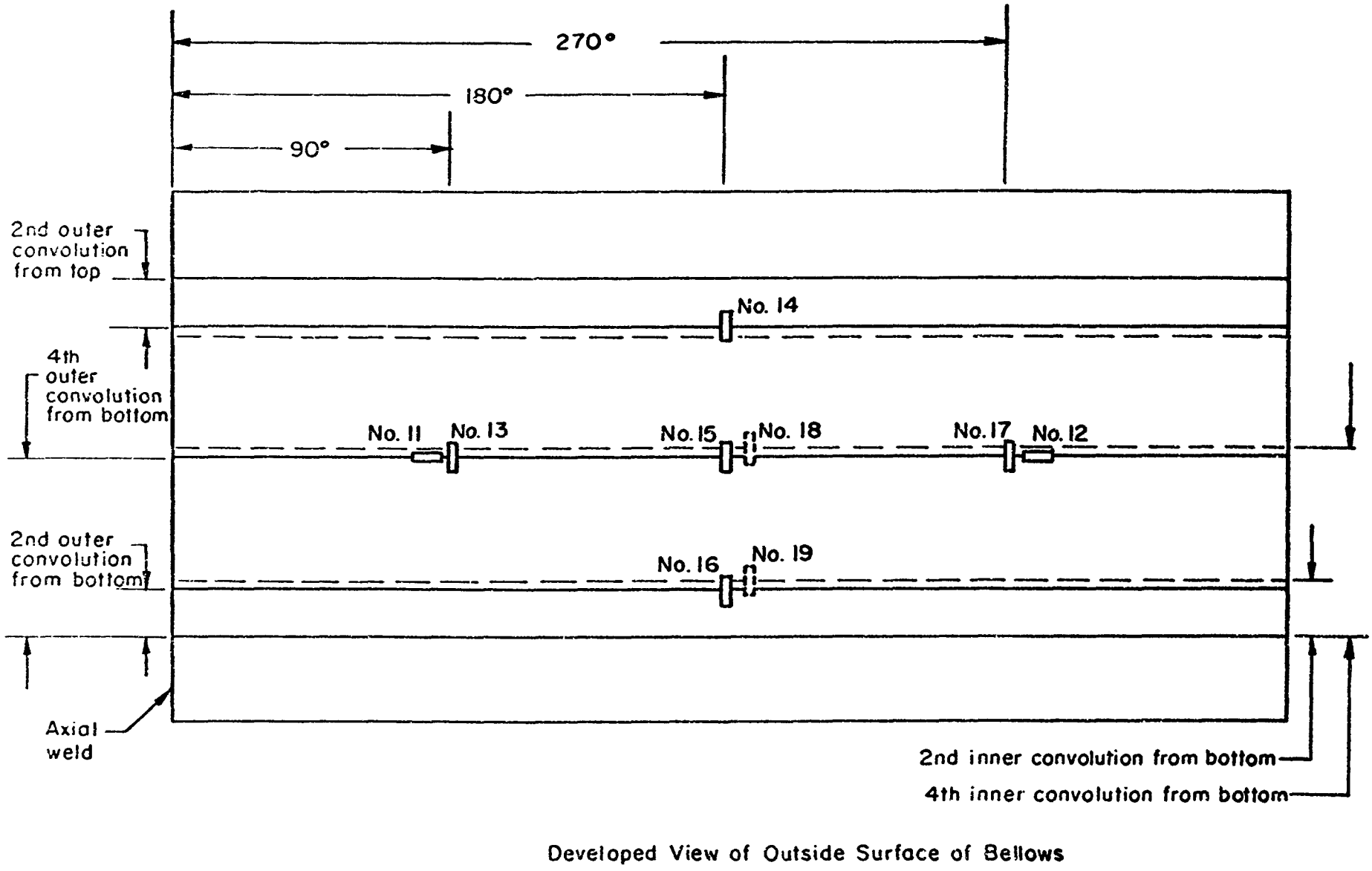

FIGURE F-7. STRAIN GAGE LOCATIONS FOR 1-INCH FORMED BELLOWS – TYPE 321 STAINLESS STEEL

APPENDIX G

STRESS ANALYSIS OF A 3- AND A 1-INCH TWO-PLY FORMED BELLOWS - TYPE 321 STAINLESS STEEL

APPENDIX G

STRESS ANALYSIS OF A 3- AND A 1-INCH TWO-PLY FORMED BELLOWS - TYPE 321 STAINLESS STEEL

The exact analysis of a two-ply bellows is believed to be beyond the present state of the art of bellows analysis. Early in the program, an approximate theoretical model was developed to incorporate some of the features of two-ply bellows. In the modeling technique, each two-ply bellows was to be replaced with a multilayer shell having the same shape and having equivalent membrane and bending stiffnesses. This approach was based on information obtained during the state-of-the-art survey in which it was reported that with low pressure the plies of a multiple-ply bellows move relatively independently, but with sufficiently high pressure, the plies "lock up" and the bellows behaves more like a one-ply bellows having a thickness equal to the total thickness of all the plies.

The multilayer model chosen to represent the two-ply bellows was to be a three-layer sandwich shell with layers of equal thickness. It was intended that fictitious values for Young's modulus, for the different layers, would be utilized to adjust the bending stiffness of each multilayer-bellows model so that it would have the same spring rate and stresses as the experimentally determined values for the bellows of interest. It was determined that such an approach would permit a sufficient variation in the bending stiffness that the case in which the two plies were completely free to slide could be analyzed, as well as the case in which the plies were completely locked together. Any intermediate bending stiffness could also be selected to correspond to partial sliding between the plies. Because the amount of friction was expected to vary with configuration and internal pressure, it was recognized that design nomographs might have to be developed for typical conditions.

Mathematical Models

When the order was placed for the formed bellows, it was requested that the one- and two-ply, 3- and 1-inch bellows be made as similar as possible. An examination of the cross-sectioned specimens showed that the shapes of the two-ply bellows were essentially the same as for the one-ply bellows. Also, checks of the thickness variations at typical locations showed that the forming process had produced essentially the same variations in the one- and two-ply bellows. The one significant difference noted was the fact that the plies of the 3-inch two-ply bellows, as shown in Figures G-1 and G-2, were significantly separated over much of their length, while the plies of the 1-inch two-ply bellows, as shown in Figures G-3 and G-4, were quite close together. This difference, however, proved to be beneficial because it permitted an evaluation of the effect of ply separation.

Following these examinations, it was decided that the geometries used for the one-ply 3- and 1-inch bellows would be sufficiently accurate for the geometries of the two-ply bellows. (Tables E-1 and E-2 and Figures E-3 and E-4 of Appendix E describe the geometric properties of the 3-inch one-ply bellows, while Tables F-1 and F-2 and Figures F-3 through F-6 of Appendix F describe the geometric properties of the 1-inch one-ply bellows.)

Theoretically Predicted Bounds for Stresses and Spring Rates

The multiple-ply shell was assumed to have the same membrane rigidity and a bending rigidity of k times the rigidity of a single-ply shell of the same total thickness, where k was some number less than 1. The value of k was expected to decrease as the number of plies increased and increase with increasing friction between the plies. For two-ply bellows, k was expected to lie between 1/4 and 1. If the plies were completely free to slide, k would be 1/4, while if the plies were completely locked, k would equal 1.

To facilitate analysis of the experimental results, calculations were made of the theoretical spring rates and typical theoretical meridional stresses for the 3- and 1-inch two-ply bellows for k = 1/4, 5/8, and 1. The results are shown in Tables G-1 and G-2.

Determination of k by Spring-Rate Measurement

An examination of Table G-1 shows the effect on spring rate of a change in k. When there is no interference between the plies (k = 1/4) the spring rate of the two-ply bellows should be twice the spring rate of the corresponding 1-ply bellows. As k increases with increasing interaction between the plies, the spring rate also increases. Thus, a comparison of the measured spring rates of the one- and two-ply bellows was expected to give an indication of the value of k. Further, a comparison of the spring rates of each bellows at different deflections and at different pressures was expected to give an indication of the effects of pressure or deflection on the interaction between the plies.

The experimental spring rates for the 3-inch one- and two-ply bellows are shown in Table G-3. For the one-ply bellows, tests were conducted at 0 psi and at 25 psi. The tests were conducted at two deflections (corresponding to those used for the fatigue tests), with equal extension and compression. The two-ply 3-inch bellows was tested at 0, 8, 16, and 25 psi to provide data concerning the effect of pressure on ply interaction. Table G-4 shows similar test results for the one- and two-ply 1-inch bellows. The pressure values were selected sufficiently low to eliminate the problem of squirming which was found at higher pressures (see Appendix J).

An examination of Tables G-3 and G-4 shows that there was no apparent effect of pressure or deflection on the spring rate of either two-ply bellows. This indicated that no increase in friction occurred for the pressures or deflections considered.

A comparison of the experimental spring rates for the 3-inch one- and two-ply bellows (see Table G-3) shows a ratio of 2.06 and 2.08 for the bellows in compression and tension respectively. As shown in Table G-4, the ratios of the experimental spring rates for the 1-inch bellows were 1.75 for compression and 1.95 for tension. The lower ratios, which were not possible theoretically if the one- and two-ply bellows cross sections were identical, were probably the result of slight differences in the cross section geometries. For instance, a check of the thickness at all of the crowns of the 1-inch one- and two-ply cross-sectioned bellows showed that the two-ply bellows were slightly thinner than the one-ply bellows. This would at least partially account for the lower spring-rate ratio.

It was concluded that the relative values of the spring rates indicated that there was no interaction between the plies for axial deflection of either the 3-inch or the 1-inch two-ply bellows.

Determination of k by Deflection-Strain Measurement

As shown in Table G-2, the stresses due to deflection increase as k increases. Because of the similarity of the one- and two-ply bellows for each size, it was believed that another check on the value of k could be obtained by a direct comparison of the measured deflection strains for the one- and two-ply bellows.

Tables G-5 through G-8 show the strains due to deflection in the 3- and 1-inch two-ply bellows as determined by tests conducted similarly to those described in Appendixes E and F. The locations of the gages on the two-ply bellows were the same as the locations of the gages on the one-ply bellows. Tables G-9 and G-10 summarize the strains at the "middle" convolution for the 3- and 1-inch one- and two-ply bellows. Gages 11 and 12 were circumferential gages and Gages 13, 15, and 17 were meridional gages on the crown of the same convolution for each bellows.

Table G-9 shows that the strains in the 3-inch one- and two-ply bellows were essentially the same for equal deflections. This indicated that the plies of the two-ply bellows moved independently during deflection and that $k = 1/4$ for the 3-inch two-ply bellows.

Table G-10 shows that the strains in the 1-inch one- and two-ply bellows were similar for the two circumferential gages and one meridional gage. For the two other meridional gages, the strains in the two-ply bellows were significantly less than those in the one-ply bellows. The reason for these differences is unexplained. The high meridional strains for the one-ply bellows were close to those predicted by the mathematical model (see Appendix F) Further, all gages gave consistent readings for compression and extension, with and without pressure, indicating that no interaction between the plies was apparent. Consequently, the reduced deflection strains were apparently the results of some other factor. However, since no significant increase in deflection strain was noted in either two-ply bellows as compared with the one-ply bellows, the experimentally determined deflection strains indicated that $k = 1/4$ for the 3- and 1-inch two-ply bellows.

Determination of k by Pressure-Strain Measurement

As shown in Table G-2, the calculated stresses due to pressure decrease with increasing k. Again, because of the similarity of the one- and two-ply bellows for each size, another check on k for each two-ply bellows was provided by a direct comparison of the measured pressure strains for the one- and two-ply bellows.

Tables G-11 through G-14 show the strains due to pressure in the 3- and 1-inch two-ply bellows as determined by tests conducted similarly to those described in Appendixes E and F. Tables G-15 and G-16 summarize the pressure strains at the middle convolution for 10-psi increments of internal pressure in the 3-inch one- and two-ply bellows, respectively. The results of three tests and the averages of the readings are given. Gage No. 18 was a meridional gage on the inside surface of the root of the convolution on the crown of which the other gages were located. The strain increments of the one-ply bellows were approximately the same for each increment of pressure, while the strain increments of the two-ply bellows decreased somewhat as the pressure increased. This indicated an interaction between the plies. Further, a comparison of Tables G-15 and G-16 shows that the pressure strains in the two-ply bellows were

approximately 30 percent of the pressure strains in the one-ply bellows. As shown in Table G-2, this reduction in pressure stresses implied that k was close to 1.

Tables G-17 and G-18 show the strains for 10-psi pressure increments in the 1-inch one- and two-ply bellows, respectively. These readings were somewhat more difficult to evaluate than the results for the 3-inch bellows, particularly since the strain-gage readings for the 1-inch one-ply bellows were not as consistent as the results for the 3-inch bellows. However, the ratios between the recorded strains for the two-ply 1-inch bellows and the strains for the one-ply bellows were apparently nearer to 0.5 than 0.3. This indicated that there was less friction between plies in the one-inch bellows under pressure than in the 3-inch bellows. However, since the plies of the 3-inch bellows were more widely separated than the plies of the one-inch bellows, this appeared to be a direct contradiction of the friction model.

Discussion of the Behavior of Two-Ply Bellows

After considerable study of the experimental data for the one- and two-ply 3-inch and 1-inch bellows, and after a comparison of the results with the predictions of the theoretical models, it was concluded that there was no significant frictional interaction between the plies of the two-ply bellows for any of the test conditions. A possible explanation of the absence of appreciable friction is the fact that a bellows shell can support only a small normal load. (For instance, the pressure loads on the bellows were only 50 psi or less.) It was concluded that the principal interaction between the plies in a two-ply bellows probably occurs because of restrictions to the normal deflection of the plies when they contact. This will be discussed in terms of deflection and pressure.

Behavior During Deflection. Ply interaction will not normally occur during axial deflection because both plies tend to act as individual bellows and to deform in the same manner. As noted previously, the absence of ply interaction during deflection for the 3- and 1-inch two-ply bellows was indicated by the spring-rate measurements and by the measured strains.

Behavior During Pressure Loading. The behavior of the two-ply bellows under pressure loading can be explained by the assumption that interaction between the plies tends to restrict deflections due to pressure. A comparison of Tables G-15 and G-16 shows that the measured meridional surface strains at the inside surface of the root and the outside surface of the crown of the 3-inch two-ply bellows convolutions were significantly lower than for the one-ply bellows. An examination of the two-ply bellows cross section in Figure G-2 shows there was a considerable gap between the plies near the crown of the bellows but not at the root of the bellows. Thus, reduced load transference between the inner and outer plies at the bellows crown would explain the low strains on the crown of the outer ply with internal pressure, and the high strains on the crown of the outer ply with external pressure. At the bellows root, the interference between the plies might permit the outer ply to share the load and reduce the stress level at the inner-ply root. Note that there was also a gap between the plies over the flat-plate portion of the bellows. This could have permitted the interaction between the plies to be localized at the root. This conclusion is supported by theoretical calculations which showed that the normal deflection of the pressurized inner ply in the flat-plate area are barely sufficient to close the gap between the plies, even if the inner ply were completely free to deform.

In contrast, Figure G-4 shows that the 1-inch two-ply bellows was in contact over essentially the entire bellows cross section even in the unloaded condition. Therefore, under internal pressure the two plies would contact over the entire cross section. In this case both plies would share the load equally and the surface stresses everywhere in both plies would be about one-half the stresses in the one-ply bellows. This is supported by the data in Tables G-17 and G-18 which show that the pressure strains in the two-ply bellows were approximately one-half the pressure strains in the single-ply bellows.

Conclusions

The experimental data obtained for the 3- and 1-inch two-ply bellows indicate that the interaction between the plies is considerably more complex than the assumptions made for the theoretical model. Thus, the model was not sufficiently general to explain all of the observed behavior. Eventually it may be possible to develop an exact theory of a two-ply bellows. Such a theory would probably involve the iterative solution of a very nonlinear problem. The solution would have to be obtained by starting with an exact model of the undeformed bellows cross section as determined by sectioning. Then the deformed state of the bellows would have to be determined by applying the load in small increments with a determination of the new contact area between the plies at each step. Even if the bellows was assumed to contact uniformly over a progressively larger area with increasing deformation, this would be a formidable problem.

Fortunately, on the basis of similar experimental data for a two-ply bellows with closely spaced plies and for a two-ply bellows with significantly separated plies, it is believed that useful estimates can be made of some of the critical performance characteristics of two-ply bellows (at least in the intermediate pressure range).

It is recommended that the behavior of a two-ply bellows be related to a corresponding one-ply bellows with the same cross-sectional shape, and with a thickness equal to the thickness of one ply. The stresses and spring rate of this single-ply bellows can be found with the analysis procedure described in Appendix B. The spring rate of the two-ply bellows will be approximately twice the spring rate of the single-ply bellows. The deflection stresses in the two-ply bellows can be conservatively estimated as being equal to the stresses in the single-ply bellows. This is particularly true for estimating fatigue life under axial deflection. The fatigue lives of the single- and two-ply test bellows were essentially equal for equal deflection strains (see Appendix L).

For pressure loading, the stresses in the bellows will vary between 0.5 and 1.0 times the stresses in the single-ply bellows, depending on the amount of separation of the plies. Unless the plies can be determined by sectioning to be as close together as those for the 1-inch two-ply bellows, it is believed that the values of the pressure stresses for the one-ply bellows should be used as the maximum stresses in the two-ply bellows. Fortunately the fatigue tests have shown that a constant pressure does not affect the fatigue life of a stainless steel bellows provided the bellows is not excessively deformed.

TABLE G-1. THEORETICAL SPRING RATES FOR 3-AND 1-INCH TWO-PLY STAINLESS STEEL FORMED BELLOWS FOR SELECTED VALUES OF k

Bellows	Minimum, Intermediate, and Maximum Values of k		
	0.25	0.625	1.0
3-inch, JD77	324 lb/in	723 lb/in	1120 lb/in
1-inch, JD18	173 lb/in	391 lb/in	607 lb/in

TABLE G-2. THEORETICAL MERIDIONAL STRESSES* IN 3- AND 1-INCH TWO-PLY STAINLESS STEEL BELLOWS FOR SELECTED VALUES OF k

			Minimum, Intermediate, and Maximum Values of k					
			0.25		0.625		1.0	
		Position	Membrane Stress	Bending Stress, Outer Surface	Membrane Stress	Bending Stress, Outer Surface	Membrane Stress	Bending Stress, Outer Surface
Stresses in 3" Bellows	Axial Compress.	Root	-4538.6	-518,400	-10,120.0	-757,840	-15,691.8	-1,003,430
		Crown	-4284.3	+415,358	- 9,553.9	+676,600	-14,812.7	+920,740
	Internal Pressure	Root	-11.146	-881.627	-11.274	-360.113	-11.306	-226.211
		Crown	+11.573	-731.502	+11.452	-307.363	+11.422	-194.574
Stresses in 1" Bellows	Axial Compression	Root	-5323.3	-522,126	-12,039.8	-774,172	-18,712.2	-1,028,220
		Crown	-4586.8	+353,159	-10,374.3	+621,514	-16,120.0	+864,192
		Root	-5483.1	-591,203	-12,401.1	-872,054	-19,273.4	-1,155,540
	Internal Pressure	Root	-9.646	-566.607	-9.793	-238.104	-9.836	-150.489
		Crown	+10.313	-434.824	+10.186	-208.579	+10.148	-136.938
		Root	-10.966	-736.877	-11.117	-317.778	-11.162	-202.815

* Plus values are tensile stresses, minus values are compressive stresses;

TABLE G-3. SUMMARY OF EXPERIMENTAL SPRING RATES FOR 3-INCH ONE- AND TWO-PLY STAINLESS STEEL FORMED BELLOWS

	Deflection Mode	Stroke, in.	Spring Rate at 0 psi, lb/in.	Spring Rate at 8 psi, lb/in.	Spring Rate at 16 psi, lb/in.	Spring Rate at 25 psi, lb/in.	Comb. Av., lb/in.
3-Inch One-Ply Bellows JD69	Compression	.205	145.9			152.9	
		.340	133.3			147.6	
		av.	139.6			150.3	145.0
	Tension	.205	170.5			188.8	
		.340	173.7			189.6	
		av.	172.1			189.2	180.7
3-Inch Two-Ply Bellows JD78	Compression	.240	306.2	317.2	312.9	285.2	
		.385	273.4	304.2	298.3	292.7	
		av.	289.8	310.7	305.6	289.0	298.8
	Tension	.240	364.6	385.0	383.3	368.3	
		.385	366.2	388.4	389.9	364.7	
		av.	365.4	386.7	386.6	367.0	376.4

TABLE G-4. SUMMARY OF EXPERIMENTAL SPRING RATES FOR 1-INCH ONE- AND TWO-PLY STAINLESS STEEL FORMED BELLOWS

	Deflection Mode	Stroke, in	Spring Rate at 0 psi, lb/in	Spring Rate at 16 psi, lb/in	Spring Rate at 50 psi, lb/in	Comb. Av., lb/in
One-Inch One-Ply Bellows JD28	Compression	.100	67.5		68.0	
		.175	68.2		65.7	
		av.	67.9		66.9	67.4
	Tension	.100	76.3		73.0	
		.175	79.4		76.9	
		av.	77.8		75.0	76.4
One-Inch Two-Ply Bellows JD17	Compression	.090	122.9	119.7	120.0	
		.150	115.9	115.6	114.5	
		av.	119.4	117.7	117.3	118.1
	Tension	.090	144.4	147.2	140.8	
		.150	151.7	150.9	151.9	
		av.	148.1	149.1	146.4	148.9

TABLE G-5. DEFLECTION STRAINS FOR COMPRESSION AND EXTENSION OF 3-INCH TWO-PLY FORMED BELLOWS--NO INTERNAL PRESSURE[c]

Gage No.	Microinches of Strain[a], Bellows in Compression						Microinches of Strain[b], Bellows in Extension						Combined Average
	Test No. 1	Test No. 2	Test No. 3	Test No. 4	Test No. 5	Compression Average	Test No. 1	Test No. 2	Test No. 3	Test No. 4	Test No. 5	Extension Average	
11	160	157	180	172	180	170	188	193	185	185	183	187	179
12	172	172	182	185	190	180	195	190	198	198	195	195	188
13	372	380	417	407	422	400	410	423	405	418	408	413	407
14	360	362	375	380	392	374	375	393	380	480	398	405	390
15	372	377	402	400	420	394	380	390	390	393	393	389	392
16	375	375	400	407	410	393	410	420	405	408	408	410	402
17	425	422	477	460	447	446	445	455	455	453	463	454	450
18	507	620	575	557	562	564	582	693	590	593	578	607	586
19	527	522	580	575	575	556	585	595	590	590	585	589	573

(a) All measured strains in compression were tensile--deflection was 0.060 inch.
(b) All measured strains in extension were compressive--deflection was 0.060 inch.
(c) Compression and extension tests were alternated.

TABLE G-6. DEFLECTION STRAINS FOR 3-INCH TWO-PLY FORMED BELLOWS COMPRESSED AND EXTENDED, AND PRESSURIZED INTERNALLY AND EXTERNALLY TO 30 PSI

	Gage No.	Microinches of Strain[a], Bellows in Compression					Microinches of Strain[b], Bellows in Extension					Combined Average
		0 psi	10 psi	20 psi	30 psi	Compression Average	0 psi	10 psi	20 psi	30 psi	Extension Average	
Internal Pressure	11	157	165	165	175	166	183	183	185	190	185	176
	12	185	180	182	185	183	200	200	205	195	200	192
	13	377	397	395	393	391	408	415	415	423	415	403
	14	337	332	380	392	360	380	375	398	425	395	378
	15	370	380	412	422	396	390	383	418	420	403	400
	16	395	400	397	402	399	410	395	413	418	409	404
	17	447	427	452	462	447	450	450	455	458	453	450
	18	607	592	575	565	585	570	560	543	548	555	570
	19	550	547	542	537	544	563	543	575	533	554	549
External Pressure	11	207	200	200	208	204	200	200	198	193	198	201
	13	455	450	435	430	443	423	435	425	413	424	434

(a) All measured strains in compression were tensile--deflection was 0.060 inch.
(b) All measured strains in extension were compressive--deflection was 0.060 inch.

TABLE G-7. DEFLECTION STRAINS FOR COMPRESSION AND EXTENSION OF 1-INCH TWO-PLY FORMED BELLOWS--NO INTERNAL PRESSURE[c]

Gage No.	Microinches of Strain[a], Bellows in Compression: Test No. 1	Test No. 2	Test No. 3	Test No. 4	Test No. 5	Compression Average	Microinches of Strain[b], Bellows in Extension: Test No. 1	Test No. 2	Test No. 3	Test No. 4	Test No. 5	Extension Average	Combined Average
11	467	470	477	452	462	466	503	500	513	435	495	489	478
12	447	460	452	435	462	451	495	460	503	425	483	473	462
13	637	807	870	733	757	761	678	610	723	595	688	659	710
14	795	890	872	892	872	864	745	663	695	643	725	694	779
15	588	632	625	580	610	607	545	490	573	473	538	524	566
16	620	492	600	515	585	562	608	523	605	458	520	543	553
17	645	610	655	617	637	635	570	530	583	495	553	546	591
18	1262	1285	1267	1242	1282	1268	1210	1115	1255	1065	1208	1171	1220
19	1535	1570	1620	1640	1602	1593	1650	1620	1568	1425	1625	1578	1586

(a) All measured strains in compression were tensile--deflection was 0.060 inch.
(b) All measured strains in extension were compressive--deflection was 0.060 inch.
(c) Compression and extension tests were alternated.

TABLE G-8. DEFLECTION STRAINS FOR 1-INCH TWO-PLY FORMED BELLOWS COMPRESSED AND EXTENDED, AND PRESSURIZED INTERNALLY AND EXTERNALLY TO 50 PSI

	Gage No.	Microinches of Strain[a], Bellows in Compression: 0 psi	10 psi	20 psi	30 psi	40 psi	50 psi	Compression Average	Microinches of Strain[b], Bellows in Extension: 0 psi	10 psi	20 psi	30 psi	40 psi	50 psi	Extension Average	Combined Average
Internal Pressure	11	239	234	235	238	238	237	237	249	247	249	247	243	240	246	242
	12	241	235	240	237	235	244	239	249	247	242	239	237	247	244	242
	13	345	360	346	374	349	374	358	354	337	340	327	344	326	336	347
	14	432	424	429	433	439	440	433	371	373	370	368	368	379	372	403
	15	290	286	287	291	291	287	289	281	283	279	275	284	274	279	274
	16	260	258	259	256	253	253	256	273	272	269	266	268	267	269	263
	17	299	295	299	287	290	292	296	297	302	282	287	269	291	288	292
	18	614	624	614	615	619	625	619	620	610	608	602	599	603	607	613
	19	804	815	813	820	826	823	817	798	790	801	803	797	805	799	808
External Pressure	11	246	242	250	246	258	244	248	261	251	244	243	238	245	247	248
	13	349	334	330	341	325	335	337	320	307	309	302	311	305	309	323

(a) All measured strains in compression were tensile--deflection was 0.030 inch--average of two tests.
(b) All measured strains in extension were compressive--deflection was 0.030 inch--average of two tests.

TABLE G-9. DEFLECTION STRAINS* FOR 0.060-INCH COMPRESSION OF 3-INCH ONE- AND TWO-PLY BELLOWS (CROWN OF CONVOLUTION NO. 5)

	Gage No.	Microinches of Tensile Strain, μin./in. Test No. 1	Test No. 2	Test No. 3	Test No. 4	Test No. 5	Average
3" One-Ply Bellows JD9 (See Table E-5)	11	175	177	180	187	182	180
	12	180	175	180	182	180	179
	13	375	397	392	395	395	391
	15	410	425	397	405	402	408
	17	417	400	405	407	405	407
3" Two-Ply Bellows JD8 (See Table G-5)	11	160	157	180	172	180	170
	12	172	172	182	185	190	180
	13	372	380	417	407	422	400
	15	372	377	402	400	420	394
	17	425	422	477	460	447	446

* All measured strains were tensile.

TABLE G-10. DEFLECTION STRAINS* FOR 0.060-INCH COMPRESSION OF 1-INCH ONE- AND TWO-PLY BELLOWS (CROWN OF CONVOLUTION NO. 4)

	Gage No.	Microinches of Tensile Strain, μin./in. Test No. 1	Test No. 2	Test No. 3	Test No. 4	Test No. 5	Average
1-Inch One-Ply Bellows JD8 (See Table F-5)	11	490	480	487	490	480	485
	12	390	375	365	370	380	376
	13	805	775	632	792	765	794
	15	1127	1122	1125	1125	1117	1123
	17	1052	1047	1047	1042	1030	1044
1-Inch Two-Ply Bellows JD 17 (See Table G-7)	11	467	470	477	452	462	466
	12	447	460	452	435	462	451
	13	637	807	870	733	757	761
	15	588	632	625	580	610	607
	17	645	610	655	617	637	633

* All measured strains were tensile.

TABLE G-11. PRESSURE STRAINS FOR 3-INCH TWO-PLY FORMED BELLOWS PRESSURIZED INTERNALLY AND EXTERNALLY--NO DEFLECTION

Gage No.	Microinches of Strain[a], Internal Pressure, 50 psi: Test No. 1	Test No. 2	Test No. 3	Average	Average per 10 psi	Microinches of Strain[a], External Pressure, 50 psi: Test No. 1	Test No. 2	Test No. 3	Average	Average per 10 psi
11	-085	-095	-095	-092	-018.4	+310	+315	+310	+312	+062.4
12	-068	-060	-060	-063	-012.6	-	-	-	-	-
13	-400	-438	-433	-424	-084.8	+1185	+1167	+1150	+1167	+233.4
14	-430	-440	-425	-432	-086.4	-	-	-	-	-
15	-348	-365	-368	-360	-072.0	-	-	-	-	-
16	-280	-285	-290	-285	-057.0	-	-	-	-	-
17	-245	-258	-263	-255	-051.0	-	-	-	-	-
18	+442	+447	+445	+445	+089.0	-	-	-	-	-
19	+677	+690	+687	+685	+137.0	-	-	-	-	-

Plus values indicate measured tensile strain; minus values indicate measured compressive strain.

(a) Tests were run in 10-psi increments ascending and descending--values shown are differences between readings at 50 psi (maximum pressure) and average readings for zero pressure before and after test.

TABLE G-12. PRESSURE STRAINS FOR 3-INCH TWO-PLY FORMED BELLOWS COMPRESSED, EXTENDED, AND PRESSURIZED INTERNALLY AND EXTERNALLY TO 30 PSI

		Gage No.	Microin. of Strain[a] for Pressure Increments: Deflection--0.0 in.[b] 0-10 psi	10-20 psi	20-30 psi	Deflection--0.030 in.[b] 0-10 psi	10-20 psi	20-30 psi	Deflection--0.060 in. 0-10 psi	10-20 psi	20-30 psi	Average Change per 10 psi
Compression	Internal Pressure	11	-028	-025	-035	-023	-023	-028	-020	-025	-025	-026
		12	-005	-018	-013	-003	-023	-010	-010	-015	-010	-012
		13	-075	-098	-118	-060	-103	-103	-055	-100	-115	-092
		14	-080	-133	-078	-080	-103	-073	-075	-095	-065	-087
		15	-070	-118	-075	-068	-100	-060	-060	-085	-065	-078
		16	-035	-053	-065	-030	-058	-058	-030	-055	-060	-049
		17	-030	-095	-045	-038	-073	-043	-050	-070	-035	-053
		18	+085	+113	+085	+075	+098	+080	+070	+095	+075	+085
		19	+088	+155	+140	+078	+155	+135	+080	+150	+135	+124
	External Pressure	11	+043	+080	+063	+035	+073	+055	+035	+080	+055	+057
		13	+115	+260	+285	+120	+240	+270	+115	+245	+280	+214
Extension	Internal Pressure	11	-0 [illegible]	-023	-030	-023	-028	-030	-025	-025	-035	-027
		12	-0 [illegible]	-020	-015	-003	-025	-008	-005	-025	-005	-012
		13	-0 [illegible]	-105	-118	-073	-098	-123	-075	-105	-125	-099
		14	-0[illegible]5	-118	-068	-083	-125	-078	-080	-140	-095	-097
		15	-073	-105	-073	-070	-123	-073	-065	-140	-075	-089
		16	-035	-053	-065	-023	-063	-068	-020	-070	-070	-052
		17	-030	-090	-033	-043	-080	-040	-030	-095	-035	-053
		18	+080	+103	+080	+085	+103	+078	+090	+120	+075	+090
		19	+085	+148	+138	+100	+143	+138	+100	+165	+130	+127
	External Pressure	11	+035	+078	+060	+033	+083	+060	+035	+080	+065	+059
		13	+113	+260	+278	+103	+268	+280	+105	+270	+290	+219

(a) Plus values indicate tensile strains; minus values indicate compressive strains.
(b) Average of two readings.

TABLE G-13. PRESSURE STRAINS FOR 1-INCH TWO-PLY FORMED BELLOWS PRESSURIZED INTERNALLY AND EXTERNALLY--NO DEFLECTION

Gage No.	Microinches of Strain[a], Internal Pressure, 50 psi: Test No. 1	Test No. 2	Test No. 3	Average	Average per 10 psi	Microinches of Strain[a], External Pressure, 50 psi: Test No. 1	Test No. 2	Test No. 3	Average	Average per 10 psi
11	-150	-140	-145	-145	-029.0	+257	+257	+250	+255	+051.0
12	-170	-160	-160	-162	-032.4	-	-	-	-	-
13	-455	-415	-475	-448	-089.6	+450	+452	+455	+452	+090.4
14	-493	-460	-478	-477	-095.4	-	-	-	-	-
15	-465	-475	-470	-470	-094.0	-	-	-	-	-
16	-508	-508	-518	-511	-102.2	-	-	-	-	-
17	-500	-500	-500	-500	-100.0	-	-	-	-	-
18	+455	+455	+460	+457	+091.4	-	-	-	-	-
19	+670	+660	+682	+671	+134.2	-	-	-	-	-

(a) Plus values indicate measured tensile strain; minus values indicate measured compressive strain.

Tests were run in 10-psi increments ascending and descending--values shown are differences between readings at 50 psi (maximum pressure) and average readings for zero pressure before and after test.

TABLE G-14. PRESSURE STRAINS FOR 1-INCH TWO-PLY FORMED BELLOWS COMPRESSED AND EXTENDED, AND PRESSURIZED INTERNALLY AND EXTERNALLY TO 50 PSI

		Gage No.	Microinches of Strain[a] for 10-psi Pressure Increments: First Test 0-10 psi	10-20 psi	20-30 psi	30-40 psi	40-50 psi	Average	Second Test 0-10 psi	10-20 psi	20-30 psi	30-40 psi	40-50 psi	Average	Combined Average
Compression--0.030 inch	Internal Pressure	11	-035	-030	-035	-030	-045	-035	-030	-030	-050	-020	-040	-034	-035
		12	-010	-050	-025	-040	-015	-028	-015	-045	-025	-045	-015	-029	-029
		13	-085	-120	-115	-085	-110	-103	-100	-090	-125	-100	-110	-105	-104
		14	-045	-110	-100	-105	-065	-085	-055	-115	-100	-095	-070	-087	-086
		15	-060	-105	-105	-105	-110	-097	-055	-105	-105	-105	-105	-095	-096
		16	-065	-120	-115	-120	-115	-107	-065	-115	-125	-115	-115	-107	-107
		17	-050	-110	-125	-115	-105	-101	-045	-120	-100	-130	-095	-098	-100
		18	+055	+090	+080	+105	+100	+086	+055	+095	+105	+095	+090	+088	+087
		19	+085	+150	+150	+160	+145	+138	+070	+150	+155	+150	+145	+134	+136
	External Pressure	11	+020	+065	+050	+060	+045	+048	+040	+055	+050	+060	+055	+052	+050
		13	+090	+090	+090	+090	+130	+098	+055	+100	+070	+120	+100	+089	+094
Extension--0.030 inch	Internal Pressure	11	-030	-025	-050	-015	-025	-029	-030	-025	-045	-020	-045	-033	-031
		12	-010	-040	-025	-035	-030	-028	-005	-040	-025	-040	-030	-028	-028
		13	-100	-080	-125	-100	-125	-106	-085	-095	-155	-065	-115	-103	-104
		14	-045	-110	-100	-110	-075	-088	-045	-120	-095	-110	-085	-091	-090
		15	-060	-100	-105	-125	-090	-096	-055	-105	-105	-100	-100	-093	-095
		16	-060	-115	-115	-120	-115	-105	-055	-115	-115	-110	-120	-103	-104
		17	-045	-110	-110	-095	-120	-096	-055	-095	-100	-120	-125	-099	-098
		18	+060	+105	+095	+105	+075	+088	+055	+105	+095	+095	+095	+089	+089
		19	+080	+135	+145	+165	+135	+132	+080	+155	+140	+140	+145	+132	+132
	External Pressure	11	+055	+060	+050	+055	+060	+056	+040	+050	+055	+055	+050	+049	+053
		13	+060	+085	+085	+090	+135	+091	+050	+100	+070	+110	+100	+086	+089

(a) Plus values indicate tensile strains; minus values indicate compressive strains--compression and extension tests were alternated.

TABLE G-15. PRESSURE STRAINS[a] FOR CONVOLUTION NO. 5 OF 3-INCH ONE-PLY STAINLESS STEEL BELLOWS JD69 PRESSURIZED INTERNALLY

		Gage No.	Microinches of Strain for 10-psi Increments 0-10 psi	10-20 psi	20-30 psi	30-40 psi	40-50 psi
Meridional Crown Gages	Test No. 1	13	-265	-310	-280	-290	-280
		15	-250	-250	-260	-190	-240
		17	-290	-230	-260	-235	-260
	Test No. 2	13	-250	-280	-235	-290	-260
		15	-245	-230	-235	-215	-235
		17	-270	-220	-265	-220	-270
	Test No. 3	13	-255	-285	-240	-290	-250
		15	-250	-230	-240	-210	-230
		17	-200	-215	-250	-220	-260
	Average		-264	-250	-255	-240	-254
Circumferential Crown Gages	Test No. 1	11	-40	-60	-45	-55	-60
		12	-60	-30	-50	-30	-55
	Test No. 2	11	-55	-50	-50	-50	-50
		12	-50	-35	-50	-25	-50
	Test No. 3	11	-45	-50	-40	-60	-50
		12	-50	-30	-50	-30	-55
	Average		-50	-42	-49	-43	-53
Meridional Root Gage	Test No. 1	18	+375	+380	+405	+355	+405
	Test No. 2	18	+340	+340	+365	+375	+365
	Test No. 3	18	+355	+350	+355	+370	+370
	Average		+357	+357	+375	+367	+380

(a) Plus values indicate tensile strains; minus values indicate compressive strains. The strains for 50-psi internal and external pressure for all gages and with averaged zero pressure readings are given in Table E-7.

TABLE G-16. PRESSURE STRAINS[a] FOR CONVOLUTION NO. 5 OF 3-INCH TWO-PLY STAINLESS STEEL BELLOWS JD78 PRESSURIZED INTERNALLY

		Gage No.	Microinches of Strain for 10-psi Increments 0-10 psi	10-20 psi	20-30 psi	30-40 psi	40-50 psi
Meridional Crown Gages	Test No. 1	13	-60	-125	-60	-50	-70
		15	-60	-100	-70	-50	-55
		17	-55	-30	-60	-25	-65
	Test No. 2	13	-70	-105	-105	-90	-70
		15	-85	-90	-85	-55	-50
		17	-60	-50	-60	-30	-65
	Test No. 3	13	-65	-115	-100	-90	-65
		15	-85	-105	-75	-50	-55
		17	-50	-55	-50	-40	-60
	Average		-65	-86	-74	-53	-62
Circumferential Crown Gages	Test No. 1	11	-5	-35	-15	-20	-5
		12	-25	-10	-15	-5	-20
	Test No. 2	11	-10	-30	-25	-20	-10
		12	-20	0	-20	-10	-10
	Test No. 3	11	-15	-30	-20	-25	-5
		12	-20	-5	-15	-10	-10
	Average		-16	-18	-18	-15	-10
Meridional Root Gage	Test No. 1	18	+80	+110	+95	+85	+80
	Test No. 2	18	+85	+110	+100	+85	+80
	Test No. 3	18	+90	+110	+95	+85	+80
	Average		+85	+110	+97	+85	+80

(a) Plus values indicate tensile strains; minus values indicate compressive strains. The strains for 50-psi internal and external pressure for all gages and with averaged zero pressure readings are given in Table G-11.

TABLE G-17. PRESSURE STRAINS FOR CONVOLUTION NO. 4 OF 1-INCH CRS-PLY STAINLESS STEEL BELLOWS JD28 PRESSURIZED INTERNALLY

		Gage No.	Microinches of Strain(a) for 10-psi Increments 0-10 psi	10-20 psi	20-30 psi	30-40 psi	40-50 psi
Meridional Crown Gages	Test No. 1	13	-150	-190	-120	-210	-155
		15	-220	-205	-215	-200	-215
		17	-175	-115	-215	-130	-180
	Test No. 2	13	-145	-140	-135	-205	-150
		15	-250	-190	-180	-220	-215
		17	-240	-100	-195	-135	-175
	Test No. 3	13	-120	-190	-120	-190	-110
		15	-220	-215	-190	-215	-215
		17	-205	-130	-205	-130	-200
	Average		-192	-164	-175	-182	-179
Circumferential Crown Gages	Test No. 1	11	-50	-70	-60	-80	-60
		12	-40	-60	-30	-65	-15
	Test No. 2	11	-60	-65	-55	-70	-60
		12	-55	-65	-20	-70	-20
	Test No. 3	11	-55	-65	-60	-70	-60
		12	-45	-65	-30	-65	-25
	Average		-51	-69	-43	-70	-40
Meridional Root Gage	Test No. 1	18	+235	+185	+190	+200	+200
	Test No. 2	18	+215	+175	+190	+195	+200
	Test No. 3	18	+205	+205	+210	+205	+200
	Average		+219	+188	+196	+200	+200

(a) Plus values indicate tensile strains; minus values indicate compressive strains. The strains for 50-psi internal and external pressure for all gages and with averaged zero pressure readings are given in Table F-7.

TABLE G-18. PRESSURE STRAINS FOR CONVOLUTION NO. 5 OF 1-INCH TWO-PLY STAINLESS STEEL BELLOWS JD17 PRESSURIZED INTERNALLY

		Gage No.	Microinches of Strain(a) for 10-psi Increments 0-10 psi	10-20 psi	20-30 psi	30-40 psi	40-50 psi
Meridional Crown Gages	Test No. 1	13	-25	-130	-100	-155	-45
		15	-65	-90	-115	-105	-105
		17	-70	-85	-135	-100	-120
	Test No. 2	13	-40	-170	-170	-138	-80
		15	-20	-60	-95	-105	-95
		17	-45	-95	-155	-115	-90
	Test No. 3	13	-50	-125	-120	-105	-105
		15	-55	-100	-105	-105	-105
		17	-65	-105	-90	-110	-130
	Average		-48	-107	-121	-115	-97
Circumferential Crown Gages	Test No. 1	11	0	-55	-35	-45	-25
		12	-50	-35	-50	-20	-35
	Test No. 2	11	-15	-55	-25	-30	-25
		12	-20	-25	-55	-20	-40
	Test No. 3	11	-10	-50	-25	-40	-25
		12	-20	-30	-45	-30	-35
	Average		-21	-42	-38	-34	-31
Meridional Root Gage	Test No. 1	18	+50	+80	+110	+95	+105
	Test No. 2	18	+105	+60	+105	+90	+95
	Test No. 3	18	+60	+100	+95	+100	+100
	Average		+72	+80	+103	+95	+100

(a) Plus values indicate tensile strains; minus values indicate compressive strains. The strains for 50-psi internal and external pressure for all gages and with averaged zero pressure readings are given in Table G-13.

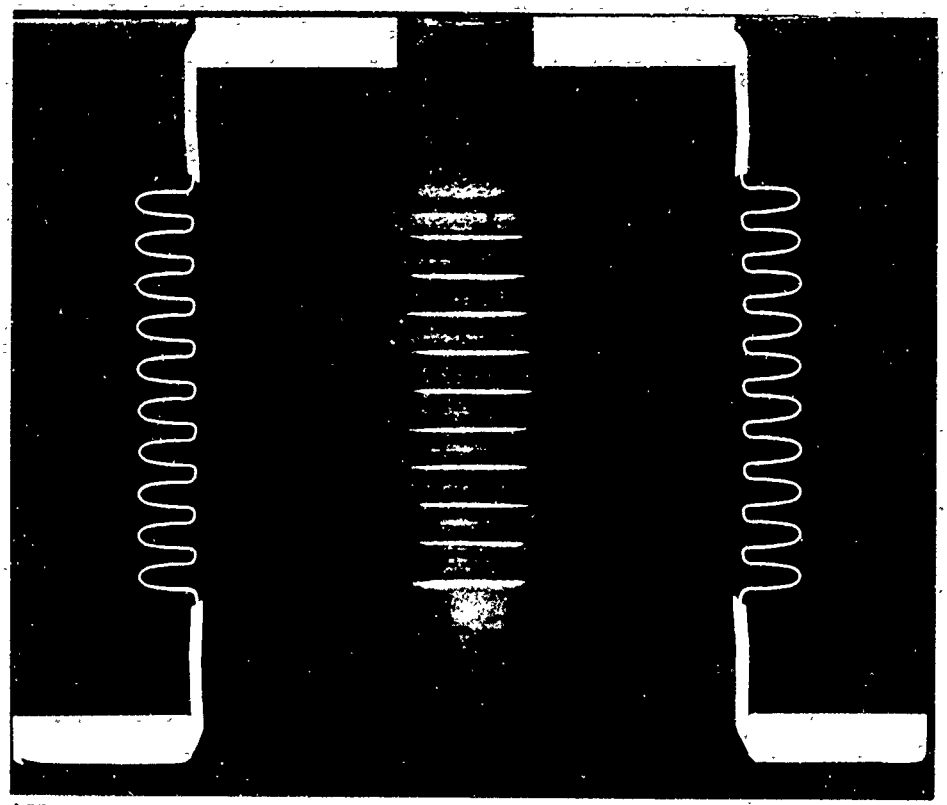

1X As Polished 4A541

FIGURE G-1. CROSS SECTION OF 3-INCH, 2-PLY FORMED BELLOWS JD77 – TYPE 321 STAINLESS STEEL

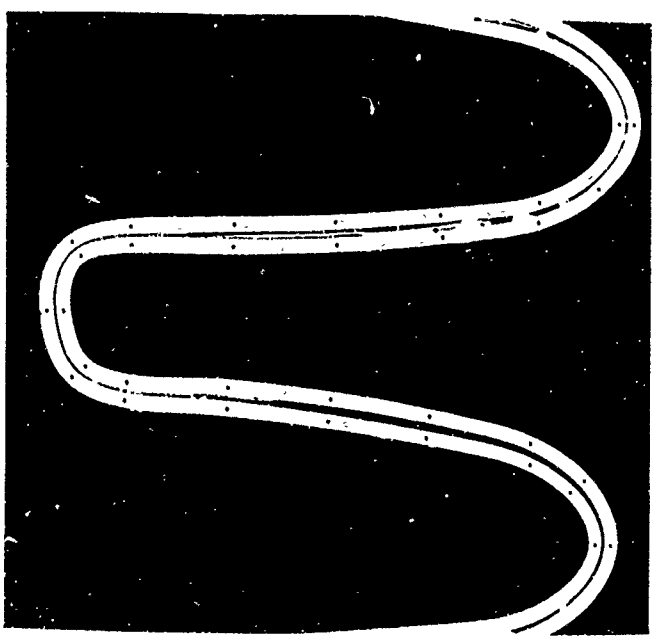

10X As Polished 4A542

FIGURE G-2. ENLARGED VIEW OF CONVOLUTIONS OF CROSS-SECTIONED 3-INCH, 2-PLY FORMED BELLOWS JD77 -- TYPE 321 STAINLESS STEEL

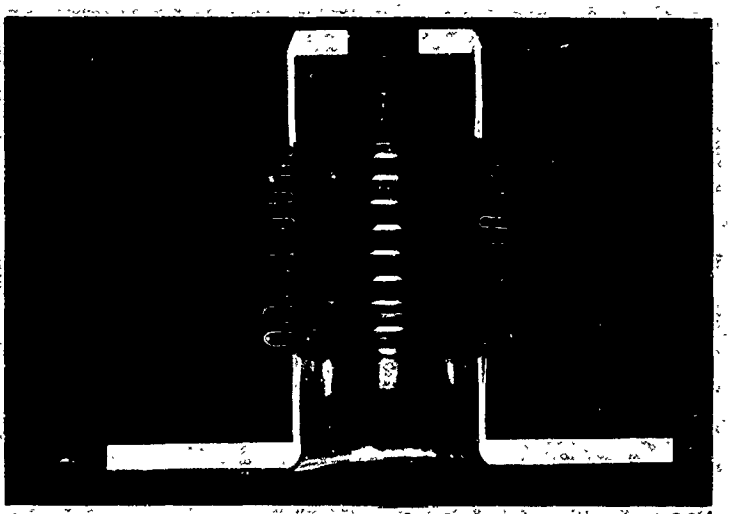

1X As Polished 4A836

FIGURE G-3. CROSS SECTION OF 1-INCH, 2-PLY FORMED BELLOWS JD18 – TYPE 321 STAINLESS STEEL

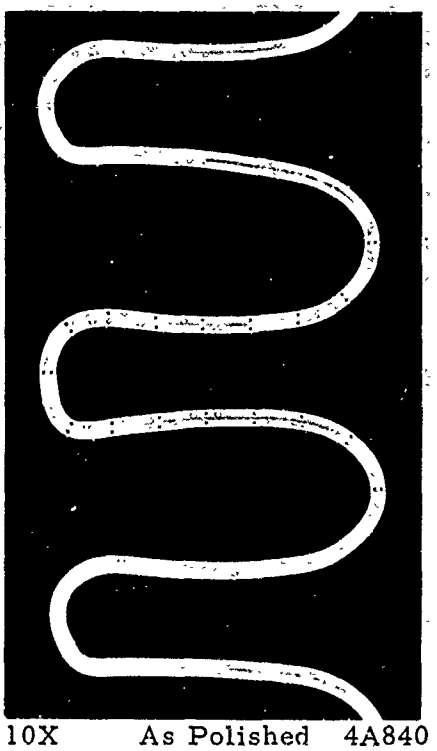

10X As Polished 4A840

FIGURE G-4. ENLARGED VIEW OF CONVOLUTIONS OF CROSS-SECTIONED 1-INCH, 2-PLY FORMED BELLOWS JD18 – TYPE 321 STAINLESS STEEL

APPENDIX H

STRESS ANALYSIS OF A 3-1/2-INCH WELDED BELLOWS – TYPE 347 STAINLESS STEEL

APPENDIX H

STRESS ANALYSIS OF A 3-1/2-INCH WELDED BELLOWS - TYPE 347 STAINLESS STEEL

Theoretical Stress Analysis

Mathematical Model

Since the analysis of the 3-inch formed bellows (see Appendix E) showed that the wall thickness variation is an important factor in obtaining an accurate description of stress distribution, detailed thickness measurements were made on the encapsulated and cross-sectioned bellows shown in Figure H-1. Measurements, which accurately determined the diaphragm centerline and thickness, were made on six diaphragms, three upper and three lower. The points at which the measurements were taken are shown in Figure H-2. The welds on the right-hand side of Figure H-2 are those on the outside diameter (crown), while the welds on the left-hand side are those on the inside diameter (root). Reading 1 corresponds to the first indentation on the inside diameter of the uppermost diaphragm. The measurements are shown in Table H-1. In order to simplify the analysis, the results for the three upper diaphragms were averaged as were the results for the three lower diaphragms.

The mathematical models of the upper and lower diaphragms which were obtained from this averaging process are shown in Figures H-3 and H-4. The values of the various parameters are listed in Table H-2. The mathematical model used in the computer computations consisted of two convolutions, i.e., it contained two upper and two lower diaphragms. This was done so that the influence of the boundary conditions on the stress state would be minimized in most parts of the bellows. The thicknesses measured at the various points on the bellows are also tabulated in Table H-1. The values for the upper and lower diaphragms were averaged. Plots of the thickness variations are given in Figures H-5 and H-6. The circled points indicate the value from the average of three readings, while the solid line indicates the variation used in the actual computations.

Theoretical Stresses

The meridional surface stresses for the upper and lower diaphragms are shown in Figures H-7 through H-10, for an axial compression of $\delta/L = 0.3$ and an internal pressure of 10 psi. The length of the mathematical model was 0.1062 inch. Figures H-11 through H-14 give the circumferential outer surface stresses for the upper and lower diaphragms for the same loading conditions. In these figures, the stresses are superimposed on the shape of the diaphragm so that the diaphragm cross section corresponds to a zero stress level. The dotted line gives the results for the linear calculations while the solid line indicates the results from the nonlinear bending theory.

Modified Theoretical Stresses

Table H-3 shows typical theoretical stresses for the 3-1/2-inch Type 347 welded bellows modified to reflect the thickness of the strain gages (as described in Appendix Q).

In accordance with the location of the gages, as described in the next section, the theoretical stresses selected for modification were those calculated for a location on the outer surface of the lower diaphragm, 0.0455 inch from the edge of the weld bead. From Figure H-5, a thickness of 0.0052 inch was selected for that location.

Experimental Stress Analysis

Strain-Gage Locations

Appendix Q gives a description of the type of strain gages used, the techniques for instrumentation, and the philosophy underlying the location of the gages on the welded bellows. As shown in Figure H-15, two pairs of gages were placed on the underside of the "middle" or fourth convolution from the flanged end. Because the strain increased to a maximum at the weld bead, it was necessary to measure the distance from the center of the gages to the edge of the weld bead. This was done with a calibrated microscope with calculations to allow for the angle of observation. A third pair of gages was placed on the underside of the 7th convolution. As shown in Figure H-15, these gages were placed 90° from the primary pairs of gages.

Strains Due to Axial Deflection

Two types of tests were conducted with the 3-1/2-inch welded bellows in which the strains due to axial deflection could be determined. In the first type of test, the bellows was deflected alternately in increments of compression (0.060 inch and 0.120 inch) and extension (0.060 inch and 0.120 inch), and strain-gage readings were taken at each deflection increment and at the intermediate zero deflection. In the second type of test, in which pressure was combined with deflection, the bellows was deflected alternately in increments of compression (0.060 inch and 0.120 inch) and extension (0.060 inch and 0.120 inch) and, at each deflection increment, the internal (and subsequently the external) pressure of the bellows was increased in 10-psi increments to 20 psi. By subtracting the readings obtained at each pressure level in the latter type of test, the strains due to deflection could be determined.

Table H-4 shows the results of the deflection tests with no pressure. (None of the tabulated values are corrected for gage thickness.) Table H-5 shows the strains due to deflection when the bellows was pressurized. An examination of the data led to the following observations: (1) the deflection strains were essentially the same with and without pressure, (2) the strains were quite uniform despite the flexibility of the bellows, (3) the magnitude of the meridional strains was related to the distance of the gages from the edge of the weld bead, and (4) extension of the bellows caused a slight increase in the circumferential strains.

Strains Due to Pressure

Two types of tests were conducted in which the strains due to pressure could be determined. In the first type of tests, the bellows was pressurized at zero deflection: (1) in 10-psi increments of internal pressure to 20 psi, and (2) in 10-psi increments of external pressure to 20 psi. The second type of test, combining deflection and pressure, was described above.

Table H-6 shows the strains due to 20-psi pressure at zero deflection. Table H-7 shows the strains due to increments of 10 psi at different deflection increments. These data showed that (1) the strains due to external pressure were generally higher than the strains due to internal pressure, (2) the average strains per 10 psi were similar for similarly mounted gages in both tables.

Experimentally Determined Stresses and Strains

The method of calculating stresses from experimentally determined strains is explained in Appendix Q. The strains as given by the gages on the "middle" convolution were used as representative strains in the bellows, and the values were selected from tests which did not combine deflection and pressure. Because the theory for the formed bellows did not predict a difference in strain magnitude for compression and tension, the experimental values for each were averaged for all formed-bellows calculations. Since the theory did predict a difference for the welded bellows, only the compression averages were used from Table H-4 to calculate representative stresses for the 3-1/2-inch stainless steel welded bellows.

Table H-8 shows the representative deflection strains and the representative pressure strains for the primary gages as given in Tables H-4 and H-6. Also shown are the stresses calculated using these strains. Because the strains were averaged, the distances from the strain gages to the edge of the weld bead also were averaged. Thus, the average distance of the meridional strain gage was calculated to be 0.0455 inch from the edge of the weld bead, and the average distance of the circumferential strain gage was calculated to be 0.445 inch from the edge of the weld bead. Because the meridional strain showed a much greater change in relation to location, 0.0455 inch was selected as the average distance for all gages from the edge of the weld bead.

Comparison of Theoretically and Experimentally Determined Stresses and Strains for 3-1/2-Inch Type 347 Welded Bellows

As shown in Table H-9, the experimentally determined deflection stresses and strains showed excellent agreement with the deflection stresses and strains which were calculated using the mathematical model. The experimentally determined pressure stresses and strains showed good agreement wiht the theoretically determined pressure stresses and strains.

TABLE H-1. COORDINATES AND THICKNESSES FOR 3-1/2-INCH SINGLE-PLY STAINLESS STEEL BELLOWS JD136

(Nominal thickness = 0.006 in.; 1 unit = 0.001 in.)

Reading	Coordinates x	Coordinates y	Thickness, in.	Reading	Coordinates x	Coordinates y	Thickness, in.
1	0	0	.00527	100	365	85.5	.00535
2	20	2	.00523	101	335	87	.00518
3	40	3	.00535	102	315	87.5	.00527
4	60	3	.00506	103	305	87	.00523
5	65	3.5	.00462	104	295	85	.00539
6	70	5	.00466	105	285	83	.00535
7	75	7.5	.00510	106	275	81.5	.00531
8	85	11	.00503	107	265	81.5	.00518
9	95	13	.00503	108	255	83	.00514
10	105	13	.00494	109	245	87	.00499
11	115	11	.00510	110	235	92.5	.00499
12	125	7	.00503	111	225	97	.00510
13	135	3.5	.00499	112	215	99.5	.00510
14	145	2	.00523	113	205	100.5	.00507
15	155	2	.00527	114	195	99	.00503
16	165	3	.00515	115	185	97	.00518
17	175	5.5	.00499	116	175	93	.00494
18	185	11.5	.00515	117	165	90	.00514
19	195	17	.00523	118	155	89.5	.00514
20	205	21	.00523	119	145	90	.00527
21	215	22.5	.00507	120	135	91.5	.00527
22	225	22.5	.00510	121	125	95.5	.00523
23	235	21	.00503	122	115	100.5	.00518
24	245	17	.00494	123	105	105	.00510
25	255	13.5	.00494	124	95	107.5	.00514
26	265	12.5	.00503	125	85	107.5	.00518
27	275	12.5	.00494	126	75	106.5	.00535
28	285	14.5	.00490	127	70	105	.00535
29	295	17.5	.00503	128	65	103.5	.00518
30	305	21	.00503	129	60	102.5	.00510
31	315	23	.00523	130	40	102	.00527
32	335	23.5	.00510	131	220	102	.00510
33	365	24	.00523	132	0	101	.00527
34	365	29	.00518	133	0	108.5	.00543
35	335	31	.00503	134	20	109.5	.00518
36	315	31	.00527	135	40	111.5	.00539
37	305	30	.00523	136	60	112.5	.00514
38	295	28.5	.00518	137	65	113	.00462
39	285	26	.00507	138	70	115.5	.00486
40	275	25	.00503	139	75	117.5	.00518
41	265	26	.00507	140	85	121.5	.00514
42	255	29	.00503	141	95	123	.00514
43	245	34.5	.00507	142	105	122.5	.00518
44	235	40	.00503	143	115	120	.00523
45	225	43	.00503	144	125	116	.00514
46	215	44.5	.00495	145	135	113	.00518
47	205	45	.00507	146	145	111.5	.00518
48	195	42.5	.00503	147	155	111.5	.00527
49	185	39	.00494	148	165	113	.00507
50	175	35.5	.00490	149	175	116.5	.00503
51	165	34	.00514	150	185	123.5	.00507
52	155	34	.00518	151	195	128.5	.00507
53	145	35	.00510	152	205	131.5	.00503
54	135	38.5	.00507	153	215	133	.00503
55	125	44.5	.00507	154	225	132.5	.00503
56	115	49.5	.00499	155	235	130.5	.00514
57	105	52	.00490	156	245	126.5	.00494
58	95	53	.00486	157	255	124	.00507
59	85	52.5	.00490	158	265	123	.00507
60	75	50.5	.00490	159	275	123.5	.00510
61	70	49	.00474	160	285	125.5	.00499
62	65	48	.00490	161	295	129	.00518
63	60	48	.00499	162	305	132	.00527
64	40	48	.00518	163	315	133.5	.00523
65	20	48.5	.00507	164	335	133.5	.00514
66	-7	50	.00518	165	365	134.5	.00514
67	-7	55	.00547	166	365	140	.00535
68	20	57.5	.00531	167	335	140.5	.00527
69	40	58.5	.00503	168	315	141	.00527
70	60	58.5	.00503	169	305	141	.00535
71	65	59	.00474	170	295	138.5	.00551
72	70	60.5	.00478	171	285	136.5	.00539
73	75	62.5	.00490	172	275	135	.00543
74	85	66.5	.00499	173	265	135	.00531
75	95	68.5	.00499	174	255	137	.00523
76	105	68.5	.00503	175	245	140.5	.00514
77	115	66.5	.00503	176	235	146.5	.00527
78	125	63	.00510	177	225	150.5	.00510
79	135	59	.00507	178	215	153	.00510
80	145	57	.00486	179	205	154	.00514
81	155	57	.00514	180	195	153	.00510
82	165	58	.00499	181	185	150.5	.00507
83	175	61	.00503	182	175	146.5	.00503
84	185	67	.00503	183	165	143.5	.00323
85	195	72	.00507	184	155	142.5	.00527
86	205	76	.00510	185	145	143	.00535
87	215	78	.00490	186	135	145	.00523
88	225	78.5	.00499	187	125	149	.00514
89	235	76.5	.00499	188	115	154.5	.00518
90	245	73	.00490	189	105	158	.00527
91	255	70	.00486	190	95	160.5	.00523
92	265	69	.00494	191	85	161	.00523
93	275	69	.00494	192	75	159.5	.00523
94	285	70	.00490	193	70	158	.00527
95	295	74	.00507	194	65	157	.00510
96	305	77.5	.00499	195	60	156	.00514
97	315	79.5	.00507	196	40	155	.00518
98	335	75.3	.00510	197	20	154.5	.00523
99	365	80.5	.00514	198	-2	154.5	.00527

TABLE H-2. DIMENSIONS OF MATHEMATICAL MODEL OF 3-1/2-INCH SINGLE-PLY STAINLESS STEEL WELDED BELLOWS JD136

Part	Shell Type	a, in.	b, in.	Coordinates, Degree Initial	Final
1	Conical[a]	1.7973	0.0609	180.0	-
2	Toroidal	1.7364	0.0458	180.0	199.75
3	Toroidal	1.7004	-0.0620[b]	199.75	148.5
4	Toroidal	1.6339	0.0653	148.5	204.5
5	Toroidal	1.5814	-0.0610	204.5	147.5
6	Toroidal	1.5159	0.0610	147.5	197.25
7	Toroidal	1.4849	-0.0435	197.25	181.75
8	Conical	1.4864	0.02	181.75	-
9	Conical	1.4664	0.02	180.0	-
10	Conical	1.4464	0.0277	177.75	-
11	Conical	1.4193	0.0472	4.0	-
12	Conical	1.4664	0.02	1.0	-
13	Toroidal	1.4861	0.0243	1.0	27.0
14	Toroidal	1.5254	-0.0627	27.0	-25.0
15	Toroidal	1.5774	0.0605	-25.0	34.5
16	Toroidal	1.6464	-0.0605	34.5	-23.5
17	Toroidal	1.6954	0.0617	-23.5	25.0
18	Toroidal	1.7474	-0.0617	25.0	1.0
19	Conical	1.7464	0.0509	1.0	-

(a) a is the radial distance from the center of the bellows to the outer edge for Shells 1, 8, 9, and 10, and to the inner edge for Shells 11, 12, and 19. b is the slant length of the conical shell. The initial cordinate is the cone angle.

(b) A negative radius indicates that the normal to the shell midsurface is pointing toward the center of curvature.

TABLE H-3. MODIFIED THEORETICAL DEFLECTION AND PRESSURE STRESSES AND STRAINS FOR 3-1/2-INCH TYPE 347 STAINLESS STEEL WELDED BELLOWS JD136

		Membrane Stress	Bending Stress, Outer Surface	Modified Bending Stress,* Outer Surface	Stress, psi, Calculation for 0.120-in. Compression, or 10-psi Internal Pres.	Strain, μin/in, Calculation for 0.120-in. compression or 10-psi Internal Pressure
Deflection Stresses	Meridional	-66.2	+18,503	+28,107	+28,040	+830
	Circumferential	+2987	+4,881	+7,415	+10,402	+167
Pressure Stresses	Meridional	-24.7	-9,520	-14,461	-14,486	-441
	Circumferential	-496.6	-2,404	-3,652	-4,149	+007

* Bending stresses at outer surface multiplied by 1.519.

TABLE H-4. DEFLECTION STRAINS FOR COMPRESSION AND EXTENSION OF 3-1/2-INCH TYPE 347 STAINLESS STEEL WELDED BELLOWS--NO INTERNAL PRESSURE[a]

Gage No.	Microin. of Strain[b], Bellows in Compression: Test No. 1	Test No. 2	Test No. 3	Test No. 4	Test No. 5	Compression Average	Microin. of Strain[c], Bellows in Extension: Test No. 1	Test No. 2	Test No. 3	Test No. 4	Test No. 5	Extension Average	Combined Average
1	162	162	165	160	160	162	205	200	200	200	200	201	182
2	157	142	145	145	145	147	198	198	200	200	200	199	173
3	157	165	162	167	170	164	203	208	208	205	205	206	185
4	945	850	898	952	940	917	890	790	975	840	915	882	900
5	677	680	675	680	677	678	663	665	668	663	660	664	671
6	795	757	775	827	825	796	783	658	848	753	815	771	784
7	1090	1050	1050	1050	1085	1065	980	980	985	978	978	980	1023

(a) Compression and extension tests were alternated. (b) All measured strains in compression were tensile--deflection was 0.120 inch. (c) All measured strains in extension were compressive--deflection was 0.120 inch.

TABLE H-5. DEFLECTION STRAINS FOR 3-1/2-INCH TYPE 347 STAINLESS STEEL WELDED BELLOWS COMPRESSED AND EXTENDED, AND PRESSURIZED INTERNALLY AND EXTERNALLY TO 20 PSI

	Gage No.	Microin. of Strain[a], Bellows in Compression: 0 psi	10 psi	20 psi	Compression Average	Microin. of Strain[b], Bellows in Extension: 0 psi	10 psi	20 psi	Extension Average	Combined Average
Internal Pressure	1	162	157	172	164	198	203	213	205	185
	2	150	155	165	167	200	205	205	203	185
	3	170	180	185	178	215	210	215	213	196
	4	960	947	897	935	863	843	943	883	909
	5	685	672	625	661	653	650	620	641	651
	6	855	865	815	845	795	783	760	779	812
	7	1055	1052	975	1027	958	1013	1068	1013	1020
External Pressure	1	220	180	227	209	200	225	250	225	217
	4	925	1025	1152	1034	945	955	1020	973	1004

(a) All measured strains in compression were tensile--deflection was 0.120 inch.
(b) All measured strains in extension were compressive--deflection was 0.120 inch.

TABLE H-6. PRESSURE STRAINS FOR 3-1/2-INCH TYPE 347 STAINLESS STEEL WELDED BELLOWS PRESSURIZED INTERNALLY AND EXTERNALLY--NO DEFLECTION

Gage No.	Microin. of Strain[a], Internal Pressure, 20 psi: Test No. 1	Test No. 2	Test No. 3	Average	Average per 10 psi	Microin. of Strain[a], External Pressure, 20 psi: Test No. 1	Test No. 2	Test No. 3	Average	Average per 10 psi
1	-5	-20	-18	-14	-7	+40	+70	+35	+48	+24
2	-13	-18	-20	-17	-8.5	-	-	-	-	-
3	-33	-25	-25	-28	-14	-	-	-	-	-
4	-875	-855	-870	-876	-433.5	+1045	+1082	+1067	+1065	+532.5
5	-585	-580	-595	-587	-293.5	-	-	-	-	-
6	-800	-750	-763	-771	-385.5	-	-	-	-	-
7	-993	-1013	-1030	-1012	-506	-	-	-	-	-

Plus values indicate measured tensile strain; minus values indicate measured compressive strain.

(a) Tests were run in 10-psi increments ascending and descending--values shown are differences between readings at 20 psi (maximum pressure) and average readings for zero pressure before and after tests.

TABLE H-7. PRESSURE STRAINS FOR 3-1/2-INCH TYPE 347 STAINLESS STEEL WELDED BELLOWS COMPRESSED, EXTENDED AND PRESSURIZED INTERNALLY AND EXTERNALLY TO 20 PSI

		Gage No.	Microin. of Strain[a] for Pressure Increments: Deflection, 0.0 inch[b] 0-10 psi	Deflection, 0.0 inch[b] 10-20 psi	Deflection, 0.060 inch[b] 0-10 psi	Deflection, 0.060 inch[b] 10-20 psi	Deflection, 0.120 inch 0-10 psi	Deflection, 0.120 inch 10-20 psi	Average Change per 10 psi
Compression	Internal Pressure	1	-5	-15	-8	-10	-10	0	-8
		2	-5	-15	-8	-8	0	-5	-7
		3	-10	-30	-18	-15	0	-25	-16
		4	-363	-525	-358	-563	-375	-575	-460
		5	-248	-363	-255	-353	-260	-410	-315
		6	-330	-485	-320	-505	-320	-535	-416
		7	-413	-598	-425	-570	-415	-675	-516
	External Pressure	1	+20	+23	+8	+30	-20	+70	+22
		4	+405	+658	+460	+708	+460	+830	+587
Extension	Internal Pressure	1	-10	-15	-8	-18	-15	-25	-15
		2	-10	-15	-13	-15	-15	-15	-14
		3	-15	-25	-20	-23	-10	-30	-20
		4	-355	-530	-370	-533	-335	-630	-459
		5	-243	-360	-248	-355	-240	-330	-296
		6	-323	-488	-335	-478	-310	-465	-400
		7	-405	-595	-420	-605	-460	-650	-523
	External Pressure	1	-10	+28	-23	+25	-15	0	+1
		4	+425	+640	+438	+598	+415	+575	+515

(a) Plus values indicate tensile strains; minus values indicate compressive strains.
(b) Average of two readings.

TABLE H-8. EXPERIMENTALLY DETERMINED REPRESENTATIVE STRAINS AND STRESSES IN 3-1/2-INCH TYPE 347 STAINLESS STEEL WELDED BELLOWS

		Gage No. 1	Gage No. 2	Gage No. 4	Gage No. 5	Average Representative Strains, μin/in	Average Representative Stresses, psi
Strains for 0.120-inch Compression, From Table H-4	Meridional	-	-	+917	+678	+798	+28,166
	Meridional	-	-	-	-	-	-
	Circumferential	+162	+147	-	-	+155	+13,133
Strains for 10 psi Internal Pressure, from Table H-6	Meridional	-	-	-434	-294	-364	-12,067
	Meridional	-	-	-	-	-	-
	Circumferential	-7	-9	-	-	-8	-3,858

TABLE H-9. COMPARISON OF THEORETICALLY DETERMINED AND EXPERIMENTALLY DETERMINED STRESSES AND STRAINS FOR 3-1/2-INCH TYPE 347 STAINLESS STEEL WELDED BELLOWS

		Comparison of Strains		Comparison of Stresses	
		Experimental	Theoretical	Experimental	Theoretical
0.120" Compr. Deflection Stresses and Strains	Meridional	+798	+830	+28,166	+28,040
	Circumferential	+155	+167	+13,133	+10,402
10 psi Pressure Stresses and Strains	Meridional	-364	-441	-12,067	-14,486
	Circumferential	-8	+7	-3,858	-4,149

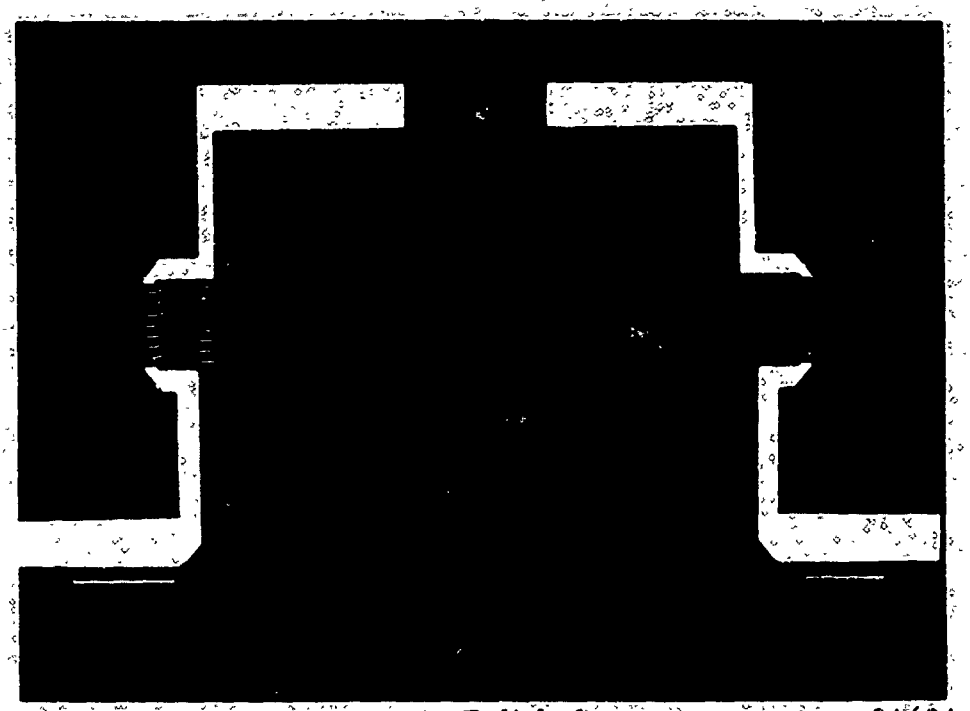

FIGURE H-1. CROSS SECTION OF 3-1/2-INCH TYPE 347 STAINLESS STEEL WELDED-BELLOWS JD136

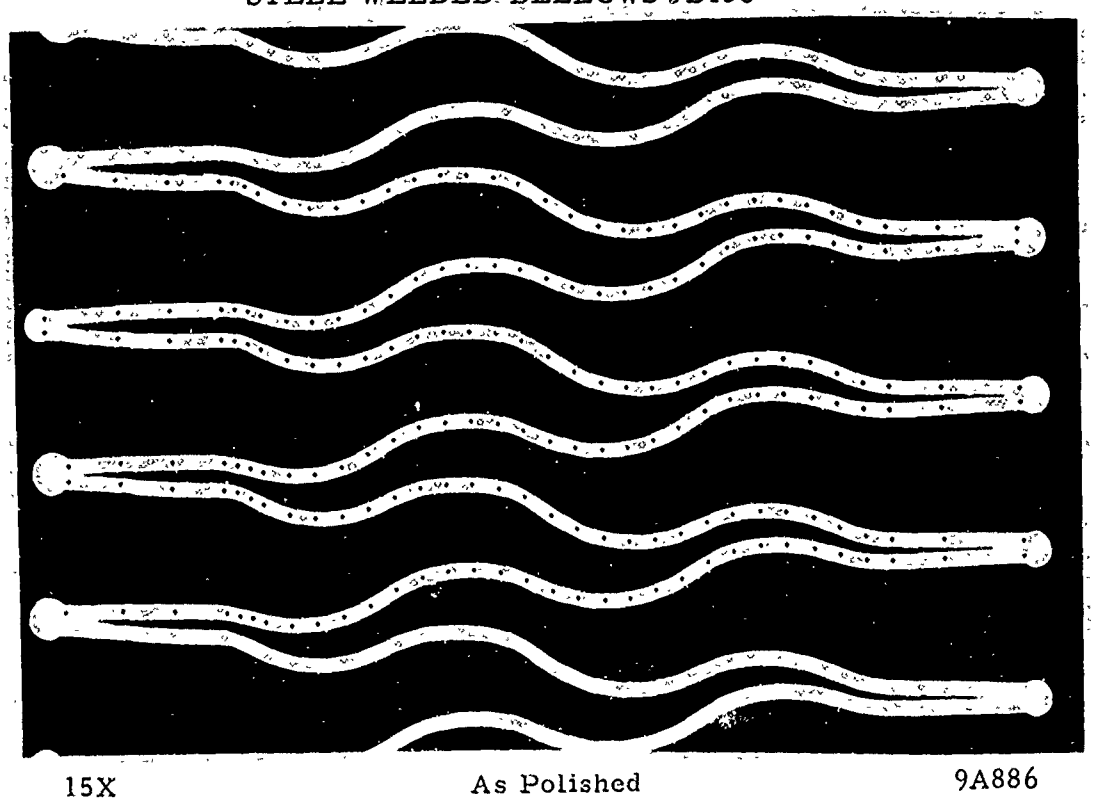

FIGURE H-2. ENLARGED VIEW OF CONVOLUTIONS OF CROSS-SECTIONED 3-1/2 INCH TYPE 347 STAINLESS STEEL WELDED-BELLOWS JD136

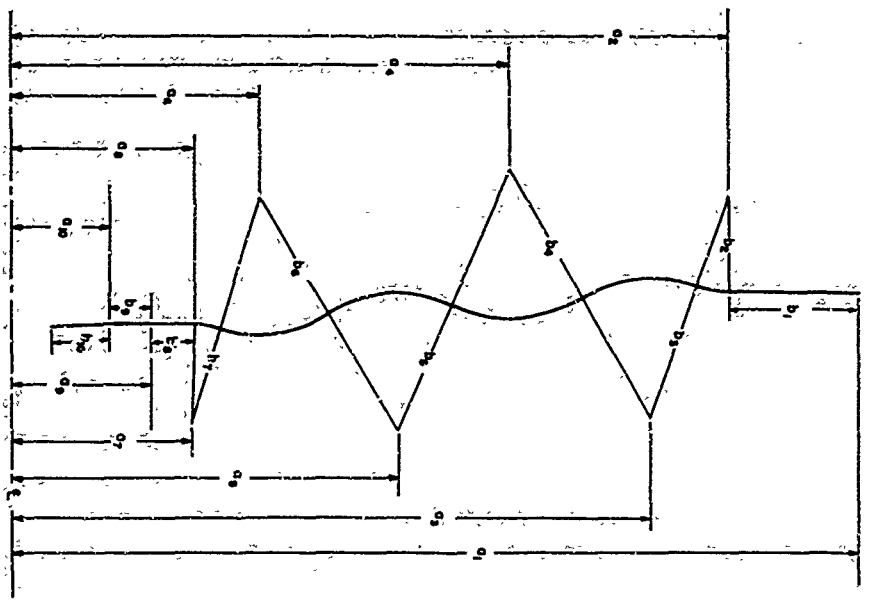

FIGURE H-3. MATHEMATICAL MODEL OF UPPER LEAF OF 3-1/2-INCH SINGLE-PLY STAINLESS STEEL WELDED BELLOWS JD136

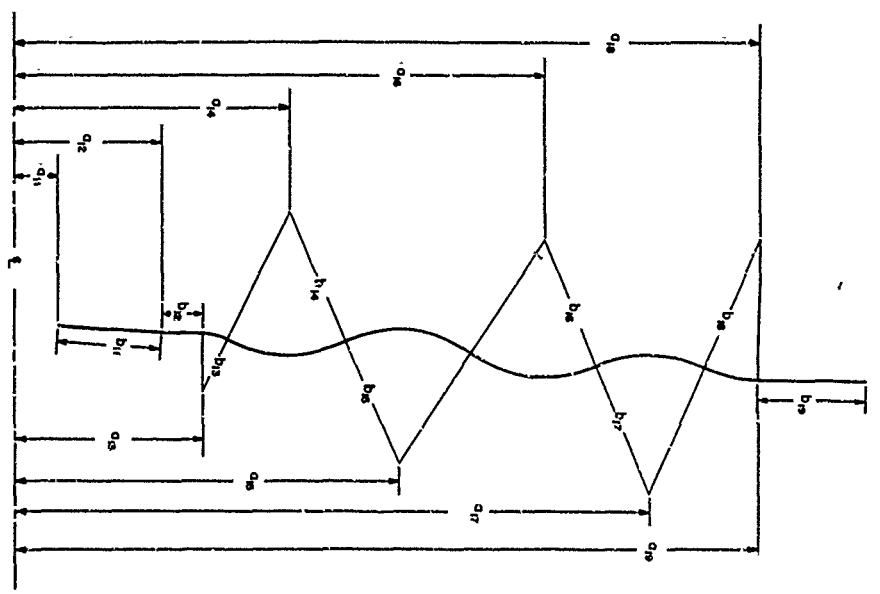

FIGURE H-4. MATHEMATICAL MODEL OF LOWER LEAF OF 3-1/2-INCH SINGLE-PLY STAINLESS STEEL WELDED BELLOWS JD136

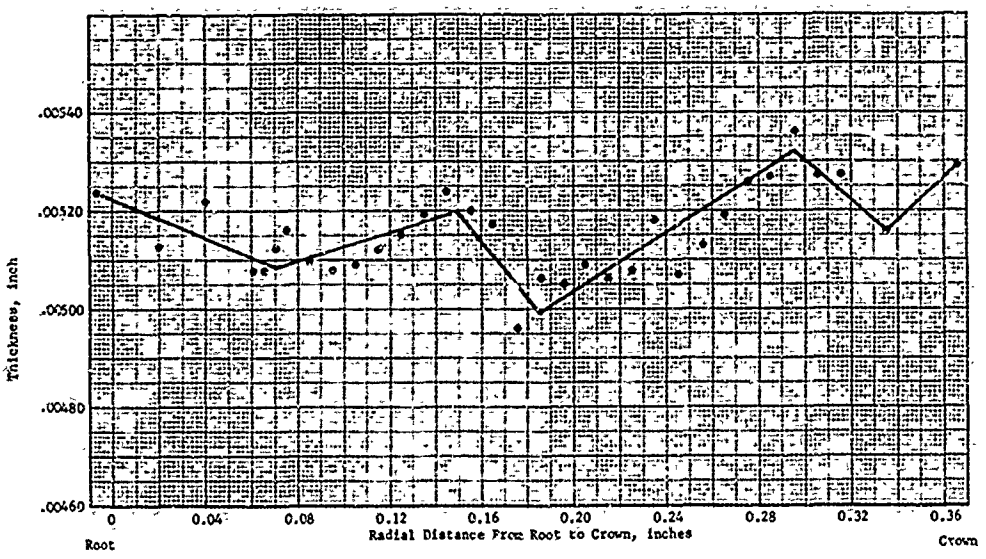

FIGURE H-5. THICKNESS VARIATION FOR PARTS 1-10 FOR 3-1/2-INCH SINGLE PLY STAINLESS STEEL WELDED BELLOWS JD136 (nominal thickness = 0.005 inch)

Circled points indicate average of three measured thicknesses and solid line is thickness variation used for parts 1-10 in mathematical model shown in Figure H-3.

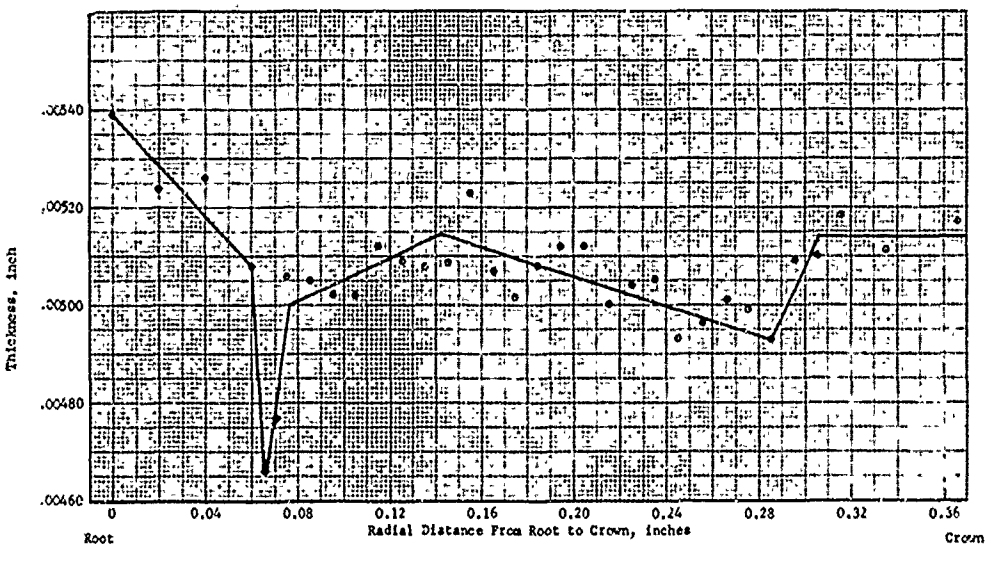

FIGURE H-6. THICKNESS VARIATION FOR PARTS 11-19 FOR 3-1/2-INCH SINGLE-PLY STAINLESS STEEL BELLOWS JD136 (nominal thickness = 0.005 inch)

Circled points indicate average of three measured thicknesses and solid line is thickness variation used for parts 11-19 in mathematical model shown in Figure H-4.

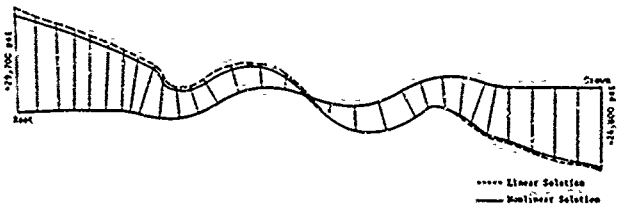

FIGURE H-7. MERIDIONAL INNER SURFACE STRESS FOR UPPER LEAF OF 3-1/2-INCH SINGLE-PLY STAINLESS STEEL WELDED BELLOWS JD136 DUE TO AN AXIAL DEFLECTION OF $\delta/L = 0.3$

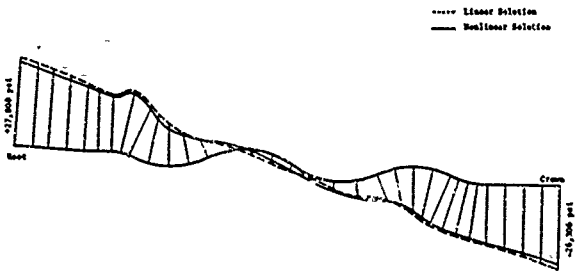

FIGURE H-8. MERIDIONAL INNER SURFACE STRESS FOR LOWER LEAF OF 3-1/2-INCH SINGLE-PLY STAINLESS STEEL WELDED BELLOWS JD136 DUE TO AN AXIAL DEFLECTION OF $\delta/L = 0.3$

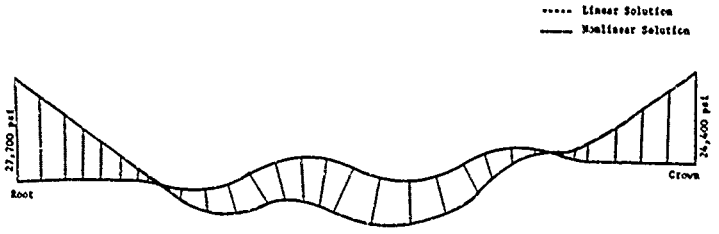

FIGURE H-9. MERIDIONAL INNER SURFACE STRESS FOR UPPER LEAF OF 3-1/2-INCH SINGLE-PLY STAINLESS STEEL WELDED BELLOWS JD136 DUE TO AN INTERNAL PRESSURE OF 10 PSI

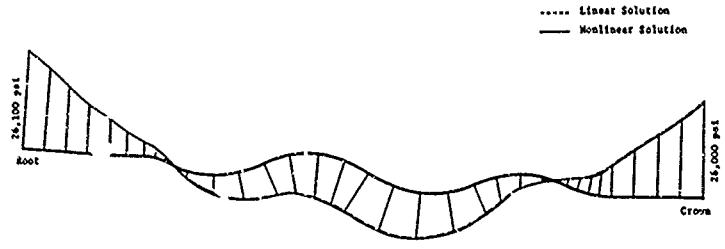

FIGURE H-10. MERIDIONAL INNER SURFACE STRESS FOR LOWER LEAF OF 3-1/2-INCH SINGLE-PLY STAINLESS STEEL WELDED BELLOWS JD136 DUE TO AN INTERNAL PRESSURE OF 10 PSI

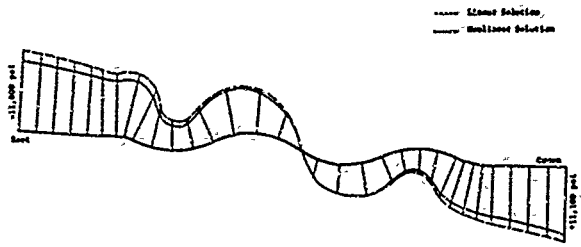

FIGURE H-11. CIRCUMFERENTIAL OUTER SURFACE STRESS FOR LOWER LEAF OF 3-1/2-INCH SINGLE-PLY STAINLESS STEEL WELDED BELLOW JD136 DUE TO AXIAL DEFLECTION OF $\delta/L = 0.3$

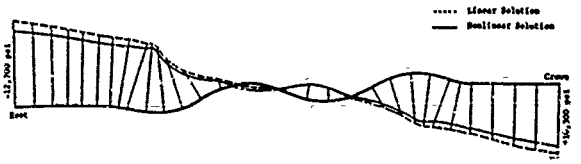

FIGURE H-12. CIRCUMFERENTIAL OUTER SURFACE STRESS FOR UPPER LEAF OF 3-1/2-INCH SINGLE-PLY STAINLESS STEEL WELDED BELLOWS JD136 DUE TO AXIAL DEFLECTION OF $\delta/L = 0.3$

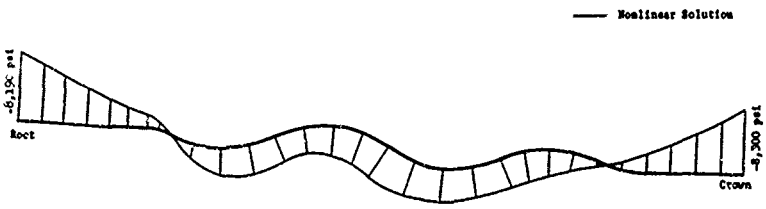

FIGURE H-13. CIRCUMFERENTIAL OUTER SURFACE STRESS FOR LOWER LEAF OF 3-1/2-INCH SINGLE-PLY STAINLESS STEEL WELDED BELLOWS JD136 DUE TO INTERNAL PRESSURE OF 10 PSI

(Linear and nonlinear results were the same for this loading.)

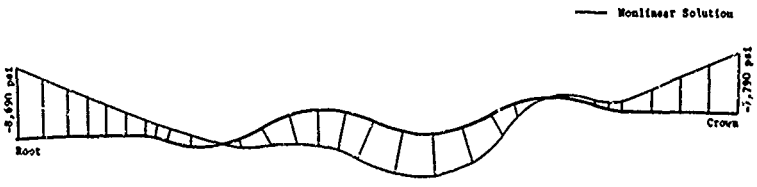

FIGURE H-14. CIRCUMFERENTIAL OUTER SURFACE STRESS FOR UPPER LEAF OF 3-1/2-INCH SINGLE-PLY STAINLESS STEEL WELDED BELLOWS JD136 DUE TO INTERNAL PRESSURE OF 10 PSI

(Linear and nonlinear results are identical for this loading.)

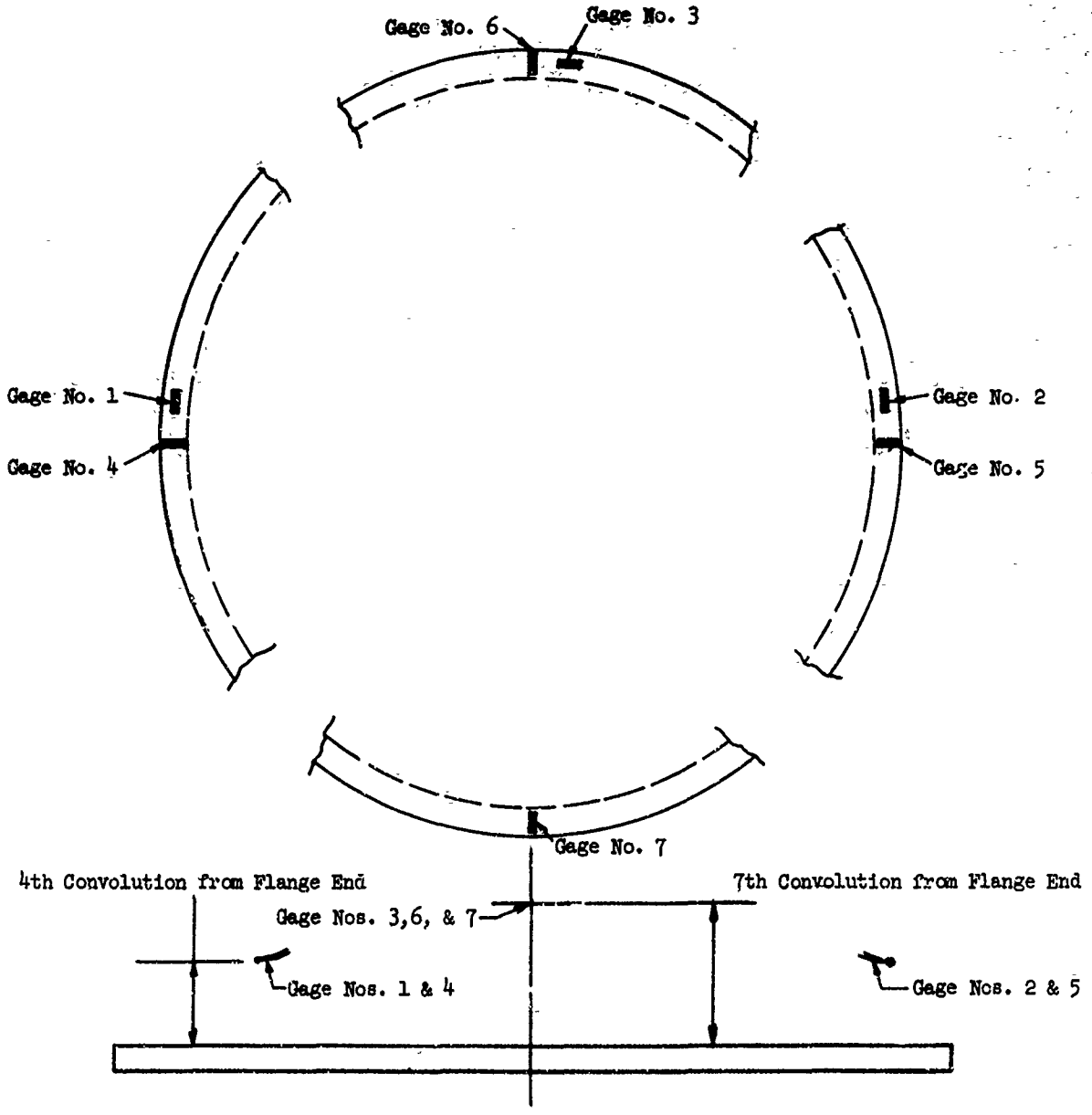

Gage No.	Type	X*
1	Circumferential	0.040
2	Circumferential	0.049
3	Circumferential	0.045
4	Meridional	0.042
5	Meridional	0.049
6	Meridional	0.046
7	Meridional	0.031

*X = Distance from the edge of the weld bead to the center of the gage, in.

FIGURE H-15. LOCATION OF STRAIN GAGES ON 3-1/2-INCH TYPE 347 STAINLESS STEEL WELDED BELLOWS

APPENDIX I

STRESS ANALYSIS OF 4-INCH STAINLESS STEEL DIAPHRAGMS

ABBREVIATIONS AND SYMBOLS

θ Angle measured in the circumferential direction, deg

δ Total axial deflection of the diaphragm hub, in.

k Axial spring rate, lb/in.

P Axial force imposed on the diaphragm hub, lb

ϵ_ϕ Meridional strain at gage position, in./in.

ϵ_θ Circumferential strain at gage position, in./in.

p Internal pressure, psi

M_y Bending moment in diaphragm when material yields, in-lb/in.

σ_y Yield stress of diaphragm material, psi

h Diaphragm wall thickness, in.

M_ϕ Bending moment resultant in meridional direction, in-lb/in.

P_c Critical axial force causing plastic collapse of the diaphragm, lb

p_c Critical internal pressure causing plastic collapse of the diaphragm, psi

b Beam width (Figure I-29), in.

APPENDIX I

STRESS ANALYSIS OF 4-INCH STAINLESS STEEL DIAPHRAGMS

Theoretical and experimental stress analyses of 4-inch stainless-steel convoluted diaphragms were conducted for the following loadings: upward deflection, downward deflection, and upward (internal) pressure. In this Appendix, these elastic analyses are described, and the theoretical and experimental results are compared. In addition, overload-deflection experiments, overpressure experiments and related plastic-collapse analyses are described.

Theoretical Stress Analysis

Mathematical Model

To obtain an accurate mathematical model for best description of the stress distribution, detailed dimensional measurements were made on an encapsulated and cross-sectioned diaphragm, shown in Figure I-1. Measurements were made on the left-side cross section of the diaphragm to accurately locate the diaphragm centerline as well as to determine its thickness. The points at which the measurements were made are shown in Figure I-2. The values of the measurements are shown in Table I-1. Reading 1 in Table I-1 corresponds to the first indentation on the outside diameter of the diaphragm. In order to simplify the analysis, the measured x coordinates were translated to make the first indentation on the outside diameter the origin for the x coordinates.

The 13-part mathematical model of the diaphragm obtained from the dimensional measurements is shown in Figure I-3. The values of the various parameters are listed in Table I-2. The thicknesses measured at the various points on the diaphragm are also tabulated in Table I-1. Plots of the thickness variations are given in Figure I-4. The circled points indicate the actual readings while the solid line indicates the variation assumed in the mathematical model used in the actual computations.

The 13-part mathematical model described above extends from the outside weld to the inside weld shown in Figure I-2. Shell Part 1 (of Table I-2 and Figure I-3) extends over the rim and Shell Parts 12 and 13 extend under the hub. For upward deflection loading, the diaphragm will move away from the rim and the hub. Therefore, the 13-part mathematical model was used for this loading. However, for downward deflection loading, the diaphragm will impinge on the rim as well as on the hub and the effective length of the diaphragm will be reduced. Therefore, for downward deflection loading, a 10-part mathematical model was used which was assumed to be clamped at the edges of the hub and rim. Dimensions for this model are given in Table I-3. This 10-part model is the same as the 13-part model, Table I-2, except that Shell Parts 1, 12 and 13 have been eliminated and Shell Part 11, Table I-2, has been reduced in length (i.e., ϕ_f changed from 178 to 194 degrees).

For upward pressure loading, the diaphragm will receive support at the hub, but not at the rim. Therefore, an 11-part mathematical model was used for this loading –

it was the same as the 10-part model except that Part 1 of the 13-part model, Table I-2, again was included, in order that the outer flat portion of the diaphragm could be allowed to lift off the rim. Dimensions of the 11-part model are given in Table I-4.

Theoretical Results

The computer program NONLIN was used for the theoretical calculations. The meridional upper-surface stresses predicted by both the linear and nonlinear theory for the deflection loadings are shown in Figures I-5 and I-6. For these loadings, the diaphragm was assumed clamped (zero slope and zero horizontal deflection) at the hub and rim, and the hub was moved upward (0.0150 inch) and downward (0.020 inch) with respect to the rim. Appreciable differences between the linear and nonlinear theory were found even at fairly small deflections corresponding to maximum bending stresses of only ±20,000 psi to ±30,000 psi as shown in Figures I-5 and I-6. (On these figures, the stresses are superimposed on the shape of the diaphragm so that the diaphragm cross section corresponds to a zero stress level). Although the stresses are small, the hub deflections of 0.0150 inch and 0.0200 inch are three to four times the thickness, and this amount of geometry change in shell theory is considered a geometrical nonlinearity. A 0.0200-inch downward deflection gives about twice the magnitude of stress as does a 0.0150-inch upward deflection -29,691 psi and +15,750 psi, respectively, near the inside edge as shown in Figures I-5 and I-6.

Figure I-7 shows the upper-surface meridional stresses due to an upward pressure of 2.45 psi (5 inches Hg). (The value 5 inches of Hg was used in order to later directly compare the experimental results.) The plot shown in Figure I-7 represents the stresses from both the linear and nonlinear theory (i.e., there was little difference in results at this pressure). For example, the stresses at the inside and outside edges were -32,359 psi and -19,915 psi, respectively, from the nonlinear theory, and -31,399 psi and -19,303 psi for the linear theory. These results reflect a lack of geometrical nonlinearity in this case. The diaphragm was clamped at both the inside and outside edges. The maximum deflection at 2.45 psi was only 0.0049 inch (in Shell Part 6, Table I-4), which is about one-third the deflection imposed in the deflection experiments. (Of course, geometrical nonlinearity would be expected to have a greater effect at higher pressures.)

Experimental Stress Analysis

Strain-Gage Instrumentation of Diaphragm JD190

Linear theoretical calculations on Diaphragm JD181 indicated that maximum surface strains occur at the tops and bottoms of some of the convolutions and also on the flat near the rim. Accordingly, on Diaphragm JD190, 13 such locations on 3 radial lines were chosen for installation of a total of 22 strain gages as shown in Figures I-8 and I-9. One radial line (the $\theta = 0°$ meridion in Figure I-8) was selected for installation of 9 pairs of radial and circumferential gages on each root and crown of the convolutions, as shown in a close-up view in Figure I-10. To check later on the uniformity of response around the circumference, two radial gages were installed on two crowns on two other radial lines, the $\theta = 120$-degree and $\theta = 240$-degree meridions as noted in Figure I-8.

The strain gages selected for the instrumentation were 1/64-inch gage-length gages, Types EA-09-015EH-120 and EA-09-015DJ-120, obtained from Micro-Measurements, Inc. The EH-type gages were used to measure circumferential strains and the DJ type to measure radial strains. The two types can be seen in Figure I-10.

Deflection Experiments

Deflection experiments were conducted on an Instron machine. The rim of the diaphragm (Figure I-8) was clamped to the base of the machine and the hub was clamped to the movable crosshead of the machine. It was observed that the hub of Diaphragm JD190 was initially tilted with respect to the rim in the unclamped position. Clamping straightened the diaphragm out so that the hub was parallel to the rim, but this produced some initial strains which varied around the circumference as shown in Table I-5. The diaphragm was clamped at zero net upward load. In all the further experiments, the strain gages were zeroed at the clamped position under zero load in order to have Diaphragm JD190 correspond as closely as possible to a perfect unloaded diaphragm with an initially parallel hub and rim.

Initial experiments were run to maximum measured strains of 800 μin./in. in order to avoid damaging the diaphragm by (unknown) overstrain at the more critical weld locations where no strain gages could be applied. For upward deflection runs, 800 μin./in. maximum corresponded to an upward deflection $\delta = 0.020$ in., which is nearly 4 times the diaphragm thickness and is considered a nonlinear deformation. Although the deflection was relatively large compared to the thickness, the strain-versus-deflection curves, shown in Figure I-11, were found to be only slightly nonlinear. The load-deflection curve in Figure I-12 was found to be approximately linear up to $\delta = 0.020$ in., and corresponded to a spring constant for upward deflection of

$$k = \frac{P}{\delta} = 212 \text{ lb/in.} \qquad \text{(I-1)}$$

Downward deflection experiments were also conducted to a deflection of $-\delta = 0.020$ in. maximum. Measured strains are shown in Figure I-13. The diaphragm has a different shape when observed from below than when observed from the top, i.e., Location 9 in Figure I-8 appears convex from above, but concave from below. Consequently, nonlinear response of the diaphragm to downward deflections can be expected to be different from its response to upward deflections. Comparison of Figures I-13 and I-14 shows that lower magnitudes of maximum strain occurred under downward deflection, i.e., at Location 8, $\epsilon_\phi = 820$ μin./in. for $\delta = 0.020$ and $\epsilon_\phi = -650$ μin./in. for $\delta = -0.020$. The lower strain results for downward deflection are believed to be also partially due to some support of the diaphragm by the rim and hub (Figure I-8). An increased stiffness under downward deflection is also noted in the load-deflection plot in Figure I-14 where the spring constant was determined to be

$$k = \frac{-P}{-\delta} = 234 \text{ lb/in. for downward deflection.} \qquad \text{(I-2)}$$

Pressure Experiments

For the pressure experiments, the diaphragm was initially clamped in the Instron machine at zero net upward deflection and load. Of course, the load changed when pressure was applied, but the hub was kept fixed with respect to the rim.

Standard pressure gages did not have a small enough scale in (psi) for the very sensitive diaphragm. Therefore, a mercury manometer was used to control the pressure in increments of inches of Hg (mercury). The pressurizing medium was helium.

Figure I-15 shows the strain results for upward pressures up to 5.0 inches Hg. Whereas maximum strains were measured at Location 8 in the deflection experiments, maximum strains were measured at Location 1 in the pressure experiments. The strain-versus-pressure curves in Figure I-15 are more linear than are the strain-deflection curves, Figures I-11 and I-13. This is related to the deflections and the corresponding changes in geometry: in the pressure experiments, the hub was kept fixed relative to the rim, but in the deflection experiments, the hub was moved 0.020 in. relative to the rim. In the pressure experiments, p = 5.0 in. Hg resulted only in a upward deflection of about 0.007 in. at Location 5 (Figure I-8) midway between the rim and the hub. Consequently, there was less geometry change and less nonlinearity in the response observed in the pressure experiments than in the deflection experiments. (This result agrees with the results of the theoretical analysis).

Circumferential Variation of Strains

It was noted earlier that strain gages at Locations 10 through 13, Figure I-8, were installed to check the symmetry response of the diaphragm. Results for these locations and Locations 3 and 7 are shown in Table I-6. It was found that the circumferential variation of response was small. The largest variation was measured for the downward deflection response, but in this case the magnitudes of measured strains were small. Thus, a fairly uniform response was achieved as desired.

Combined Pressure and Deflection Loadings

Since some geometrical nonlinearity was evidenced in the deflection experiments, it was questionable whether or not individual deflection results and pressure results could be superimposed to give the correct result for combined pressure and deflection loadings. Therefore, combined loading experiments were run. Figure I-16 shows the measured strain ϵ_ϕ at Location 8 for two experiments: one with upward deflection first followed by upward pressure, and the other with upward pressure first followed by upward deflection. The same final strain value was reached for each loading path, in this case, ϵ_ϕ = 380 μin./in. Also, the results for the individual loadings can be superimposed in this case to give approximately the same net result: from Figure I-16, ϵ_ϕ = 820-410 = 410 μin./in. The difference 410-380 = 30 μin./in. is small compared with the accuracy of reading of the gages – about ±20 μin./in.

(The experimental data in Figures I-16 and I-17 are the average data for three runs.)

Figure I-17 shows another combined loading experiment, but with downward deflection instead of upward deflection. In this case, the final result again was independent of loading path; the difference in final strains was negligible, 765-750 = 15 μin./in. However, the more significant result in this case was that the individual loadings could not be superimposed to give the correct combined value of net strain; i.e., ϵ_ϕ = 520 + 300 = 820 μin./in., which was appreciably different from the values of 765 or 750 μin./in. for each path for the combined loadings. This result is attributed to larger net strains in this case and consequently to greater nonlinear effects. The strains from downward deflection add to the strains from upward pressure to give a larger magnitude of net strains, but the strains from upward deflection in the previous case, Figure I-16, subtracted from the pressure strains to give lower net strains.

The greater nonlinearity in the combined downward deflection and upward pressure loadings was also partially attributed to hub support of the diaphragm. Both of these loadings force the hub and diaphragm together over a short radial length near the inside edge, as can be noted in Figure I-8. This contact was believed to have increased with increasing load and thus contributed to the nonlinear response.

Comparison of Theoretical and Experimental Results

The theoretical and experimental results for the spring constant (k) for the deflection loadings were first compared. As shown in Table I-7, the theoretical values for Diaphragm JD181 are somewhat higher than the experimental values for Diaphragm JD190.

The experimental spring constant was found to be higher for downward deflection (k = 234 lb/in.) than for upward deflection (k = 212 lb/in.), as noted earlier in Figures I-12 and I-14. However, the theoretical spring constants, using the 13-part mathematical model of Table I-2, were found to be essentially the same for both upward and downward deflections. The difference noted in the experiments was believed due to hub and rim support of the diaphragm over small regions near the inside and outside edges, respectively, for downward deflections. (This is apparent in Figure I-8.) However, the 10-part mathematical model, Table I-3, theoretically accounts for these supporting effects for downward deflections. The theoretical results for the spring constant (k) for the 10-part mathematical model are also shown in Table I-7. An increase in k by a factor of $\frac{312}{256}$ = 1.22 was found theoretically for downward deflections over upward deflections. The experimental factor is $\frac{234}{212}$ = 1.10. Thus, the 10-part mathematical model accounted for increased stiffness for downward deflections due to hub and rim support, but it seemed to somewhat overaccount for the increase. This may have been due to differences in geometry of the Diaphragms JD181 and JD190, or it may have been due to incomplete support at the hub as evidenced by a small gap between the diaphragm and the hub in Figure I-2.

Theoretical and experimental strains were also compared, but the bending part of the experimentally measured strains had to be first corrected for the effect of gage and cement thickness. In Appendix Q, this thickness measurement was reported for the same type of gages used here in the diaphragm. The midsurface of the strain gages was found to be 0.00135 in. above the diaphragm surface. Assuming a linear strain gradient through the diaphragm thickness and taking an average diaphragm thickness

of 0.0055 in., the measured bending strains were reduced by the factor (0.0055/2)/(0.00135 + 0.0055/2) = 0.671, i.e.,

$$\left(\epsilon_{\text{bending}}\right)_{\text{corrected}} = 0.671 \left(\epsilon_{\text{bending}}\right)_{\text{measured}} \quad . \tag{I-3}$$

The measured strains, however, were total strains and not bending strains. In order to calculate the experimental bending strain from the experimental total strain, the theoretical ratio of membrane strain to bending strain was used, i.e.,

$$\left(\epsilon_{\text{bending}}\right)_{\text{experimental}} = \left(\frac{\epsilon_{\text{bending}}}{\epsilon_{\text{total}}}\right)_{\text{theoretical}} \times \left(\epsilon_{\text{total}}\right)_{\text{experimental}}, \tag{I-4}$$

where, in general

$$\epsilon_{\text{total}} = \epsilon_{\text{membrane}} + \epsilon_{\text{bending}} \quad .$$

Thus, the total corrected experimental strains were found from the formula

$$\epsilon_{\text{total}} = 0.671\ \epsilon_{\text{bending}} + \epsilon_{\text{membrane}} \quad . \tag{I-5}$$

A comparison of theoretical and experimental strains was made for the meridional strain (ϵ_ϕ) at Location 8 and for the circumferential strain (ϵ_θ) at Location 7. The locations are shown in Figure I-8. The theoretical and experimental strains are shown in Tables I-8 and I-9. For a downward deflection of δ = -0.020 inch, a larger magnitude of total meridional strain at Location 8, Table I-8, was found for the 10-part mathematical model than for the 13-part mathematical model. (The theoretical circumferential strains, Table I-8, were about the same for each model). The results of these two models bracket the experimental results. Therefore, it is concluded that the 10-part model accounts for hub and rim support of the diaphragm which was evidently present in the downward deflection experiments.

Comparison of the total theoretical and total corrected experimental meridional strains in Table I-8 for the pressure loading p = 2.45 psi shows that the theoretical strain predicted for the 11-part mathematical model is almost exactly the same as the experimental strain, viz., -358 μin./in. as compared with -360 μin./in. Evidently, the hub again supported the diaphragm during the upward pressure experiments as it did in the downward deflection experiments and the 11-part mathematical model correctly accounts for this hub support for upward pressure loading. The rim does not offer support when the diaphragm is subjected to upward pressure as can be observed in Figure I-8. This result again confirms the presence of hub support when the diaphragm and hub are forced together. For comparison, the results obtained using a 13-part mathematical model are included in Table I-8 for p = 2.45 psi. As evident, the 13-part model, which does not account for hub support, shows a much lower theoretical strain (-248 μin./in.).

Further comparisons of theory and experiment are made in Figures I-18, I-19, and I-20, where upper-surface meridional stresses calculated from corrected strain-gage data are shown superimposed on the theoretical curves (shown previously in Figures I-5, I-6, and I-7). As can be observed, the experimental points are close to the theoretical predictions.

The above comparisons of theoretical and experimental results show that the computer program NONLIN enables an accurate prediction of strains and stresses when the diaphragm is correctly modeled for specific loadings.

Overload Experiments and Plastic-Collapse Analysis

Overload Deflection Experiments

Instrumented Diaphragm JD190 was also subjected to upward deflections to cause strains in the plastic range. Upward deflections were chosen rather than downward deflections because of the complication of hub and rim support to the diaphragm in the latter case. Also, the response to upward deflections was considered to be of more importance to the fatigue behavior than response to upward pressure. Therefore, the upward-deflection experiments were carried into the plastic range on Diaphragm JD190 which had been kept free of plastic deformation up to this time. Once these experiments were carried out, the diaphragm became permanently deformed and was not used further for any other type of experiments.

Figures I-21, I-22, and I-23 show load-versus-deflection curves for 9 overload runs. The first three runs were made to a deflection of $\delta = 0.050$ inch and then unloaded to zero deflection as shown in Figure I-21. The first load reached was 13.7 lb. Shakedown* occurred after three runs; i.e., repetitive data were measured for a shakedown load varying between +13.2 lb and -0.90 lb. Figures I-22 and I-23 show subsequent runs to higher deflections of $\delta = 0.070$ in. and $\delta = 0.08$ in. Again, shakedown was achieved after three runs to the maximum deflection. The shakedown loads were (+19.0 lb, -1.40 lb), and (+25.3 lb, -2.05 lb), respectively.

Figure I-24 shows the experimentally measured strains at Locations 1 and 8 for the three overload deflection experiments. Results for Runs 1, 4, and 7 are shown. Strain results for the subsequent two runs were essentially the same in each of the three cases, i.e., there were only small changes for subsequent runs. For example, the maximum strains measured at Location 8 were 4560, 4535, and 4510 μin./in. for Runs 7, 8, and 9 respectively. These results indicate that the diaphragm can be cycled into the plastic range, with shakedown occurring after very few cycles.

Overpressure Experiments

Two diaphragms JD188 and JD189 were subjected to overpressures up to 60 psi and 300 psi, respectively. In these experiments, dial indicators were used to measure upward deflections of the crowns of convolutions at the Locations 3, 5, 7, and 9 shown in Figure I-8. Deflection-versus-pressure results are shown in Figures I-25 and I-26. The deflections reached were almost entirely retained as a permanent set upon unloading as shown. For Location 9, Figure I-25 shows a maximum deflection of 0.040 in. at 60 psi and a permanent set of 0.027 in. The difference 0.040 - 0.027 = 0.013 in. repre nts a recoverable elastic deflection. On the loading curve, 0.013 in. corresponds to p = 12 psi. This pressure can be used as an estimate of the "initially plastic

*Shakedown is defined as that condition of elastic loading and unloading subsequent to a loading causing plastic flow to occur. Shakedown loads are not unique; they depend upon the loading program.

collapse" pressure. However, because elastic behavior is nonlinear and elastic loading and elastic unloading behavior may differ, this estimate is approximate. Different estimates would be obtained for locations other than Location 9, but for Location 9, the unloading curve is most nearly parallel to the elastic part of the loading curve, and consequently the estimate of p = 12 psi is considered best.

Diaphragm JD189 was pressurized to 100 psi first, then unpressurized, and then pressurized to 300 psi as indicated in Figure I-26. The second loading curves follow closely the first unloading curves. From the first loading and unloading curves for Location 9 in Figure I-26, the recoverable elastic deflection from unloading is 0.039 - 0.026 = 0.013 in., which corresponds to an initial plastic collapse pressure of p = 17 psi on the first loading curve.

The second loading of Diaphragm JD189, Figure I-26, is really the loading of a new shape of diaphragm which may have been further strain hardened in addition to its initial forming operation. However, the second loading curves appear to become tangent to the initial loading curves.

Although the initial plastic collapse pressures are relatively small, the diaphragm can withstand much higher pressure without burst (up to 300 psi), but it does so with a great change in shape. This can be observed in Figures I-27 and I-28, which show photographs of cross-sectioned and encapsulated Diaphragms JD188 and JD189 after deformation.

Plastic Collapse Analysis

First the method of using the linear elastic solution for predicting plastic collapse is considered. As observed from the theoretical analysis described above, the maximum stresses are predominantly bending stresses which occur at the inside and outside edges. Consequently, the maximum bending moment predicted by the elastic theory can be scaled up to the yield moment value in order to give a lower bound to the collapse load. The yield moment M_y in a shell is

$$M_y = \frac{\sigma_y h^2}{4} \quad , \tag{I-6}$$

where

σ_y = yield tensile stress, psi

h = thickness, in.

From the linear computer calculations the maximum bending moments for upward deflection (P) and upward pressure (p) loadings for 13-part and 11-part mathematical models are, respectively,

$$\left| M_\phi \right| = 0.0222\ P,$$
$$\left| M_\phi \right| = 0.0553\ p\ . \tag{I-7a, b}$$

Equating Equations (I-7a, b) and (I-6) for $\sigma_y = 40,000$ psi and $h = 0.0055$ in. average gives the following values for the lower bounds P^- and p^- to the collapse load P_c and collapse pressure p_c:

$$P_c \geq P^- = 13.6 \text{ lb} \quad , \qquad (I\text{-}8a, b)$$

$$p_c \geq p^- = 5.48 \text{ psi} \quad .$$

The value $P^- = 13.6$ lb is very close to the value $P = 13.7$ lb, in Figure I-21, at which plastic deformation was first recorded, but the value $p^- = 5.48$ psi is appreciably different from the initial collapse values $p = 12$ psi and $p = 17$ psi estimated from experimental results on Diaphragms JD188 and JD189. However, the lower bound estimate (Equation I-8b) is certainly a lower bound relative to the experimental estimates. The yield-strength value, $\sigma_y = 40,000$ psi, is for annealed sheet material. In the cold-drawn condition, $\sigma_y = 65,000$ psi. The exact amount of cold work in forming the diaphragms is unknown. Using $\sigma_y = 65,000$ psi gives higher values for the lower bounds: $P = 22.1$ lb and $p = 8.9$ psi.

Battelle has recently developed two computer codes for the plastic collapse of thin shells of revolution: one based upon the Tresca yield condition, the other on the von Mises yield condition. The codes embody a rigid perfectly plastic analysis, so they do not account for progressive strain hardening of the shell material. However, the codes do serve to predict initial plastic collapse of shells of strain-hardening materials such as Type 347 stainless steel if the correct value of the yield strength is used. At present the codes employ small deformation theory. The computer program based upon the von Mises yield condition was used to calculate collapse loads for upward deflection and upward pressure on the mathematical models of Diaphragm JD181. For upward deflection, the 13-part mathematical model (Table I-2) was used, and for upward pressure, the 11-part mathematical model (parts 12 and 13 eliminated) was used. Clamped boundary conditions were imposed at both the inside and outside edges. A yield strength of 40,000 psi in tension was assumed for the Type 347 stainless steel. An average thickness of 0.0055 in. was assumed. An upper bound, P_c^+, to the collapse load, P_c, for upward deflection was calculated:

$$P_c \leq P_c^+ = 21.0 \text{ lb} \quad .$$

This is somewhat higher than the load $P = 13.7$ lb, Figure I-21, at which plastic deformation became significant in Diaphragm JD190, but it is in between the load values in Figures I-22 and I-23.

An upper bound, p_c^+, to the collapse pressure, p_c, was also calculated:

$$p_c \leq p_c^+ = 16 \text{ psi} \quad .$$

From the experimental results on Diaphragms JD188 and JD189, initial plastic collapse pressures of 12.0 psi and 17 psi, respectively, were estimated. Thus, the theoretical value of 16 psi is in close agreement with the experimental results.

More accurate calculations are possible using the Battelle plastic collapse computer programs. Actually, "exact" values of initial collapse loads are possible (satisfying both the lower bound and upper bound conditions) for shells with thickness and strength varying along the meridion. Thus, the effect of increased strength from

strain hardening at roots and crowns of convolutions can be included. The detailed analysis is complicated, however, and was beyond the scope of the present program. However, such future detailed efforts are recommended.

Although the initial plastic collapse pressure is relatively small, $p_c \simeq 16$ psi, the diaphragms can withstand much higher pressures without burst, as noted previously. This behavior is attributed to the favorable geometry change during deformation. As noted in Figures I-27 and I-28, the diaphragms deform from the corrugated shape toward a semitoroidal shape with flattening of the corrugations. Thus, large deformations are possible without appreciable stretching, but with appreciable bending at the tops and bottoms of the convolutions; i.e., material is available in the corrugations to permit a grossly deformed shape without reducing the thickness. This type of behavior is illustrated by the hinged beam model in Figure I-29, where the collapse load curve is shown for two rigid beams joined by a yield hinge at the center and pulled apart at the ends. As shown, the initial collapse load (for rectangular cross-sectioned beams) for predominantly bending collapse is only $1/28.3 = 0.0353$ times the final collapse load for pure tension collapse when the hinged beam model straightens out. It is noted that this curve, Figure I-29 for the hinged beam, is concave upward similar to the pressure loading curves, Figures I-25 and I-26 (up to 100 psi), and also the upward deflection curves, Figures I-21, I-22, and I-23.

The overload experiments and the above simplified beam analysis indicate that corrugated diaphragms can withstand loads much beyond their initial plastic collapse loads. Accurate prediction of this kind of behavior will require an elastic-plastic theoretical analysis. Battelle is currently developing an elastic-plastic computer code for shells. It is recommended that this code be applied in future analysis of diaphragms.

TABLE I-1. COORDINATES AND THICKNESSES FOR 4-INCH CONVOLUTED DIAPHRAGM JD181
(1 unit = 0.001 inch)

Reading	Coordinates y	Coordinates x	Translated Coordinate, x	Thickness
1	33	-316	0	586
2	33	-296	20	590
3	33	-276.5	39.5	566
4	29	-264	52	578
5	22.5	-250	66	578
6	17.5	-235	81	574
8	15	-217	99	578
7	17.5	-194.5	121.5	582
9	22.5	-179.5	136.5	574
10	29.5	-165.5	150.5	582
11	36	-151	165	574
12	40.5	-135.5	180.5	570
13	42	-118	198	562
14	40.5	-100	216	562
15	36	-84	232	558
16	29.5	-70.5	245.5	570
17	21	-57	259	578
18	12.5	-43.5	272.5	570
19	6	-30	286	566
20	1.5	-14.5	301.5	562
21	0	0	316	570
22	1.5	15	331	570
23	5.5	30	346	574
24	12.5	45	361	574
25	19.5	60	376	566
26	25.5	75	391	550
27	29.5	90	406	550
28	31	105	421	554
29	29.5	120	436	550
30	25.5	136	452	566
31	19.5	150	466	562
32	12.5	162	478	546
33	5.5	175.5	491.5	550
34	0	190	506	554
35	-2.5	209	525	558
36	0	230	546	554
37	5.5	246.5	562.5	550
38	12.5	258.5	574.5	550
39	20.5	270	586	542
40	29	283	599	538
41	36	299	615	538
42	40	326.5	642.5	538
43	36	352.5	668.5	546
44	29	369	685	554
45	21.5	381.5	697.5	554
46	15	396	712	554
47	10	411.5	727.5	538
48	8.5	426.5	742.5	534
49	10	441	757	538
50	15	458	774	538
51	21.5	470	786	538
52	29.5	480.5	796.5	542
53	36	490	806	546
54	43	501.5	817.5	546
55	49	515.5	831.5	546
56	52	538.5	854.5	542
57	49	561	877	534
58	43	577	893	546
59	37	591.5	907.5	514
60	36	608.5	924.5	554
61	37.5	628.5	944.5	550
62	37.5	648.5	964.5	566

TABLE I-2. DIMENSIONS OF 13-PART MATHEMATICAL MODEL OF 4-INCH CONVOLUTED DIAPHRAGM JD181 FOR UPWARD DEFLECTION LOADING

Part	Shell Type	a, inches	b, inches	Meridional Coordinates, φ, deg. Initial	Final
1	Conical	1.982	0.03300	180.0	-
2	Toroidal	1.949	0.04830	180.0	210.0
3	Toroidal	1.8805	-0.08900	210.0	149.6
4	Toroidal	1.7835	0.10100	149.6	219.0
5	Toroidal	1.6655	-0.08720	219.0	146.3
6	Toroidal	1.5615	0.09950	146.3	215.5
7	Toroidal	1.4555	-0.08304	215.5	139.3
8	Toroidal	1.341	0.09180	139.3	214.5
9	Toroidal	1.2405	-0.08630	214.5	139.0
10	Toroidal	1.126	0.08860	139.0	208.5
11	Toroidal	1.063	-0.04210	208.5	178.0
12	Conical	1.061	0.02490	178.0	-
13	Conical	1.0365	0.02000	180.0	-

TABLE I-3. DIMENSIONS OF 10-PART MATHEMATICAL MODEL OF 4-INCH CONVOLUTED DIAPHRAGM JD181 FOR DOWNWARD DEFLECTION LOADING

Part	Shell Type	a, inches	b, inches	Meridional Coordinates, φ, degree Initial	Final
1	Toroidal	1.949	0.04830	180.0	210.0
2	Toroidal	1.8805	-0.08900	210.0	149.6
3	Toroidal	1.7835	0.10100	149.6	219.0
4	Toroidal	1.6655	-0.08720	219.0	146.3
5	Toroidal	1.5615	0.09950	146.3	215.5
6	Toroidal	1.4555	-0.08304	215.5	139.3
7	Toroidal	1.341	0.09180	139.3	214.5
8	Toroidal	1.2405	-0.08630	214.5	139.0
9	Toroidal	1.126	0.08860	139.0	208.5
10	Toroidal	1.063	-0.04210	208.5	194.0

TABLE I-4. DIMENSIONS OF 11-PART MATHEMATICAL MODEL OF 4-INCH CONVOLUTED DIAPHRAGM JD181 FOR UPWARD PRESSURE LOADING

Part	Shell Type	a, inches	b, inches	Meridional Coordinates, φ, degree Initial	Final
1	Conical	1.982	0.03300	180.0	-
2	Toroidal	1.949	0.04830	180.0	210.0
3	Toroidal	1.8805	-0.08900	210.0	149.6
4	Toroidal	1.7835	0.10100	149.6	219.0
5	Toroidal	1.6655	-0.08720	219.0	146.3
6	Toroidal	1.5615	0.09950	146.3	215.5
7	Toroidal	1.4555	-0.08304	215.5	139.3
8	Toroidal	1.341	0.09180	139.3	214.5
9	Toroidal	1.2405	-0.08630	214.5	139.0
10	Toroidal	1.126	0.08860	139.0	208.5
11	Toroidal	1.063	-0.04210	208.5	194.0

TABLE I-5. CHANGE IN EXPERIMENTAL STRAINS AT DIFFERENT CIRCUMFERENTIAL LOCATIONS AFTER CLAMPING OF DIAPHRAGM JD190

	Meridional Strain[a], μin./in., at Location Number[b]					
	3 (θ = 0°)	11 (θ = 120°)	13 (θ = 240°)	7 (θ = 0°)	10 (θ = 120°)	12 (θ = 240°)
	60	105	-100	65	35	-30
	30	120	-100	55	-15	-30
	25	115	-75	60	30	-30
Average	38	113	- 92	60	17	-30

(a) Change from the unclamped position. At the unclamped position the hub was observed to be tilted with respect to the rim. The hub was clamped to be parallel to the rim.

(b) Locations shown in Figure I-8.

TABLE I-6. EXPERIMENTAL STRAINS MEASURED AT DIFFERENT CIRCUMFERENTIAL LOCATIONS ON DIAPHRAGM JD190

	Meridional Strain, in./in., at Location Number					
Loading	3 (θ = 0°)	11 (θ = 120°)	13 (θ = 240°)	7 (θ = 0°)	10 (θ = 120°)	12 (θ = 240°)
Upward Deflection, δ = 0.020 in.	-250	-210	-270	-215	-235	-215
	-250	-210	-290	-215	-215	-215
	-250	-215	-255	-210	-210	-220
Average	-253	-212	-272	-213	-220	-217
Downward Deflection, δ = -0.020 in.	15	75	45	30	-(a)	55
	15	80	70	30	-	55
	15	80	75	30	-	60
Average	15	78	63	30		57
Internal Pressure p = 5 in. Hg,	130	155	140	500	545	535
	115	155	145	475	515	525
	115	160	145	475	520	540
Average	120	157	143	483	527	533

(a) The gage at Location 10 showed an open circuit at this time in the experiments.

TABLE I-7. COMPARISON OF THEORETICAL AND EXPERIMENTAL SPRING CONSTANTS

Direction of Loading	Mathematical Model	Spring Constant, k, lb/in.		
		Theoretical (JD181)		
		Linear	Nonlinear	Experimental (JD190)
Upward	13-part	254	256	212
Downward	13-part	258	254	234
	10-part(a)	305	312	

(a) The 10-part model accounted for both hub support and rim support at the inside and outside edges, respectively, of the diaphragm.

TABLE I-8. COMPARISON OF THEORETICAL AND EXPERIMENTAL MERIDIONAL STRAINS ON UPPER SURFACE AT LOCATION 8

Loading	Mathematical Model	Theoretical Strain (JD181), ϵ_φ, microin./in. Membrane	Bending	Total	Total Experimental Strain, (JD190), ϵ_φ, microin/in. Measured	Corrected[a]
δ = 0.015 in.	13	78	313	391	602	390
δ = -0.020 in.	10[b]	-122	-448	-570	-670	-497
δ = -0.020 in.	13	-120	-333	-453		-509
p = 2.45 psi	11[c]	- 95	-263	-358	-475	-360
p = 2.45 psi	13	-106	-142	-248		-386

(a) The bending part of the measured experimental strains was corrected for the effect of gage and cement thickness according to Equation (I-5) in the text. The measured strains are the average values for 3 experiments.

(b) The 10-part model accounted for both hub support and rim support for downward-deflection loading.

(c) The 11-part model accounted for hub support at the inside edge for upward-pressure loading.

TABLE I-9. COMPARISON OF THEORETICAL AND EXPERIMENTAL CIRCUMFERENTIAL STRAINS ON UPPER SURFACE AT LOCATION 7

Loading	Mathematical Model	Theoretical Strain, (JD181), ϵ_θ, microin./in. Membrane	Bending	Total	Total Experimental Strain, (JD190), ϵ_θ, microin./in. Measured	Corrected[a]
δ = 0.015 in.	13	230	40	270	288	274
δ = -0.020 in.	10[b]	-363	-64	-427	-410	-390
δ = -0.020 in.	13	- 33	-59	-392		-390
p = 2.45 psi	11[c]	-178	-32	-210	-207	-197
p = 2.45 psi	13	-162	-30	-192		-197

(a) The bending part of the measured experimental strains was corrected for the effect of gage and cement thickness according to Equation (I-5) in the text. The measured strains are the average values for 3 experiments.

(b) The 10-part model accounted for both hub support and rim support for downward-deflection loading.

(c) The 11-part model accounted for hub support at the inside edge for upward-pressure loading.

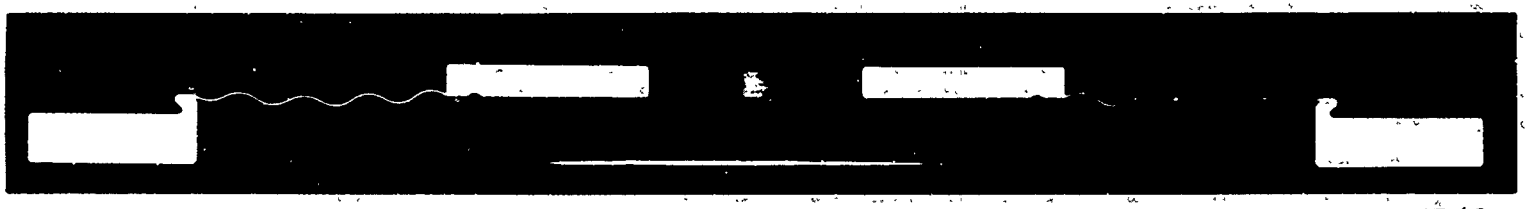

1X 5B685

FIGURE I-1. CROSS SECTION OF 4-INCH CONVOLUTED STAINLESS STEEL DIAPHRAGM (JD181)

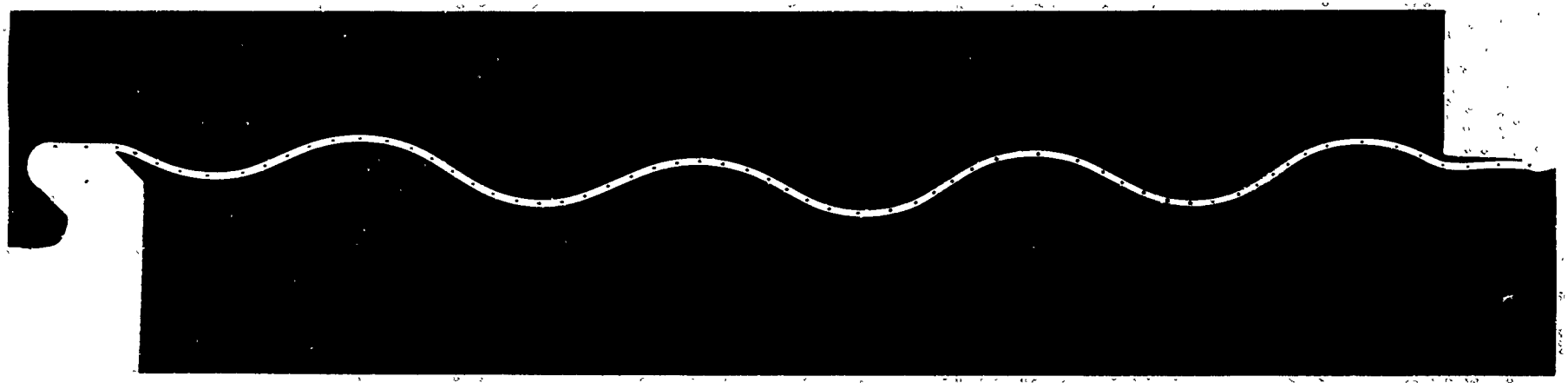

10X 8B248

FIGURE I-2. ENLARGED VIEW OF THE CONVOLUTIONS OF 4-INCH CONVOLUTED DIAPHRAGM (JD181)

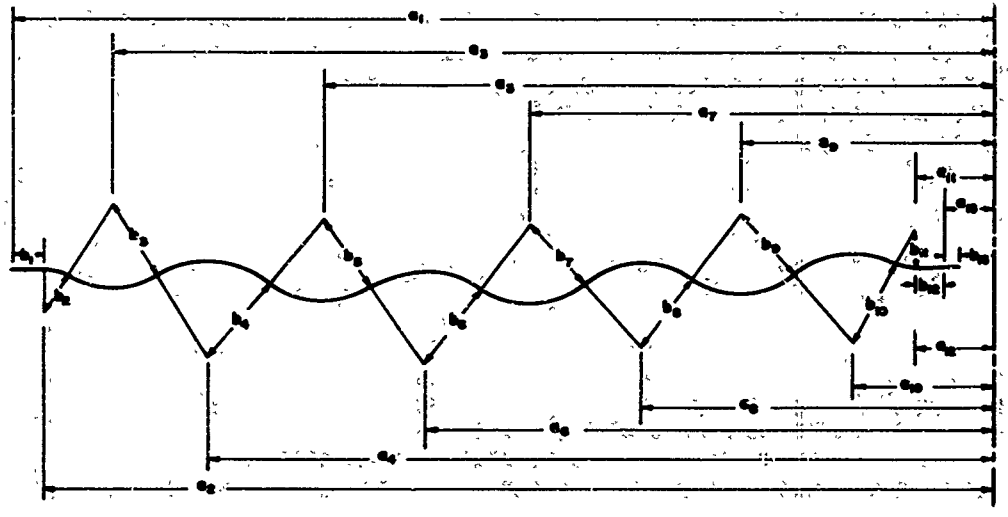

FIGURE I-3. 13-PART MATHEMATICAL MODEL OF 4-INCH DIAPHRAGM (JD181)

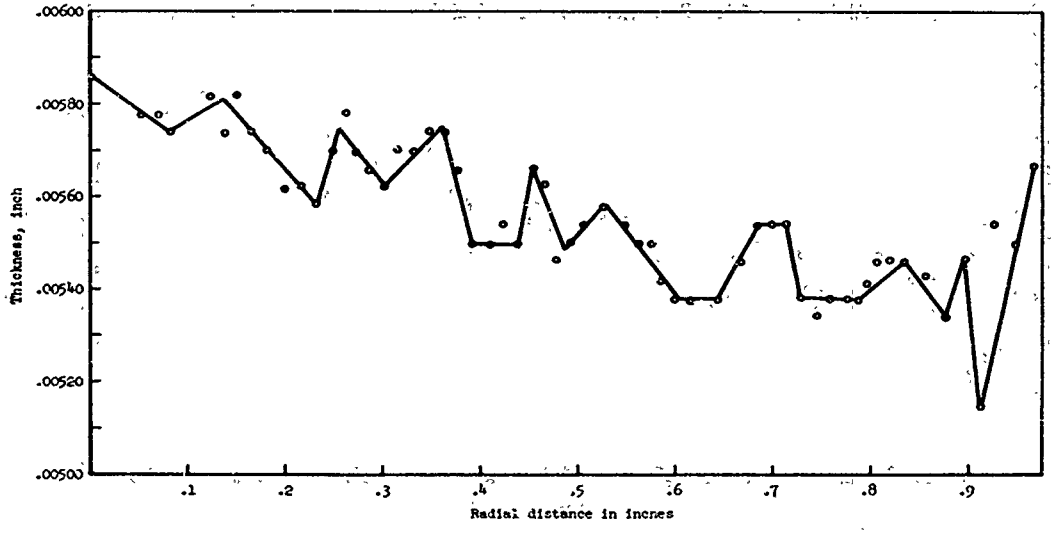

FIGURE I-4. THICKNESS VARIATION FOR 4-INCH CONVOLUTED DIAPHRAGM (JD181)

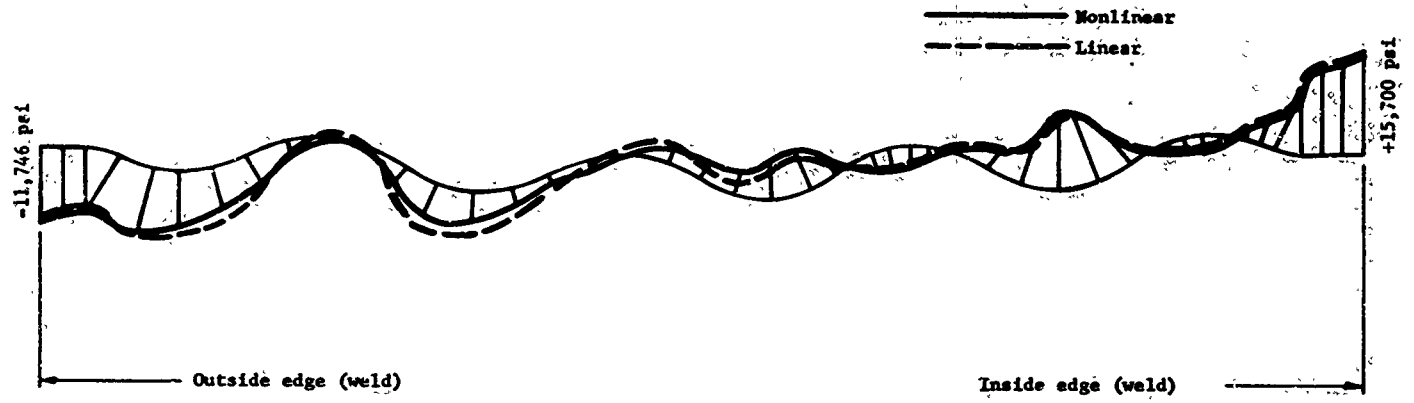

FIGURE I-5. UPPER-SURFACE MERIDIONAL STRESSES ON 4-INCH DIAPHRAGM (JD181) DUE TO UPWARD DEFLECTION OF 0.0150 INCH

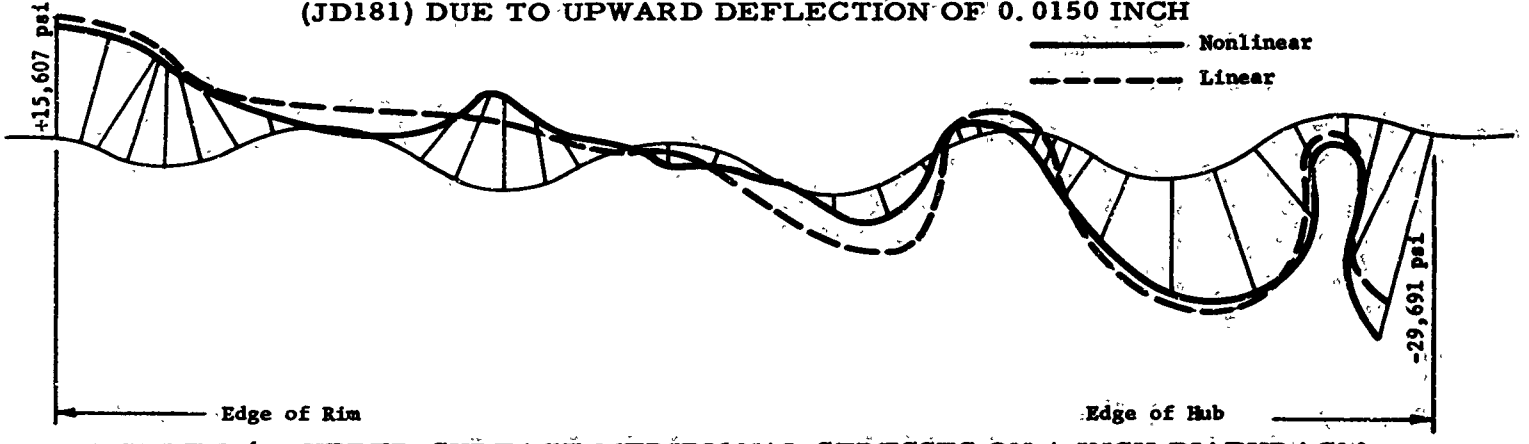

FIGURE I-6. UPPER-SURFACE MERIDIONAL STRESSES ON 4-INCH DIAPHRAGM (JD181) DUE TO DOWNWARD DEFLECTION OF 0.020 INCH – EFFECT OF HUB AND RIM SUPPORT

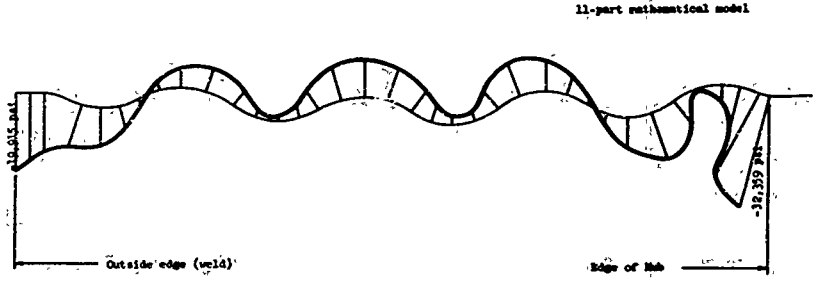

FIGURE I-7. UPPER-SURFACE MERIDIONAL STRESSES ON 4-INCH DIAPHRAGM (JD181) DUE TO UPWARD PRESSURE OF 2.45 PSI

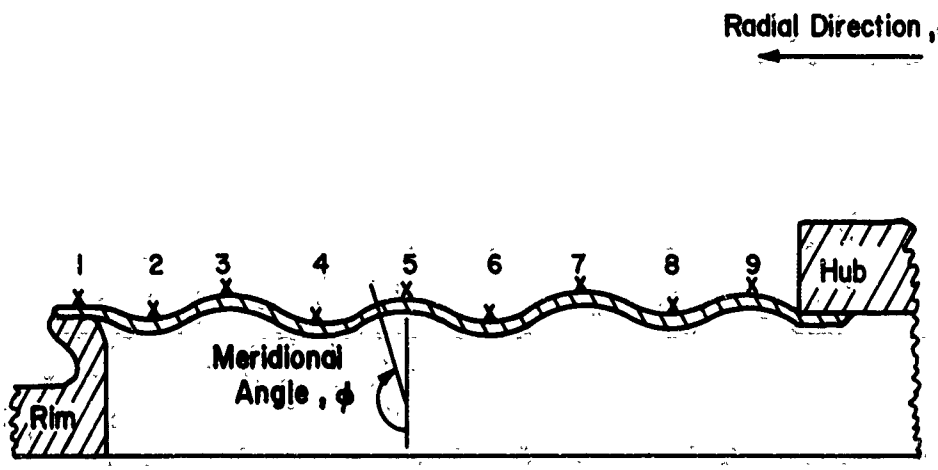

(a) Locations along $\theta = 0°$ meridion

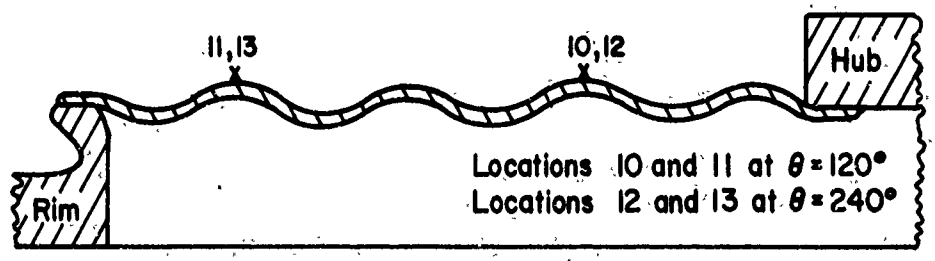

(b) Locations along $\theta = 120°$ and $\theta = 240°$ meridions

FIGURE I-8. STRAIN-GAGE LOCATIONS ON DIAPHRAGM JD190

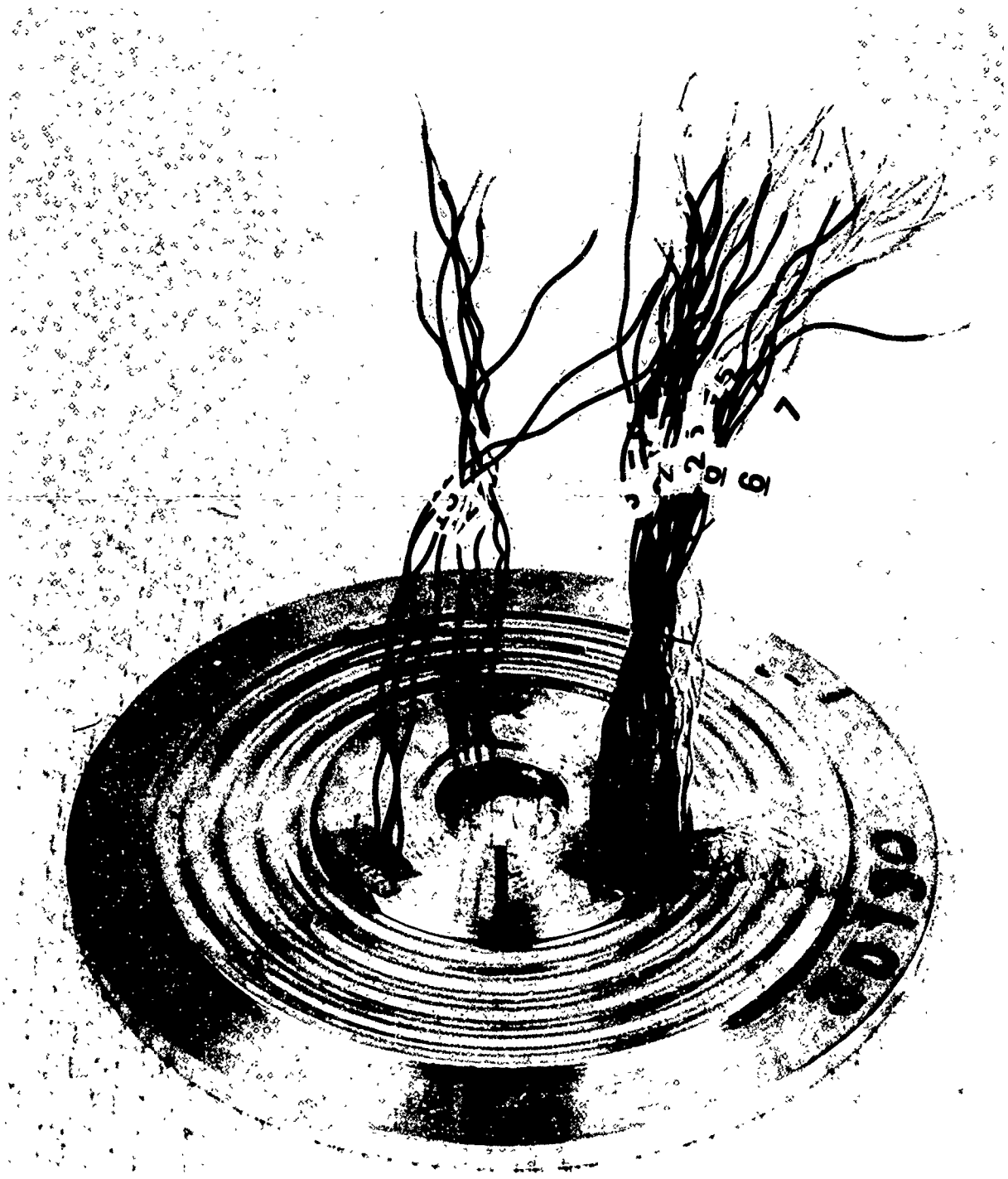

FIGURE I-9. STRAIN-GAGE INSTRUMENTATION OF DIAPHRAGM JD190

1C063

FIGURE I-10. CLOSE-UP VIEW OF THE 18 STRAIN GAGES INSTALLED ALONG ONE RADIAL LINE (θ=0°) OF DIAPHRAGM JD190

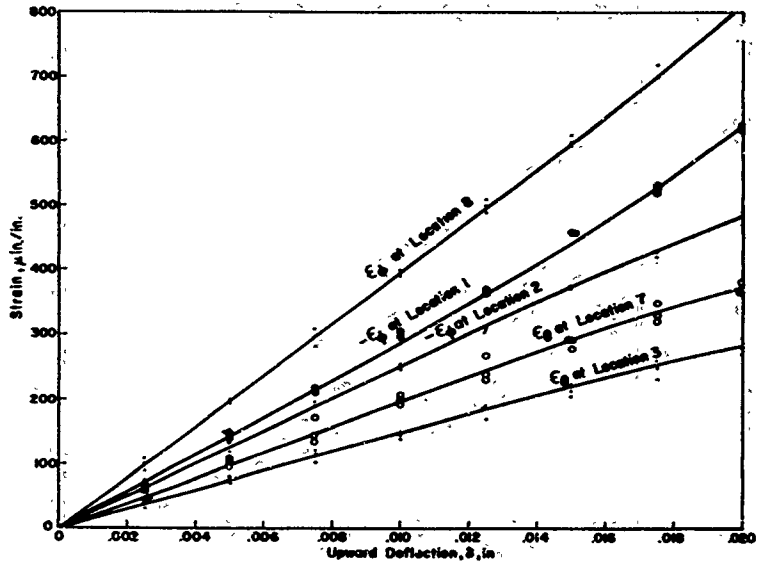

FIGURE I-11. EXPERIMENTAL STRAINS MEASURED ON DIAPHRAGM JD190 FOR UPWARD DEFLECTION

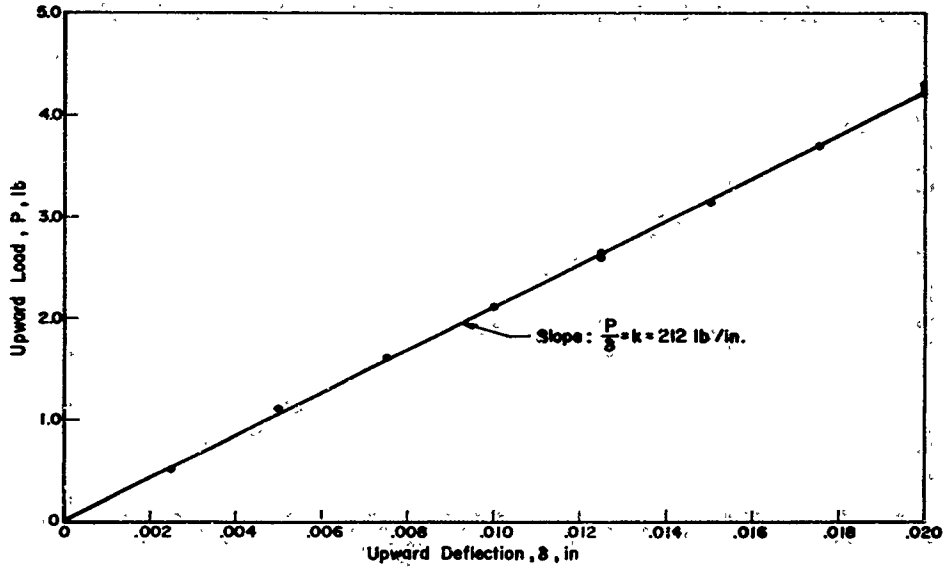

FIGURE I-12. EXPERIMENTAL LOAD-DEFLECTION CURVE FOR DIAPHRAGM JD190 FOR UPWARD DEFLECTIONS

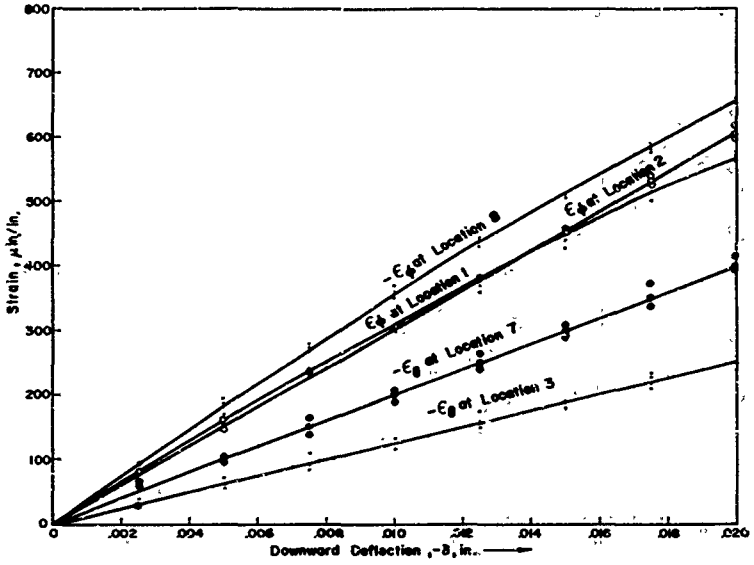

FIGURE I-13. EXPERIMENTAL STRAINS MEASURED ON DIAPHRAGM JD190 FOR DOWNWARD DEFLECTION

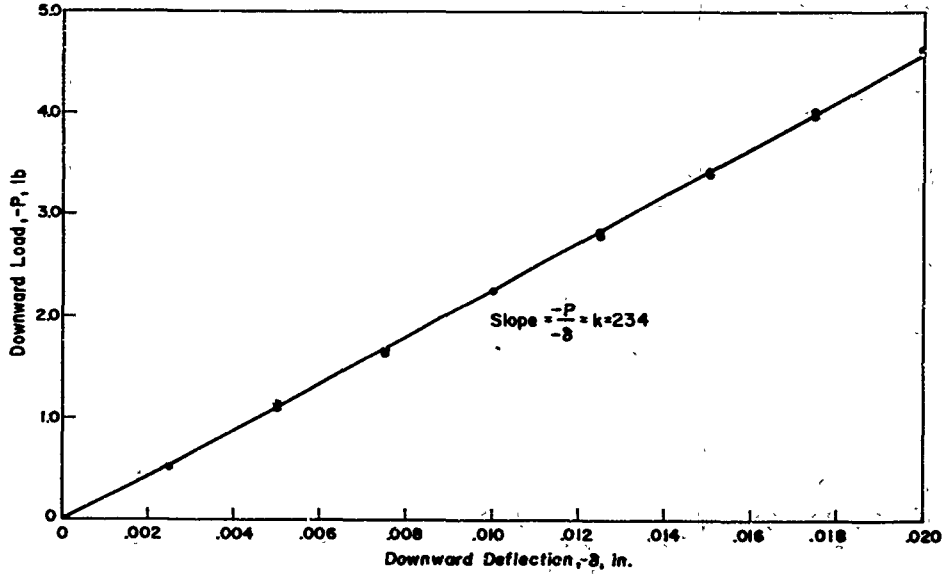

FIGURE I-14. EXPERIMENTAL LOAD-DEFLECTION CURVE FOR DIAPHRAGM JD190 FOR DOWNWARD DEFLECTIONS

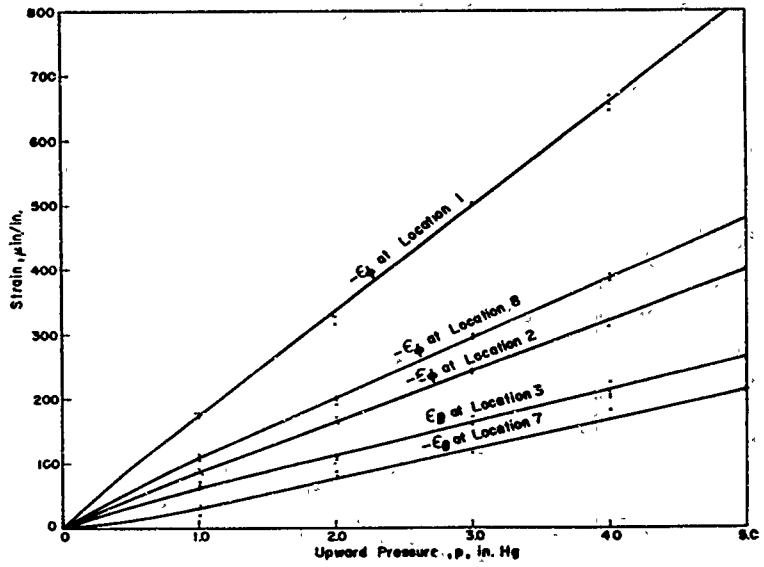

FIGURE I-15. EXPERIMENTAL STRAINS MEASURED ON DIAPHRAGM JD190 FOR UPWARD PRESSURE

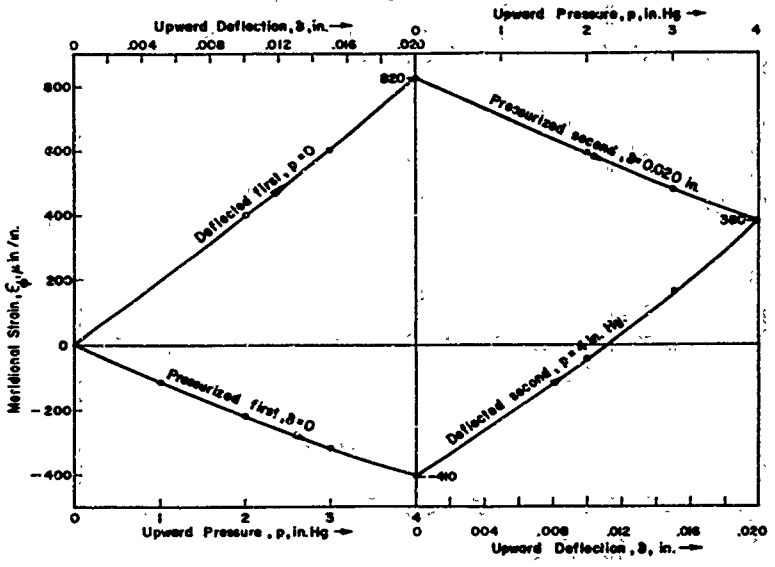

FIGURE I-16. EXPERIMENTAL STRAIN MEASURED AT LOCATION 8 ON DIAPHRAGM JD190 FOR COMBINED UPWARD PRESSURE AND UPWARD DEFLECTION LOADINGS

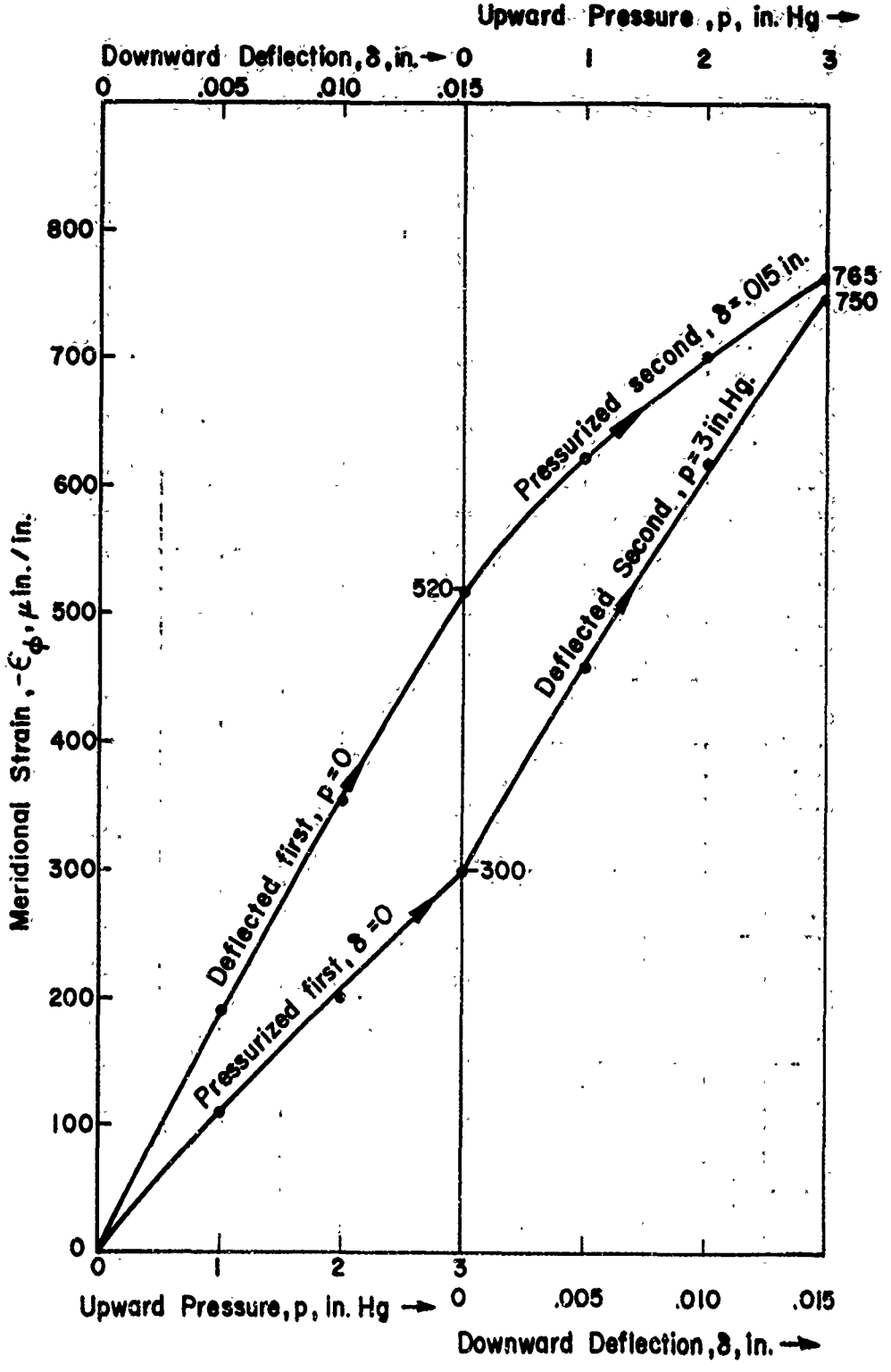

FIGURE I-17. EXPERIMENTAL STRAIN MEASURED AT LOCATION 8 ON DIAPHRAGM JD190 FOR COMBINED UPWARD PRESSURE AND DOWNWARD DEFLECTION

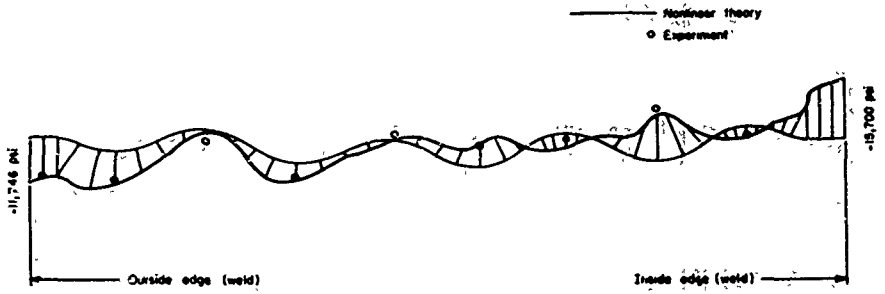

FIGURE I-18. COMPARISON OF THEORETICAL AND EXPERIMENTAL UPPER-SURFACE MERIDIONAL STRESSES DUE TO UPWARD DEFLECTION OF 0.0150 INCH

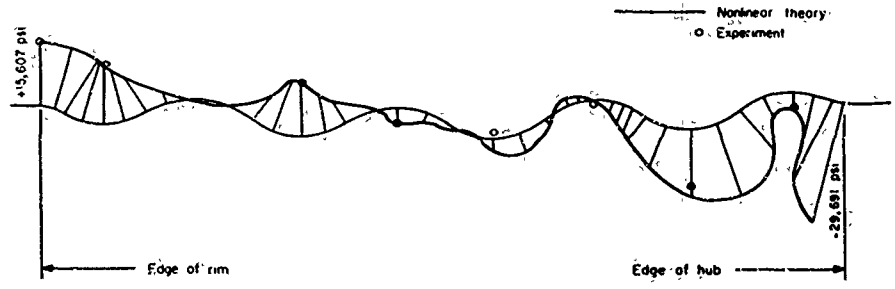

FIGURE I-19. COMPARISON OF THERORECTICAL AND EXPERIMENTAL UPPER-SURFACE MERIDIONAL STRESSES DUE TO DOWNWARD DEFLECTION OF 0.020 INCH

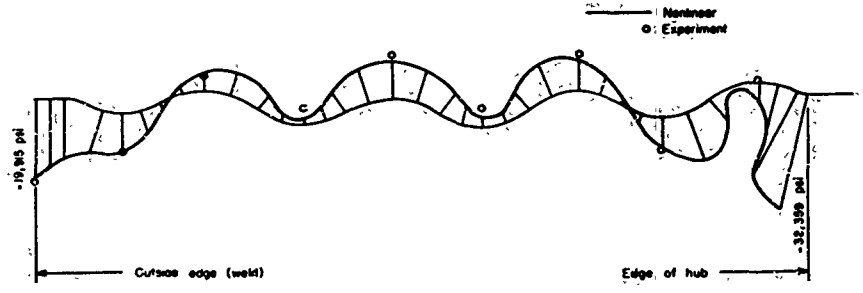

FIGURE I-20. COMPARISON OF THEORETICAL AND EXPERIMENTAL UPPER-SURFACE MERIDIONAL STRESSES DUE TO UPWARD PRESSURE OF 2.45 PSI

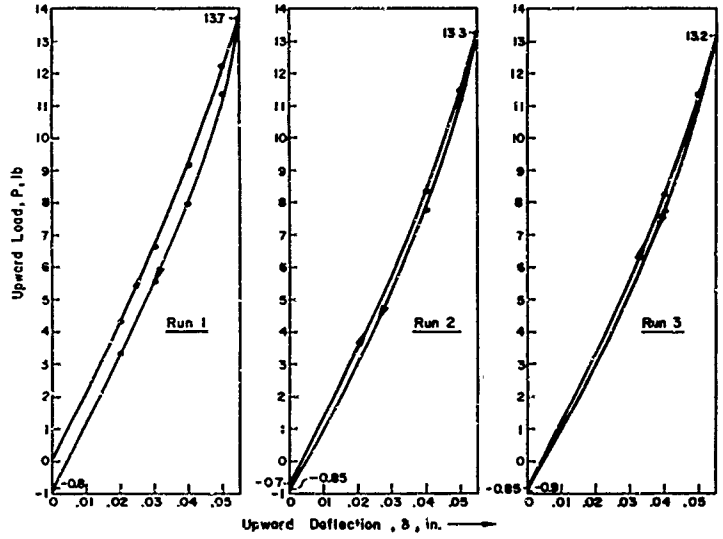

FIGURE I-21. EXPERIMENTAL OVERLOAD UPWARD-DEFLECTION RUNS ON DIAPHRAGM JD190, δ_{max} = 0.055 in.

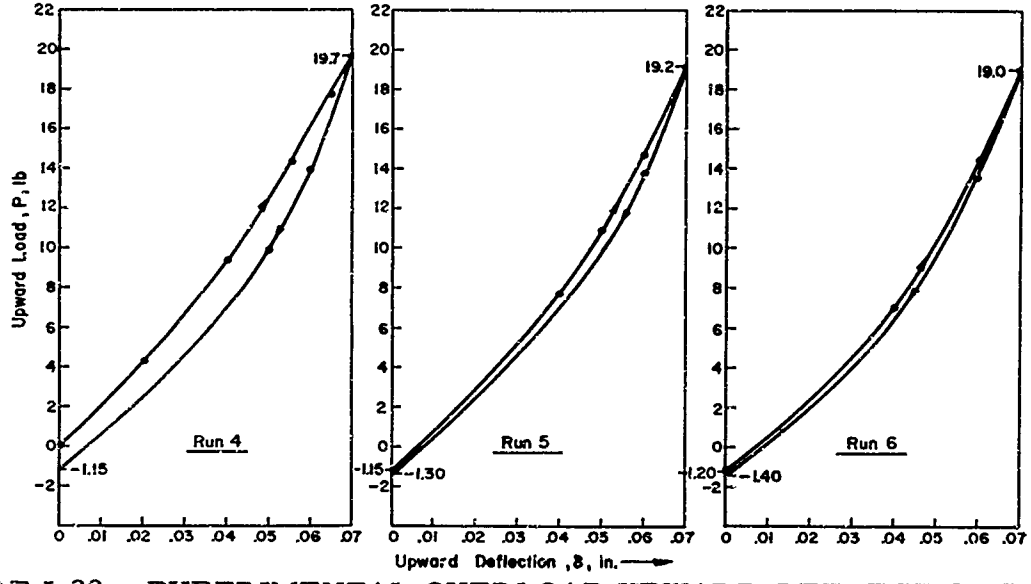

FIGURE I-22. EXPERIMENTAL OVERLOAD UPWARD-DEFLECTION RUNS ON DIAPHRAGM JD190, δ_{max} = 0.70 in.

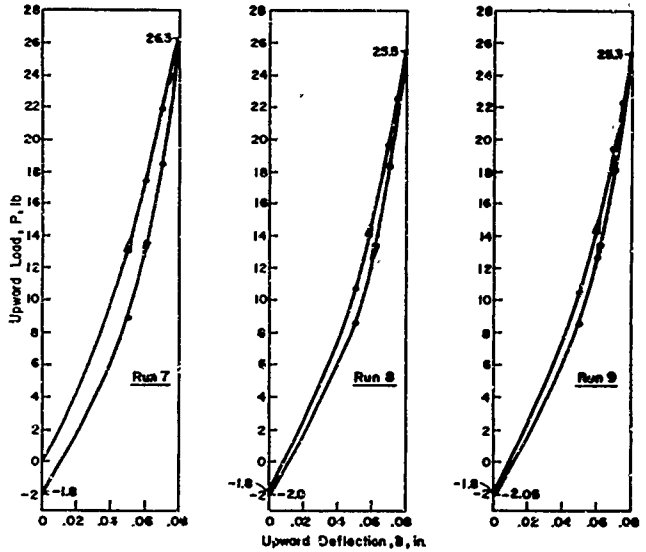

FIGURE I-23. EXPERIMENTAL OVERLOAD UPWARD DEFLECTION RUNS ON DIAPHRAGM JD190, δ_{max} = 0.080 in.

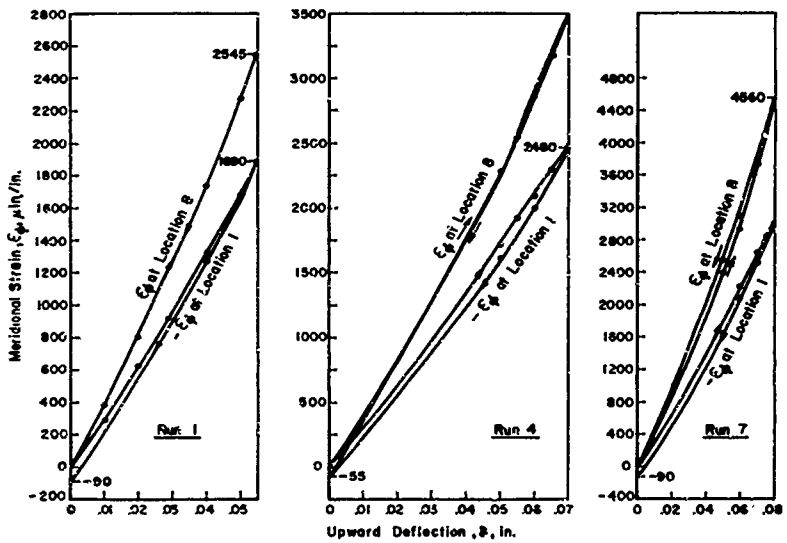

FIGURE I-24. EXPERIMENTAL STRAINS MEASURED ON DIAPHRAGM JD190 DURING OVERLOAD UPWARD-DEFLECTION RUNS

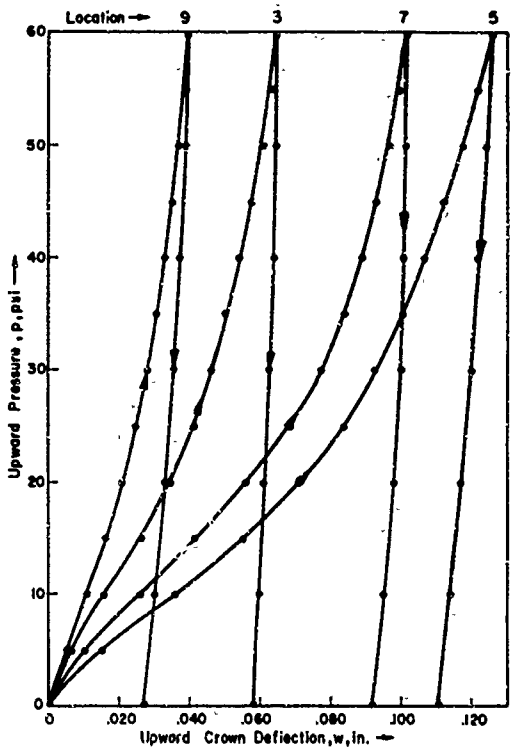

FIGURE I-25. DEFLECTIONS MEASURED ON DIAPHRAGM JD188 DURING OVERPRESSURE EXPERIMENT

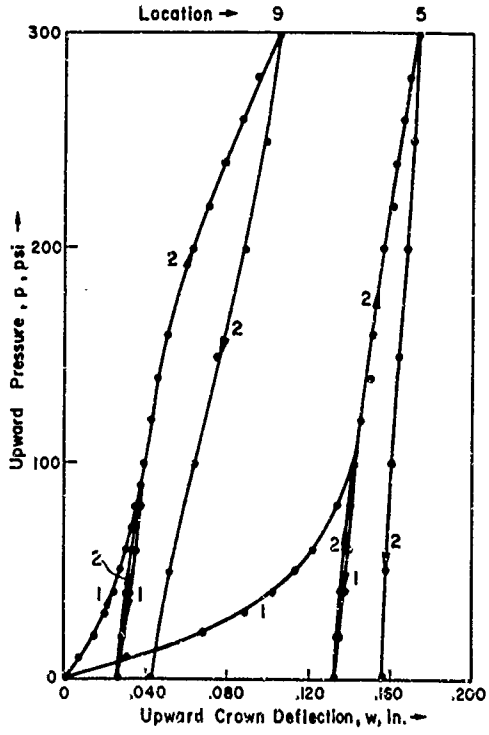

FIGURE I-26. DEFLECTIONS MEASURED ON DIAPHRAGM JD189 DURING OVERPRESSURE EXPERIMENT

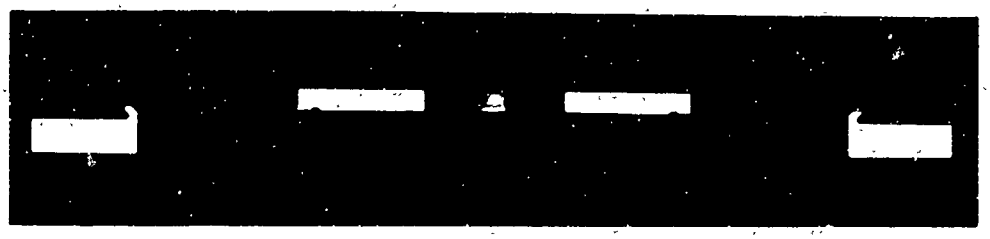

1X 2C492

(a) Diaphragm JD188 After Over-Pressure to 60 psi

1X 2C493

(b) Diaphragm JD189 After Over-Pressure to 300 psi

FIGURE I-27. DISTORTED SHAPES OF DIAPHRAGMS JD188 AND JD189 AFTER OVER-PRESSURE EXPERIMENTS

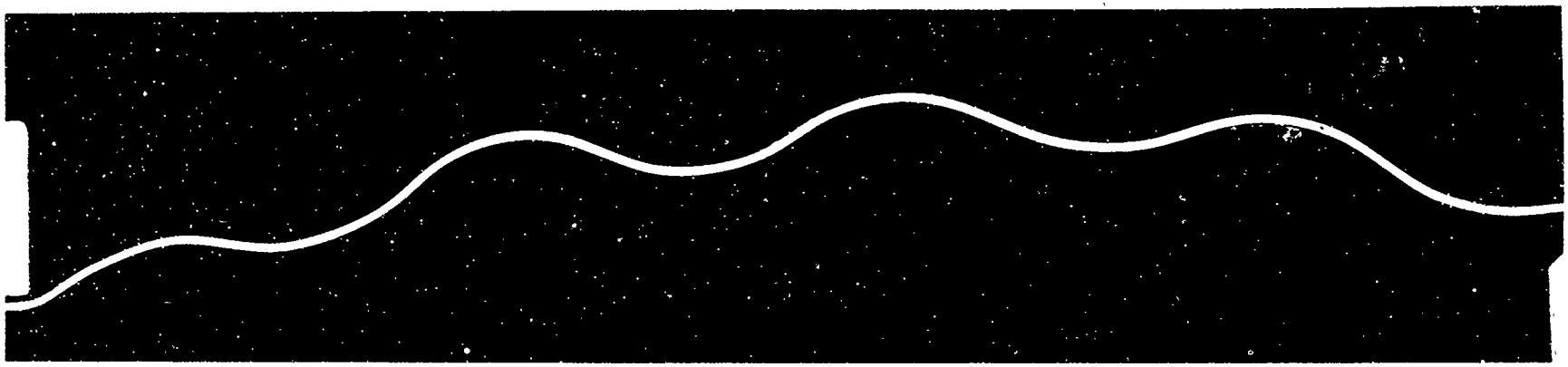

10X 2C494

(a) Diaphragm JD188 After Over-Pressure to 60 psi

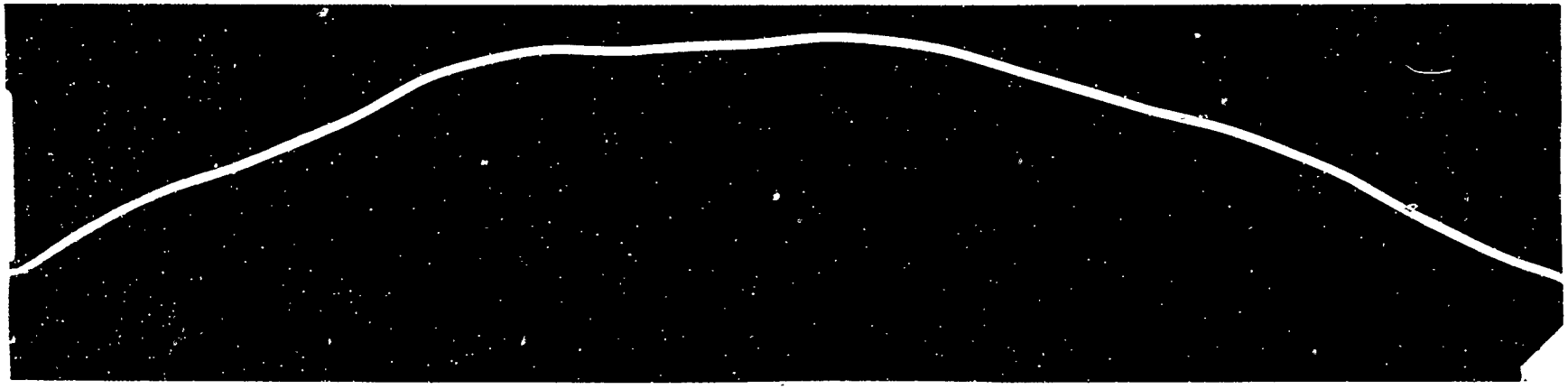

10X 2C495

(b) Diaphragm JD189 After Overpressure to 300 psi

FIGURE I-28. DISTORTED SHAPES OF DIAPHRAGMS JD188 AND JD189 AFTER OVERPRESSURE EXPERIMENTS

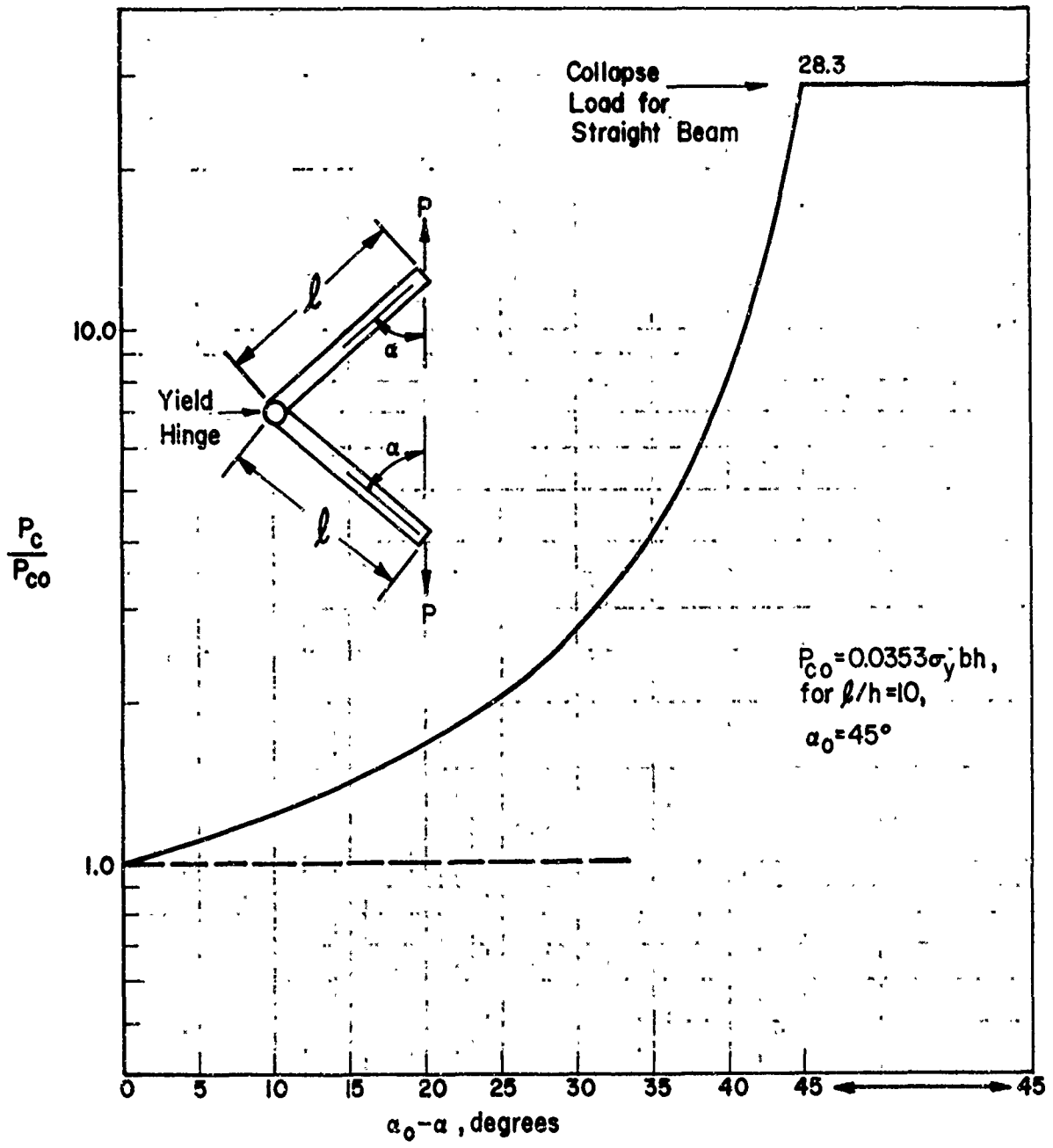

FIGURE I-29. INCREASE OF PLASTIC COLLAPSE LOAD P_c WITH DEFORMATION FOR A HINGED BEAM MODEL

APPENDIX J

ELASTIC BUCKLING AND PLASTIC COLLAPSE OF BELLOWS

ABBREVIATIONS AND SYMBOLS

D	Lateral bending stiffness of bellows, lb-in.^{2}
I	Moment of inertia of bellows area, in.^{4}
E	Modulus of elasticity, psi
θ	Angle of rotation of free end of cantilevered bellows loaded laterally, deg
W	Weight applied to free end of cantilevered bellows in bending test, in-lb/in.
L_c	Total live length of bellows, in.
L	Total length of bellows assembly, in.
M	Lateral bending moment applied to bellows, in-lb
S	Slope of load rotation curves in bending tests ($S = W/\theta$)
ϕ	Angle between normal to bellows surface and its axis of revolution, deg
Q	Effective shear resultant force in direction normal to the shell, lb/in.
u_ϕ	Displacement in the meridional direction, in.
θ_ϕ	Angle of rotation of bellows normal in meridional direction, deg
u_θ	Displacement in the circumferential direction, in.
$\bar{\beta}$	Small rotation imposed on free end of mathematical model of bellows, deg
M_ϕ, M_θ	Bending moment resultants in meridional and circumferential directions, respectively, in-lb/in.
Q_ϕ, Q_θ	Effective shear resultant forces in direction normal to shell and measured along midsurface arcs normal to the meridional and circumferential directions, respectively, lb/in.
N_ϕ, N_θ	Membrane resultant forces in meridional and circumferential directions, lb/in.
$N_{\theta\phi}$	Membrane resultant shearing force, lb/in.
$M_{\theta\phi}$	Resultant twisting moment, in-lb/in.
R	Radius of a cylinder or radius to edge of bellows, in.
V	Transverse shear force applied to bellows, lb
N_1	Maximum value of N_ϕ on edge of bent bellows ($N_\phi = N_1 \cos \theta$), lb/in.
M_1	Maximum value of M_ϕ on edge of bent bellows ($M_\phi = M_1 \cos \theta$), in-lb/in.
N	Effective shear resultant force in the circumferential direction, lb/in.
N_2	Maximum value of circumferential shear resultant force N due to transverse shear force on bent bellows ($N = N_2 \sin \theta$), in-lb/in.
α	Reduction factor relating Seide's Formula to bellows bending analysis
Δ	Axial compressive deflection imposed on bellows in buckling experiments, in.
Δ_{cr}	Critical deflection at which bellows buckles, in.
p	Internal pressure in bellows, psi
P_{cr}	Critical Euler load (compressive) for column buckling of beam, lb
p_{cr}	Critical internal pressure for bellows buckling, psi
A	Mean cross-sectional area of bellows, in.^{2}
k	Axial spring rate of bellows, lb/in.
$k_p p_{cr}$	Compressive load buildup at end of clamped bellows resulting from internal pressure acting on convolutions, lb
(a), (e), (s)	Measures of the deviation of actual bellows from a perfectly straight ideal bellows: (a) is the central deviation, (e) is the eccentricity, and (s) is the slant offset, in.
δ_e	Allowable sidewise deflection of bellows in buckling experiment, in.
δ_s	Sidewise deflection of axially compressed bellows due to eccentricity (e), in.
δ_c	Uniform radial expansion of bellows crown due to axial compression Δ, in.
δ_p	Uniform expansion of bellows crown due to internal pressure, in.
σ_ϕ	Meridional surface stress, psi
σ_o	Material yield stress in tension, psi
h	Shell thickness, in.

APPENDIX J

ELASTIC BUCKLING AND PLASTIC COLLAPSE OF BELLOWS

Theoretical and experimental studies of both elastic buckling and plastic collapse of bellows were included in the research program. The results of these studies are described in this appendix.

A potential failure mode of most bellows is sidewise beam-column buckling (squirm) at relatively low internal pressures and small axial deflections. This overall lateral buckling of the bellows is to be distinguished from higher order modes of shell buckling which involve local buckling of the wall of the convolutions. The former is easily analyzed using beam-bending theory of shells. The latter is very complicated and necessitates the use of shell theory not fully developed as yet for shells of such variable geometry as a bellows. Although the use of shell theory for the higher modes of buckling was beyond the scope of the present program, local shell buckling appears to be less critical than the beam buckling of bellows.

Analysis of Beam-Column Buckling of Bellows

This type of analysis is concerned with the elastic instability of the bellows as a beam column. The buckling strength of a beam column is proportional to its lateral bending stiffness, D. For conventional beams, $D = EI$ lb-in.^{2} where E = modulus of elasticity, psi, and I = moment of inertia of area, in.^{4}. Generally, the stiffness is sufficiently large that short columns do not buckle. However, bellows are quite flexible and short bellows can buckle. Furthermore, D is not easily determined for bellows. Accordingly, experimental and theoretical analyses were conducted with the test specimens in order to find typical values for D for bellows. These analyses, and experimental and theoretical analyses of buckling of the test specimens are described.

Experimental Determination of Lateral Bending Stiffness D

The experimental method for determining the lateral bending stiffness of bellows is shown in Figure J-1. The bellows was oriented horizontally, clamped at its base, and loaded at the other end with weights, as shown. The change in angle θ was measured for each change in weight, W. Loadings were kept sufficiently small that no significant permanent deformation due to plastic strain occurred.

Experiments were conducted on specimens of the 5-, 3-, and 1-inch single-ply stainless steel formed bellows, on specimens of the 3- and 1-inch single-ply Inconel formed bellows, on specimens of the 3-inch double-ply stainless steel formed bellows, on one specimen each of the 3-1/2- and 1-1/2-inch stainless steel welded bellows, and on one specimen each of the 3- and 1-1/2-inch AM350 welded bellows (see Appendix P for descriptions of the test bellows). The formed bellows had a longitudinal welded seam. The effect of orientation of the specimens with respect to the seam was investigated by rotating the 5-inch bellows JD90 between experiments. The results are shown in Figure J-2, where little effect of seam orientation was found. Additional

results on other specimens confirmed this, although an occasional specimen exhibited some seam effect. Thereafter, the effect of seam orientation was neglected and tests were performed with the specimen oriented with the seam to the right, i.e., with the seam in the horizontal plane containing the neutral axis.

As shown in Figure J-1, the bellows was mounted as a cantilever beam with a load W and a moment M = WL at the free end. It was assumed that bending occurred only over the total convolution length L_c, i.e., the cylindrical parts of the specimens were assumed to be relatively rigid. From beam formulas, then, the bending stiffness D was calculated as follows:

$$D = \frac{ML_c}{\theta} + \frac{WL_c^2}{2\theta} = \frac{WL_c}{\theta}\left(L + \frac{L_c}{2}\right) = 57.296\ SL_c\left(L + \frac{L_c}{2}\right) \qquad (J\text{-}1)$$

where S is the slope, lb/deg of the experimental curves as shown in Figure J-2, and the factor 57.296 accounts for the change from degrees to radians.

The measurements of S, L_c, and D for the formed bellows are shown in Tables J-1 to J-6. The average bending stiffness, D = 15.4 lb-in.^{2}, for the 1-inch Inconel bellows (Table J-4) was higher than it was for the 1-inch stainless steel bellows, D = 12.2 lb-in.^{2} (Table J-3). But for the 3-inch single-ply bellows the reverse was true. The average bending stiffness, D = 413.4 lb-in.^{2} for the 3-inch Inconel bellows (Table J-5) was lower than the value D = 586.3 lb-in.^{2}, for the 3-inch stainless steel bellows (Table J-2). These results are attributed to the different number of convolutions per unit length, to different thicknesses, and to other differences in geometry. For example, the convolutions and thicknesses were as follows:

Single-Ply Bellows	Number of Convolutions	Nominal Thickness, inch
1-inch Inconel	16	0.004
1-inch stainless steel	8	0.005
3-inch Inconel	14	0.006
3-inch stainless steel	10	0.008

It was also found that the bending stiffness D of the two-ply bellows was approximately twice that of the single-ply bellows. This is indicated in Table J-6. These data, average D = 1007 lb-in.^{2}, are about twice the average, D = 586 lb-in.^{2}, found previously for the 3-inch single-ply stainless steel bellows (Table J-2). Thus, D, as well as the spring constant k, can be estimated for double-ply bellows by taking twice the respective values of single-ply bellows.

Theoretical Determination of Lateral Bending Stiffness D

The lateral bending stiffnesses of the test bellows were also determined theoretically using the shell computer codes MOLSA and NONLIN (see Appendixes A, B, and C). MOLSA was used initially, but when NONLIN was extended to include nonsymmetric loadings it was used for these calculations.

In order to find D theoretically, the length L of the mathematical model of the bellows was given a (small) pure rotation $\bar{\beta}$, as shown in Figure J-3. Analogous to beam theory, it was assumed that plane sections remained plane, and that there was no extension of the axial centerline of the bellows. Also, it was assumed that the transverse shear force Q = 0 at the boundaries. This is analogous to the resultant transverse shear stress over the cross section going to zero at the top and bottom of a beam. Thus, relative to Figure J-3, the following boundary conditions were derived for a (small) pure rotation of a bellows (or other axisymmetric shell):

$$\text{at} \quad \phi = 0, \; Q = 0, \; u_\phi = 0, \; \beta_\phi = 0, \; u_\theta = 0, \tag{J-2}$$

$$\text{at} \quad \phi = \bar{\beta}, \; Q = 0, \; u_\phi \simeq \bar{u} \cos\theta, \; \beta_\phi = \bar{\beta} \cos\theta, \; u_\theta = \bar{y} \sin\theta, \tag{J-2}$$

where

$$\bar{y} = \frac{L}{\bar{\beta}} (1 - \cos\bar{\beta}), \; \bar{u} = R \sin\bar{\beta} \quad . \tag{J-3}$$

In the calculations, the value of the rotation was taken as $\bar{\beta} = 0.01$ radian.

The computer input data for program NONLIN corresponding to these boundary conditions are shown in Table J-7 for bellows JD68, as an example. Input data for this bellows have been described in Appendix B. The same data can be used here except for the boundary data. For this nonsymmetric problem, boundary data in Table J-7 for Cards 2 and 3 in Columns 61-80 for the displacement u_θ are needed in addition to the data previously described in Appendix B for symmetric problems. (A symmetric problem requires three boundary conditions at each edge, but the nonsymmetric beam-bending problem requires four boundary conditions.) Also Data Card 5 is changed to have a 1 in Column 64 to signify Fourier harmonic mode No. 1 for a beam-bending type solution.

This method of computer calculation of beam-bending stiffness of a shell was first checked out for the cylindrical shell for which closed-form analytical solutions are known[1, 2, 3]*. For small rotations of a cylinder, the membrane solution is applicable. This is:

$$M_\phi = M_\theta = Q_\phi = Q_\theta = N_\theta = M_{\theta\phi} = N_{\theta\phi} = 0, \; N_\phi = N_1 \cos\theta, \tag{J-4}$$

and corresponds to a lateral beam-bending moment

$$M = 4 \int_0^{\pi/2} R \cos\theta \, N_\phi \cdot r d\theta = \pi R^2 N_1 \tag{J-5}$$

where R = radius of cylinder. Application of the boundary conditions (J-2), enables determination of the relation between M and the rotation $\bar{\beta}$. Defining the stiffness D by the curvature relation,

$$D = M \cdot \frac{L}{\bar{\beta}} \quad , \tag{J-6}$$

*References for Appendix J are listed on page J-16

the membrane solution for a cylinder gives

$$N_1 = ERh \cdot \bar{\beta}/L,$$

and consequently,

$$D = E\pi R^3 h \quad , \tag{J-7}$$

where h = thickness of shell and E = Young's modulus.

The same result (J-7) for cylindrical shells was also found from the computer calculation using boundary conditions (J-2). Therefore, these boundary conditions were taken to be appropriate for the computer calculation of the beam bending stiffnesses of the bellows as well. However, it was found that the bending of a bellows is not as simple as that of a cylinder. Nonzero values of M_ϕ, M_θ, N_θ, $M_{\theta\phi}$, and $N_{\theta\phi}$ result as contrasted to the zero values of the cylinder equations (J-4). Therefore, for a bellows the equation for the beam-bending moment M is different from Equation (J-5) and includes contribution of the shell-wall moment M_ϕ. For the bellows:

$$M = 4\int_0^{\pi/2} [\cos\theta\, M_\phi + R\cos\theta\, N_\phi]\, Rd\theta \quad ,$$

$$M = \pi R\,(M_1 + RN_1) \tag{J-8}$$

where $M_\phi = M_1 \cos\theta$ and where now R is the radius to a root or crown of a convolution depending on which occurs at a boundary. In addition, in a bellows it is found that a transverse shear force V, lb., does occur even though Q = 0 [boundary conditions (J-2)]. V results from nonzero $N_{\theta\phi}$ and $M_{\theta\phi}$; i.e., from N where

$$N = N_{\theta\phi} + \frac{\sin\phi}{r} M_{\theta\phi} = N_2 \sin\theta \quad , \tag{J-9}$$

and

$$V = 4\int_0^{\pi/2} (N \sin\theta) \cdot Rd\theta = \pi N_2 R \quad . \tag{J-10}$$

Thus, the rotation $\bar{\beta}$ of a bellows is caused partly by a shear force V in addition to the moment M as shown in Figure J-4. Therefore, in this case (analogous to bending of a beam),

$$D = M\frac{L}{\bar{\beta}} + V\frac{L^2}{2\bar{\beta}} \quad . \tag{J-11}$$

[Note correspondence with Equation (J-1) used for the experiments on bellows.]

The following example calculation is now given for 3-inch bellows JD68 to illustrate the method of theoretical determination of D. Boundary data have been given in Table J-7. The following results were found from a computer calculation:

$$N_1 = 5.61732, \quad M_1 = -0.492724, \quad N_2 = -26.7542. \tag{J-12}$$

From Equation (J-8)

$$M = \pi\,(1.8208)\,[-0.492724 + 1.8208\,(5.61732)] = 55.67887,$$

and from Equation (J-10)

$$V = \pi\,(-26.7542)\,1.8208 = -153.039564.$$

Substitution of these values of M and V into (J-11) gives:

$$D = 55.687886\,\frac{(0.10)}{0.01} - 153.039564\,\frac{(0.01)}{2(0.01)} = 480.35908 \qquad \text{(J-13)}$$

where $L = 0.100$ and $\bar{\beta} = 0.01$. This value of D is listed in Table J-2 along with the experimental data. Although the theoretical value for JD68, $D = 480.4$, is relatively low compared to the experimental average, $D = 586.3$, it is close to the experimental value for JD63 ($D = 470.5$). This is an indication of fairly good accuracy of the computer calculations for the bending stiffness D.

Computer values for D for the other formed stainless steel bellows are also listed in Tables J-1, J-3, J-6, and J-9. These values also agree fairly well with the experimental data.

Computer calculations were made for the bending stiffnesses of the following welded bellows: 3-1/2-inch stainless steel bellows JN136, 1-1/2-inch stainless steel bellows JN150, 3-inch AM350 bellows JN158, and 1-1/2 inch AM350 bellows JN171. The computer results are shown in Table J-8, together with experimentally determined values.

Relation Between Bending Stiffness D and Axial Spring Constant k

The experimental results were compared with the prediction of the Seide formula[4]. This formula relates the bending stiffness D to the axial spring constant k as follows:

$$D = \alpha k \bar{R}^2 L_c \qquad \text{(J-14)}$$

where $\bar{R}$ is the average bellows radius, $\frac{R_o + R_i}{2}$, and the factor $\alpha = 0.500$. This formula can be shown to be exact for a cylindrical shell if the rotation θ is sufficiently small, i.e., when linear membrane theory is accurate, but its application was questionable for complicated shells such as bellows.

Tables J-9 through J-14 show the results for the factor $\alpha = \frac{D}{k\bar{R}^2 L_c}$ for the formed bellows for which k and D have both been determined experimentally. Instead of the factor $\alpha = 0.500$ as predicted in Reference (4), the range of α found experimentally on all the sizes of formed bellows tested was $0.365 \leq \alpha \leq 0.643$. It was concluded that the factor α is not directly proportional to the mean diameter of the bellows, but must be a more complicated function of the geometry of the convolutions.

Although α varies appreciably, it can be found quite accurately from a computer calculation for an individual bellows, as indicated in Tables J-9, J-10, and J-11. For example, in Table J-11, the experimental range of α for nine 1-inch bellows was 0.365 to 0.483. The theoretical value for one bellows was 0.480.

The factor α was also determined by computer calculation for the four welded bellows of Table J-8. The values of α given in Table J-15 range from 0.457 to 0.699. The value $\alpha = 0.699$ was the highest found on any bellows formed or welded. Table J-15 also gives experimentally determined values for α for one specimen of each type of welded bellows. The reason for the poor correlation for the small bellows was not determined.

Experimental Beam-Column Buckling

Experiments were conducted on the bellows to determine their susceptibility to beam-column buckling under combinations of internal pressure and axial compression. The fatigue machine (see Appendix Q) was used for these experiments. In this machine the bellows were clamped at both ends. For the buckling experiments the machine was not cycled; only static axial displacements were imposed.

In order to detect the sidewise beam-column-type deflection, the equipment illustrated schematically in Figure J-5 was employed. Six contacts were positioned at 60-degree intervals around the circumference. Each of the six contacts was separately wired in series with a 1.5-volt battery and the bellows. Whenever the bellows touched a contact a bulb would light. The contacts were set at the neutral position (pressure and axial displacement both zero) with gaps, δ, of about 0.004, 0.0025, and 0.002 inch for the 5-, 3-, and 1-inch bellows, respectively. These small gaps allowed for elastic buckling; upon removal of the loads the bellows would return to its original position and tests could be repeated at one loading condition with the same response occurring in the bellows. The procedure for setting the gaps was to turn in the adjusting screws until the bulbs lighted and then to turn the screws out a fraction of a turn after the bulbs went out.

The equipment shown in Figure J-5 allowed for evaluation of the buckling strength of bellows at a standard (preset) buckling deflection, δ. The procedure was to first apply a compressive displacement Δ (inch) to the bellows. Then the internal pressure (psi) was slowly increased until either buckling was detected or the maximum allowable pressure $p_{max} = 100$ psi was reached. The maximum compression applied was $\Delta_{max} = 0.1\ L_c$ where L_c is the total convolution length. These maximums p_{max} and Δ_{max} were chosen so that the maximum combined bending strain (symmetrical without buckling) did not exceed 4000 μin./in.

Representative buckling data are presented in Tables J-16 through J-21 for the various formed bellows tested. All of these bellows had been previously fatigue tested. The 3-inch bellows JD72, Table J-17, and three of the 1-inch bellows in Table J-18 had a large fatigue crack and did not hold pressure. Therefore, buckling experiments were not conducted on these bellows. As can be seen, some of the bellows buckled and some did not. Buckling is highly sensitive to initial imperfections, as shown later in the theoretical analysis.

Specimen JD23, Table J-18, did not buckle in the usual beam-column mode, but it did buckle in a local-shell mode as shown in Figure J-6. There was no sidewise beam

deflection, but only one side of the bellows buckled and it moved inward. It is possible that higher modes of buckling occurred in some of the other bellows, but if so it was not detected.

Only two out of nine 1-inch single-ply Inconel bellows and only two out of eight 3-inch single-ply Inconel bellows buckled, as indicated in Tables J-19 and J-20. The Inconel bellows on the whole appeared to be less susceptible to buckling than the stainless steel bellows.

Double-ply bellows also buckle but they can withstand larger axial compression, up to 0.360 inch, before buckling, as is evident from the data for the 3-inch double-ply bellows in Table J-21. Three-inch single-ply bellows buckled at lower axial compressions, $\Delta \leq 0.220$ inch, as reported in Table J-17.

The welded bellows specimens were so short, as evident in Table J-15, that they were not expected to buckle as a beam. However, a limited number of experiments were conducted on three of the larger size welded bellows, the 3 and 3-1/2-inch sizes. Depth micrometer readings on the outside edge of the leaves from a fixed vertical were used as an indication of possible buckling of the welded bellows. The results are shown below.

Specimen	Nominal Size, in.	Compression (Δ), in.	Pressure (p), psi	Sidewise Deflection (δ_e), in.
JN135	3-1/2	0.150	11	0.0003
JN156	3	0.100	14	0.0006
JN165	3	0 to 0.120	0 to 40	No noticeable deflection

Some amount of deflection did occur on two of the bellows at relatively small pressures, 11 and 14 psi, but at relatively large axial compressions, $\Delta/L_c \approx 1/3$. The deflections shown above were relatively small, and the occurrence of buckling is open to question. Part of the deflection was due to axisymmetric deformation and, therefore, the data cannot be taken as proof of buckling until examined further, as done in the next section.

Because of the greater flexibility of welded bellows, buckling is expected to be much more critical for longer length welded bellows than for the formed bellows; e.g., D = 58.5 lb-in.^{2} for 3-inch AM350 welded bellows, JN158, Table J-8, but D = 586.3 lb-in. for 3-inch stainless steel formed bellows, Table J-2.

Experiments were not conducted on 1-inch double-ply bellows. These were also believed to be less susceptible to buckling, as were the 3-inch double-ply bellows. This belief was supported by beam-column theory which predicted a buckling load proportional to the beam bending stiffness D.

Theoretical Beam-Column Buckling of Bellows

A theoretical analysis of the elastic buckling of bellows was conducted. The analysis was approximate; each bellows was approximated as a beam column with initial imperfections. The buckling strength of a beam column is proportional to its lateral bending stiffness D, lb-in.^{2}, and is inversely proportional to its length squared (L^2), in.^{2}.

Efforts were concentrated on the theoretical analysis of the buckling of clamped bellows under internal pressure (p, psi) and axial compression (Δ, in.). It was found that the beam-column approximation results in a close prediction of the magnitude of p and Δ that cause buckling of bellows if initial imperfections are included in the analysis.

Buckling of Perfect Bellows. Beam-column theory was employed to determine the theoretical buckling strength of bellows. For a perfectly straight beam with clamped ends and axially loaded with zero eccentricity, the Euler critical load (compressive) at which buckling occurs is:

$$P_{cr} = \frac{4\pi^2 D}{L^2} \quad . \tag{J-15}$$

For a bellows the equivalent axial load P_{cr} is a combination of internal pressure forces and a compression force, i.e.,

$$P_{cr} = p_{cr}(A + k_p) + k\Delta_{cr} \quad , \tag{J-16}$$

where

A = mean cross-sectional area = $\pi \bar{R}^2$ (in.^{2})

p_{cr} = critical value of internal pressure (psi), in combination with Δ_{cr}

$k_p p_{cr}$ = compressive load buildup at end of clamped bellows (lb), resulting from internal pressure acting on the area (depth) of the convolutions

Δ_{cr} = critical value of axial compression (in.), in combination with p_{cr}

k = axial spring constant (lb/in.).

For perfectly straight bellows (bellows having perfectly straight axial alignment) the equality of Equations (J-15) and (J-16) gave the critical pressures, p_{cr}, tabulated in Table J-22 for the test bellows for compressions of $\Delta_{cr} = 0.1\ L_c$ ($L = L_c$ in (J-15)). As seen in Table J-22, the critical internal pressure causing beam-column collapse of "perfectly" straight-formed bellows were fairly high, in the range of 300 to 500 psi for single-ply bellows and about twice as much for double-ply bellows. Similar data are presented in Table J-23 for the welded test bellows. The first length L_c corresponds to the length of the specimens tested, Table J-15. Because these lengths were so short, they did not give a realistic indication of expected buckling pressures. Therefore, lengths equal to one-half the nominal diameter and equal to the nominal diameter were also considered. The great reduction in critical buckling pressure with increased length is evident.

The pressure coefficients k_p in Table J-23 (defined in Equation (J-16)) are negative for the welded bellows. This is favorable because it tends to increase the critical buckling pressure. A negative k_p corresponds to a tensile end load at the end of the bellows from internal pressure acting on the leaves which were clamped at the outside diameter in the specimens analyzed in this program.

A comparison of Tables J-22 and J-23 shows that the 3- and 3-1/2-inch welded bellows had an appreciably lower critical buckling pressure than did the 3-inch formed

bellows. Even for a shorter length welded bellows, L_c = 1.500 in. for the 3-inch bellows in Table J-23, the pressure was lower, p_{cr} = 143 psi as compared to 400 and 481 psi for the 3-inch Inconel and 3-inch stainless steel formed bellows, respectively.

In Tables J-24 and J-25 the individual load terms, $p_{cr}A$, $p_{cr}k_p$, and $k\Delta_{cr}$, of Equation (J-16) are listed for comparison with the total load, P_{cr}, for $\Delta_{cr} = 0.1\ L_c$. It was found that the axial compression $k\Delta_{cr}$ contributes only about 1 to 2 percent of the total critical load, P_{cr}. Thus, buckling of perfect bellows as a beam column is caused primarily by the internal pressure loading. The pressure-load term, $p_{cr}A$, is most important, but the pressure-load term, $p_{cr}k_p$, should not be neglected for it does represent 10 to 25 percent of the total buckling load. This is a significant result, and when related to the different sign of k_p for welded bellows clamped at the outer diameter, than for formed bellows clamped at the minimum diameter, leads to the following conclusion: clamping of bellows at their outer diameter gives a significant increase in their critical buckling pressures.

Buckling of Imperfect Bellows. Although internal critical buckling pressures were predicted to be 300 to 500 psi (for single-ply formed bellows), much lower pressures, below 100 psi, were found to cause buckling in the experiments. This reduction in the buckling strength was caused by initial imperfections of the bellows. The kinds of imperfections measured on the bellows are shown in Figure J-7. The eccentricity (e) in Figure J-7a is really part of the maximum central deviation (a) in Figure J-7b. In a clamped bellows the eccentricity does not add an end moment as it does in a pinned-end column. Thus, the important imperfections of clamped bellows are the total maximum central deviation (a), which includes eccentricity (e), and the slant offset (s). These quantities are tabulated in Table J-26 for some formed bellows and in Table J-27 for some welded bellows. The quantities (a) and (e) were measured in the plane corresponding to the direction of observed buckling.

The imperfection (a) is represented by either of the following two sine functions:

$$y_o(x) = a_1 \sin \alpha_1 x, \text{ with } a_1 = (a),\ \alpha_1 = \frac{\pi}{L_c}, \tag{J-17}$$

or

$$y_o(x) = a_1 \sin \alpha_1 x + a_3 \sin \alpha_3 x, \tag{J-18}$$

with

$$a_1 - a_3 = (a),\ \alpha_1 = \frac{\pi}{L_c},\ \alpha_3 = \frac{3\pi}{L_c} \text{ and } a_1 = \frac{-1}{3} a_3 \quad .$$

The differential equation to be solved is the following:[4]

$$\frac{d^4y}{dx^4} + \alpha^2 \frac{d^2y}{dx^2} = \frac{d^4y_o}{dx^4} \quad , \tag{J-19}$$

where $\alpha^2 = \dfrac{pA + pk_p + k\Delta}{D}$. [The solution (J-15): $P_{cr} = \dfrac{D\alpha^2}{L^2}$, with $\alpha^2 = 4\pi^2$, is for $y_o \equiv 0$.] The solutions of Equation (J-19) for clamped bellows for imperfections (J-17 and J-18) are plotted in Figure J-8 where ' is the sidewise beam-column deflection at midlength (at x = L/2) and

$$\alpha^* \equiv \frac{L^2}{D}\left[k\Delta + p(k_p + A)\right] \quad . \tag{J-20}$$

(The curves in Figure J-8 are asymptotic to $\alpha^* = 4\pi^2$.) In the buckling experiments δ_e was preset as a gap, as shown in Figure J-5. In order to correlate theoretical and experimental results, it was necessary to determine how much of the experimental deflection δ_e (of Figure J-5) was due to sidewise beam-column buckling (δ of Figure J-8), how much was due to the slant (s) (Figure J-7), and how much was due to local axisymmetric shell deformation. The slant causes a sidewise deflection δ_s when the bellows is subject to compression Δ which can be calculated as follows:

$$\delta_s = \frac{1}{2}\Delta \sin\alpha \quad , \tag{J-21}$$

where $\sin\alpha \approx \alpha \approx \frac{s}{L_c}$. This deflection is shown in Figure J-9.

The compression Δ also causes a local shell deflection of the crown of the convolutions which can be determined from axisymmetric shell computer-code calculations, i.e.,

$$\delta_c = w\frac{\Delta}{L_c} \text{ for formed bellows,} \tag{J-22}$$

$$\delta_c = u_\phi \frac{\Delta}{L_c} \text{ for welded bellows.}$$

(This is a uniform expansion of the crown around the circumference.)

In addition, there is a uniform deflection (δ_p) due to axisymmetric deformation under internal pressure, which can also be determined from shell computer-code calculations. It was found that the deflection (δ_p) is negligible compared to (δ_c) for the formed bellows, but (δ_p) is included in the calculation for the welded bellows. The w and u_ϕ of Equation (J-22) are tabulated in Tables J-28 and J-29 for the bellows considered. Also included in Table J-29 are the deflections (δ_p) for the welded bellows. Thus, the actual sidewise deflection δ caused by beam-column buckling is

$$\delta = \delta_e - \delta_s - \delta_c - \delta_p \quad . \tag{J-23}$$

Equation (J-23) was used to correlate experimental buckling data for δ_e with theoretical beam-column predictions for δ. For example, consider the case of 5-inch bellows JD95, the imperfection of which is plotted in Figure J-10 and represented (approximately) by

$$y_o(x) = a_1 \sin\alpha_1 x = 0.0177 \sin\frac{\pi}{4.053}x \quad . \tag{J-24}$$

For $\Delta = 0.2$ inch the following are determined:

$$\delta_s = \frac{1}{2}\frac{s}{L_c}(0.2) = \frac{1}{2}\left(\frac{0.0275}{4.053}\right)(0.2) = 0.00068,$$

$$\delta_c = \frac{w}{L_c}(0.2) = \frac{0.0210}{4.053}(0.2) = 0.001036,$$

$$\delta = 0.004 - 0.00068 - 0.001036 = 0.00228,$$

$$\frac{\delta}{a} = \frac{0.00228}{0.0177} = 0.178,$$

α^* = 6.8 from Figure J-8,

and p = 46.7 psi from Equation (J-20).

The experimental pressure causing buckling (with $\delta_e = 0.004$) at $\Delta = 0.2$ in. was p = 72 psi. This indicates that the beam-column theory enables a very good approximation (conservative) to the buckling of bellows with imperfections of the form $y_o = a_1 \sin \alpha_1 x$, i.e., relative to p_{cr} = 380 psi for a "perfectly straight" 5-inch bellows (Table J-22), the theory predicts the correct order of magnitude of buckling pressure for an imperfect 5-inch bellows.

Further comparisons of theory and experiment are shown in Figures J-11 to J-18 for 1-, 3-, and 5-inch formed bellows. Generally, there is good agreement. (Each experimental data point is the average of three tests at one loading condition. The response was usually identical for the three tests.) The theory is most often conservative for small compression Δ. For larger compression Δ, there appear to be other modes of buckling that occur, as indicated by the experimental results. These modes would be affected by higher order imperfections. Some of these modes are believed to be higher order elastic-shell modes involving local dimples superimposed on the beam-column mode. (Reference, experimental result on bellows JD23, Figure J-6). Analysis of the higher order buckling is very complicated and was beyond the scope of the present program. However, the shell analysis of buckling of bellows under large compression ($\Delta \geq 0.05\ L_c$) appears to be critical and is, therefore, recommended as a future investigation.

Experimental data were presented on page J-7 for welded bellows under axial compression and internal pressure. It is now shown that these data do not represent buckling, but primarily axisymmetric deformation. Calculation of (δ_s), (δ_c), and (δ_p) and substitution into Equation (J-23) gives the following predicted sidewise deflections (δ):

for Specimen JN135,

$$\delta = 0.0003 - 0.00036 + 0.000086 + 0.000036 = 0.000062,$$

and for Specimen JN156,

$$\delta = 0.0006 - 0.000415 - 0.000087 - 0.000124 = -0.000026.$$

These net deflections, less than 0.0001 inch, are smaller than the accuracy of micrometer readings. Therefore, it was concluded that beam-column buckling of these very short welded bellows did not occur, but that the measured deflections represented primarily axisymmetric deformation.

The nominal stresses (in the absence of buckling) for compressions of $\frac{\Delta}{L_c} \approx 0.1$ in formed bellows are predicted to be in the plastic range, e.g., for 5-inch bellows JD92 the meridional stress at the surface of the inner convolution calculated from the elastic analysis is

$$\sigma_\phi = 768,500 \frac{\Delta}{L_c} = 76,350 \text{ psi for } \frac{\Delta}{L_c} = 0.1 \quad .$$

This is about twice the yield stress of 40,000 psi for annealed 347 stainless steel sheet material and also exceeds the yield stress of 65,000 psi for this material in the cold-drawn condition*. The elastic limit is reached for $\frac{\Delta_e}{L_c} = 0.0520$ for JD92. Therefore, a theoretical stress analysis for compressions of $\frac{\Delta}{L_c} \geqq 0.05$ should involve elastic-plastic constitutive laws for the material. (Strain-hardening during fatigue testing may have also increased the yield strength.) This may account for the agreement with elastic theory in Figures J-17 and J-18 for large Δ. The more critical modes of buckling for large Δ in Figures J-11, J-12, J-15, J-17, and J-18 may have been caused by a reduced bending stiffness D for the bellows material in the elastic-plastic state.

Thus, there appear to be two possible reasons for the low buckling pressures at large compression:

(1) Higher order shell modes of elastic buckling superimposed on the beam-column mode

(2) Elastic-plastic buckling.

It is highly recommended that an extensive theoretical analysis be made of these two possible kinds of buckling of bellows.

Analysis of Plastic Collapse of Bellows

The plastic collapse of a bellows results in gross permanent deformation of the bellows which makes it unfit for further use. At the limit load at which collapse occurs, a sufficiently large region of the bellows convolutions becomes wholly plastic through the thickness that adjacent elastic or elastic-plastic regions of the convolutions no longer restrain the plastic region. Whereas initial buckling deflections can be analyzed using elasticity theory, the terminal collapse state necessitates the use of the plasticity theory. Only the axisymmetric plastic collapse (burst) under internal pressure was considered in this program. (Nonsymmetric plastic collapse can also occur. For example, if the elastic beam-column buckling loads are exceeded, a state of permanent squirm deformation results.)

*The bellows may be in the cold-drawn condition after forming. The exact amount of cold work of the bellows during forming is unknown.

Experimental Analysis

Experiments were initially conducted on the plastic collapse of 5-inch formed bellows JD96 and JD90 under internal pressure. It was found that these bellows collapsed at internal pressures of about 260 and 270 psi, respectively, when they were restrained from beam-column buckling. These pressures were much larger than the elastic buckling pressures (<100 psi) shown in Figures J-17 and J-18, and thus beam-column buckling was found to be the more critical mode of failure.

The fixture constructed for the internal-pressure tests is shown in Figure J-19. To find the axisymmetric plastic-collapse mode for a straight bellows, modifications had to be made in the fixture to prevent the bellows from buckling in the beam-column mode. The imperfect bellows (imperfect either from manufacture or from prior fatigue testing) were restrained from sidewise motion by six restraints spaced equally around the circumference as shown in Figure J-19. The restraints were positioned with initial gaps of about 0.002 inch to allow the bellows to expand uniformly from the internal pressure. Two of these restraints are also shown in Figure J-20, which is a photograph of Bellows JD96 at 250 psi.

During the experiments, the thickness of the 7th convolution (from the bottom) and the diameter change of this convolution were measured. The measured data are plotted in Figures J-21, J-22, J-23, and J-24. As is evident in these figures, the deformation increased fairly linearly until the pressure exceeded 250 psi, when the deformation rapidly increased. A surprising result was found: the diameter of the crown of the convolutions decreased at the plastic-collapse pressure, as shown in Figures J-22 and J-24, whereas it was increasing at smaller pressures.

Photographs were made of the 7th convolution during the experiments and magnified. Tracings of the magnified positives are shown in Figure J-25 for Bellows JD96. As indicated, the convolution expanded outward prior to collapse, but then the crown moved in and the convolution grew wider at collapse. In Figure J-26, the 270-psi deformation curve is translated vertically so that the roots coincide. It can be seen that the root area of the convolution remained relatively rigid while the flat and crown areas plastically deformed.

The restraints were removed from Bellows JD96 at 270 psi. It momentarily remained straight, but then snapped sidewise. Figure J-27 shows the permanent deformation after release of pressure. The restraints were kept on Bellows JD90 and the pressure was released from 280 psi. Figure J-28 shows its deformation. As shown, the deformation of the convolution contains a cos 2θ (or sin 2θ Fourier variation) around the circumference. Bellows JD96 also appeared the same way before removal of the restraints. This circumferential variation can be explained in this manner: consider the crown of the convolution as a curved beam under a compressive force (corresponding to the decrease in diameter in Figure J-24), then the circumferential variation, exhibiting an axial movement, is the result of a plastic buckling of the curved beam (analogous to Euler column buckling).

Internal pressure experiments were also conducted on 3-inch Inconel formed bellows JD125, and on 1-inch Inconel formed bellows JD111. Because of a smaller diameter-to-thickness ratio for these bellows than for the 5-inch bellows, and because of the greater yield strength of Inconel 718, collapse pressures in excess of 300 psi were expected. Internal pressures up to 300 psi in the 3-inch bellows and up to 750 psi in the 1-inch bellows did not cause any observable plastic deformation.

Because the plastic-collapse pressures were so much higher than the elastic beam-column buckling pressures, further experiments were not considered warranted under the present program.

Approximate Theoretical Analysis

The elastic solution for stresses in shells can be used to obtain a lower bound on the collapse pressure. This method has been employed by Marcal and Turner[5] to obtain limit pressures for bellows. As a first approximation this method is also employed here.

Examination of the computer results for the elastic solution for 5-inch bellows JD92 under internal pressure shows that the maximum stresses occur at the roots of the convolutions. This stress is predominantly a bending stress corresponding to a bending moment of

$$M_\phi = 0.008624\ p,\ \text{in.-lb/in. at the root.} \tag{J-25}$$

The plastic-collapse bending moment M_o in a shell is

$$M_o = \frac{\sigma_o h^2}{4} \tag{J-26}$$

where σ_o = yield stress in tension, psi

h = shell thickness, in.

Equating (J-25) and (J-26) the following lower bound is obtained:

$$p_c \geqq \frac{\sigma_o h^2}{4(M_\phi/p)} \tag{J-27}$$

This equation gives the collapse pressure for a predominately bending-type collapse (Method I).

For σ_o = 40,000 psi (yield strength of 347 annealed stainless steel sheet material) and h = 0.010 in. (nominal thickness of 5-inch bellows), the following lower bound to the collapse pressure p_c is calculated from Equation (J-27):

$$p_c \geqq \frac{40,000\ (0.0001)}{4\ (0.008624)} = 116\ \text{psi.}$$

This is not a very good lower bound relation to the experimentally observed collapse pressure of 250 to 270 psi in Figures J-21 to J-24. Even if account is made of strain hardening due to forming and fatigue test cycling at the root, it does not appear that this accounts for the larger observed collapse pressure - particularly since the root area was also observed to remain relatively rigid at collapse as previously shown in Figure J-26.

Thus, use of the elastic solution to predict lower bounds based upon the maximum elastic stress is not sufficiently accurate. Marcal and Turner[5], however, had much better success. The reason for this is believed to be due to two different kinds of

plastic collapse which are related to two different ranges of diameter-to-thickness ratios. The diameter-to-thickness ratio for the 5-inch bellows is d/h = 5.0/0.010 = 500, whereas the ratio for the bellows tested in Reference (4) ranged from 8.2 to 23.4. It is believed that a membrane stress state predominates at plastic collapse of the thin-walled bellows (d/h $\simeq$ 500), and that a bending-stress state predominates at plastic collapse of thick-walled bellows (d/h $\simeq$ 10).

Accordingly, if the above reasoning is correct, then the maximum membrane stress calculated elastically may result in a better prediction of the collapse pressure. The membrane stress resultants N_ϕ and N_θ from the elastic computer solution are taken at the inflection point where the bending moment $M_\phi \simeq 0$. For 5-inch bellows JD92 these are

$$N_\phi = -0.0259\ p,\ N_\theta = 1.253\ p \quad . \tag{J-28}$$

In order to use the Tresca yield criterion, the difference is taken,

$$N_\theta - N_\phi = 1.279\ p \quad . \tag{J-29}$$

Equating this result to the yield value,

$$N_o = \sigma_o h \quad , \tag{J-30}$$

for σ_o = 40,000 psi and h = 0.010 inch, the following result is obtained:

$$p_c \approx \frac{\sigma_o h}{[(N_\theta - N_\phi)/p]} = \frac{40,000(0.010)}{1.279} = 313 \text{ psi.}$$

This result is quite close to the experimental values of 260 to 270 psi shown in Figures J-21 to J-24. It is believed that this is as close an approximation as can be made without conducting a complete detailed theoretical plastic analysis.

In other thin-walled bellows, N_θ rather than $N_\theta - N_\phi$ may be maximum. Therefore, according to the Tresca yield criterion, for the membrane type of collapse (Method II) the collapse pressures are:

$$p_{cr} \approx \frac{\sigma_c h}{(N_\theta/p)}\ ,\ \text{for } N_\theta > N_\theta - N_\phi \tag{J-31}$$

and

$$p_{cr} \approx \frac{\sigma_o h}{[(N_\theta - N_\phi)/p]}\ ,\ \text{for } N_\theta - N_\phi > N_\theta \tag{J-32}$$

where N_θ and N_ϕ are values from an elastic computer calculation. Formulas (J-31) and (J-32) and also formula (J-27) were used to predict collapse pressures for 1- and 3-inch stainless steel bellows. The results are given in Table J-30. Collapse pressures in excess of 400 psi were predicted for the 1- and 3-inch stainless steel bellows by Method II, for the membrane type of collapse. The Inconel bellows were predicted to have higher collapse pressures because of higher yield strengths. Inconel bellows JD111 (1-inch) was tested to 750 psi without collapse.

Summary

In summary, the significance of the results of this section are related to design analysis. It has been found that the plastic-collapse pressure of bellows can be estimated approximately by either of two methods, depending on the diameter-to-thickness ratio d/h. These methods, I and II, Equations (J-27), and (J-31, 32), apply for the predominantly bending and the predominantly membrane type of deformation, respectively, and appear to be valid for $d/h \approx 10$ to 20, and $d/h \approx 200$ to 500, respectively. Bellows with $20 \leq d/h \leq 200$ are in the intermediate range where estimation is difficult. It is recommended that both methods be applied here to bracket the collapse pressure. However, for a more accurate plastic-collapse analysis of any bellows, Battelle has computer codes which can be applied. This is recommended.

REFERENCES

J-1. Brazier, L. G., "On the Flexure of Thin Cylindrical Shells and Other 'Thin' Sections", Proc. of the Royal Society of London, Series A, 116, pp 104-114 (1927).

J-2. Reissner, E., and Weinitschke, H. J., "Finite Pure Bending of Circular Cylindrical Tubes", Quart. Appl. Math., XX (4), pp 305-319 (January, 1963).

J-3. Reissner, E., "On Finite Pure Bending of Cylindrical Tubes", Österr. Ing. Arch., 5, pp 165-172 (1961).

J-4. Seide, P., "The Effect of Pressure on the Bending Characteristics of an Actuator System", ASME Trans., J. Appl. Mech., 82, pp 429-437 (1960).

J-5. Marcal, P. V. and Turner, C E., "Elastic Solution in the Limit Analysis of Shells of Revolution With Special Reference to Expansion Bellows", J. Mech. Eng. Sci., 3 (3), pp 252-257.

TABLE J-1. EXPERIMENTAL DETERMINATION OF LATERAL BENDING STIFFNESS D FOR 5-INCH SINGLE-PLY STAINLESS STEEL BELLOWS

Specimen	Slope of Force-Rotation Curve, S, lb/degree[(a)]	Total Convolution Length, L_c, in.[(b)]	Bending Stiffness, D[(c)], lb-in.^{2}
JD90	1.44	4.153	4412
JD93	1.36	3.907	3883
JD94	1.55	4.110	4692
JD95	1.33	4.053	3962
JD96	1.33	4.140	4060
JD97	1.31	4.111	3997
JD98	1.28	4.115	3880
		Average	4124
Theoretical bending stiffness from computer calculation on JD92			4507

(a) Average of experimental data as shown in Figure J-2.
(b) L_c = average bellows length + average pitch.
(c) The length L in Figure J-1 is 10.80 in. D calculated with formula (J-1).

TABLE J-2. EXPERIMENTAL DETERMINATION OF LATERAL BENDING STIFFNESS D FOR 3-INCH SINGLE-PLY STAINLESS STEEL BELLOWS

Specimen	Slope of Force-Rotation Curve, S, lb/degree[(a)]	Total Convolution Length, L_c, in.[(b)]	Bending Stiffness, D[(c)], lb-in.^{2}
JD62	0.439	2.120	625.5
JD63	0.348	2.023	470.5
JD64	0.404	2.070	554.7
JD66	0.421	2.153	610.8
JD67	0.389	2.096	547.6
JD70	0.437	2.098	615.6
JD71	0.410	2.128	586.6
JD72	0.465	2.168	679.4
		Average	586.3
Theoretical bending stiffness from computer calculation on JD68			480.4

(a) Average of experimental data as shown in Figure J-2.
(b) L_c = average bellows length + average pitch.
(c) The length L in Figure J-1 is 10.68 in. D calculated with formula (J-1).

TABLE J-3. EXPERIMENTAL DETERMINATION OF LATERAL BENDING STIFFNESS D FOR 1-INCH SINGLE-PLY STAINLESS STEEL BELLOWS

Specimen	Slope of Force-Rotation Curve, S, lb/degree[a]	Total Convolution Length, L_c, in.[b]	Bending Stiffness, D[c], lb-in.^{2}
JD23	0.0330	0.979	12.2
JD25	0.0290	1.059	11.6
JD26	0.0285	1.056	11.4
JD27	0.0330	1.077	13.5
JD30	0.0360	1.033	14.1
JD31	0.0349	0.965	12.7
JD32	0.0250	1.057	10.0
JD33	0.0275	1.039	10.9
JD34	0.0321	1.104	13.5
		Average	12.2
Theoretical bending stiffness from computer calculation on JD29			13.8

(a) Average of experimental data similar to that shown in Figure J-2.
(b) L_c = average bellows length + average pitch.
(c) D calculated with L = 6.103 in. in Formula (J-1)

TABLE J-4. EXPERIMENTAL DETERMINATION OF LATERAL BENDING STIFFNESS D FOR 1-INCH SINGLE-PLY INCONEL BELLOWS

Specimen	Slope of Force-Rotation Curve, S, lb/degree[a]	Total Convolution Length, L_c, in.[b]	Bending Stiffness, D[c], lb-in.^{2}
JD107	0.0320	1.217	15.0
JD109	0.0310	1.229	14.7
JD111	0.0365	1.211	17.0
JD112	0.0320	1.201	14.7
JD113	0.0315	1.244	15.1
JD114	0.0325	1.252	15.7
JD115	0.0331	1.243	15.8
JD116	0.0315	1.195	14.4
JD118	0.0345	1.237	16.4
		Average	15.4

(a) Average of experimental data similar to that shown in Figure J-2.
(b) L_c = average bellows length + average pitch.
(c) D calculated with L = 6.103 in. in Formula (J-1).

TABLE J-5. EXPERIMENTAL DETERMINATION OF LATERAL BENDING STIFFNESS D FOR 3-INCH SINGLE-PLY INCONEL BELLOWS

Specimen	Slope of Force-Rotation Curve, S, lb/degree[a]	Total Convolution Length, L_c, in.[b]	Bending Stiffness, D[c], lb-in.^{2}
JD119	0.321	2.037	438.2
JD120	0.292	2.034	397.4
JD121	0.300	2.055	413.8
JD123	0.300	2.099	423.4
JD125	0.308	2.042	422.3
JD126	0.296	2.084	414.4
JD127	0.272	2.072	377.9
JD129	0.300	2.082	419.7
		Average	413.4

(a) Average of experimental data similar to that shown in Figure J-2.
(b) L_c = average bellows length + average pitch.
(c) D calculated with L = 10.68 inches in Formula (J-1).

TABLE J-6. EXPERIMENTAL DETERMINATION OF LATERAL BENDING STIFFNESS D FOR 3-INCH DOUBLE-PLY STAINLESS STEEL BELLOWS

Specimen	Slope of Force-Rotation Curve, S, lb/degree[a]	Total Convolution Length, L_c, in.[b]	Bending Stiffness, D[c], lb-in.^{2}
JD74	0.669	2.139	962.7
JD75	0.713	2.121	1016.4
JD76	0.671	2.141	966.8
JD79	0.758	2.207	1130.1
JD80	0.625	2.163	911.1
JD81	0.688	2.134	987.4
JD82	0.733	2.148	1060.6
JD83	0.721	2.111	1023.3
		Average	1007.3
		Theoretical value[d] D_2 =	960.8

(a) Average of experimental data similar to that shown in Figure J-2.
(b) L_c = average bellows length + average pitch.
(c) D calculated with L = 10.68 in. in Formula (J-1).
(d) $D_2 = 2D_1$ where D_1 is the theoretical value for a single-ply bellows and D_2 = estimated value for a double-ply bellows. D_1 = 480.4 lb-in.^{2} from computer calculation on JD68.

TABLE J-7. INPUT DATA CARDS FOR CALCULATION OF THE BEAM BENDING STIFFNESS OF 3-INCH BELLOWS JD68

DATA SET 1 (three title cards)

```
3-INCH SINGLE-PLY STAINLESS STEEL FORMED BELLOWS JD68
VARIABLE THICKNESS MODEL
BENDING STIFFNESS CALCULATION, ROTATION PRESCRIBED
```

DATA SET 2 (boundary data at initial edge)

type	value	type	value	type	value	type	value
FORCE	0.0	DISPLACEMENT	0.0	SLOPE	0.0	DISPLACEMENT	0.0

DATA SET 3 (boundary data at final edge)

type	value	type	value	type	value	type	value
FORCE	0.0	DISPLACEMENT	0.01821	SLOPE	0.01	DISPLACEMENT	0.00050

DATA SET 4 (angle between support and shell)

α initial, degrees	α final, degrees
0.	0.

DATA SET 5 (control set)

parts	iter	ridummy	plot	intprn	intval	level 1	level 2	error control	convergence	Fourier Harmonic Data: No.	Fourier Harmonic Data: Values
	6	0		0	0			1.0E06	1.0E-04	1	1

DATA SET 6 (Young's Modulus and Poisson's Ratio)

constant?	Young's Modulus		nu
	E		

DATA SET 7 (loading parameters)

constant?	pressure, psi	unit weight, lb./in.^{3}	dead weight, psi

TABLE J-8. THEORETICAL DETERMINATION OF LATERAL BENDING STIFFNESS D FOR WELDED BELLOWS

Specimen	Nominal Size, in.	Material	Bending Stiffness D, lb-in.^{2}	Experimental[a] Values for D, lb-in.^{2}
JD136	3-1/2	347 stainless steel	37.9046	44.5
JD150	1-1/2	347 stainless steel	9.4382	6.80
JD158	3	AM350	58.4983	63.5
JD171	1-1/2	AM350	12.8310	8.02

(a) Determined from experiments on Specimens JD134, JD143, JD155, and JN167, respectively.

TABLE J-9. EXPERIMENTAL RELATION BETWEEN BENDING STIFFNESS D AND AXIAL SPRING CONSTANT k FOR 5-INCH SINGLE-PLY STAINLESS STEEL BELLOWS

Specimen	Axial Spring Constant, k, lb-in.	Average Bellows Radius, $\bar{R}$, in.	α Factor, $\frac{D^{(a)}}{k\bar{R}^2 L_c}$
JD90	310	2.673	0.479
JD93	287	2.672	0.484
JD94	297	2.672	0.538
JD95	301	2.673	0.454
JD96	305	2.672	0.450
JD97	300	2.674	0.452
JD98	300	2.673	0.439
		Average	0.471
Theoretical factor from computer calculation[b]			0.536

(a) Bending stiffness D and convolution length L_c given in Table J-1.
(b) Theoretical result using calculated D of 4507 and k of 325 for bellows JD92.

TABLE J-10. EXPERIMENTAL RELATION BETWEEN BENDING STIFFNESS D AND AXIAL SPRING CONSTANT k FOR 3-INCH SINGLE-PLY STAINLESS STEEL BELLOWS

Specimen	Axial Spring Constant, k, lb/in.	Average Bellows Radius, $\bar{R}$, in.	α Factor, $\frac{D^{(a)}}{k\bar{R}^2 L_c}$
JD62	167	1.658	0.643
JD63	173	1.654	0.492
JD64	161	1.659	0.605
JD66	178	1.658	0.580
JD67	169	1.659	0.562
JD70	172	1.658	0.621
JD71	185	1.656	0.543
JD72	184	1.656	0.621
		Average	0.583
Theoretical factor from computer calculation[b]			0.540

(a) Bending stiffness D and convolution length L_c given in Table J-2.
(b) Theoretical result using calculated D of 480.4 and k of 161 for bellows JD68.

TABLE J-11. EXPERIMENTAL RELATION BETWEEN BENDING STIFFNESS D AND AXIAL SPRING CONSTANT k FOR 1-INCH SINGLE-PLY STAINLESS STEEL BELLOWS

Specimen	Axial Spring Constant, k, lb/in.	Average Bellows Radius, $\bar{R}$, in.	α Factor, $\frac{D^{(a)}}{k\bar{R}^2 L_c}$
JD23	77	0.579	0.483
JD25	85	0.579	0.384
JD26	84	0.579	0.383
JD27	82	0.577	0.459
JD30	81	0.579	0.503
JD31	83	0.577	0.476
JD32	75	0.576	0.380
JD33	86	0.578	0.365
JD34	76	0.579	0.480
		Average	0.434
Theoretical factor from computer calculation on JD29[b]			0.480

(a) Bending stiffness D and convolution length L_c given in Table J-3.
(b) Theoretical result using calculated D of 13.8 and k of 86 for bellows JD29.

TABLE J-12. EXPERIMENTAL RELATION BETWEEN BENDING STIFFNESS D AND AXIAL SPRING CONSTANT k FOR 1-INCH SINGLE-PLY INCONEL BELLOWS

Specimen	Axial Spring Constant, k lb/in.	Average Bellows Radius, $\bar{R}$, in.	α Factor, $\frac{D^{(a)}}{k\bar{R}^2 L_c}$
JD107	75.6	0.563	0.513
JD109	77.5	0.562	0.488
JD111	90.0	0.563	0.492
JD112	77.0	0.562	0.505
JD113	77.9	0.561	0.495
JD114	80.2	0.563	0.493
JD115	81.9	0.561	0.494
JD116	79.4	0.562	0.482
JD118	89.2	0.562	0.472
		Average	0.493

(a) Bending stiffness D and convolution length L_c given in Table J-4.

TABLE J-13. EXPERIMENTAL RELATION BETWEEN BENDING STIFFNESS D AND AXIAL SPRING CONSTANT k FOR 3-INCH SINGLE-PLY INCONEL BELLOWS

Specimen	Axial Spring Constant, k, lb/in.	Average Bellows Radius, $\bar{R}$, in.	α Factor, $\frac{D^{(a)}}{k\bar{R}^2 L_c}$
JD119	142.5	1.632	0.567
JD120	128.2	1.636	0.569
JD121	140.0	1.631	0.541
JD123	142.0	1.630	0.535
JD125	131.8	1.647	0.578
JD126	138.4	1.641	0.533
JD127	135.6	1.632	0.505
JD129	138.9	1.633	0.544
		Average	0.547

(a) Bending stiffness D and convolution length L_c given in Table J-5.

TABLE J-14. EXPERIMENTAL RELATION BETWEEN BENDING STIFFNESS D AND AXIAL SPRING CONSTANT k FOR 3-INCH DOUBLE-PLY STAINLESS STEEL BELLOWS

Specimen	Axial Spring Constant, k, lb/in.	Average Bellows Radius, $\bar{R}$, in.	α Factor, $\frac{D^{(a)}}{k\bar{R}^2 L_c}$
JD74	361	1.648	0.459
JD75	337	1.649	0.523
JD76	360	1.649	0.461
JD79	333	1.647	0.567
JD80	297	1.652	0.520
JD81	359	1.648	0.475
JD82	360	1.648	0.505
JD83	360	1.647	0.496
		Average	0.501

(a) Bending stiffness D and convolution length L_c given in Table J-6.

TABLE J-15. THEORETICAL RELATION BETWEEN BENDING STIFFNESS D AND AXIAL SPRING CONSTANT k FOR WELDED BELLOWS

Specimen	Nominal Size, inch	Axial Spring Constant $k^{(a)}$, lb/in.^{2}	Average Bellows Radius, $\bar{R}^{(b)}$, in.	Total Convolution Length, L_c, inch	α Factor, $\frac{D^{(c)}}{k\bar{R}^2 L_c}$	Experimental$^{(d)}$ Values for
JD136	3-1/2	57	1.6084	0.480	0.537	0.575
JD150	1-1/2	101	0.6567	0.373	0.581	0.406
JD158	3	152	1.5710	0.341	0.457	0.495
JD171	1-1/2	124	0.6612	0.338	0.699	0.430

(a) The theoretical value for compression reported in Table 6 of the Report body.
(b) Average radius as measured on sectional and encapsulated specimens.
(c) α defined in Equation (J-14).
(d) Determined from experiments on Specimens JD134, JD143, JD155, and JD167.

TABLE J-16. BUCKLING DATA ON 5-INCH SINGLE-PLY STAINLESS STEEL BELLOWS

Specimen	Compression, Δ, in.	Test Pressure, p, psi	Remarks
JD90	0.300	100	Did not buckle
	0.340	90	Buckled
JD93	0 to 0.410	100	Did not buckle
JD94	0.300	100	Did not buckle
	0.370	90	Buckled
JD95	0.298	14	Buckled
JD96	0.291	49	Buckled
JD97	0.300	100	Did not buckle
	0.390	80	Buckled
JD98	0.284	89	Buckled

TABLE J-17. BUCKLING DATA ON 3-INCH SINGLE-PLY STAINLESS STEEL BELLOWS

Specimen	Compression, Δ, in.	Test Pressure, p, psi	Remarks
JD61	0.220	100	Did not buckle
JD62	0.149	32	Buckled
JD63	0.220	100	Did not buckle
JD64	0.145	59	Buckled
JD65	0.220	100	Did not buckle
JD66	0.146	54	Buckled
JD67	0.143	88	Buckled
JD70	0.147	64	Buckled
JD71	0.150	100	Did not buckle
	0.210	100	Buckled
JD72 - had large fatigue crack--did not hold pressure			

TABLE J-18. BUCKLING DATA ON 1-INCH SINGLE-PLY STAINLESS STEEL BELLOWS

Specimen	Compression, Δ, in.	Test Pressure, p, psi	Remarks
JD23	0.100	100	Did not buckle*
JD25	0.100	100	Did not buckle
JD26 - had large fatigue crack--did not hold pressure			
JD27	0.015	73	Buckled
	0.042	0	Buckled
JD30	0.0725	100	Buckled
	0.0815	0	Buckled
JD31	0.100	100	Did not buckle
JD32 - had large fatigue crack--did not hold pressure			
JD33 - had large fatigue crack--did not hold pressure			
JD34	0.100	100	Did not buckle

* Specimen JD23 did not buckle in the usual beam-column mode, but it did buckle into a local shell mode as shown in Figure J-6. The depth of this buckle was about 0.001 in. at both $\Delta = 0$ in. and $p = 100$ psi and $\Delta = 0.100$ in. and $p = 0$ psi, and was about 0.002 in. at $\Delta = 0.100$ in. and $p = 100$ psi.

TABLE J-19. BUCKLING DATA ON 1-INCH SINGLE-PLY INCONEL BELLOWS

Specimen	Compression, Δ, in.	Pressure, p, psi	Remarks
JD107	0.100	100	Did not buckle
JD109	0.100	100	Did not buckle
JD111	0.080	67	Buckled
	0.100	0	Buckled
JD112	0.100	99	Buckled
JD113	0.100	100	Did not buckle
JD115	0.100	100	Did not buckle
JD116	0.100	100	Did not buckle
JD118	0.100	100	Did not buckle

TABLE J-20. BUCKLING DATA ON 3-INCH SINGLE PLY-INCONEL BELLOWS

Specimen	Compression, Δ, in.	Pressure, p, psi	Remarks
JD119	0.220	100	Did not buckle
JD120	0.155	67	Buckled
JD121	0.220	100	Did not buckle
JD123	0.220	100	Did not buckle
JD125	0.220	100	Did not buckle
JD126	0.159	23	Buckled
JD127	0.220	100	Did not buckle
JD129	0.220	100	Did not buckle

TABLE J-21. BUCKLING DATA ON 3-INCH DOUBLE-PLY STAINLESS STEEL BELLOWS

Specimen	Compression, Δ, in.	Pressure, p, psi	Remarks
JD73	0.358	79	Buckled
JD74	0.358	39	Buckled
JD75	0.360	100	Did not buckle
JD76	0.360	100	Did not buckle
JD79	0.360	100	Did not buckle
JD80	0.360	100	Did not buckle
JD81	0.356	91	Buckled
JD82	0.356	88	Buckled
JD83	0.360	100	Did not buckle

TABLE J-22. CRITICAL INTERNAL PRESSURES CAUSING BUCKLING OF PERFECTLY STRAIGHT FORMED TEST BELLOWS[a]

Size of Bellows[b]	Material	Total Convolution Length, L_c, in.[c]	Mean Area A[c], in.^{2}[d]	Axial Spring Constant, k[c], lb/in.^{2}	Bending Stiffness, D[c], lb-in.^{2}	Pressure Coefficient, k_p[e], in^2	Critical Pressure, p_{cr}[f], psi
1-inch, single-ply	Stainless steel	1.041	1.050	81	12.2	0.266	331
1-inch, single-ply	Inconel	1.226	0.992	81	15.4	0.175	338
3-inch, single-ply	Stainless steel	2.107	8.62	174	559.2	1.59	481
3-inch, single-ply	Inconel	2.063	8.39	137	413.4	1.10	400
3-inch, double-ply	Stainless steel	2.145	8.52	346	1007.3	1.60	845
5-inch, single-ply	Stainless steel	4.084	22.45	300	4124.0	2.87	380

(a) For $\Delta_{cr} = 0.1\ L_c$ in Equation (J-16); (b) Nominal diameter;

(c) Average of experimental data. (d) $A = \pi \bar{R}^2$; (e) Determined from computer calculation of a mathematical shell model of bellows with p = 1 psi; (f) Calculated from Equations (J-15) and (J-16).

TABLE J-23. CRITICAL INTERNAL PRESSURES CAUSING BUCKLING OF PERFECTLY STRAIGHT WELDED TEST BELLOWS[a]

Size of Bellows[b], inch	Material	Total Convolution Length, L_c, in.[c]	Mean Area, A[d], in.^{2}	Axial Spring Constant, k, lb/in.^{2}	Bending Stiffness, D, lb-in.^{2}	Pressure Coefficient, k_p[e], in.^{2}	Critical Pressure, p_{cr}[f], psi
3-1/2	347 Stainless steel	0.480 1.750 3.500	8.127	57	37.9	-1.009	909 67 14
1-1/2	347 Stainless steel	0.373 0.750 1.500	1.355	101	9.44	-0.162	2242 549 126
3	AM350	0.341 1.500 3.000	7.753	152	58.5	-0.720	2823 143 30
1-1/2	AM350	0.338 0.750 1.500	1.3735	124	12.8	-0.283	4054 812 189

(a), (b), (c), and (f) the same as in Table J-23. (c) The first L_c listed corresponds to the specimen lengths in Table J-15. The other L_c are taken as 1/2 and equal to the nominal diameter, respectively. (d) $A = \pi \bar{R}^2$; $\bar{R}$ from Table J-15.

TABLE J-24. COMPARISON OF INDIVIDUAL LOAD TERMS[a] CONTRIBUTING TO TOTAL BUCKLING LOAD FOR PERFECTLY STRAIGHT FORMED TEST BELLOWS

Size of Bellows[b]	Material	Load Term, $p_{cr}A$, lb	Load Term, $p_{cr}k_p$, lb	Load Term, $k\Delta_{cr}$[c], lb	Total Critical Load, P_{cr}[d], lb
1-inch, single-ply	Stainless steel	348	88	8.45	445
1-inch, single-ply	Inconel	335	59	9.92	405
3-inch, single-ply	Stainless steel	4150	765	36.7	4960
3-inch, single-ply	Inconel	3360	440	28.3	3830
3-inch, single-ply	Stainless steel	7200	1350	74.4	8650
5-inch, single-ply	Stainless steel	8540	1090	122.5	9750

(a) In Equation (J-16). (b) Nominal diameter. (c) $\Delta_{cr} = 0.1\ L_c$.

(d) $P = \frac{4\pi^2 D}{L_c^2}$, Equation (J-15).

TABLE J-25. COMPARISON OF INDIVIDUAL LOAD TERMS [a] CONTRIBUTING TO TOTAL BUCKLING LOAD FOR PERFECTLY STRAIGHT WELDED TEST BELLOWS LENGTHS OF ONE-HALF THE NOMINAL DIAMETER

Size of Bellows[b]	Material	Load Term, $p_{cr}A$, lb	Load Term, $p_{cr}k_p$, lb	Load Term, $k\Delta_{cr}$[c], lb	Total Critical Load, P_{cr}[d], lb
3-1/2 in.	347 Stainless steel	545	-68	10	487
1-1/2 in.	347 Stainless steel	744	-89	8	663
3-inch	AM350	1109	-103	23	1029
1-1/2 in.	AM350	1115	-230	9	894

(a) In Equation (J-16). (b) Nominal diameter. (c) $\Delta_{cr} = 0.1\ L_c$.

(d) $P = \frac{4\pi^2 D}{L_c^2}$, Equation (J-15).

TABLE J-26. IMPERFECTIONS MEASURED ON FORMED BELLOWS[a]

Specimen	Size of Bellows[b], inch	Material		Number of Plies	Total Maximum Central Deviation (a), in.	Slant Offset (s)[c], inch
		Stainless Steel	Inconel			
JD27	1	x		1	0.0090	0.0285
JD111	1		x	1	0.00975	0.0095
JD62	3	x		1	0.0368	0.0025
JD64	3	x		1	0.0197	-0.02125
JD126	3		x	1	0.0105	0.0050
JD74	3	x		2	0.0085	0.0230
JD95	5	x		1	0.0177	0.0275
JD96	5	x		1	0.0188	0.0030

(a) Imperfections shown in Figure J-7.
(b) Nominal diameter
(c) (s) is positive in the direction of positive (a) as shown in Figure J-7.

TABLE J-27. IMPERFECTIONS MEASURED ON WELDED BELLOWS[a]

Specimen	Nominal Diameter of Bellows, in.	Material	Total Maximum Central Deviation, (a), in.	Slant Offset, (s)[b], in.
JD135	3-1/2	347 stainless steel	0.0017	0.0023
JD156	3	AM350	0.0006	0.0031
JD164	3	AM350	0.0011	0.0025

(a) Imperfections shown in Figure J-7.
(b) (s) is positive in the direction of positive (a) as shown in Figure J-7.

TABLE J-28. THEORETICAL CROWN DEFLECTIONS (w, INCH) FOR FORMED BELLOWS UNDER AXIAL COMPRESSION (Δ, INCH)[a]

Specimen	Size of Bellows[b], inch	Material: Stainless Steel	Material: Inconel	Number of Plies	Crown Deflection (w), in.[c]
JD29	1	X		1	0.00424
JD117	1		X	1	0.00168
JD68	3	X		1	0.00102
JD124	3		X	1	0.02785
JD77	3	X		2	0.01022
JD92	5	X		1	0.00210

(a) Determined from computer calculations on exact mathematical models.
(b) Nominal diameter.
(c) Deflection used in Equation (J-22).

TABLE J-29. THEORETICAL OUTER LEAF DEFLECTIONS (u_φ, INCH) FOR WELDED BELLOWS UNDER AXIAL COMPRESSION (Δ, INCH) AND INTERNAL PRESSURE (p)[a]

Specimen	Nominal Diameter, inch	Material	Outer Leaf Deflections, in.[b]: u_φ for $\frac{\Delta}{L_c} = 1$	u_φ for p = 10 psi
JD136	3-1/2	347 Stainless steel	-0.000274	-0.0000323
JD158	3	AM350	0.000325	0.0000886

(a) Determined from computer calculations on exact mathematical models.
(b) Deflections used in Equation (J-22).

TABLE J-30. PREDICTIONS OF INTERNAL PLASTIC COLLAPSE PRESSURE FOR STAINLESS STEEL BELLOWS

Specimen	Nominal Diameter, inch	Nominal Thickness, inch	Diameter-to-Thickness Ratio	Predicted Collapse Pressure, psi[a]: Method I	Method II
JD29	1	0.005	200	138	402
JD68	3	0.008	375	131	456
JD92	5	0.010	500	116	313

(a) Method I employs Equation (J-27) for a predominantly bending type of collapse; Method II employs Equations (J-31) or (J-32) for a predominantly membrane-type of collapse.

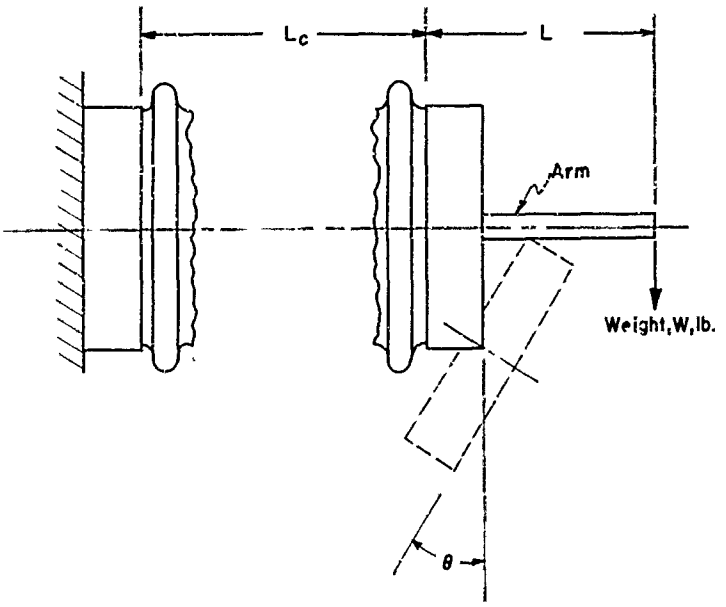

FIGURE J-1. EXPERIMENTAL METHOD FOR LATERAL BENDING OF BELLOWS

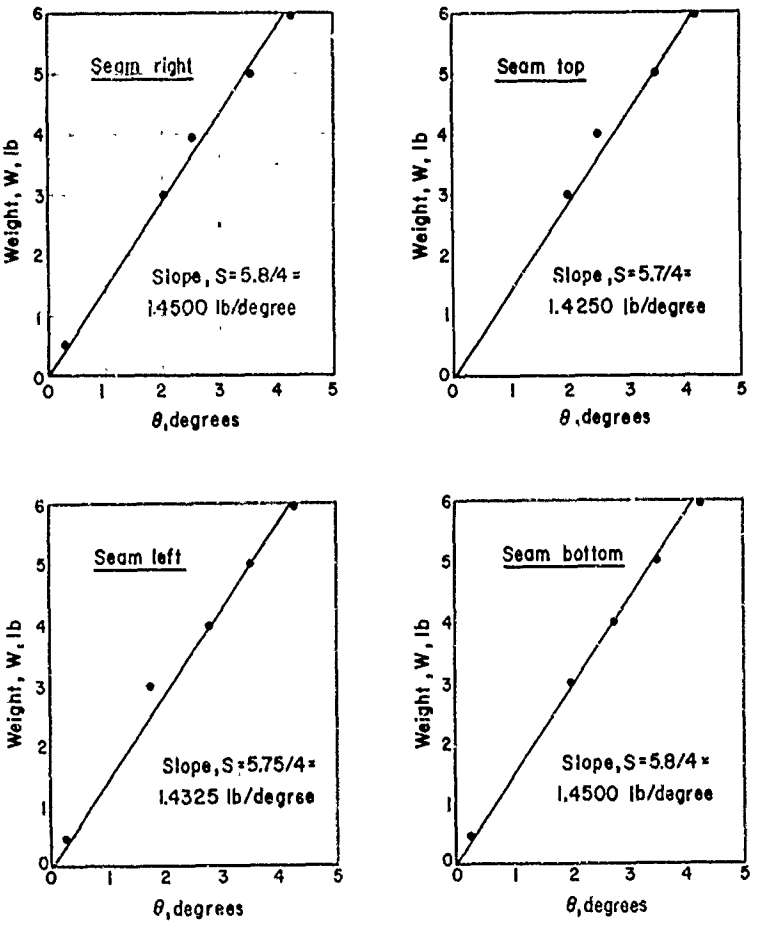

FIGURE J-2. EXPERIMENTAL DATA ON BENDING OF 5-INCH BELLOWS, JD90

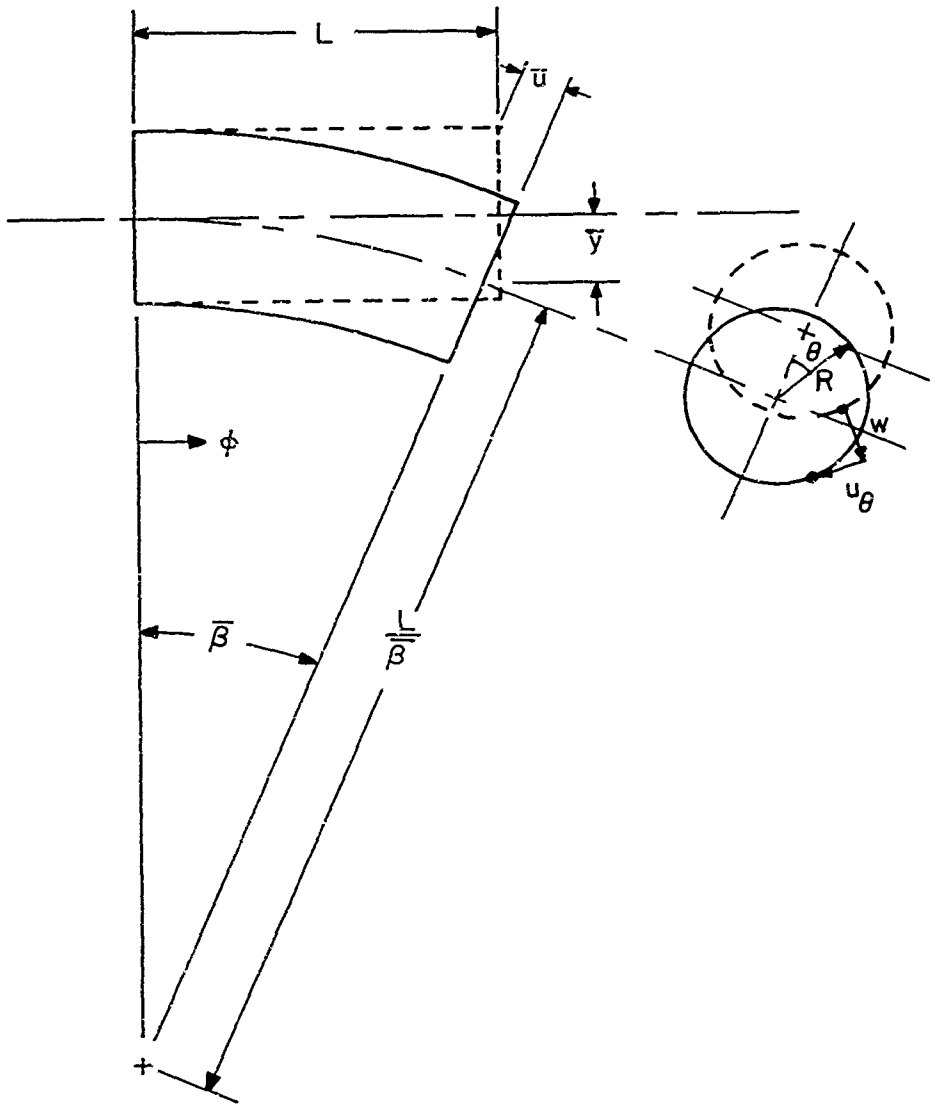

FIGURE J-3. PURE ROTATION OF BELLOWS AND RESULTING DISPLACEMENTS USED FOR THEORETICAL DETERMINATION OF BENDING STIFFNESS

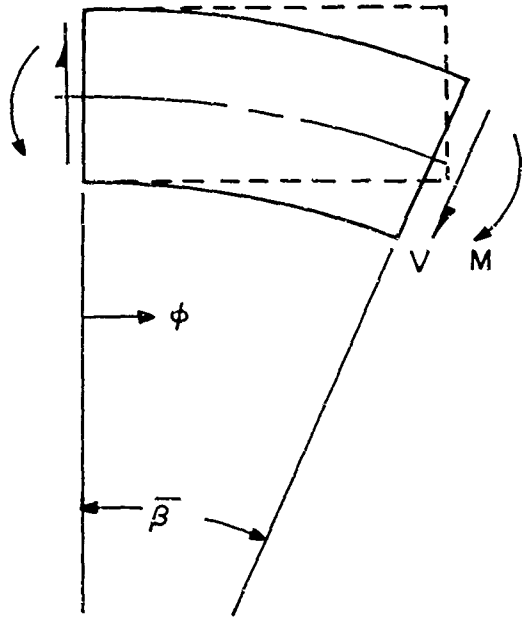

FIGURE J-4. RESULTANT SHEAR V AND MOMENT M ON A BELLOWS SUBJECTED TO A PURE ROTATION $\bar{\beta}$

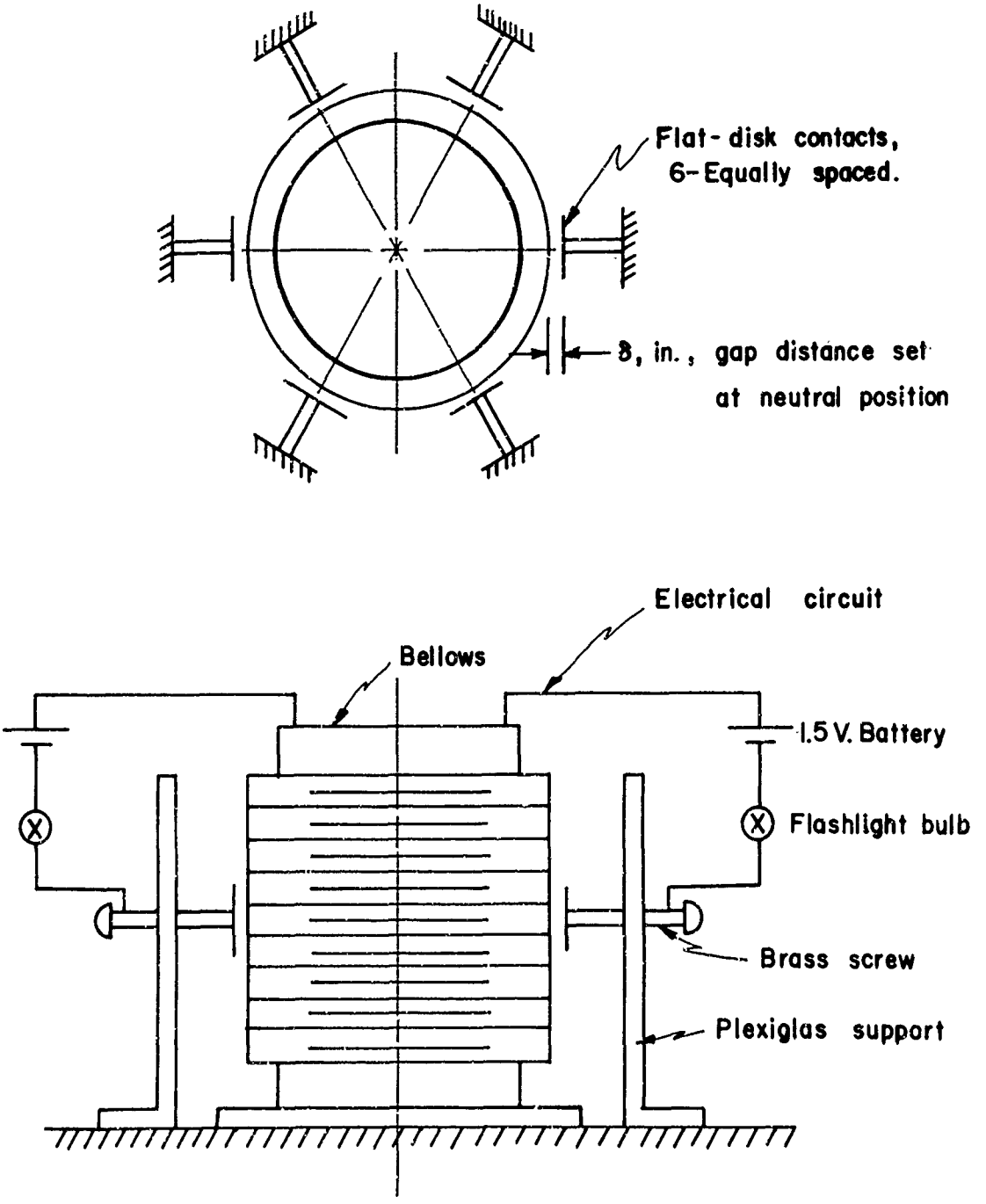

FIGURE J-5. SCHEMATIC OF EQUIPMENT FOR BUCKLING EXPERIMENTS ON FORMED BELLOWS

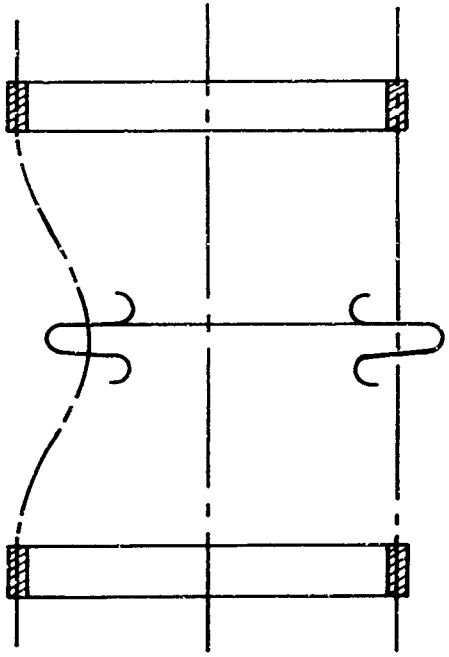

FIGURE J-6. ATYPICAL BUCKLING MODE OBSERVED ON 1-INCH BELLOWS JD23

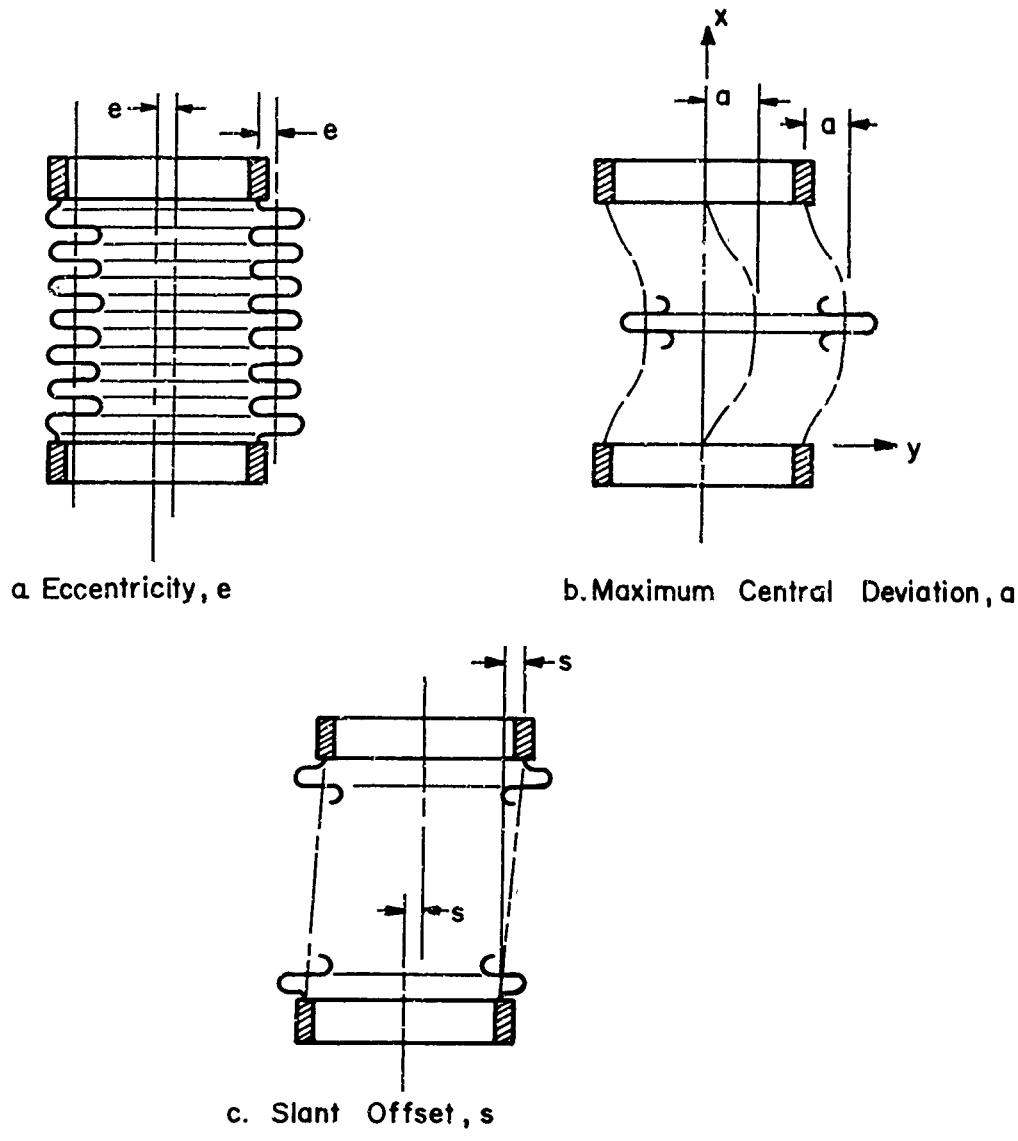

FIGURE J-7. IMPERFECTION MEASUREMENT ON BELLOWS

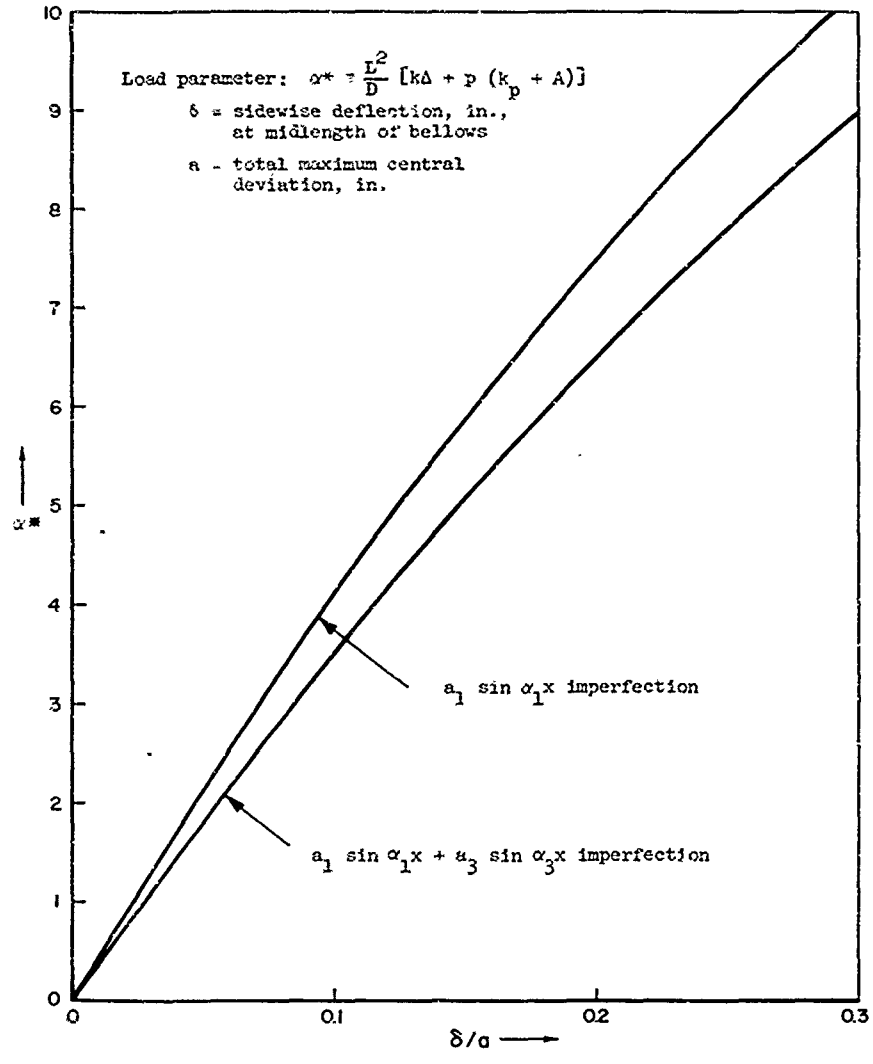

FIGURE J-8. THEORETICAL BEAM-COLUMN BUCKLING OF CLAMPED BELLOWS-EFFECT OF IMPERFECTIONS

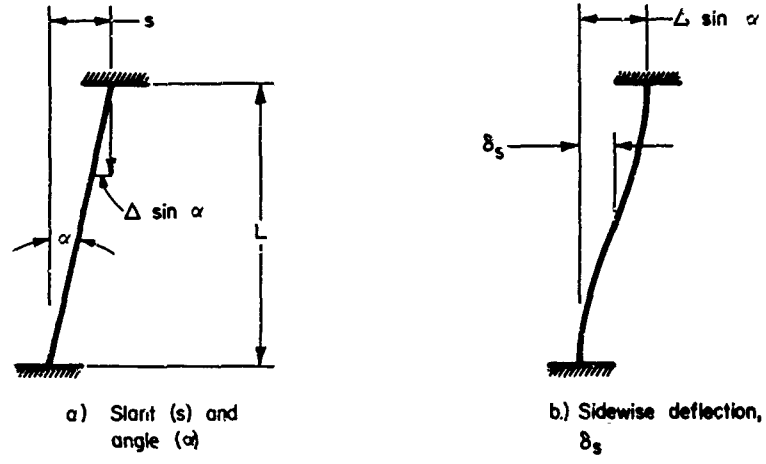

a) Slant (s) and angle (α)

b.) Sidewise deflection, δ_s

FIGURE J-9. SIDEWISE DEFLECTION δ_s CAUSED BY SLANT (s) IN COMBINATION WITH COMPRESSION Δ

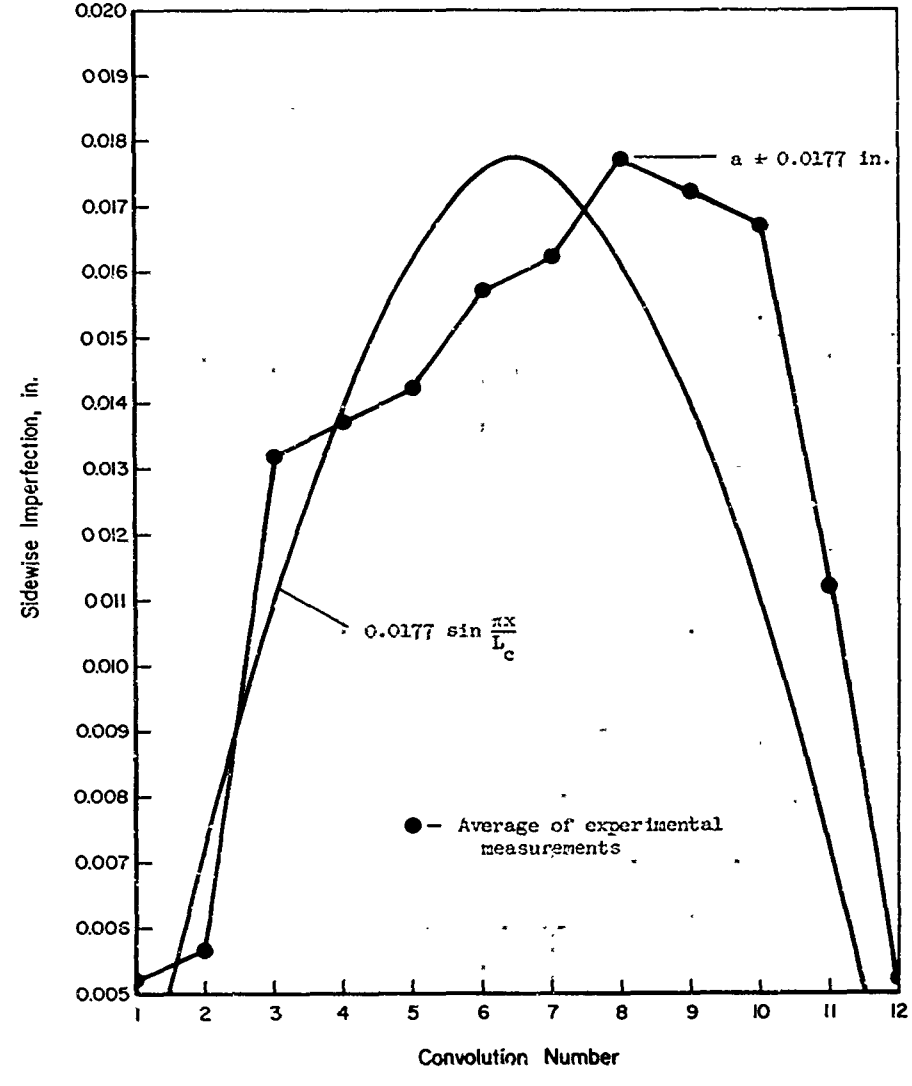

FIGURE J-10. SIDEWISE IMPERFECTION OF BELLOWS JD95

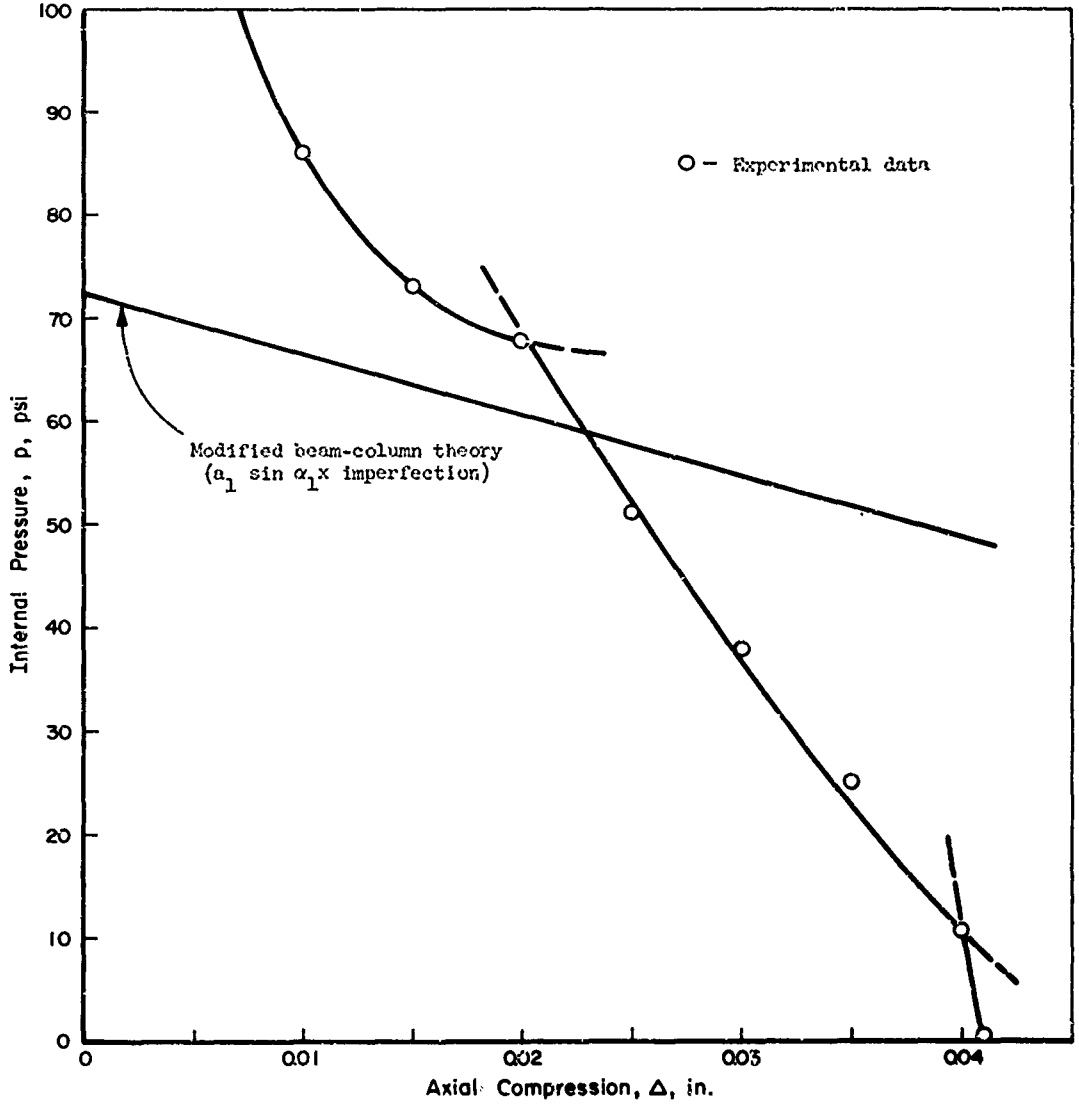

FIGURE J-11. EXPERIMENTAL AND THEORETICAL BUCKLING OF 1-INCH BELLOWS JD27

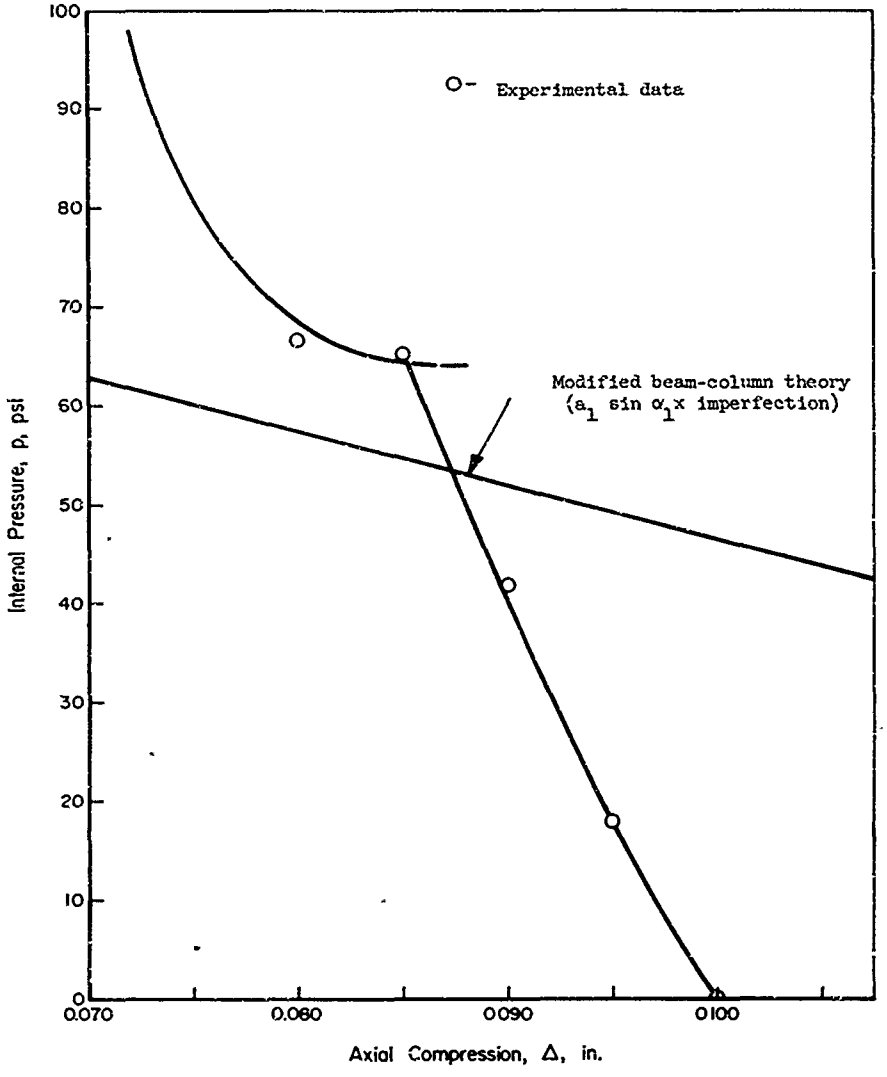

FIGURE J-12. EXPERIMENTAL AND THEORETICAL BUCKLING OF 1-INCH BELLOWS JD111

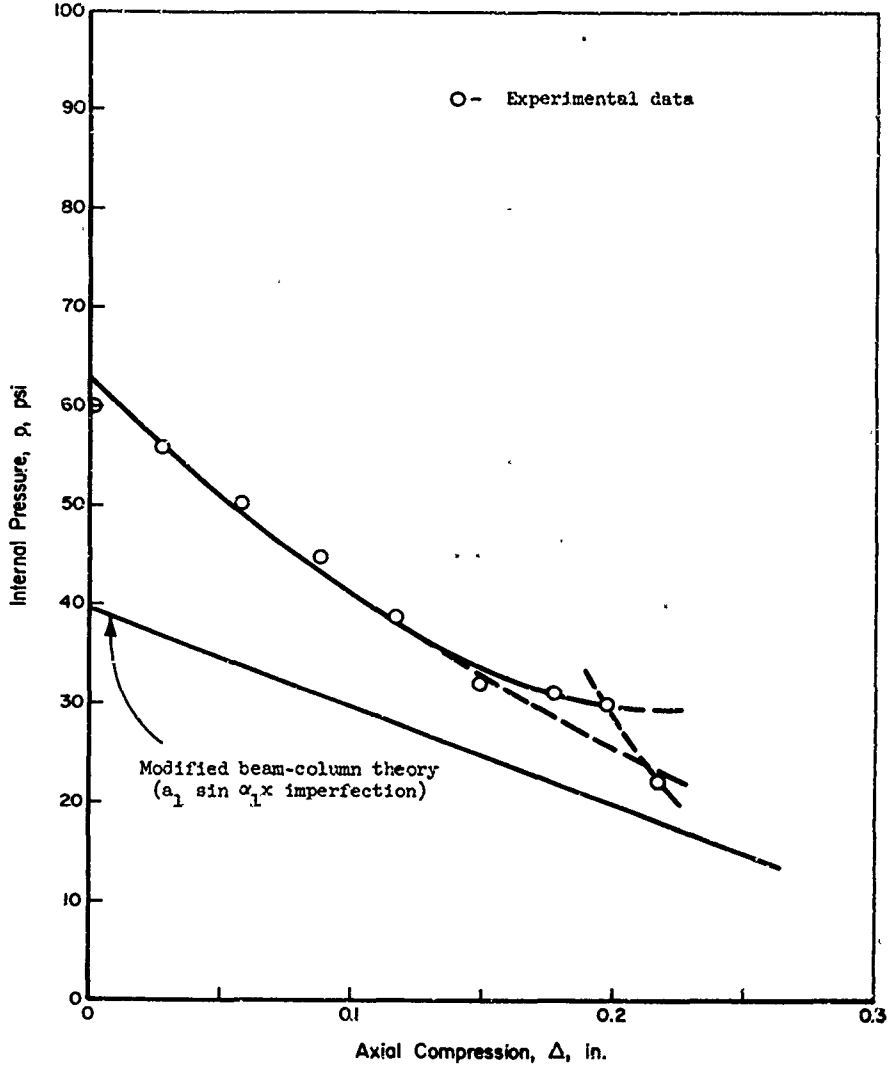

FIGURE J-13. EXPERIMENTAL AND THEORETICAL BUCKLING OF 3-INCH BELLOWS JD62

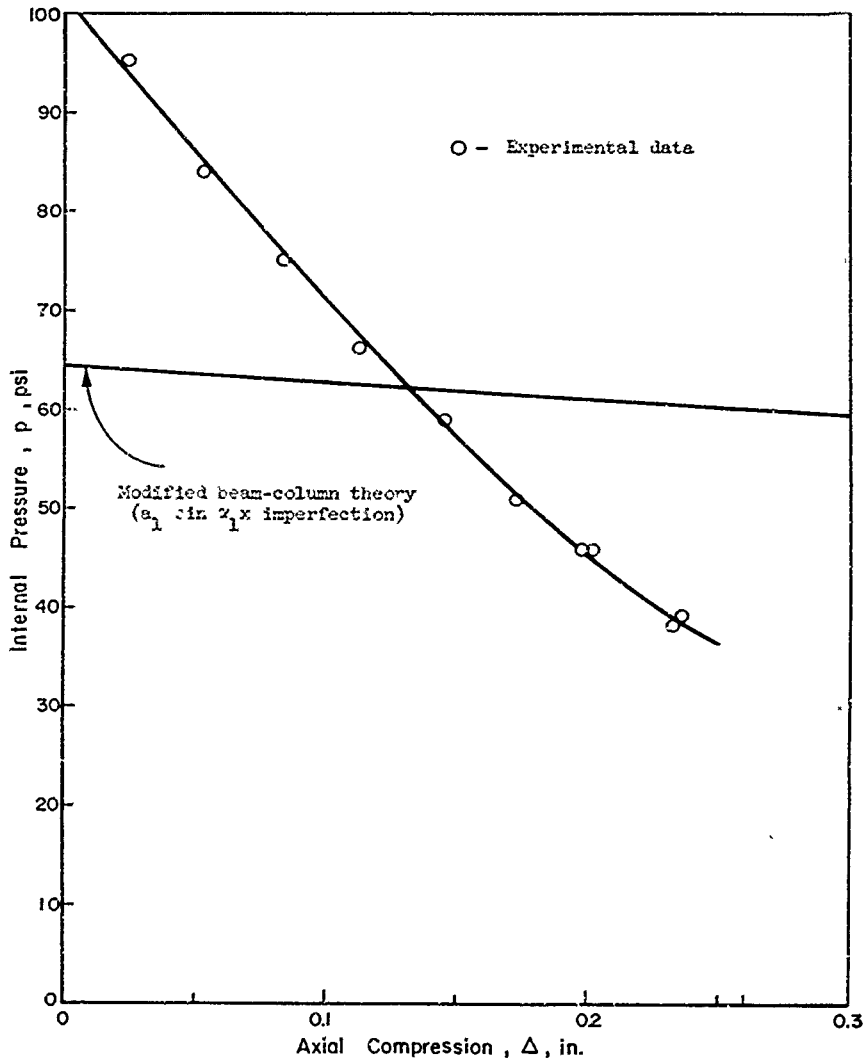

FIGURE J-14. EXPERIMENTAL AND THEORETICAL BUCKLING OF 3-INCH BELLOWS JD64

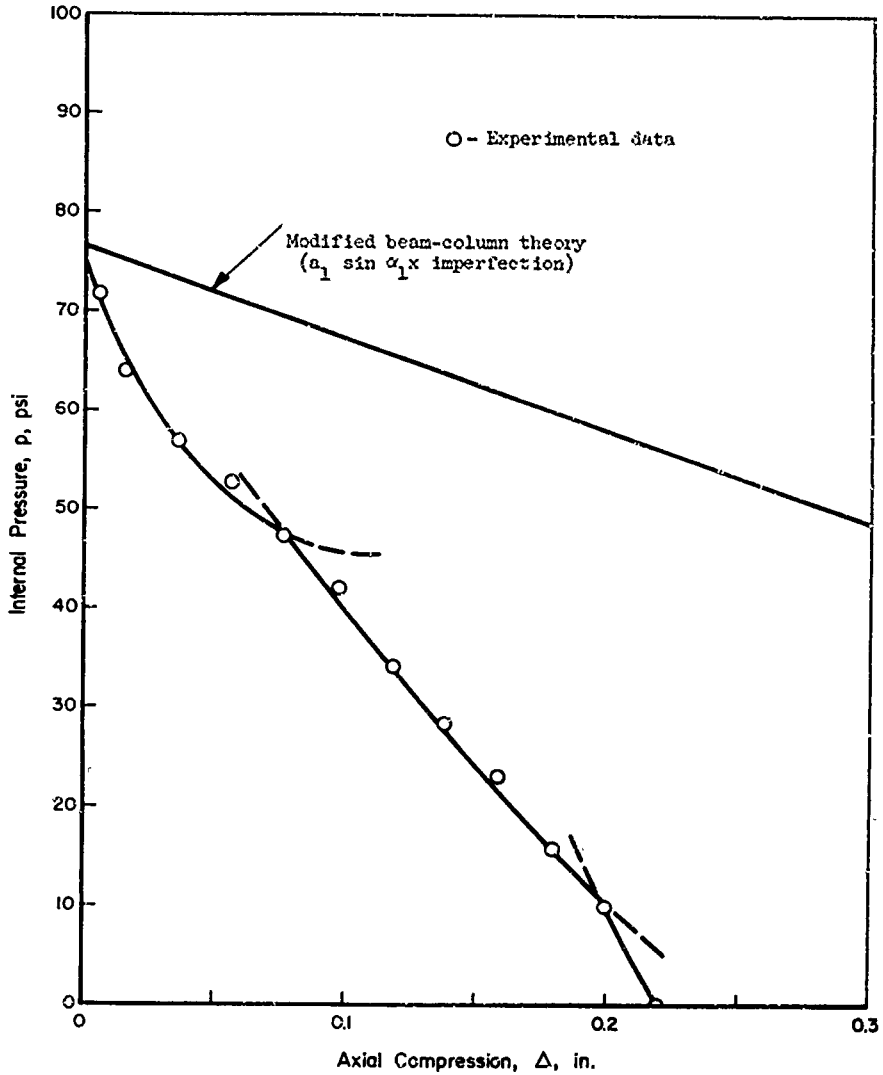

FIGURE J-15. EXPERIMENTAL AND THEORETICAL BUCKLING OF 3-INCH BELLOWS JD126

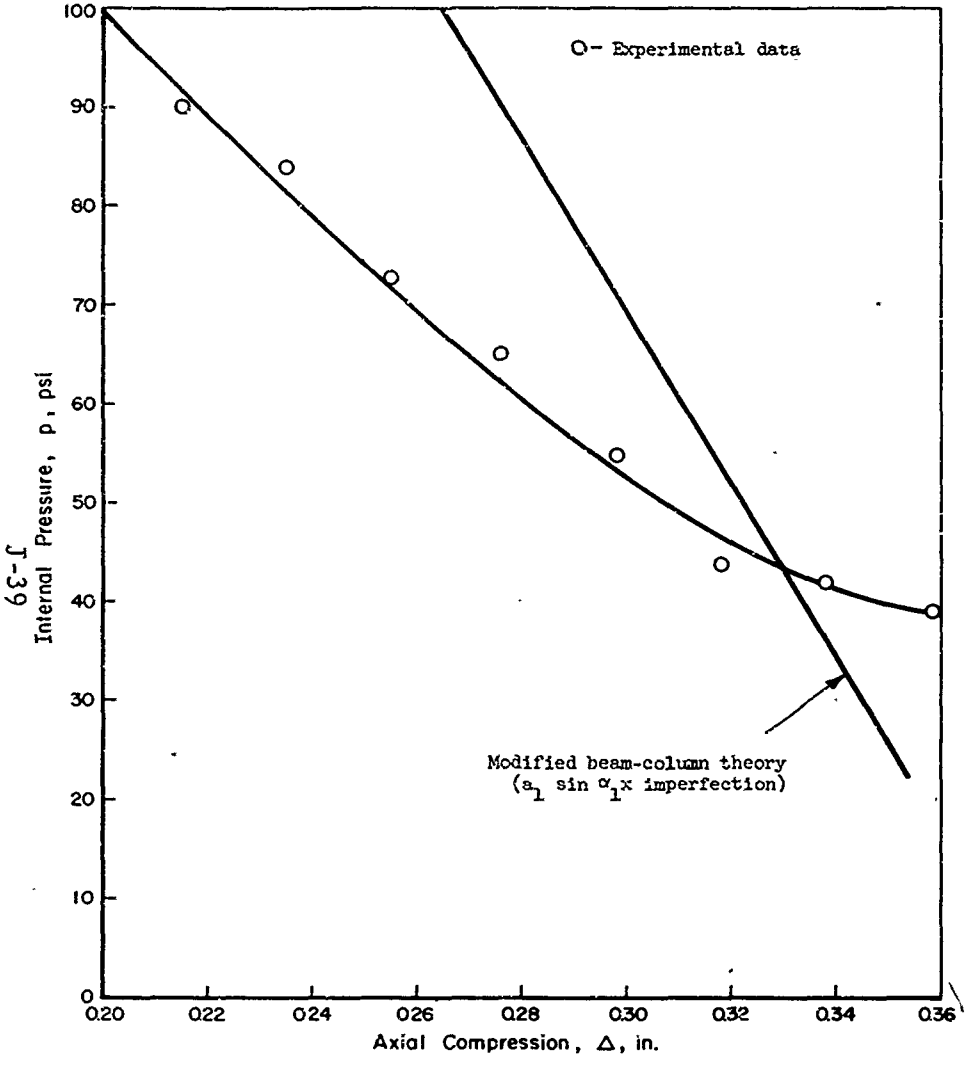

FIGURE J-16. EXPERIMENTAL AND THEORETICAL BUCKLING OF 3-INCH BELLOWS JD74

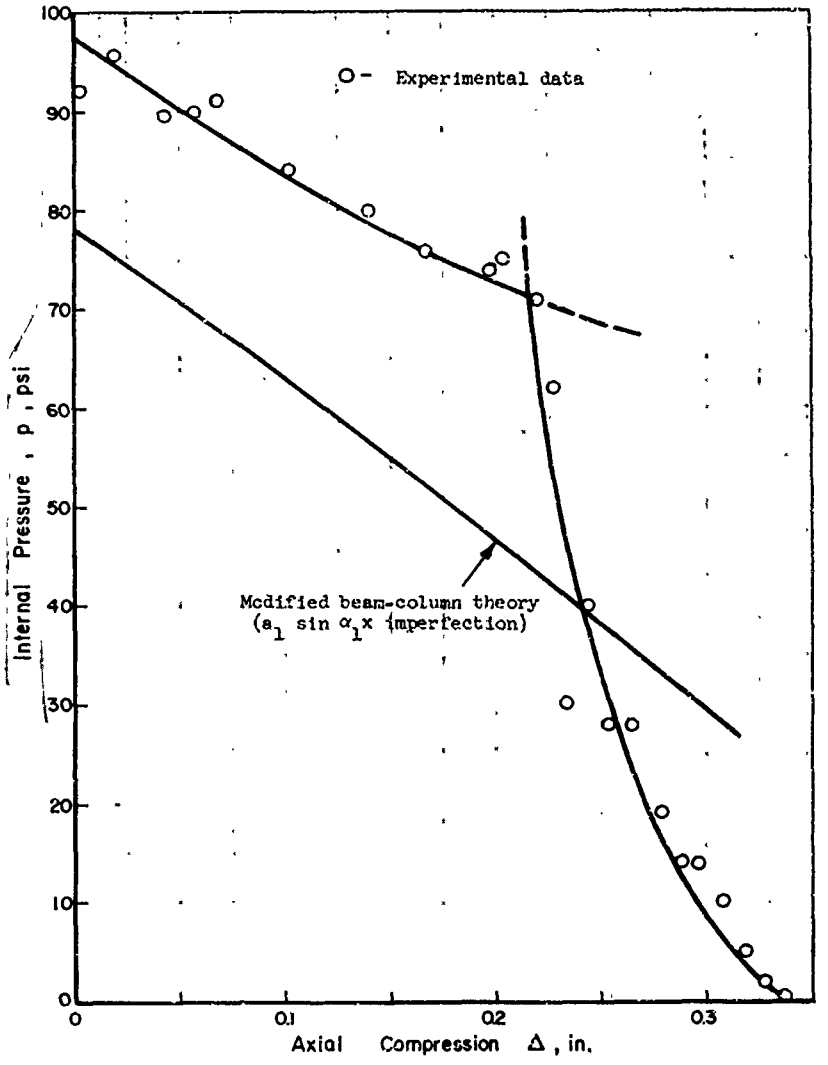

FIGURE J-17. EXPERIMENTAL AND THEORETICAL BUCKLING OF 5-INCH BELLOWS JD95

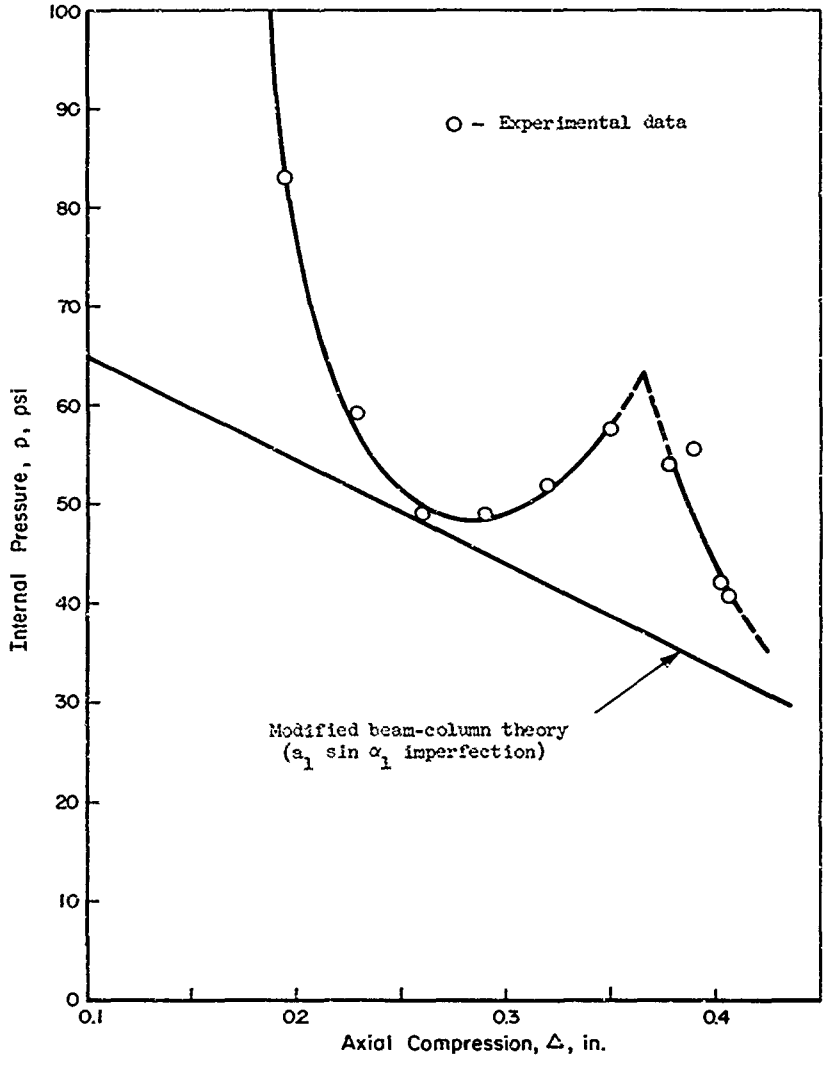

FIGURE J-18. EXPERIMENTAL AND THEORETICAL BUCKLING OF 5-INCH BELLOWS JD96

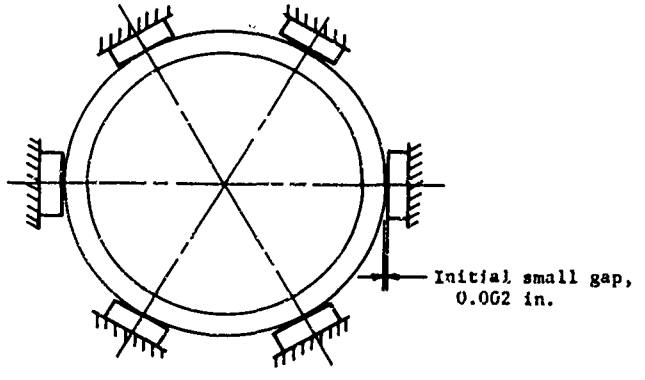

FIGURE J-19. SCHEMATIC OF SETUP OF BELLOWS JD90 AND JD96 FOR INTERNAL PRESSURE-COLLAPSE EXPERIMENTS

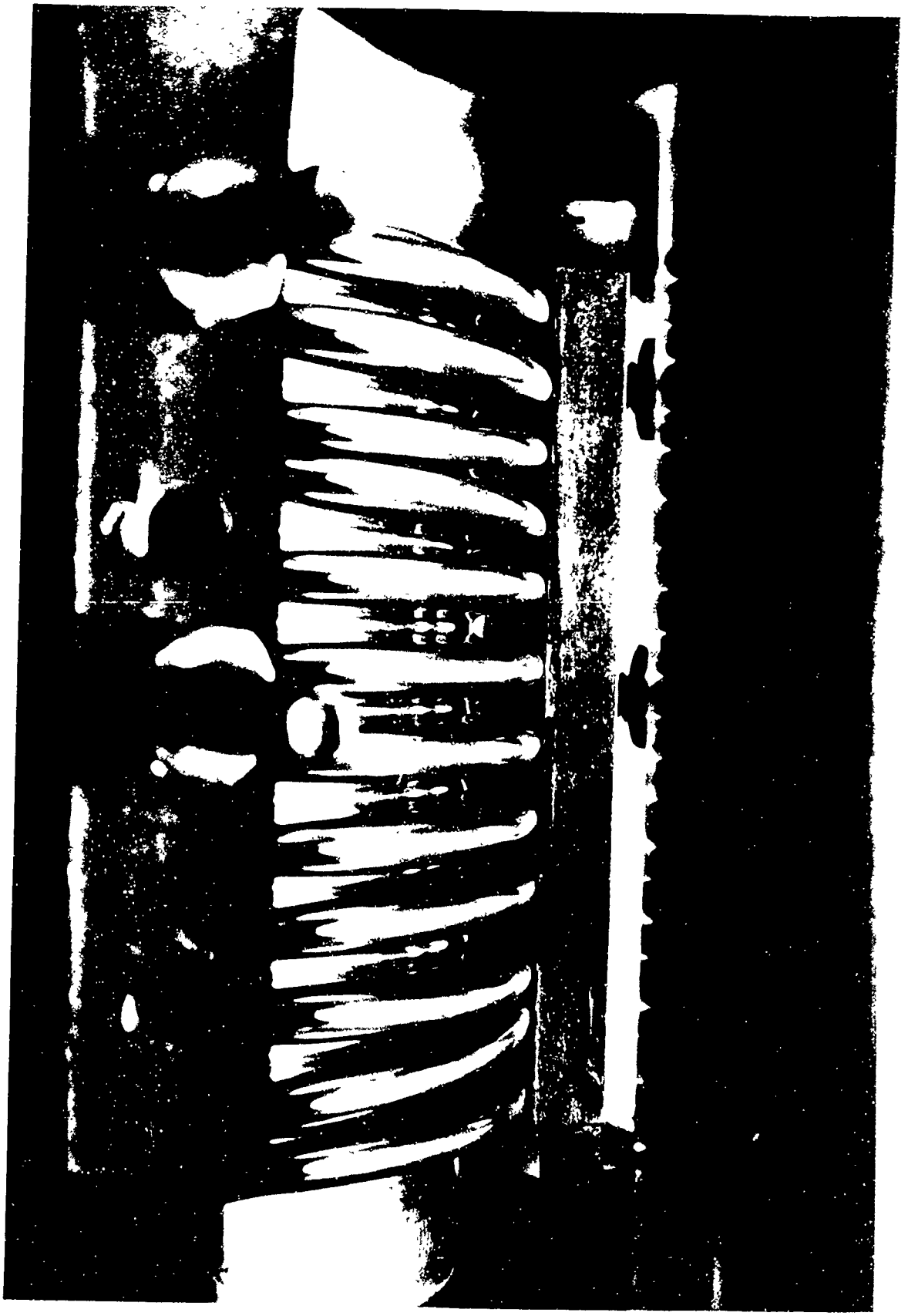

N35236

FIGURE I-20. PHOTOGRAPH OF BELLOWS JD96
AT 250 PSI INTERNAL PRESSURE

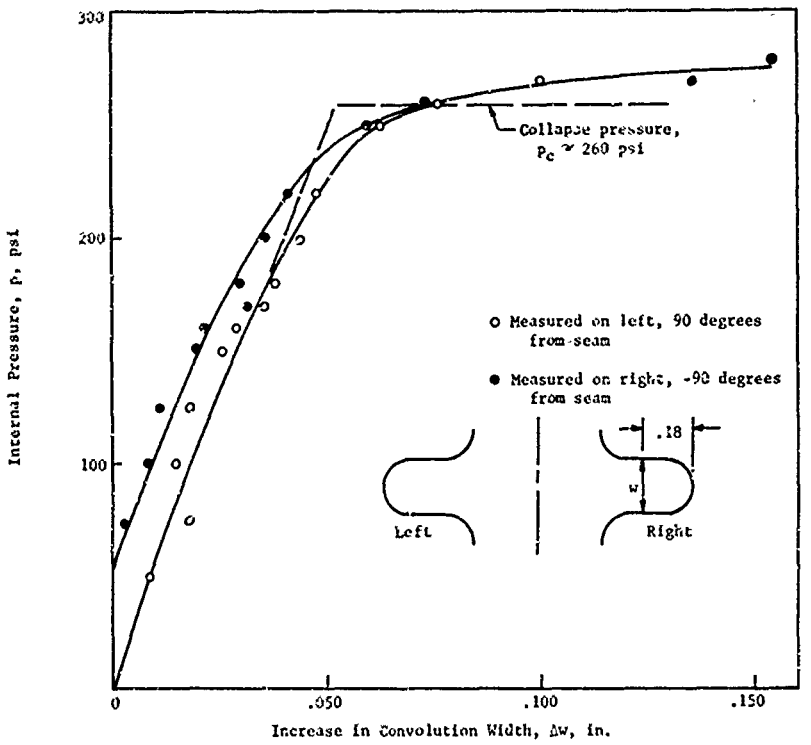

FIGURE J-21. EXPERIMENTAL PRESSURE-DEFLECTION CURVE FOR COLLAPSE OF 5-INCH BELLOWS JD96

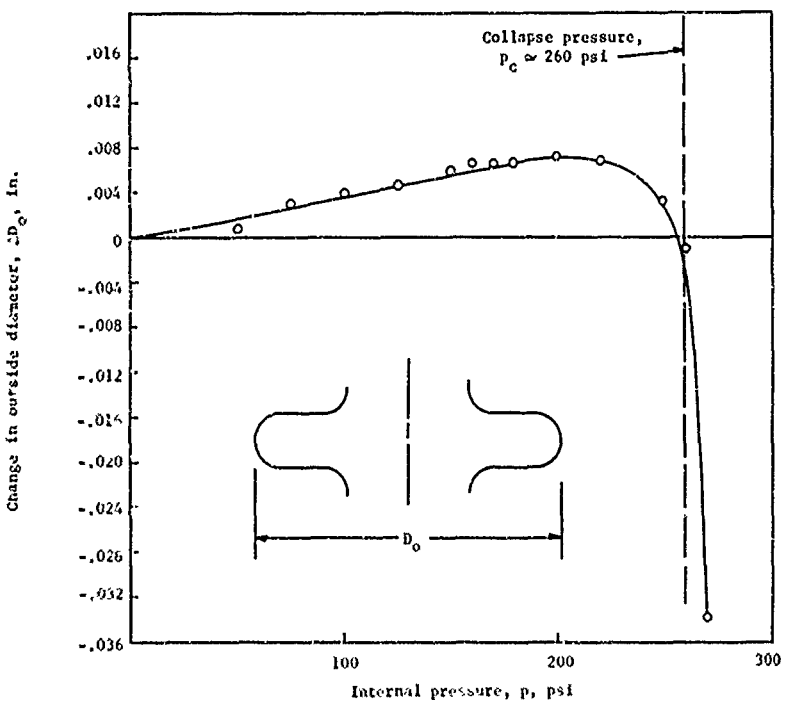

FIGURE J-22. EXPERIMENTAL DIAMETER CHANGE-PRESSURE CURVE FOR COLLAPSE OF BELLOWS JD96

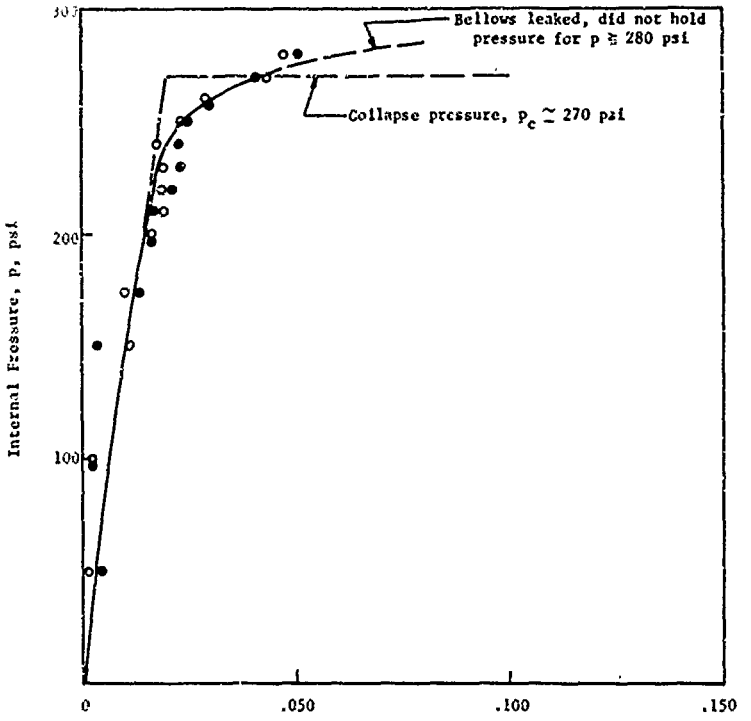

FIGURE J-23. EXPERIMENTAL PRESSURE-DEFLECTION CURVE FOR COLLAPSE OF 5-INCH BELLOWS JD90

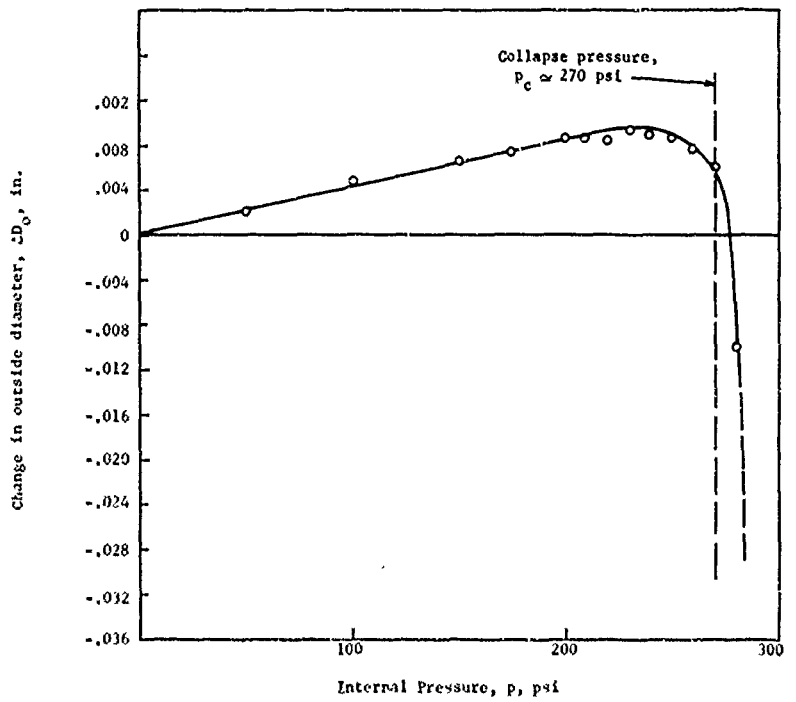

FIGURE J-24. EXPERIMENTAL DIAMETER CHANGE-PRESSURE CURVE FOR COLLAPSE OF 5-INCH BELLOWS JD90

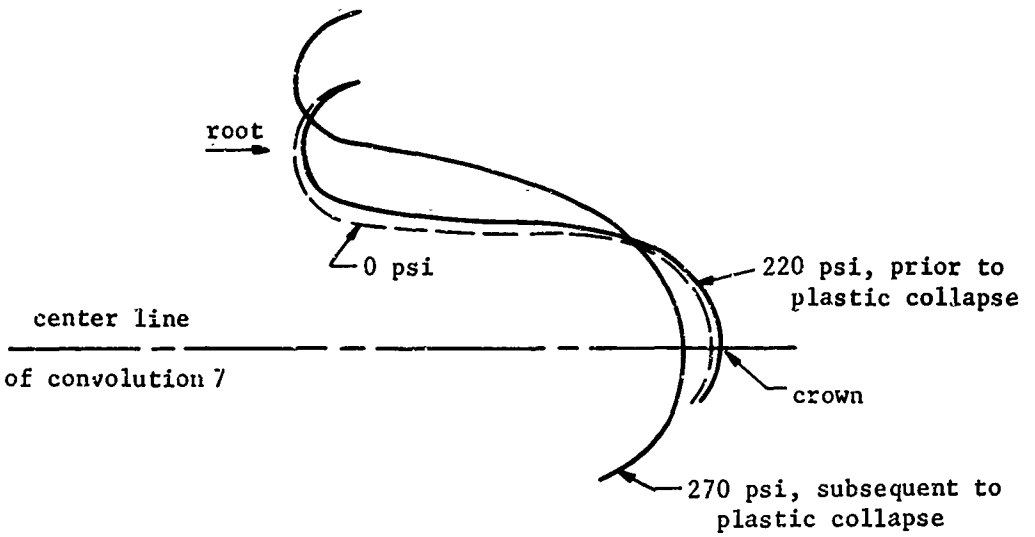

FIGURE J-25. DEFORMATION OF BELLOWS JD96 PRIOR TO AND SUBSEQUENT TO PLASTIC COLLAPSE

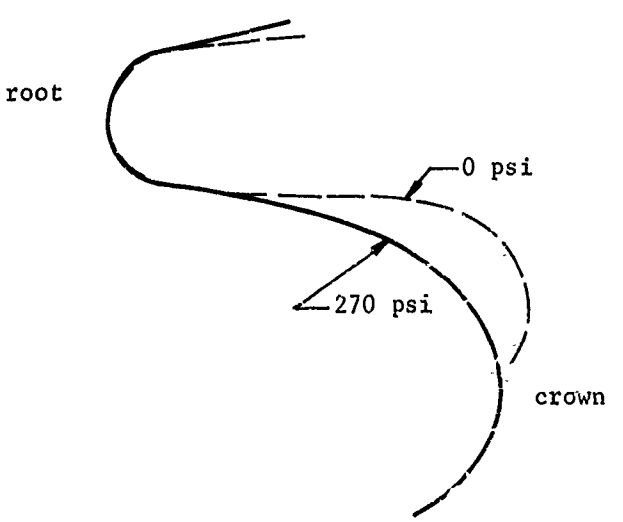

FIGURE J-26. TRANSLATION OF 270 PSI DEFORMATION CURVE TO THE ZERO-PSI REFERENCE SO THAT ROOTS COINCIDE

N35223

FIGURE J-27. PERMANENT DEFORMATION OF BELLOWS JD96 AFTER REMOVAL OF RESTRAINTS AT 270 PSI, SIDEWISE BUCKLING, AND THEN RELEASE OF PRESSURE

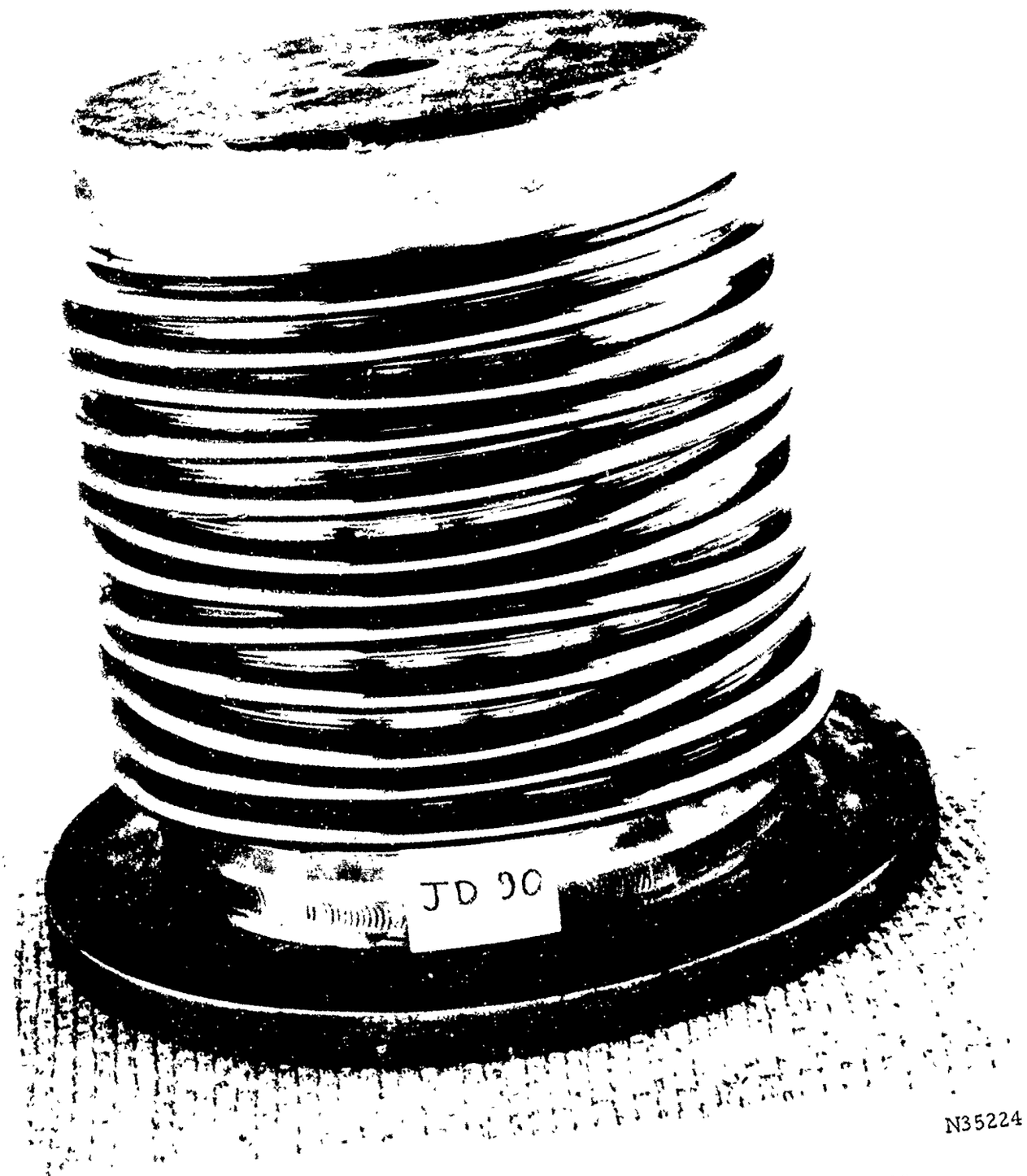

FIGURE J-28. PERMANENT DEFORMATION OF BELLOWS JD90 AFTER INTERNAL PRESSURE COLLAPSE

APPENDIX K

LOW-CYCLE FATIGUE AND FATIGUE-LIFE PREDICTION

ABBREVIATIONS AND SYMBOLS

$\Delta\epsilon_t$ Total strain range

$\Delta\epsilon_p$ Range of plastic strain

$\Delta\epsilon_e$ Range of elastic strain

N Total cycles of fatigue life

APPENDIX K

LOW-CYCLE FATIGUE AND FATIGUE-LIFE PREDICTION

Until 30 or 40 years ago, design to prevent the fatigue failure of structural parts was generally based upon stresses so low that the material would not fail in millions of stress repetitions. Stress ranges were kept below the fatigue limit (then called the endurance limit) of the material. In more recent years – particularly in the aircraft industry – to avoid weight penalties of possible overdesign, it has been recognized that higher stress ranges can be allowed in parts that must withstand only a finite number of stress repetitions. In some instances, the required number of loadings the part must withstand may be very small, and design is said to be concerned with "low-cycle" fatigue. There is no sharp dividing line between low-cycle fatigue and long-life fatigue upon which experts agree. In this report, the term "low-cycle fatigue" is used for the range of lifetimes (5,000 to 50,000 cycles) of interest to the bellows and diaphragm program.

While there have been many approaches to seeking a basic mechanism (or basic mechanisms) for the development of fatigue cracking, present understanding remains uncertain. Knowledge applicable to engineering design comes primarily from empirical formulations based upon laboratory tests of material specimens. A brief review of some of this work is given to provide a framework for considering the fatigue behavior that might be expected in bellows and diaphragms submitted to cycling deformations due to varying deflection and/or pressure.

Methods of Correlating Low-Cycle-Fatigue Data

Suppose a metal specimen is cycled between two values of total uniaxial strain so that the material traces, after the first quarter-cycle loading, the hysteresis loop ABCDA in the stress-strain diagram of Figure K-1. If the stress-strain cycle is known, the loading may be characterized by any one of the three parameters:

$\Delta\epsilon_t$ = total strain range

$\Delta\epsilon_p$ = range of plastic strain

$\Delta\epsilon_e$ = range of elastic strain.

It has been found in laboratory tests(K-1, K-2)* that material fatigue behavior can be described, with one provision: the stress-strain curve under cyclic loading may vary in the first few cycles before settling down to a "saturation" curve which may be higher (for strain-hardening materials) or lower (for strain-softening materials) than that obtained in a monotonic loading. Figure K-2 illustrates behavior observed for a strain-hardening material (Inconel 713C-LC).

A fatigue test may be run by subjecting specimens to various ranges of total strain and recording the corresponding lifetimes to fracture. The results may be plotted in

References for Appendix K are listed on p K-6.

terms of the logarithm of $\Delta\epsilon_t$ or of $\Delta\epsilon_p$ or of $\Delta\epsilon_e$ against the logarithm of lifetime. This is illustrated in Figure K-3, where the strain values were determined from a cyclic stress-strain curve taken at about half the lifetime to fracture. Note that the curve ln $\Delta\epsilon_p$ vs. ln N is approximately a straight line with a slope about -1/2; the curve for ln $\Delta\epsilon_e$ vs. ln N is also a straight line with a much lower (negative) slope. Thus it appears that, to a good approximation,

$$N = A\,(\Delta\epsilon_p)^{-m} = B\,(\Delta\epsilon_e)^{-n} \quad ,$$

where A, B, m, and n can be considered material parameters.

Since $\Delta\epsilon_t = \Delta\epsilon_p + \Delta\epsilon_e$, the curve for ln $\Delta\epsilon_t$ vs. ln N will be asymptotic to that for ln $\Delta\epsilon_p$ vs. N at low values of N and to that for ln $\Delta\epsilon_e$ vs. ln N at large values of N.

The behavior illustrated in Figure K-3 is characteristic of materials commonly used in bellows and diaphragms. Note that, in the range of lifetimes (5000 to 50,000 cycles) of interest in this study, values of $\Delta\epsilon_p$ and $\Delta\epsilon_e$ are of about the same order of magnitude, so that neither can, in general, be neglected with respect to the other. For this reason, as well as because measurements (for example, with bonded electric strain gages) give values of total strain, it is convenient to use values of ln $\Delta\epsilon_t$ vs. ln N to correlate fatigue data for bellows and diaphragms.

Differences Between Strains in Material Specimens and Strains in Bellows and Diaphragms

Material data such as those illustrated in Figure K-3 are usually obtained under controlled and intentionally simplified conditions, while material at critical locations in a bellows or diaphragm may be under complex conditions. Some of the differences in conditions are:

	Material Specimen	Material at Critical Location in Bellows or Diaphragm
(1)	Uniaxial stress and strain	Biaxial stress and strain
(2)	Fully reversed strain	Possible significant mean strain
(3)	Constant strain range	Local strain range possibly changing
(4)	No strain concentration	Strain concentration
(5)	Failure criterion – rupture	Failure criterion – cracking.

Other complications exist in the bellows or diaphragm: the initial condition of material in regard to such items as residual stresses and local strain hardening from forming is seldom accurately known, the local strains and strain ranges can be estimated (by elastic theory) but evaluated only approximately in regard to plastic components, etc. Such factors mean that identification of bellows or diaphragm fatigue behavior with material fatigue data requires careful consideration and cannot be expected to be quantitatively precise.

The best present engineering practice in estimating fatigue life of bellows or diaphragms seems to be: (1) use material information (such as Figure K-3) as a guide, (2) consider, at least qualitatively, such items as are listed above to minimize bellows or diaphragm fatigue testing, and (3) depend upon fatigue tests of coupons of similar material for approximate life prediction, but (4) utilize test data from similar bellows or diaphragms to verify or adjust the prediction.

With regard to this general approach, the five strain-condition differences listed above are discussed briefly. [For more extensive discussion of some of these items, see Reference (K-2)]

Uniaxial vs. Biaxial Stresses and Strains

Data on the relation of fatigue behavior under biaxial stress to fatigue behavior under uniaxial stress are not yet extensive in the range of low-to-intermediate cycle fatigue, and there is no universal agreement concerning engineering design rules. However, the principal stress or strain range has a dominant effect on fatigue life, and a simple approach is to interpret results in terms of the largest principal strain range.

Variations in Mean Strain

There are few data concerning the effect of mean strain on the strain range that can be endured without failure in the range of lifetimes from 5000 to 100,000 cycles, particularly for the materials and the loading conditions pertinent to bellows and diaphragms. Figure K-4 shows some results obtained in constant-stress-amplitude fatigue tests on an aluminum alloy that may be indicative of the general behavior of metal alloys. In these tests, the stress range endured for a specified lifetime decreased with increasing mean tensile stress. Particularly for long lifetimes and relatively low mean stresses, the rate of decrease is less than indicated by a linear approximation which, in the absence of experimental data, is often used as an engineering guide. A few experiments [see, for example, Reference (3)] have shown a decrease in the range of plastic strain endurable for a specified lifetime with increase in mean tensile strain in constant-strain-amplitude fatigue tests.

Although there are few data on thin materials in the lifetime range from 5000 to 100,000 cycles under such conditions as constant-strain-amplitude tests with parametric variation of mean strain, it can be inferred, from the type of information described above, that increased mean strain in a bellows material would decrease the strain range allowable for a lifetime of concern in this study. The amount of decrease cannot be estimated with accuracy, but it may be small for low mean strains.

Possible Changes in Local Strain Range

Related to the possible effect of mean strain upon the fatigue lifetime of a bellows is the question of the actual strain history at the critical location where a crack may ultimately occur. Figure K-5 illustrates two possibilities of local behavior of material (for example, at a convolution root in a formed bellows) when the bellows is deflected from an initial condition considered as having zero stress and strain to some deflection involving a high local strain in tension, and then this deflection range is repeated. In Figure K-5a it is supposed that, after the first loading, the material returns to zero

stress, but, because the local stress at maximum deflection exceeded the elastic limit, not to zero strain. Such behavior is generally unlikely if the bulk of the bellows material stays within the elastic limit because the elastic surrounding material will force the small region that has undergone plastic deformation back toward zero strain (and a compressive residual stress), as indicated in Figure K-5b. This behavior of the local region may be called "elastically controlled". Note that, in the first case, both the strain range and the mean strain after the first quarter cycle are different from values expected if the material all behaved elastically. In the second case, the mean strain is decreased, but the strain range is the same as if all the material behaved elastically.

The actual behavior at a critical location in a bellows cannot be evaluated with certainty except by an analytical elastic-plastic solution, which is beyond the present state of the art, or by local strain measurements. These are difficult and are not feasible for some high-strain locations. However, it may be expected that a close approximation can be obtained by assuming elastic control when the highly stressed regions are small compared to the bulk of the material, and when the loading is not so high that the bulk of the bellows material behaves inelastically. Then $\Delta\epsilon$ obtained from an elastic calculation may be an approximation to that existing in the critical highly stressed regions. In some bellows it is feasible to examine the validity of this procedure by using very small strain gages at locations considered critical. (Such an investigation is described in Appendix L.)

Strain Concentration

The use of a detailed theoretical calculation may circumvent the strain-amplification consideration at some locations, such as the roots and crowns of formed bellows. However, there remains a question as to the effect on fatigue life of a very high strain gradient such as may occur at the juncture of the diaphragms in the weld bead of a welded bellows. At present, the quantitative effect of such configurations can only be checked experimentally.

Failure Criterion

The failure criterion in laboratory tests of materials is commonly complete rupture of the specimen. In tests of bellows, the criterion may be a small leak or a tiny crack. In general, this difference in failure criteria will make the observed bellows fatigue life shorter than that of otherwise corresponding material coupons, although the difference may not be large.

Investigation of the Fatigue Life of Bellows and Diaphragms

Based on the preceding information, it appeared that a reasonable procedure for investigating the fatigue behavior of bellows was as follows:

(1) The tests were to be run in terms of total strain range as calculated by elastic theory.

(2) It was anticipated that the calculated strain range would, on account of "elastic control", approximate the range of local strains. This approximation was expected to be quite good for relatively low strains (and long lifetimes) and possibly less good at high strains (and very short lifetimes). The approximation was to be examined to some extent by the use of small strain gages.

(3) A number of items made it likely that bellows lifetime on this basis would be somewhat less than that of small material specimens. There was, however, expected to be a correlation between the bellows behavior and that of material coupons.

(4) Among parameters expected to have an effect was mean strain, and therefore, the mean deflection and the internal pressure in the bellows tests. The amount of this effect was to be examined by experiment. At least for moderate values of mean strain, the lifetime was expected to be less sensitive to this than to strain range.

Fatigue-Life Prediction

It is well-known that careful laboratory fatigue tests of metal specimens show considerable scatter in lifetime at a selected stress (or strain) level – a range of 7 to 1 is not uncommon for a modest number (say, 15 to 20) of specimens. When a somewhat complex structural part is made out of the same metal, the variance may be less (although the median value is lower) than for carefully polished fatigue specimens. One reason for this is that the structural part has a built-in stress raiser often as high as "random" weak spots in a carefully polished "unnotched" fatigue specimen. In addition, however, the structural part is likely to have variations induced in manufacture, such as stress concentrations, residual stresses, and local spots of strain hardening (or softening). These will increase scatter in fatigue tests of a number of supposedly similar parts. Thus, fatigue tests of fabricated parts may show less scatter than tests of material or more scatter, dependent upon the variations introduced in manufacture.

The statistics of fatigue test results are still being explored.[K-4] Data are still being accumulated and are presently scarce in regard to materials used in bellows, at the lifetimes of interest in this study. Nevertheless, scatter may be anticipated both from material and from fabrication. The amount must be estimated from bellows tests. One important concern is that the minimum value determined in any small number of tests is not completely safe for design use – some kind of safety factor must be applied. For purposes of consistency in deriving tentative design recommendations from the bellows fatigue tests, the scheme illustrated in Figure K-6 may be used. This is to quote a strain range corresponding to the minimum strain range observed at twice the lifetime of interest. This "safety factor" was selected arbitrarily and can be altered when sufficient statistical data are available to define the class of bellows of interest to the designer.

REFERENCES

(K-1) Morrow, JoDean, and Tuller, F. R., "Low Cycle Fatigue of Inconel 713C and Waspaloy", J. Basic Eng., June, 1965, pp 275-289.

(K-2) Manson, S. S., Thermal Stress and Low Cycle Fatigue, McGraw-Hill Book Company, New York (1966).

(K-3) Pian, T. H., and D'Amato, R., "Low Cycle Fatigue of Notched and Unnotched Specimens of 2024 Aluminum Allow Under Axial Loading", WADC Tech Note 58-57 (February, 1958).

(K-4) "A Tentative Guide for Fatigue Testing and the Statistical Analysis of Fatigue Data", ASTM STP 91A (Note: this is currently being revised).

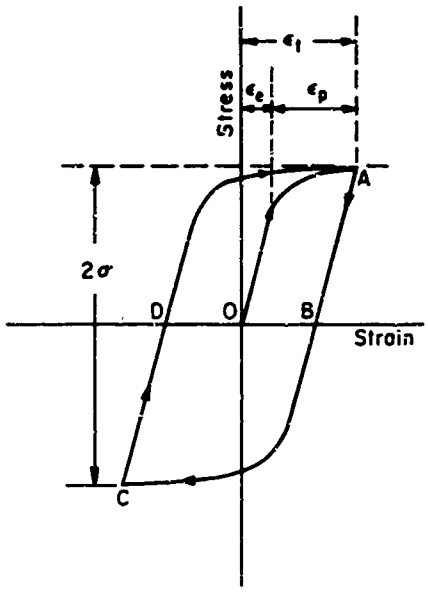

For cycling between $+\epsilon_t$ and $-\epsilon_t$,

$$\Delta\epsilon_t = \Delta\epsilon_p + \Delta\epsilon_e$$
$$= 2\epsilon_p + 2\sigma/E$$

where E = elastic modulus

FIGURE K-1. SCHEMATIC BEHAVIOR OF MATERIAL LOADED WELL BEYOND ITS ELASTIC LIMIT

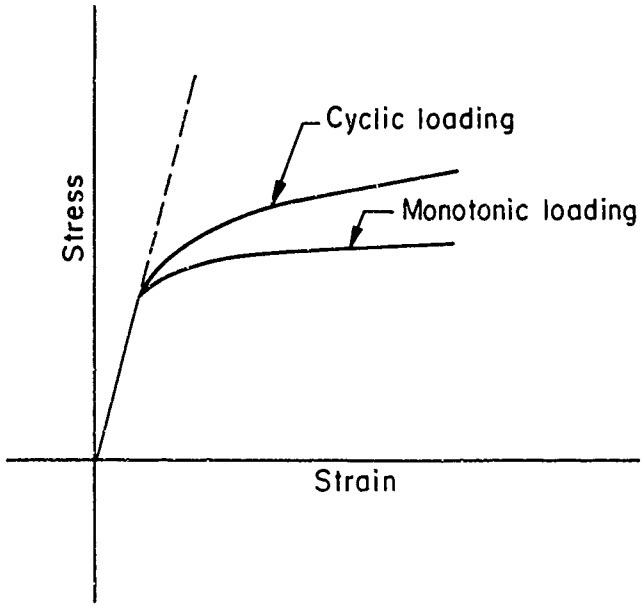

FIGURE K-2. STRESS-STRAIN CURVES FOR A STRAIN-HARDENING MATERIAL

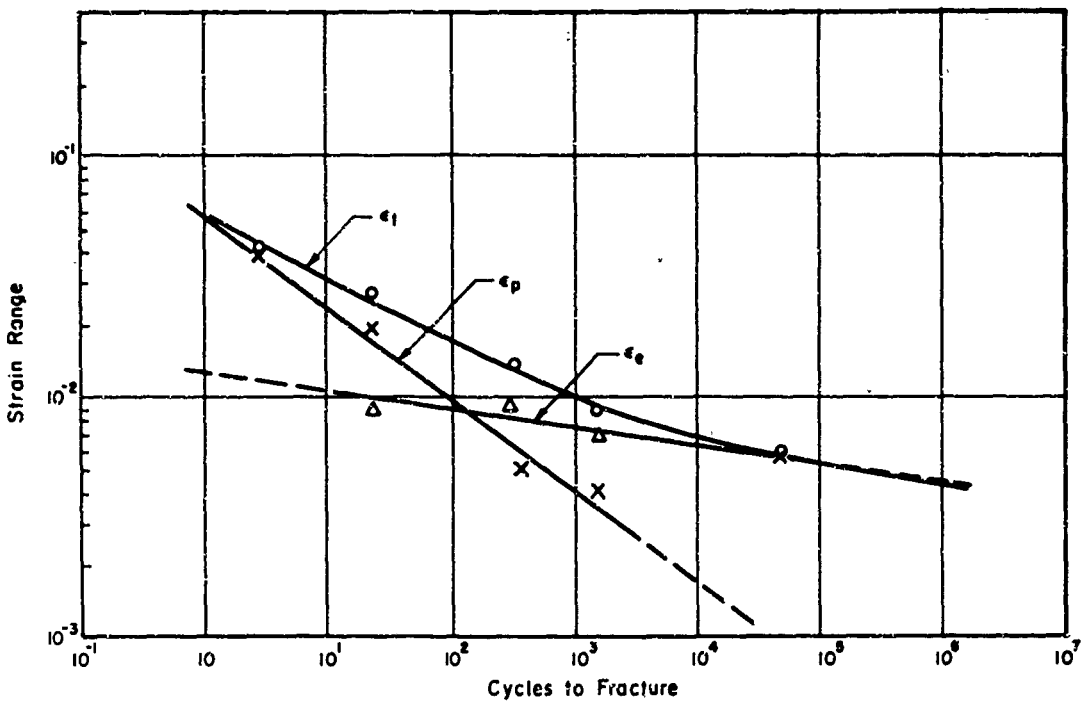

FIGURE K-3. ILLUSTRATION OF DIFFERENT WAYS OF PLOTTING FATIGUE TEST RESULTS

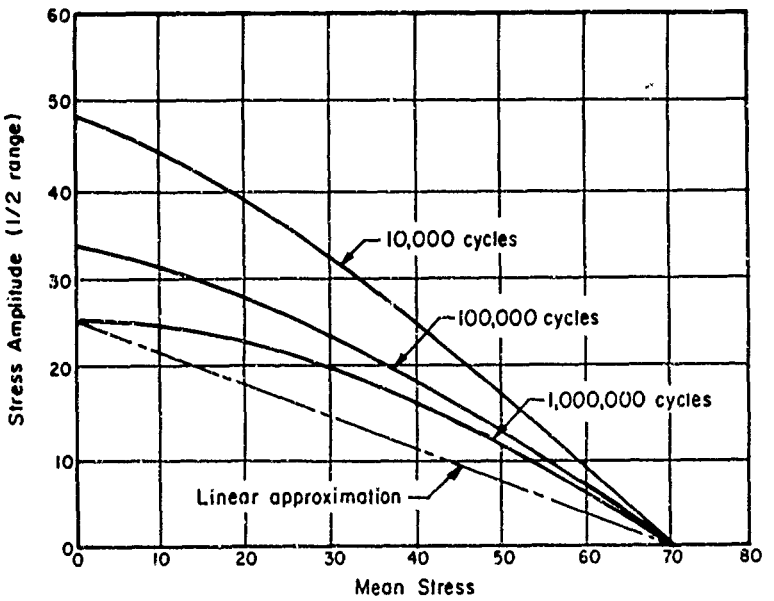

FIGURE K-4. EFFECT OF MEAN STRESS IN STRESS-CONTROLLED FATIGUE TESTS OF A MATERIAL (AN ALUMINUM ALLOY)

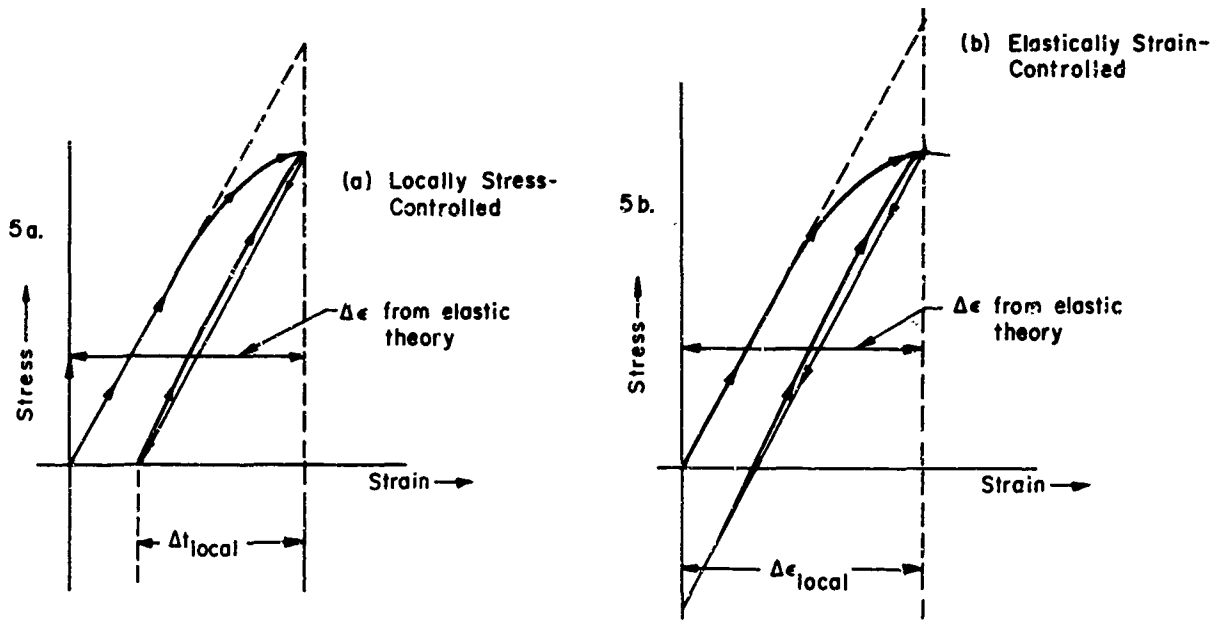

FIGURE K-5. TWO POSSIBLE EXTREMES OF LOCAL STRAIN BEHAVIOR

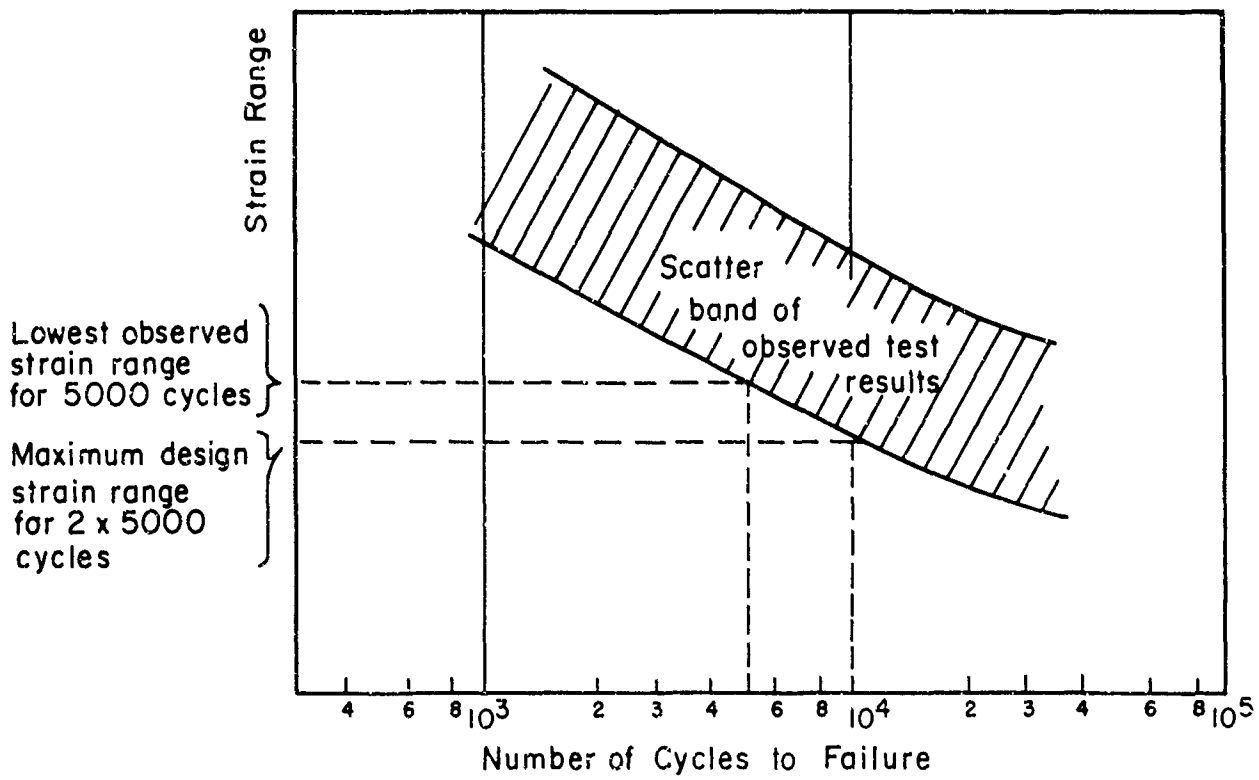

FIGURE K-6. ILLUSTRATION OF ARBITRARY "SAFETY FACTOR" QUOTED FOR BELLOWS

APPENDIX L

FATIGUE ANALYSIS OF FORMED BELLOWS - TYPE 321 STAINLESS STEEL

APPENDIX L

FATIGUE ANALYSIS OF FORMED BELLOWS - TYPE 321 STAINLESS STEEL

As discussed in Appendix K, the decision was made to investigate the usefulness of a selected method for designing bellows and diaphragms to attain a minimum fatigue life. This method is based on the analytical prediction of the operational strain ranges in bellows and diaphragms, and the correlation of the fatigue life of bellows and diaphragms with the fatigue life of metal coupons under equivalent strain ranges.

It was mutually agreed with the Technical Monitor that the bellows and diaphragm applications of interest require a minimum fatigue life of about 20,000 cycles. For some rocket-propulsion components, a minimum fatigue life of 5000 cycles is satisfactory, while for other components a minimum fatigue life of 50,000 cycles is required. Based on these requirements, it was decided that the bellows and diaphragms should be tested at two general strain-range values: (1) a strain range to provide a minimum life of 5000 cycles, and (2) a strain range to provide a minimum life of 50,000 cycles.

An examination of coupon fatigue data for Type 321 stainless steel showed that a strain range of approximately 9000 μin./in. gives an average fatigue life of about 10,000 cycles, and a strain range of approximately 5400 μin./in. gives an average fatigue life of about 50,000 cycles. Based on these data, a strain range of 8000 μin./in. was selected as the initial test value to provide a minimum life of 5000 cycles. Selection of other strain values for the test bellows was based on the results of tests of the first few bellows.

With a strain range of 8000 μin./in., and with an annealed material with an elastic limit equal to a strain amplitude of approximately $\pm$1500 μin./in., a bellows would undergo significant plastic strain. For this condition it was difficult to envision the relation between strain and bellows deflection. Therefore, it was decided that this relationship should be examined before the fatigue tests of the bellows were initiated.

When the initial strain-deflection tests had been conducted, 50 Type 321 stainless steel formed bellows were tested to failure in fatigue under different conditions of deflection and pressure.

Investigation of Large-Strain-Deflection Characteristics in Type 321 Stainless Steel Formed Bellows

A bellows may be compared to several fatigue specimens (one for each convolution) connected in series. With all of the material in the elastic state, the strains could be determined by the elastic stress analysis described in Appendix B. As the material began to yield at the high-stress locations, however, the effect of continued deflection on the various strains in the bellows was not clear. The major questions concerning the partially plastic behavior of a bellows were:

(1) Once yielding started, would continued deflection of the bellows be accommodated for the most part at the yielding locations, or would nonyielding portions continue to show significant increases in strain?

(2) If the bellows were compressed or extended sufficiently to cause local yielding, would the return of the bellows to zero deflection result in zero local strain?

(3) How much difference in local strain range would occur for the same range of deflection obtained by two different loadings, such as zero to compression, and compression to tension?

(4) How closely could a local strain range of 8000 μin. /in., associated with a minimum life of 5000 cycles, be approximated from the elastic theory?

(5) In a bellows undergoing significant yielding, would the strain range at the points of yielding remain constant during successive cycles? Work hardening, for instance, might result in increased resistance to yielding and a change in local strain range.

(6) Would the introduction of significant constant pressure in a bellows alter the relationship between total strain range and cycles to failure because of the resulting change in the mean strain level?

Tests were made with a strain-gaged 5-inch formed bellows to investigate these questions. Figure L-1 shows a cross section of a similar bellows, while Figure L-2 shows an enlarged view of the bellows convolutions. Figure L-3 shows the location of the 1/64-inch strain gages which were used to measure representative meridional and circumferential strains in the bellows.

The tests were conducted in a Baldwin-Lima-Hamilton universal testing machine. Pressures were measured to within ±0.50 percent, while deflections were measured to within ±0.0001 inch. One bellows end fitting was clamped to the bottom platen of the machine. The other end fitting pushed against a steel ball centered in the upper platen. An internal pressure of 10 psi was used for one series of tests to simulate the fatigue tests that would be run with a low internal pressure. A second type of test was made with 50-psi internal pressure to simulate fatigue tests to be conducted with 50-psi internal pressure. A third type of test to be conducted with 100-psi internal pressure was not run because the bellows squirmed during the first compression stroke.

Figure L-4 summarizes the strain conditions at the gage showing maximum strain (Gage No. 18). To simplify reporting the values plotted in Figure L-4 and the values tabulated in the pertinent tables are the actual readings of the strain gages. To make the results in Figure L-4 more generally meaningful, a scale has been added to the x-axis showing the corrected strain occurring at the surface of the metal. The tests are discussed chronologically because the strain-gage readings at the start of each test were somewhat influenced by the conditions of the preceding test.

Investigation of Nonlinearity

The first test was conducted to investigate the degree of nonlinearity in the maximum strain-bellows-compression relationship for a strain amplitude (1/2 strain range) approximately that required (4000 μin. /in.) for a bellows life of 5000 cycles. Table L-1 shows the increments of change for each strain gage as the bellows was compressed in increments of 0.0625 inch. (Gages Nos. 11 and 12 measured circumferential strains while Gages Nos. 13 through 19 measured meridional strains.) The increments of change for Gage No. 18 are plotted in Figure L-4.

It was apparent that yielding occurred at the roots of the inner convolutions where Gages Nos. 18 and 19 were located. However, in answer to the first question, an examination of all gages showed that, despite substantial yielding at the inner convolutions, the other locations in the bellows continued to experience significant increases in strain, although at a reduced rate of increase.

As shown in Figure L-4, a significant departure from linearity occurred at a compression of about 0.375 inch at a surface strain of about 2500 μin. /in. – corresponding to a stress of about 72,500 psi ($S = E\epsilon = 29 \times 10^6 \times 0.0025$). This was well above the yield strength of annealed Type 321 stainless steel and presumably was due to combinations of: (1) work hardening, (2) differences between the development of plastic strain due to bending as compared to that in tension, and (3) biaxiality of stress, inhibiting yielding.

Investigation of Residual Strain

Following the first test, the bellows was returned to zero deflection. The gage readings at this point are shown in Column 3 (Second 0 Deflection) of Table L-2. The reading for Gage No. 18 is plotted in Figure L-4.

It was apparent that Gages Nos. 18 and 19 registered significant amounts of residual tensile strain. However, the other gages, which had registered tensile strain during compression, showed some residual compressive strain. (These measured residual strains were, of course, in addition to whatever residual strains existed in the as-received bellows.) These readings were compatible with the existence of a significant residual compressive stress at the convolution crowns and at the convolution roots.

Investigation of Strain Repeatability

A test of strain repeatability was conducted by deflecting the bellows three additional times between zero deflection and the final compression value (0.492 inch). The strain-gage readings for the cycles are recorded in Table L-2. For clarity, only the first of these additional cycles is plotted in Figure L-4.

A comparison of Gages Nos. 11 through 17 shows a remarkable similarity between the readings at the second zero deflection, and the readings at the fifth zero deflection. Even for Gage No. 18, a change of 160 μin. /in. between these two readings did not seem to be significant as compared with the strain range for this gage of approximately 4115 μin. /in. Further, a comparison of successive readings for Gage No. 18 showed that the differences were successively smaller – there was a difference of only 25 μin. / in. between the fourth and fifth zero deflection.

Comparison of Strains Due to Compression and Strains Due to Extension

It was not clear because of the residual stresses what strains would be generated when the bellows deflection was reversed. To investigate this condition, the bellows was extended in increments, and after each increment of extension, the bellows was returned to a specified initial amount of compression. A compression value of 0.469 inch was selected. Table L-3 shows the gage readings for incremental additions of extension to a total extension of 0.375 inch. Since the strain at Gage No. 18 had exhibited the strain range of interest, no further extension was tested. The first cycle and part of the final cycle are shown in Figure L-4.

The meaning of these cycles is further understood if comparisons are made for each cycle of the strain per unit deflection for Gage No. 18 – the gage showing the largest strain. These values are shown in Table L-4. The first column represents elastic strain at Gage No. 18. An examination of Tables L-3 and L-4 and Figure L-4 leads to the following conclusions concerning the questions asked previously: (1) within a maximum strain range of 6300 μin. /in. (8000 μin. /in. at the gage) all gage locations of the bellows continued to experience strains essentially within 10 percent as predicted by the elastic theory, (2) at a location experiencing a strain range of 6300 μin. /in., the strain-bellows-deflection curve (see Figure L-4) showed a slight hysteresis effect, (3) within the deflection conditions investigated, after the first few cycles, the amount of strain was determined by the total bellows stroke, not by the percent of stroke in tension or compression, and (4) for a maximum strain range of 6300 μin. /in., all strain ranges remained relatively constant during successive bellows cycles.

Investigation of Effect of 50-Psi Internal Pressure

To investigate the effects of a higher constant internal pressure (causing changes in mean stress level and possible changes in bellows shape), gage readings were taken as the bellows was deflected between 0.375-inch compression and 0.375-inch tension with 50-psi internal pressure. The results are shown in Table L-5. The values for Gage No. 18 are plotted on Figure L-4. Examination of these results shows that the strain-deflection characteristics of the bellows with 50-psi internal pressure were generally similar to those of the bellows with 10-psi internal pressure. The largest difference noted was that Gage No. 18 showed, for 50 psi, a corrected strain difference of 5600 μin. /in. (uncorrected 7120 μin. /in.) for a deflection from 0.375-inch tension to 0.375-inch compression, in comparison to a corrected strain difference with 10-psi internal pressure of 5460 μin. /in. (uncorrected 6940 μin. /in.) for a deflection from 0.3125-inch tension to 0.4687-inch compression. This represented an increase in strain/deflection rate of about 6 percent with an increase in internal pressure from 10 psi to 50 psi.

Investigation of Effect of 100-Psi Internal Pressure

An attempt was made to deflect the bellows between 0.375-inch compression and 0.375-inch tension with 100-psi internal pressure. At a compression of 0.370 inch, the bellows squirmed, as shown in Figure L-5. At the time it was thought that the bellows

squirmed because the upper end fitting was not rigidly attached to the platen of the testing machine. As determined subsequently, however, an internal pressure of 100 psi was sufficient to cause deformation in the bellows even with both bellows end fittings rigidly fastened, when the stroke was fairly large.

Investigations With 3- and 1-Inch Formed Bellows

Tests with the 5-inch bellows showed that, up to deflections producing strains approximately 6300 μin./in., the strain-deflection behavior was approximately linear. The results of similar tests with 3-inch bellows and 1-inch bellows, summarized in Table L-6, were generally similar. It was decided that the 3-inch bellows probably showed higher nonlinearity with internal pressure because the more flexible convolutions were deformed more by the pressure, resulting in a somewhat altered convolution shape.

Fatigue Tests of 5-, 3-, and 1-Inch One-Ply, and 3- and 1-Inch Two-Ply Bellows

The details of the fatigue-test equipment are contained in Appendix Q, while the test bellows are described in Appendix P. Although the tests described above indicated that there was little effect on local strain behavior due to different amounts of constant internal pressure or to different amounts of percent stroke in compression, the state-of-the-art survey that was completed earlier in the program indicated that these two factors had been found to affect bellows fatigue life. Therefore, the fatigue test program was planned to include examination of these effects. The program had three primary objectives: (1) the determination of the correlation between the strain and fatigue life of metal coupons, and the strain and fatigue life of bellows at two general life values – 5000 cycles and 50,000 cycles, (2) the determination of the effect on bellows fatigue life caused by the percent stroke in compression, and (3) the determination of the effect on bellows fatigue life caused by constant internal pressure. (The fatigue program did not include direct studies of cyclic pressure because the stress-analysis program makes it possible to calculate the total strain range due to cyclic deflection and/or cyclic pressure. Thus, the tests simulated combinations of cyclic deflection and pressure.)

Three basic test conditions were established: (1) bellows were to be tested at two general strain levels: at a level commensurate with a minimum life of 5000 cycles, and at a level commensurate with a minimum life of 50,000 cycles, (2) bellows were to be tested with 50 percent of the stroke in compression, and with 100 percent of the stroke in compression, and (3) bellows were to be tested with negligible internal pressure, and with a reasonably high constant internal pressure. The bellows were tested in pairs. In each pair, all test conditions were identical except that one bellows was mounted so 50 percent of the stroke would be in compression from the relaxed position, and the other bellows was mounted so 100 percent of the same stroke would be in compression from the relaxed condition. In successive pairs of bellows the internal pressure was changed from a very low value to as high a value as the bellows would permit without deformation. When one bellows of a pair failed the other bellows was kept on test, even though the internal pressure fluctuated somewhat because of deflection. This procedure greatly reduced the cost of the test specimens, and the amount of pressure fluctuation did not seem to cause early failure of the remaining bellows.

During the first tests with the 5-inch bellows, it was apparent that the fatigue life of the bellows was significantly shorter for a given strain range than the fatigue life indicated by available coupon data. Therefore, as the subsequent tests were conducted, the selection of the test strain ranges was based on the preceding bellows tests, rather than on the coupon data.

The results of the fatigue tests of all the Type 321 stainless steel bellows are listed in Tables L-7 through L-11. The results are plotted in Figure L-6 in terms of logarithm of strain range vs. logarithm of number of cycles to failure. Figure L-6 also shows the results of reversed-bending fatigue tests of sheet specimens of materials of the class of the Type 321 stainless steel used in the bellows (fatigue data on the actual bellows materials were not available).

Results of Bellows Fatigue Tests in Comparison to Results of Metal-Coupon Fatigue Tests

In Figure L-6, the results of fatigue tests on metal coupons are indicated as falling within a "scatter band" having a significantly large width in lifetime. This is a convenience in the subsequent discussion, but it should not be considered to have fundamental significance because: (1) the available data are for varied materials and heats, (2) the condition of each material is not known precisely (although most are believed to have been annealed), and (3) there are not enough data for any material to provide statistically significant measures of variance.

Considering the scatter band drawn for the coupons as a reference, it may be noted that the results of the fatigue tests on the bellows fall in a still wider band (the extent of scatter observed in the bellows is discussed subsequently) that is lower than, but slightly overlaps, the coupon band. There are several reasons why the values for the bellows would be expected to be different from those for the coupons: (1) variations in convolution shape and in material thickness may result in strain ranges different from those calculated by the representative model, (2) each failure would be expected to occur at the "weakest" convolution (analogous to the shortest fatigue lifetime of several specimens tested at once), (3) the strains in the bellows were biaxial, in contrast to the uniaxial straining of the metal coupons, (4) in some bellows tests there was a nonzero mean strain, and (5) the surface finish of the bellows was not the highly polished condition of some of the coupons. Most of these factors would be expected to result in bellows lifetimes less than those for coupons undergoing the same range of cylic strain.

In general, it might be anticipated that the bellows fatigue-test results would fall within a band lower than (or overlapping the low edge of) the band for the coupons. However, factor (2) of the five listed above would suggest a relatively narrow band for the bellows – since there would usually be a weak spot among the several convolutions in each bellows. The wide range of scatter may be attributed to factors (1) and (4), and this is discussed subsequently.

Comparison of Results of Various Bellows Fatigue Tests

Although it is possible to note that the results for one group of bellows (for example, the 5-inch, one-ply bellows) indicate apparently lower life for a particular strain

range than another group (for example, the 3-inch, one-ply bellows), in view of the considerable scatter such speculation has questionable value. It is interesting to note that the values for the two groups of two-ply bellows fit in with the values for the three groups of single-ply bellows. This observation substantiates the discussion in Appendix G, which concludes that the deflection strains for the one- and two-ply bellows were essentially the same.

Of the 20 pairs (40 bellows) of different degrees of stroke in compression in which at least one failure occurred, 5 pairs showed negligible differences in lifetime, 8 pairs showed shorter lifetime for the bellows with 100 percent compression, and 7 pairs showed shorter lifetime for the bellows with 50 percent compression. It is concluded that, within the test specimens and conditions investigated, there was no clear effect of varying the stroke from 100 percent compression to 50 percent compression (with the same strain range). It may be noted that there is some limited evidence in the literature that within the range of lifetime (5000 cycles to 50,000 cycles) for this material (Type 321 stainless steel) the range of strain that can be withstood to a specified lifetime is not sensitive to the level of mean strain. Hence, possible effects of changing the degree of stroke in compression might be masked by scatter.

For the 13 pairs of bellows for which effects of pressure may be compared, six show higher life at the lower pressure, one shows the reverse, and five show negligible effect. There appears to be a slight indication that an increase in internal pressure causes a decrease in fatigue lifetime. It will be recalled that for a significant increase in internal pressure (10 to 50 psi), the 5-inch bellows showed a small (4 percent) increase in strain range for a particular stroke. In general, the tendency for slight decrease in lifetime with increasing pressure seems compatible with the small effect of mean strain, and a small effect on strain-deflection characteristics, and the masking of such effects by the scatter in the bellows fatigue tests. It should be noted that this tendency (for a specified deflection stroke) cannot be safely extrapolated beyond the conditions of these tests. Further, as previously noted, large internal pressures can cause excessive deformations.

The scatter of results of the bellows fatigue tests is largely attributable to variations in geometry (even from one convolution to another in a specific bellows). Related to variations in geometry may be variations in local thinning and local work hardening of material. The computed strain ranges are based upon models of the bellows geometry, and details of geometry can influence greatly the values of the computed strains (see Appendix E). Hence, if any convolution differs in detail from the model selected for that bellows, the actual strain range it undergoes for a specified stroke and internal pressure may differ significantly from the value assigned in the fatigue test.

Conclusions

(1) The results of the fatigue tests are compatible with available strain-range-cycle data on the materials and with values of strain ranges computed by elastic theory.

(2) In nearly every case (26 out of 29), failure was at a convolution root, where theory predicted the highest strains. In three exceptions failures were at the locations (crowns) of next highest theoretical strain.

(3) There was no significant difference between the behavior of one-ply and of two-ply bellows under strain ranges determined by elastic theory.

(4) Within the test specimens and conditions investigated, there was no clear effect on bellows fatigue life of variations in internal pressure (provided the bellows was not deformed), or of varying the stroke from 100 percent compression to 50 percent compression (with the same strain range).

(5) Based upon the lower broken line in Figure L-6 (minimum observed lifetime) and the arbitrary use of a factor of 2 times the design lifetime, these Type 321 stainless steel bellows should not be operated over a strain range more than 4200 μin. /in. for a minimum expected lifetime of 5000 cycles, nor at a strain range of more than 3000 μin. / in. for a minimum expected lifetime of 50,000 cycles. These values could probably be increased for bellows that are very uniform and can be modeled accurately. On the other hand, it is equally probable that the values should be decreased for some bellows that are commercially available.

TABLE L-1. INCREMENTS OF STRAIN FOR INCREMENTS OF COMPRESSION OF 5-INCH FORMED BELLOWS--10-PSI INTERNAL PRESSURE

Gage No.	Strain Increments,[a] μin/in., for Indicated Bellows Compression Increments, inch: 0 to 0.063	0.063 to 0.125	0.125 to 0.188	0.188 to 0.250	0.250 to 0.313	0.313 to 0.375	0.375 to 0.438	0.438 to 0.492	Total Strain, μin/in., for 0 to 0.492 in. Compression
11	135	135	140	140	130	115	105	100	1000
12	135	135	125	125	130	115	090	110	965
13	350	355	385	380	370	355	315	315	2825
14	295	295	300	290	285	265	220	210	2160
15	340	330	340	350	340	335	300	290	2625
16	355	355	365	370	355	345	295	295	2735
17	350	335	325	355	335	324	285	290	2600
18	505	520	500	550	560	750	915	1055	5355[b]
19	495	495	505	520	560	705	760	810	4850

(a) All strain increments were tensile and uncorrected for strain-gage thickness.
(b) Corrected total strain at the metal surface was 4217 μin/in. (see Appendix Q).

TABLE L-2. STRAINS IN 5-INCH FORMED BELLOWS DURING SUCCESSIVE DEFLECTIONS BETWEEN 0 AND 0.492-INCH COMPRESSION--10-PSI INTERNAL PRESSURE

Gage No.	Strain-Gage Readings at Each Deflection Extreme: First 0 Deflection	First 0.492 in. Compression	Second 0 Deflection	Second 0.492 in. Compression	Third 0 Deflection	Third 0.492 in. Compression	Fourth 0 Deflection	Fourth 0.492 in. Compression	Fifth 0 Deflection	Difference Between 1st and 5th 0 Deflec., μin/in.[a]
11	11,450	12,450	11,430	12,450	11,425	12,440	11,430	12,440	11,425	-025
12	11,035	12,000	11,035	12,005	11,040	12,010	11,030	12,010	11,030	-005
13	16,575	19,400	16,490	19,385	16,500	19,390	16,490	19,370	16,490	-085
14	15,030	17,190	14,860	17,170	14,845	17,155	14,840	17,150	14,830	-200
15	13,305	15,930	13,140	15,950	13,170	15,940	13,175	15,940	13,175	-130
16	14,335	17,070	14,240	17,060	14,230	17,050	14,230	17,050	14,230	-105
17	15,090	17,690	15,015	17,695	14,985	17,670	14,980	17,680	14,980	-110
18	14,655	20,010	15,915	20,135	16,000	20,170	16,050	20,190	16,075	+1420
19	16,650	21,500	17,485	21,580	17,550	21,590	17,570	21,595	17,570	+920

(a) Plus values indicate tensile strains; minus values indicate compressive strains. Strain values are uncorrected for strain-gage thickness (see Appendix Q).

TABLE L-3. STRAIN-GAGE READINGS FOR INCREMENTAL INCREASES IN DEFLECTION OF 5-INCH FORMED BELLOWS; UNIFORMITY OF READINGS AFTER 6 FINAL DEFLECTION CYCLES--10 PSI INTERNAL PRESSURE

		Strain-Gage Readings at Deflection Extremes, inch								
Gage No.	Original 0 Readings	Fifth 0 Deflection	New 0 Deflection	0.469 Compression	0 Deflection	0.625 Tension	0.469 Compression	0.125 Tension	0.469 Compression	0.188 Tension
11	11,450	11,425	11,440	12,410	11,450	11,295	12,395	11,125	12,400	10,975
12	11,035	11,030	11,070	12,000	11,050	10,910	12,000	10,780	11,980	10,620
13	16,575	16,490	16,590	19,320	16,595	16,210	19,300	15,845	19,305	15,500
14	15,030	14,830	15,010	17,210	14,990	14,700	17,190	14,405	17,175	14,120
15	13,305	13,175	13,370	15,875	13,340	13,040	15,865	12,700	15,820	12,360
16	14,335	14,230	14,390	17,080	14,390	14,025	17,070	13,665	17,055	13,310
17	15,090	14,980	15,090	17,640	15,065	14,735	17,630	14,400	17,600	14,040
18	14,655	16,075	16,205	20,185	16,290	15,740	20,225	15,205	20,250	14,635
19	16,650	17,570	17,740	21,580	17,770	17,250	21,590	16,730	21,600	16,180

	Strain-Gage Readings at Deflection Extremes, inch									
Gage No.	0.469 Compression	0.250 Tension	0.469 Compression	0.313 Tension	0.469 Compression	0.375 Tension	0.469 Compression	0 Deflection	6th Reading 0.375 Tension	6th Reading 0.469 Compression
11	12,380	10,820	12,385	10,650	12,390	10,490	12,385	11,430	10,470	12,380
12	11,985	10,470	11,990	10,310	11,970	10,150	11,980	11,045	10,140	11,975
13	19,270	15,150	19,270	14,770	19,270	14,425	19,230	16,530	14,395	19,210
14	17,170	13,850	17,170	13,580	17,150	13,310	17,155	14,960	13,295	17,145
15	15,835	12,070	15,870	11,725	15,805	11,415	15,780	13,300	11,335	15,735
16	17,045	12,960	17,050	12,610	17,025	12,255	17,015	14,340	12,235	16,995
17	17,605	13,710	17,605	13,380	17,570	13,030	17,575	15,015	13,010	17,555
18	20,275	14,030	20,330	13,420	20,360	12,760	20,440	16,505	12,865	20,550
19	21,610	15,625	21,655	15,060	21,660	14,450	21,715	17,900	14,510	21,760

TABLE L-4. STRAIN/DEFLECTION RATES[a] FOR SELECTED CONDITIONS OF DEFLECTION OF THE 5-INCH FORMED BELLOWS--10-PSI INTERNAL PRESSURE

	Selected Bellows Deflections, inch								
	0 Deflection to 0.250 Compression	0 Deflection to 0.313 Compression	0 Deflection to 0.469 Compression	0.125 Tension to 0.469 Compression	0.188 Tension to 0.469 Compression	0.250 Tension to 0.469 Compression	0.313 Tension to 0.469 Compression	0.375 Tension to 0.469 Compression	0.438 Tension to 0.438 Compression
Maximum Gage Reading	16,730	17,290	20,135	20,250	20,275	20,330	20,360	20,550	20,290
Minimum Gage Reading	14,655	14,655	16,205	15,205	14,635	14,030	13,420	12,865	12,250
Difference in Readings	2,075	2,635	3,980	5,045	5,640	6,300	6,940	7,685	8,040
Corrected Strain[b], μin/in.	1,635	2,070	3,135	3,970	4,440	4,950	5,500	6,060	6,320
Bellows Deflection, in.	0.250	0.313	0.469	0.594	0.657	0.719	0.782	0.844	0.876
Strain per Deflection, μin/in.^{2}	6,540	6,630	6,670	6,700	6,770	6,920	6,990	7,160	7,220
Diff. in Strain per Deflection from 1st Col., μin/in.^{2}	-	+102	+142	+257	+236	+388	+465	+637	+701
% Diff., Strain per deflection, from 1st Col.	-	1.6	2.2	2.4	3.6	5.8	7.1	9.8	10.1

(a) At the location of maximum observed strain, Gage No. 18.
(b) See Appendix Q (readings divided by 1.273).

TABLE L-5. EFFECT OF 50-PSI INTERNAL PRESSURE ON STRAINS OF COMPRESSED AND EXTENDED 5-INCH FORMED BELLOWS

Gage No.	Original 10-psi 0 Deflect.	New[a] 10-psi 0 Deflect.	Gage Readings at Deflection Extremes, inch: 50-psi 0 Deflect.	50-psi 0.375 Compr.	50-psi 0.375 Tension	50-psi 0.188 Tension	50-psi 0.188 Compr.	50-psi 0.375 Compr.	50-psi 0.188 Compr.	50-psi 0.188 Tension	50-psi 0.375 Tension	50-psi 0 Deflec.
11	11,450	11,420	11,370	12,145	10,410	10,885	11,750	12,110	11,720	10,870	10,390	11,330
12	11,035	11,070	11,045	11,780	10,135	10,610	11,410	11,760	11,410	10,585	10,130	11,015
13	16,575	16,540	15,830	17,950	13,570	14,590	16,665	17,730	16,685	14,605	13,565	15,645
14	15,030	15,015	14,305	16,000	12,525	13,400	15,070	15,860	15,065	13,395	12,560	14,285
15	13,305	13,330	12,670	14,570	10,525	11,545	13,450	14,365	13,395	11,505	10,565	12,515
16	14,335	14,360	13,680	15,780	11,440	12,480	14,560	15,600	14,575	12,500	11,460	13,550
17	15,050	15,050	14,425	16,410	12,330	13,330	15,300	16,285	15,310	13,350	12,370	14,330
18	14,655	16,620	17,455	20,745	13,945	15,575	18,975	21,065	19,485	16,050	14,130	17,390
19	16,650	17,960	18,600	21,710	15,330	16,900	20,100	21,880	20,290	17,090	15,365	18,475

(a) After tests described in Tables L-1 through L-4.

TABLE L-6. SUMMARY OF DEFLECTION CONDITIONS AND STRAINS FOR 3- AND 1-INCH BELLOWS

	3-inch Bellows						1-inch Bellows					
	0.060 Tension to 0.060 Compr. 0 psi	0.205 Tension to 0.205 Compr. 0 psi	0.340 Tension to 0.340 Compr. 0 psi	0.205 Tension to 0.205 Compr. 25 psi	0.205 Tension to 0.205 Compr. 50 psi	0.340 Tension to 0.340 Compr. 25 psi	0.060 Tension to 0.060 Compr. 0 psi	0.100 Tension to 0.100 Compr. 0 psi	0.175 Tension to 0.175 Compr. 0 psi	0.100 Tension to 0.100 Compr. 50 psi	0.175 Tension to 0.175 Compr. 25 psi	0.175 Tension to 0.175 Compr. 50 psi
Maximum Gage Reading	22,935	24,265	25,400	33,550	35,055	35,035	18,360	19,250	21,060	20,415	21,820	23,090
Minimum Gage Reading	21,680	19,850	17,560	28,690	30,070	26,200	15,655	14,720	13,365	15,810	13,730	14,900
Difference in Readings	1,255	4,415	7,840	4,860	4,985	8,885	2,705	4,530	7,695	4,605	8,090	8,190
Corrected Strain(a), μin/in.	912	3,210	5,690	3,535	3,620	6,450	1,690	2,830	4,790	2,880	5,050	5,110
Bellows Deflection, in.	0.120	0.410	0.680	0.410	0.410	0.680	0.120	0.200	0.350	0.200	0.350	0.350
Strain per Deflection, μin/in.	7,560	7,800	8,360	8,640	8,800	9,490	14,100	14,150	13,700	14,400	14,450	14,600
Diff in Strain per Deflection, from 1st Col., μin/in.	-	+140	+800	+1,080	+1,240	+1,930	-	+50	-400	+300	+350	+500
% Diff., Strain per Deflection, from 1st Column	-	+1.9	+10.6	+14.3	+16.4	+25.5	-	+0.3	-2.8	+2.1	+2.5	+3.5

(a) See Appendix Q (readings divided by 1.375 for 3-inch bellows, and 1.600 for 1-inch bellows).

TABLE L-7. RESULTS OF FATIGUE TESTS OF 5-INCH ONE-PLY FORMED BELLOWS (12 CONVOLUTIONS)
(Test Conditions: Room temperature, 60 cpm--see text for other details)

Bellows No.	Total Stroke, inch	% Stroke in Compression	Internal Pressure, psi	Local(a) Strain Range, μin/in.	Cycles to Failure	Failure Location(b), Remarks
JD89	0.875	50	8	4437	10,847	Crown No. 7, 100° from weld--low stress region, corrosion pit
JD97	0.875	100	8	4437	20,677	Root No. 2, 140° to 205° from weld
JD90	0.875	50	8	4437	17,771	Root No. 10, 350° from weld
JD98	0.875	50	50	4437	14,954	Root No. 7, 150° from weld, corrosion pit
JD95	0.875	100	50	4437	7,728	Root No. 1, 255° to 260° from weld
JD94	0.875	100	50	4437	>7,226	Did not fail--was used to replace JD95 while JD98 was tested
JD87	0.875	50	100, 8	4437	360 at 100 psi +2,461 at 8 psi	Root No. 11, 285° to 300° from weld; deformed after 360 cycles at 100 psi, and test was completed at 8 psi
JD91	0.875	100	100, 8	4437	360 at 100 psi +6256 at 8 psi	Root No. 1, 185° to 200° from weld. Deformed after 360 cycles at 100 psi and test was completed at 8 psi
JD93	0.532	50	8	2698	282,928	Root No. 1, 30° from weld
JD96	0.532	100	8	2693	>764,324	Did not fail

(a) Maximum strain range at convolution root, calculated from elastic theory.
(b) Range of angle indicates approximate length of crack. Absence of limited range denotes small crack.

TABLE L-8. RESULTS OF FATIGUE TESTS OF 3-INCH ONE-PLY FORMED BELLOWS (10 CONVOLUTIONS)

(Test Conditions: Room temperature, 60 cpm--see text for other details)

Bellows No.	Total Stroke, inch	% Stroke in Compression	Internal Pressure, psi	Local[a] Strain Range, μin/in.	Cycles to Failure	Failure Location[b], Remarks
JD66	0.680	50	8	5773	6,273	Root No. 9, 80° to 130° from weld
JD65	0.680	100	8	5773	10,777	Root No. 2, 270° to 280° from weld, and Root No. 9, 230° to 240° from weld
JD72	0.680	50	25	5773	4,624	Root No. 1, 270° to 300° from weld
JD71	0.680	100	25	5773	5,728	Root No. 9, 200° to 210° from weld
JD62	0.610	50	5	5178	52,539	Root No. 9, 0° to 2° from weld (transverse heat-affected zone crack)
JD63	0.610	100	5	5178	22,012	Root No. 2 at weld and Root No. 4 at weld
JD61	0.410	50	8	3480	500,008	Crown No. 10 at weld
JD67	0.410	100	8	3480	136,537	Root No. 2 at weld, and Root No. 3 at weld--longitudinal-weld centerline crack
JD64	0.410	50	25	3780	306,727	Crown No. 10 at weld
JD70	0.410	100	25	3480	357,790	Root No. 6, longitudinal-weld centerline crack

(a) Maximum strain range at convolution root, calculated from elastic theory.
(b) Range of angle indicates approximate length of crack. Absence of listed range denotes small circumferential crack (transverse to the weld).

TABLE L-9. RESULTS OF FATIGUE TESTS OF 1-INCH ONE-PLY FORMED BELLOWS (8 CONVOLUTIONS)

(Test Conditions: Room temperature, 60 cpm--see text for other details)

Bellows No.	Total Stroke, inch	% Stroke in Compression	Internal Pressure, psi	Local[a] Strain Range, μin/in.	Cycles to Failure	Failure Location[b], Remarks
JD32[c]	0.350	50	8	5931	25,430	Root No. 7, 200° to 305° from weld
JD26	0.350	100	8	5931	5,610	Root No. 4, 230° to 335° from weld
JD30	0.350	50	50	5931	1,607	Root No. 7, 120° to 155° from weld
JD27	0.350	100	50	5931	3,529	Root No. 4, 40° to 75° from weld
JD25	0.300	50	8	5084	33,359	Root No. 2, at 270° from weld
JD33	0.300	100	8	5084	6,773	Root No. 2, 240° to 315° from weld
JD24	0.200	50	8	3389	>524,200	Did not fail
JD23	0.200	100	8	3389	>524,200	Did not fail
JD31	0.200	50	50	3389	>549,000	Did not fail
JD34	0.200	100	50	3389	185,814	Root No. 7, 345° to 15° from weld, and Root No. 4, 185° to 225° from weld

(a) Maximum strain range at convolution root, calculated from elastic theory.
(b) Range of angle indicates approximate length of crack.
(c) Bellows No. JD32 contained 9 convolutions instead of 8--not plotted in Figure L-6.

TABLE L-10. RESULTS OF FATIGUE TESTS OF 3-INCH TWO-PLY FORMED BELLOWS (10 CONVOLUTIONS)

(Test Conditions: Room temperature, 80 cpm--see text for other details)

Bellows No.	Total Stroke, inch	% Stroke in Compression	Internal Pressure, psi	Local[a] Strain Range, μin/in.	Cycles to Failure	Failure Location[b]; Remarks
JD83	0.770	50	8	6537	4,033	Root No. 9, 60° to 200° from weld
JD76	0.770	100	8	6537	4,597	Root No. 9, 340° to 120° from weld
JD75	0.770	50	50	6537	3,336	Root No. 1, 160° to 330° from weld
JD74	0.770	100	50	6537	4,271	Root No. 9, 220° to 40° from weld
JD80	0.680	50	8	5773	17,215	Root No. 1, 40° to 80° from weld
JD81	0.680	100	8	5773	7,175	Root No. 1, 265° to 45° from weld
JD79	0.480	50	8	4075	211,977	Root No. 8, 40° to 80° from weld
JD82	0.480	100	8	4075	76,389	Root No. 1 and Root No. 5, at weld
JD73	0.480	50	50	4075	37,889	Root No. 8, 75° to 140° from weld, and Root No. 9, 110° to 255° from weld
JD84	0.480	100	50	4075	65,244	Root No. 1, 320° to 50°, No. 3, 355° to 10°, and No. 4, 355° to 5° from weld

(a) Maximum strain range at convolution root, calculated from elastic theory.
(b) Range of angle indicates approximate length of crack.

TABLE L-11. RESULTS OF FATIGUE TESTS OF 1-INCH TWO-PLY FORMED BELLOWS (8 CONVOLUTIONS)

(Test Conditions: Room temperature, 80 cpm--see text for other details)

Bellows No.	Total Stroke, Inch	% Stroke in Compression	Internal Pressure, psi	Local[a] Strain Range, μin/in.	Cycles to Failure	Failure Location[b]; Remarks
JD20	0.350	50	8	5931	13,747	Root No. 2, 60° to 155° from weld
JD14	0.350	100	8	5931	16,808	Root No. 6, 170° to 15° from weld
JD16	0.300	50	8	5084	15,569	Root No. 3, 275° to 320° from weld
JD15	0.300	100	8	5084	26,350	Root No. 2, 290° to 315° from weld
JD21	0.300	50	50	5084	<24,001	Root No. 2, 285° to 340° from weld
JD13	0.300	100	50	5084	24,001	Root No. 6, 20° to 110° from weld
JD12	0.180	50	8	3050	>581,000	Did not fail
JD22	0.180	100	8	3050	>581,000	Did not fail
JD19	0.180	50	50	3050	>588,900	Did not fail
JD11	0.180	100	50	3050	>588,900	Did not fail

(a) Maximum strain range at convolution root, calculated from elastic theory.
(b) Range of angle indicates approximate length of crack.

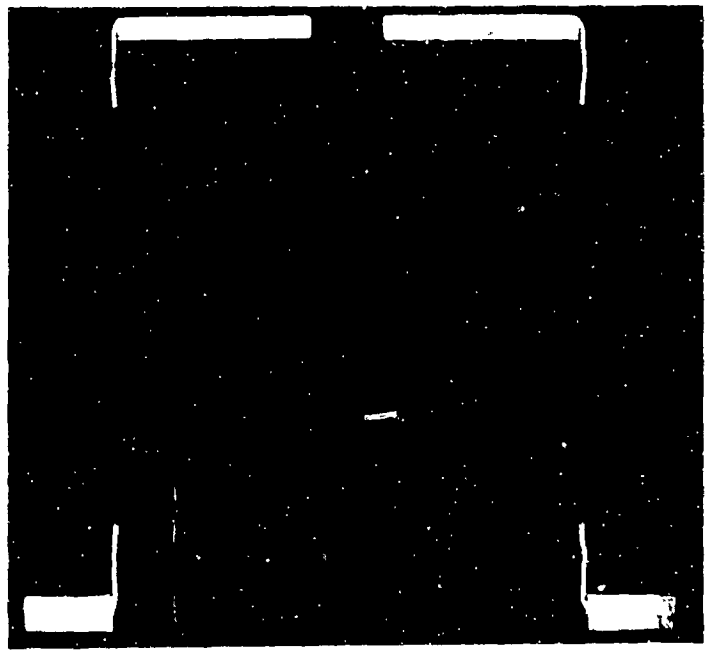

FIGURE L-1. CROSS SECTION OF 5-INCH FORMED BELLOWS JD92

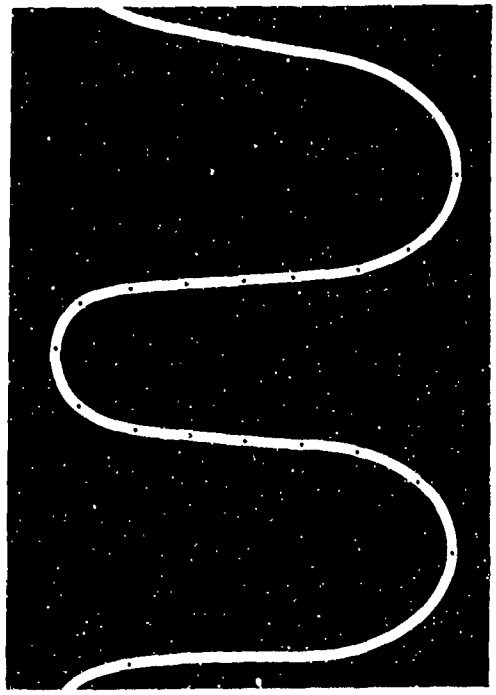

FIGURE L-2. ENLARGED VIEW OF CONVOLUTIONS OF CROSS-SECTIONED 5-INCH FORMED BELLOWS JD92

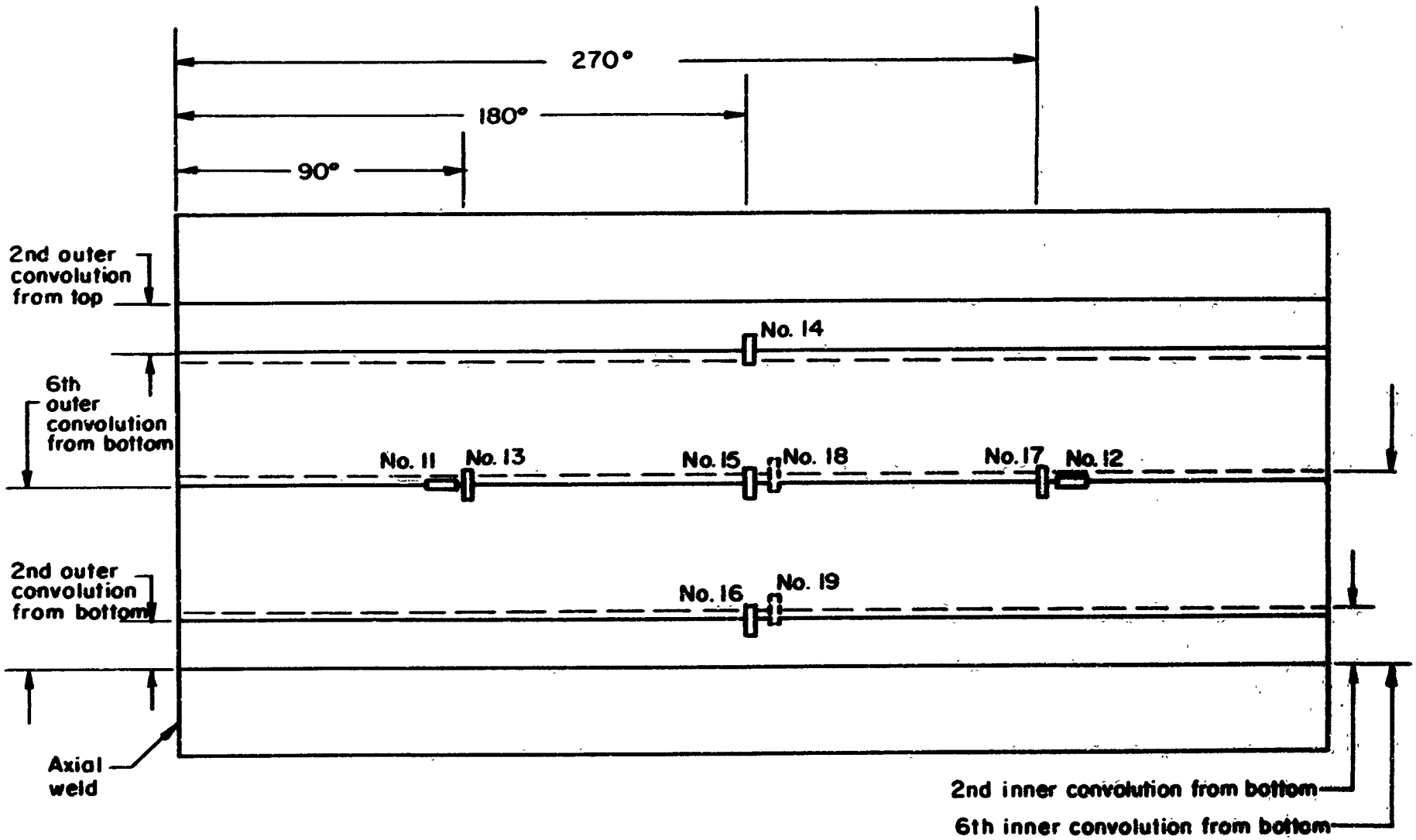

FIGURE L-3. STRAIN GAGE LOCATIONS FOR 5-INCH FORMED BELLOWS

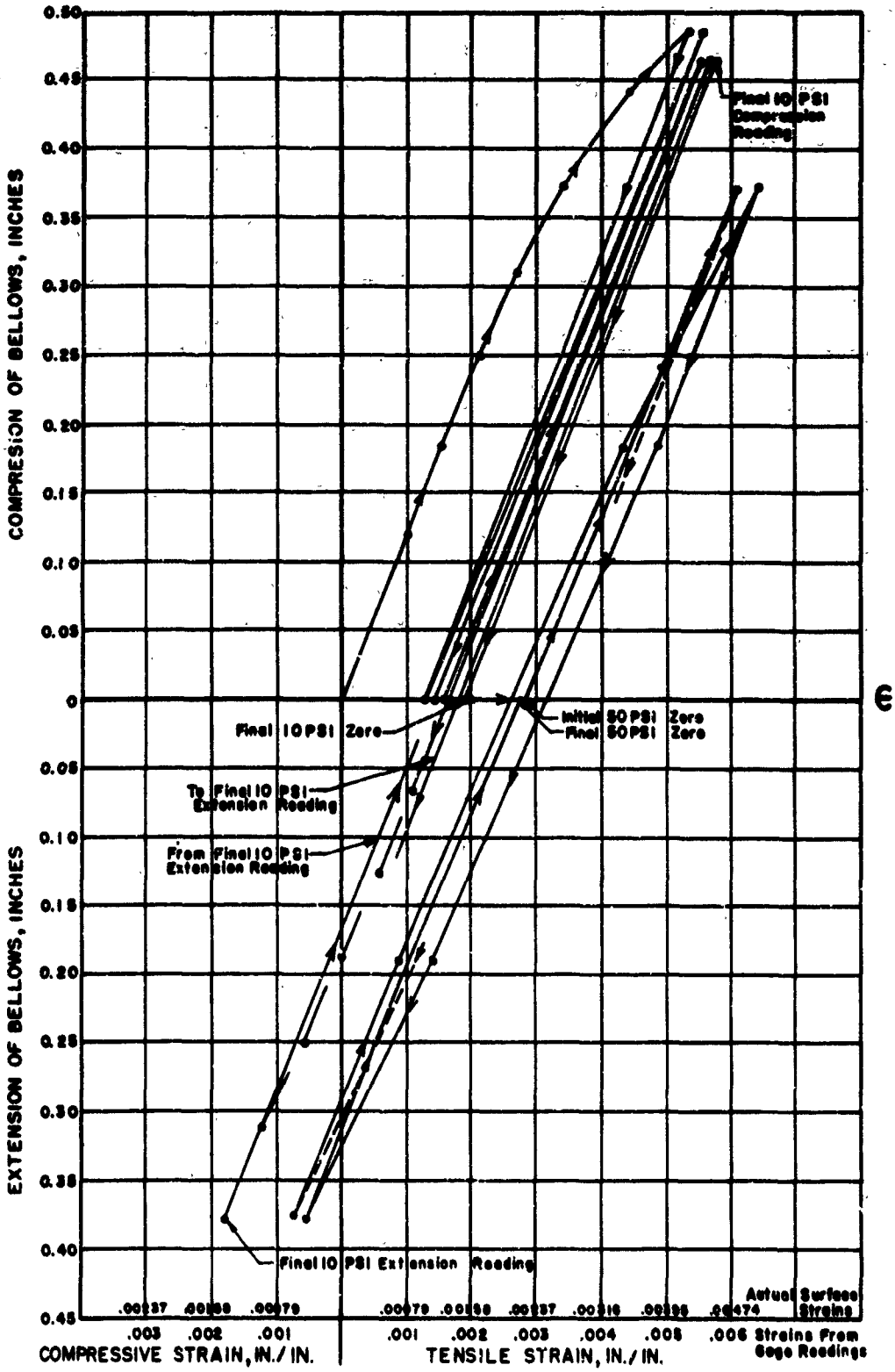

FIGURE L-4. STRAIN ON GAGE NO. 18 OF 5-INCH FORMED BELLOWS JD88 DURING SUCCESSIVE COMPRESSION AND EXTENSION CYCLES WITH 10 PSI AND 50 PSI INTERNAL PRESSURE

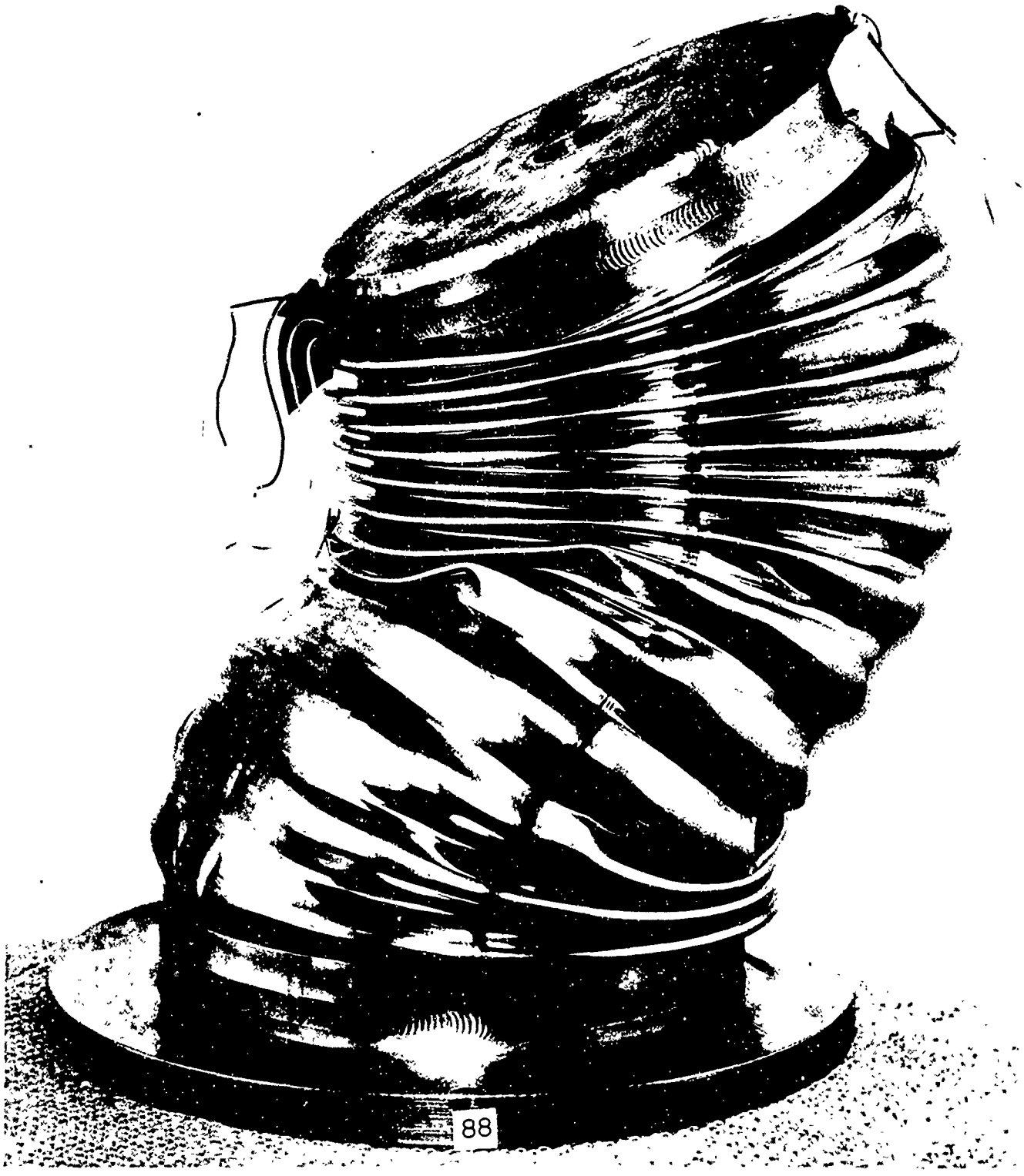

32506

FIGURE L-5. SQUIRMED 5-INCH FORMED BELLOWS

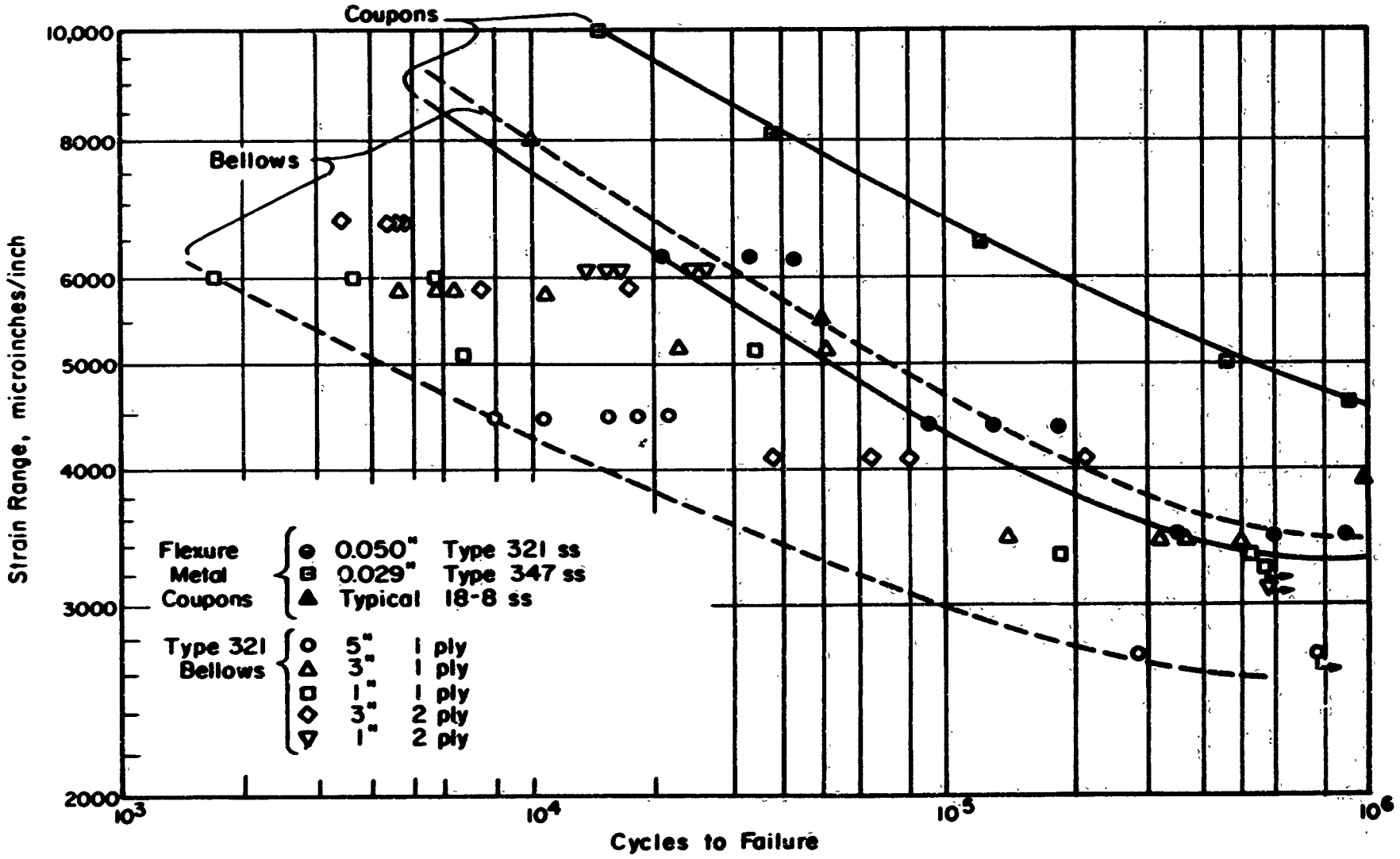

FIGURE L-6. FATIGUE RESULTS OF STAINLESS STEEL FORMED BELLOWS AND STAINLESS STEEL COUPONS

APPENDIX M

FATIGUE ANALYSIS OF FORMED BELLOWS - INCONEL 718

APPENDIX M

FATIGUE ANALYSIS OF FORMED BELLOWS – INCONEL 718

Fatigue tests were made on the 3-inch and the 1-inch Inconel 718 bellows described in Appendix P. The procedure was essentially that described in Appendix L for stainless steel bellows.

Strain gages were applied, at locations shown in Figure M-1, to a 3-inch bellows, and values were observed, with particular attention given to Gage No. 18 at a convolution root (where elastic theory indicated there was maximum strain). Table M-1 shows several values of strain range observed in comparison with values computed from elastic theory; Table M-2 gives more details in regard to the theoretical evaluation. It was concluded that:

(1) The values from the strain-gage readings agreed, to within better than 10 percent, with values calculated from the elastic theory

(2) The effect of varying the internal pressure from 0 to 50 psi upon the range of deflection strain was very small (less than 9 percent)

(3) Strain-deflection values as determined by the elastic theory should be used as a basis for fatigue tests of the bellows.

Strain ranges essentially the same as those used for the fatigue tests of Type 321 stainless steel bellows were selected for first tests of the 3-inch bellows, on the basis of limited information about the fatigue behavior of Inconel 718 metal coupons. In subsequent tests, somewhat different values of strain range were used on the basis of experience in the early tests.

Tables M-3 and M-4 show the results of fatigue tests of the 3-inch bellows and the 1-inch bellows, respectively. These results are plotted in Figure M-2, in which are also shown fatigue-test results for coupons of 0.050-inch-thick Inconel 718 sheet, and fatigue-test results for 1-1/2-inch Inconel 718 bellows investigated on another program.

From Figure M-2 and Tables M-3 and M-4, the following observations can be made:

(1) The results of the bellows fatigue tests show considerable scatter and fall within a band lower than the S-N curve for the limited test data on Inconel 718 sheet material. The trend is compatible with expectations from the theory.

(2) In nearly every case (15 out of 16), failure was at a convolution root where the theory predicted the highest strains. In the one exception, failure was at a crown – the location of next-highest predicted strain.

(3) There was no clear effect of the degree of compression on fatigue lifetime. Of eight pairs of bellows in which at least one failure occurred, one pair showed no significant difference in lifetime, four pairs showed shorter lifetime for 100 percent of the stroke in compression, and three pairs showed shorter lifetime for 50 percent of the stroke in compression.

(4) There was a trend toward shorter lifetime with higher internal pressure (seven out of eight pairs showed this).

(5) Based upon the lower broken line in Figure M-2 (minimum observed lifetime) and the arbitrary use of a factor of 2 times the design lifetime, these Inconel 718 bellows should not be operated over a strain range more than 4000 μin/in. for a minimum expected lifetime of 5000 cycles nor at a strain range more than 3000 μin/in. for a minimum expected lifetime of 50,000 cycles. Possibly somewhat larger values of strain range could be used for unusually well formed bellows for which a more accurate mathematical model could be used. (An indication of this is given by the three 1-1/2-inch bellows.) Smaller values should be used for bellows having less uniformity in detail geometry.

TABLE M-1. EXPERIMENTALLY DETERMINED STRAIN RANGES AT CONVOLUTION ROOT ON 3-INCH INCONEL BELLOWS

Deflection Range, in.	Internal Pressure, psi	Strain Range, μin./in.	
		Gage[a]	Elastic Theory[b]
0.670	0	5360	5873
	25	5320	5873
	50	5500	5873
0.380	0	3020	3331
	25	2760	3331
	50	3060	3331

(a) Corrected to value at metal surface.
(b) See Table M-2.

TABLE M-2. THEORETICAL DEFLECTION STRESSES AND STRAINS AT INNER CONVOLUTIONS FOR 3- AND 1-INCH INCONEL 718 FORMED BELLOWS

		Membrane Stress	Bending Stress, Outer Surface	Total Stress, Inner Surface	Stress[a], psi, Calculated for 1-inch Deflection	Strain, μin./in., Calculated for 1-inch Deflection	Strain Calculated for Deflection for Fatigue Tests	
							Deflection, in.	Strain, μin./in.
3-inch Inconel Bellows, Stresses	Meridional Stresses and Strains	-5,509.45	-584,670	+579,168	+282,793	+8765	0.670	+5873
	Circumferential Stresses	-99,991.7	-175,680	+75,688	+36,957	-	0.600	+5259
							0.380	+3331
1-inch Inconel Bellows, Stresses	Meridional Stresses and Strains	-1027.76	-774,380	+773,352	+623,168	+19,638	0.204	+4000
	Circumferential Stresses	-172,765	-232,314	+59,549	+47,985	-	0.[illegible]3	+3000

(a) Total stress multiplied by the deflection (1 inch) and divided by the live length of the bellows. The live lengths were: 2.048 in. for the 3-inch bellows, and 1.241 in. for the 1-inch bellows.

TABLE M-3. RESULTS OF FATIGUE TESTS OF 3-INCH INCONEL FORMED BELLOWS (14 CONVOLUTIONS)

(Test Conditions: Room temperature, 80 cpm--see Appendix L for other details)

Bellows No.	Total Stroke, inch	% Stroke in Compression	Internal Pressure, psi	Local[a] Strain Range, μin/in.	Cycles to Failure	Failure Location[b], Remarks
JD123	0.670	50	8	5873	37,007	Root No. 13, 190° to 205° from weld
JD119	0.670	100	8	5873	11,521	Root No. 13, 65° to 75° and 90° to 95° from weld
JD129	0.670	50	50	5873	2,305	Root No. 13, 20° to 35° from weld
JD126	0.670	100	50	5873	12,848	Root No. 13, 355° to 5° from weld
JD130	0.600	50	50	5259	82,578	Root No. 13, 130° to 135° from weld
JD121	0.600	100	50	5259	3,477	Root No. 1, 330° to 340° from weld
JD125	0.380	50	8	3331	>619,000	Did not fail
JD128	0.380	100	8	3331	114,539	Root No. 13, 265° to 275° from weld
JD120	0.380	50	50	3331	152,714	Crown No. 1, small hole 10° from weld
JD127	0.380	100	50	3331	74,871	Root No. 1, 355° to 5° from weld

(a) Maximum strain range at convolution root, calculated from elastic theory.
(b) Range of angle indicates approximate length of crack.

TABLE M-4. RESULTS OF FATIGUE TESTS OF 1-INCH INCONEL FORMED BELLOWS (16 CONVOLUTIONS)

(Test Conditions: Room temperature, 80 cpm--see Appendix L for other details)

Bellows No.	Total Stroke, inch	% Stroke in Compression	Internal Pressure, psi	Local[a] Strain Range, μin/in.	Cycles to Failure	Failure Location[b], Remarks
JD107	0.204	50	8	4000	17,949	Root No. 15, 60° to 105° from weld
JD118	0.204	100	8	4000	262,690	Root No. 6, 355° to 0° from weld
JD116	0.204	50	25	4000	13,500	Root No. 16, 0° to 70° from weld--in straight-end section of bellows
JD115	0.205	100	25	4000	117,774	Root No. 2, 230° to 240° from weld
JD113	0.204	50	25	4000	63,483	Root No. 1, 55° from weld
JD111	0.153	50	8	3000	>861,000	Did not fail
JD109	0.153	100	8	3000	>861,000	Did not fail
JD112	0.153	50	25	3000	151,171	Root No. 1, 75° to 85° from weld
JD114	0.153	100	25	3000	114,561	Root No. 1, at weld

(a) Maximum strain range at convolution root, calculated from elastic theory.
(b) Range of angle indicates approximate length of crack.

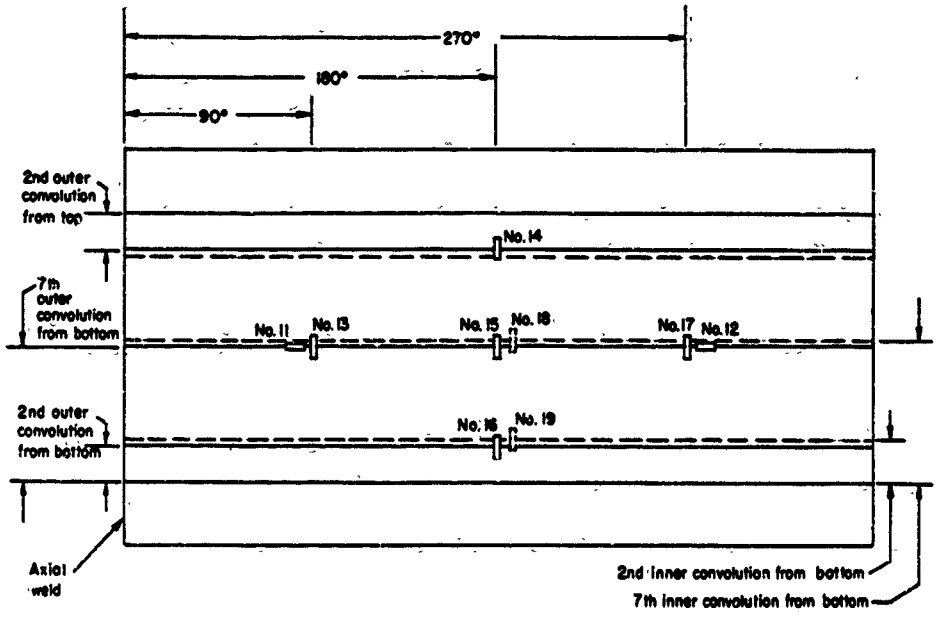

FIGURE M-1. STRAIN GAGE LOCATIONS FOR 3-INCH INCONEL FORMED BELLOWS

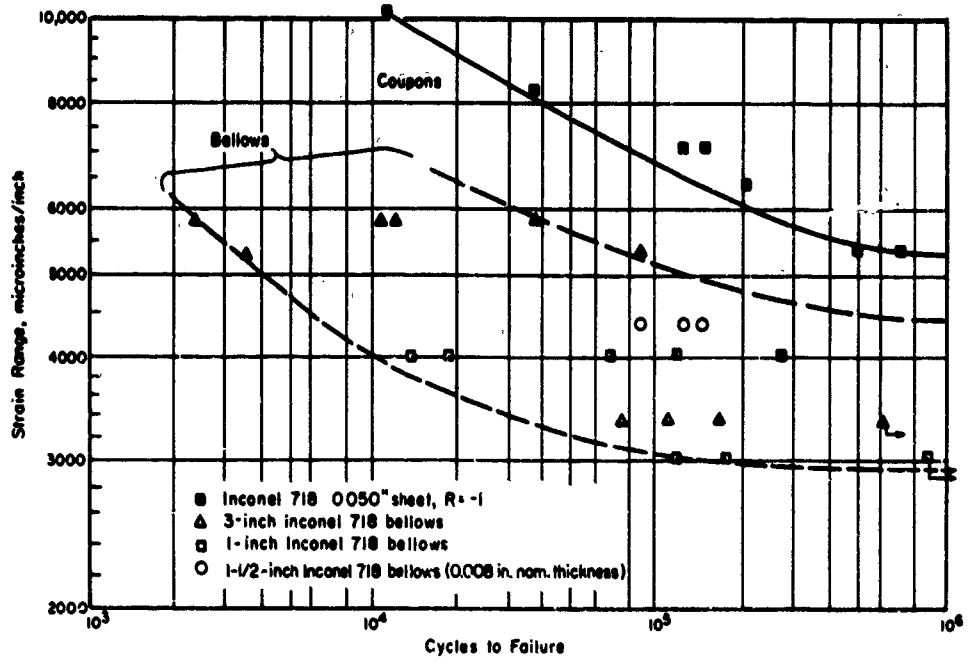

FIGURE M-2. FATIGUE RESULTS OF INCONEL FORMED BELLOWS AND INCONEL COUPONS

APPENDIX N

FATIGUE ANALYSIS OF WELDED BELLOWS AND DIAPHRAGMS

APPENDIX N

FATIGUE ANALYSIS OF WELDED BELLOWS AND DIAPHRAGMS

It was established early in this research program that premature fatigue failures of welded bellows and diaphragms constitute a critical problem to the Air Force. Such failures almost invariably occur in weld areas at the convolution roots or crowns, or at the end fittings. Detailed characterization of the fatigue behavior of such areas involves the consideration of additional factors not associated with the fatigue of formed bellows.

One such additional factor is the notch at the weld bead. At these locations, significant variations of stress and strain occur over distances smaller than the order of the material thickness, and the analysis of the localized stresses in such a configuration is outside the realm of shell theory. The stress analysis described in Appendix B can, with the use of a reasonable model for the weld-bead stiffness, provide values for nominal stresses and strains that afford useful predictions of such properties as spring rates of welded bellows in addition to the accurate values of surface stresses at points of the bellows that are not influenced by the notch effect. It is possible that analytical methods can be applied to obtain the stresses at the weld-bead notch, but such analyses require development beyond the theory developed in the current research program.

Another factor in the welded bellows and diaphragms is the local material variation that results even with the best current welding practice: possible weld defects of several kinds, local variations in metallurgical microstructure in and near the weld, residual stresses, etc. Such variations have been observed to influence significantly the fatigue resistance of welded joints in other structures as well as in bellows.

Consequently, fatigue tests of typical welded bellows and diaphragms were conducted to find out how such additional parameters as the weld notch geometry and the metallurgical variations in weld material might influence the analysis of fatigue lifetimes in terms of strain ranges computed by shell theory for a model with a reasonable allowance for weld-bead stiffness.

Fatigue Test Specimens and Conditions

The test specimens (bellows and diaphragms) were ordered in batches of 12. It was requested that the specimens in each batch be made as nearly identical as was reasonably possible within the state of the art (see Appendix P). All of the welded bellows had been inspected carefully by each manufacturer and by Battelle prior to test and were judged to be of good quality. Examinations of typical cross-sectioned bellows after test showed that they were made with good manufacturing techniques.

In general, 10 specimens of each batch were used for the fatigue tests. Three batches of bellows of Type 347 stainless steel, three of AM350, and one batch of diaphragms of Type 347 stainless steel were tested in fatigue. Early tests were conducted in pairs, with one bellows deflected 100 percent in compression and one 50 percent in compression and 50 percent in tension; this was the procedure used for the formed

bellows. However, the life of welded bellows with 100 percent compression was so much longer than that of welded bellows in tension-compression that this procedure resulted in the fatigue machine operating a large percentage of the time with only one specimen. Hence, to expedite the tests, bellows were subsequently tested either singly or with both experiencing the same degree of compression and tension. On account of some long test times, the cycling speed was sometimes increased during a test. Usually a test was started at 80 cpm; after 300,000 cycles the speed was increased up to 120 cpm; in no instance was the speed high enough that dynamic response significantly increased strain.

Test conditions of deflection and pressure were generally chosen to produce selected values of strain, as calculated by elastic theory, at a convolution root.

Results of Fatigue Tests

Tables N-1 through N-7 give the results of the fatigue tests. If these are plotted in terms of a single parameter, such as the calculated strain range at a convolution root, against lifetime, the points show such scatter that it seems clear that a single parameter is an inadequate criterion for prediction of fatigue lifetime. Some insight into this inadequacy can be obtained by considering some of the apparent trends.

Scatter in Lifetimes

Even under identical conditions of loading of supposedly identical bellows, there were instances of very great variation in lifetime. Examples are shown in Table N-8. These were presumably (and sometimes identifiably*) due to variations in material properties and in manufacturing processes.

The scatter in results of the fatigue tests has another important limitation. As noted subsequently, some loading variables (the pressure, the degree of compression) have apparently more influence on the lifetimes of welded bellows than they have on the lifetimes of formed bellows. In view of the large scatter for supposedly identical testing conditions and of the effects of loading variables, a quantitative assessment of factors influencing lifetime would require a much larger number of specimens of welded bellows than of formed bellows. For this reason, analysis of the results of the finite number of tests in this research program is qualitative.

Effect of Pressure

Considerable difficulty was experienced in the interpretation of the initial fatigue results of the Type 347 stainless steel bellows because internal pressure caused the bellows diaphragms to deform, and at certain values of pressure and compression, the diaphragms touched and increased local strains in the bellows. This effect had not been encountered in the state-of-the-art survey. When this failure mode was suspected, it was easily verified by careful spring-rate measurements made with incrementally compressed bellows containing a constant internal pressure. Diaphragm interference was

*For example, the early failure of JD141 through the weld bead was ascribed to insufficient burn-down. Although other failures were examined as described in Appendix P, it was beyond the scope of this program to determine the exact cause of failure of every bellows.

detected by an increase in spring rate at various values of compression, depending on the amount of internal pressure. Considerable diaphragm interference was demonstrated for the combinations of test conditions used for bellows JD133, JD142, JD149, and JD147, and significant reductions in fatigue life were experienced by these bellows, as is shown in Table N-9.

The fact is generally known that welded bellows have a longer fatigue life in compression than in tension. Thus, there is a natural tendency to use a welded bellows as much as possible in compression. However, diaphragm interference must be avoided because of the possibility of encountering a large reduction in fatigue life. Although this condition cannot be estimated by the analysis procedures described in Appendix B, it can easily be determined experimentally as described above.

On the basis of the brief evaluation that was possible, the pressurized bellows must not be compressed beyond the point at which the spring rate is increased 10 percent, if the bellows fatigue life is to be unaffected by diaphragm interference. Engineering judgment must be used to determine the actual amount of compression that can be permitted and still provide an adequate margin of safety to avoid this condition.

Even without diaphragm interference, a change in internal pressure has two effects: (1) a possible change in diaphragm shape not included in the stress analysis program and (2) a change in the mean strain during a cycle that may be large enough to affect the fatigue lifetime. Such effects were noted in the behavior of formed bellows, but they seemed small enough that they could be neglected as a first approximation in estimating fatigue lifetime. The entries in Table N-10 indicate a very definite trend for increasing internal pressure to decrease the lifetime of welded bellows and diaphragms.

The larger effect of pressure on the fatigue life of welded bellows than on the fatigue life of formed bellows may be due in part to the strain concentration at the welds being influenced by internal pressure.

Effect of Percent of Stroke in Tension

Examination of the entries in Tables N-1 through N-7 (some examples are shown in Tables N-11 and N-12), shows that, for a specific stroke, the greater the percent of this stroke in tension the shorter is the fatigue lifetime. This effect was pronounced for welded bellows, in contrast to observations for formed bellows. It seems likely that the effect can be associated with the notch formed by the weld bead. This localized behavior might be accounted for by a strain concentration factor considered to be different in tension than in compression. A plausible mechanistic description would require an analysis (probably elastic-plastic) of the weld bead area. A useful numerical factor can probably be obtained for a given material and a given manufacturer's process if enough tests are conducted. Some of the manufacturers offer this type of correlation for their bellows, and the Type 347 bellows and diaphragms tested during this program could be closely correlated with selected factors. However, the same factors did not apply to the AM350 bellows, and it is believed that empirical factors must be developed for each material and each manufacturer.

Fatigue Failure Location

Examination of Tables N-1 and N-2 shows that there were more failures at crown welds than at root welds despite calculated strain ranges being higher at the root areas. This indicates either more severe weld defects in this location or a higher local strain concentration (or, of course, some combination of these). Tables N-1 through N-7 show a general inconsistency of failure location for all of the batches of bellows, with many failures at end-fitting joints. Such variations emphasize the need for more detailed understanding of local conditions in these areas.

Conclusions and Recommendations

(1) The results of fatigue tests on typical welded bellows and diaphragms were not nearly so well correlated with strain ranges computed by shell theory as were the results of fatigue tests on formed bellows.

(2) One factor that made attempts at correlation difficult was the apparent scatter in fatigue lifetime and failure location for each batch of specimens. It is believed this was due to variations in fabrication (particularly in welding) that seem unavoidable in the present state of the art. Allowance for these would require the testing of many specimens to afford statistically significant measures.

(3) Correlation was also made difficult by another factor – local strain concentration not derivable on the basis of shell theory. The presence of this factor was shown by the dependence of lifetime upon internal pressure and upon the percent of stroke in tension, and by the prevalence of failure at the crown weld beads despite larger calculated stresses at the root weld beads. A strain concentration factor, larger for crown welds than for root welds and larger for tension than for compression, could be applied to calculated strain ranges to make the test results under different loading conditions more consistent. Obtaining numerical values for such a factor would be aided by a more elaborate theoretical analysis, and, for engineering purposes, would require many tests to provide statistical significance.

(4) Until further research is conducted, the practical considerations where welded bellows or diaphragms must be used are:

   (a) Utilize the stress-analysis procedure described in Appendix B to calculate spring rate and effective area, and to evaluate the comparative effects of different deflection and pressure loadings for a given material and a given manufacturer.

   (b) Recognize the probability of larger scatter than for formed bellows and allow for this by tests of a relatively large number of units of a specific lot of material fabricated by a specific process to provide some statistical measure of probability of "premature" failure.

(c) Test under conditions (high internal pressure and high percentage of stroke in tension) that, within the range of necessary usage, seem most critical.

(d) Monitor weld burn-down during manufacture to assure that the weld bead has a diameter at least 3 times the thickness of the diaphragm.

TABLE N-1. RESULTS OF FATIGUE TESTS OF 3-1/2-INCH TYPE 347 STAINLESS STEEL WELDED BELLOWS[a]

(Test Conditions: Room temperature, 80 cpm--see Appendix L for other details.)

Bellows	Total Stroke, in.	% Stroke in Tension	Internal Pressure, psi	Strain Range[b] at Root Weld Bead, μin./in.	Strain Range[b] at Crown Weld Bead, μin./in.	Cycles to Failure	Failure Location[c]; Remarks
JD141	0.240	0	20	2000	1800	453[e]	Crown No. 7, 355° to 10°, crack through weld bead
JD135	0.250	0	20	2000	1800	1,747,069	Did not fail
JD132	0.240	50	20	2000	1800	73,322[e]	Crown No. 1, 175° to 195°, crack through weld bead
JD140	0.240	50	20	2000	1800	282,346	Crown No. 5, 200° to 205°, crack through weld bead
JD131[d]	0.240	50	20	2000	1800	768,870	Did not fail
JD138[d]	0.240	0	20	2000	1800	768,870	Did not fail
JD137	0.240	50	40	2000	1800	95,590	Crown No. 1, 215° to 220°, crack through weld bead
JD138[d]	0.480	50	4	4000	3600	158,115	Lower end fitting, 100° to 110°, crack through weld bead
JD131[d]	0.480	50	4	4000	3600	158,520	Crown No. 5, 190° to 195°, crack through weld bead
JD139	0.480	50	10	4000	3600	195,600	Crown No. 1, 100° to 115°, crack through heat-affected zone
JD133	0.480	50	20	4000	3600	11,382[f]	Lower end fitting, 10° to 20°, crack through weld bead
JD142	0.480	50	40	4000	3600	4,219[f]	Crown No. 3, 145° to 150°, crack through weld bead

(a) Manufacturer A. (b) Maximum strain range calculated from elastic theory. (c) Range of angle indicates approximate length of crack. (d) These bellows were tested in two modes. (e) These fatigue failures were considered to be abnormally short. (f) These early-fatigue failures were caused by pressure-induced diaphragm interference.

TABLE N-2. RESULTS OF FATIGUE TESTS OF 1-1/2-INCH TYPE 347 STAINLESS STEEL WELDED BELLOWS[a]

(Test Conditions: Room temperature; 80-120 cpm--see Appendix L for other details.)

Bellows	Total Stroke, in.	% Stroke in Tension	Internal Pressure, psi	Strain Range[b], at Root Weld Bead, μin./in.	Strain Range[b] at Crown Weld Bead, μin./in.	Cycles to Failure	Failure Location[c]; Remarks
JD145	0.160	0	4	3760	3340	831,864	Crown No. 3, 3/8 in. crack in heat-affected zone
JD146	0.160	0	30	3760	3340	776,163	Crown No. 3, 1/8 in. crack in heat-affected zone
JD149	0.160	0	60	3760	3340	27,694[d]	Crown No. 1, 55° to 70°, crack in heat-affected zone
JD147	0.160	0	90	3760	3340	4,010[d]	Crown No. 4, 300° to 315°, crack in heat-affected zone
JD148	0.160	50	4	3760	3340	94,800	Root No. 2, 190° to 330°, crack in heat-affected zone
JD144	0.160	50	4	3760	3340	74,087	Root No. 1, 25° to 70°, crack in heat-affected zone
JD153	0.160	50	30	3760	3340	63,751	Crown No. 1, 3/8 in. crack in heat-affected zone
JD152	0.160	50	60	3760	3340	55,620	Crown No. 1, 330° to 340°, crack in heat-affected zone
JD151	0.160	50	90	3760	3340	28,145	End fitting, 210° to 250°, crack in heat-affected zone
JD154	0.080	100	4	1880	1670	1,501,500	Did not fail

(a) Manufacturer A.
(b) Maximum strain range, calculated from elastic theory.
(c) Range of angle indicates approximate length of crack; specimens without angular measurements had been destroyed for fractographic examination.
(d) These early-fatigue failures were caused by pressure-induced diaphragm interference.

TABLE N-3. RESULTS OF FATIGUE TESTS OF 1-1/2-INCH TYPE 347 STAINLESS STEEL WELDED BELLOWS[a]

(Test Conditions: Room temperature, 80-120 cpm--see Appendix L for other details)

Bellows	Total Stroke, in.	% Stroke in Tension	Internal Pressure, psi	Strain Range[b] at Root Weld Bead, μin./in.	Strain Range[b] at Crown Weld Bead, μin./in.	Cycles to Failure	Failure Location[c]; Remarks
JD203	0.160	50	4	2740	1580	1,216,345	Root No. 6, 35° to 55°, crack through heat-affected zone
JD204	0.160	50	4	2740	1580	204,920	Upper end fitting, 270° to 190° crack through heat-affected zone
JD205	0.120	100	4	2055	1185	412,322	Root No. 2, 105° to 135°, crack through weld bead
JD206	0.120	100	4	2055	1185	214,636	Crown No. 4, 60° to 85°, crack through weld bead
JD207	0.240	50	4	4110	2370	53,598	Crown No. 3, 120° to 140°, crack through weld bead
JD208	0.240	50	4	4110	2370	48,336	Upper end-ftg. weld, 25° to 65°, crack through heat-affected zone
JD209	0.180	100	4	3425	1975	47,530	Crown No. 5, 210° to 235°, and crown No. 6, 175° to 210°, crack through weld bead
JD210	0.180	100	4	3425	1975	51,916	Upper end-fitting weld, 270° to 325°, crack through heat-affected zone
JD211	0.240	100	4	4110	2370	17,588	Crown No. 7, 10° to 50°, crack through weld bead
JD212	0.240	100	4	4110	2370	22,380	Crown No. 2, 35° to 55°, crack through weld bead
JD213	0.360	100	4	6165	3555	4,496	Root No. 7, 165° to 245°, crack through weld bead

(a) Manufacturer B.
(b) Maximum strain range, calculated from elastic theory.
(c) Range of angle indicates approximate length of crack.

TABLE N-4. RESULTS OF FATIGUE TESTS OF 3-INCH AM350 WELDED BELLOWS[a]

(Test Conditions: Room temperature, 80-100 cpm--see Appendix L for other details.)

Bellows	Total Stroke, in.	% Stroke in Tension	Internal Pressure, psi	Strain Range[b] at Root Weld Bead, μin./in.	Strain Range[b] at Crown Weld Bead, μin./in.	Cycles to Failure	Failure Location[c]; Remarks
JD191[d]	0.240	100	4	1940	1220	1,900,000	Did not fail
JD192[d]	0.240	100	4	1940	1220	1,900,000	Did not fail
JD191[d]	0.480	100	4	3880	2440	580,000	Did not fail
JD192[d]	0.480	100	4	3880	2440	580,000	Did not fail
JD191[d]	0.640	100	4	5173	3253	29,539	Root No. 1, 95° to 120°, crack in heat-affected zone
JD192[d]	0.640	100	4	5173	3253	26,394	Root No. 1, 290° to 320°, crack in heat-affected zone
JD195	0.735	100	2	5935	3735	15,220	Root No. 1, 80° to 110°, crack in heat-affected zone
JD196	0.735	100	2	5935	3735	16,774	Root No. 6, 203° to 205° and 235° to 240°, crack in heat-affected zone
JD199	0.600	80	2	4850	3050	54,878	Root No. 1, 15° to 40° , crack in heat-affected zone
JD200	0.600	80	2	4850	3050	32,103	Upper end-fitting weld, 20° to 55°, crack in heat-affected zone
JD201	0.600	80	2	4850	3050	76,759	Root No. 1, 160° to 175°, crack in heat-affected zone
JD197	0.720	66-2/3	3	5820	3660	44,207	Root No. 7, 265° to 285°, crack in heat-affected zone
JD198	0.720	66-2/3	3	5820	3660	39,469	Lower end-fitting weld, 10° to 40°, crack in heat-affected zone
JD193	0.960	66-2/3	4	7760	4880	7,938	Lower end-fitting weld, 255° to 285°, crack in heat-affected zone
JD194	0.960	66-2/3	4	7760	4880	16,460	Lower end-fitting weld, 0° to 360°, crack in heat-affected zone

(a) Manufacturer C.
(b) Maximum strain range calculated from elastic theory.
(c) Range of angle indicates approximate length of crack.
(d) These bellows were tested in more than one mode.

TABLE N-5. RESULTS OF FATIGUE TESTS OF 3-INCH AM350 WELDED BELLOWS[a]

(Test Conditions: Room temperature, 80 - 100 cpm--see Appendix L for other details.)

Bellows	Total Stroke, in.	% Stroke in Tension	Internal Pressure, psi	Strain Range[b] at Root Weld Bead, μin./in.	Strain Range[b] at Crown Weld Bead, μin./in.	Cycles to Failure	Failure Location[c]; Remarks
JD156	0.240	50	4	1700	2940	1,612,266	Did not fail
JD164	0.240	50	40	1700	2940	1,000,000	Did not fail
JD166	0.240	50	40	1700	2940	37,145	Upper end fitting, 5° to 45°, crack in heat-affected zone
JD157	0.240	100	4	1700	2940	26,321	Upper end fitting, 55° to 140°, crack in heat-affected zone
JD159	0.240	100	4	1700	2940	104,518	Root No. 7, 165° to 240°, crack in heat-affected zone
JD161	0.240	100	4	1700	2940	140,137	Root No. 6, 100° to 140°, crack in heat affected zone
JD162	0.240	100	40	1700	2940	37,779	Crown No. 1, small crack at 90°
JD163	0.240	100	40	1700	2940	27,339	Upper end fitting, 150° to 180°, crack in heat-affected zone
JD160	0.240	100	80	1700	2940	20,394	Upper end fitting, 5° to 30°, crack in heat-affected zone
JD165	0.240	100	80	1700	2940	26,219	Upper end fitting, 5° to 45°, crack in heat-affected zone

(a) Manufacturer D.
(b) Maximum strain range at convolution root, calculated from elastic theory.
(c) Range of angle indicates approximate length of crack.

TABLE N-6. RESULTS OF FATIGUE TESTS OF 1-1/2-INCH AM350 WELDED BELLOWS[a]

(Test Conditions: Room temperature, 80 - 120 cpm-- see Appendix L for other details.)

Bellows	Total Stroke, inch	% Stroke in Tension	Internal Pressure, psi	Strain Range[b] at Root Weld Bead, μin./in.	Strain Range[b] at Crown Weld Bead, μin./in.	Cycles to Failure	Failure Location[c]; Remarks
JD168[d]	0.100	100	4	2550	1640	2,005,000	Did not fail
JD168[d]	0.150	100	4	3825	2460	829,500	Did not fail
JD169[d]	0.200	50	4	5100	3280	3,695,000	Did not fail
JD172	0.250	60	4	6375	4100	257,373	Lower end fitting, 135° to 165°, crack in heat-affected zone
JD173	0.250	60	4	6375	4100	117,450	Root No. 7, 270° to 330°, crack in heat-affected zone
JD174	0.250	60	4	6375	4100	211,987	Root No. 7, 165° to 210°, crack in heat-affected zone
JD177	0.250	60	60	6375	4100	41,015	Root No. 5, 350° to 10°, crack in heat-affected zone
JD178	0.250	60	60	6375	4100	32,203	Upper end fitting, 195° to 210°, crack in heat-affected zone
JD168[d]	0.200	100	4	5100	3280	24,670	Root No. 7, 110° to 150°, crack in heat-affected zone
JD169[d]	0.200	100	4	5100	3280	46,230	Root No. 7, 115° to 125°, crack in heat-affected zone
JD170	0.200	100	4	5100	3280	37,160	Crown No. 7, 80° to 140°, crack in heat-affected zone
JD175	0.300	66-2/3	4	7650	4920	18,234	Upper end ftg, 155° to 185°, crack in heat-affected zone
JD176	0.300	66-2/3	4	7650	4920	21,244	Root No. 7, 345°to 355°, crack in heat-affected zone

(a) Manufacturer D. (b) Maximum strain range at convolution root, calculated from elastic theory.
(c) Range of angle indicates approximate length of crack. (d) These bellows were tested in more than one mode.

TABLE N-7. RESULTS OF FATIGUE TESTS OF 4-INCH TYPE 347 DIAPHRAGMS[a]

(Test Conditions: Room temperature, 80 cpm--see Appendix L for other details)

Diaphragm	Total Stroke, inch	% Stroke in Tension	Internal Pressure, psi	Local Strain Range[b], μin./in.	Cycles to Failure	Failure Location[c]; Remarks
JD186	0.080	50	0.5	2600	625,000	Did not fail
JD187	0.080	50	0.5	2600	625,000	Did not fail
JD179	0.080	100	0.3	2600	227,456	Hub weld, crack through heat-affected zone, 180° to 230°
JD180	0.080	100	0.3	2600	115,730	Hub weld, crack through heat-affected zone, 0° to 360°
JD184	0.160	50	0.5	5200	7,335	Hub weld, crack through heat-affected zone, 170° to 230°
JD185	0.160	50	0.5	5200	4,787	Hub weld, crack through heat-affected zone, 55° to 125°
JD182	0.160	100	0.5	5200	2,173	Fatigue crack in trough of center corrugation (Dim. S), 125° to 220°
JD183	0.160	100	0.5	5200	2,436	Fatigue crack in trough of center corrugation (Dim. S), 85° to 125°

(a) Manufacturer E.
(b) Maximum strain range at diaphragm ID, calculated from elastic theory.
(c) Range of angle indicates approximate length of crack.

TABLE N-8. EXCESSIVE VARIATION IN THE FATIGUE LIFE OF WELDED BELLOWS

Bellows	OD, inch	Bellows Material	Internal Pressure, psi	Stroke, inch	% Stroke in Tension	Fatigue Life
JD141	3-1/2	347 S.S.	20	0.240	0	453
JD135	3-1/2	347 S.S.	20	0.240	0	NF 1,747,069
JD132	3-1/2	347 S.S	20	0.240	50	73,322
JD131	3-1/2	347 S.S.	20	0.240	50	NF 768,870
JD166	3	AM350	40	0.240	50	37,145
JD164	3	AM350	40	0.240	50	NF 1,000,000

TABLE N-9. REDUCTION IN THE FATIGUE LIFE OF TYPE 347 STAINLESS STEEL WELDED BELLOWS DUE TO PRESSURE-INDUCED DIAPHRAGM INTERFERENCE

Bellows	OD, inch	Internal Pressure, psi	Stroke, inch	% Stroke in Tension	Fatigue Life
JD138	3-1/2	4	0.480	50	158,115
JD131	3-1/2	4	0.480	50	158,520
JD139	3-1/2	10	0.480	50	195,600
JD133	3-1/2	20	0.480	50	11,382
JD142	3-1/2	40	0.480	50	4,219
JD145	1-1/2	4	0.160	50	831,864
JD146	1-1/2	30	0.160	50	776,163
JD149	1-1/2	60	0.160	50	27,694
JD147	1-1/2	90	0.160	50	4,010

TABLE N-10. EFFECT OF INCREASING INTERNAL PRESSURE ON THE FATIGUE LIFE OF WELDED BELLOWS

Bellows	OD, inch	Bellows Material	Internal Pressure, psi	Stroke, inch	% Stroke in Tension	Fatigue Life
JD148	1-1/2	347 SS	4	0.160	50	94,800
JD144	1-1/2	347 SS	4	0.160	50	74,087
JD153	1-1/2	347 SS	30	0.160	50	63,751
JD152	1-1/2	347 SS	60	0.160	50	55,620
JD151	1-1/2	347 SS	90	0.160	50	28,145
JD161	3	AM350	4	0.240	100	140,137
JD159	3	AM350	4	0.240	100	104,518
JD162	3	AM350	40	0.240	100	37,779
JD163	3	AM350	40	0.240	100	27,339
JD165	3	AM350	80	0.240	100	26,219
JD160	3	AM350	80	0.240	100	20,394
JD172	1-1/2	AM350	4	0.250	60	257,373
JD174	1-1/2	AM350	4	0.250	60	211,987
JD173	1-1/2	AM350	4	0.250	60	117,450
JD177	1-1/2	AM350	60	0.250	60	41,015
JD178	1-1/2	AM350	60	0.250	60	32,203

TABLE N-11. EFFECT OF PERCENT STROKE IN TENSION ON THE FATIGUE LIFE OF 1-1/2-INCH TYPE 347 STAINLESS STEEL BELLOWS

Bellows	OD, inch	Internal Pressure, psi	Stroke, inch	% Stroke in Tension	Fatigue Life
JD145	1-1/2	4	0.160	0	831,864
JD146	1-1/2	30	0.160	0	776,163
JD148	1-1/2	4	0.160	50	94,800
JD144	1-1/2	4	0.160	50	74,087
JD153	1-1/2	30	0.160	50	63,751

TABLE N-12. COMPARISON OF THE EFFECT OF INCREMENTS OF TENSION AND COMPRESSION ON THE FATIGUE LIFE OF WELDED BELLOWS

Bellows	OD, inch	Bellows Material	Internal Pressure, psi	Basic Stroke in Tension, inch	Additional Stroke Increment, inch	Fatigue Life
JD205	1-1/2	347 SS	4	0.120	-	412,322
JD206	1-1/2	347 SS	4	0.120	-	214,636
JD207	1-1/2	347 SS	4	0.120	0.120 (compr.)	53,598
JD208	1-1/2	347 SS	4	0.120	0.120 (compr.)	48,336
JD209	1-1/2	347 SS	4	0.120	0.060 (tens.)	47,530
JD210	1-1/2	347 SS	4	0.120	0.060 (tens.)	51,916
JD168[a]	1-1/2	AM350	4	0.150	-	NF829,550
JD172	1-1/2	AM350	4	0.150	0.100 (compr.)	257,373
JD173	1-1/2	AM350	4	0.150	0.100 (compr.)	117,450
JD174	1-1/2	AM350	4	0.150	0.100 (compr.)	211,987
JD168[a]	1-1/2	AM350	4	0.150	0.050 (tens.)	24,670
JD169	1-1/2	AM350	4	0.150	0.050 (tens.)	46,230
JD170	1-1/2	AM350	4	0.150	0.050 (tens.)	37,160

(a) This bellows was tested in more than one mode.

APPENDIX O

EVALUATION OF THE CORROSION BEHAVIOR OF BELLOWS AND DIAPHRAGM MATERIALS FOR AEROSPACE APPLICATIONS

APPENDIX O

EVALUATION OF THE CORROSION BEHAVIOR OF BELLOWS AND DIAPHRAGM MATERIALS FOR AEROSPACE APPLICATIONS

The application of a bellows or diaphragm in a particular environment must necessarily take into account the corrosion behavior of the material of construction in order to assure the planned life expectancy. Of the various rocket fuels, oxidizers, and other fluids of interest to the Air Force, many are reactive and require special handling techniques and special materials of construction.

One objective of the program was the study of the corrosion behavior of selected metals and alloys on the basis of their use as bellows and diaphragm materials in missile fluids. The results of this work are presented in four categories:

(1) Forms of Corrosion - The various forms of corrosion pertinent to missile systems are discussed in relation to bellows and diaphragms.

(2) Compatibility to Fluid Media - The general compatibility of metals and alloys is discussed for the fluids of interest.

(3) Literature Survey - A summary is given of a literature survey for pertinent corrosion data.

(4) Experimental Program - A summary is given of a laboratory investigation conducted to obtain corrosion-fatigue data for selected metal coupons tested in representative fluids.

Forms of Corrosion

Corrosion manifests itself in a number of ways. The attack may be uniform or it may be localized in the form of pits. Corrosion may combine with other deteriorating factors such as static or cyclic stresses and result in particularly severe damage. It is not uncommon for several forms of corrosion to occur at the same time, although one form usually predominates.

Corrosion and oxidation resistance are often considered as entirely separate characteristics. However, in many ways they are very similar. Fortunately, many of the commercial alloys noted for good oxidation resistance are equally resistant to corrosive attack in many media. To be considered useful, a material must have adequate corrosion and/or oxidation resistance in the service media when subjected to the service conditions.

The following sections discuss several forms of corrosion and their relationship to the performance of bellows in the candidate environments. These forms are:

(1) Uniform attack

(2) Pitting

(3) Corrosion fatigue

(4) Stress-corrosion cracking

(5) Intergranular attack

(6) Preferential phase dissolution

(7) Erosion corrosion

(8) Galvanic attack

(9) Concentration cell corrosion

(10) Oxidation.

Uniform Attack

Uniform attack of metal systems is the most common form of metal corrosion caused by chemical or electrochemical reaction. It is typified by uniform wastage of the metal and can be measured by loss of weight or thickness. Since highly corrosion-resistant materials will normally be selected, this type of attack will present no great problem in the design of bellows and diaphragms. When less resistant materials are considered, then weight change data can be used to establish adequate corrosion allowances to insure satisfactory equipment life.

Pitting

Pitting is one of the most detrimental forms of corrosion, since failure can occur owing to perforation of metals with relatively little overall weight loss. Pitting is a localized form of attack and is often initiated as a result of the presence of impurities, inclusions, rough spots, nicks on the metal surface, crevices, etc., which promote localized breakdown of protective surface films. Pits can also be points of initiation for other forms of attack such as stress-corrosion cracking or corrosion fatigue.

The choice of materials for bellows and diaphragms must be restricted to those materials in which little or no pitting has been observed in the required environments.

Corrosion Fatigue

Corrosion fatigue can be defined as the combination of the effects of corrosion and cyclic stress occurring at the same time. Many metals are said to have a "fatigue limit"

or a limit of stresses below which failures caused by cyclic loading are not expected. This is true only in the absence of corrosion, since no fatigue limit exists when corrosion is present.

Fatigue tests are most often conducted in air. After a sufficient number of cycles at high enough loads, fatigue cracking will occur. Corrosion is usually considered to play no part in this process, although air and moisture do cause some corrosion. However, in general, corrosion in air has only a moderate effect on fatigue properties. When attack is more severe, corrosion fatigue must be measured in terms of "endurance limit" or the highest stress which can be withstood without failure in a particular number of cycles, say 10^7 cycles.

With corrosion fatigue, the total time duration of the exposure is important as well as the number of cycles to failure, since corrosion is time dependent. For instance, if the rate of cyclic stressing is high, failure may occur before significant corrosion has taken place. In this case, the endurance limit will be nearly the same as that for air. On the other hand, if cyclic stressing rates are low, the specimen may be severely corroded before a large number of stress cycles is reached. In this instance there will be a large difference between the endurance limit with and without corrosion. Thus, in corrosion-fatigue studies there are two variables: stress and cyclic rate.

The corrosion resistance of many metals is a function of the corrosion-product film on the metal surface. Cyclic stresses tend to rupture or render more permeable these protective films which usually retard corrosion. Also, fatigue produces worked or distorted areas on the metal surfaces. These worked areas are more susceptible to corrosive attack while undergoing distortion, and a change in the local area ratios of anode to cathode may cause a variation in polarization, with accompanying accelerated attack. In either case, fatigue increases localized corrosion rates and promotes the formation of notches. In turn, the notches accelerate the fatigue damage.

From the standpoint of bellows and diaphragm applications, corrosion fatigue can be a serious limitation to the choice of materials of construction. Some materials may be eliminated and the allowable stress for others may be drastically reduced in very reactive oxidizing media. Since corrosion fatigue data were not available for many combinations of materials and propellants of interest to the program, representative data were obtained by selected laboratory tests.

Stress-Corrosion Cracking

Stress-corrosion cracking can be described as an interaction between static tensile stress and corrosion, causing more rapid failure than the sum of the individual effects of stress and corrosion acting separately. The failure is characterized by a brittle-type fracture in an otherwise ductile material. Often severe cracking occurs in the absence of any significant general corrosion. Stress-corrosion cracking is believed to occur only with alloy systems and generally not with pure metals. Microscopically small branched cracks, either transgranular or intergranular, promote stress-corrosion cracking.

Tensile stresses must be present at the surface for stress-corrosion cracking to occur. Both residual and applied stresses must be considered. The magnitude of the stress is also critical, since the rate of failure increases with an increase in stress levels.

The environments which initiate stress-corrosion cracking are often specific. For instance, some high-strength steels fail rapidly under conditions of atmospheric exposure. Table O-1 lists a number of environments known to cause stress-corrosion cracking. For bellows and diaphragms, both high residual-tensile and high applied-tensile stresses could be present during long-term storage. Thus, susceptible materials exposed under certain environments might fail with little or no warning.

In the fuel and oxidizer systems under consideration, the role of stress-corrosion cracking has not been completely defined. To date, stress-corrosion cracking has not been found to be a problem in most of the systems. However, many of the high-strength alloys suffer severe stress-corrosion cracking under atmospheric conditions. For this reason, adequate stress-corrosion-cracking data would be required for candidate materials under exposure to the anticipated fluid media, as well as under atmospheric exposure.

Intergranular Attack

Intergranular attack results when the grain boundaries of an alloy are selectively attacked in a given environment. In this manner, whole grains can fall out, or disintegration of the whole metal can occur, even though a relatively small percentage of the metal is removed. A crystalline or sugary appearance is produced.

Welding or improper heat treatment of alloys is a common cause of intergranular attack. For instance, on the 18-8 stainless steels, corrosion can be intergranular when chromium carbides are allowed to precipitate in the grain boundaries. This is minimized by using an extra-low-carbon grade of steel or by the addition of carbon stabilizers such as columbium or titanium.

With some metals, an intergranular type of corrosion is the usual mode of attack. In these cases, the depth of penetration and the severity must be considered. In most of the selected environments, severe intergranular attack has not been reported and should not affect the choice of materials for bellows and diaphragms.

Preferential Phase Dissolution

Preferential phase dissolution occurs when a less resistant phase is selectively removed from an alloy, leaving a porous structure. Usually the dimensions of the structure do not change, and attack is not detected until failure occurs. Dezincification of brasses in water and decobaltization of Stellite in sulfuric acid are examples.

This type of attack is not often encountered and is not expected to complicate the selection of materials in the anticipated environments for bellows and diaphragms.

Erosion Corrosion

Erosion can be combined with corrosion to produce severe attack, often of a local nature. Many metals owe their corrosion resistance to protective films. The removal of these films by erosion exposes fresh metal to attack. As a result, the metal corrodes more rapidly than it does in the absence of erosion. Special terms are applied to

different forms of attack, such as erosion corrosion, impingement attack, cavitation, and fretting corrosion. The surface of the metal often appears worn or abraded by the attack.

Because of the thin materials of construction, care should be taken to prevent high velocities and direct impingement on bellows and diaphragms.

Galvanic Attack

Galvanic attack is often termed two-metal corrosion. When two dissimilar metals are connected in a corrosive liquid or conductive solution, a potential is set up between them and a current flows. Attack of the less resistant metal is accelerated, while the more resistant metal is protected. Since the current density is proportional to the area exposed, the area of the more resistant or more noble material should be kept small in relation to that of the less resistant metal. Metal loss is usually greatest at the point of contact with the noble metal.

Galvanic corrosion should not be a problem in bellows and diaphragms, since, in general, dissimilar metals will not be used in their construction. When they are used, those chosen will be near to each other in the galvanic series so that severe galvanic attack should be prevented. In addition, many of the proposed fluids are nonconductive, so that a flow of current, necessary for galvanic corrosion, will not occur.

Concentration-Cell Corrosion

Concentration cells between areas of different concentrations in an ionic solution can cause a potential difference and a current flow. An example of the result of this is the corrosion occurring in crevices and cracks. In aqueous solutions, a concentration cell can be set up by a buildup of ions in a stagnant area, or by depletion of the corrodant by corrosion. In systems which are open to the atmosphere, concentration cells of high and low oxygen contents are often found.

Although crevices may be common in bellows and diaphragms, crevice corrosion is not expected in the anticipated environments because: (1) many of the fluids are non-ionic and (2) the fluids will be completely closed to outside contaminants.

Oxidation

Oxidation attack can be considered a type of corrosion in which oxygen in the air is the corrosive medium. Oxidation resistance will be extremely important in selecting materials for high-temperature service where a portion of the component is exposed to air. Oxidation attack may proceed by most of the mechanisms previously discussed for general corrosion.

The rate of oxidation of any alloy depends on the access of oxygen atoms available to the metallic surface. The initial growth rate of the oxide film follows a parabolic relationship, since growth is controlled by the diffusion rate of metal ions through any existing film. After the initial growth period, further oxidation depends greatly on the oxide-film characteristics. If the film is tight and adherent, growth may essentially

stop. Such oxide films are usually referred to as protective oxides. Aluminum, for example, forms such a film. Oxide films that crack or spall are nonprotective. Oxidation rates also are highly temperature dependent, increasing rapidly with increasing temperature. Small alloy additions may cause significant changes in the nature of the oxide film. For example, aluminum additions to nickel-base alloys greatly increase high-temperature-oxidation resistance.

In some alloys, oxidation may occur selectively at grain boundaries, accelerating the effective rate of penetration. Other alloys may have the mechanical properties of their surfaces altered significantly by oxidation. While such surface effects are not normally of concern, they are very important in the thin elements of bellows and diaphragms.

Compatibility With Fluid Media

In missiles, bellows and diaphragms are usually used in fluid systems. Thus, the environments for the bellows and diaphragms are determined by the fluid media. For missiles, these media can be divided into three groups:

(1) Cryogenic propellants – hydrogen, oxygen, fluorine, FLOX, and possibly diborane

(2) Storable propellants – UDMH-hydrazine blends, MMH, pentaborane, N_2O_4, ClF_3, NF_3, and N_2F_4

(3) Gases – helium, nitrogen, hydrogen, methane, fluorine, and combustion products.

Selected physical properties of these fluids are listed in Table O-2.

The exposure conditions of a given bellows or diaphragm vary considerably for the three groups. Under current Air Force practice, materials exposed to the cryogenic propellants can be in service at temperatures ranging from -423 to 200 F. Storable propellant systems have service temperatures from -65 F to 600 F. In some systems, such as for combustion gases, temperatures above 1000 F can be encountered.

Materials are selected for corrosive applications on the basis of: (1) overall corrosion resistance, (2) impact sensitivity of the metal to reaction with the environment, and (3) catalytic effect of the metal on the decomposition of the environment.

Another important consideration is the behavior of the metals and alloys in the atmosphere. For example, many of the ultrahigh-strength, low-alloy steels and precipitation-hardening stainless steels will experience stress-corrosion cracking in marine atmospheres. Similar conditions may promote pitting of other alloy systems. The proper selection of materials of construction and/or protective treatment can do much to minimize the corrosion problem.

The following sections discuss the known corrosion data and the limitations imposed by the fluids of interest.

Cryogenic Propellants

With cryogenic propellants, the first consideration is the mechanical properties of the candidate materials. Failure often results from loss of ductility at low temperatures. Face-centered cubic metals, and alloys which form solid solutions do not exhibit brittle fracture at low temperature and thus can be used to -423 F. Some hexagonal close-packed metals, such as magnesium and titanium, can be used in special cases.

There is essentially no corrosion of metals at the low temperatures of the cryogenic propellants. However, in the oxidizer systems, sensitivity to reactions caused by energy inputs, such as impact, must be considered. For instance, in LOX, titanium alloys can be ignited by impact or by puncture, resulting in violent reactions. In such cases the reaction continues until the metal or the oxygen is consumed. Contamination of the oxidizer systems with reactive organic materials can also cause severe damage. If the organic material is ignited, the intense heat can trigger rapid oxidation which may consume the system.

Hydrogen. Corrosion is not considered to be a problem with liquid hydrogen. Materials such as the austenitic stainless steels and the nickel-base, aluminum-base, and copper-base alloys are frequently used. Some magnesium alloys and titanium alloys, Ti-6Al-4V and Ti-5Al-2.5Sn, are used with care.

Room-temperature and high-temperature considerations for hydrogen are discussed under gases.

Diborane. Diborane, B_2H_6, is a relatively noncorrosive gas which is readily stored in low-alloy-steel containers. Since it decomposes slowly at room temperature and rapidly above about 290 F, it is generally stored at 32 F or below.

Oxygen. Little corrosion occurs in liquid oxygen. Most of the common aircraft metals are satisfactory for use. Titanium and its alloys are not recommended for LOX service because of their impact sensitivity in LOX.

With gaseous oxygen at temperatures up to about 200 F, the stainless steels and the nickel-base, copper-base, and aluminum-base alloys all give good service even at high pressures. At temperatures up to 1500 F, the materials of construction are limited to a few of the high-strength alloys with good oxidation resistance, such as those containing chromium, nickel, and cobalt.

Most of the available information on oxygen is either at high pressure and low temperature or low pressure and high temperature. The combination of both high temperature and high pressure is a severe condition, since the reactivity of oxygen increases with increase of both temperature and pressure. Many of these data will have to be developed as required.

Fluorine. High-purity liquid fluorine is not corrosive to most of the common metals used in the aerospace industry. If moisture is present, HF can form. In this case, Monel is the best choice; the stainless steels show a low corrosion rate, but they

tend to scale up. Titanium is slightly impact sensitive in liquid fluorine, but the reaction does not propagate and the damage is about the same as that from the impact alone. Owing to the reactivity of fluorine, fluorine systems are particularly susceptible to erosion corrosion. Corrosion considerations for gaseous fluorine are discussed under gases.

FLOX. FLOX, a solution of fluorine and oxygen, is generally handled with the same care as fluorine, although it may be slightly less corrosive. The same general comments for oxygen and fluorine apply to FLOX.

Storable Propellants

The storable propellants are generally those fuels and oxidizers which can be stored at moderate temperatures and pressures without extensive supervision. While many of the propellants, such as hydrazine or N_2O_4, are truly storable, other propellants such as ClF_3, NF_3, and N_2F_4 are storable only under pressure or at temperatures below room temperature (see Table O-2).

UDMH-Hydrazine Blends. The hydrazine fuels are slightly alkaline in nature and many common metals, with certain exceptions, can be used. The stainless steels, nickel, and titanium alloys, many aluminum alloys, and many cobalt alloys are quite resistant. Magnesium alloys have poor resistance to the fuel blend.

Decomposition of the fuel blend can readily occur with certain materials such as copper, iron, and possibly molybdenum acting as catalysts. Therefore, copper and iron alloys are not used for general service. Some early data indicated that the molybdenum-bearing stainless steels, such as Type 316, would catalyze decomposition of the fuel. More recent data have shown Type 316 to be as good as other stainless steels.

The hydrazine fuel can also decompose with temperature and the maximum service temperature is about 200 F.

Monomethylhydrazine. Monomethylhydrazine is similar to the UDMH-hydrazine blends. Metals suitable for the fuel blend are also suitable for MMH.

Pentaborane. Pentaborane is an extremely toxic liquid which is compatible with the common metals of the aerospace industry, including carbon steels and stainless steels, and nickel-base, aluminum-base, titanium-base, and copper-base alloys. Decomposition of pentaborane occurs at about 300 F.

No difficulties from corrosion are anticipated with bellows and diaphragms used with pentaborane.

Nitrogen Tetroxide. N_2O_4 is an oxidizer which forms nitric acid in the presence of water. When N_2O_4 is dry, most common metals can be used, including stainless steels, titanium alloys, steels, nickel alloys, and aluminum alloys. Magnesium alloys

show only fair resistance to dry N_2O_4. In moist N_2O_4, only those materials which are resistant to nitric acid can be used. The metals are limited to the stainless steels (including PH alloys) and titanium alloys. Titanium is slightly impact sensitive in N_2O_4, but this is not considered to affect its compatibility with liquid N_2O_4. At high temperature and high pressure, the oxidation-resistant chromium-nickel stainless steels probably will be required. In order to prevent stress-corrosion cracking of titanium alloys, green N_2O_4, containing 0.4 to 0.8 percent NO as an inhibitor is specified.

Chlorine Trifluoride. Chlorine trifluoride can be handled by many common metals. As with fluorine, a coating is formed on metals, which provides protection from corrosive attack. Among the metals which are resistant to ClF_3 are steel, stainless steel, nickel, Monel, and copper-base alloys. Monel and nickel are preferred because of their resistance to HF and HCl which are formed by the reaction of ClF_3 with water. Titanium is rapidly attacked by ClF_3.

Nitrogen Trifluoride. NF_3 is an oxidizer similar to fluorine and is generally stored below room temperature. It is handled by the same metals as those used with fluorine and oxygen. It is less reactive, however, than fluorine. It is a relatively stable gas at room temperature and can be stored in steel cylinders at room temperature at pressures of 600 psi. Stainless steel or nickel would be required for handling above room temperature. Stainless steel has been used for short periods of time at temperatures as high as 750 F at 500 psi. Additional corrosion data are needed to determine adequately the high-temperature and high-pressure service for NF_3.

Tetrafluorohydrazine. N_2F_4 is handled in a manner similar to NF_3. At temperatures of 840 F, copper and stainless steels show attack, as would be expected on the basis of fluorine data. Mild steel at 840 F is heavily attacked but the corrosion product appears to be adherent. Additional corrosion data for high-temperature and high-pressure service are required for N_2F_4.

Gases

High-temperature and high-pressure service may be experienced for certain gases. As temperatures and pressures are increased, the physical properties of the metals become especially important, and high-strength metals are required. The following sections discuss the temperature and pressure limitations of the gases from the standpoint of corrosion.

Helium. Helium does not react with metals and corrosion is not a problem.

Nitrogen. Nitrogen is not corrosive to most common metals at moderate temperatures and pressures. At atmospheric pressures, steels, stainless steels, nickel, or cobalt-base alloys show little corrosion at temperatures of the order of 1000 F. At 1500 F, some metals can become embrittled with nitrogen.

At temperatures of about 1500 F and higher, high-chromium-nickel stainless steels are required for nitrogen service. At pressures above atmospheric, the corrosion is expected to be more severe. The relationship between maximum temperatures and pressures on the corrosion of metal is not well defined.

Hydrogen. Materials can be embrittled at elevated temperatures and pressures when in contact with hydrogen. Thus, titanium alloys are not recommended for such use above about 200 F. Copper-base alloys are not subject to attack; however, when they contain oxides, the formation of water from reaction with hydrogen can cause rupture of the metal at temperatures as low as 750 F. Chromium-nickel stainless steel alloys (18-8 and 25-20) of low carbon content are not embrittled up to 3000 psi at 930 F, while at 3700 psi, 18-8 stainless steel becomes embrittled at 840 F. Cobalt-base alloys are considered resistant to hydrogen at least up to 1800 F. High-nickel alloys, free from oxides, are not adversely affected by hydrogen. Under conditions of higher temperatures or pressures, additional data will be required.

Methane. At room temperature, methane is not corrosive to common materials of construction. Methane is a reducing gas and at high temperatures will tend to disassociate into carbon and hydrogen. Metals resistant to both hydrogen embrittlement and to carburization will be required. In general, stainless steels are used for service at temperatures of 1000 F and above.

The effects of high-pressure methane on the corrosion of metals at high temperature are not fully known. High pressures may tend to depress the dissociation of methane and may reduce its corrosiveness.

Fluorine. Fluorine gas can be contained in many common metals because a tightly adherent fluoride film is formed. The temperature to which a metal is usually resistant appears to be related to the vapor pressure of its fluoride film. Thus, nickel is resistant to about 1200 to 1300 F, aluminum and copper to 700 F, steels (including stainless steels) to 400 to 600 F, and titanium to 300 F. Alloys containing silicon, molybdenum, columbium, or carbon may be susceptible to pitting owing to the high vapor pressure of their fluorides.

The reactivity of fluorine increases rapidly with pressure as well as temperature. The handling of fluorine above 1000 psi is difficult. Gas cylinders normally are used for only 400 psi.

Combustion Products. The exhaust from solid- and liquid-propellant motors contains a variety of combustion products. These products may vary from water, CO, and CO_2, to more corrosive media containing oxides of nitrogen, HF, or HCl. In addition, solid-propellant exhaust may contain oxides of various metals such as Al_2O_3.

In most cases, the general class of materials known as high-temperature oxidation-resistant alloys will be required. (See the discussion on oxygen.) Where chlorides and fluorides are found, alloys containing molybdenum and/or high nickel will be preferred. Where nitrates are present in solid-propellant exhaust, titanium might be useful up to about 1000 F.

Atmospheric Environment. Though the environment of rocket propellants on the inside of missile hardware is an important consideration for bellows and diaphragms, the atmospheric conditions must also be considered. The atmospheric environment may take several forms: ordinary air, marine atmosphere, air contaminated with small amounts of propellant, and any of the first three with moisture, depending upon the storage conditions.

Many of the materials of construction that might be selected on the basis of propellant compatibility will be resistant to ordinary or salt-contaminated atmospheric corrosion as well. Examples are cobalt alloys, nickel alloys, titanium alloys, and some copper alloys. The two main groups which may not be compatible with the possible atmospheric environments are the high-strength, low-alloy steels and the high-strength aluminum alloys. The steel alloys, heat-treated to their highest strength levels, are susceptible to stress-corrosion cracking in relatively mild conditions, and are very susceptible if chlorides are present.

Though the group of resistant alloys discussed above is not subject to stress-corrosion cracking in ordinary air, these alloys may be in propellant-contaminated air. Some data are available on stress-corrosion cracking caused by propellant contaminants, but very little corrosion-fatigue data are available.

Oxidation resistance will be a required property for components exposed to air at high temperatures. Nickel-base alloys will be most useful at temperatures between about 1200 and 1800 F. Since the refractory alloys exhibit very poor oxidation resistance, they will require protection from air by some suitable means.

Literature Search

A search was made of the literature for corrosion data for candidate bellows materials. Although general corrosion data were found for most media, corrosion-fatigue data relating to the requirements of this program were scarce.

The abstract series utilized included the National Association of Corrosion Engineers (1945 to 1967) and Chemical Abstracts (1957 to 1967). Many of the references contained extensive bibliographies, and some of these "subreferences" provided pertinent material.

The search was conducted under several headings. The headings fell essentially into three groups:

(1) General - Typical headings searched were "Corrosion Fatigue" and "Fatigue".

(2) Metals - Corrosion data were sought for the metals listed in Tables O-3 and O-4.

(3) Environments - Corrosion data were sought for the pertinent metals by environment.

The combined literature of fatigue and corrosion fatigue for metals is quite extensive. The researches on fatigue are far more numerous, however. In reality, many of the fatigue data are corrosion-fatigue data because the tests were conducted in air, and it has been shown that the fatigue limit of a metal is higher in vacuum than in air. Accordingly, in this report, corrosion fatigue is taken to mean failure in any atmosphere other than a vacuum. However, air data are given only where data in other media were available. In many cases, the reports did not fully describe the conditions under which fatigue life was determined. For example, where the testing was done in air, no relative-humidity data were included and it is known that this can have an influence on fatigue life.

Table O-5 contains data on the general corrosion of the pertinent metals. Most of these data were taken from DMIC Memorandum 201[1]* This table is included because there are few data on corrosion fatigue, and Table O-5 serves to screen those metals which corrode moderately or severely. The entries in Table O-5 follow the system used in DMIC Memorandum 201. The significance of the Digits 1, 2, 3, and 4 is explained in Table O-5. Compositions or types for various alloys are also entered in Table O-5. For example, under brass, the type "red", or composition "70-30", is given. In addition, the temperature at which the corrosion resistance was determined is given in Fahrenheit.

Table O-6 contains the available corrosion-fatigue data. In some cases, the data follow, in general, the rule that the fatigue limit in a corrosive medium is less than that in air. For low temperatures, the data equally indicate that the fatigue limit increases with a decrease in temperature.

Experimental Program

The combined effect of corrosion and cycle stress (corrosion fatigue) is a critical factor in the selection of materials for bellows and diaphragms. As described in the previous section, such data are not readily available for the more common rocket-propellant fluids. Consequently, it was decided that representative corrosion-fatigue data should be obtained by fatigue tests conducted with coupons of selected metal exposed to representative rocket-propellant fluids.

Selected Test Fluids

The fluid media of interest to the Air Force were divided into five groups on the basis of chemical properties and availability of corrosion data (see Table O-7). Chlorine trifluoride, a storable propellant, was selected to represent Group I, which included fluorine, nitrogen trifluoride, tetrafluorohydrazine, and FLOX mixtures. Nitrogen tetroxide, the only propellant in Group 2, was chosen because it is chemically quite different from the other oxidizers, and because of its importance in fluid systems. The 50/50 UDMH-hydrazine blend (Group 3) was selected to represent the hydrazine-type fuels such as UDMH, hydrazine, and monomethylhydrazine. The compositions of the purchased fluids are shown in Table O-8. No evaluation was made of materials from Group IV since inert-gas fatigue data or moderate-temperature air-fatigue data could be used in place of actual corrosion-fatigue data. In addition, no materials from

*References for Appendix O are listed on pp O-17, O-18, and O-19.

Group V were studied since some quantitative or at least qualitative corrosion-fatigue data are available for some temperature ranges. However, tests were conducted in air at 200 F to obtain more precise baseline data against which the data for the fluids of interest could be compared.

A temperature of 200 F was used for all tests. This temperature was selected as being a representative worst condition for a storable propellant system. The vapor pressure at 200 F was about 235 psia for N_2O_4, 215 psia for ClF_3, and 35 psia for A-50. Some decomposition of the A-50 was detected in three experiments, with the pressure in one experiment reaching about 345 psia.

Selected Test Metals

It was believed that the many classes of alloys available to designers of aerospace bellows and diaphragms could be represented by three types of materials: aluminum, stainless alloys, and nickel alloys. Aluminum 6061-T6, Type 347 stainless steel, and Inconel 718 were selected as being representative of these materials. Table O-9 gives the chemical and physical-property data for the selected metals.

Standard bending-fatigue specimens, Figure O-1, were machined from 51 to 53-mil sheet stock. After machining, the flat surfaces were polished by hand to a standard polished finish. Table O-10 gives the measured surface finishes of duplicate specimens of each material. The average surface finishes for 6061-T6 aluminum, Type 347 stainless steel, and Inconel 718 were 8.5, 2.6, and 4.7 microinches rms, respectively.

Experimental Equipment and Procedures

Experimental Equipment. The standard reversed-bending sheet specimens were exposed to the liquid propellants and to air at 200 F in specially designed chambers. Two chambers, shown schematically in Figure O-2, were constructed of Type 304 stainless steel. A stainless steel bellows permitted movement of the specimen by an external motor-driven eccentric cam. Teflon O-rings were used to seal the system; these were replaced after each run.

One chamber, used exclusively with ClF_3, employed Monel diaphragm valves with nickel tubing. The second chamber was used alternately (after cleaning) for either N_2O_4 or Aerozine 50 (A-50). Figure O-3 gives an overall view of the equipment, showing the insulation-wrapped chamber. Standard high-pressure fittings were used for the N_2O_4 and A-50 unit.

Prior to the experiments, the equipment and specimens were specially cleaned by soap and water, followed by an acetone rinse. The ClF_3 chamber was given an initial exposure to ClF_3 to decompose any residual organic matter and to provide a light fluoride film.

To begin an experiment, a specimen was placed in the chamber and the desired deflection was set. This was done by adjusting the eccentric cam, taking into account the

expansion of the system during heat-up to 200 F. The system was then sealed and evacuated.

The required amount of propellant, 250 cc, needed to cover the specimen was metered from the bulk-storage system into a bomb of the calculated volume. This amount was then added to the evacuated test chamber.

The system was heated to 200 F by electrical heating tapes within the insulation. The cyclic deflection was begun by starting the motor on the eccentric cam. Deflection of the specimen was detected by two small semiconductor strain gages placed in a machined groove behind the specimen, but outside the propellant environment. One such unit measured 5 by 30 mils, and employed 2-mil gold leads. The output signal was recorded by a 5 or 10-mv recorder.

The deflection applied to each specimen was designed to cause failure after 10,000 or 100,000 cycles (based on 200 F-air data). In order to allow equivalent time for corrosion fatigue, the rate of deflection was set at either 1.4 or 13.7 cpm. Thus, failure could be expected after 5 days of exposure for either 10,000- or 100,000-cycle experiments.

The 200 F-air experiments were performed in the equipment described above. A cyclic rate of 15 cpm was employed.

Experimental Procedures

The experimental procedures employed provided a safe and effective means of determining the time to failure for the three types of specimens in the four environments. For the experiments in air, attachment of a control device enabled exact measurement of the cycles to failure.

For the other environments, recording of the strain applied to each specimen provided a measure of the time to failure, although the equipment did not automatically shut off as with the runs in air. The cycles to failure were calculated by determining the time of failure as recorded on chart paper. In this manner, the low-cycle runs, of about 10,000 cycles, could be determined with an accuracy of about ±10 cycles (±0.1 percent). In the high-cycle (100,000 cycles) runs, time to failure was recorded within about ±1/2 hour or ±400 cycles (±0.4 percent). The specimen strain measurement for the high cycle (about 14 cpm) was made only 10 minutes out of each hour. Continuous measurement was not made since a continuous "band" was painted on the chart at the high-cycle rate.

For the most part, the equipment functioned satisfactorily, although occasional leaks developed in the bellows, resulting in loss of the environment. The bellows was then replaced, although in one case a small pinhole in the 5-mil wall was TIG welded. One bellows failure occurred with ClF_3 while at temperature during start-up. Since no combustible material was available, the ClF_3 boiled harmlessly away until transfer was accomplished into the storage system.

Some galling of the guide pins at the bottom of the chambers occurred during the experiments. This resulted in uneven application of load on the downstroke of the eccentric. Type 304 pins were, therefore, replaced midway in the program with harder

Type 410 stainless steel. This wear is believed to result from the poor lubrication properties of the fluids, especially ClF_3 and N_2O_4.

Some wear of all specimens under the knife edge also resulted from ClF_3 exposure. This effect is described in detail later.

Corrosion-Fatigue Results

Air. Air at 200 F was selected as a baseline for the corrosion-fatigue studies. Available room-temperature data were not believed to be applicable because of the difference in surface finish between the Battelle specimens and those of other investigators. In addition, some difference in the physical properties of the test specimens might result from the temperature increase from 70 to 200 F.

Table O-11 gives the cycle fatigue-failure data for the three materials in the test program. A plot of these data is shown in Figure O-4. Also shown are 70 F-air data from a previous fatigue study.[2]

Rather good agreement is indicated between these data. It appeared that the surface finish was the most important property, in the temperature range of 70 to 200 F. As expected, the smoother specimens attained a greater number of cycles before failure.

The stress-deflection calibration and stress-strain data for Al-6061-T6, Type 347, and Inconel 718 obtained during a previous program[2] are believed to be valid for the sheet material used in this program. These data, plotted in Figures O-5 through O-10, were used to relate deflection of the specimens to stress and strain.

N_2O_4. Excellent agreement was shown among the specimens of Al-6061-T6 and Type 347 stainless steel fatigue in liquid N_2O_4 at 200 F. The results of five experiments for each material are given in Table O-12. The deflection applied to each specimen and its expected cycles to failure were determined from the air-fatigue data previously discussed, Figure O-4. The applied strain was determined from calibration curves from a previous program.[2] Note that the specimens were strained in the plastic region during the low-cycle (10,000 cycles) experiments.

No significant corrosion could be detected for any specimens exposed to N_2O_4, as is to be expected for these highly resistant materials. Figure O-11 shows the typical appearance of the Al-6061-T6 and Type 347 specimens after failure. Note that a network of cracks can be detected around the point of failure. The line at the tip of the specimen is a scoring line from the knife edge.

A plot of these data is given in Figure O-12, along with the corresponding 200 F-air data (dashed line). It can be readily seen that the N_2O_4 data, especially for Type 347, fall below the air-fatigue values. This indicates a reduction in fatigue life for these metals when exposed to this oxidizer at 200 F. A loss of about 43 percent of fatigue life is shown at a strain of 6000 μin./in. and 19 percent at 3000 μin./in. for Al-6061-T6. For Type 347, this loss is 57 percent at 7000 μin./in. and 45 percent at 3000 μin./in. strain.

Aerozine 50. The fatigue life for Al-6061-T6 and Type 347 stainless steel was found to be identical to that obtained in 200 F air. The data are given in Table O-12, and plotted in Figure O-13. Excellent agreement among the experiments was found in the total of nine experiments with both materials.

No corrosion of the test specimens was indicated. Some decomposition of the hydrazine mix was detected during the last three experiments, with Specimens A-14, S-18, and S-4. It was believed to be the result of catalytic decomposition of the fuel caused by finely divided corrosion products trapped in the test chamber. This powder apparently remained from the previous N_2O_4 experiments, even though stringent cleaning procedures were employed. The powder probably came from wear of the guide pin, and several slightly rusty areas observed after disassembly.

This decomposition became progressively worse, generating a pressure rise of 0.75, 0.85, and 1.7 psi/hr for the three experiments. An estimated pressure of 345 psia was formed during the final run.

It is not believed that this decomposition and formation of gaseous products had any great effect on the fatigue specimen submerged in the liquid. Note the good agreement obtained for all the fatigue data.

Chlorine Trifluoride. Corrosion-fatigue data for four specimens each of Al-6061-T6, Type 347 stainless steel, and Inconel 718 in 200 F liquid ClF_3 are given in Table O-12. Corrected values of deflection, strain, and expected cycles to failure are also given. These corrected values are applied to take care of the wear which resulted under the knife edge of all specimens in ClF_3 runs. A plot of these data in presented in Figure O-14. Figure O-11 shows the typical appearance of Inconel 718 after exposure to ClF_3.

Little or no difference in fatigue behavior can be detected for Al-6061-T6 in 200 F ClF_3 compared with that in 200 F air. Inconel 718 also exhibits a similar behavior in life to failure between ClF_3 and air at 200 F. Some reduction in fatigue life is evident, however, for Type 347 stainless steel in ClF_3 at the very high strain rates of about 4000 to 7000 μin./in. These values are essentially in the plastic region (see Figure O-8). The reduction in life at 7000 μin./in. appears to be of the order of 45 percent. At a strain of about 3000 μin./in. , no reduction in fatigue is noted.

All specimens deflected in ClF_3 became deeply gouged at the point of contact with the knife edges as previously mentioned. This wear caused a reduction in the deflection of the specimen and lowering of the strain, as noted in Table O-12.

The depth of wear measured for the top and bottom of each specimen is given in Table O-13. A total of from 7 to 21 mils was thus removed from the 51 to 53-mil-thick specimens at the knife edges. Figure O-15 shows the typical wear pattern as viewed from each edge. In every case, the metal removal was greater from the top of the specimen. This may have been caused by the galling of the guide pin and subsequent side movement at the end of the downward stroke.

The load on the specimen at the knife edge, which is at a maximum at the point of highest deflection, was approximated by the following equation:

$$P = \frac{E\epsilon}{l} \times 1/6\ wt^2 \quad ,$$

where

w = 0. 378 at l = 0. 70 (Figure O-1)

E = modulus of elasticity

ϵ = strain

t = thickness

P = load at knife edge.

This equation assumes a linear stress-strain relationship, which is not true for the specimen at the high deflection, when it actually is in plastic deformation. The calculated values are given in Table O-13.

From a plot of the wear versus the load, Figure O-16, it appears that rapid increase in wear results when the maximum load is increased above 5 pounds for the aluminum and 20 pounds for the stainless steel and Inconel 718. Thus, it appears that the fluoride film found on the metal surface may have some lubricating effect on the specimen below these critical loads. Above the critical load, the film is not an effective lubricant and may be physically penetrated by the knife edge. On the basis of a contact area measured as about 0. 03 by 0. 04 inch for the specimens, the critical force is about 4000 psi for Al-6061-T6 and about 16,000 psi for Type 347 and Inconel 718.

In N_2O_4 and A-50, the area of contact by the knife edge on the Al-6061-T6 is about the same as in ClF_3, but for Type 347 stainless steel, the area is about half that found in ClF_3. Thus, a force of 5000 to 10,000 psi on the aluminum and 30,000 to 80,000 psi on Type 347 produces only light scoring of the surfaces in N_2O_4 or A-50, but severe damage in ClF_3. This indicates that a basic difference exists between the films formed in N_2O_4 or A-50 and ClF_3. Therefore, it must be assumed that the fluoride film formed in ClF_3 on the three types of metals is softer and much less wear resistant than the normal oxide films found on the surface.

Other than the wear on the specimens, no indication of corrosive attack was revealed by the three alloys exposed in ClF_3.

REFERENCES

O-1. Boyd, W. K. , Berry, W. E. , and White, E. L. , "Compatibility of Materials with Rocket Propellants and Oxidizers", DMIC Memo 201 (January 29, 1965), Defense Metals Information Center, Battelle Memorial Institute, Columbus Laboratories.

O-2. Mindlin, Harold, and Hyler, W. S., "Fatigue Properties of Sheet and Bar Materials for Cryogenic Applications", Battelle Memorial Institute, for Rocketdyne Division, North American Aviation, Incorporated, pp 8-19 (January 21, 1966).

O-3. Clark, J. D., Boyce, A. E., and Mobley, S. P., Technical Report 3115, Picatinny Arsenal, Dover, New Jersey (October, 1963).

O-4. Lorkovic, W. M., Varallyay, D., and Daniels, R. D., Materials Protection, 3(3), p 16 (November, 1964).

O-5. Karlashow, A. V., Gnatzuk, A. D., and Tokarev, V. P., Soviet Materials Science, 1(4), 344-347 (July-August, 1965).

O-6. Corrosion Handbook, H. H. Uhlig, Editor, John Wiley and Sons (1948), Section on Corrosion Fatigue by B. B. Wescott, p 578; from original data by McAdam, D. J., Jr., Proc. ASTM 27(II), p 102 (1927).

O-7. McGammon, R. D., and Rosenberg, H. M., Proc. Royal Soc., A242, p 203 (1957).

O-8. Gideon, D. N., et al., Technical Documentary Report No. ASD-TDR-62-351 (April, 1962), available on ASTIA AD 286480.

O-9. Favor, R. J., Roberts, D. A., and Achback, W. P., DMIC Report 132 (July 20, 1960), Defense Metals Information Center, Battelle Memorial Institute, Columbus Laboratories.

O-10. Heitzman, R. J., Grumman Aircraft Engineering Corp. Report No. ADRO2-09-64.1 (February, 1964).

O-11. Zambrow, J. L., and Fontana, M. G., Trans. ASM, 41, p 480 (1949).

O-12. Spretnak, J. W., Fontana, M. G., and Brooks, H. E., Trans. ASM, 43, p 547 (1951).

O-13. Haven, Hugh E., Trans. Am. Soc. Mech. Engrs., 54, p 109 (1932).

O-14. Cotton, J. B., and Downing, B. P., Trans. Inst. Marine Engrs., 69, p 311 (1957).

O-15. Metals Handbook, American Society for Metals, Cleveland, Ohio (1961), p 530.

O-16. Guard, R. W., Product Engineering, p 160 (October, 1956).

O-17. Klima, Stanley J., Nachtigall, A. J., and Hoffman, C. A., NASA TN D1458.

O-18. Cryogenic Materials Data Handbook, Air Force Materials Laboratory, Research and Technology Division, Air Force Systems Command, Wright-Patterson Air Force Base, Ohio, ML-TDR-64-280, prepared under Contract AF 33(657)-9161 by the Martin Co., Denver, Colorado.

O-19. Avery, C. H., and Turley, R. V., Douglas Aircraft Co., Inc., Technical Documentary Report No. ML-TDR-64-44, Vol. II (May, 1964). Note: The data taken from this report are preliminary and subject to correction at a later date.

O-20. McKinnell, W. P., Beck, F. H., and Fontana, M. G., News in Engineering, p 28 (November, 1956).

TABLE O-1. ENVIRONMENTS IN WHICH STRESS-CORROSION CRACKING HAS BEEN OBSERVED

Alloy	Sensitive Environment
Low-alloy steels	Nitrates, caustic, hydrogen sulfide
Chromium stainless steels (greater than 12 percent chromium)	Halides, hydrogen sulfide, steam
Austenitic stainless steels (of the 18 percent chromium - 8 percent nickel type)	Chlorides, caustic
PH stainless steels	Chlorides, marine atmosphere
Aluminum alloys	Air, sea water, sodium chloride, tropical environments
Copper alloys	Ammonia, mercurous nitrate, steam
Gold alloys	Iron chlorides, potassium cyanide
Magnesium alloys	Sodium chloride--potassium chromate, fluorides
Nickel alloys	Caustic, hydrofluorosilicic acid
Titanium alloys	Red fuming nitric acid, chlorinated hydrocarbons, fused salts, HCl, red N_2O_4, Methanol, liquid cadmium, liquid mercury

TABLE O-2. PHYSICAL PROPERTIES OF FLUID MEDIA

Propellant	Melting Point, F	Boiling Point, F	Critical Temperature, F	Critical Temperature, psia
Helium	-457[a]	-452	-450	33
Nitrogen	-346	-320	-233	492
Hydrogen	-434	-423	-400	189
Diborane	-266	-135	62	581
Methane	-299	-259	-116	673
Oxygen	-361	-297	-182	730
Fluorine	-369	-306	-200	820
FLOX	-363[b]	-299[b]	-188[b]	760[b]
UDMH	-71	146	480	880
Hydrazine	35	236	716	2135
MMH	-62	189	561	1195
Pentaborane	-52	140	441	572
N_2O_4	11	70	317	1469
ClF_3	-105	53	345	838
NF_3	-358	-184	-	687
N_2F_4	-263	-100	100	794

(a) 382 psi.
(b) Approximate values.

TABLE O-3. TYPICAL FORMED BELLOWS MATERIALS

Alloy	Crystal Structure
Solution-Strengthened Alloys	
Alpha brass	Face-centered cubic
Copper	"
Stainless steels, Types 304, 321, and 347	"
Titanium, commercially pure and Alpha alloys	Hexagonal close packed
Inconel	Face-centered cubic
Precipitation-Hardened Alloys	
Beryllium copper	Face-centered cubic
Inconel 718	"
Aluminum, 7075 alloy	"
Transformation-Hardened Alloys	
Titanium, Alpha-Beta alloys	Hexagonal close packed; body-centered cubic

TABLE O-4. TYPICAL WELDED BELLOWS ALLOYS

Alloy	Crystal Structure
Precipitation-Hardened Alloys	
Inconel X	Face-centered cubic
René 41	"
René 62	"
17-7 PH	"
17-4PH	"
PH 15-7 Mo	"
M-252	"
Waspaloy	"
Udimet 700	"
Solution-Strengthened Alloys	
19-9 DL	Face-centered cubic
A-286	Body-centered cubic

TABLE O-5. COMPATIBILITY OF POTENTIAL BELLOWS AND DIAPHRAGM MATERIALS WITH PROPELLANTS AND OXIDIZERS

(Note: Ratings 1, 2, 3, and 4 are defined at the end of the Table; all data taken from Reference 1 except as noted in superscript parentheses.)

	304	321	347	PH15-7Mo	PH17-4	PH17-7	Titanium	Titanium Alloys	René 41	A286
ClF_3(gas)			1(85F) (Welded)	1(85F) (Welded)			100A 4(75F)			
ClF_3(liq)	1(85F) 1(160F)(3)	1(160F)(3)	1(85F) 1(85F) (Welded) 1(160F)(3)	1(85F) (RH95C) 1(85F) (TH1050)			100A 4(75F)	(C120AV) (A-110AT) 4(75F)	2(75F)	2(75F)
FLOX(liq) 40% F_2, 60% O_2	1(-320F)		1(-320F)							
FLOX(liq) 20% F_2, 80% O_2			2(-320F) (Oxylube 701 on 347)							
Fluorine (gas)	1(400F) 2(400F) 3(500F) 4(>500F) 304L 1(>70F) 2(>406F)		1(390F) 4(500F)					A55 1(212F) 2(100F) 3(>350) 6AL4V 2(350F) B120VCA 2(350F) 4(>350F) 16V-2.5Al 2(300F) 8 Mn 2(300F)		
Fluorine (liq)	1(-320F) 2(-320F) 3(-310F)	3(-310F)	1(-310F) 3(-320F)	1(-320F)			75A 4(-310F)	A-55 4(-310F) A-70 4(-320F) 6AL-4V 1(-320F) 2(-320F) 4(-310F) A-110AT 1(-320F) 2(-320F) 8Mn 4(-310F)		
Hydrazine (gas)	1(140F)	1(140F)	1(200F)		1(140F)					
Hydrazine (liq)	1(140F)	1(140F) 4(68F)	1(200F)		1(140F) 4(160F)	1(75F)		6Al-4V 1(160F) A-110AT 1(140F)		
MMH										
UDMH(gas)	1(140F)	1(140F)	1(160F)			1(160F)		C120AV 1(160F)		
UDMH(liq)	1(160F)	1(160F)	1(160F)	1(85F)		1(160F)		A55 1(145F) A110-AT 1(130F) B120VCA 1(145F)	1(85F)	1(85F)
50:50 N_2H_4: UDMH (gas)	304L 1(160F)	1(160F)	1(160F)	Cond A 1(160F)	1(160F)	Cond A 1(160F)		B120VCA 1(160F) A110AT 1(160F) C120AV 1(160F)		
50:50 N_2H_4: UDMH (liq)	304L 1(160F) 304L Welded 1(160F)	1(160F) Welded 1(160F)	1(160F) Welded 1(160F) AMS4775 Microbraze 1(160F) Easy-Flo Silver Braze 1(160F) C62 Braze 1(160F)	Cond A 1(160F)	1(160F)	Cond A 1(160F)		B120VCA 1(160F) A110-AT 1(160F) C120AV 1(160F)		

TABLE O-5. (CONTINUED)

	304	321	347	PH15-7Mo	PH17-4	PH17-7	Titanium	Titanium Alloys	René 41	A286
N_2O_4 (gas)	1(65F) 4(<215F)	1(65F)	1(65F)			TH950 1(60F)		A110-AT 1(65F)(a) RC130B(a) 1(150F)		
N_2O_4 (liq)	1(140F) 304L 1(165F) 304L Welded 1(65F)	1(65F) 347 Welded 1(65F)	1(130F) 347 Welded 1(65F) Easy-Flo Braze on 347 1(65F) AMS4775 Nickel Braze on 347 1(65F) C62 Brass on 347 2(100F)	Cond A 1(165F)	Cond A 1(65F) H1000 1(100F)	TH950 1(100F) H950 1(100F)	6Al-4V 1(100F)(a) 75A 1(165F)(a)	A110-AT 1(65F)(a) B120VCA 1(6CF)(a) C-120AV 1(165F)(a) RC130AV 1(150F)(a)		Annealed 1(100F) Aged 1(60F)
N_2O_4 (liq) 0.2 to 1% H_2O	1(140F) 304L 1(165F)		1(130F)	1(165F)			75A 1(165F)	6Al-4V 1(165F)		Annealed 1(60F)
N_2O_4 (liq) 3.2% H_2O	304L 1(165F)			1(165F)			75A 1(165F)	6Al-4V 1(165F)		
Pentaborane (liq)	1(75F)	1(75F)	1(75F)					C-110-M 1(75F) C-130-AM 1(75F)		

	AL6061	Al6061T6	AL7075	AL7075T6	Brass	Copper	Be Copper	Inconel	Inconel X
ClF_3 (gas)	1(85F) Welded				1(85F)	ETP 1(85F) 3(590F)			
ClF_3 (liq)	1(85F) Welded		1(160F)(3)		1(85F)	ETP 1(85F) DHP 1(85F) 1(160F)(3)	2% Be 1(85F)	1(85F) 1(160F)(3)	3(75F)
FLOX (liq) 40% F_2 - 60% O_2		1(-320F)							1(-320F)
FLOX (liq) 20% F_2 - 80% O_2									
Fluorine (gas)					70-30 2(200F) 4(400F) Red 1(200F) 2(400F) 3(600F) 4(>600F) 243 1(200F) 3(500F) 4(>500F)	Deoxidized 4(<400F) Commercial 1(200F) 2(400F) 3(800F) 4(>800F) ETP Same as commercial		2(1000) 4(<750F)	
Fluorine (liq)	1(-320)				Red 4(-310F) 243 3(-310F) Low Leaded 4(-310F) Yellow 1(-320) Cartridge 1(-320F)	Commercial 1(-320F) 3(-310F)			
Hydrazine (gas)	1(140F)							4(200F)	
Hydrazine (liq)	1(160F)		3(150F) 4(75F)		1(80F) 2(140F) 4(140F)	Commercial 1(68F) 2(80F) 4(140F)		1(200F) 3(140F)	1(80F) 3(140F)
MMH									
UDMH(gas)	1(75F) 2(160F)		1(160F)					1(140F)	

TABLE O-5. (CONTINUED)

	Al6061	Al6061T6	Al7075	AL7075T6	Brass	Copper	Be Copper	Inconel	Inconel X
UDMH(liq)	1(160F) 2(160F)	1(145F)	1(160F)	1(145F)	1(75F) 4(75F)	1(145F)			
50:50 N_2H_4: UDMH (gas)		1(160F) H_2SO_4 ANOD 1(150F) Alodine 1(160F)		1(160F)					
50:50 N_2H_4: UDMH (liq)		1(160F) Welded 1(160F) H_2SO_4 ANOD 1(160F) Alodine 1(150F)		1(160F) Stressed to 80% of yield 1(160F)		Copper Plate 4(60 F)			
N_2O_4(gas) <0.2% Moisture		1(150F)	1(60F)		Yellow 3(75F) Red 3(75F)	2(80F) 3(80F) 4(80F)		1(65F)	1(75F)
N_2O_4(liq) 0.2 to 1% H_2O		1(130F)		1(60F) 3(160F)	Yellow 4(80F) Red 4(80F)	2(80F)			
Pentaborane (liq)		6061-ST6 1(75 F)		1(75F)	1(75F)	1(75F)			

(a) Titanium ignites under impact but does not spread.

Compatibility Classifications for Metals (based on the lowest rating of any one of the three properties)

Class	Rating	Corrosion Resistance Penetration rate, mils/yr.	Decomposition of Propellant	Shock Sensitivity
1	Excellent	< 1	no	no
2	Good	< 5	no	no
3	Fair	5 to 50	some	no
4	Poor	> 50	extensive	yes

TABLE O-6. FATIGUE STRENGTH OF SELECTED METALS OR ALLOYS IN VARIOUS ENVIRONMENTS

Metal or Alloy	Analysis	Condition	Tensile Strength, psi	Diameter of Specimen, inch	Type of Fatigue Stress	Frequency, cps	Endurance Basis, Cycles	Temp., F	Corrosive Medium	Fatigue Limit, psi	Remarks	Reference
7075-T6				0.25	flexure	2000	10^6	ambient	air, 3% NaCl solution	17,500 10,000		4 4
7075-T6			90,000	0.394	Rotating, bending	6000	10^5 10^6 10^7 10^5 10^6 10^7 10^7	ambient ambient ambient ambient ambient ambient ambient	air air air 3% NaCl 3% NaCl 3% NaCl 3% NaCl	32,700 23,500 18,500 24,900 12,000 5,700		5 5 5 5 5 5 5
7075-T6			83,900	0.750 rod	flexure		10^4 10^5 10^6 10^7 10^4 10^5 10^6 10^7	70 -320 	air liq N_2 	68,000 45,000 33,000 90,000 71,000 59,000		18 18 18 18 18 18
7075-T6			78,800	0.190 sheet	axial		10^4 10^5 10^6 10^7 10^4 10^5 10^6 10^7 10^4 10^5 10^6 10^7 10^8	70 -320 -423 	air liq N_2 liq N_2 	44,000 23,000 14,000 12,000 54,000 39,000 21,000 20,000 73,000 56,000 36,000 35,000		18 18 18 18 18 18 18 18 18 18 18 18
Brass	60 Cu, 40 Zn	Annealed	53,000			1450 1450	10^8 10^8	ambient ambient	air well water(a)	21,000 18,000		6 6
		Cold rolled	84,000			1450	10^8	ambient	air well water(a)	24,000 18,000		6 6
Copper	99.99 Cu	Annealed (1200 F)	31,200			1450	10^8	ambient	air well water(a) salt water(b)	9,800 10,000 10,000		6 6 6
		Annealed (250 F)	46,500						air well water(a) salt water(b)	16,500 17,500 17,500		6 6 6
	0.03% O_2	Annealed (112 F)		0.02	Axial	13,500	10^5	ambient -297 -423 -452	air liq O_2 liq H_2 liq He	21,280 29,120 39,200 42,560		7 7 7 7
Be-copper	Berylco 25	Sheet, AT	178,000	0.020 sheet	flexure	1,800 1,800 3,450 	10^4 10^5 10^6 10^7 10^5 10^6 10^5 10^6	70 -320 -423 	air liq N_2 liq H_2 	138,000 92,000 59,000 44,000 112,000 74,000 154,000 113,000		8 8 8 8 8 8 8 8
Inconel			106,000			3,450	10^8	ambient 800 1000 1200 1400 1600 1800	air	49,000 47,200 41,800 26,500 15,500 10,000 7,000		9 9 9 9 9 9 9
		Cold rolled	132,000	0.035 sheet	flexure	1,800 1,800 	10^4 10^5 10^6 10^7 10^5 10^6 10^5 10^6	70 -320 -423 	air liq N_2 liq H_2 	158,000 106,000 62,000 42,000 112,000 84,000 130,000 96,000	estimated from strain data ditto " " " "	18 18 18 18 18 18 18 18
Inconel X							10^8	1200 1350 1500	air	47,000 44,000 38,000		16 16 16
Inconel X		Solution treated and aged	177,000	0.020 sheet	flexure	1800 1800 1450	10^4 10^5 10^6 10^7 10^5 10^6 10^7 10^5 10^6 10^7	70 70 -320 -423 	air liq N_2 liq H_2 	160,000 102,000 64,000 110,000 86,000 150,000 110,000	Estimated from strain data ditto " " "	18 18 18 18 18 18 18

Best Available Copy

Metal or Alloy	Analysis	Condition	Tensile Strength, psi	Diameter of Specimen, inch	Type of Fatigue Stress	Frequency, cpm	Endurance Basis, Cycles	Temp., F	Corrosive Medium	Fatigue Limit, psi	Remarks	Reference
Inconel 718							10^7	ambient	sea water	97,700		10
							10^7			85,800		10
		Solution treated		0.100 sheet	axial		10^3	70	air	90,000		18
							10^4			84,000		18
							10^5	70	air	81,000		18
							10^6			72,000		18
							10^4	-320	liq N_2	99,500		18
							10^5			95,500		18
							10^6			71,000		18
							10^3	-423	liq H_2	112,500		18
							10^4			112,000		18
							10^5			107,500		18
							10^6			101,500		18
Inconel 718 (weld fatigue)		Solution treated, AS-TIG weld, 718 filler		0.100 sheet	axial		10^3	70	air	77,500		18
							10^5			59,500		18
							10^6			44,000		18
							10^4			35,000		18
							10^5	-320	liq N_2	97,000		18
							10^6			66,000		18
							10^4			52,000		18
							10^5	-423	liq H_2	99,500		18
							10^6			73,000		18
							10^6			57,000		18
René 41		20% CR + aged		0.025 sheet	axial	100 + 1800	2×10^4 10^5	ambient	air & synth. sea water (results same)	130,000 87,000	preliminary data; subject to correction. Notched K_t = 2.33	9 19
Stainless steel Type 304		cold drawn	210,000	0.5 or 0.3	reciprocal beam	750 - 2000	10^6	77	air	112,000		11
								-321	liq N_2	155,000		11
				0.3	vibrating beam	2000	10^4	77	air	168,000		12
							10^5	77	air	118,000		12
							10^7	77	air	110,000		12
							10^4	-321	liq N_2	222,000		12
							10^5	-321	liq N_2	181,000		12
							10^7	-321	liq N_2	155,000		12
		not rolled	125,300			1450	10^7	ambient	air	50,000		6
									well water(a)	50,000		6
									salt water(b)	25,000		6
18-8	C 0.1; Cb 0.1		180,200	elliptical, .185 x .750	alt. torsion	360	10^6	ambient	air	53,000		13
							10^7			33,000		13
							10^8			28,000		13
							10^5		salt water(b)	27,500		13
							10^6			44,000		13
							10^7			16,000		13
							10^8			12,000		13
							10^8			12,000		13
Type 321 (see remarks)		age hardened	180,000	0.5			10^6	77	air	95,000	data are for type 322	12
							10^6	-321	liq N_2	160,000		12
Type 321		annealed	[illegible]	axial			[illegible]	70	air	38,000		18
							[illegible]			33,000		18
							[illegible]			31,000		18
							10^5	-320	liq N_2	62,000		18
							10^6			45,000		18
							10^4	-423	liq H_2	111,000		18
							10^5			80,000		18
							10^6			55,000		18
Type 347		annealed	92,500	0.129 sheet	flexure		10^5	70	air	51,000	These data	18
							10^6			14,000	should be	18
							10^5	-320	liq N_2	138,000	used with	18
							10^6			94,000	care; speci-	18
							10^5	-423	liq H_2	126,000	mens stressed	18
							10^6			96,000	beyond proportional limit	
Type [illegible] (weld fatigue)		annealed AS-TIG weld [illegible]		[illegible]	axial		[illegible]	70	air	46,000		18
							[illegible]			34,000		18
							[illegible]			23,000		18
							[illegible]			20,000		18
							[illegible]	-320	liq N_2	97,000		18
							[illegible]			71,000		18
							[illegible]			42,500		18
							[illegible]			30,000		18
							[illegible]	-423	liq H_2	108,000		18
							[illegible]			85,000		18
							[illegible]			55,000		18
							[illegible]			31,000		18

Best Available Copy

TABLE 0-6. (CONTINUED)

Metal or Alloy	Analysis	Condition	Tensile Strength, psi	Diameter of Specimen, inch	Type of Fatigue Stress	Frequency, cps	Endurance Basis, Cycles	Temp., F	Corrosive Medium	Fatigue Limit, psi	Remarks	Reference
17-7PH		TH1050	196,000	0.063 sheet	flexure	1800	10^5	70	air	114,000		18
							10^6			88,000		18
							10^7			82,000		18
							10^5	-380	liq H_2	160,000		18
							10^6			140,000		18
						3450	10^5	-423	liq H_2	157,000		18
							10^6			130,000		16
							10^6			113,000		18
17-7PH		RH950	169,000	0.063 sheet	flexure	1725	10^5	70	air	187,000		18
							10^6			116,000		18
							10^6			82,000		16
							10^5	-380	liq H_2	174,000		18
							10^6			156,000		18
							10^5	-423	liq H_2	213,000		18
							10^6			134,000		18
							10^6			105,000		18
17-7PH					vibrating beam	2000	10^5	ambient	air	116,000		20
							10^6			90,000		20
							10^7			86,000		20
							10^5	ambient	white fum. nitr. acid	94,000		20
							10^6			80,000		20
							10^7			70,000		20
PH15-7 Mo		RH 1075		0.025 sheet	axial	100 and 1800	10^4	ambient	air	127,000	Notched K_t = 2.33, no freq. effect. Prelim. data subj to correction.	19
							7×10^4			86,000		19
							10^4		synth. seawater	110,000		19
							2×10^4			85,000		19
Titanium	Commer. pure	hot rolled			rotating beam		10^5	ambient	air	55,000		14
							10^7			53,000		14
							10^8			52,500		14
							10^6			52,500		14
							10^7		dist. H_2O	57,500		14
							10^8			56,250		14
							10^6			56,000		14
							10^6		synth. sea water	57,500		14
							10^7			55,500		14
							10^8			54,500		14
							10^8			54,500		14
Titanium		hot swaged	93,000	0.25	vibrating beam	2000	10^4	77	air	101,000		12
							10^5			76,000		12
							10^7			73,500		12
							10^4	-321	liq H_2	139,000		12
							10^5			106,000		12
							10^7			100,000		12
Titanium	RC-70		93,000	0.25	vibrating beam	2000	10^5	ambient	white fum. nitr. acid	76,000		20
							10^6			76,000		20
							10^7			76,000		20
Ti-6Al-4V		annealed	144,500	0.25	axial	1800	10^6	ambient	sea water	112,700		10
							10^7			66,000		10
											Load Ratio(c)	
		annealed	136,000		axial		10^5	75	air	134,000	0.6	15
							10^6			122,000	0.6	15
							10^7			112,000	0.6	15
							10^5			114,000	1.7	15
							10^6			102,000	1.7	15
							10^7			92,000	1.7	15
							10^5			104,000	inf.	15
							10^6			86,000	inf.	15
							10^7			74,000	inf.	15
							10^5	750	air	94,000	0.6	15
							10^6			82,000	0.6	15
							10^7			-	0.6	15
							10^5			60,000	1.7	15
							10^6			72,000	1.7	15
							10^7			64,000	1.7	15
							10^5			57,000	inf.	15
							10^6			50,000	inf.	15
							10^7			45,000	inf.	15
		heat treated	170,000		axial		10^5	75	air	152,000	0.6	15
							10^6			144,000	0.6	15
							10^7			-	0.6	15
							10^5			143,000	1.7	15
							10^6			135,000	1.7	15
							10^7			128,000	1.7	15
							10^6			94,000	inf.	15
							10^6			85,000	inf.	15
							10^7			85,000	inf.	15

TABLE O-6. (CONTINUED)

Metal or Alloy	Analysis	Condition	Tensile Strength psi	Diameter of Specimen, inch	Type of Fatigue Stress	Frequency, cps	Endurance Basis, Cycles	Temp., F	Corrosive Medium	Fatigue Limit, psi	Remarks	Reference
Ti-6Al-4V (cont)							10^5	730	air	104,000	0.6	15
							10^6			90,000	0.6	15
							10^7			80,000	0.6	15
							10^5			90,000	1.7	15
							10^6			82,000	1.7	15
							10^7			80,000	1.7	15
							10^5			65,000	inf.	15
							10^6			64,000	inf.	15
							10^7			62,000	inf.	15
		annealed	136,000	0.072 sheet	flexure	1800	10^4	70	air	102,000		8
							10^5			64,000		8
							10^6			50,000		8
							10^7			44,000		8
		annealed	136,000	0.072 sheet	flexure	1800	10^5	-320	liq N_2	98,000		8
							10^6			80,000		8
						3450	10^6	-423	liq N_2	102,000		8
							10^7			76,000		8
		low interstit., solution treated and aged	165,000	0.100 sheet	axial		10^4	70	air	155,000		18
							10^5			86,000		18
							10^6			71,000		18
							10^4	-320	liq N_2	171,000		18
							10^5			96,000		18
							10^6			96,000		18
							10^4	-423	liq N_2	196,000		18
							10^5			129,000		18
							10^6			129,000		18
Ti-6Al-4V, weld fatigue		low interstit; solution treated & aged AS-TIG weld, parent metal filler	165,000	0.100 sheet	axial		10^4	70	air	125,000		18
							10^5			87,500		18
							10^6			85,000		18
Ti-6Al-4V		annealed		0.025 sheet	axial	100	10^4	500	air	82,000		19
						100	10^4	600		81,000		19
						1800	3×10^4	600		61,000		19
						100	10^5	800		82,000	prelim. data	19
						100	10^5	500	salt	53,000	subj. to correction, noted $K_t = 2.33$	19
						100	10^5	600	coated	53,000		19
						1800	10^5	600		53,000		19
						100	10^5	800		53,000		19
A-286		1800 F, 1 hr oil quench, 1300 F, 16 hr air-cool		0.355 OD 0.285 ID	alt. load	1970	29.1×10^6	1200	air	50,000		17
							24.5×10^6	1200	hydrogen	50,000		17
		solution treated		0.125 sheet	axial		10^3	70	air	52,500		18
							10^4			50,000		18
							10^5			43,500		18
							10^6			35,500		18
							10^3	-320	liq N_2	86,000		18
							10^4			85,000		18
							10^5			78,000		18
							10^6			59,000		18
							10^3	-423	liq N_2	89,000		18
							10^4			81,500		18
							10^5			79,000		18
							10^6			71,000		18
A-286 (weld fatigue)		solution treated AS-TIG weld, Hastelloy w filler		0.125 sheet	axial		10^3	70	air	47,000		18
							10^4			40,000		18
							10^5			23,500		18
							10^6			17,000		18
							10^4	-320	liq N_2	59,000		18
							10^5			36,000		18
							10^6			20,000		18
							10^4	-423	liq N_2	70,000		18
							10^5			45,500		18
							10^6			32,000		18
M252							10^8	1200	air	70,000		16
								1350		61,000		16
								1500		45,000		16
Waspaloy		aged		0.025 sheet	axial	100 & 1800	2×10^4	ambient	air and synth. sea water (same results)	132,000	prelim. data	19
							10^5			90,000	subj. to correction	19

(a) $CaSO_4$ 2ppm, $CaCO_3$ 200 ppm, $MgCl_2$ 17 ppm, NaCl 140 ppm.

(b) River water having about 1/6 salinity of seawater.

(c) Load Ratio, $A = \frac{\text{Maximum load - mean load}}{\text{Mean load}}$.

TABLE O-7. GROUPING OF FLUIDS WITH RESPECT TO CORROSION-FATIGUE STUDIES

Group I	Group II	Group III	Group IV	Group V
Chlorine trifluoride*	Nitrogen tetroxide*	UDMH-hydrazine*	Helium	Oxygen
Fluorine				
FLOX mixtures		Hydrazine	Nitrogen	Hydrogen
Nitrogen trifluoride		UDMH	Methane	water vapor
Tetrafluorohydrazine		Monomethylhydrazine	Carbon monoxide	
			Carbon dioxide	

* Fluids selected for use in corrosion-fatigue tests.

TABLE O-8. COMPOSITION OF PURCHASED FLUIDS

Fluid	Composition	Percent
Green N_2O_4(1)		
(Hercules Chemical Company)	N_2O_4	100.16
	NO	0.59
	H_2O equiv.	0.03
	Cl	<0.01
	Particulate	<0.8 mg/liter
A-50(2)		
(Olin-Mathieson Chemical Corporation)	N_2H_4	51.0 ± 0.8
	UDMH + amines	47.0 (min)
	H_2O	1.8 (max)
	N_2H_4 - UDMH + amines	98.2 (min)
ClF_3 (Chlorine Trifluoride)		
(Allied Chemical Company, General Chemicals Division)	ClF_3	99.0 (min.)
	HF	0.5 (max)
	Chlorine-oxyfluorides	0.5 (max)

(1) Analysis by procedure in MIL-P26539A and MIL-P27408.
(2) Analysis by procedure in MIL-P27402.

TABLE O-9. NOMINAL PHYSICAL PROPERTIES AND CHEMICAL ANALYSIS OF TEST MATERIALS

	6061-T6	Type 347[1]	Inconel 718
Heat number		89551	
Tensile, psi	42,000	95,230	185,000
Yield, psi	35,000	44,530	155,000
Elongation, percent	8	50.0	12
Hardness, Rockwell		B/86	
Thickness, mils	51	52	53
Analysis, percent			
Cr	0.25	17.74	19.0
Ni		9.87	52.5
Fe	0.70		18.0
Si	0.60	0.74	0.20
Mn	0.15	1.59	0.20
Cu	0.30	0.12	0.10
C		0.050	0.04
Mg	1.0		
Zn	0.25		
Ti	0.15		0.80
P		0.024	
Cb			5.20
Mo		0.24	3.00
Cb/Ta		0.88	
Al	Balance		0.60
S		0.015	0.007

(1) Actual analysis.

TABLE O-10. SURFACE FINISH OF REPRESENTATIVE COUPONS

Alloy	Specimen Number	Surface Finish, μin. rms
6061-T6	A-1	9.1
6061-T6	A-3	7.9
Type 347 stainless steel	S-7	2.3
Type 347 stainless steel	S-13	2.9
Inconel 718	I-2	2.3
Inconel 718	I-3	7.1

TABLE O-11. REVERSED BENDING-FATIGUE DATA FOR POLISHED Al-6061-T6, TYPE 347 STAINLESS STEEL, AND INCONEL 718 IN AIR AT 200 F (51-53 MIL SHEET)

Specimen Number	Alloy	Deflection, mils	Strain[1], μin./in.	Failure, Cycles	Surface Finish[2], μin. rms
A-13	6061-T6	95	4450	16,530	8.5
A-18	6061-T6	86	4000	15,870	8.5
A-3	6061-T6	70	3250	62,445	8.5
S-2	347	100	7250	10,275	2.6
S-10	347	88	6250	13,035	2.6
S-13	347	70	4800	35,000	2.6
S-1	347	60	4000	58,000	2.6
I-14	718	120	6000	13,200	4.7
I-7	718	112	5600	13,185	4.7
I-3	718	90	4500	28,420	4.7
A	718 (3)	80	4000	33,000	4.7
B	718 (3)	70	3500	48,000	4.7
C	718 (3)	60	3000	86,500	4.7

(1) Based on calibration curves from previous program (Reference 2).
(2) Estimate based on average of 2 specimens.
(3) Specimens obtained from previous fatigue program (Reference 2), polished to same surface finish.

TABLE O-12. REVERSED-BENDING FATIGUE OF 6061-T6, TYPE 347 STAINLESS STEEL AND INCONEL 718 SHEET[1] IN LIQUID N_2O_4, A-50, OR ClF_3 AT 200 F

Specimen Number	Alloy	Media	Deflection, mils	Strain[2], μin./in.	Failure, Cycles Actual	Expected
A-8	6061-T6	N_2O_4	67	3100	74,000	90,000
A-4	6061-T6	N_2O_4	67	3100	54,000	90,000
A-10	6061-T6	N_2O_4	96	4500	6,900	12,000
A-12	6061-T6	N_2O_4	96	4500	6,413	12,000
A-11	6061-T6	N_2O_4	100	4700	4,550	10,000
S-7	347	N_2O_4	50	3200	63,700	100,000
S-15	347	N_2O_4	50	3200	43,300	100,000
S-11	347	N_2O_4	97	7000	5,100	11,000
S-8	347	N_2O_4	97	7000	4,911	11,000
S-6	347	N_2O_4	100	7200	5100-6100	10,000
A-14	6061-T6	A-50	67	3100	107,000	90,000
A-9	6061-T6	A-50	67	3100	84,750	90,000
A-6	6061-T6	A-50[3]	96	4500	11,700	12,000
A-16	6061-T6	A-50	96	4500	9,384	12,000
S-18	347	A-50	50	3200	150,000	100,000
S-4	347	A-50	50	3200	118,000	100,000
S-19	347	A-50	100	7200	10,844	10,000
S-14	347	A-50	100	7200	9,020	10,000
S-20	347	A-50	100	7200	7,615	10,000
A-15	6061-T6	ClF_3	67(58)[4]	3100(2700)[5]	148,000	90,000(200,000)[5]
A-2	6061-T6	ClF_3	73(66)[4]	3400(3050)[5]	56,500	59,000(90,000)[5]
A-7	6061-T6	ClF_3	100(95)[4]	4700(4450)[5]	10,740	10,000(13,000)[5]
A-17	6061-T6	ClF_3	100(96)[4]	4700(4500)[5]	9,780	10,000(12,000)[5]
S-5	347	ClF_3	50(44)[4]	3200(2750)[5]	196,700NF[6]	100,000(150,000)[5]
S-12	347	ClF_3	67(64)[4]	4500(4350)[5]	21,200	38,000(44,000)[5]
S-3	347	ClF_3	100(94)[4]	7200(6700)[5]	9,310	10,000(12,000)[5]
S-17	347	ClF_3	100(99)[4]	7200(7100)[5]	7,270	10,000(10,200)[5]
I-8	Inc. 718	ClF_3	56(48)[4]	2800(2400)[5]	211,000NF[6]	100,000(150,000)[5]
I-11	Inc. 718	ClF_3	56(46)[4]	2800(2300)[5]	191,800NF[6]	100,000(170,000)[5]
I-1	Inc. 718	ClF_3	130(125)[4]	6500(6250)[5]	10,870	10,000(11,000)[5]
I-10	Inc. 718	ClF_3	130(125)[4]	6500(6250)[5]	8,890	10,000(11,000)[5]

(1) 51-53 mil sheet.
(2) Determined from calibration curves of previous program.[2]
(3) Leaked after 8600 cycles, after which exposure was A-50 vapor.
(4) Excessive wear of specimen at knife edge lowered effective deflection to the value in parentheses by the end of the run.
(5) Based on deflection in parentheses.
(6) No failure.

TABLE O-13. DEPTH OF WEAR AT KNIFE EDGE ON SPECIMENS DEFLECTED IN ClF_3

Specimen Number	Alloy	No. of Cycles	Depth of Wear Mils[1]	Mils/100,000 cycles	Calculated Load, lb
A-15	6061-T6	148,000	10, 9	13	7.3 - 6.3
A-2	6061-T6	56,500	8, 5	23	8.0 - 7.1
A-7	6061-T6	10,749	8, 1	84	11 - 10.4
A-17	6061-T6	9,780	6, 1	72	11 - 10.5
S-5	347 S.S.	196,700	7, 6	7	22 - 19
S-12	347 S.S.	21,200	4, 3	33	31 - 29.6
S-3	347 S.S.	9,310	6, 6	129	49 - 45.5
S-17	347 S.S.	7,270	7, 5	165	49 - 48
I-8	Inconel 718	211,000	10, 7	8	20 - 17
I-11	Inconel 718	191,800	14, 7	11	20 - 16.5
I-1	Inconel 718	10,870	9, 2	101	47 - 45.0
I-10	Inconel 718	8,890	7, 3	113	45 - 45.0

(1) Wear on top of specimen listed first.

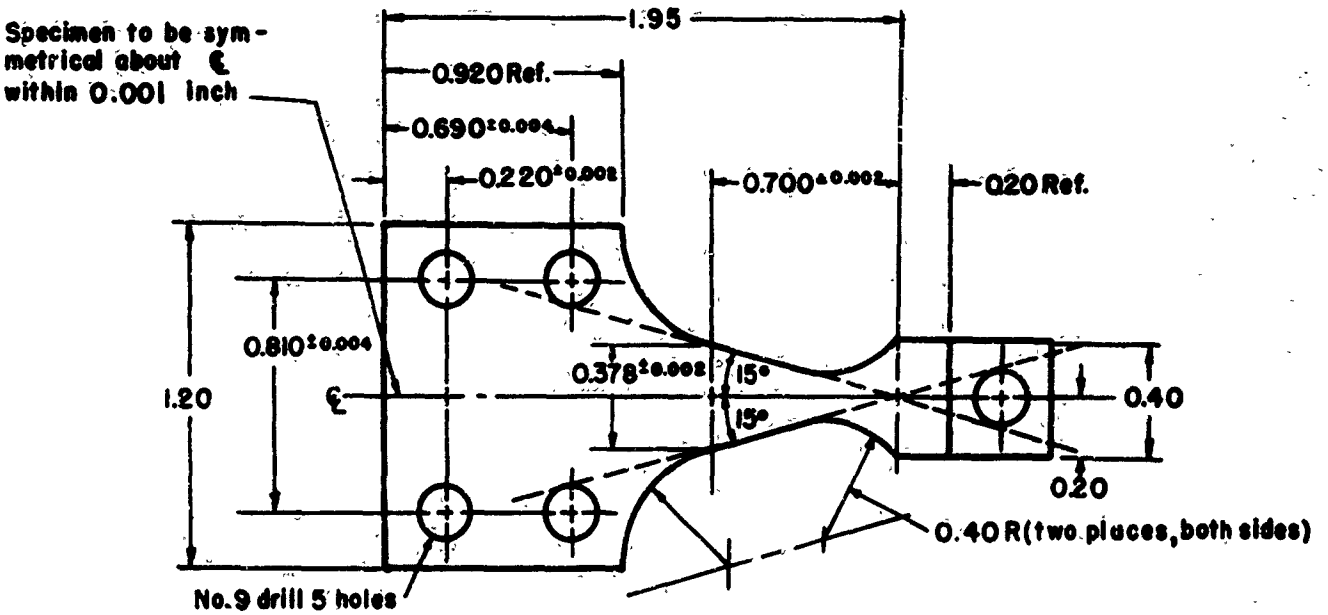

FIGURE O-1. BENDING-FATIGUE SPECIMEN

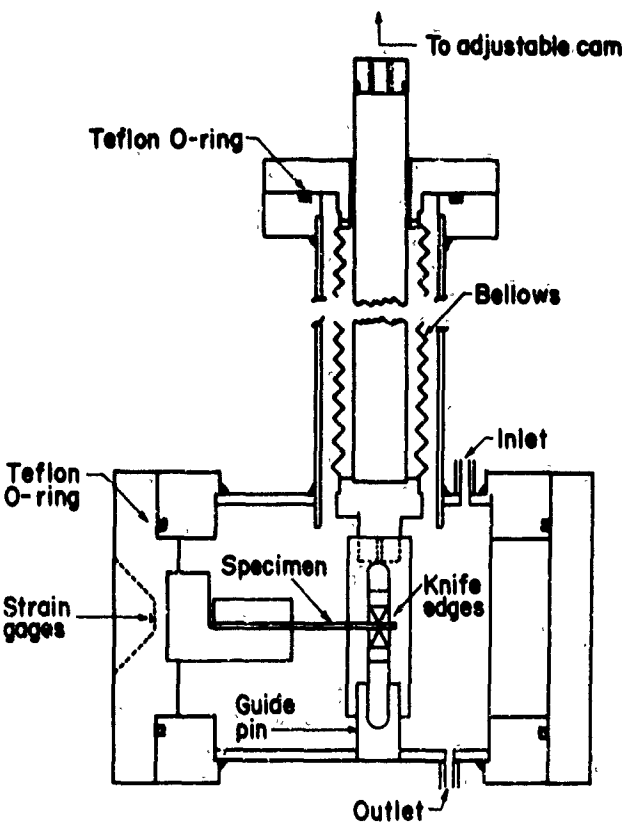

FIGURE O-2. SCHEMATIC OF STAINLESS STEEL CORROSION-FATIGUE CHAMBER

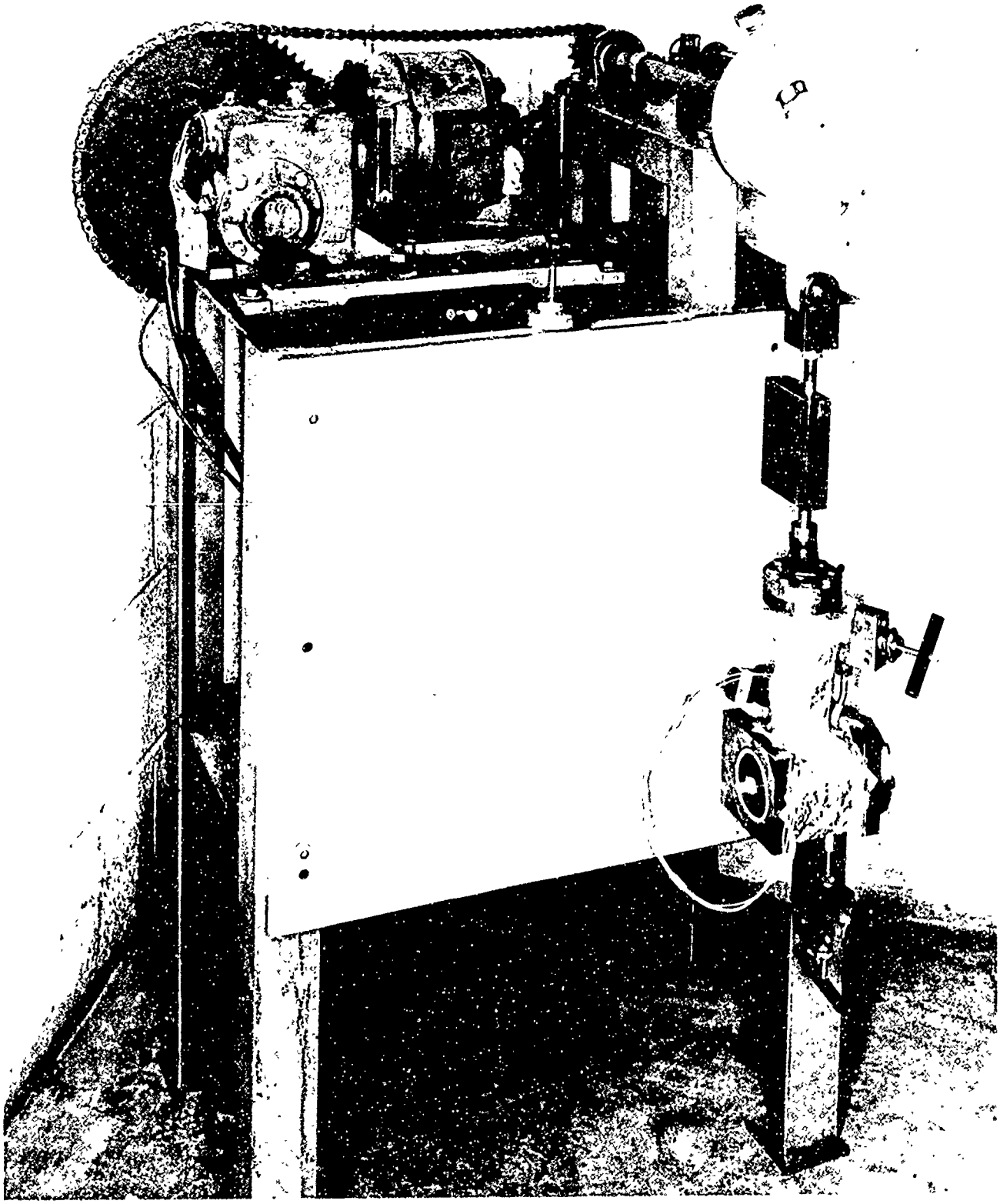

36995

FIGURE O-3. ENVIRONMENTAL CHAMBER AND MOTOR DRIVE FOR REVERSED-BENDING CORROSION-FATIGUE STUDIES

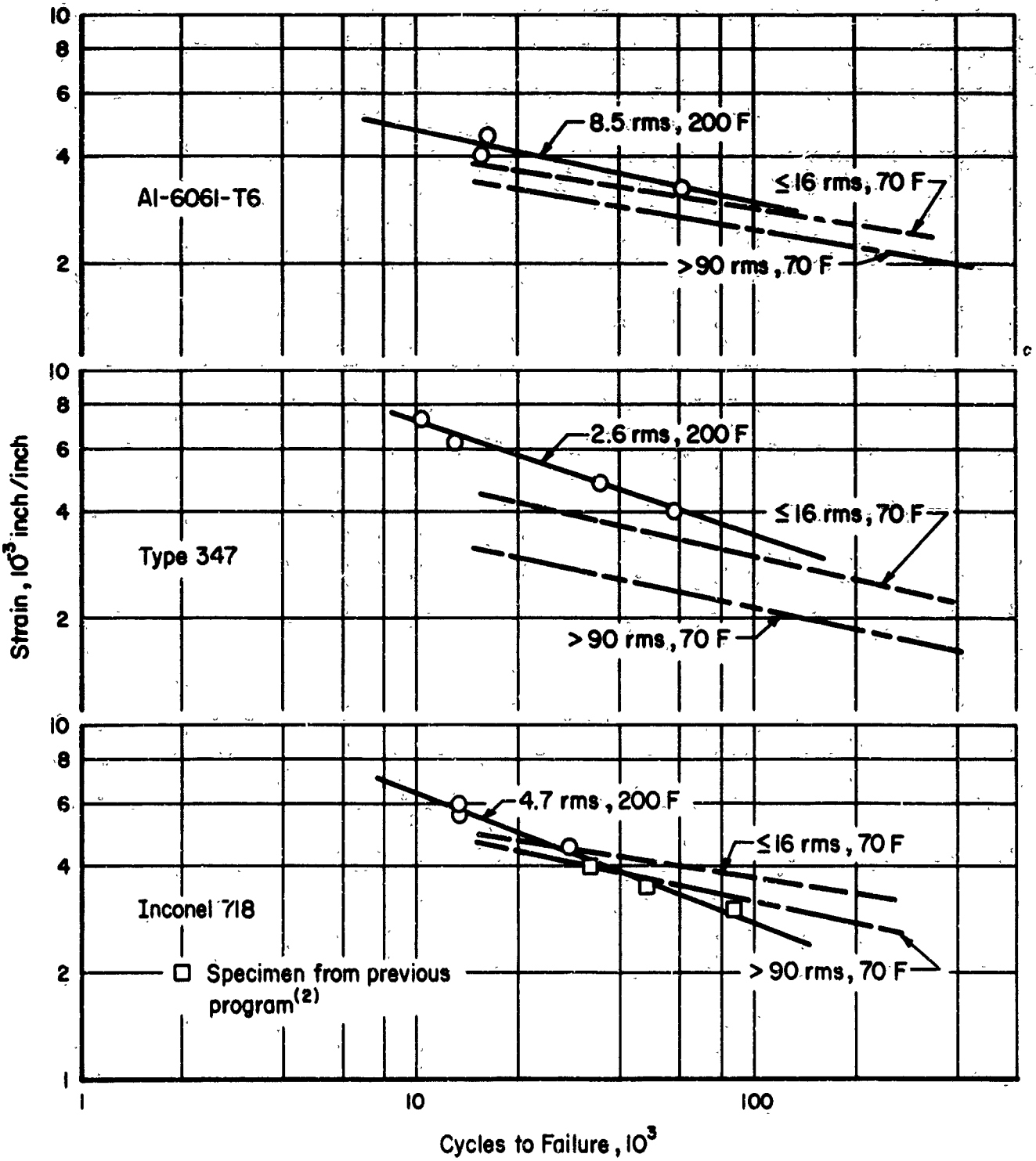

FIGURE O-4. REVERSED-BENDING-FATIGUE DATA FOR POLISHED Al-6061-T6, TYPE 347, AND INCONEL 718 IN AIR

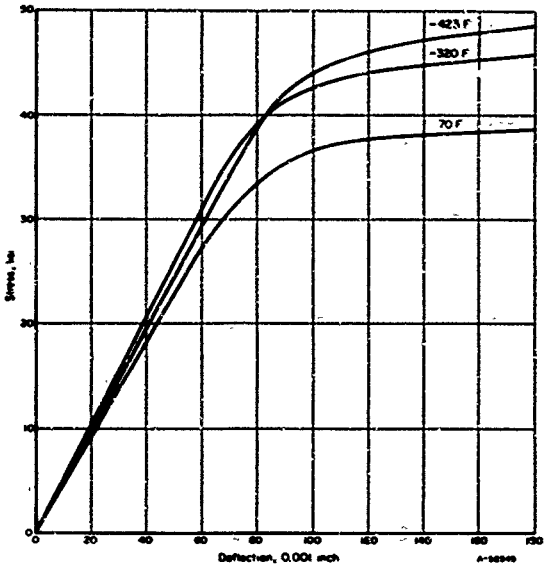

FIGURE O-5. STRESS-DEFLECTION CALIBRATION CURVES FOR REVERSED-BENDING FATIGUE OF 6061-T6 ALUMINUM SHEET AT THREE TEMPERATURES(2)

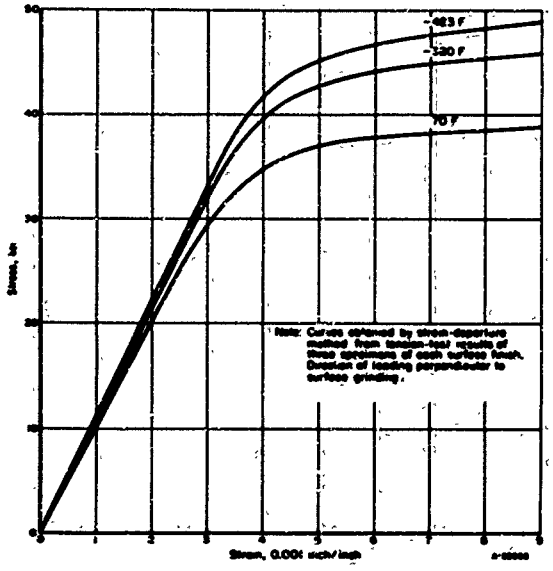

FIGURE O-6. TYPICAL STRESS-STRAIN CURVES FOR 6061-T6 ALUMINUM SHEET AT THREE TEST TEMPERATURES(2)

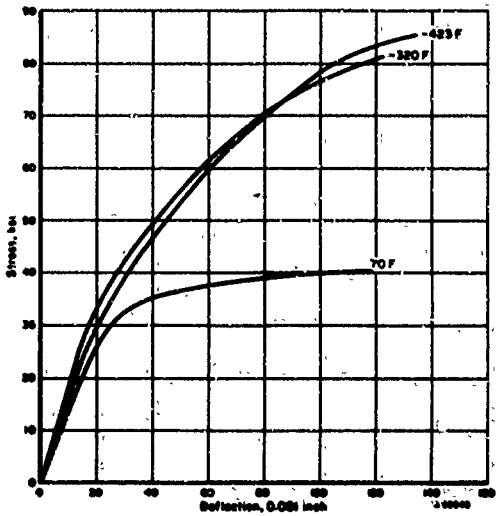

FIGURE O-7. STRESS-DEFLECTION CALIBRATION CURVES FOR REVERSED-BENDING FATIGUE OF 347 STAINLESS STEEL SHEET AT THREE TEMPERATURES(2)

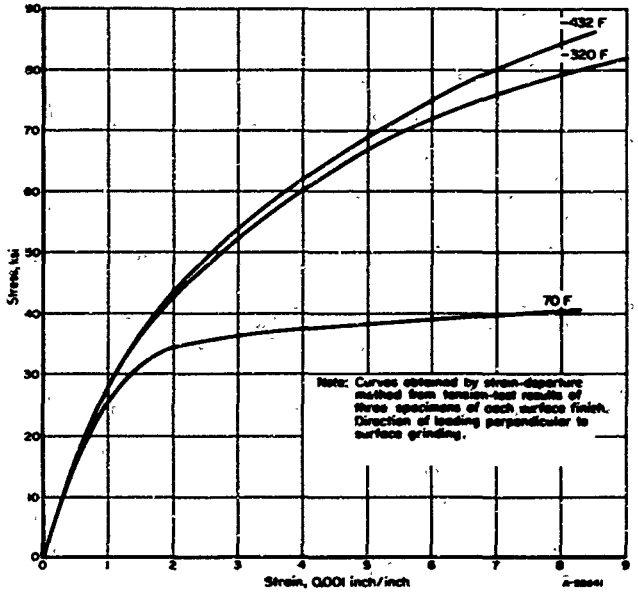

FIGURE O-8. TYPICAL STRESS-STRAIN CURVES FOR 347 STAINLESS STEEL SHEET AT THREE TEMPERATURES[2]

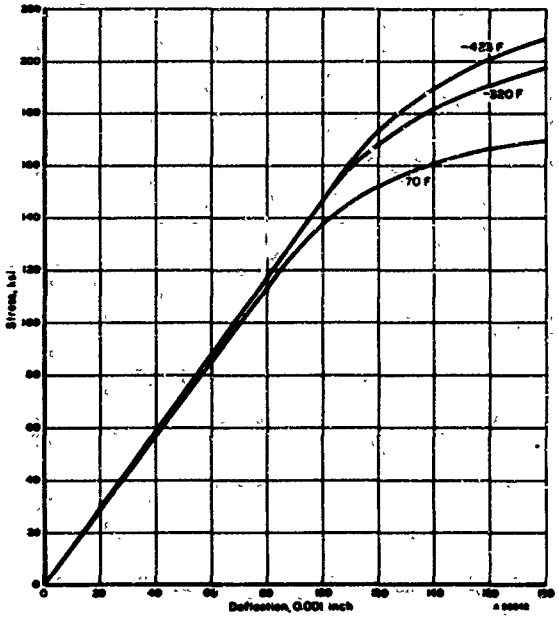

FIGURE O-9. STRESS-DEFLECTION CALIBRATION CURVES FOR REVERSED-BENDING FATIGUE OF INCONEL 718 SHEET AT THREE TEMPERATURES[4]

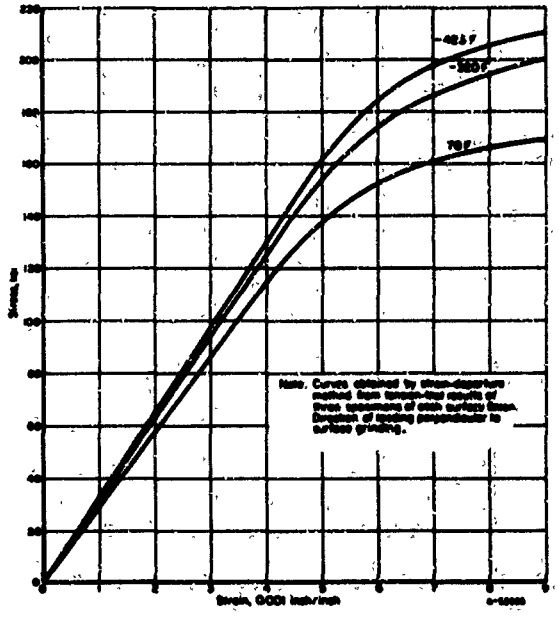

FIGURE O-10. TYPICAL STRESS-STRAIN CURVES FOR INCONEL 718 SHEET AT THREE TEMPERATURES[3]

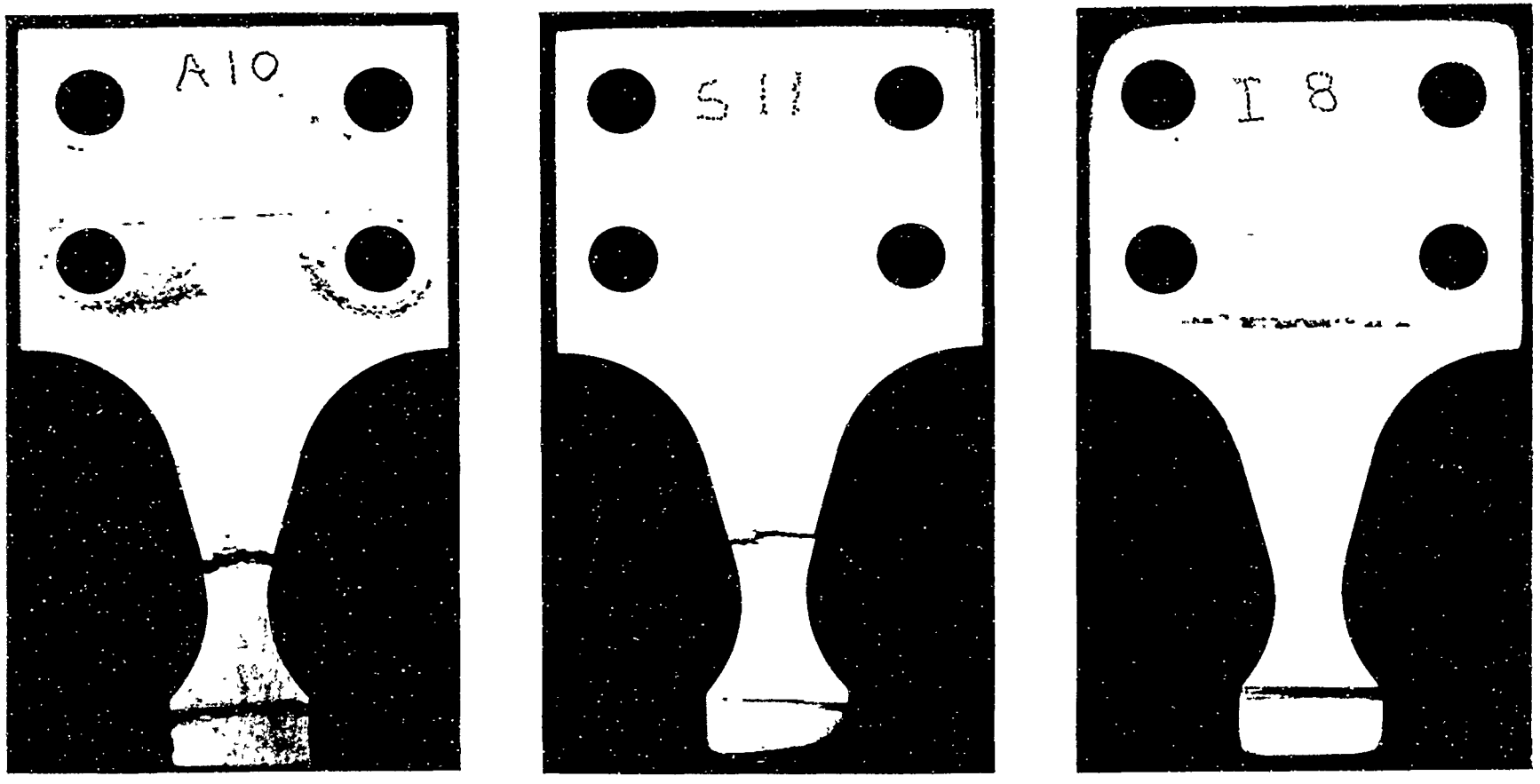

2X 6061-T6 C-2639
6900 cycles in N_2O_4

2X 347 C-2639
5100 cycles in N_2O_4

2X Inconel 718 C-2640
211,000 cycles in ClF_3

FIGURE O-11. REPRESENTATIVE CORROSION FATIGUE SPECIMENS AFTER EXPOSURE TO 200 F N_2O_4 OR ClF_3

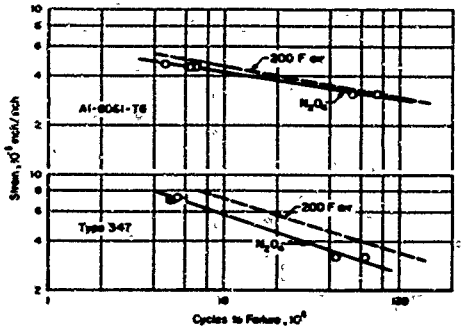

FIGURE O-12. REVERSED-BENDING-FATIGUE DATA FOR POLISHED Al-6061-T6 AND TYPE 347 IN N_2O_4 AT 200 F

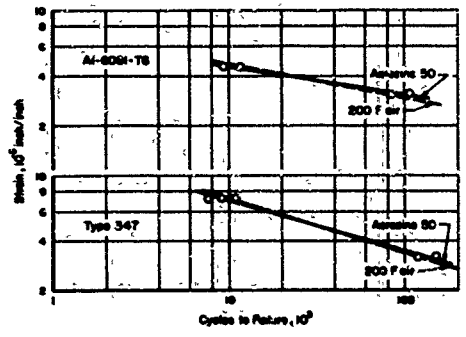

FIGURE O-13. REVERSED-BENDING-FATIGUE DATA FOR POLISHED Al-6061-T6 AND TYPE 347 IN AEROZINE 50 AT 200 F

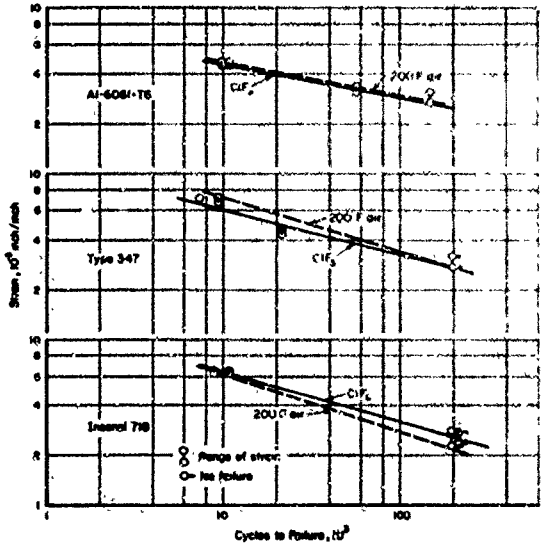

FIGURE O-14. REVERSED-BENDING-FATIGUE DATA FOR POLISHED Al-6061-T6, TYPE 347, AND INCONEL 718 IN ClF_3 AT 200 F

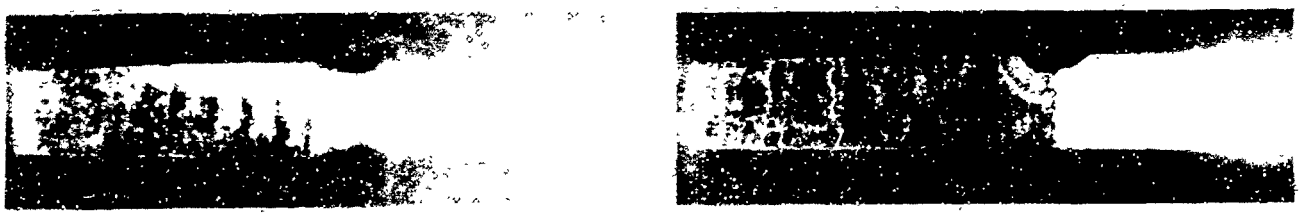

9X 2C641 9X 2C642

FIGURE O-15. WEAR UNDER KNIFE EDGES OF INCONEL 718 FATIGUE SPECIMEN I-8 AFTER 211,000 CYCLES IN ClF_3

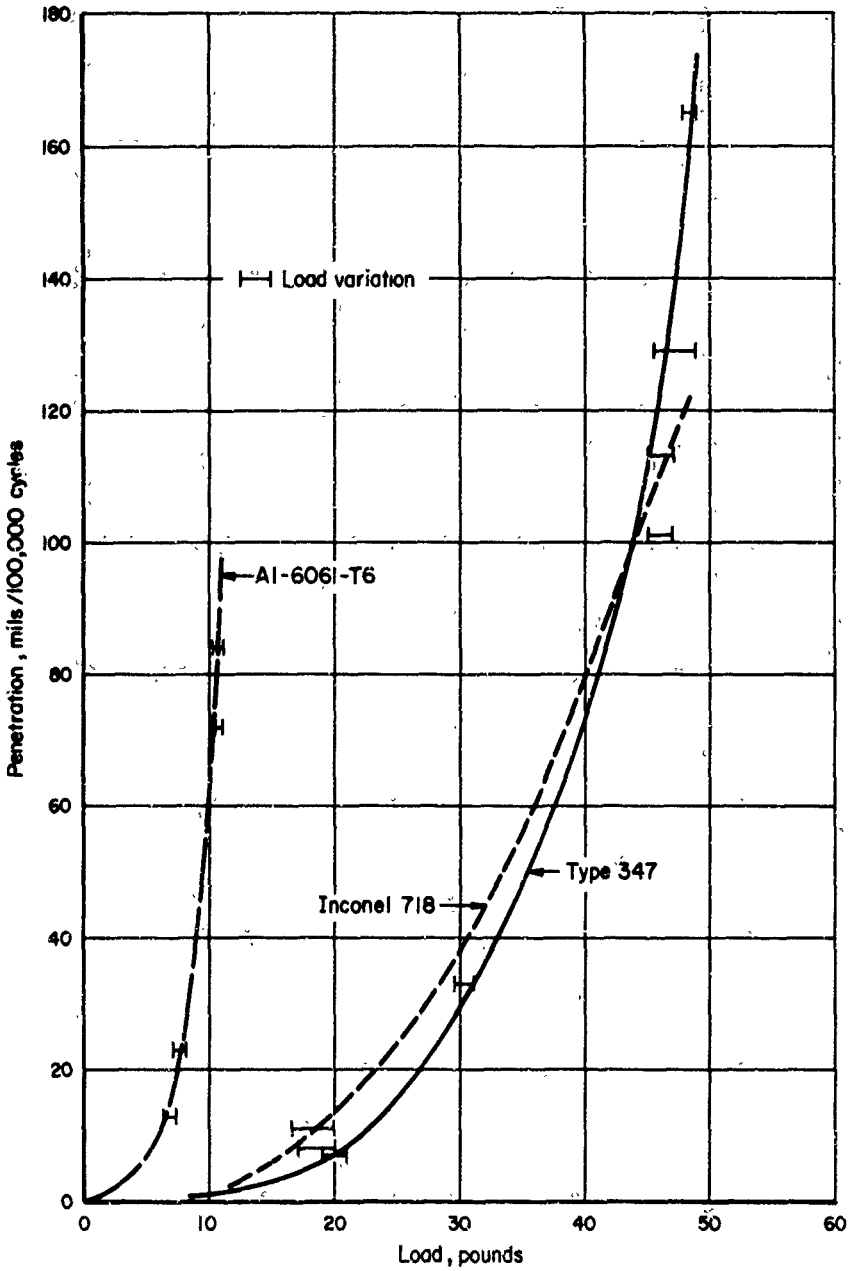

FIGURE O-16. PLOT OF WEAR VERSUS LOAD FOR Al-6061-T6, TYPE 347, AND INCONEL 718 EXPOSED IN 200 F ClF_3

O-39 and O-40

APPENDIX P

INSPECTION AND MEASUREMENT OF BELLOWS AND DIAPHRAGMS

ABBREVIATIONS AND SYMBOLS

$\bar{X}$	Mean of a set of n samples X_1, X_2, ... X_n
s	Standard deviation of a set of samples from its mean
$\bar{\bar{X}}$	Grand mean of a bellows parameter averaged over an entire set of bellows
$s_{\bar{X}}$	Standard deviation of the means from the grand mean
$\bar{s}$	Average standard deviation of a bellows parameter within each bellows

APPENDIX P

INSPECTION AND MEASUREMENT OF BELLOWS AND DIAPHRAGMS

The test bellows and diaphragms were carefully examined and measured prior to testing. It had been hoped at the beginning of the program that nondestructive measurements of dimensions could be used to establish values of torus radii, convolution depths, cone angles, average convolution radii, pitch, free length, etc., for use in the stress-analysis computer program. It became apparent early in the program that analyses of stresses and strains based on approximate convolution shapes are not sufficiently accurate for the prediction of actual strains and bellows cycle lives (see Appendix D). The accuracy of prediction was much improved when more accurate representations of the convolution shapes were used than could be obtained from nondestructive measurements. The more precise mathematical model had to be generated from cross-sectioned bellows in which true convolution shapes could be observed and on which the shell dimensions and wall thickness could be measured. The procedures used for encapsulating, sectioning, and measuring the bellows and diaphragms are described in detail in this appendix.

Nondestructive bellows and diaphragm measurements of the test items were useful for purposes other than the mathematical modeling of convolution shapes, however. First, knowledge of the measurable dimensions of a batch of bellows permitted the selection of individual bellows for cross sectioning and for strain gaging that were as near to the average dimensions of the batch as possible. Also, on the basis of the assumption that the bellows and diaphragms supplied by the several manufacturers for test in the Battelle program were at least as carefully made as is customary in the bellows industry, the accumulated dimensions constitute a useful record of achievable dimensional uniformity using present bellows and diaphragm manufacturing processes. Since the end use of the items ordered was generally known by the bellows and diaphragm suppliers, it is probable that greater than average care was taken in their manufacture.

Tests by the Manufacturers

The only tests conducted by the manufacturers were pressure and mass-spectrometer helium-leak tests performed on some bellows after attachment of the end fittings. All bellows and diaphragms received during the program were checked at Battelle and found to be helium leaktight, and no difficulties were encountered with premature leakage.

Receiving Procedure

It seems to be a universal human tendency to want to pick up and compress or extend a bellows on sight. Cases were brought to Battelle's attention by bellows manufacturers in which personnel who were unfamiliar with the often very limited allowable strokes of metal bellows have caused irreparable damage by overstraining them. A receiving procedure was therefore set up whereby incoming cartons of bellows were to be opened only in the presence of a designated program engineer.

Packaging

The receiving procedure also included noting the condition and effectiveness of the packaging. There were wide variations among suppliers in the care with which their bellows and diaphragms had been packaged for shipment. As might be expected, the welded bellows, being more expensive than the formed bellows and the diaphragms, were more securely packed. All welded-bellows manufacturers used individual rigid packages for each item. Packages used by some manufacturers contained internal supports for the bellows. Typical practice for formed-bellows packing was for the manufacturer to have covered the active portions of the bellows with a strip of pasteboard held in place with a rubber band, wrapped the bellows in kraft paper, and placed them in a large pasteboard shipping carton.

Although no bellows were damaged or lost during shipment, several cartons from one manufacturer arrived in an extremely battered condition and it was only through good fortune that some bellows had not been crushed or lost. Clear polystyrene boxes used by another manufacturer were slightly small for the bellows flanges, and all of the polystyrene boxes shattered during shipment or after arrival owing to the high internal stress from the flanges. Where advanced packaging materials such as air-cell plastic sheeting were used, the quantities were too small to be reliably effective in protecting the bellows. None of the manufacturers used such packaging techniques as vacuum-formed plastic sheets, foamed polystyrene, or foamed polyurethane.

Visual Examination

Each bellows and diaphragm was given an identification number, which was engraved on the top of the lower flange. For the welded bellows and the diaphragms, this number was taken as the arbitrary zero azimuth for recording the angular positions of features observed in the visual examination. For formed bellows, the longitudinal weld seam served as the zero azimuth point.

A bellows to be examined was first centered on a rotatable pedestal to which a 360-degree protractor had been affixed. Centering of the bellows was simplified by a series of concentric circles scribed on the top surface of the pedestal.

The exterior surface of the active portion of each bellows was carefully examined using a lighted 1-1/2X magnifying viewer. Additional sidelighting was provided by a floodlight. A white background was preferred.

The visual-examination procedure was further improved during the posttesting examinations by substitution of a stereo microscope for the magnifier. A magnification no greater than about 15X is recommended for general use.

The results of the visual examinations were recorded on charts depicting the developed surface of the bellows (see Figure P-1). Stains, scratches, dents, nicks, bulges, etc., were denoted by pencilled shading and a simple letter code.

Visual observation of the interior surfaces of the bellows became increasingly difficult with smaller bellows diameters. It was possible to examine the inner surfaces of 5-inch and 3-inch formed bellows using a dental mirror. A flexible fiber optic viewer

proved unsatisfactory because it had insufficient resolution, and a conventional borescope had such a limited field of view that the inspector had great difficulty in relating observed features to their locations on the bellows. Inner surface features were recorded in the same way as those on the exterior. The 1-inch and 1-1/2-inch bellows were too small to permit insertion of the dental mirror. These bellows were therefore not examined in detail on their interiors. In the case of welded bellows, it was possible to examine the external weld beads and the adjacent portions of the diaphragms, but the corrugations blocked much of the view between diaphragms. Such observations as could be made regarding size, shape, and uniformity of the weld beads were recorded.

Although some features were frequently visible on the surfaces of formed bellows such as stained areas, die marks, small scratches, dents, and nicks, there was no case in which any of these features appeared to have been related in any way to the fatigue fractures. The question of when a visible surface feature becomes a rejectable defect is complex, and there is need for the establishment of equitable acceptance standards in the industry.

Nondestructive Measurement of Dimensions

Each batch of 12 nominally identical bellows and diaphragms received during the program was subjected to a series of dimensional measurements. As in the case of the preceding visual examinations, the formed bellows permitted more complete measurement than the welded bellows. Specialized measurement methods and recording techniques were considered for use on the program, but it soon became apparent that considerable effort and time would be required to develop measuring systems having assured capability, accuracy, and reliability. Dimensions of the test bellows and diaphragms were therefore measured using conventional methods, including a dial indicator and height gages, micrometers, and a 50X optical comparator. Since use of these devices is common machine-shop practice, only the specific techniques believed to be unusual in any way are included in this report.

Figure P-2 shows the dimensions of the formed bellows that were measured. The convolution details presented in Figure P-2B are expressed in terms of constant-radius torus and straight cone sections. The inadequacy of such approximations compared with detailed convolution-shape measurements has already been pointed out. Of the convolution-shape parameters, only the average outer torus radii could be measured with a satisfactory accuracy. Some inner torus radii were measured, but shielding of the roots by cone sections sometimes prevented their accurate observation, and inner torus radii measurements are not considered to be sufficiently accurate to warrant their presentation. Even approximate determination of the cone angles and true shapes of the "flat" portions of the convolutions could not be made from the unsectioned bellows. A few average cone angles were measured from bellows cross sections, but they were not suitable for the more detailed mathematical modeling technique developed during the program, so the measurements were discontinued. The average outer torus radii, on the other hand, were relatively easy to measure and these measurements helped to provide an indication of manufacturing variability.

Of the dimensions shown in Figure P-2 that could be obtained nondestructively, five are considered to be of major importance: outside diameter, inside diameter, average outer torus radius, pitch, and bellows length. The values of these dimensions for the test bellows are summarized in this appendix. Note that the bellows length as

defined is smaller than the free length by about one pitch distance. The crown-to-crown length measurement could be made more accurately than the free length measurement, since it did not require the operator to judge the beginning of the end convolution. The major bellows dimensions that were measured, both nondestructively and destructively, are listed in Table P-1, along with the measurement methods and pertinent remarks.

The dimensions listed in Table P-1 are summarized in Tables P-2 through P-13. Because of the volume of data taken, it was not feasible to present the individual observations. Instead, each measured dimension is presented for each bellows or diaphragm in terms of an average and an associated standard deviation. The numbers of observations contained in each average dimension are also presented. Since the analysis of the dimensional data depends heavily on the statistical approach, the concepts and the statistical quantities involved in the analysis will be summarized before proceeding to the results of the analysis.

Statistical Principles

If a dimension of an object, say the outside diameter of a bellows convolution, is measured several times by the same operator using the same measuring device and at the same location on the bellows, it will be found that there will be some small amount of scatter among the individual (replicate) measurements. If the operator makes his measurements at different locations, the scatter will be larger. Usual practice when making such measurements is to calculate the arithmetic mean value, often loosely called the average, of n measurements according to the formula:

$$\overline{X} = \frac{X_1 + X_2 + \ldots + X_n}{n} .$$

It can be shown for the vast majority of measurements of dimensions of the sort under consideration in this program that if large numbers of replicate measurements are taken and the results plotted as a frequency histogram, their values will be distributed in a characteristic bell-shaped curve known as a Normal distribution. The assumption that dimensions measured during this program are Normally distributed could therefore be made with good confidence, and it was not considered necessary to make statistical tests to establish Normality.

For Normally distributed measurements, a second statistic other than the arithmetic mean serves to measure the scatter, or dispersion, of the individual observations about the mean. This statistic is the standard deviation of the observations. It is defined by the following formula, though more convenient forms of the equation are available for calculation purposes:

$$s = \sqrt{\frac{(X_1 - \overline{X})^2 + (X_2 - \overline{X})^2 + \ldots + (X_n - \overline{X})^2}{n - 1}} .$$

Because of the properties of the Normal distribution, the standard deviation is extremely useful for determining the natural tolerances of a manufacturing process. For a Normally distributed dimension, 68.2 percent of the measurements of that dimension, on the average, will fall within one standard deviation of the mean value, or $\overline{X} \pm 1s$; 95.4 percent of the measurements will fall within the range $\overline{X} \pm 2s$; and 99.7 percent will fall within $\overline{X} \pm 3s$. Knowing $\overline{X}$ and s for his process, a manufacturer can state with confidence what tolerance he can comfortably work to or what fraction of his product will have

to be rejected if he is required to work to any particular closer tolerance. For further discussion of such applications of statistics, the reader is referred to books on the subject. The percentage points of the Normal distribution were included above, however, to assist the reader in making comparisons of dimensions of other bellows and diaphragms with those used on this program. The quantities $\bar{X}$, s, and n as just defined appear in Tables P-2 through P-12 for each dimension of each bellows under the column headings "Mean", "Std. Dev.", and "No. of Observ."

The bellows and diaphragms used in the program were obtained in lots of twelve that were made sequentially from the same heat of material on a single piece of manufacturing equipment.

Even so, it can be seen from the tables that there are variations among the bellows in a lot. It is appropriate again to use the arithmetic mean and the standard deviation to measure a best single value for each dimension and the variation in this dimension among bellows. These two numbers are presented in the lower portions of the tables for each dimension under the headings "Grand Mean, $\bar{\bar{X}}$" and "Standard Deviation of Means, $s_{\bar{X}}$". The quantity $s_{\bar{X}}$ is a measure of the scatter in dimensions resulting from three possible causes: bellows-to-bellows variation, convolution-to-convolution variation within bellows, and scatter due to measurement inaccuracy, operator techniques, etc.

Among the pertinent questions for both manufacturers and users of bellows and diaphragms are the following:

(1) What are the actual, rather than the nominal, dimensions of the bellows or diaphragm?

(2) What variations in dimensions exist among the convolutions or corrugations of a single bellows or diaphragm?

(3) Are the variations in the corresponding dimensions of different bellows or diaphragms from the same lot significantly different from the convolution-to-convolution variations within a single item?

For the test bellows and diaphragms, Question 1 is answered by the values of $\bar{X}$ and $\bar{\bar{X}}$ in the tables for the dimensions that could be measured. If more replicate measurements had been made, confidence in the degree to which the averages of the measurements approach the true mean values would of course have been increased.

Question 2 is an important one, since local strains, and therefore mechanical performance, have been shown to be strongly dependent on convolution geometry. Although the nondestructive measurements that could be made on the program items do not completely define the convolution shapes, the values of the standard deviations, s, do give some indication of the convolution-to-convolution variations within a single item, although the values of s also contain the scatter due to measurement inaccuracy and operator variations. If a duplicate set of measurements in all respects had been made, it would have been possible to separate these two sources of scatter. However, to have made duplicate measurements would have added significantly to the program costs.

Question 3 can be answered by comparing the standard deviation of the means, $s_{\bar{X}}$, with a single number representing the average standard deviation within a bellows, $\bar{s}$. A valid estimate of $\bar{s}$ for a particular dimension cannot be obtained by simply taking the

average of the standard deviations for that dimension associated with each bellows. For a set of k items, the formula for determining $\bar{s}$ from the individual values of s for each item is:

$$\bar{s} = \sqrt{\frac{(n_1 - 1)\, s_1^2 + (n_2 - 1)\, s_2^2 + \ldots + (n_k - 1)\, s_k^2}{n_1 + n_2 + \ldots + n_k - k}} \quad .$$

Values of $\bar{s}$ for each dimension of each set of bellows for which more than a single measurement had been made are given in the tables under the heading "Mean Standard Deviation, $\bar{s}$". Because the individual values of s contain variations arising from more than one source, as noted above, the values of $\bar{s}$ are measures of average variation among the convolutions of single bellows plus the measurement inaccuracies and operator effects.

A statistical test known as the F-test is available to determine whether a statistically significant difference exists between any pair of values of $s_{\bar{X}}$ and $\bar{s}$. To perform an F-test it is necessary also to know the number of degrees of freedom associated with $s_{\bar{X}}$ and with $\bar{s}$. In the present case, the number of degrees of freedom for $s_{\bar{X}}$ is one less than the number of bellows or diaphragms in the set, or k - 1. For $\bar{s}$, the number of degrees of freedom is the total number of observations minus the number of items in the set, or $n_1 + n_2 + \ldots + n_k - k$. It will be noted that this number is also the denominator in the expression for calculating $\bar{s}$. Knowing these four numbers, the F-test is made by consulting a table of the F-distribution. Such tables are included in most books on statistics. The one used in the calculations made in this program was Table D in Statistical Methods in Research and Production, by O. L. Davies, published by Oliver and Boyd (London), 1949, pp 272-275.

In making the F-test, the squared ratio of the theoretically larger standard deviation, in this case $s_{\bar{X}}$, to the smaller, $\bar{s}$, is calculated for the measurement in question. The F-table gives the minimum value of the ratio F between the squared standard deviations, or variances, having any particular degrees of freedom for which a statistically significant difference between the standard deviations can be presumed to exist. If the calculated value of F is larger than the corresponding tabular value, one can say in the present case that there is significantly more variation among bellows in the dimension for which F was calculated than there is variation in the same dimension within individual bellows.* A value of the F-ratio less than unity also means that there is no statistically significant difference between $s_{\bar{X}}$ and $\bar{s}$. Although the true value of $s_{\bar{X}}$ must always be equal to or greater than the true value of $\bar{s}$, since it contains the additional item-to-item scatter, experimental estimates of the F-ratio may be less than unity.

As with all statistical statements, the results of the F-test can only be stated in terms of probability. F-tables are usually constructed containing ratio values for 0.90, 0.95, and 0.99 probabilities of significance. Given a value of the ratio shown by the F-table to be significant at the 95 percent level, the proper interpretation is that 95 times out of 100, on the average, the tabular value of the ratio is correct in indicating that a difference exists between the standard deviations in question. If one examines an F-table, he will note that as the number of observations, and therefore the number of degrees of freedom, is increased, the test is able to distinguish statistical significance

*As has been noted, the values of $s_{\bar{X}}$ and $\bar{s}$ obtained in this program also contain the error term, which is small with respect to the variations in the dimensions in most cases, but which cannot be separated.

when smaller and smaller differences exist between the standard deviations being compared. Tables P-2 through P-13 include the calculated F-ratios between $\bar{s}$'s and $s_{\bar{X}}$'s for each dimension with their associated significance statements.

Analysis of Nondestructive Dimension Data

The procurement of test bellows and diaphragms for the program was different from the usual procurement. Instead of the bellows and diaphragms being required to perform under a set of operating conditions, "standard" items were ordered that were of convenient size and general performance capability. The closeness with which the performance of the items could be predicted by the theory was then determined. The use of standard bellows and diaphragms significantly reduced the testing cost in the program. Although there were no tolerance standards against which the dimensions could be compared, the mean values of the measured dimensions permit a number of conclusions to be drawn concerning the "typical" manufacturing processes. The different dimensions will be discussed in turn.

Convolution Outer Diameter. In all of the formed bellows tested, the convolutions were formed radially outward, beginning with a uniform longitudinally butt-welded cylindrical tube having the approximate diameter of the finished-bellows inside diameter. The behavior of the mean standard deviations, $\bar{s}$, and the standard deviations of the means, $s_{\bar{X}}$, are shown in Figure P-3, as functions of the outer diameter. The mean standard deviation for the single-ply Type 321 stainless steel formed bellows, the only program bellows series having three diameters, was linearly related to diameter. This indicated that the tolerance on individual convolutions of a bellows is naturally greater, the larger the bellows when manufactured by the particular hydraulic process used. The standard deviation of the means for these bellows was not a function of bellows diameter, however, indicating that the average outside diameter taken over all the convolutions of a bellows was likely to deviate from the average outside diameter for all the bellows in the group by about the same amount, whatever the size of the bellows. Furthermore, $s_{\bar{X}}$ was significantly smaller than $\bar{s}$ for the 5-inch and 3-inch bellows. For the 1-inch bellows, $s_{\bar{X}}$ and $\bar{s}$ were equal. This suggests that if bellows much smaller than 1-inch outside diameter were made with the same manufacturing process, the resulting bellows might have $\bar{s}$ significantly greater than $s_{\bar{X}}$.

For the two-ply Type 321 bellows, $\bar{s}$ was smaller than for the single-ply bellows. The two-ply bellows appeared to show the same sort of size dependence as the single-ply bellows, though this cannot be stated definitely because only two sizes of two-ply bellows were measured. The $\bar{s}$ data indicate that the convolution-to-convolution uniformity was better for the two-ply bellows, probably because their doubled wall thickness made them less critical to form than the single-ply bellows. The two-ply bellows as a group were not as uniform as the single-ply bellows, as shown by their higher values of $s_{\bar{X}}$. A possible reason might be that it was more difficult to control the higher hydraulic pressures required to form the two-ply bellows.

The Inconel 718 formed bellows showed a greater size dependence of $\bar{s}$ for the outside diameter than did the Type 321 bellows, and these bellows also showed a size dependence of $s_{\bar{X}}$, in contrast to the Type 321 bellows.

As might have been expected, the standard deviations of the outside diameters for the welded bellows (see Tables P-9 through P-12) were generally smaller than those of the formed bellows, reflecting greater uniformity. The smaller welded bellows appeared to have slightly larger standard deviations than did the larger ones, however. This might have been the result of the weld burn-down being a larger fraction of the diameter in the smaller welded bellows.

Inside Diameter. The standard deviations for the inside-diameter measurements of the formed bellows are shown in Figure P-4. Behavior was generally similar to the outside-diameter standard deviations. The abnormally high value for the standard deviation of the means for the 3-inch single-ply Type 321 bellows was entirely due to the results for bellows JD61 and JD67. If the inside diameters of these two bellows are neglected, $s_{\bar{X}}$ becomes 0.0036 for the remaining 10 bellows, and a linear relationship with diameter results. These values indicate the type of statistical basis on which bellows could be rejected.

As has already been noted, nondestructive inside-diameter measurements of welded bellows could be obtained only for the 3-inch Type 347 bellows. Only single observations were made, so it was not possible to calculate $\bar{s}$. The value of $s_{\bar{X}}$ obtained, 0.0015, fell below the corresponding formed-bellows values, as would be expected.

Outer Torus Radius. Standard deviations for the outer torus radii of the formed bellows are plotted against torus radius in Figure P-5 (note the smaller vertical scale than that of Figures P-3 and P-4). They could equally well have been plotted against a bellows-diameter measurement, since smaller bellows had smaller convolutions and smaller torus radii. For the single-ply Type 321 bellows, $\bar{s}$ showed almost no dependence on torus radius, while $s_{\bar{X}}$ was erratic. The $s_{\bar{X}}$ value for the 3-inch set of bellows looks suspiciously low, owing to a remarkably uniform set of mean values (Table P-3). Matching of torus radii to the master templates was possibly not done carefully enough on this set of bellows.

Pitch. Standard deviations for pitch are plotted against pitch in Figure P-6. The mean standard deviation for the 5-inch bellows was markedly high, and on the bellows themselves, the convolution-to-convolution pitch variations and even variations with azimuth around adjacent convolutions were visible to the practiced eye. For the 3-inch and 1-inch single-ply Type 321 bellows, pitch variations along the bellows were no greater than pitch variations from one bellows to another. There was very little size dependence of $s_{\bar{X}}$ for either the single-ply or the two-ply Type 321 bellows. The two-ply bellows were significantly more uniform in pitch than were the corresponding single-ply bellows.

The Inconel 718 formed bellows were supplied by a different manufacturer. Mean standard deviation of pitch in these bellows showed a strong dependence on size, the 3-inch Inconel 718 bellows being second only to the 5-inch Type 321 bellows in convolution-to-convolution pitch variation. The situation was reversed for the 1-inch size, the Inconel 718 being the more uniform in pitch.

Pitch measurements were made on the welded bellows and are presented in Tables P-9 through P-12. The standard deviations ranged somewhat lower than those for most of the formed bellows and did not appear to show any significant trends.

Bellows Length. Standard deviations for the lengths of the formed bellows, measured between crowns of the end convolutions, are shown in Figure P-7. In almost every case, $s_{\bar{X}}$ was significantly larger than $\bar{s}$. This is perhaps to be expected, since only a gross lack of parallelism between the end convolutions of a bellows could produce a large value of $\bar{s}$. The amount by which $s_{\bar{X}}$ exceeds $\bar{s}$ for the single-ply Type 321 bellows is somewhat surprising, however. It can be accounted for only as the result of accumulated variations in pitch summed over the bellows lengths.

Diaphragm Dimensions. After visual examination, diameters of the diaphragm corrugations were measured with the same optical comparator used throughout the program for measurements of bellows pitch, free length, and torus radii. In the case of the diaphragm measurements, however, the comparator was used in the reflected-light mode, rather than in the transmitted-light or shadow mode. The specular reflections from the crests and troughs of the corrugations were easily observed, and accurate measurements were obtained of the corrugation diameters.

Heights and depths of the diaphragm corrugations were measured using a conventional metallurgical microscope having a 4-mm focal-length objective lens and a calibrated rack-and-pinion focusing arrangement. The microscope was focused on the crest of a corrugation, the calibrated drum was read, and the diaphragm was traversed along a diameter to the trough of the corrugation. The microscope was again focused, the drum was read, and the top-to-bottom corrugation height was determined by difference. Corrugation diameters and heights were measured across two orthogonal diameters on each diaphragm.

Measured dimensions of the diaphragms appear in Table P-13 and the associated figure, P-8. From the F-test significance statements in the table, it will be noted that there are significant variations in the diameters of the innermost and outermost corrugation crests. The item-to-item variations thus revealed are most likely attributable to minor heating variations associated with making the end fitting welds.

Measurement of Dimensions Requiring Destruction of the Bellows or Diaphragm

One bellows or diaphragm from each lot of 12 was selected for encapsulation and cross sectioning upon completion of the nondestructive measurements. Insofar as possible, a bellows or diaphragm was selected that had dimensions close to the grand means of the measured dimensions. The remaining items of the lot were held until the dimensions from the cross sections had been obtained, the mathematical model had been constructed, and the predictions of mechanical behavior had been made using the stress-analysis procedure described in Appendix B. The items were then released for testing to verify the predictions.

To obtain the dimensions required for the mathematical model, the items were encapsulated in a plastic matrix and accurately cross sectioned along their longitudinal

axes. The exposed cross-sectioned surfaces were then polished, and indentations or bench marks were located on appropriate convolutions. The X-Y coordinates of each bench mark were then determined so the shape of the convolutions could be reproduced for the mathematical model. The instructions presented in this section not only describe the procedures followed during the program, but also outline the steps required to obtain dimensions for the stress-analysis procedure described in Appendix B.

Encapsulation

A hard plastic such as Epon 815* should be used for encapsulation to minimize metal smearing in the polishing process. If the curing process is exothermic, the proper accelerator must be used or a runaway cure may result in large bubbles, unsound plastic, and distortion of the bellows. An accelerator that will produce good results with Epon 815 is DEAPA (diethylaminopropylamine)**. Although a mixture ratio of 6 parts of accelerator to 100 parts of resin by weight is recommended, with experience this ratio may be adjusted in accordance with the mass of plastic material required.

The bellows can be encapsulated in any convenient rigid container. For a large bellows, e.g., 5 inches OD, a water-cooled polyethylene bottle may be inserted inside the bellows to reduce the mass of plastic material and minimize the possibility of a runaway cure.

The resin must be thoroughly mixed with the accelerator, using a power stirrer, just prior to encapsulation. After mixing, the plastic should be degassed in a vacuum before casting. Degassing should take only a few minutes. A second degassing should be performed immediately after the plastic is poured into the mold. Epon 815 will require from 1 to 3 days to cure at room temperature, depending on the mass of plastic and the ambient temperature.

Preparation of the Cross Section

After the plastic matrix has cured sufficiently (the exposed surfaces are no longer tacky), it can be removed from the mold. Then it is necessary to section the plastic block along the longitudinal axis of the bellows. This can be accomplished readily with a resin-bonded abrasive cutoff wheel. It is important that the exposed surface be parallel to the longitudinal axis of the bellows, and that the surface be slightly off center (about 0.005 inch) to allow material for the subsequent grinding and polishing operations. Care must be exercised during the casting process so that both diametral ends of the bellows are exposed or are visible. This makes it possible to locate and scribe the true centerline of the bellows on the plastic mass. The centerline then serves as a guide for cross sectioning the mass.

The base of the plastic block should be machined parallel to the cross-sectioned surface. If it is desirable to square off the plastic block all over to facilitate subsequent polishing and measuring operations, this can be accomplished in a standard milling machine with a fly cutter or end mill. In any case, it is advisable to grind the surface

* A product of the Shell Chemical Corporation.

** Experience has shown that this accelerator should be stored in a refrigerator since erratic and runaway curing may occur if the accelerator ages on the shelf.

exposed by the cutoff wheel to give an initially flat surface and to reduce the amount of polishing required. This can be done with a standard surface grinder using a large-grit, open-face grinding wheel.

In the final step of preparation, the cross-sectioned surface is polished. A mirror finish, free of grinding scratches, is required. This is accomplished by first polishing the surface with a rotating disk of felt cloth charged with a 1-micron diamond paste. The final polish is achieved with an aluminum oxide abrasive of 0.03 micron size. Photomacrographs of polished bellows and diaphragm cross sections are shown in Figures P-9 through P-14.

Location of Bench Marks

As a part of the stress-analysis procedure, a series of X-Y coordinates is used to draw the enlarged portion of the bellows. To obtain X-Y coordinates, it is first necessary to establish the midplane of the shell of the selected convolution(s) on the bellows cross section. This can be done with a Tukon microhardness tester. Diamond pyramid hardness impressions (bench marks) are indented into the shell along the midplane at regular intervals using a Vickers diamond penetrator and a 300-gram load. Generally, an experienced operator can visually place an indentation within 0.0005 inch of the midplane, especially with materials approximately 0.005 inch thick. For thicker materials it may be necessary to locate the midplane by making measurements from the edges of the material.

Measurement of Bench Marks

After hardness impressions have been placed along the midplane of the convolution, the block containing the sectioned bellows is mounted on a calibrated X-Y micrometer stage under a microscope equipped with a cross-hair reticle. As each hardness impression is brought under the cross hairs, its X and Y coordinates are read from the stage drums.

The specimen is then examined under a microscope equipped with a Vickers image-splitting measuring eyepiece, and the wall thickness is measured at all of the hardness impressions. Wall-thickness data are also an input to the computer program.

Hardness Measurement

Finally, the hardness impressions can be read to determine the hardness number associated with each impression. It was found that there is a noticeable increase in microhardness of the bellows wall material that is approximately proportional to the amount of wall thinning. Although not much use can be made of this observation within the state of the art, it is mentioned because of the relationship that exists between the tensile strength and hardness of metals. The gain in limiting material properties with hardness acts to offset at least partially the increase in membrane stress that accompanies wall thinning.

Metallurgical Examinations of Bellows and Diaphragm Cross Sections

After the convolution shapes had been determined from the bellows and diaphragm cross sections, they were examined microscopically in the unetched and etched conditions. Unetched examinations showed that inclusion contents of all bellows, diaphragm, and end-fitting materials were satisfactorily low. Etched examinations showed that grain size relative to wall thickness was small in all cases, signifying good control by the metal fabricators. Examples of typical microstructures are shown in the photomicrographs accompanying the following discussion of the end fittings and convolution welds.

End Fittings – Formed Bellows

All formed bellows tested during the program had their end fittings attached by overlapping spot-resistance seam welding. One manufacturer first seam-welded inner and outer reinforcement rings to the ends of the bellows and then gas-tungsten-arc welded the flanges to the rings (Figures P-9 and P-10). The other formed-bellows manufacturer made the inner reinforcement ring an integral part of the machined end fitting (Figure P-11). Figure P-15 shows an enlarged view of a cross section of a formed-bellows end-fitting weld. The weld nugget is properly sized and is symmetrically located. Note that the small amount of distortion of the reinforcement rings accompanying seam welding tends to separate the rings from the bellows slightly. This separation may be beneficial, since it makes it less likely that the edges of the rings could cause a stress concentration in the bellows wall. The gap between the bellows and the reinforcement rings is a potential point of contamination entrapment, however, and would be very difficult to clean.

No difficulties were encountered during the program with either leakage or mechanical failure of a formed-bellows end fitting. It must be stated, however, that the program specimen requirements did not impose any serious restrictions on end-fitting design or attachment. Manufacturers were therefore able to employ their best practice in attaching the end fittings.

End Fittings – Welded Bellows

Two sizes of Type 347 welded bellows were obtained from one manufacturer, and two sizes of AM-350 welded bellows were obtained from another manufacturer. These bellows were examined in detail and the results are presented in the following section. Welded bellows from two other manufacturers were obtained late in the program. Although the fatigue results for these last bellows are included in Appendix N, the examinations of the bellows were very brief and the results are not included here.

The welded bellows that were examined in detail had end fittings that required an edge burn-down, gas-tungsten-arc weld to attach the outer circumference of the last diaphragm to a portion of the end fitting that had been previously machined to about 3 to 4 times the diaphragm thickness. The manufacturer of the Type 347 stainless steel bellows favored a conically tapered fitting, as shown in Figure P-12.

The manufacturer of the AM-350 bellows used an end-fitting design requiring a machined flange as shown in Figure P-13. The use by the latter manufacturer of a tilted inner edge on his convolutions made it necessary for him to increase the end-fitting clearance on the female (flange-side) end fitting. An etched photomicrograph of one of the AM-350 end-fitting welds is shown in Figure P-16. The amount of burn-down appears adequate and the weld microstructure is fine rather than coarse. A rather substantial heat-affected zone is visible in the end fitting, but the section size is sufficient to keep the stress low in that region. Machining marks are visible on the mating surface of the end fitting. These marks were not present on all of the end fittings sectioned. Also visible in the end-fitting microstructure are stringers of delta ferrite, which are to be expected in the AM-355 end-fitting alloy. These stringers, which are oriented parallel to the plane of rolling, are not known to be harmful in themselves. When the stringers are accompanied by large inclusions in the rolling plane, as in a dirty heat of AM-355 (which this one is not), it is easy to see from Figure P-16 how a brittle inclusion that opens because of the heat of welding can create a leak path through the flange portion of the end fitting. The manufacturer has some control over the orientation of the ferrite stringers and inclusions, if any, by his design and his materials selection. For example, in some cases there is a choice between making end fittings from bar or from plate.

Convolution Welds. An etched photomicrograph of a typical outer-diameter weld in a 3-1/2-inch Type 347 welded bellows is shown in Figure P-17. The weld bead is symmetrical and well formed. The diameter of the bead, about 2-1/2 to 3 times the diaphragm thickness, is of a size that offers sufficient reinforcement to avoid failure through the bead. The diaphragms are approximately tangent at the edge of the fusion zone of the weld. The edge of the fusion zone is not the edge of the columnar region, but is defined by the intersection points of the circular weld bead with the outer diaphragm surfaces and the point of initial tangency of the inner diaphragm surfaces. A small amount of epitaxial grain growth occurred before solidification proceeded far enough into the bead to establish the unidirectional heat-flow pattern necessary for columnar solidification. The grain size of the columnar portion of the fusion zone is relatively fine. There was also very little grain growth in the heat-affected zone. In short, the weld in Figure P-17 was a good one, and was typical of the inner- and outer-diameter welds on the 3-1/2-inch Type 347 cross section.

On the 1-1/2-inch Type 347 bellows welds in thinner material, however, the manufacturer appeared to have had some difficulty in maintaining a close fitup between diaphragms, so there was sometimes, though not always, a gap such as that visible in Figure P-18. Whether the geometrical effect of such a gap is good or bad is debatable. In cases where the notch at the base of the weld is its weakest point, the blunting of its end might be beneficial in reducing the stress concentration. Insofar as the gap between the diaphragms may represent a nonuniformity in the manufacturing process, however, it is bad.

An example of an outer-diameter weld in a 3-inch AM-350 welded bellows is shown in Figure P-19. The weld uniformity in both sizes of the AM-350 bellows, both inner- and outer-diameter, was excellent. Fitup was good on all welds examined in cross section. The particular photomicrograph presented in Figure P-19 was selected because one of the diaphragms happened to have its rolling direction very near the plane of polish, revealing the stringer-like nature of the delta ferrite regions. A small "tail", presumably surface oxide that has been entrapped in the weld, is visible at the base of the notch in this figure, and in the Type 347 stainless steel in Figure P-17. Tails of this

size are not reported to be harmful, though the presence of excessive amounts of such oxide as could result from poor cleaning or welding practice can cause a plane of weakness in the weld bead.

Hardness. Microhardness traverses across convolution welds in the welded bellows showed that there was only slight hardness variation across the welds in the Type 347 stainless steel (Figure P-20). The Type 347 welds were all within a 50-point band of Knoop Hardness Numbers (KHN). There were no apparent differences between traverses of inside- and outside-diameter welds. In general, the hardnesses of the fusion and heat-affected zones of the Type 347 welds were slightly less than the base-metal hardness.

Convolution welds in the AM-350 welded bellows, hardnesses of which are also shown in Figure P-20, had a spread of 100 points of hardness, about twice that of the Type 347 welds. However, hardnesses of the AM-350 welds and base metal were at a much higher level than were those of the Type 347 stainless steel. There appeared to be a slight drop in hardness across the heat-affected zone and into the fusion zone, but in AM-350 the peak hardness in the fusion zone equalled or exceeded the base-metal hardness by a small amount.

Examinations of Fatigued Bellows and Diaphragms

Following fatigue testing, the bellows were visually examined, and certain bellows were subjected to destructive examinations of the fracture regions.

Posttesting Visual Examination

As described in Appendix Q, the approximate locations and lengths of fatigue fractures had already been determined using internal pressurization and soap solution immediately after the testing. Visual examinations were made later at 15X of the entire visible exterior surfaces of all fatigue-tested bellows, and this was found to be the preferred method of posttest examination. There were several cases in which the soap-bubble tests gave misleading results, despite the care used in making the tests. In a few cases, fractures were observed with the soap solution that could not be observed visually. These difficulties occurred on the 1-inch formed Inconel 718 bellows, which had dull gray-black oxide surfaces, and on two or three of the welded bellows, where the convolution geometry prevented good observation. In these cases, locations of the fractures were confirmed by dye-penetrant tests in which the dye was sprayed on the bellows inner surfaces and the developer was sprayed on the outside surfaces. Dye seeping through the fractures revealed them in all but three or four cases, in which pressure had to be used to force the dye through the very small cracks. The fracture locations and lengths are summarized in Appendixes L, M, and N, which treat the fatigue results.

With the exception of two corrosion-initiated failures and possibly some failures in formed-bellows longitudinal welds, points of initiation of the fatigue fractures could not be located or associated with any visual or microscopic surface features. It is reassuring that the minor scratches, nicks, die marks, oxide films, stains, etc., observed visually did not contribute to failure, since their entire elimination from commercial

bellows would be very difficult. Significant details of the fatigue fractures will be discussed for each group of test bellows.

Type 321 Stainless Steel Formed Bellows. With three exceptions, the fatigue failures were at the points of highest stress as predicted by the theory, viz., at the convolution roots. The remaining three failures were in the crowns. Of these, two were small cracks that probably initiated in the weld. The third, in a 5-inch bellows, JD89, was at a corrosion pit. A similar corrosion failure occurring at a root was observed in another 5-inch bellows, JD98. The cause of the corrosion was determined to have been stress corrosion due to the soap solution. The 5-inch bellows were the first series tested, at which time the manometer system was not available to determine which of the two test bellows had failed, so the procedure was to soap both bellows. The unfailed bellows was left on test with no attempt being made to remove the soap. This procedure resulted in extensive pitting. Fortunately, in both cases where this occurred, the bellows were very near the end of their cycle lives before the bellows in the other test chamber happened to have failed, so there was no noticeable effect on the fatigue results obtained from JD89 and JD98. This experience is cited as a reminder that soaps and detergents can be highly corrosive to mechanically stressed stainless steels, and that such a routine procedure as using soap solution repeatedly during a bellows test may vitiate the test results by introducing an extraneous mode of failure.

Figure P-21 shows a typical fatigue fracture in a 1-inch single-ply Type 321 bellows. Inclusion content of the material is also typical. The presence of two parallel cracks growing from the bellows inner (convex) surface is not unusual in fatigue. The fatal crack can also be observed to have branched near the center of material, also not unusual. The sudden change in direction of the fatal crack might have been passed by without comment if it had not been for the occurrence of an unsuspected condition in the root of the adjacent convolution, shown in Figure P-22. Here it is seen that there were separate fatigue cracks growing from both the inner and outer surfaces. The change in crack direction in Figure P-21 was in all likelihood the intersection of two oppositely directed cracks.

It was observed during the posttest visual examination that single-ply bellows failed at a single convolution, although the fractures sometimes appeared to be composed of smaller cracks that had linked up at, or just prior to, failure. The presence of an undetected crack such as the one in Figure P-22 suggests that there were probably other cases among the single-ply bellows where more than one convolution was very near failure.

The presence of secondary cracks in several convolutions of the outer ply of the two-ply bellows was very common. Some, if not all, of these cracks were entirely through the outer ply. Failures were at the one point in each bellows where both the inner and outer plies had fractured at the same location. Rupture of the outer ply over a substantial arc (fractures in two-ply bellows were significantly longer than those in single-ply bellows) may have increased the loading on the inner ply, which then failed.

The prevalence of fatigue fractures in the vicinity of the longitudinal seam welds of the 3-inch single-ply Type 321 bellows (Appendix L, Table L-8) suggests that there was something amiss in the manufacture of this series. Failures in the other Type 321 bellows showed no tendency to occur in any fixed relation to the weld. A possible cause of the localization of the failures in the 3-inch bellows might have been a slightly excessive amount of planishing, since there was nothing about the appearance of the welds to suggest a cause.

Inconel 718 Formed Bellows. With one exception, JD120, all fatigue failures in the Inconel 718 bellows occurred in the roots. The failure in JD120 was a small crack or hole in a crown not associated with the weld. Since the cycle life of the bellows fell within the range of bellows having normal failures, cause of the crown failure was not determined. Fractures in the Inconel 718 bellows were very similar to those in the Type 321 bellows, and the same comments apply.

Type 347 Welded Bellows. There were three failures in the heat-affected zones of the end-fitting welds. Out of a total of 18 failures in the Type 347 welded-bellows test items, three end-fitting failures is probably not excessive. Of the remaining failures, 13 were in outer diameters of the convolutions. Only two failures occurred along inner diameters, and both of these were in the smaller, 1-1/2-inch bellows. Three of the outer-diameter failures in the 3-1/2-inch bellows were through the weld bead itself. The others were classified as heat-affected-zone failures.

A photomicrograph of a typical failure in a Type 347 welded-bellows convolution weld is shown in Figure P-23. The fracture path was either in the very high-temperature edge of the heat-affected zone or at the fusion line. A comparison of this figure with Figure P-17 shows that the welds were very similar. Both show tails of about the same size. There is no evidence of any deformation associated with the notch formed by the incoming diaphragms.

Figure P-24 shows a photomicrograph of one of the three fractures through the weld beads. It is obvious from the configuration that there was insufficient melting to produce an adequate weld bead in this case. Failure to have discovered the existence of such regions of reduced burn-down in the pretest inspection must be partly attributed to inexperience of the inspecting personnel, but it is also true that inspection of these small welds is difficult. The regions might have been discovered if the 15X stereo microscope used in the posttest inspection had been used on the pretest inspection. They would not have been discovered on either inspection if they had been on the inside diameter. Cause of the regions of insufficient burn-down may have been momentary variations in welder power-supply output, an increased arc-path length due to radial motion of the torch or the welding fixture, or slightly undersize diaphragms.

A limited fractographic study was conducted on several of the fatigued Type 347 welded bellows. The fractures were confirmed to be due to fatigue. Figure P-25 shows a photomicrograph of the fracture surface of bellows JD145, a heat-affected zone failure. The fracture surface is neatly divided into two zones by a line running parallel to the diaphragm surfaces some distance from the presumed neutral axis. The larger portion of the fracture surface was the zone of fatigue fracture, while the smaller zone was the region of final shear fracture that occurred at the termination of the test, possibly over a single load cycle. This change in fracture mode is very commonly observed in fatigue-specimen fractures.

The nature of the fractures was further confirmed using electron fractography. Replicas of a similar fracture surface of Bellows JD148 were made and examined in the electron microscope at much higher magnifications than are possible with the optical microscope. Figure P-26 shows the nature of the fracture in the fatigue portion of the fracture surface. The striations, or "beach marks", are characteristic of fatigue fractures. They are caused by the stopping and restarting of the crack that takes place on the reversal of the load cycles. For comparison, a portion of the shear fracture region is shown in Figure P-27. It gives the impression of having been torn apart, which in fact it was.

The beach marks visible on the fatigue fracture surface were found to be parallel to the diaphragm surface, showing that the fatigue crack propagated perpendicularly across the diaphragm thickness rather than spreading circumferentially around the outer diameter from one or two crack nuclei. The perpendicular propagation direction is further confirmed by the demarcation line in Figure P-25, which shows that at the moment of transition to the shear fracture mode, the fatigue crack front was straight and parallel to the diaphragm surface. These observations explain the existence of very long fractures in a few of the bellows such as JD148. If the crack growth had been circumferential, it was difficult to see how the fracture could have grown so large without the failure detection system's having shut down the testing machine (see Appendix Q). Having recognized the propagation direction of the fracture to be perpendicular to the diaphragm surface, however, it is clear that there was no perforation of the diaphragm until the moment of final shear fracture. The presence of a long fracture under such conditions is actually a sign of uniformity of manufacture that resulted in a uniform stress over a large region of the outer diameter.

AM-350 Welded Bellows. Of the eight fatigue failures in the 3-inch AM-350 bellows, five occurred in end-fitting welds, one in an outer-diameter weld, and two in inner-diameter welds. In the 1-1/2-inch AM-350 bellows, there were three end-fitting weld failures, one outer-diameter-weld failure, and six inner-diameter-weld failures. All failures appeared to have taken place in the heat-affected zones, although this is not absolutely certain in five of the cases. In these five, the fractures were too small and too inaccessible to flex the diaphragms to reveal the exact crack location. There were no fractures through weld beads in the AM-350 bellows, however.

Absence of fractures through the weld beads correlates with the excellent convolution-weld uniformity in these series of bellows that was noted in the pretest inspection. The frequency of failures in the end-fitting welds was not expected. A cross section of a typical end-fitting-weld failure is shown in Figure P-28. Failure was at or near the edge of the fusion zone. Figure P-29 is an enlarged view of the end-fitting weld shown in Figure P-16 and is typical of several such undamaged end-fitting welds examined in both sizes of AM-350 welded bellows. One feature of the end-fitting welds that was not observed in the AM-350 convolution welds is a narrow band of enlarged grains in the diaphragm just at the edge of the weld bead. A hardness traverse of the end-fitting-weld cross section of Figure P-28 is plotted in Figure P-20. It shows that the band of larger grains had lower hardness than was typically observed in convolution weld traverses (KHN 417). It is possible that this soft zone was incapable of strain-hardening sufficiently on cycling to prevent localization of the fractures there. Presence of the zone of grain growth in the end-fitting welds but not in the convolution welds may have been associated with the higher heat input necessary to burn down the relatively thick end-fitting section and the relatively poor heat sinking between the diaphragm and the warm end-fitting mass.

Diaphragms. Visual examination of the diaphragms after testing to failure confirmed that all of the failures obtained at relatively low strain levels occurred at the inner-diameter-weld heat-affected zone. Figure P-30 shows that the nature of the fractures did not differ from similarly located failures in welded bellows. Diaphragm JD182, which had been tested at a high strain level, failed by fatigue in the trough of a center corrugation (Dimension S in Figure P-8). There were no unusual or unexpected features in the diaphragm failures.

TABLE P-1. MAJOR MEASURED BELLOWS DIMENSIONS

Dimension	Method	Remarks
	Nondestructive Measurements (all Items)	
Outside Diameter	Micrometer	--
Indide Diameter	Micrometer; Optical Comparator (Ex-Cell-0 Model 14-808 Contour Projector)	Inside micrometer was used on formed bellows. Comparator was used on 3-1/2-inch Type 347 welded bellows. Other welded bellows could not be measured.
Pitch	Optical Comparator, 10X	--
Bellows Length	Optical Comparator, 10X	Note that length measurements for formed bellows were from crown to crown and are not the free bellows length.
Outer Torus Radius	Optical Comparator and Radius Template Transparencies, 50X	Formed bellows only.
Flange Thickness	Micrometer	--
Corrugation Diameter (Diaphragm)	Optical Comparator, 10X	Used in reflection mode.
Corrugation Height (Diaphragms)	Metallurgical Microscope; 4-mm Objective	Focused successively on tops and bottoms of corrugations.
	Destructive Measurements (Mounted Cross Sections)	
Convolution Shape	Microhardness Tester; Microscope; X-Y Stage	Locations of hardness impressions made along convolutions were measured.
Wall Thickness	Microscope; Vickers Image-Splitting Measuring Eyepiece	Thickness measurements were at locations of hardness impressions.
Hardness	Microhardness Tester	Hardness impressions made to determine convolution shape were read.

TABLE P-2. DIMENSIONS OF 5-INCH, 1-PLY, TYPE 321 STAINLESS STEEL FORMED BELLOWS

Bellows No.	Outside Diameter Mean	Std. Dev.	No. of Observ.	Inside Diameter Mean	Std. Dev.	No. of Observ.	Outer Torus Radius Mean	Std. Dev.	No. of Observ.	Pitch Mean	Std. Dev.	No. of Observ.	Bellows Length Mean	Std. Dev.	No. of Observ.
JD87	5.7167	0.0108	24	4.9898	0.0059	22	0.0657	0.0009	21	0.3467	0.0312	20	3.8023	0.0020	4
JD88	5.7144	0.0128	24	4.9881	0.0057	22	0.0659	0.0007	21	0.3544	0.0303	20	3.7865	0.0570	4
JD89	5.6993	0.0102	12	4.9735	0.0080	10	0.0770	0.0009	6	0.3454	0.0081	5	3.7508	0.0332	4
JD90	5.7070	0.0064	24	4.9835	0.0053	22	0.0765	0.0012	6	0.3470	0.0014	5	3.8068	0.0265	4
JD91	5.7023	0.0089	12	4.9860	0.0040	10	0.0778	0.0008	6	0.3450	0.0038	5	3.8168	0.0176	4
JD92	5.7043	0.0089	12	4.9827	0.0056	10	0.0760	0.0006	6	0.3385	0.0118	15	3.8000	0.0179	4
JD93	5.7047	0.0054	24	4.9793	0.0056	22	0.0755	0.0014	6	0.3286	0.0063	5	3.5775	0.0364	4
JD94	5.7054	0.0149	12	4.9813	0.0066	10	0.0767	0.0014	6	0.3412	0.0122	5	3.7685	0.0219	4
JD95	5.7058	0.0199	12	4.9829	0.0091	10	0.0763	0.0012	6	0.3250	0.0310	5	3.7283	0.0243	4
JD96	5.7026	0.0160	12	4.9816	0.0059	10	0.0767	0.0010	6	0.3386	0.0114	5	3.8013	0.0151	4
JD97	5.7080	0.0099	12	4.9847	0.0037	10	0.0773	0.0010	6	0.3408	0.0075	5	3.7695	0.0176	4
JD98	5.7057	0.0058	12	4.9835	0.0033	10	0.0770	0.0018	6	0.3364	0.0092	5	3.7688	0.0238	4
Total Observations			192			168			102			100			48
Mean Standard Deviation, $\bar{s}$			0.0111			0.0058			0.0010			0.0223			0.0277
Standard Deviation of Means, $s_{\bar{X}}$			0.0049			0.0042			0.0043			0.0081			0.0634
Grand Mean, $\bar{\bar{X}}$			5.7064			4.9830			0.0749			0.3406			3.7473
Variance Ratio, F			<1			<1			18.49			<1			5.24
Significance Level, percent			N.S.(a)			N.S.			99			N.S.			99

(a) No statistically significant difference.

TABLE P-3. DIMENSIONS OF 3-INCH, 1-PLY, TYPE 321 STAINLESS STEEL FORMED BELLOWS

Bellows No.	Outside Diameter Mean	Std. Dev.	No. of Observ.	Inside Diameter Mean	Std. Dev.	No. of Observ.	Outer Torus Radius Mean	Std. Dev.	No. of Observ.	Pitch Mean	Std. Dev.	No. of Observ.	Bellows Length Mean	Std. Dev.	No. of Observ.
JD61	3.6360	0.0089	12	3.0118	0.0076	6	0.0380	0.0014	4	0.1963	0.0060	3	1.7575	0.0040	4
JD62	3.6413	0.0072	12	2.9873	0.0043	6	0.0383	0.0013	4	0.2163	0.0040	3	1.9040	0.0148	4
JD63	3.6340	0.0057	12	2.9820	0.0036	6	0.0393	0.0025	4	0.2050	0.0078	3	1.8183	0.0373	4
JD64	3.6418	0.0088	12	2.9938	0.0038	6	0.0380	0.0008	4	0.2060	0.0164	3	1.8593	0.0100	4
JD65	3.6388	0.0109	12	2.9952	0.0033	6	0.0380	0.0008	4	0.2170	0.0070	3	1.9125	0.0152	4
JD66	3.6377	0.0052	12	2.9913	0.0031	6	0.0385	0.0006	4	0.2147	0.0064	3	1.9383	0.0165	4
JD67	3.6377	0.0069	12	2.9963	0.0084	6	0.0380	0.0008	4	0.2083	0.0091	3	1.8878	0.0188	4
JD68	3.6436	0.0138	12	2.9883	0.0054	6	0.0383	0.0012	4	0.2090	0.0039	3	1.8280	0.0264	4
JD69	3.6470	0.0021	8	2.9900	0.0026	6	0.0378	0.0005	4	0.2070	0.0024	3	1.8478	0.0059	4
JD70	3.6430	0.0028	8	2.9862	0.0031	6	0.0383	0.0009	4	0.2123	0.0061	3	1.8960	0.0009	4
JD71	3.6301	0.0044	8	2.9925	0.0028	6	0.0373	0.0005	4	0.2133	0.0065	3	1.9135	0.0152	4
JD72	3.6336	0.0050	8	2.9902	0.0024	6	0.0365	0.0003	4	0.2197	0.0076	3	1.9480	0.0223	4
Total Observations			128			72			43			36			48
Mean Standard Deviation, $\bar{s}$			0.0079			0.0046			0.0011			0.0077			0.0184
Standard Deviation of Means, $s_{\bar{X}}$			0.0049			0.0074			0.0007			0.0065			0.0355
Grand Mean, $\bar{\bar{X}}$			3.6387			2.9971			0.0380			0.2104			1.8759
Variance Ratio, F			< 1			2.59			< 1			< 1			9.10
Significance Level, percent			N.S.(a)			99			N.S.			N.S.			99

(a) No statistically significant difference.

TABLE P-4. DIMENSIONS OF 3-INCH, 2-PLY, TYPE 321 STAINLESS STEEL FORMED BELLOWS

Bellows No.	Outside Diameter Mean	Std. Dev.	No. of Observ.	Inside Diameter Mean	Std. Dev.	No. of Observ.	Outer Torus Radius Mean	Std. Dev.	No. of Observ.	Pitch Mean	Std. Dev.	No. of Observ.	Bellows Length Mean	Std. Dev.	No. of Observ.
JD73	3.6183	0.0031	8	2.9737	0.0034	6	0.0370	0.0008	4	0.2160	0.0009	3	1.9503	0.0185	4
JD74	3.6175	0.0020	8	2.9728	0.0027	6	0.0395	0.0020	4	0.2167	0.0015	3	1.9218	0.0344	4
JD75	3.6225	0.0028	8	2.9690	0.0035	6	0.0388	0.0005	4	0.2120	0.0040	3	1.9085	0.0091	4
JD76	3.6196	0.0034	8	2.9747	0.0031	6	0.0368	0.0005	4	0.2143	0.0040	3	1.9273	0.0112	4
JD77	3.6189	0.0030	8	2.9720	0.0039	6	0.0368	0.0005	4	0.2123	0.0094	3	1.9155	0.0119	4
JD78	3.6203	0.0021	8	2.9717	0.0040	6	0.0375	0.0006	4	0.2100	0.0034	3	1.9400	0.0215	4
JD79	3.6181	0.0073	8	2.9685	0.0033	6	0.0453	0.0009	4	0.2137	0.0045	3	1.9925	0.0251	4
JD80	3.6403	0.0035	8	2.9657	0.0043	6	0.0493	0.0009	4	0.2183	0.0049	3	1.9195	0.0513	4
JD81	3.6170	0.0053	8	2.9740	0.0034	6	0.0403	0.0013	4	0.2130	0.0017	3	1.9210	0.0037	4
JD82	3.6193	0.0026	8	2.9717	0.0033	6	0.0380	0.0008	4	0.2130	0.0029	3	1.9350	0.0074	4
JD83	3.6163	0.0038	8	2.9727	0.0036	6	0.0360	0.0000	4	0.2113	0.0011	3	1.9223	0.0468	4
JD84	3.6206	0.0024	8	2.9737	0.0045	6	0.0383	0.0004	4	0.2193	0.0012	3	1.9493	0.0169	4
Total Observations			96			72			48			36			48
Mean Standard Deviation, $\bar{s}$			0.0037			0.0036			0.0009			0.0040			0.0261
Standard Deviation of Means, $s_{\bar{X}}$			0.0064			0.0027			0.0039			0.0026			0.0227
Grand Mean, $\bar{\bar{X}}$			3.6207			2.9717			0.0395			0.2142			1.9336
Variance Ratio, F			2.99			< 1			18.74			< 1			< 1
Significance Level, percent			99			N.S.(a)			99			N.S.			N.S.

(a) No statistically significant difference.

TABLE P-5. DIMENSIONS OF 1-INCH, 1-PLY TYPE 321 STAINLESS STEEL FORMED BELLOWS

Bellows No.	Outside Diameter Mean	Std. Dev.	No. of Observ.	Inside Diameter Mean	Std. Dev.	No. of Observ.	Outer Torus Radius Mean	Std. Dev.	No. of Observ.	Pitch Mean	Std. Dev.	No. of Observ.	Bellows Length Mean	Std. Dev.	No. of Observ.
JD23	1.3384	0.0049	8	0.9763	0.0047	6	0.0295	0.0009	6	0.1204	0.0019	5	0.9593	0.0060	4
JD24	1.3473	0.0049	8	0.9748	0.0022	6	0.0323	0.0008	6	0.1338	0.0029	5	0.9328	0.0039	4
JD25	1.3330	0.0048	8	0.9780	0.0041	6	0.0289	0.0010	6	0.1306	0.0029	5	0.9280	0.0066	4
JD26	1.3330	0.0049	8	0.9788	0.0039	6	0.0297	0.0008	6	0.1298	0.0011	5	0.9255	0.0113	4
JD27	1.3329	0.0026	8	0.9743	0.0036	6	0.0292	0.0003	6	0.1330	0.0044	5	0.9435	0.0044	4
JD28	1.3331	0.0026	8	0.9770	0.0018	6	0.0305	0.0009	6	0.1318	0.0058	5	0.9448	0.0113	4
JD29	1.3295	0.0045	8	0.9775	0.0058	6	0.0292	0.0014	6	0.1260	0.0165	5	0.8860	0.0016	4
JD30	1.3330	0.0074	8	0.9797	0.0057	6	0.0308	0.0014	6	0.1316	0.0011	5	0.9010	0.0164	4
JD31	1.3310	0.0034	8	0.9753	0.0022	6	0.0297	0.0013	6	0.1208	0.0051	5	0.8440	0.0149	4
JD32	1.3295	0.0037	8	0.9710	0.0014	6	0.0282	0.0008	6	0.1170	0.0053	5	0.9400	0.0093	4
JD33	1.3318	0.0031	8	0.9773	0.0031	6	0.0302	0.0008	6	0.1264	0.0022	5	0.9215	0.0138	4
JD34	1.3337	0.0031	8	0.9793	0.0025	6	0.0297	0.0018	6	0.1114	0.0050	5	0.7930	0.0150	4
Total Observations			96			72			72			60			48
Mean Standard Deviation, $\bar{s}$			0.0043			0.0037			0.0011			0.0060			0.0107
Standard Deviation of Means, $s_{\bar{X}}$			0.0048			0.0025			0.0028			0.0071			0.0482
Grand Mean, $\bar{\bar{X}}$			1.3339			0.9766			0.0291			0.1260			0.9100
Variance Ratio, F			1.25			< 1			6.48			1.40			20.3
Significance Level, percent			N.S.(a)			N.S.			99			N.S.			99

(a) No statistically significant difference.

TABLE P-6. DIMENSIONS OF 1-INCH, 2-PLY TYPE 321 STAINLESS STEEL FORMED BELLOWS

Bellows No.	Outside Diameter Mean	Std. Dev.	No. of Observ.	Inside Diameter Mean	Std. Dev.	No. of Observ.	Outer Torus Radius Mean	Std. Dev.	No. of Observ.	Pitch Mean	Std. Dev.	No. of Observ.	Bellows Length Mean	Std. Dev.	No. of Observ.
JD11	1.3406	0.0037	8	0.9742	0.0030	6	0.0323	0.0009	6	0.1294	0.0048	5	0.9017	0.0130	3
JD12	1.3228	0.0037	8	0.9677	0.0062	6	0.0313	0.0014	6	0.1304	0.0049	5	0.9180	0.0117	4
JD13	1.3433	0.0018	8	0.9767	0.0027	6	0.0337	0.0012	6	0.1342	0.0088	5	0.9408	0.0068	4
JD14	1.3440	0.0015	8	0.9722	0.0019	6	0.0330	0.0019	6	0.1328	0.0041	5	0.9338	0.0069	4
JD15	1.3473	0.0032	8	0.9767	0.0022	6	0.0327	0.0005	6	0.1336	0.0059	5	0.9465	0.0149	4
JD16	1.3525	0.0026	8	0.9748	0.0026	6	0.0327	0.0004	6	0.1255	0.0027	5	0.8853	0.0079	4
JD17	1.3524	0.0031	8	0.9773	0.0021	6	0.0327	0.0012	6	0.1344	0.0064	5	0.9605	0.0087	4
JD18	1.3469	0.0018	8	0.9756	0.0015	6	0.0322	0.0008	6	0.1336	0.0025	5	0.9293	0.0035	4
JD19	1.3476	0.0028	8	0.9757	0.0024	6	0.0308	0.0008	6	0.1316	0.0040	5	0.9268	0.0080	4
JD20	1.3485	0.0015	8	0.9760	0.0016	6	0.0316	0.0004	6	0.1274	0.0046	5	0.9058	0.0051	4
JD21	1.3448	0.0021	8	0.9787	0.0015	6	0.0323	0.0010	6	0.1358	0.0037	5	0.9555	0.0084	4
JD22	1.3468	0.0018	8	0.9736	0.0024	6	0.0320	0.0015	6	0.1316	0.0029	5	0.9235	0.0058	4
Total Observations			96			72			72			60			47
Mean Standard Deviation, $\bar{s}$			0.0025			0.0028			0.0011			0.0051			0.0088
Standard Deviation of Means, $s_{\bar{X}}$			0.0077			0.0029			0.0008			0.0031			0.0223
Grand Mean, $\bar{\bar{X}}$			1.3447			0.9749			0.0328			0.1317			0.9273
Variance Ratio, F			9.49			1.07			< 1			< 1			6.42
Significance Level, percent			99			N.S.(a)			N.S.			N.S.			99

(a) No statistically significant difference.

TABLE P-7. DIMENSIONS OF 3-INCH, 1-PLY INCONEL 718 FORMED BELLOWS

Bellows No.	Outside Diameter Mean	Std. Dev.	No. of Observ.	Inside Diameter Mean	Std. Dev.	No. of Observ.	Outer Torus Radius Mean	Std. Dev.	No. of Observ.	Pitch Mean	Std. Dev.	No. of Observ.	Bellows Length Mean	Std. Dev.	No. of Observ.
JD119	3.4877	0.0137	3	3.0370	0.0087	3	0.0300	0.0013	6	0.1523	0.0069	3	1.8853	0.0194	4
JD120	3.5047	0.0058	3	3.0393	0.0050	3	0.0317	0.0025	6	0.1503	0.0071	3	1.8863	0.0115	4
JD121	3.4870	0.0060	3	3.0340	0.0017	3	0.0302	0.0020	6	0.1527	0.0119	3	1.9023	0.0100	4
JD122	3.4977	0.0021	3	3.0407	0.0040	3	0.0298	0.0031	6	0.1500	0.0175	3	1.9043	0.0337	4
JD123	3.4877	0.0127	3	3.0343	0.0015	3	0.0302	0.0018	6	0.1613	0.0184	3	1.9383	0.0121	4
JD124	3.4917	0.0093	3	3.0373	0.0021	3	0.0315	0.0019	6	0.1520	0.0169	3	1.8973	0.0107	4
JD125	3.4943	0.0085	3	3.0453	0.0015	3	0.0300	0.0024	6	0.1570	0.0113	3	1.8550	0.0196	4
JD126	3.4960	0.0010	3	3.0283	0.0035	3	0.0297	0.0010	6	0.1570	0.0157	3	1.9270	0.0058	4
JD127	3.4877	0.0078	3	3.0370	0.0046	3	0.0302	0.0019	6	0.1467	0.0021	3	1.9248	0.0151	4
JD128	3.4887	0.0180	3	3.0383	0.0038	3	0.0297	0.0020	6	0.1493	0.0021	3	1.9115	0.0088	4
JD129	3.4930	0.0044	3	3.0360	0.0035	3	0.0322	0.0026	6	0.1557	0.0160	3	1.9258	0.0126	4
JD130	3.4807	0.0025	3	3.0403	0.0038	3	0.0288	0.0005	4	0.1523	0.0040	3	1.9063	0.0014	4
Total Observations			36			36			70			36			48
Mean Standard Deviation, $\bar{s}$			0.0091			0.0041			0.0021			0.0123			0.0155
Standard Deviation of Means, $s_{\bar{X}}$			0.0063			0.0042			0.0010			0.0040			0.0229
Grand Mean, $\bar{\bar{X}}$			3.4914			3.0373			0.0303			0.1531			1.9054
Variance Ratio, F			< 1			1.05			< 1			< 1			2.18
Significance Level, percent			N.S.(a)			N.S.			N.S.			N.S.			95

(a) No statistically significant difference.

TABLE P-8. DIMENSIONS OF 1-INCH, 1-PLY INCONEL 718 FORMED BELLOWS

Bellows No.	Outside Diameter Mean	Std. Dev.	No. of Observ.	Inside Diameter Mean	Std. Dev.	No. of Observ.	Outer Torus Radius Mean	Std. Dev.	No. of Observ.	Pitch Mean	Std. Dev.	No. of Observ.	Bellows Length Mean	Std. Dev.	No. of Observ.
JD107	1.2355	0.0007	2	1.0110	0.0000	3	0.0237	0.0009	6	0.0753	0.0021	3	1.1422	0.0106	4
JD108	1.2370	0.0014	2	1.0093	0.0015	3	0.0240	0.0015	6	0.0783	0.0045	3	1.1558	0.0088	4
JD109	1.2365	0.0007	2	1.0100	0.0026	3	0.0233	0.0020	6	0.0757	0.0006	3	1.1525	0.0158	4
JD110	1.2380	0.0014	2	1.0110	0.0000	3	0.0242	0.0014	6	0.0787	0.0029	3	1.1638	0.0048	4
JD111	1.2365	0.0035	2	1.0123	0.0032	3	0.0245	0.0022	6	0.0757	0.0094	3	1.1348	0.0048	4
JD112	1.2365	0.0021	2	1.0063	0.0012	3	0.0248	0.0022	6	0.0743	0.0091	3	1.1273	0.0211	4
JD113	1.2325	0.0007	2	1.0103	0.0006	3	0.0238	0.0020	6	0.0787	0.0015	3	1.1655	0.0097	4
JD114	1.2365	0.0021	2	1.0107	0.0025	3	0.0252	0.0025	6	0.0807	0.0045	3	1.1705	0.0132	4
JD115	1.2335	0.0007	2	1.0103	0.0015	3	0.0249	0.0028	6	0.0790	0.0020	3	1.1635	0.0046	4
JD116	1.2345	0.0021	2	1.0110	0.0000	3	0.0240	0.0013	6	0.0733	0.0036	3	1.1215	0.0087	4
JD117	1.2365	0.0007	2	1.0073	0.0035	3	0.0242	0.0019	6	0.0760	0.0017	3	1.1513	0.0062	4
JD118	1.2350	0.0000	2	1.0113	0.0040	3	0.0252	0.0016	6	0.0797	0.0031	3	1.1568	0.0194	4
Total Observations			24			36			72			36			48
Mean Standard Deviation, $\bar{s}$			0.0016			0.0020			0.0019			0.0046			0.0119
Standard Deviation of Means, $s_{\bar{X}}$			0.0016			0.0017			0.0006			0.0023			0.0158
Grand Mean, $\bar{\bar{X}}$			1.2357			1.0101			0.0243			0.0771			1.1504
Variance Ratio, F			1.00			< 1			< 1			< 1			1.76
Significance Level, percent			N.S.(a)			N.S.			N.S.			N.S.			N.S.

(a) No statistically significant difference.

TABLE P-9. DIMENSIONS OF 3-1/2-INCH TYPE 347 STAINLESS STEEL WELDED BELLOWS

Bellows No.	Outside Diameter Mean	Std. Dev.	No. of Observ.	Inside Diameter Mean	Std. Dev.	No. of Observ.	Pitch Mean	Std. Dev.	No. of Observ.	Bellows Length Mean	Std. Dev.	No. of Observ.
JD131	3.5986	0.0022	5	2.815	-	1	0.0552	0.0053	5	0.4220	0.0055	4
JD132	3.5990	0.0019	5	2.818	-	1	0.0556	0.0051	5	0.4158	0.0015	4
JD133	3.5998	0.0032	5	2.816	-	1	0.0566	0.0027	5	0.4253	0.0017	4
JD135	3.5978	0.0021	5	2.813	-	1	0.0632	0.0034	5	0.4213	0.0040	4
JD136	3.6010	0.0029	4	2.996(a)	-	1	0.0592	0.0044	5	0.4213	0.0040	4
JD137	3.5986	0.0021	5	2.815	-	1	0.0510	0.0053	5	0.4253	0.0015	4
JD138	3.5982	0.0025	5	2.816	-	1	0.0492	0.0019	5	0.4235	0.0021	4
JD139	3.5982	0.0023	5	2.814	-	1	0.0516	0.0037	5	0.4225	0.0013	4
JD140	3.5986	0.0016	5	2.814	-	1	0.0510	0.0031	5	0.4230	0.0028	4
JD141	3.5988	0.0020	5	2.815	-	1	0.0540	0.0061	5	0.4145	0.0013	4
JD142	3.5982	0.0019	5	2.813	-	1	0.0486	0.0040	5	0.4050	0.0031	4
Total Observations			54			11			55			44
Mean Standard Deviation, $\bar{s}$			0.0023			-			0.0043			0.0029
Standard Deviation of Means, $s_{\bar{X}}$			0.0009			0.0015			0.0044			0.0060
Grand Mean, $\bar{\bar{X}}$			3.5988			2.8149			0.0541			0.4200
Variance Ratio, F			< 1			-			1.05			4.28
Significance Level, percent			N.S.(b)			-			N.S.			99

(a) Measurement apparently in error. Discarded in calculation of grand mean.

(b) No statistically significant difference.

TABLE P-10. DIMENSIONS OF 1-1/2-INCH TYPE 347 STAINLESS STEEL WELDED BELLOWS

Bellows No.	Outside Diameter Mean	Std. Dev.	No. of Observ.	Pitch Mean	Std. Dev.	No. of Observ.	Bellows Length Mean	Std. Dev.	No. of Observ.
JM43	1.5578	0.0045	5	0.0395	0.0046	6	0.2938	0.0307	4
JM44	1.5616	0.0015	5	0.0367	0.0055	6	0.3675	0.0125	4
JM45	1.5612	0.0039	5	0.0448	0.0035	6	0.3373	0.0060	4
JM46	1.5612	0.0030	5	0.0400	0.0105	6	0.3173	0.0061	4
JM47	1.5610	0.0020	5	0.0387	0.0071	6	0.3008	0.0148	4
JM48	1.5624	0.0019	5	0.0443	0.0063	6	0.3368	0.0092	4
JM49	1.5616	0.0016	5	0.0408	0.0012	6	0.3058	0.0109	4
JM50	1.5590	0.0039	5	0.0413	0.0073	6	0.3332	0.0153	4
JM51	1.5616	0.0030	5	0.0430	0.0074	5	0.3368	0.0171	4
JM52	1.5652	0.0022	5	0.0438	0.0065	5	0.3295	0.0082	4
JM53	1.5616	0.0018	5	0.0448	0.0043	5	0.3628	0.0068	4
JM54	1.5656	0.0021	5	0.0436	0.0072	5	0.3930	0.0095	4
Total Observations			60			70			48
Mean Standard Deviation, $\bar{s}$			0.0028			0.0064			0.0157
Standard Deviation of Means, $s_{\bar{x}}$			0.0022			0.0025			0.0064
Grand Mean, $\bar{\bar{X}}$			1.5617			0.0425			0.3368
Variance Ratio, F			< 1			< 1			2.83
Significance Level, percent			N.S.(a)			N.S.			99

(a) No statistically significant difference.

TABLE P-11. DIMENSIONS OF 3-INCH AM-350 WELDED BELLOWS

Bellows No.	Outside Diameter Mean	Std. Dev.	No. of Observ.	Pitch Mean	Std. Dev.	No. of Observ.	Bellows Length Mean	Std. Dev.	No. of Observ.
JM55	2.9408	0.0015	5	0.0373	0.0051	6	0.3003	0.0030	4
JM56	2.9384	0.0015	5	0.0397	0.0047	6	0.3020	0.0014	4
JM57	2.9384	0.0019	5	0.0365	0.0050	6	0.2915	0.0013	4
JM58	2.9404	0.0032	5	0.0390	0.0030	6	0.3020	0.0008	4
JM59	2.9422	0.0029	5	0.0372	0.0034	6	0.3005	0.0013	4
JM60	2.9390	0.0035	5	0.0385	0.0038	6	0.3048	0.0015	4
JM61	2.9384	0.0021	5	0.0370	0.0048	6	0.3021	0.0051	4
JM62	2.9382	0.0028	5	0.0383	0.0023	6	0.2995	0.0060	4
JM63	2.9426	0.0015	5	0.0393	0.0051	6	0.2998	0.0045	4
JM64	2.9400	0.0005	5	0.0405	0.0041	6	0.3283	0.0046	4
JM65	2.9430	0.0023	5	0.0373	0.0038	6	0.2990	0.0012	4
JM66	2.9424	0.0019	5	0.0393	0.0050	6	0.3048	0.0017	4
Total Observations			60			72			48
Mean Standard Deviation, $\bar{s}$			0.0023			0.0043			0.0029
Standard Deviation of Means, $s_{\bar{x}}$			0.0018			0.0012			0.0087
Grand Mean, $\bar{\bar{X}}$			2.9405			0.0382			0.3029
Variance Ratio, F			< 1			< 1			9.02
Significance Level, percent			N.S.(a)			N.S.			99

(a) No statistically significant difference.

TABLE P-12. DIMENSIONS OF 1-1/2-INCH AM-350 WELDED BELLOWS

Bellows No.	Outside Diameter Mean	Std. Dev.	No. of Observ.	Pitch Mean	Std. Dev.	No. of Observ.	Bellows Length Mean	Std. Dev.	No. of Observ.
JM67	1.5659	0.0044	5	0.0373	0.0027	6	0.2988	0.0015	4
JM68	1.5639	0.0021	5	0.0385	0.0041	6	0.2663	0.0022	4
JM69	1.5638	0.0021	5	0.0363	0.0023	6	0.2680	0.0026	4
JM70	1.5610	0.0028	5	0.0372	0.0012	6	0.2670	0.0008	4
JM71	1.5600	0.0040	5	0.0380	0.0031	6	0.2698	0.0043	4
JM72	1.5612	0.0028	5	0.0370	0.0025	6	0.2680	0.0009	4
JM73	1.5578	0.0031	5	0.0357	0.0029	6	0.2975	0.0010	4
JM74	1.5638	0.0015	5	0.0362	0.0017	6	0.2675	0.0038	4
JM75	1.5616	0.0061	5	0.0365	0.0019	6	0.2988	0.0015	4
JM76	1.5604	0.0042	5	0.0375	0.0036	6	0.2993	0.0033	4
JM77	1.5612	0.0031	5	0.0338	0.0026	6	0.2663	0.0065	4
JM78	1.5598	0.0042	5	0.0390	0.0015	6	0.3010	0.0014	4
Total Observations			60			72			48
Mean Standard Deviation, $\bar{s}$			0.0036			0.0024			0.0024
Standard Deviation of Means, $s_{\bar{x}}$			0.0021			0.0018			0.0157
Grand Mean, $\bar{\bar{X}}$			1.5614			0.0384			0.2842
Variance Ratio, F			< 1			< 1			43.0
Significance Level, percent			N.S.(a)			N.S.			99

(a) No statistically significant difference.

TABLE P-13. DIMENSIONS OF 4-INCH DIAPHRAGMS[a]

Diaphragm No.	Corrugation Diameters, in.[b]							Corrugation Heights, in.[c]					
	N	P	R	S	T	U	V	A&B	C&D	E&F	G&H	J&K	L&M
JD179	3.558	3.334	3.112	2.906	2.666	2.470	2.227	0.04207	0.03307	0.03640	0.04030	0.03015	0.04188
JD180	3.558	3.330	3.114	2.900	2.666	2.466	2.229	0.04072	0.03235	0.03445	0.04190	0.03120	0.04098
JD181	3.559	3.330	3.112	2.903	2.664	2.471	2.226	0.04152	0.03175	0.03355	0.04145	0.03005	0.04215
JD182	3.544	3.340	3.104	2.906	2.665	2.466	2.228	0.03237	0.03630	0.03095	0.04247	0.03117	0.04172
JD183	3.546	3.338	3.104	2.908	2.666	2.472	2.228	0.03312	0.03590	0.02975	0.04307	0.02910	0.04262
JD184	3.554	3.332	3.108	2.904	2.664	2.467	2.223	0.04110	0.03190	0.03245	0.04125	0.03115	0.04132
JD185	3.548	3.335	3.112	2.911	2.665	2.467	2.235	0.03515	0.03380	0.03035	0.04235	0.03070	0.03662
JD186	3.560	3.326	3.112	2.898	2.664	2.468	2.224	0.04190	0.03065	0.03362	0.04135	0.02972	0.04352
JD187	3.542	3.340	3.106	2.904	2.664	2.468	2.228	0.04182	0.03112	0.03337	0.04140	0.02922	0.04225
JD188	3.548	3.341	3.110	2.904	2.670	2.466	2.227	0.04085	0.03222	0.03305	0.04142	0.03005	0.04212
JD189	3.552	3.335	3.106	2.902	2.662	2.470	2.222	0.04072	0.03140	0.03317	0.04117	0.03005	0.04305
JD190	3.556	3.332	3.113	2.902	2.664	2.471	2.227	0.04155	0.03145	0.03327	0.04127	0.03017	0.04255
Mean Standard Deviation, $\bar{s}$	0.0020	0.0029	0.0028	0.0032	0.0032	0.0033	0.0016	0.0019	0.0021	0.0025	0.0008	0.0012	0.0016
Standard Deviation of Means, $s_{\bar{X}}$	0.0063	0.0047	0.0036	0.0035	0.0020	0.0022	0.0033	0.00361	0.00182	0.00182	0.00073	0.00071	0.00175
Grand Mean, $\bar{\bar{X}}$	3.5521	3.3343	3.1094	2.9040	2.6650	2.4685	2.2270	0.03941	0.03266	0.03286	0.04162	0.03023	0.04173
Variance Ratio, F	9.92	2.62	1.65	1.20	< 1	< 1	4.25	3.59	< 1	< 1	< 1	< 1	1.13
Significance Level, percent	99	90	N.S.[d]	N.S.	N.S.	N.S.	95	99	N.S.	N.S.	N.S.	N.S.	N.S.

(a) Refer to Figure P-8 for identification of dimensions.
(b) Average of two measurements at 90°.
(c) Average of four measurements at 90°.
(d) No statistically significant difference.

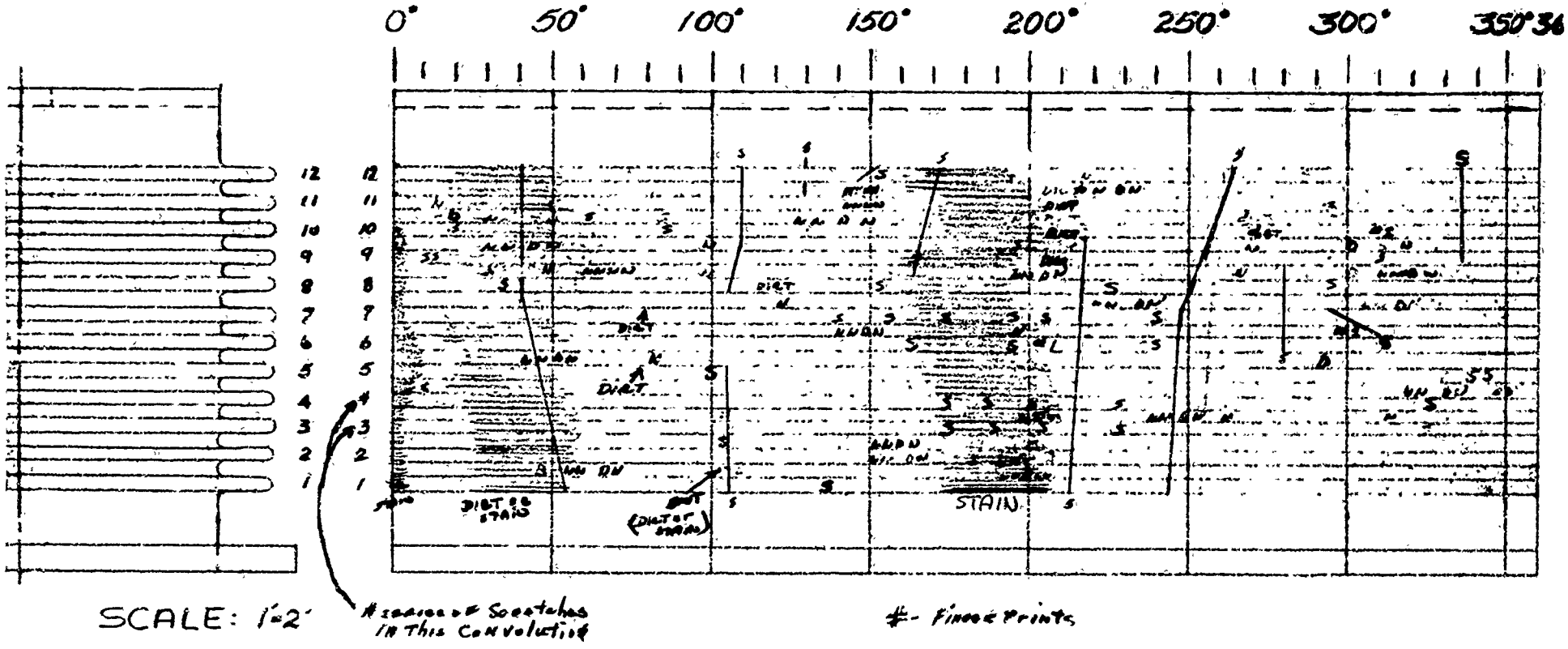

SPECIMEN NO: JD90
SIZE: 5"
PLIES: 1

S - Scratch
N - Nick
D - Dent
Shading - Stain or oxide

START 2:40
FINISH 3:40
TIME LAPSE - 1 hr

OUTSIDE

FIGURE P-1. SAMPLE VISUAL EXAMINATION RECORD SHEET

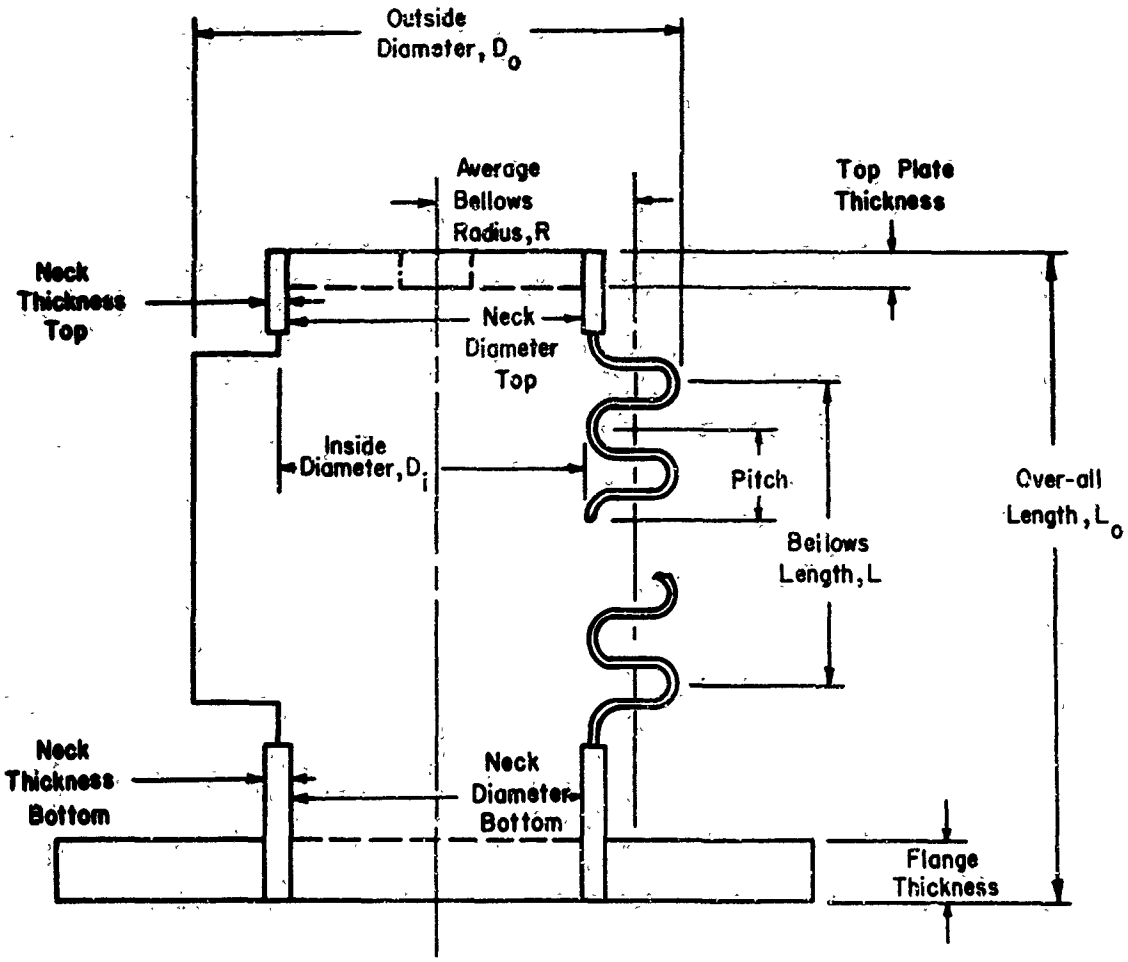

A. General View

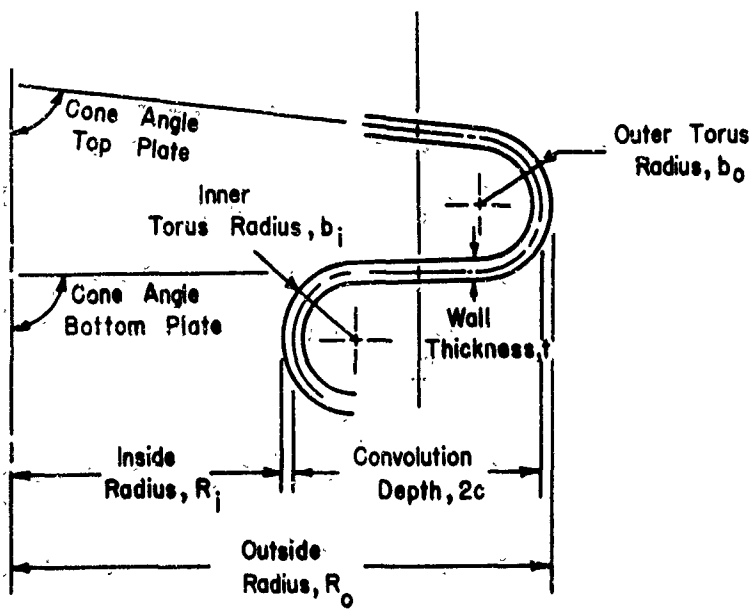

B. Convolution Details

FIGURE P-2. NOMENCLATURE FOR BELLOWS DIMENSIONS

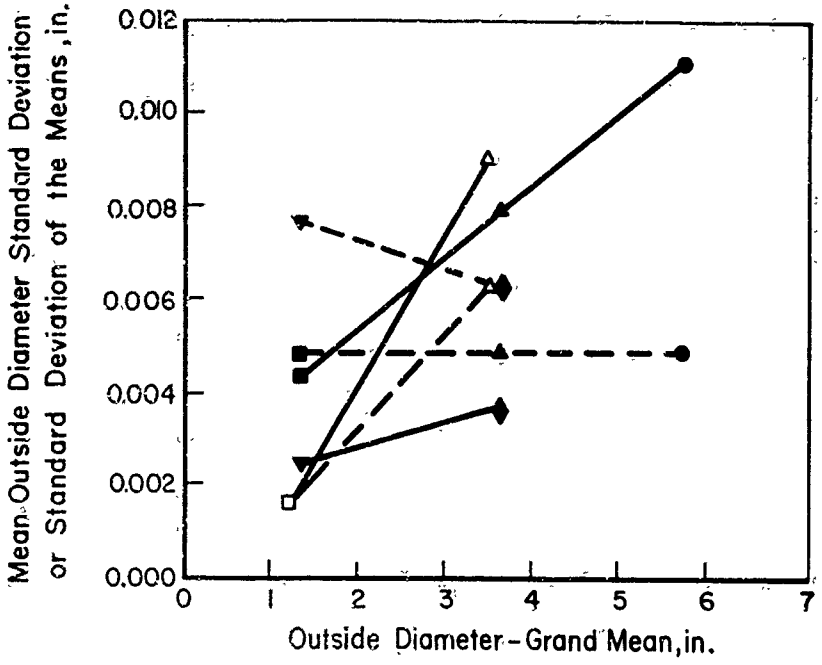

FIGURE P-3. MEAN OUTSIDE DIAMETER STANDARD DEVIATION AND STANDARD DEVIATION OF THE MEANS VS. OUTSIDE DIAMETER - FORMED BELLOWS

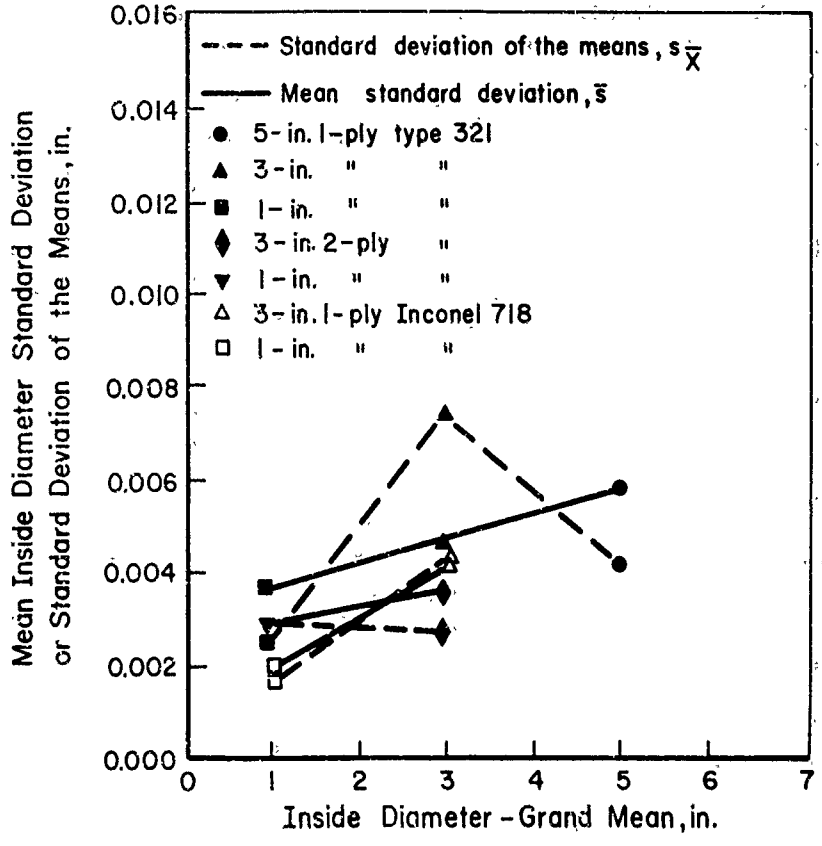

FIGURE P-4. MEAN INSIDE DIAMETER STANDARD DEVIATION AND STANDARD DEVIATION OF THE MEANS VS. INSIDE DIAMETER - FORMED BELLOWS

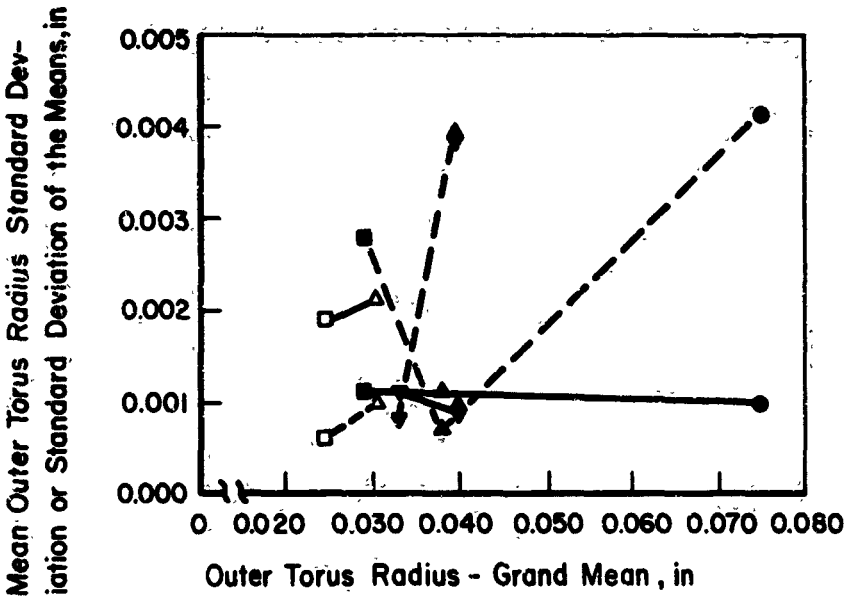

FIGURE P-5. MEAN OUTER TORUS RADIUS STANDARD DEVIATION AND STANDARD DEVIATION OF THE MEANS VS. OUTER TORUS RADIUS – FORMED BELLOWS

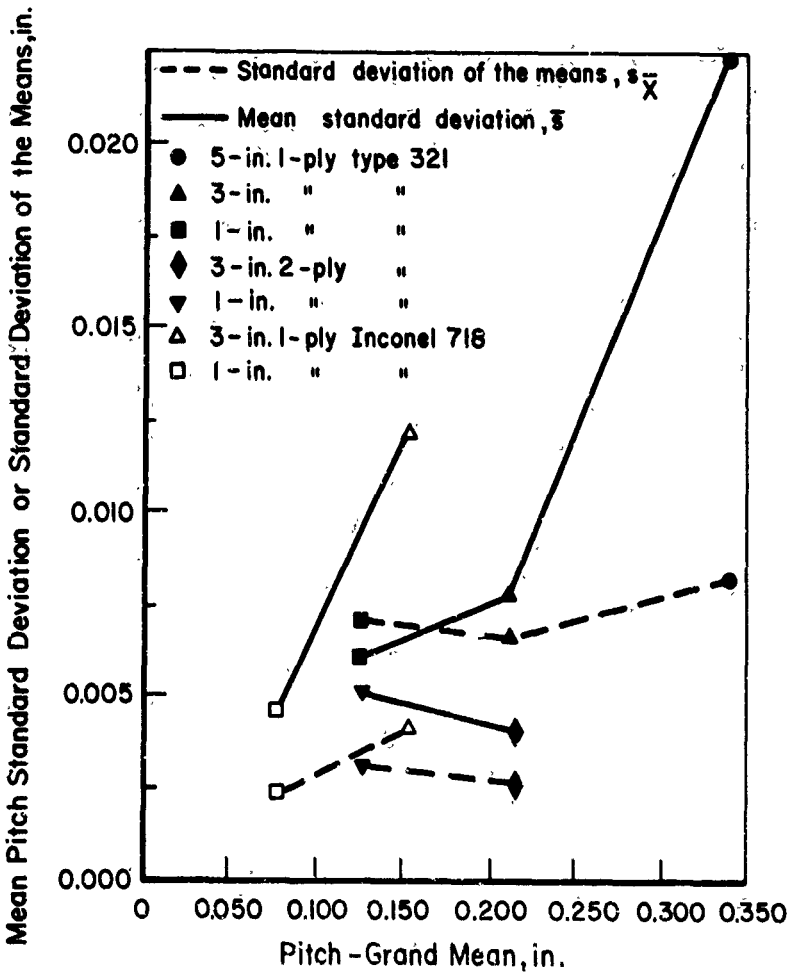

FIGURE P-6. MEAN PITCH STANDARD DEVIATION AND STANDARD DEVIATION OF THE MEANS VS. PITCH – FORMED BELLOWS

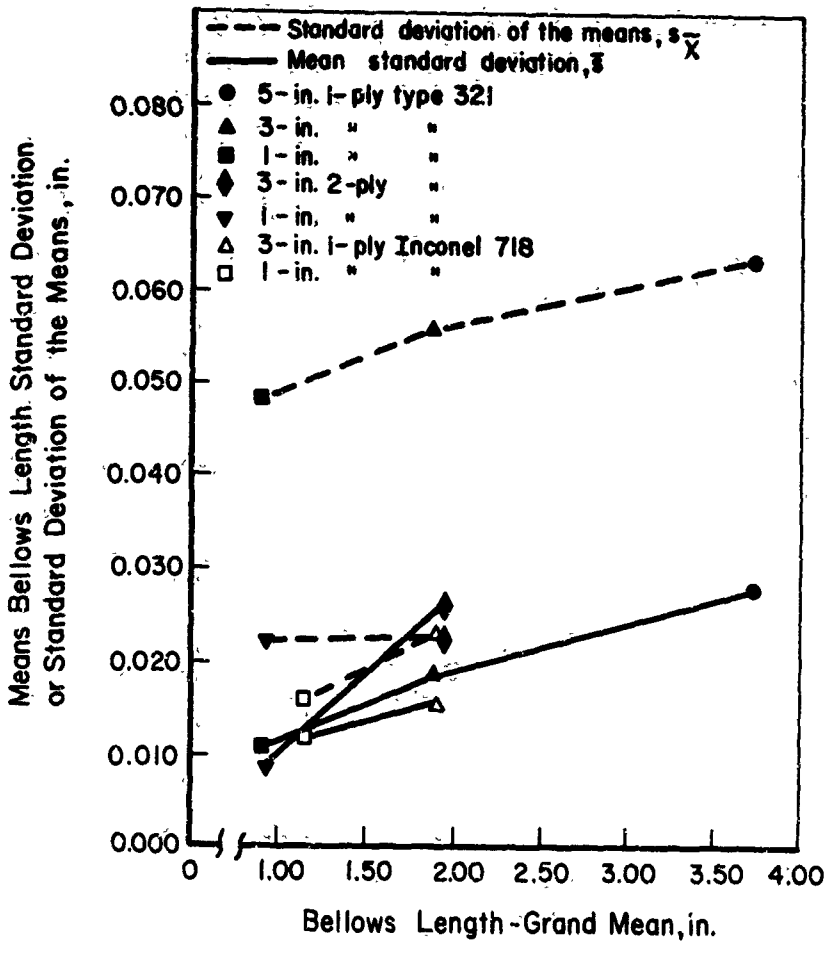

FIGURE P-7. MEAN BELLOWS LENGTH STANDARD DEVIATION AND STANDARD DEVIATION OF THE MEANS VS. BELLOWS LENGTH - FORMED BELLOWS

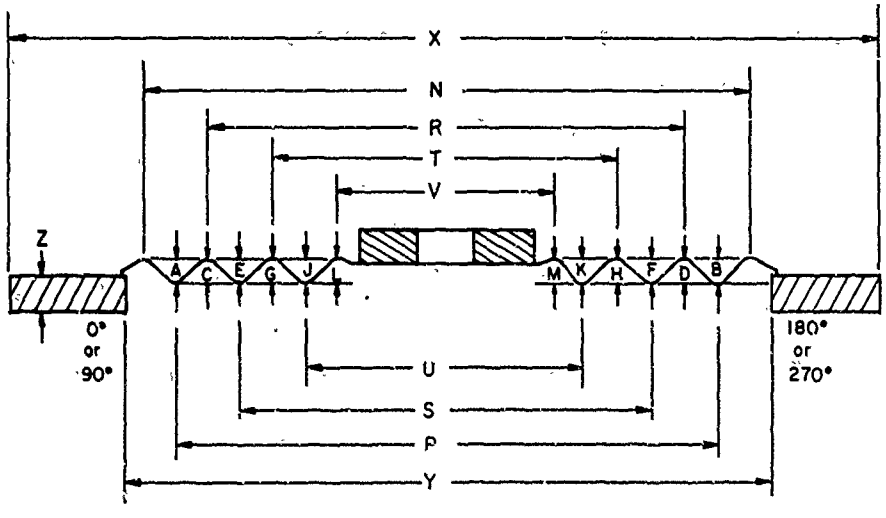

FIGURE P-8. DIMENSIONS OF DIAPHRAGMS

(Refer to Table P-13)

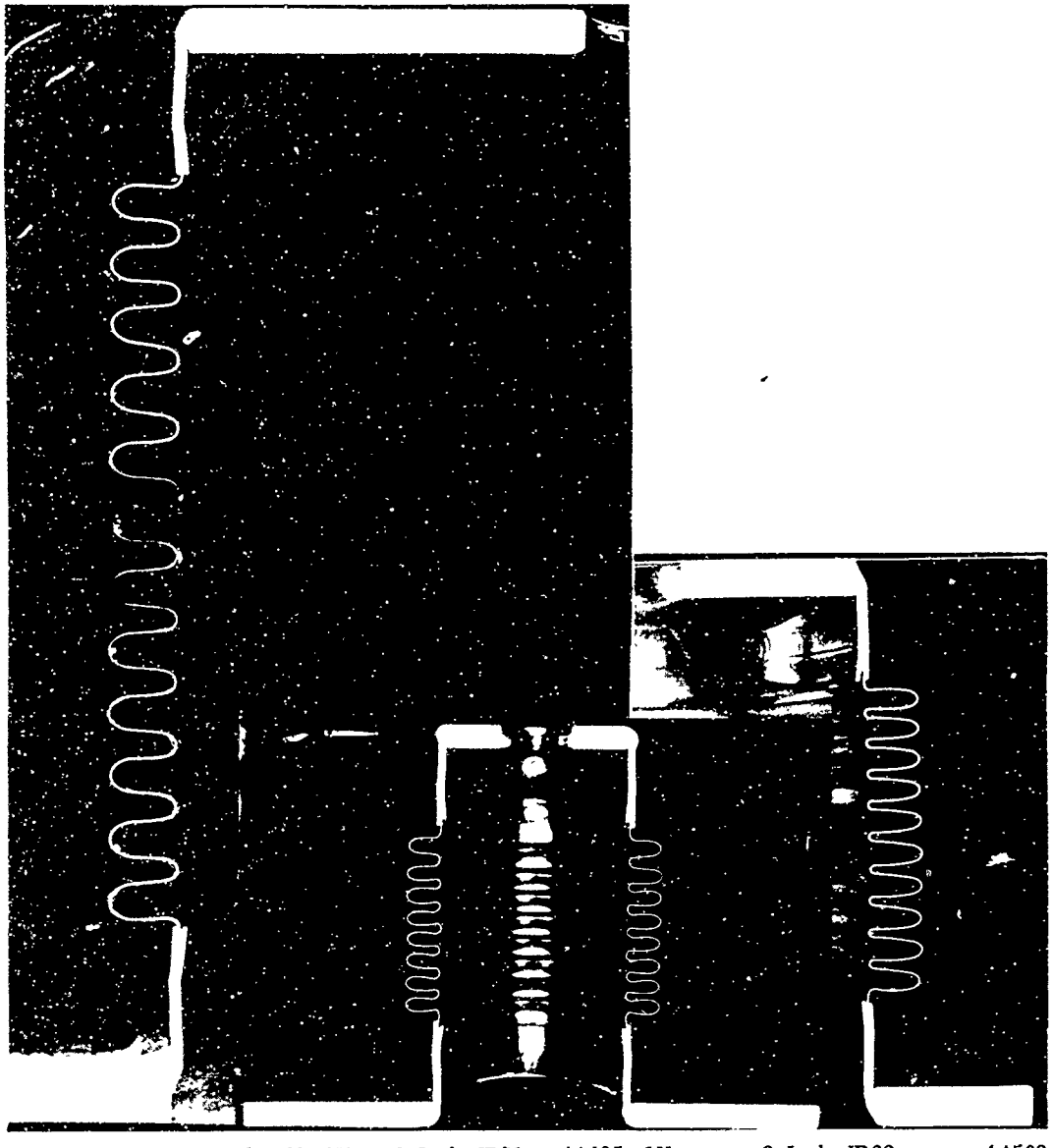

1X 5-Inch; JD92 2A889 1X 1-Inch; JD29 4A835 1X 3-Inch; JD68 4A509

FIGURE P-9. CROSS SECTIONS OF 1-PLY TYPE 321 STAINLESS STEEL FORMED BELLOWS

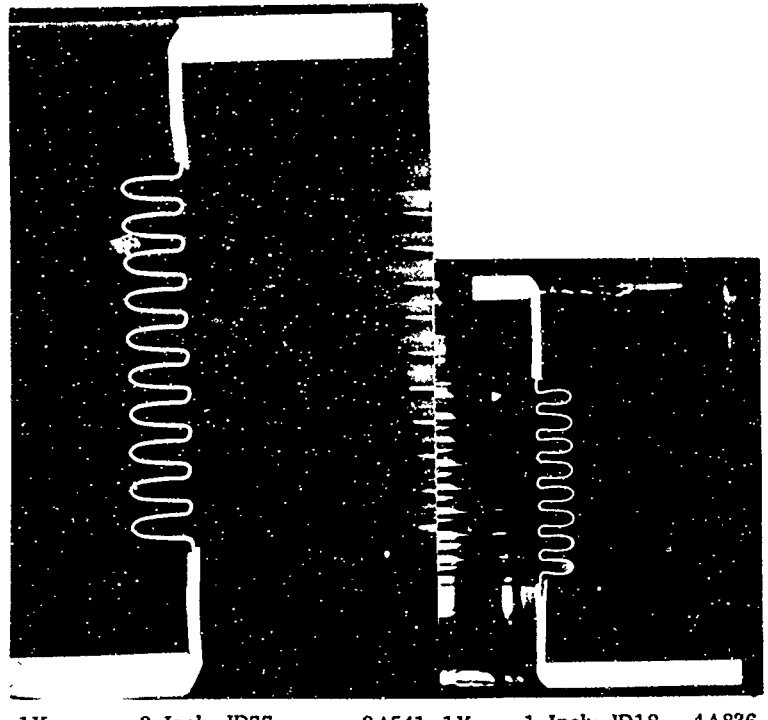

1X 3-Inch; JD77 3A541 1X 1-Inch; JD18 4A836

FIGURE P-10. CROSS SECTIONS OF 2-PLY TYPE 321 STAINLESS STEEL FORMED BELLOWS

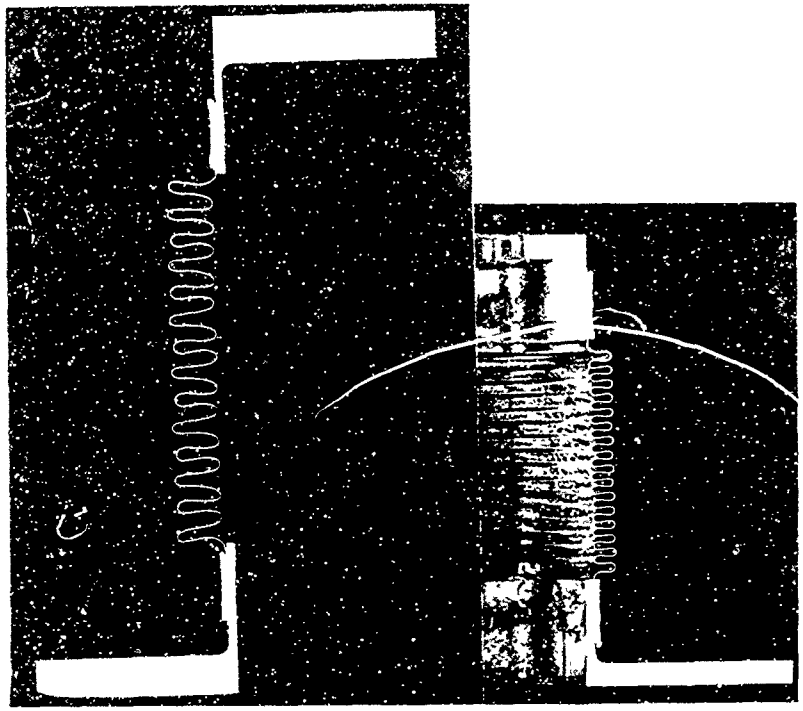

1X 3-Inch; JD124 8A893 1X 1-Inch; JD127 8A892

FIGURE P-11. CROSS SECTIONS OF INCONEL 718 FORMED BELLOWS

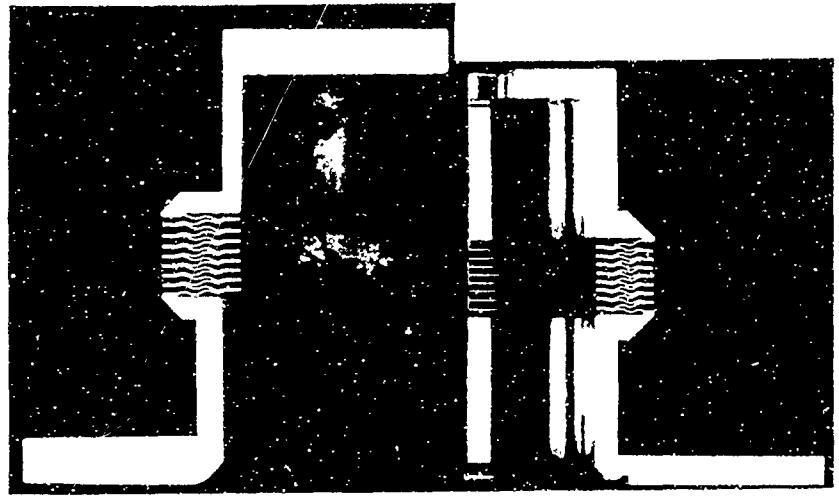

1X 3-1/2-Inch; JD136 9A694 1X 1-1/2-Inch; JD150 2B403

FIGURE P-12. CROSS SECTIONS OF TYPE 347 STAINLESS STEEL WELDED BELLOWS

1X 3-Inch; JD158 2B402 1X 1-1/2-Inch; JD171 4B197

FIGURE P-13. CROSS SECTIONS OF AM-350 WELDED BELLOWS

1X 5B685

FIGURE P-14. CROSS SECTION OF 4-INCH TYPE 347 STAINLESS STEEL DIAPHRAGM JD181

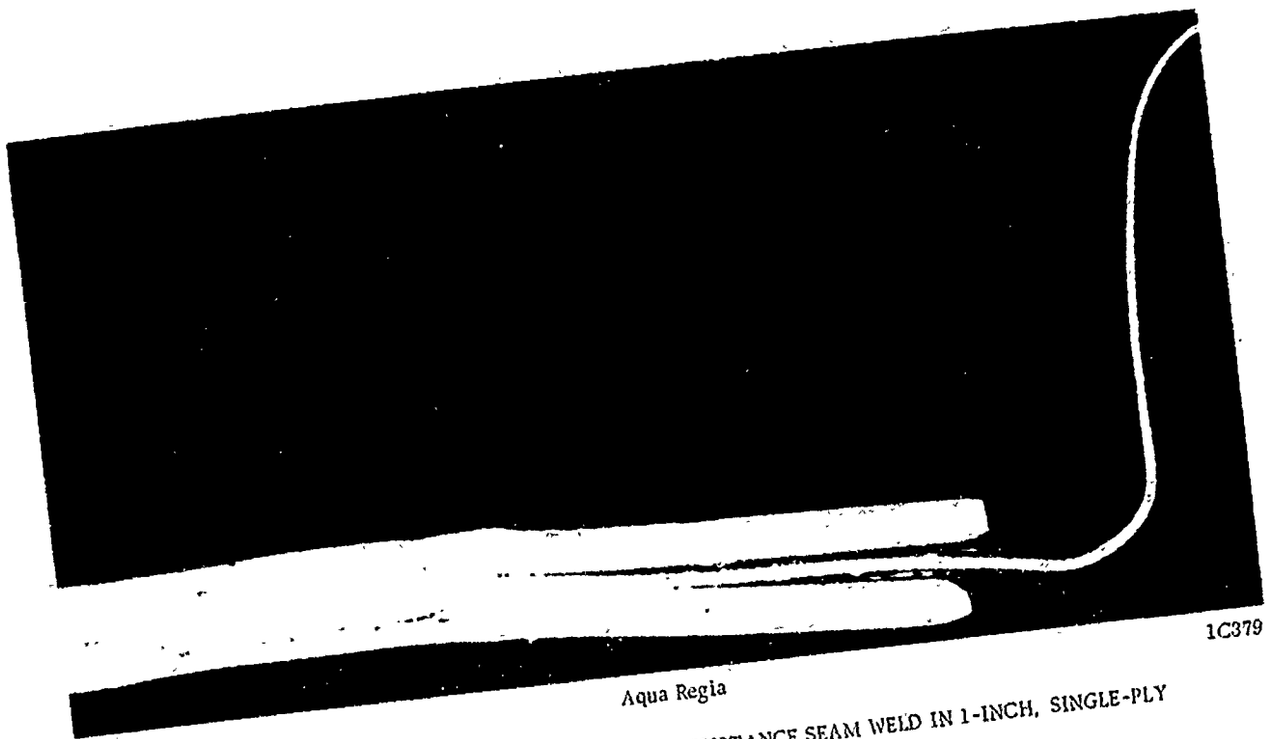

FIGURE P-15. CROSS SECTION OF END FITTING RESISTANCE SEAM WELD IN 1-INCH, SINGLE-PLY TYPE 321 STAINLESS STEEL FORMED BELLOWS JD30

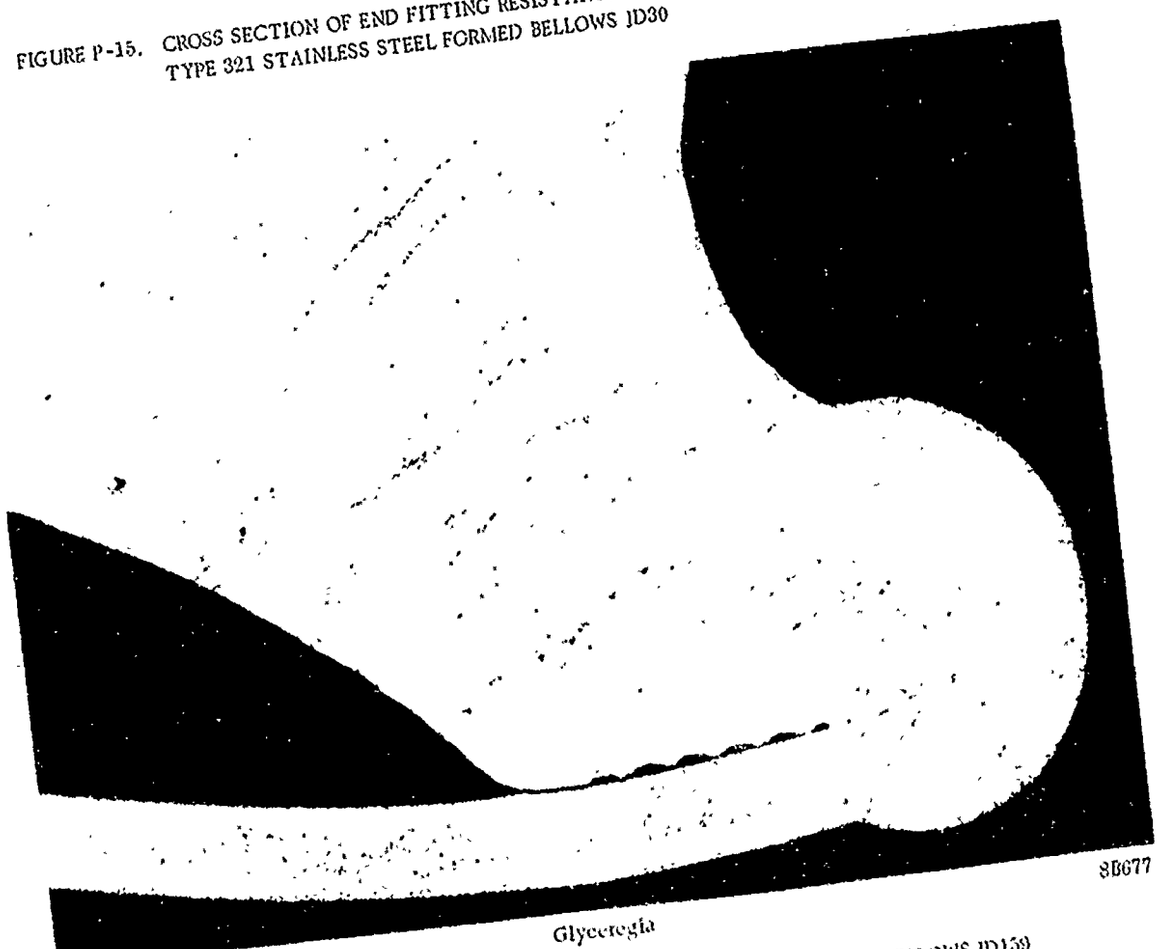

FIGURE P-16. UPPER END FITTING WELD IN 3-INCH AM-350 WELDED BELLOWS JD159

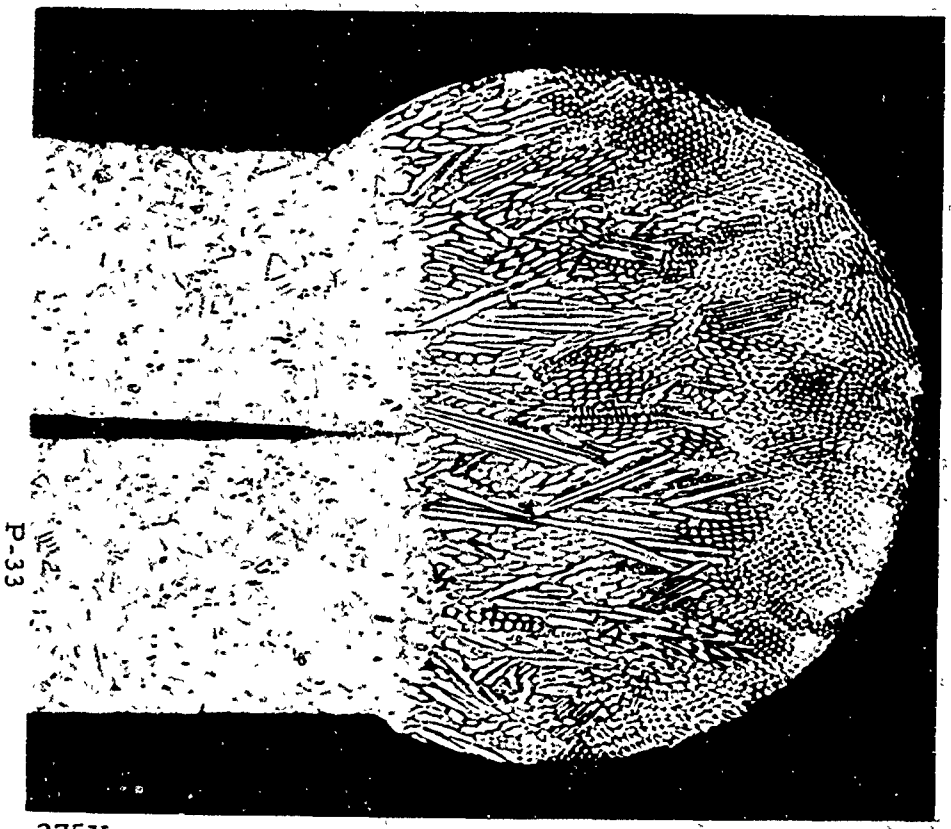

275X Glyceregia 8B674

FIGURE P-17. OUTER-DIAMETER WELD BEAD IN 3-1/2-INCH TYPE 347 STAINLESS STEEL WELDED BELLOWS JD136

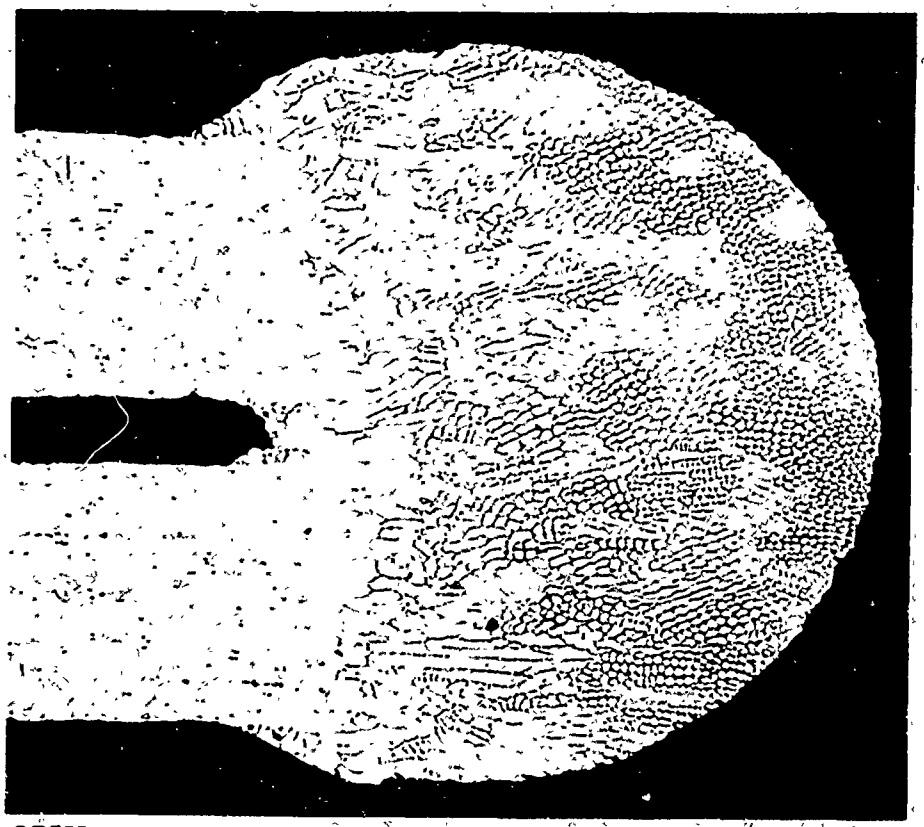

275X Glyceregia 8B671

FIGURE P-18. INNER-DIAMETER WELD BEAD IN 1-1/2-INCH TYPE 347 STAINLESS STEEL WELDED BELLOWS JD150

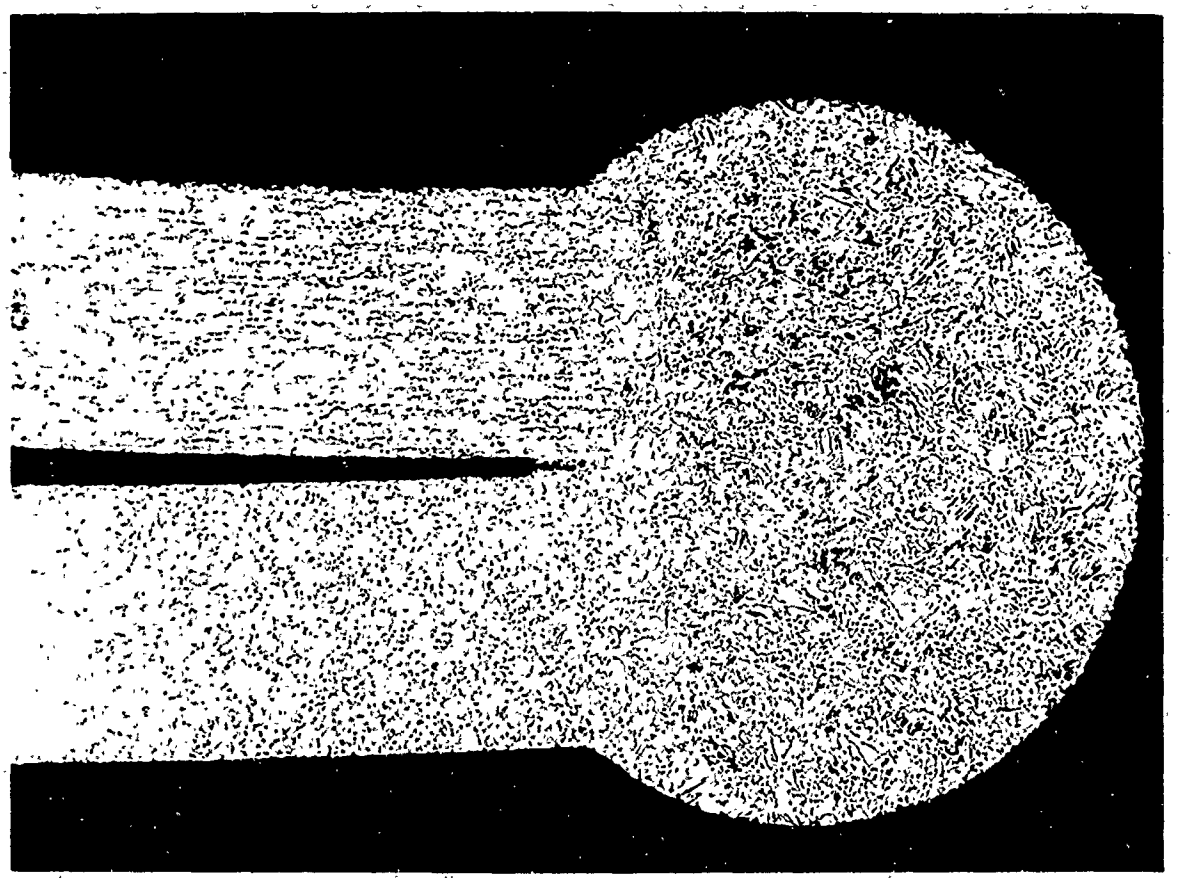

275X Glyceregia 8B676

FIGURE P-19. OUTER-DIAMETER WELD BEAD IN 3-INCH AM-350 WELDED BELLOWS JD159

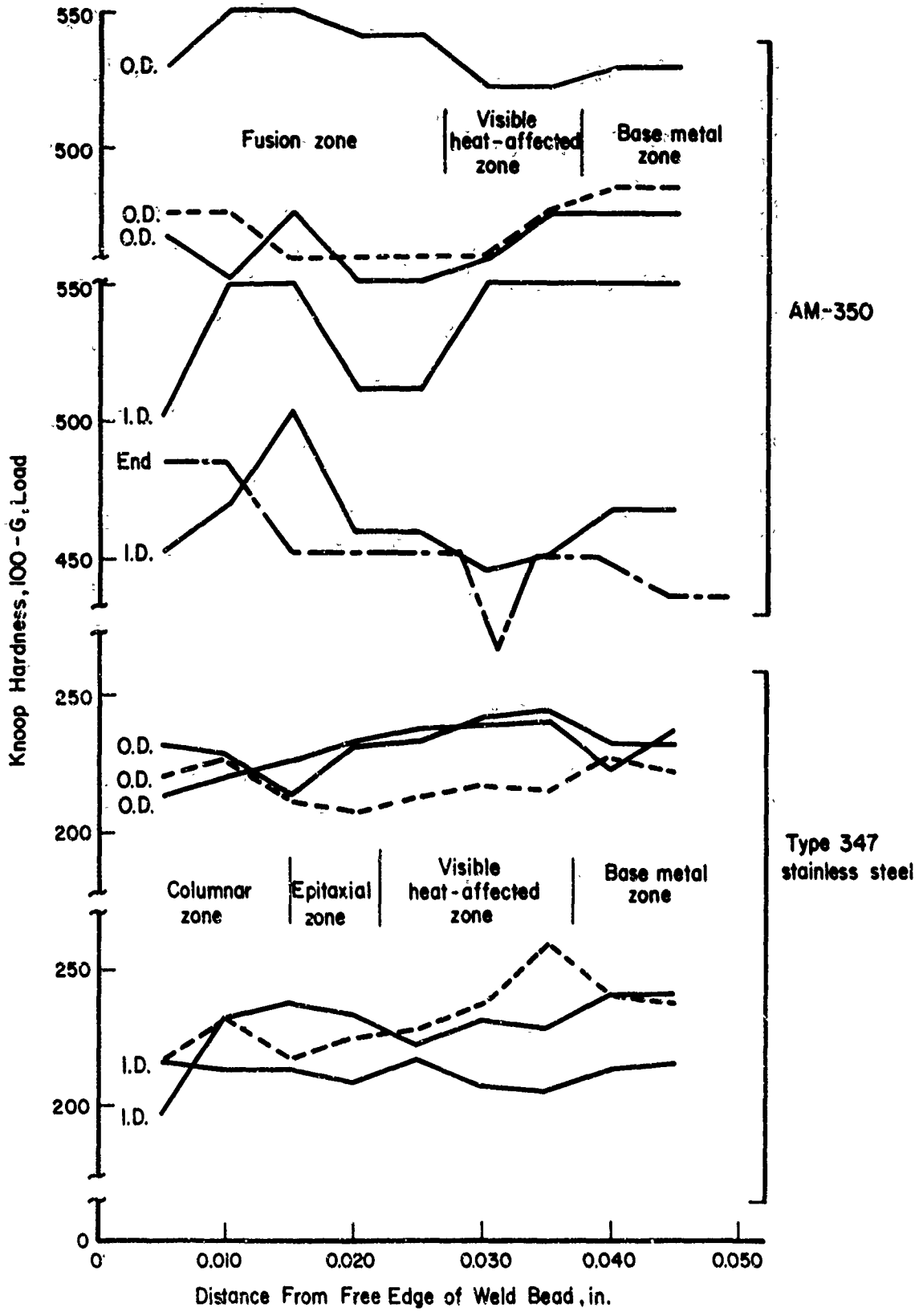

FIGURE P-20. HARDNESS TRAVERSES OF CONVOLUTION WELDS IN WELDED BELLOWS

500X (a) As Polished 1C308

500X (b) Aqua Regia 1C309

FIGURE P-21. CROSS SECTION OF FATAL FATIGUE FRACTURE IN TYPE 321 STAINLESS STEEL FORMED BELLOWS JD30 - ROOT OF SEVENTH CONVOLUTION

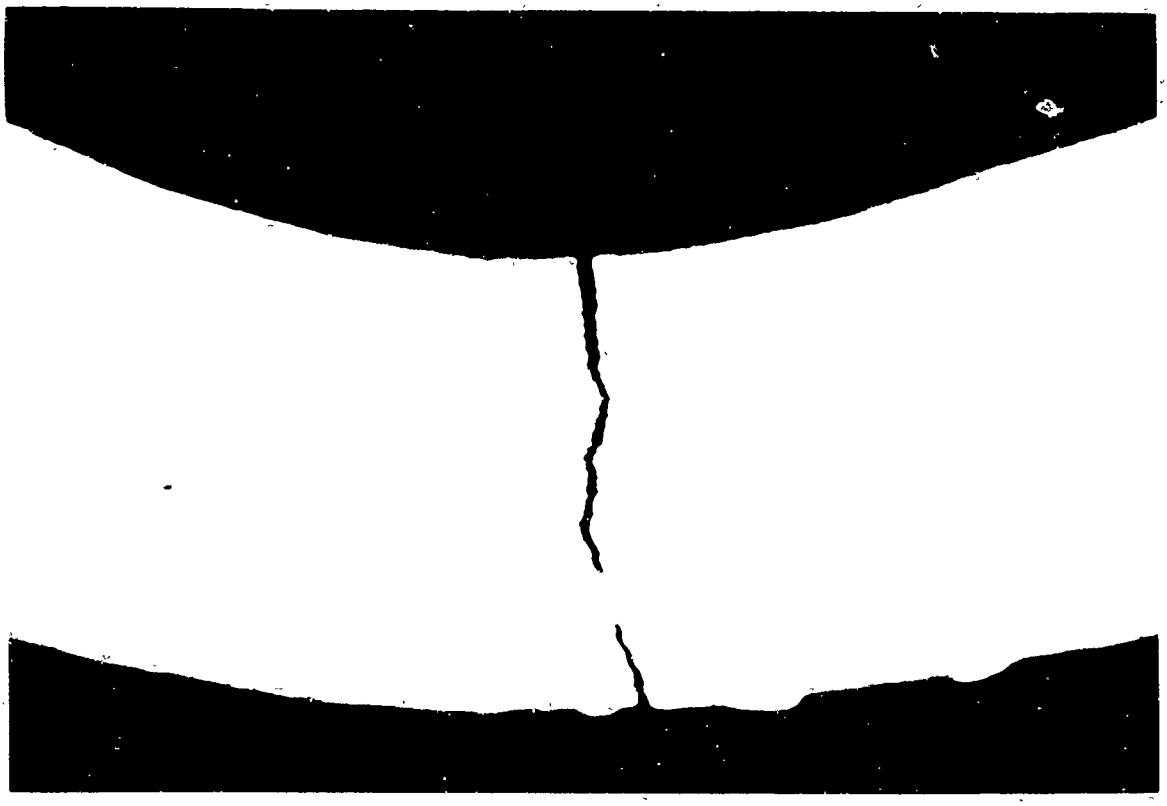

500X (a) As Polished 1C310

500X (b) Aqua Regia 1C311

FIGURE P-22. CROSS SECTION OF NONFATAL FATIGUE CRACK IN TYPE 321 STAINLESS STEEL FORMED BELLOWS JD30 - ROOT OF SIXTH CONVOLUTION

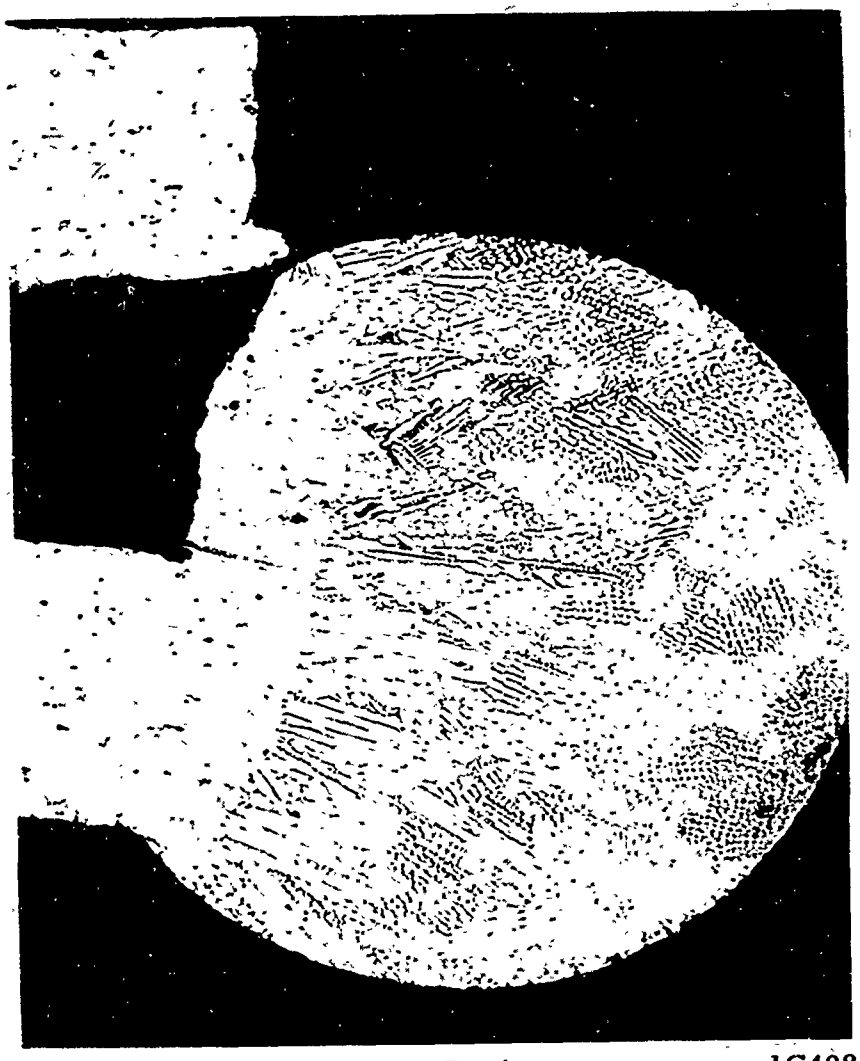

290X Aqua Regia 1C408

FIGURE P-23. CROSS SECTION THROUGH FATIGUE FRACTURE IN HEAT-AFFECTED ZONE OF TYPE 347 STAINLESS STEEL WELDED BELLOWS JD139

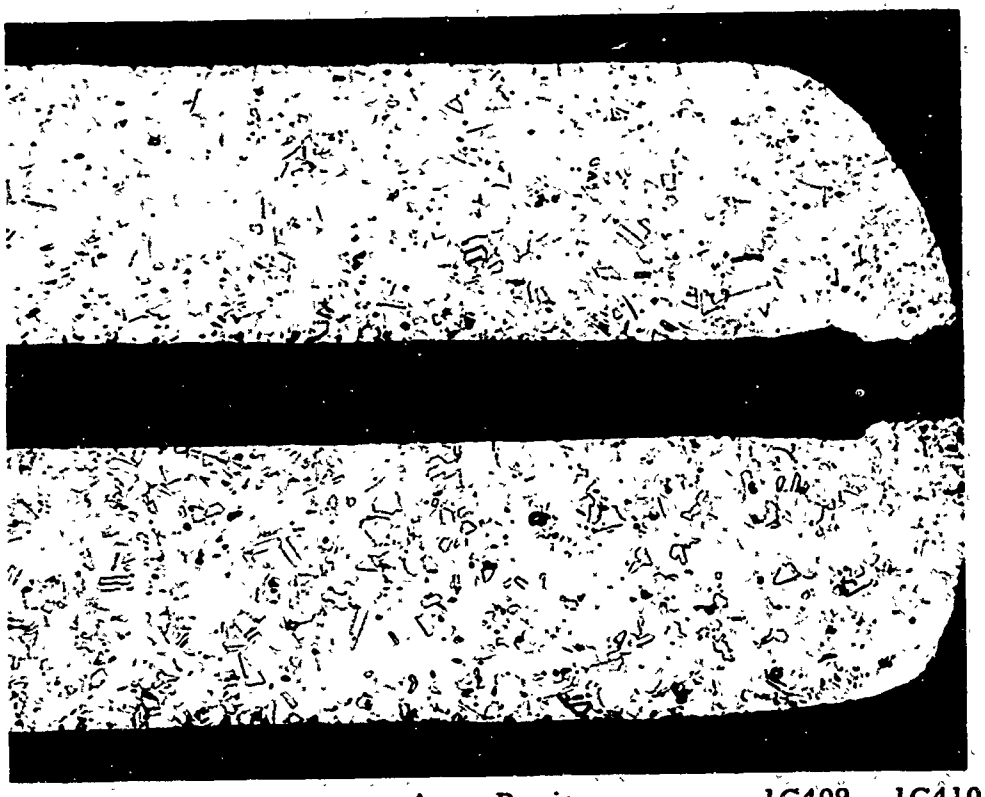

290X Aqua Regia 1C409, 1C410

FIGURE P-24. CROSS SECTION THROUGH FATIGUE FRACTURE THROUGH WELD BEAD OF TYPE 347 STAINLESS STEEL WELDED BELLOWS JD141

60X 8B761

FIGURE P-25. PHOTOMICROGRAPH OF FATIGUE FRACTURE SURFACE OF 1-1/2-INCH TYPE 347 STAINLESS STEEL WELDED BELLOWS JD145

Failure was through the weld heat-affected zone. Note the demarcation line between fatigue and shear portions of the fracture.

3800X E2296B

FIGURE P-26. ELECTRON MICROGRAPH OF FRACTURE SURFACE OF 1-1/2-INCH TYPE 347 WELDED BELLOWS JD148, SHOWING FATIGUE

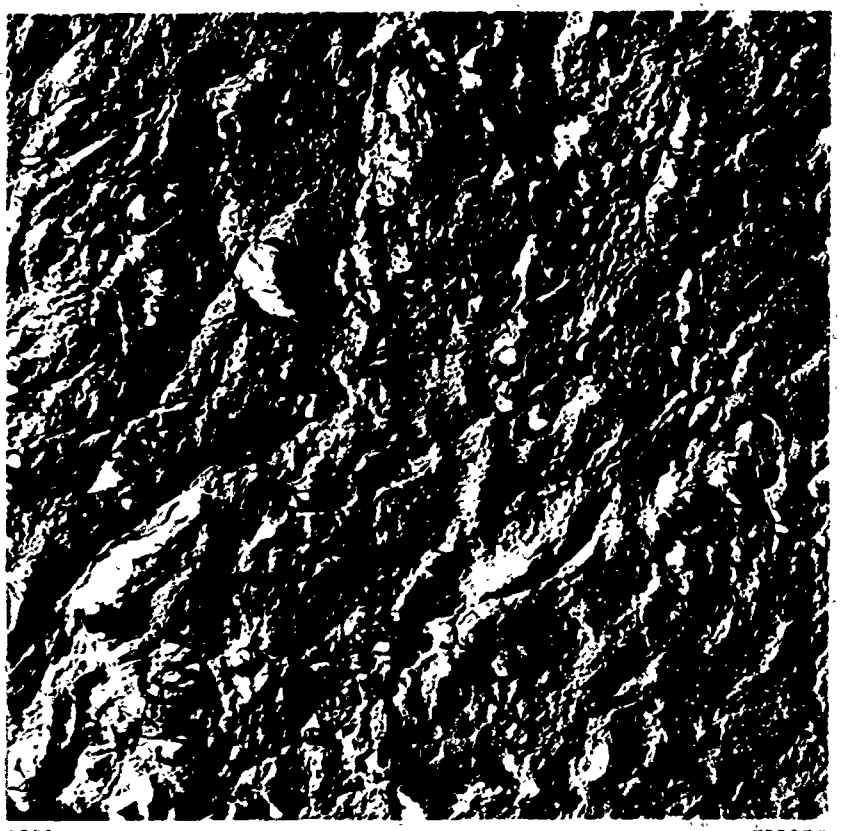

3800S E2295C

FIGURE P-27. ELECTRON MICROGRAPH OF FRACTURE SURFACE OF 1-1/2-INCH TYPE 347 WELDED BELLOWS JD148, SHOWING SHEAR

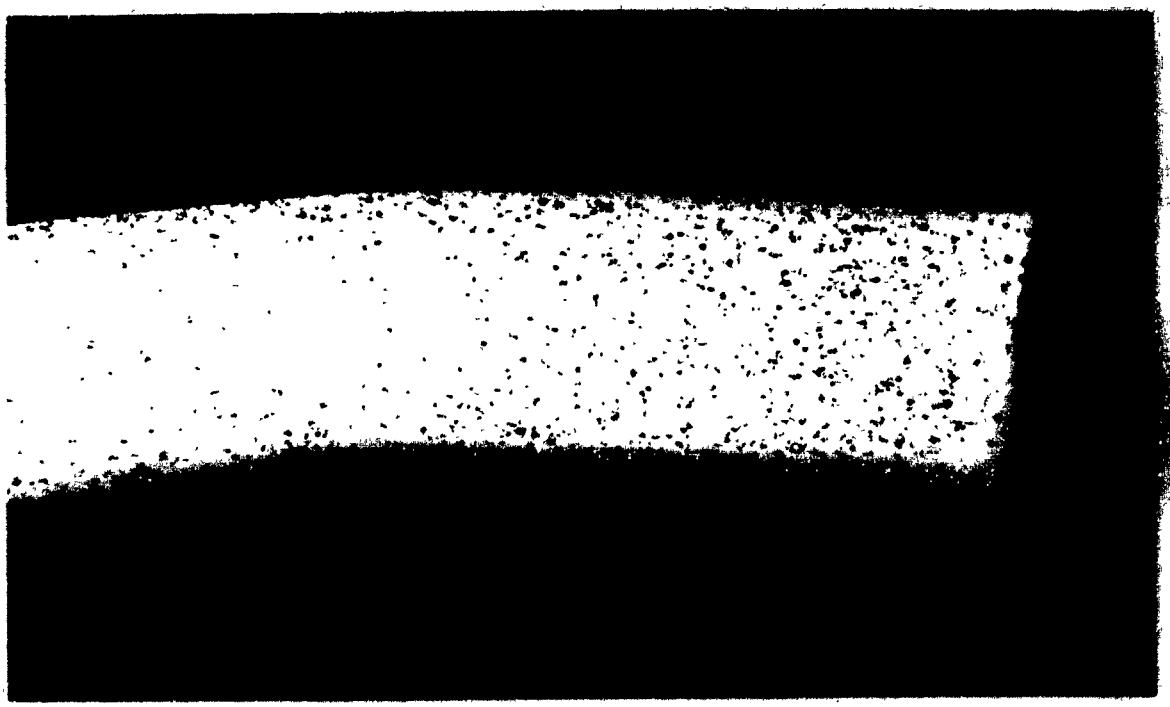

290X (a) Aqua Regia – Convolution Portion 1C412

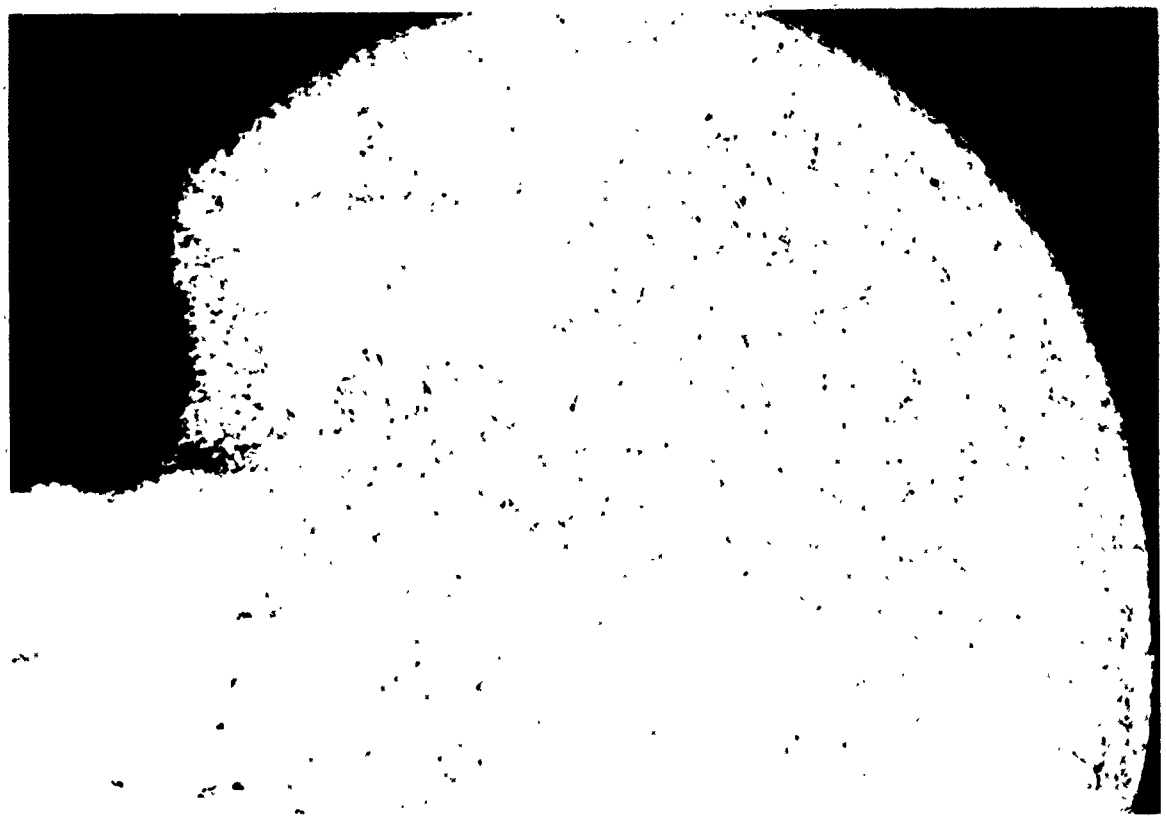

290X (b) Aqua Regia – End Fitting Portion 1C411

FIGURE P-28. CROSS SECTION THROUGH FATIGUE FRACTURE IN HEAT-AFFECTED ZONE OF END FITTING WELD IN AM-350 WELDED BELLOWS JD160

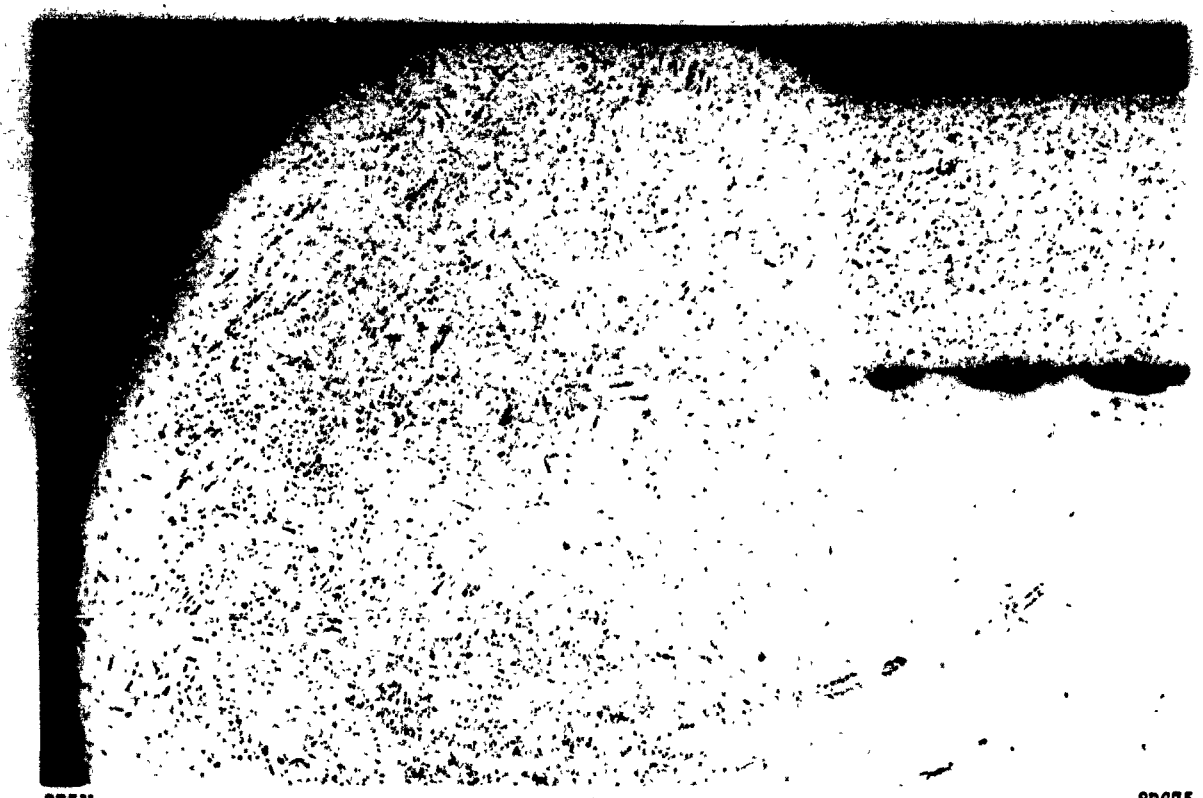

275X Glyceregia 8B675

FIGURE P-29. CROSS SECTION THROUGH UNTESTED UPPER END FITTING WELD IN 3-INCH AM-350 WELDED BELLOWS JD159

200X Aqua Regia 2C174

FIGURE P-30. CROSS SECTION THROUGH FATIGUE FRACTURE IN INNER WELD IN TYPE 347 STAINLESS STEEL DIAPHRAGM JD181

APPENDIX Q

TEST EQUIPMENT AND PROCEDURES

APPENDIX Q

TEST EQUIPMENT AND PROCEDURES

This appendix describes the equipment and procedures used for a series of tests conducted with representative bellows and diaphragms to verify the accuracy of the computerized stress-analysis procedure and to investigate the applicability of selected performance-analysis procedures. Other equipment and techniques utilized during different types of investigations are described in those report sections concerned with those investigations.

Table Q-1 shows the representative bellows and diaphragms that were tested (these items are described in some detail in Appendix P). Three basic types of tests were conducted: (1) deflection-pressure, (2) vibration, and (3) fatigue.

Deflection-Pressure Evaluation

The primary purpose of the pressure-deflection tests was to verify the accuracy of the computerized stress-analysis program for predicting elastic stresses and strains in metallic bellows and diaphragms. Because the analysis program predicts the stresses due to deflection and pressure separately, and assumes they can be combined algebraically, representative strain-gaged specimens were operated under three conditions: (1) axial deflection without pressure, (2) pressure without deflection, and (3) combined axial deflection and pressure. [Since angular deflection and offset modes of performance could be estimated by calculating an equivalent axial deflection, tests of rotational and offset (lateral) displacement were not conducted.]

The equipment and techniques used for the pressure-deflection tests are described in two categories: (1) those related to the measurement of deflection, pressure, and axial force, and (2) those related to the measurement of strain. Because the location of the strain gages on the specimens was a critical factor in the tests, the decisions relating to the strain-gage locations are included in the second category.

Measurements of Deflection, Pressure, and Axial Force

The tests were conducted in an Instron universal testing machine. Deflections were measured to within ±0.0005 inch, and axial force was measured to within ±0.10 pound. The bellows were pressurized with helium from a tank of helium, and pressures were maintained within ± 1 percent. The 4-inch diaphragm was pressurized by a column of mercury, and pressures were maintained within ± 1 percent.

Fixtures. It was necessary to design and fabricate fixtures for operation with the Instron machine. Figure Q-1 shows the major components of the fixtures. An aluminum adapter base plate was fastened to the lower, movable crosshead of the Instron machine. For internal pressure (the dashed bellows shown in Figure Q-1), one flange of the test bellows or the outside diameter of the diaphragm was clamped to the base plate against

an O-ring seal. The other flange of the bellows or the center of the diaphragm was attached to a rod fastened to an extension-compression load cell mounted in the upper crosshead. The tests of deflection without pressure were conducted by raising and lowering the lower crosshead in predetermined increments. Readings were taken at each deflection increment.

For bellows tests with internal pressure, helium was introduced through the base plate to the inside of the bellows. The tests of pressure without deflection were conducted by maintaining the null position of the lower crosshead and raising and lowering the pressure of the gas in increments by hand-operated control valves. For the tests of pressure with deflection, the lower crosshead was positioned at increments of compression and extension and the gas pressure was varied in increments. The diaphragm was pressurized by varying the height of a column of mercury contained in a manometer tube.

For bellows tests with external pressure, each bellows was surrounded by the metal cylinder shown in Figure Q-1, and pressurized gas was introduced to the volume surrounding the bellows. Tests similar to those with internal pressure were conducted with incremental variations in gas pressure and bellows deflection. By using a low-speed drive to rotate the force-rod sleeve bearing, the force needed to extend or compress the bellows under external pressure was more accurately measured than would have been possible with other types of bearings. This action was similar to the reduction of friction in hydraulic spool valves through rotation or dithering of the valve spool. Since it was not possible to pressurize the other side of the diaphragm because of strain-gage wires, "external" pressure tests were not conducted with the diaphragm.

Procedures. Because of the importance of obtaining representative strain-gage readings, the procedures used to deflect and pressurize the bellows were selected to minimize the effects of residual stress and hysteresis. For all individual and combined loadings, the stresses were kept within the elastic limit of the material. (Subsequently, as described in Appendix L, tests were conducted with some of the bellows to determine the strain distributions when the loadings were high enough to create partially plastic strains.)

To obtain strains due to deflection, a reading was first obtained at zero deflection. The specimen was then deflected in one direction to a maximum value with an intermediate reading. The specimen was then returned to the intermediate position, and then back to zero deflection. This process was repeated with deflection in the other direction to obtain a complete deflection cycle. Thus, for each deflection cycle, three readings were obtained at zero deflection, two readings were obtained at each intermediate position (one ascending and one descending), and one reading was obtained at each position of maximum deflection. Five such deflection cycles were conducted for each specimen.

To obtain strains due to pressure, readings were first obtained at zero pressure. Then the pressure was increased in 10-psi increments to a maximum value which kept all strains within the elastic limit. The pressure was then decreased in 10-psi increments to zero pressure to complete a pressure cycle. For each pressure cycle, therefore, two readings were obtained at zero pressure and at each 10-psi increment (one ascending reading and one descending reading), and one reading was obtained at the maximum pressure. At least three pressure cycles were conducted for each specimen.

To obtain strains due to deflection and pressure, the same deflection-cycle procedure was followed as described above. In addition, at each deflection increment the pressure was increased and decreased in 10-psi increments as described above. The maximum pressure for the combined loading was reduced from that used for the pressure-only tests in order to keep the combined strains within the elastic range. Only two deflection cycles were conducted for the combined loading condition because of the large number of readings required, and because the specimens had experienced considerable "settling in" during the individual loading tests.

Tests conducted for external pressure were identical to those for internal pressure. However, because the strain readings were generally similar for both types of pressure, and because the strain-gage wires required special attachments for the fixture used for external pressure, only two representative gages (one meridional and one circumferential) were read during the tests with external pressure.

Measurements of Strain

Several methods were considered for measuring strains occurring in the bellows and diaphragms. Since the stresses in each specimen were to be analyzed by the computer program as part of the analysis procedure, it was decided that the best approach would be to use very small strain gages positioned at predetermined, high-strain locations. Because of the high cost of buying and installing small strain gages, the locations of the gages were carefully selected to minimize the number of gages required.

The gages selected were 1/64-inch-long foil gages manufactured by Micro Measurements, Inc. Gages No. EA-09-015-DJ-120 were used to measure meridional strains, and Gages No. EA-09-015-EH-120 were used to measure circumferential strains. Strain readings were made with a Baldwin Lima Hamilton SR 4 Strain Indicator, Type N. Dummy gages were used for temperature compensation, and the readings were made using a bank of switches to connect each gage in turn (at each deflection and/or pressure increment) to the strain indicator. The readings were made to the nearest 5 microinches. Figure Q-2 shows a pair of gages attached to a diaphragm convolution.

Location of Strain Gages on Formed Bellows. Each formed-bellows specimen contained several convolutions. The number of convolutions was established by each manufacturer on the basis of the general size, material, and operating conditions specified by Battelle's purchase order. The number of convolutions ranged from 8 (for the 1-inch stainless steel bellows) to 16 (for the 3-inch Inconel 718 bellows).

The selection of strain-gage locations was based on two factors: (1) the theoretical stress analysis was reasonably accurate, and (2) the stresses were not expected to vary greatly from convolution to convolution. With these assumptions, the strain gages were placed (1) at the most convenient, high-strain locations, (2) at locations which would detect any gross lack of deflection symmetry, and (3) at locations which would serve as checks on other strain gages.

A "middle" convolution was selected for each bellows as the primary convolution. Because the theoretical calculations showed that the meridional stresses at the convolution roots and crowns were the largest type of stresses in each bellows, and because the convolution crown was the most convenient location, three meridional gages were placed on the "middle" convolution crown, 90, 180, and 270 degrees from the longitudinal weld.

Although the weld was avoided because of the difficulty of obtaining valid strain readings in the weld area, the three gages were expected to reveal any adverse effect on deflection symmetry caused by the weld.

One circumferential gage was paired with each of the meridional gages placed 90 and 270 degrees from the weld on the middle convolution because these were selected as the strain locations of primary interest, and biaxial strain readings were required to permit the calculation of the biaxial stresses. In addition, one meridional gage was placed on the crown of the second convolution from each end, 180 degrees from the weld. These gages were expected to reveal any significant stress variation occurring near the ends of the bellows through comparison with the gages on the middle convolution.

Finally, two meridional gages were placed 180 degrees from the weld on the inside of the root of two convolutions: the middle convolution, and the second convolution from the flanged end. These gages were essentially opposite two of the meridional gages on the convolution crowns. No circumferential gages were used at the convolution roots because of the difficulty of placing the gages on the inside diameter of the bellows. In the case of one bellows (1-inch Inconel 718), no meridional gages were used on the convolution roots because of the difficulty of installing the gages.

Figures E-21 (Appendix E) and F-7 (Appendix F) show the locations of the seven meridional and two circumferential strain gages on developed views of the 3-inch and 1-inch stainless steel bellows, respectively.

Location of Strain Gages on Welded Bellows. Calculations showed that the maximum deflection and pressure stresses in most of the welded bellows occurred at the weld beads. It was not possible to place strain gages at those locations because of the small radii of the weld beads. Therefore, a location was sought which would provide reasonably high strains and permit the use of good gage-installation techniques. The only satisfactory location was the flat portion adjacent to the crown weld bead. This area, which is clamped by the chill blocks during the welding operation, was approximately 0.060 inch wide on the 3-1/2-inch welded bellows and approximately 0.040 inch wide on the 1-1/2-inch welded bellows. It was estimated that the bellows convolutions could be separated sufficiently for meridional and circumferential gages to be installed properly.

The gages were placed generally in the middle of the flat width to avoid the heat-affected zone near the weld bead on the outside, and to avoid the radius of the first convolution on the inside. In each pair of diaphragms joined by a weld bead, the first convolution bent toward the flat in one diaphragm and away from the flat in the other diaphragm. The strain gages were mounted on that diaphragm in which the first convolution radius bent away from the mounting surface, because the gages could be more easily held in place on this flat. Gages could not be installed on the flats near the root weld beads because the working space on the inside diameter of the bellows was too small to permit separation of the convolutions and attachment of the strain gages.

Two pairs of gages were placed 180 degrees apart on the appropriate flat of the middle convolution. Because all the welded bellows were ordered with eight convolutions to keep the cost of the specimens to a minimum, the middle convolution for the welded bellows was selected as the fourth convolution from the flanged end. [Figure H-15 (Appendix H) shows the strain-gage locations selected for the 3-1/2-inch stainless steel welded bellows.] Because the strain increased to a maximum at the weld bead, it

was necessary to measure the distance from the center of each gage to the edge of the weld bead. This was done with a calibrated microscope, with calculations to allow for the angle of observation.

Although primary reliance was placed on the four gages placed on the middle convolution, two other pairs of gages were placed on the appropriate flat of the seventh convolution from the flanged end. These gages were used to determine whether deflection symmetry was maintained in the bellows.

Location of Strain Gages on the 4-Inch Diaphragm. It was decided that the 4-inch diaphragm should be highly strain gaged for two reasons: (1) it was not possible to place a sufficient number of strain gages on the welded-bellows convolutions to check the accuracy of the analysis for various locations in the welded-bellows diaphragms, even though the comparison of the experimentally determined and theoretically determined spring rates of the bellows offered a good overall check of the accuracy of the analysis, and (2) the 4-inch diaphragm offered an ideal opportunity to compare any geometrically nonlinear behavior of the diaphragm with the nonlinear analysis calculations.

Preliminary theoretical stress calculations showed that the maximum surface strains would occur at the roots and crowns of some of the convolutions and on the flat near the outside diameter, as described in Appendix I. Twenty-two strain gages were placed on one side of the diaphragm at these locations. The gages were located generally on three radial lines spaced at 120-degree intervals. On the main radial line, nine pairs of meridional and circumferential strain gages were placed on each root and crown of the convolutions. To check on the uniformity of response around the circumference, two meridional gages were installed on two crowns on the two other radial lines. Although the gages were placed carefully on the convolution roots and crowns, a calibrated microscope was used to measure the distance from the center of the diaphragm to the center of each gage as a check on the location of the gages.

Calculation of Experimentally Determined Stresses. To calculate experimentally determined stresses, it was necessary to: (1) select representative strain gages, and (2) calculate the biaxial stresses from the strain readings. For the formed bellows, the readings of two pairs of gages placed 180 degrees apart on the middle convolution were averaged, and the readings of the gage on the root of the middle convolution were used. Because no circumferential gage was placed on the convolution root and because a circumferential strain value was needed to calculate the biaxial stresses (see below), an experimental circumferential strain was determined by assuming that the ratio of the experimental stresses was the same as the ratio of the theoretical stresses at the convolution root. For the welded bellows, both the readings of the two pairs of gages on the middle convolution and the distances of the meridional gages from the weld bead were averaged. Because the circumferential stresses were smaller and the circumferential stress gradient was smaller than for the meridional stresses, the distances from the circumferential gages were selected as being the same as the distances from the meridional gages. This made it possible to obtain meridional and circumferential strain values at one location.

The equations used to calculate biaxial stresses from measured strains are:

$$S_1 = \frac{E}{1-\mu^2}(\epsilon_1 + \mu\epsilon_2) \quad (1)$$

and

$$S_2 = \frac{E}{1-\mu^2}(\epsilon_2 + \mu\epsilon_1) \quad , \quad (2)$$

where

S_1 = stress in direction of ϵ_1, psi

S_2 = stress in direction of ϵ_2, psi

ϵ_1 = strain, in./in.

ϵ_2 = strain, in./in.

E = modulus of elasticity (29×10^6 psi for stainless steel)

μ = Poisson's ratio (0.3 for stainless steel).

The problems of interpretation and approximation were minimized by using strains to the nearest microinch, and by making the stress calculations to the nearest psi. To calculate representative stresses, it was necessary to select representative deflection strain readings and representative pressure strain readings from among the readings obtained from the selected gages. For both types of strains, values were used from tests that did not combine deflection and pressure. Average values were obtained by averaging the readings of the different cycles as shown in Appendixes E and F. (The validity of adding the strains algebraically was checked by adding the individual strains and comparing them with the strains of the various combined tests.)

Comparison of Experimentally Determined Stresses and Strains With Theoretically Predicted Stresses and Strains

When the strains being measured are the result of bending stresses, and when the distance to the neutral axis is small, as it was with the bellows and diaphragm material, the strain being measured by the gage is greater than the strain at the surface of the metal. The difference is in proportion to the respective distance of the metallic surface and the center of the gage foil from the neutral axis. Thus, to compare the experimentally determined strains with the theoretically predicted strains, it was necessary either to increase the theoretical values, or to decrease the experimental values. It was decided, because the membrane strains and the bending strains were calculated independently by the computer program, that the comparison would be made more easily if the theoretical calculations were increased for comparison with the gage readings.

The deflection and pressure strains in bellows and diaphragms are the result of both membrane and bending strains. The membrane strains are constant across the entire metal thickness, and the strain gages were expected to measure the membrane strains accurately. However, since the bending strains increase in proportion to the distance from the neutral axis, the theoretical bending strains calculated for the surface of the metal had to be increased to reflect the thickness of the strain gages. The

theoretical membrane strains were then added to the corrected theoretical bending strains to calculate the "theoretical" strains at the axis of the strain-gage foil.

To determine the amount of correction necessary, the neutral axis for the bending strains in each specimen was selected as being at the middle of the metal thickness. A typical gage was mounted on a metal specimen and cross sectioned. Careful measurements showed that the middle of the foil was 0.00135 inch from the metal surface. This dimension was added to the distance from the neutral axis (half the measured bellows wall thickness), and the theoretical bending strain was multiplied by the ratio:

$$\frac{\text{distance from neutral surface to strain-gage foil*}}{\text{distance from neutral surface to metal surface}} .$$

Because of the biaxial nature of the strains, it was believed that a comparison of the experimentally determined strains with the theoretically predicted strains was not sufficient to give a clear understanding of the verification of the theory. Therefore, stresses were calculated from the modified theoretical strains, and these modified theoretically predicted stresses were compared with stresses calculated from the experimentally determined strains.

Vibration Evaluation

It was estimated that formulas from the state of the art would be adequate for predicting the longitudinal or accordion vibration mode and the transverse or beam vibration mode of formed and welded bellows for aerospace components. The applicability of these formulas was evaluated through a theoretical and experimental vibration analysis of each of the selected bellows types.

Figure Q-3 shows the design of the fixture for evaluating bellows under longitudinal and transverse vibration modes. For longitudinal vibration, the end fittings of the bellows were rigidly positioned from a base plate. Although one base plate served for all bellows sizes, separate shafts and cylindrical stiffeners were required for each of the bellows sizes and lengths. For transverse vibration testing, the longitudinal vibration fixture was turned 90 degrees and fastened to an L-shaped bracket. One L-shaped bracket was satisfactory for all bellows sizes. This arrangement minimized the cost of the fixture, and simplified the mounting of the specimens for test. The fixture was designed for use with a Caladyne Model 174.

Each bellows was subjected to accordion and lateral-mode frequency scans from 100 cps to 10,000 cps to determine resonant frequencies. Since some indications of resonance by the acceleration meter on the shaker console were produced because of fixture vibration, each indicated resonant period was checked by means of stroboscopic observation to verify that the resonant behavior was associated with the bellows and not the fixture. In some cases the amplitude of lateral response was so slight that acceleration indications of resonance were meaningless and a touch-sensing approach was used to detect the resonant periods.

*As described in Appendix L, it was occasionally necessary to estimate the strains at the metal surface from the experimentally determined strains. The reciprocal of this ratio was used to make this calculation, even though the answer was not accurate because of the inclusion of membrane strain in the measured value. However, the membrane strain was usually small compared to the bending strain, so the error in the correction was usually small.

An auxiliary test was conducted with the 5-inch formed bellows to confirm the results of the lateral-shake tests to determine the effect (if any) of fixture configuration on bellows response. The test procedure consisted of mounting the bellows in a fixture with the axis horizontal, adhesively mounting a ferrous object to the outer edge of the center convolution, and then striking the center of the bellows span with a plastic mallet. Oscillation of the bellows and ferrous target was sensed by means of a stationary magnetic pickup and taped by a recording oscillograph. Analysis of the recorded traces showed that the bellows response was identical with that obtained in the Caladyne machine.

Fatigue Evaluation

The requirements of the fatigue evaluation are described in detail in Appendixes K, L, and M. Figure Q-4 shows a layout of the machine that was designed and fabricated for the fatigue tests. Three bellows sizes (5-, 3-, and 1-inch diameter) are shown in the two views to depict the types of fixtures and special features required for mounting different specimen sizes. Figures Q-5 and Q-6 show the completed machine. A 5-inch bellows is shown mounted on the machine. Two specimens of equal size were usually mounted on the machine during test operation.

The fixture mounting surface, fulcrum-pin-support assembly, and rocker beam, together with the connecting rods, fulcrum pin, wrist pins, and bearings, were a self-contained assembly and were designed to operate with minimum structural deflection. The major portion of the forces generated in deflecting the test specimens was contained within this assembly. A mounting frame constructed from a weldment of steel angle and channel supported this assembly. Also mounted on the frame were a motor and speed-reduction unit, which provided the reciprocating motion for the rocker beam. A motor-mounted variable-speed pulley drove through a fixed-reduction gear box to provide a variation in specimen deflection rate. Because the machine was to be operated for approximately 5000 hours, provisions were made for easy adjustment and replacement of critical parts such as bearings and pins. Standard parts were used wherever possible to reduce the initial cost of the machine and the cost of machine maintenance.

The large bellows were tested at 60 cycles per minute, while the small bellows were tested at rates up to 120 cycles per minute. The rates were selected sufficiently low that no dynamic amplifications were created in the bellows.

Changes in amplitude of specimen deflection were accomplished through a micrometer adjustment incorporated in the adjustable throw-crank arm. The basic design of the machine assured that each of the two specimens under test received the same extremes of deflection and stress. Compensation for manufacturing variations in bellows height were accomplished within ±0.005 inch through the use of spacers for adjusting the length of the bellows actuator rod. With careful use of height gages and dial indicators, the bellows deflections were maintained within ±0.001 inch of the desired amount.

A leak-detection system was used which permitted the machine to be left in operation without attendance. A schematic drawing of the system is shown in Figure Q-7, and the installed system can be seen in Figures Q-5 and Q-6. The system included a source of pressurized gas which was used to pressurize the inside of the bellows. When a

bellows developed a leak during the fatigue test and gas leaked into the volume between the outside of the bellows and the inside of the bell jars, the pressure in this volume increased and an adjustable pressure switch was actuated.

With the actuation of the pressure switch, the motor on the fatigue machine was shut off, and two solenoid valves were actuated. One valve shut off the system from the source of pressurized air. The second valve opened the inside volume of the bellows to atmospheric pressure so the pressure in the bell jars could not build up because of the leak in the bellows. A test of the system showed that a helium leak of approximately 1×10^{-2} atm cc/sec actuated the pressure switch in approximately 4 minutes with the switch adjusted for 4 ounces of pressure. With this setting, the machine would automatically stop the test approximately 240 cycles (with a machine speed of 60 rpm) after a leak of this size developed in one of the bellows.

When the first of two bellows failed, a manometer was connected to each bell jar in turn (with the bellows pressurized). Movement of the water column indicated which bellows contained the leak. Soap solution was then used to find the location of the leak in the failed bellows. Each location was marked for subsequent examination, as described in Appendix P.

TABLE Q-1. REPRESENTATIVE BELLOWS AND DIAPHRAGMS

Configuration	Material
Single-Ply Formed Bellows	
5-11/16 in. OD, 5 in. ID	Type 321 stainless steel
3-5/8 in. OD, 3 in. ID	Type 321 stainless steel
1-5/16 in. OD, 1 in. ID	Type 321 stainless steel
3-1/2 in. OD, 3 in. ID	Inconel 718
1-1/4 in. OD, 1 in. ID	Inconel 718
Two-Ply Formed Bellows	
3-5/8 in. OD, 3 in. ID	Type 321 stainless steel
1-5/16 in. OD, 1 in. ID	Type 321 stainless steel
Nested-Ripple Welded Bellows	
3-1/2 in. OD, 2.812 ID	Type 347 stainless steel
3 in. OD, 2.838 ID	AM-350
1-1/2 in. OD, 1.055 ID	Type 347 stainless steel
1-1/2 in. OD, 1.060 ID	AM-350
Convoluted Diaphragms	
4 in. OD	Type 347 stainless steel

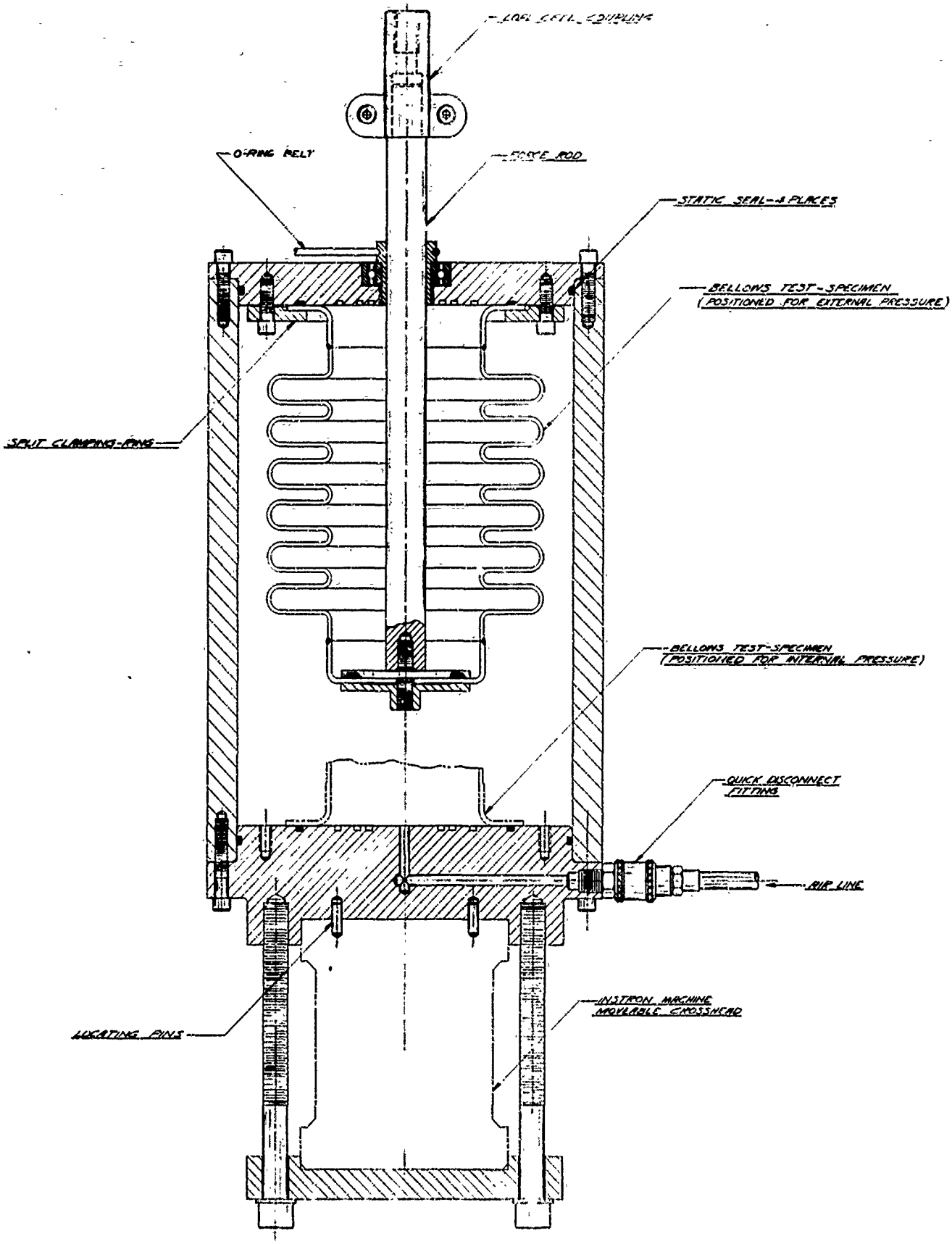

FIGURE Q-1. FIXTURE FOR PRESSURE-DEFLECTION EVALUATION OF BELLOWS

1C217

FIGURE Q-2. INSTALLATION OF A PAIR OF STRAIN GAGES – TYPES EA-09-015EH-120 (TOP) AND EA-09-015DJ (BOTTOM)

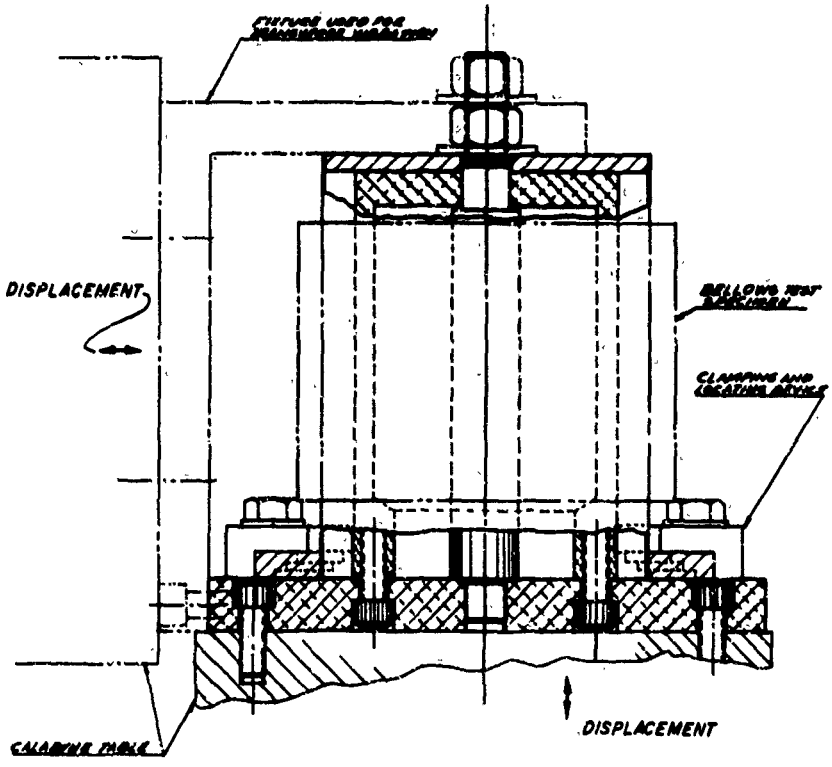

FIGURE Q-3. FIXTURE FOR VIBRATION EVALUATION OF BELLOWS

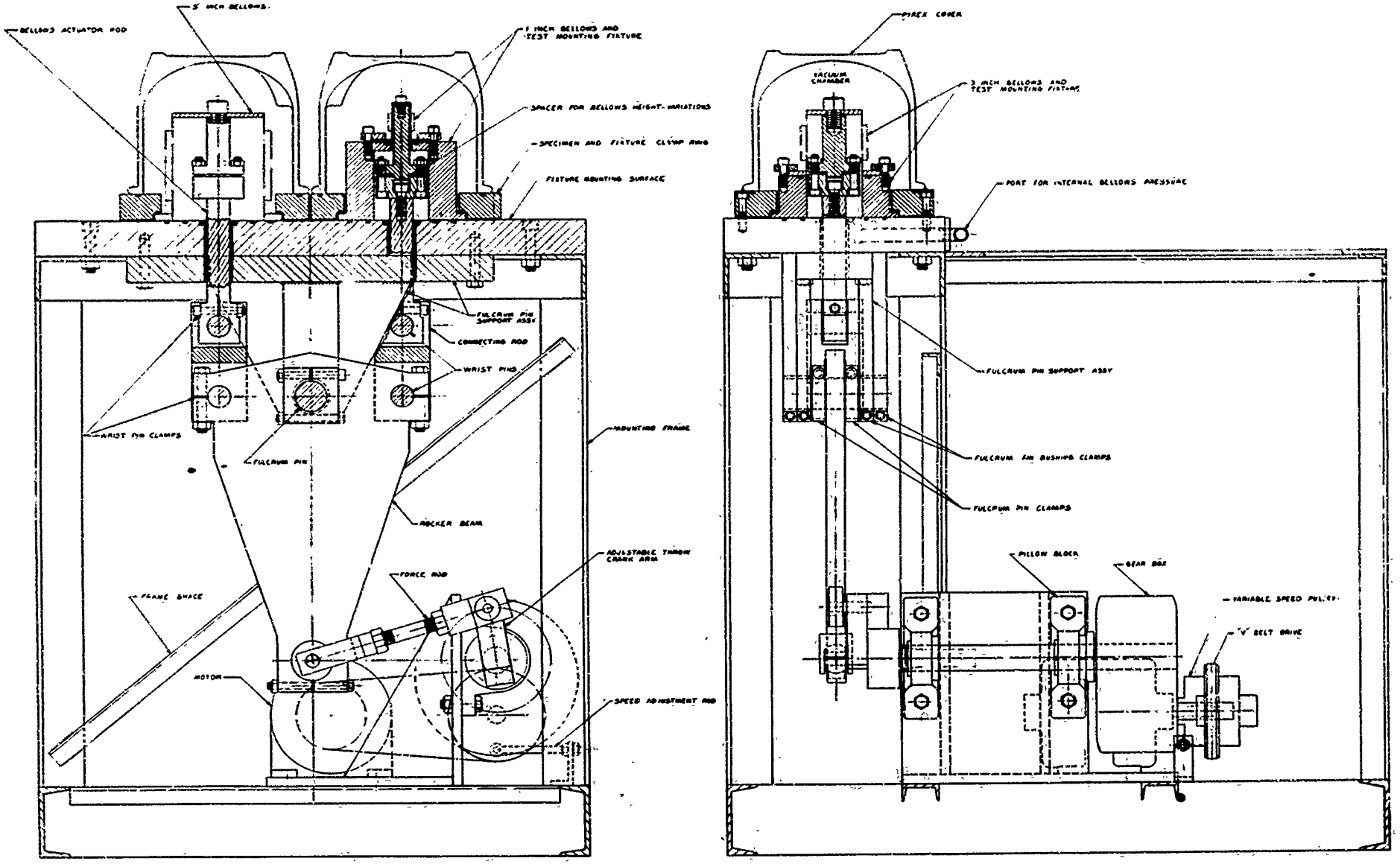

FIGURE Q-4. FATIGUE TEST MACHINE-BELLOWS AND DIAPHRAGMS

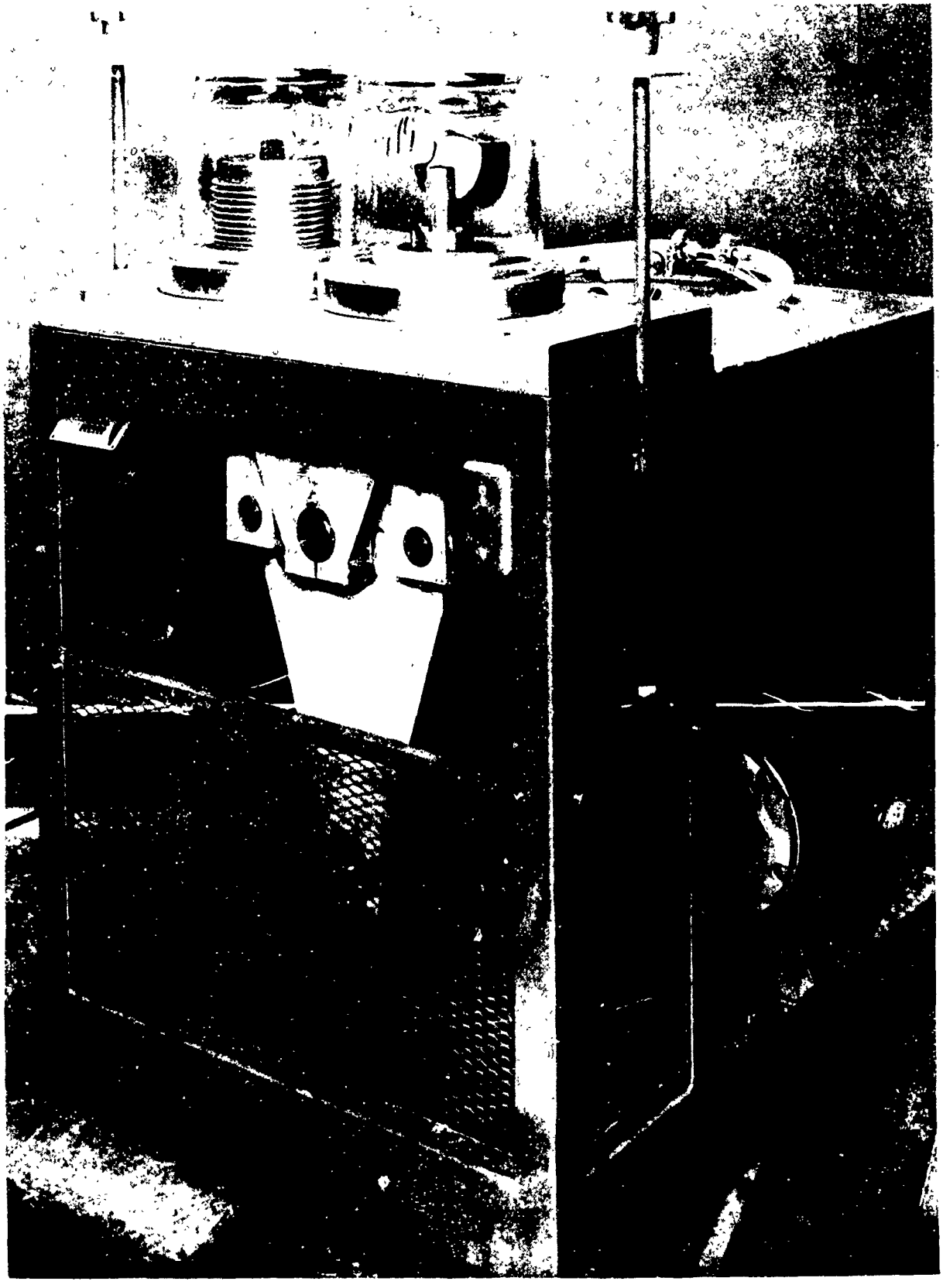

32509

FIGURE Q-5. FRONT OF FATIGUE TEST MACHINE

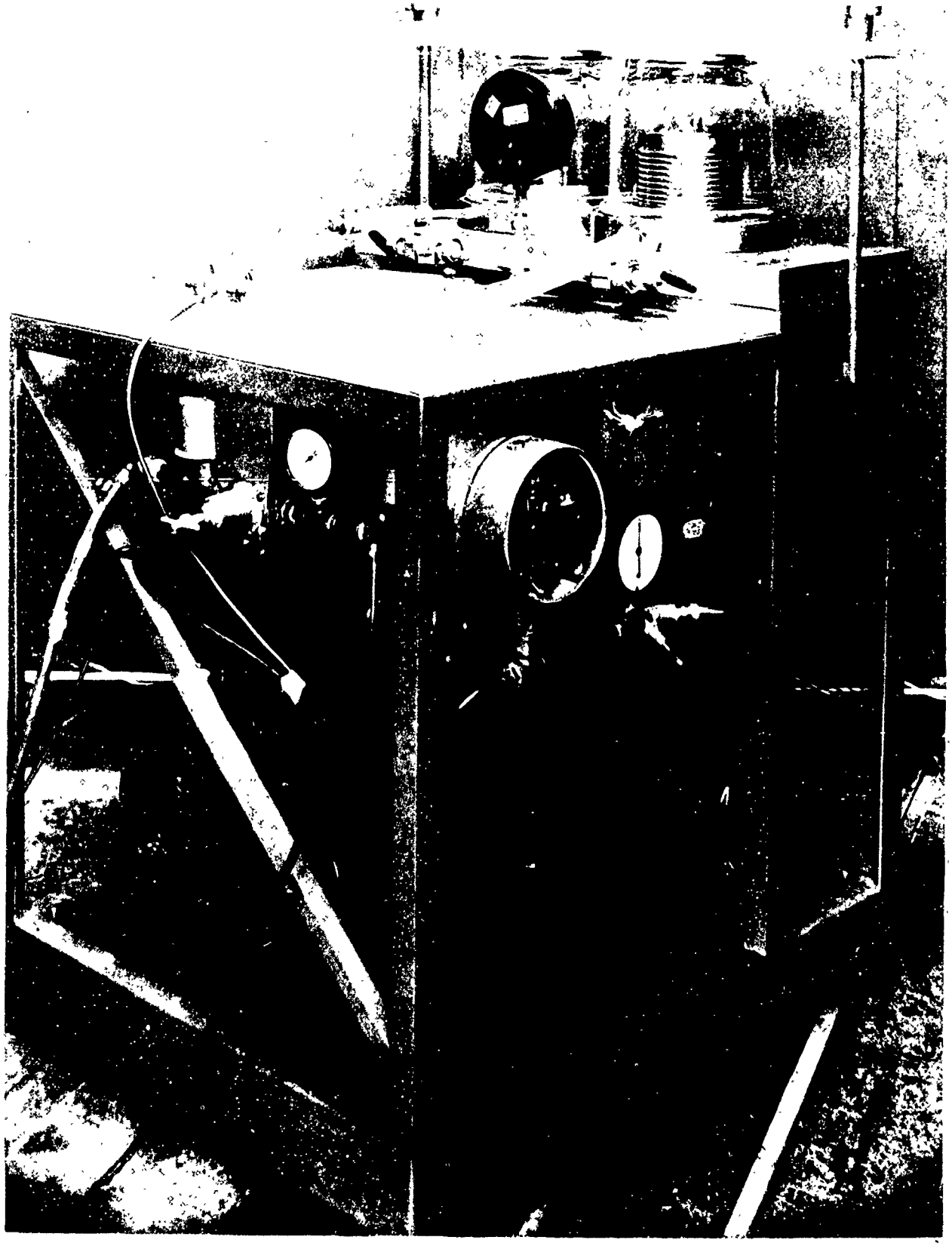

32510

FIGURE Q-6. BACK OF FATIGUE-TEST MACHINE

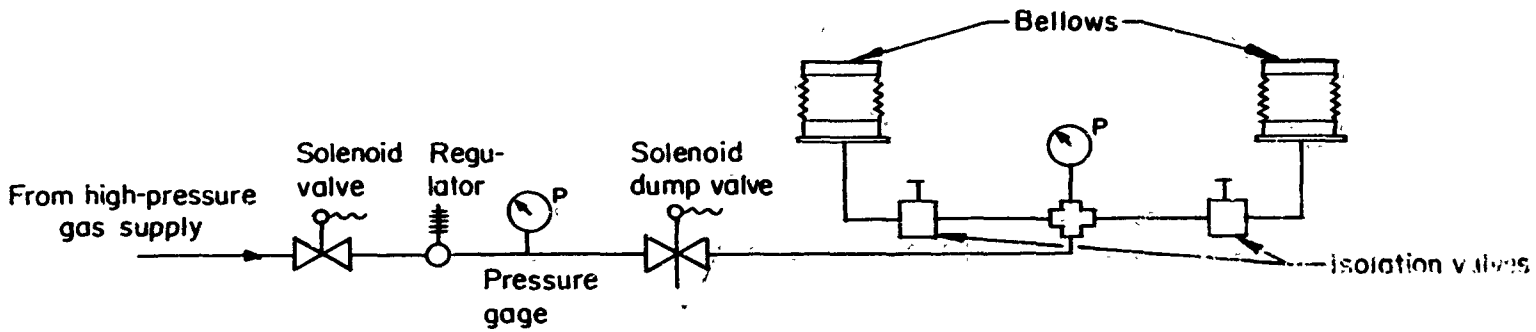

a. Pressurizing Components

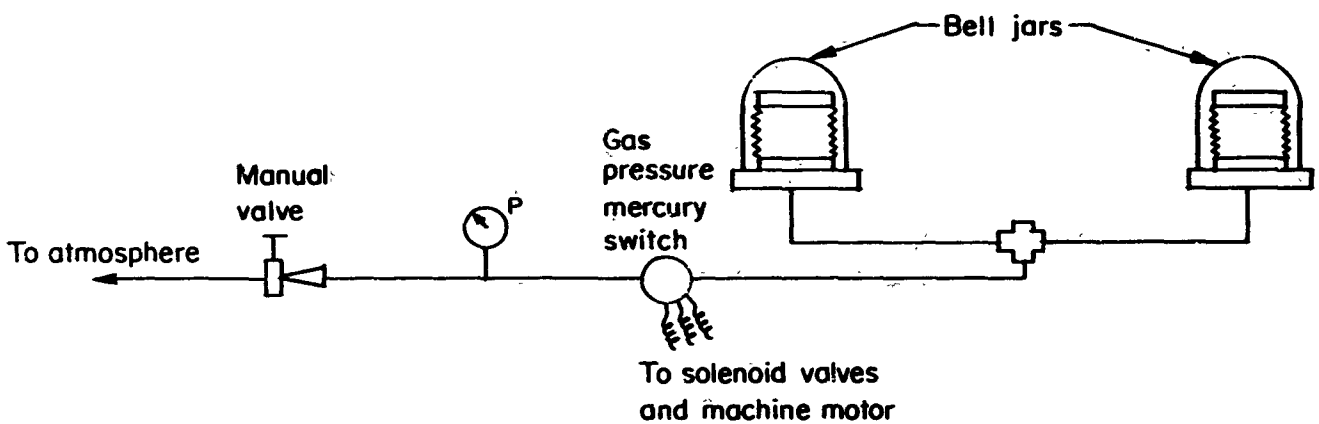

b. Leak-Detection Components

FIGURE Q-7. FATIGUE MACHINE PRESSURIZING AND LEAK-DETECTION SYSTEM